Concentrations of atmospheric reactive mercury in Australia and emissions of reactive mercury from contaminated mine materials using cation exchange membranes

Matthieu B. Miller

A dissertation submitted in fulfillment of the requirements for the degree of

Doctor of Philosophy

Department of Environmental Sciences

Faculty of Science & Engineering

November 2018

STATEMENT of CANDIDATE

Except where acknowledged in the customary manner, the material presented in this dissertation is wholly original and has not been submitted in fulfillment of a degree at this or any other university.

ABSTRACT

Mercury (Hg) is a pervasive and persistent environmental contaminant with a significant atmospheric cycle that results in distribution to all spheres of the environment. In the atmosphere Hg is found primarily as gaseous elemental Hg^0 (GEM) but under certain scenarios reactive Hg^{2+} (RM) compounds may form a significant proportion of total atmospheric Hg. Physiochemical transformation processes play a leading role in the air-surface exchange of Hg and are a major determinant of Hg mobility and longevity within the environment, including bioavailability and biological uptake into ecosystem food webs, which constitutes the primary exposure pathway to the human population. Practical differentiation of gas and particle phase RM has proven to be a profound and lasting measurement challenge, and even the broadest distinction between GEM and RM is easily confounded. In addition to the intrinsic difficulties of measurement, data on atmospheric Hg in the Southern Hemisphere (SH) suffers the further limitation of being comparatively rare, and almost non-existent for RM. Lack of data inhibits international scientific and regulatory efforts to monitor, model, and mitigate the effects of Hg exposure to human populations.

In an effort to help close some of the information gap, this study deployed a recently developed filter-based RM sampling system at two locations in Australia with existing GEM monitoring capabilities, and onboard the Australian Research Vessel Investigator (RVI) during a research voyage to the East Antarctic coast. The ground-based field sites included a remote, temperate coastal site at the Cape Grim Baseline Air Pollution Station (CGBAPS) on the northwestern point of Tasmania, and a temperate urban site at Macquarie University Automatic Weather Station (MQAWS) in Sydney, New South Wales. Measurements were undertaken between November 2015 and May 2017, constituting the most extensive dataset on RM concentrations in Australia to date. As has been shown for GEM in the SH, concentrations of RM were relatively uniform over time and between sites, despite very different environments. The overall mean RM concentration was 15.9 ± 6.7 pg m^{-3} at CGBAPS and 17.8 ± 6.6 pg m^{-3} at MQAWS. No seasonal trend in RM concentration was apparent at CGBAPS, in contrast to a small but statistically distinct difference in winter versus summer RM concentration apparent at MQAWS. The concentration of RM measured on RVI over the Southern Ocean averaged 23.7 ± 7.0 pg m^{-3} during four deployments in austral summer (January 10 – March 4, 2017). GEM was measured concurrently with the RM filter sampling, with an overall mean concentration of 0.65 ± 0.24 ng

m^{-3} MQAWS and 0.90 ± 0.35 ng m^{-3} at CGBAPS, and 0.53 ± 0.10 ng m^{-3} on the RVI voyage. Additionally, tandem measurements of GEM were performed for one year at CGBAPS using both a Tekran® 2537B and a 2537X Automatic Ambient Air Analyzer. Inter-comparison of the two instruments indicated that the 2537X unit measured systematically higher GEM concentrations versus the 2537B, with an average difference of 8.6%.

Complimentarily to the larger goal of quantifying ambient RM, the CEM material was deployed in a novel technique to measure RM air-surface exchange, in conjunction with an established method based on Teflon dynamic flux chambers (DFC) and a Tekran® 2537 mercury analyzer. Initial results using this combined CEM/DFC methodology indicate that RM flux can be detected at a minimum difference of ~ 13.5 pg m^{-3} between DFC inlet and outlet concentrations, based on the analytical detection limit of blank CEM material. Distinct differences in RM flux were observed between material types with a range of Hg concentration, and between wet and dry materials. Mercury contaminated mining materials such as tailings may have relatively large RM fluxes of several 1000 pg m^{-2} h^{-1}.

In addition to the ambient field site deployments, extensive method validation tests were undertaken in controlled laboratory conditions. As part of these tests, CEM material was exposed to high concentrations of GEM and a representative Hg^{2+} compound ($HgBr_2$), using a custom-built permeation system. The CEM material was found to take up a consistently negligible amount of GEM (0.004 ± 0.001% of total exposure) in clean laboratory air at varying levels of humidity. GEM concentrations during the permeation tests were 1.43×10^6 to 1.85×10^6 pg m^{-3}, resulting in total GEM exposures ranging from 2.7×10^6 to 7.3×10^6 pg. The low rate of GEM uptake at these high concentrations indicates that, at typically much lower ambient atmospheric concentrations, GEM uptake would be concomitantly small and essentially unobservable, an important prerequisite for the CEM material to be successfully employed in ambient air sampling. The CEM material also exhibited very little breakthrough (< 0.5%) of total permeated $HgBr_2$ at concentrations up to ~5000 pg m^{-3}, indicating a high collection efficiency for this particular gaseous oxidized Hg compound under laboratory conditions.

ACKNOWLEDGEMENTS

I extend a deep debt of gratitude to Dr. Grant C. Edwards, who in addition to providing much scientific, academic, and professional advice was also a personal friend and confidant. His warmth and generosity above all else made the completion of this dissertation possible. Dr Edwards passed away unexpectedly on September 10, 2018. He is sorely missed.

I express sincere thanks to Dr. Mae S. Gustin, an advisor not just on this dissertation but on many other classes, projects, presentations, and papers for more than a decade now. Her tireless energy has been a source of inspiration.

I also thank the students, technicians, scientists, colleagues and collaborators associated with both Dr. Edwards' and Dr. Gustin's research laboratories over the years, as well as staff from BoM and CSIRO associated with the Cape Grim research program. Many ideas have been exchanged, problems solved, and beers consumed.

The reviewers who shouldered the voluntary burden of reading and evaluating this dissertation, without remuneration nor recompense, I hail as unsung heroes.

Finally, but most importantly, I am forever indebted to and in awe of the fortitude, perseverance, and grace with which Dr. Ashley M. Pierce, my partner in this and other adventures, handled the challenges not just of my dissertation, but of her own, simultaneously. You beat me after all, Dr. Pierce.

"Always do sober what you said you'd do drunk. That will teach you to keep your mouth shut."

- Ernest Hemingway

TABLE of CONTENTS

LIST of FIGURES

LIST of TABLES

CHAPTER 1:

Opening Remarks

1.1 Introduction

Mercury (Hg) has been valued since antiquity, originally for its intriguing aesthetic qualities, but increasingly through human history for its more prosaic functional properties. Vermillion, made from the crushed Hg mineral Cinnabar, was prized for its brilliant luster in art ranging from Neolithic rock painting to elaborate classical frescoes. The Romans valued the pigment so highly that price controls were set by Senatorial decree and the first large-scale mining of Hg ore was undertaken in the vast deposits of Almadén, present day Spain. The ability of Hg to amalgamate with precious metals was first exploited at truly industrial scale in the *patio* process, developed by Bartolomé de Medina in 1554 to economically recover silver from the difficult ores of the New World Spanish provinces. Since that time Hg has been utilized in many and diverse aspects of technology and industry. The application of Hg to precision thermometry by Dutch scientist Gabriel Fahrenheit in 1714 ushered in what can be considered the first standardized calibrated measurements in early atmospheric research. It is therefore with some irony that Hg itself continues to pose serious measurement challenges for modern science.

The long legacy of anthropogenic Hg extraction, utilization, and liberation, for reasons both purposeful and incidental, and at scales ranging from the individual to industrial, has resulted in present day environmental Hg burdens many times greater than could be expected solely from natural sources. The unique volatility of Hg as a liquid metal and relatively inert monatomic gas at earth surface conditions leads to an exceptional atmospheric residence time for a metallic element, and consequently extensive cycling between all compartments of the environment. Hg

is a potent neuro-systemic toxin and its bio-accumulation and bio-magnification in aquatic ecosystems results in a significant exposure pathway to wildlife and humans, to sometimes profound detriment.

With increasing global recognition of the adverse environmental effects of Hg, the United Nations Environment Program (now UN Environment), undertook an extensive assessment and regulatory policy initiative that has culminated in widespread international commitment to the Minamata Convention on Mercury. This landmark treaty entered force on August 16, 2017, and at the time of writing had 128 signatories, including Australia, legally committed to monitoring and reducing anthropogenic emissions and releases of Hg to the environment. Within the framework of the Minamata Convention, the scientific community is urged to undertake continuous improvements in the measurement, modelling, and understanding of Hg and its complex cycle in the environment.

1.2 Dissertation Objectives

The overall objective of this dissertation was to explore novel methods in quantification of reactive mercury (RM), within the context of better overall quantification of atmospheric Hg and Hg sources. In line with this goal, a relatively new RM measurement technique using cation exchange membranes (CEM) was deployed at continuous monitoring sites in Australia (the first such long-term data for RM in Australia) and on a research cruise in the Southern Ocean, to measure ambient concentrations of RM in conjunction with gaseous elemental mercury (GEM). Mercury measurements in the Southern Hemisphere (SH) are sparse in general, so contributing to an improvement in the spatial and temporal coverage of Hg data in the SH and globally was a key motivation for the project.

The CEM material was also used to investigate a potential new method for measuring RM air-surface exchange, via the novel addition of CEM filters to a traditional dynamic flux chamber (DFC) system. The method was developed in a laboratory setting using mining-related substrates with a range of total Hg concentrations as test materials, for which a thorough data-set on GEM flux was previously compiled. This work represents the first direct measurements of RM air-surface exchange, all previous measurements being inferential. Initial results suggest this combined CEM/DFC technique could enable direct measurement of RM flux in the field, certainly at contaminated sites and possibly for background areas.

The CEM material is a promising measurement technique for atmospheric RM compounds, but method validation and quality assurance are ongoing. As such, extensive experimental quality assurance and performance verification of the CEM material was completed as part of this dissertation. This performance evaluation included an in-depth assessment of GEM uptake on the CEM filters in the active flow configurations used for measuring ambient RM concentrations, as well as an exploration of the factors controlling potential RM breakthrough or loss from the CEM material.

Lastly, a preliminary technical inter-comparison was made between two versions of the standard commercially available Hg analyzer typically employed in the ambient air monitoring capacity: the venerable Tekran® 2537B and the newer Tekran® 2537X model. The two units have been operated in tandem since June 2017 at the Cape Grim Baseline Air Pollution Station in Tasmania, Australia.

1.3 Dissertation Structure & Outline

The complete dissertation embodies nine chapters, including the introduction, a comprehensive literature review, six chapters published, submitted, or in preparation for peer-reviewed publication, and a final concluding chapter tying together results from the individual experimental studies. All research presented in this dissertation was completed while enrolled at Macquarie University, except for Chapter 3 which was completed during an interim period as a research technician at the University of Nevada Reno. This interim research period occurred post-completion of a MSc with Dr Mae Gustin at the University of Nevada, but prior to officially beginning the PhD program with Dr Grant Edwards at Macquarie University. The work presented in Chapter 3 has not been used in fulfillment of any previous academic degree. The author's relative contribution to each original research chapter is bulleted below the following short descriptions, complementarily to a detailed Statement of Authorship included at the beginning of each chapter. As the research chapters have been written and formatted as stand-alone manuscripts for submission to individual journals, some topical repetition was unavoidable.

- Chapter 2: *Origins, Characteristics, & Measurement of Mercury in the Atmosphere* provides a general overview of Hg and its origins, the basic biogeochemical processes of Hg in the environment and particularly in the atmosphere, and the techniques for measuring both atmospheric concentrations and air-surface exchange of Hg. Particular focus is given to the unknowns and uncertainties in atmospheric Hg measurement, and a concise history of the CEM methodology is presented.

- Chapter 3: "*Testing and modeling the influence of reclamation and control methods for reducing nonpoint mercury emissions associated with open pit gold mines"* is a paper published in the *Journal of the Air and Waste Management Association* describing the provenance, collection, and characterization of mining related substrate materials used in following laboratory studies of Hg flux. Potential remediation strategies for reducing GEM emissions from mining materials were explored in a laboratory setting, and a field campaign was undertaken to assess in-situ GEM fluxes from active mining locations, comparing these to a predictive model developed in previous work.

    • Study Design: 50% • Data Collection: 95% • Data Analysis: 90% • Writing: 75%

- Chapter 4: *"Evaluation of cation exchange membrane performance under exposure to high Hg^0 and $HgBr_2$ concentrations"* is a submitted manuscript currently in-discussion with *Atmospheric Measurement Techniques*. The manuscript presents the results of a quality assurance study on the CEM material using a custom-built Hg vapor permeation system. The main objectives of this study were to demonstrate high transparency of the CEM material to elemental Hg^0, as well as to test whether GOM would break through the CEM filters at high concentration. The system also enabled estimation of GOM collection efficiency by the CEM material.

    • Study Design: 90% • Data Collection: 90% • Data Analysis: 95% • Writing: 95%

- Chapter 5: *"Reactive mercury flux measurements using cation exchange membranes"* is a manuscript submitted to *Atmospheric Measurement Techniques*, presenting the results of a novel method development for measuring RM air-surface exchange using cation exchange membrane filters. In this method, dynamic flux chambers are employed in conjunction with

CEM filters for the simultaneous dual measurement of GEM and RM flux. This chapter focusses on proof of concept and quality assurance for RM flux detection, including determination of method detection limits and repeatability of measurements.

• Study Design: 65% • Data Collection: 90% • Data Analysis: 90% • Writing: 80%

- Chapter 6: *"Effect of moisture on air surface exchange of reactive mercury from mining substrates"* is a prepared manuscript presenting the results of extensive GEM and RM flux measurements, using the method developed in Chapter 5, from a series of mining-related substrate materials, under wet and dry conditions. The speciation of Hg in the mining materials was also determined via solid-phase thermal desorption, providing insight into which solid Hg compounds may contribute to RM emissions.

  • Study Design: 75% • Data Collection: 85% • Data Analysis: 85% • Writing: 95%

- Chapter 7: *"Reactive mercury concentrations in Australia and the Southern Hemisphere"* is a prepared manuscript presenting the first extended measurements of ambient RM concentrations in Australia, and some of the first reported in the Southern Hemisphere, using the CEM filter method. GOM concentrations are also reported for campaign deployments on a research cruise in the Southern Ocean. Field sites were located at the remote Cape Grim Baseline Air Pollution Station in Tasmania, and at the Macquarie University Automatic Weather Station in a suburban area of Sydney, New South Wales.

  • Study Design: 60% • Data Collection: 50% • Data Analysis: 90% • Writing: 95%

- Chapter 8: *"Inter-comparison of Tekran® 2537 B and X Ambient Air Mercury Analyzers at Cape Grim Baseline Air Pollution Station"* is a prepared manuscript that describes a

performance inter-comparison between two versions of a standard analytical platform for monitoring atmospheric Hg: the Tekran® 2537 B and X Ambient Air Mercury Analyzer. The analyzers were operated at the Cape Grim Baseline Air Pollution Station for one year.

• Study Design: 80% • Data Collection: 30% • Data Analysis: 90% • Writing: 95%

- Chapter 9 is a concluding chapter that provides a discussion of overall results and the implications for measurement of RM in the ambient atmosphere and in air-surface exchanges. The basic performance of the CEM material in capturing RM is assessed across all components of the study, from laboratory permeation to remote ambient air measurements.

CHAPTER 2:

Origins, Characteristics, & Measurement of Mercury in the Atmosphere

2.1 Geologic Origin & Basic Properties of Mercury

Mercury (Hg) is a naturally occurring metallic element, disseminated throughout the earth's lithosphere at average concentrations of 100 ng g^{-1} or less (Turekian and Wedepohl, 1961; USGS, 1970). Recent work suggests that typical igneous crustal rocks, which constitute the original geologic source of Hg before subsequent redistribution and enrichment in ore deposits and sediments, may average as low as 2 ng g^{-1} (Canil et al., 2015). However, organic rich sedimentary rocks such as shales and mudstones (and coal) may preferentially accumulate Hg at 1000's of ng g^{-1} in the depositional process, and mineralized areas can contain up to several mass % Hg (Rytuba, 2005). In primary geologic deposits, Hg predominantly occurs as the sulfide mineral Cinnabar (HgS), though it is frequently present in free elemental form, and many other minor mineral types are known (Rytuba, 2005; USGS, 1970).

Geologic concentrations of Hg are highest in zones of volcanic and geothermal activity, in which it can be readily mobilized by high temperature fluids and gases and redistributed to near-surface deposits (Bagnato et al., 2015; Rytuba, 2005; Varekamp and Buseck, 1984; White et al., 1970). Belts of such enhanced geogenic Hg concentration occur along present or former plate tectonic margins, where some deposits can be very large, such as the mining district of Almadén, Spain, where Hg has been mined for over 2 millennia (Goldwater, 1972; Parson and Percival, 2005; Rytuba, 2003). It is primarily from these zones of enrichment that Hg has entered the surface environment, either naturally from volcanic/geothermal emissions and erosive forces or facilitated, in relatively recent history, by human extraction.

Mercury is unique among metals in being liquid at ambient earth-surface temperatures and pressures, allowing vaporization into the gas phase (basic properties of elemental Hg are listed in Table 2.1). As a result, Hg is naturally present in the atmosphere as a trace gas. Elemental Hg has a low water solubility (Andersson et al., 2008; Clever et al., 1985) and is relatively chemically inert, with a first ionization potential comparable to some noble gases, reacting only slowly with most common atmospheric oxidants (Schroeder et al., 1991). Due to this relative inertness, atmospheric Hg is predominantly in the reduced monatomic elemental form (Hg^0), with an atmospheric residence time that was originally speculated at up to 2 years (Lindqvist and Rodhe, 1985; Schroeder et al., 1991; Slemr and Langer, 1992; Slemr et al., 1985) but more recently is estimated at 5-12 months (Holmes et al., 2010; Horowitz et al., 2017; Lindberg et al., 2007). The relatively long-life span of Hg in the atmosphere allows for distribution to otherwise pristine environments remote from significant sources (Fitzgerald et al., 1998; Lindberg et al., 2007).

Some fraction of atmospheric Hg can be oxidized to the divalent Hg^{2+} state, forming myriad gas-phase molecules, or sorbing to aerosols to form particulate Hg. These reactive Hg^{2+} species are more soluble and have a greater potential for both wet and dry deposition (Driscoll et al., 2013; Lindberg et al., 2007; Lindqvist and Rodhe, 1985; Schroeder and Munthe, 1998; Schroeder et al., 1991). Once distributed to an environment by such depositional processes, the ultimately irreducible elemental nature of Hg results in a long process of biogeochemical cycling throughout the various compartments of the environment, and the potential for toxic exposures to biota.

Table 2.1	
Property	**Value**
Formula	Hg^0
Atomic #	80
Atomic Mass	200.59 g mol^{-1}
Melting Point	-38.8 °C
Boiling Point	356.7 °C
Vapor Pressure (20 °C)	1.20 x 10^{-3} Torr
Saturated Air Concentration (20 °C)	13.18 ug L^{-1}
Water Solubility (20 °C)	63.9 ug L^{-1}
Specific Gravity (20 °C)	13.55
Henry's Law Coef (25 °C)	4.4 (Pa)
Ionization Potential (1st)	1008.3 kJ mol^{-1}

Table 2.1 Basic properties of elemental mercury (adapted from Schroeder et al., 1991)

2.2 Environmental Toxicity and Impacts of Mercury

Mercury is toxic to most life at a basic cellular level, where it can adversely impact cell membranes, macromolecular cell structures, and DNA (Rice et al., 2014). In aquatic environments Hg can be biotically and abiotically converted to organic methylated forms such as methyl mercury (MeHg), primarily by sulfur reducing bacteria (Compeau and Bartha, 1985), in which form it readily bio-accumulates and bio-magnifies in the food web (Benoit et al., 2002; Selin, 2009). In fish, birds, and mammals, Hg and MeHg are potent systemic toxins (Scheulhammer et al., 2007; Wolfe et al., 1998). Elevated concentrations of MeHg in seafood are the primary exposure pathway to humans (NRC, 2000).

As a human toxin, Hg is most often noted for its pronounced and grotesque neurological effects, but it is also associated with the onset of over 250 chronic and acute symptoms ranging throughout the major organ systems, including cardiovascular, immune, renal, pulmonary, and nervous (Mergler et al., 2007; Rice et al., 2014). The most graphic demonstrations of Hg toxicity have been the many industrial scale mass poisonings (Selin, 2009). In the 1950s, serious health problems in the human residents around Minamata Bay, Japan, were linked to MeHg in the local marine ecosystem. Over many years, waste effluent from a chemical plant had released MeHg to the bay, where it was concentrated in seafood and consumed by the local population, eventually resulting in over 2000 fatalities (Harada, 1995). In 1971, Iraqi farmers mistakenly used imported seed grain treated with an organo-mercury fungicide to make bread flour for human consumption, resulting in over 6000 hospitalizations (Bakir et al., 1973; Marsh et al., 1987). While graphic, industrial incidents and occupational exposures are isolated and rare, though accelerating use of Hg in small scale mining operations may portend a greater frequency of acute toxic exposures (Telmer and Veiga, 2009). Given the ubiquity of Hg in the environment, low level chronic exposure is much more pervasive, and the effects more insidious to human and ecosystem health, to great cost (Driscoll et al., 2013; Trasande et al., 2005).

Concerns about Hg toxicity have prompted national and international action on reducing Hg loading to the environment. In 2013, the United Nations Environment Minamata Convention on Mercury was promulgated with a mission to protect human health and the environment from exposure to the toxic effects of Hg and compounds thereof, through a strategy of globally coordinated control and ongoing monitoring of Hg in the environment, combined with a commitment to continuing scientific research and development (UNEP, 2013b). Meeting the goals of the Convention presents a profound challenge for the global scientific and regulatory community, as there are over 3000 known Hg contaminated sites worldwide due to mining and

industrial activity, not including legacy and small scale operations involving Hg, and existing reservoirs of Hg in all compartments of the environment are large (Kocman et al., 2013; Krabbenhoft and Sunderland, 2013; Obrist et al., 2018; Pacyna et al., 2016).

2.3 Sources of Mercury to the Atmosphere

The current atmospheric Hg burden is estimated at roughly 4.6 Gg (Streets et al., 2017). This burden is the result of Hg emissions from both anthropogenic and natural sources, including re-emission of Hg previously deposited from the atmosphere. Such deposition has resulted in an increase of Hg concentration in surface soils by a factor of 3 or more, largely attributable to anthropogenic sources (Amos et al., 2015; Biester et al., 2007), and the Hg burden in soils is now very large at 250-1000 Gg (Obrist et al., 2018; Streets et al., 2011; Streets et al., 2017).

Natural sources of Hg to the atmosphere include Hg emitted from primary geogenic sources such as volcanic and geothermal areas but are dominated to a far greater extent by emissions from reservoirs of Hg in soil, vegetation, and surface waters (Fitzgerald and Lamborg, 2014; Gustin et al., 2008; Mason, 2009; Seigneur et al., 2001). These Hg reservoirs are primarily derived from previous atmospheric deposition, which may have been either natural or anthropogenic in origin, but original sources of emitted Hg are not practicably distinguishable. Total natural emissions from both primary and re-emitted Hg are estimated at 5207 Mg yr^{-1} (Pirrone et al., 2010). Evasion of Hg from the oceans accounts for the largest part of this total at 2778 Mg yr^{-1} (Mason, 2009), while biomass burning is estimated to be the single largest natural terrestrial source at 675 Mg yr^{-1} (Friedli et al., 2009). In areas of natural geogenic Hg enrichment, primary emission may be locally or regionally dominant (Gustin, 2003; Kocman and Horvat, 2011). Despite rough estimates, uncertainties in natural Hg emission and deposition remain large, and the relative importance of different sources and sinks is not well defined (Obrist et al., 2018).

Anthropogenic sources of Hg to the atmosphere are numerous, and include fossil-fuel fired power plants, artisanal small-scale gold mining (ASGM), ferrous and non-ferrous metal production, cements production, caustic soda production, and waste incineration (Obrist et al., 2018; Pacyna et al., 2016; Pirrone et al., 2010; UNEP, 2013a). The total combined anthropogenic Hg emission is estimated to be 2320 Mg yr^{-1} (Pirrone et al., 2010). The largest single emitter is fossil fuel (primarily coal) fired electric power generation, which contributes at best estimate 800-900 Mg yr^{-1} to the atmosphere (Obrist et al., 2018; Pirrone et al., 2010). Artisanal small-scale gold mining is a large (400-700 Mg yr^{-1}) and uncontrolled source of Hg to both terrestrial and aquatic systems and the atmosphere, and it is expected to become the dominant anthropogenic source of Hg as other sources are increasingly brought under control (Obrist et al., 2018; Pacyna et al., 2016; Sundseth et al., 2017).

Specifically in regards to Australia, the most recent reporting year 2016/2017 documented 7400 kg of Hg released to the atmosphere from point source emissions (Fig. 2.1), and a further 300 kg as fugitive emissions from industrial surfaces (NPI, 2017). This is a significant decrease from 2006, when total anthropogenic emissions in Australia were estimated at 15 ± 5 Mg (Nelson et al., 2012). The overall emissions reduction is due primarily to control processes at a single smelting facility in Western Australia, Kalgoorlie Consolidated Gold, which in 2015 phased-out ore roasting and eliminated emissions of over 8000 kg yr^{-1}. The largest current Hg emission source by far in Australia is fossil fuel electricity generation (3040 kg yr^{-1}), which is up from 2006 levels of 2200 kg yr^{-1} (NPI, 2017).

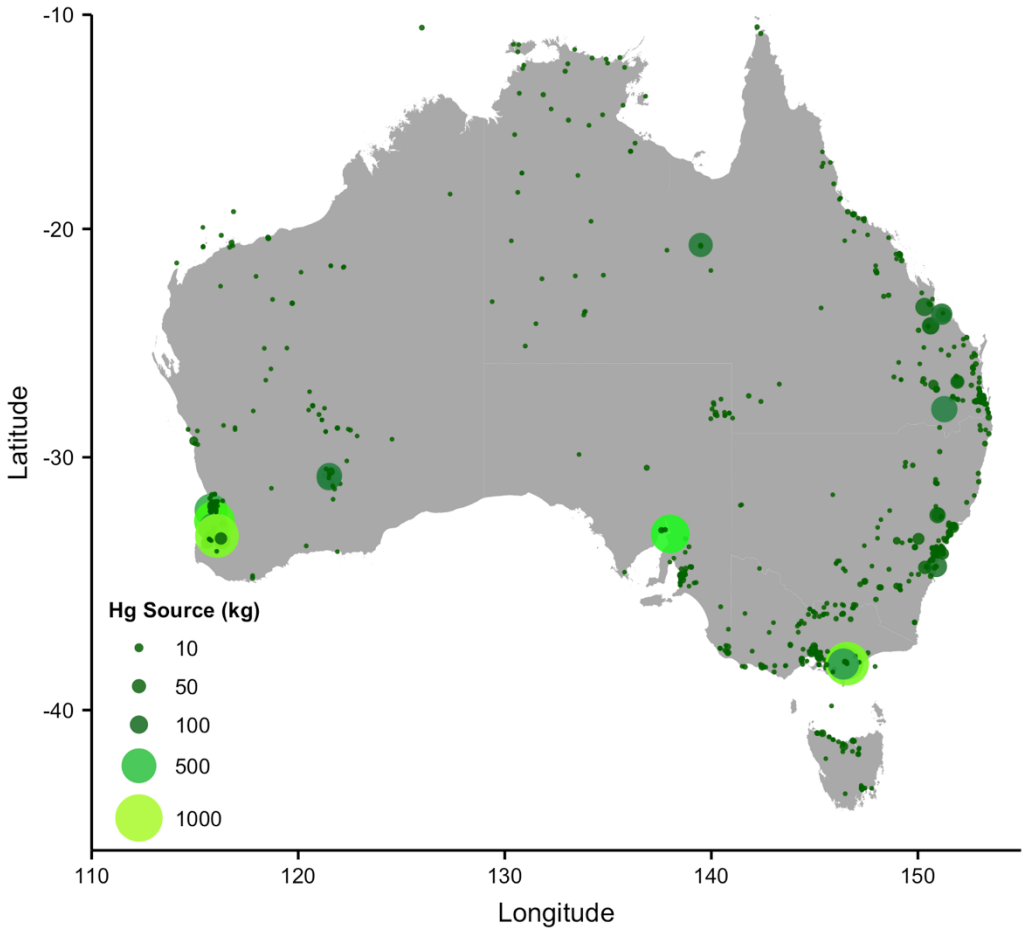

Figure 2.1 *Location and magnitude (kg yr^{-1}) of Australian point-source Hg emissions in 2016/2017. Data acquired from Australian National Pollutant Inventory (NPI, 2017).*

2.4 Mercury in the Atmosphere

Mercury in general is subject to numerous physical and chemical processes due to its unique properties, including three possible oxidation states: Hg^0, Hg^{1+}, and Hg^{2+} (Schroeder and Munthe, 1998). With a low melting point (-38.8 ºC) and high vapor pressure, Hg is highly volatile for a metal and the greatest potential for rapid transformation and cycling occurs in the atmosphere and at air-surface interfaces.

Based on physiochemical fractionation, atmospheric Hg is classified into three categories. The first and largest category is gas-phase elemental Hg^0, also known as gaseous elemental mercury (GEM), which makes up the majority (> 95%) of total gaseous mercury (TGM) and/or total atmospheric Hg (TAM) (Bloom and Fitzgerald, 1988; Gustin and Jaffe, 2010; Gustin et al., 2015; Lindqvist et al., 1991). Distribution is fairly homogenous throughout the atmosphere, with a mean Northern Hemisphere concentration of 1.3 to 1.6 ng m^{-3}, and 0.8 to 1.1 ng m^{-3} in the Southern Hemisphere (Obrist et al., 2018).

The second category is gaseous oxidized mercury (GOM), also referred to as reactive gaseous mercury (RGM), which theoretically comprises all gas-phase atmospheric Hg^{2+} species, as Hg^{1+} is assumed to be a short lived intermediate oxidation product (Ariya et al., 2015). Due to current measurement limitations, GOM cannot be directly detected and is instead operationally defined as the difference between TGM and GEM. Measurements of GOM variously place concentrations from below detection to as high as 4000 pg m^{-3}, depending on location, time of day, and season (Mao et al., 2016). A preponderance of mechanistic and observational studies currently support atomic bromine (Br) as the major initiator of atmospheric Hg oxidation, discussed below (Obrist et al., 2018).

The third category is particulate bound mercury (PBM), also referred to as particulate mercury or Hg(p). Hg^{2+} compounds sorb to existing particulates, and some potential gas-phase Hg oxidation reactions could result in a condensed Hg^{2+} aerosol product (Ariya et al., 2015; Keeler et al., 1995; Schroeder and Munthe, 1998). Observational studies suggest PBM can exist over a wide range of size fractions, from ultra-fine sub-micron to greater than 10 μm (Amos et al., 2012; Feddersen et al., 2012; Malcolm and Keeler, 2007; Talbot et al., 2011). The measurement of PBM depends heavily on physical collection parameters, such as filter pore size or inlet cut

point, and this may bias measurements (Kos et al., 2013). It is difficult to reliably separate GOM from PBM with much assurance (Gustin et al., 2015; Lu et al., 1998; Rutter et al., 2008; Zhang et al., 2017). Therefore, in cases where GOM and PBM are not convincingly distinguishable (which is almost all cases with currently available measurement methods), they can be defined together as reactive mercury (RM = GOM + PBM) or referred to as Hg^{2+} or Hg(II). Ignoring the gas/solid distinction in favor of a total RM concentration may be more meaningful given current uncertainty (Weiss-Penzias et al., 2015).

Within the Hg research community, there has and continues to be intense debate on the exact Hg^{2+} species that might realistically be expected in the atmosphere, and what the mechanisms of formation might be (Ariya et al., 2008; Ariya et al., 2015; Hynes et al., 2009; Lin and Pehkonen, 1999; Lin et al., 2006; Subir et al., 2011, 2012). In addition, uncertainties in the measurement of GOM and PBM confound experimental insight into the identification of Hg^{2+} compounds or even the basic accuracy of total RM concentrations in ambient air, a deficiency that has recently come to the forefront of discussion (Cheng and Zhang, 2017; Gustin et al., 2015; Gustin et al., 2013; Jaffe et al., 2014; Zhang et al., 2017). A major hinderance is the lack of certified, traceable standards for Hg^{2+} compounds, without which meaningful calibration and QA/QC for RM measurement is nearly impossible. Some progress has been made towards SI traceable elemental Hg vapor standards based on gravimetric calibration, and such techniques might conceivably be applied to Hg^{2+} compounds (Ent et al., 2014). However, the mass changes involved with Hg^{2+} sources at typical permeation rates are very small and meaningful gravimetric calibration standards would be very difficult to achieve.

There are many hypothetical Hg^{2+} compounds inferred from potential atmospheric oxidation reactions, a few of which are considered more likely than others (Zhang et al., 2017). Many of

these oxidation pathways have been experimentally investigated for acceptable thermochemical and kinetic parameters, and the history of this work is well summarized (Ariya et al., 2015; Hynes et al., 2009; Subir et al., 2011).

Mercuric chloride compounds were early identified as potential gas-phase Hg^{2+} species (Braman and Johnson, 1974; Schroeder and Jackson, 1985), and studies of Hg oxidation in flue gas initially strengthened the hypothesis that $HgCl_2$ and related compounds dominated GOM concentrations (Lindberg and Stratton, 1998; Prestbo and Bloom, 1995). Indeed, most early studies attempting to measure Hg speciation used $HgCl_2$ as the primary reference calibration compound (Feng et al., 2000; Landis et al., 2002; Schroeder and Jackson, 1985; Xiao et al., 1997). It now seems likely that the narrow focus on $HgCl_2$ lead to persistent unknowns in Hg speciation that are only recently being addressed (Cheng and Zhang, 2017; Gustin et al., 2015; Lyman et al., 2016).

Intensive investigation of bromine and brominated compounds as potential Hg^0 oxidants was triggered by the first observations of atmospheric mercury depletion events (AMDEs) during polar spring in both the Arctic and Antarctic, in conjunction with strongly oxidative marine air chemistries (Ebinghaus et al., 2002; Lindberg et al., 2002a; Moore et al., 2014; Schroeder et al., 1998; Temme et al., 2003). The AMDE phenomenon has since been thoroughly documented (Angot et al., 2016a; Aspmo et al., 2005; Dommergue et al., 2010; Steffen et al., 2008), including at times other than spring (Nerentorp Mastromonaco et al., 2016), and at non-polar locations including over the Dead Sea (Obrist et al., 2011; Peleg et al., 2007), an alpine area of Australia (Howard and Edwards, 2018), and in the marine boundary layer of South Africa (Brunke et al., 2010).

Observational measurement of Hg speciation in conjunction with halogen concentrations and corollary atmospheric parameters has since also favored atomic Br radicals being the primary driver of Hg^0 oxidation in the marine boundary layer (Laurier and Mason, 2007; Laurier et al., 2003; Mason and Sheu, 2002; Soerensen et al., 2010a; Wang et al., 2014), the free troposphere (Gratz et al., 2015; Shah et al., 2016; Swartzendruber et al., 2006), and the tropopause/stratosphere (Lyman and Jaffe, 2012; Talbot et al., 2007). It is now known that reaction rates for oxidation of Hg^0 by molecular halogens (Br_2, Cl_2) are too slow to account for observed Hg^0 depletion, and the concentration of Cl and Cl_2 is generally thought to be too small to account for much Hg^0 oxidation (Ariya et al., 2002; Balabanov and Peterson, 2003; Holmes et al., 2009; Subir et al., 2011; Wang et al., 2014).

Modeling studies have supported atomic Br as the main driver of Hg oxidation globally (Holmes et al., 2010; Holmes et al., 2009; Holmes et al., 2006; Horowitz et al., 2017; Soerensen et al., 2010b). In addition, mechanistic studies on Br oxidation pathways have generally shown it to be both thermo-kinetically favorable and to have sufficiently rapid reaction rates (Ariya et al., 2002; Calvert and Lindberg, 2003; Dibble et al., 2012; Donohoue et al., 2006; Goodsite et al., 2004, 2012; Khalizov et al., 2003; Raofie and Ariya, 2004; Shepler et al., 2007). A two-step process involving an intermediate HgBr oxidation product now seems likely, with the final product BrHgO (Ariya et al., 2015; Wang et al., 2014).

Many studies have explored O_3 as possible oxidant (Calvert and Lindberg, 2005; Hall, 1995; Pal and Ariya, 2004; Rutter et al., 2012; Snider et al., 2008). The bimolecular reaction $Hg + O_3$ has convincingly been demonstrated to be energetically unfavorable ($\Delta_f H \sim 90$ kJ mol^{-1}), and unlikely to occur as a homogenous gas-phase reaction in relevant environmental conditions (Calvert and Lindberg, 2005; Shepler and Peterson, 2003; Tossell, 2003). However, net

oxidation of Hg^0 by O_3 may proceed by heterogeneous surface reactions with aerosols, third-body effects from additional gas-phase reactants, and by production of intermediate oxidation products like HgO_3 (Calvert and Lindberg, 2005; Rutter et al., 2012; Snider et al., 2008).

It is well established that the primary net product of both O_3 and OH oxidation of Hg^0 would be HgO, but this is unlikely to exist in a gas phase given its low vapor pressure (Calvert and Lindberg, 2005; Schroeder and Munthe, 1998). Jones et al. (2016) were unable to generate gas-phase HgO in a heated permeation system. Reaction chamber studies have shown that 83-90 % of HgO resulting from the gas-phase reaction $Hg^0 + O_3$ either formed on or was rapidly deposited to chamber surfaces, with less than 1% recovered as an aerosol (Pal and Ariya, 2004). Indeed, agglomerated particles of 40-60 nm HgO(s) on reaction chamber surfaces have been identified by transmission electron microscopy (Snider et al., 2008), and it is speculated that these HgO chain agglomerates form in free suspension and then rapidly deposit (Rutter et al., 2012). Such HgO aerosol may form a substantial component of PBM, especially incorporated into sea-salt aerosols (Holmes et al., 2009; Subir et al., 2011).

Other possible Hg^{2+} species include mercury sulfate ($HgSO_4$) and mercury nitrate ($Hg(NO_3)_2$) (Huang and Gustin, 2015a; Huang et al., 2017; Peleg et al., 2015), and recent research has suggested HgBr + NO_2 might also be an important nighttime oxidation process (Jiao and Dibble, 2017; Wang et al., 2014).

2.5 Measurement of Atmospheric Mercury

Elemental Hg absorbs ultra-violet radiation and fluoresces at a wavelength of 253.7 nm. This characteristic allows for detection and quantification of GEM via either atomic absorption spectrometry (AAS) or atomic fluorescence spectrometry (AFS). In general, determination of Hg

at trace ambient levels (< 2 ng m^{-3}) requires pre-concentration on a trapping material, ideally a noble metal due to strong Hg amalgamating tendencies, followed by thermal desorption in an inert gas flow and quantification on an appropriate spectrophotometric detector.

Early work on atmospheric Hg measurements utilized single amalgamation and desorption directly into the detector cell (Braman and Johnson, 1974; Johnson and Braman, 1974). A dual-amalgamation technique using sample collection traps in conjunction with a carefully calibrated analytical trap was subsequently identified as the best way to separate Hg from an atmospheric sample (Fitzgerald and Gill, 1979). Gold in general, and particularly when coated onto glass beads of mesh size 60-80, demonstrates the strongest trapping behavior for Hg^0 and many other gas-phase Hg compounds, with collection efficiencies of 100%, and has long been the standard amalgamating material (Dumarey et al., 1985a; Fitzgerald and Gill, 1979; Schroeder and Jackson, 1985; Slemr et al., 1979). Temperatures from 450 °C (Schroeder and Jackson, 1985) up to 800 °C (Dumarey et al., 1985a) have been used to de-amalgamate Hg from gold traps, but 500 °C is standard in current analytical systems. Calibration of the gold traps is achieved by injection of a precise volume of air at Hg vapor saturation, based on the precisely known relationship of temperature versus saturation concentration (Dumarey et al., 1985b).

The principle automated analytical technique for measuring ambient GEM with high time resolution (2.5-5 minutes) and high precision (± 3% uncertainty) is the Tekran® 2537 A/B/X Automated Ambient Air Analyzer, which utilizes cold vapor atomic fluorescence spectrometry (CVAFS). The Tekran® 2537 analyzer employs dual gold amalgamation to allow continuous sampling, i.e. as one trap is being desorbed for analysis the other trap is sampling ambient air. As a loaded gold trapped enters the analytical cycle, the sample flow is switched to an ultra-high purity argon gas flow, to flush the trap of ambient air and possible interferences, eliminating the

need for separate collection and analytical traps. The flushed trap is heated (500 °C) and the desorbed Hg is carried in the argon flow through an optical detector path where a UV light source induces fluorescence. The fluoresced photons are counted by a high sensitivity photo-multiplier tube and converted into a voltage signal that is directly proportional to the mass of Hg in the sample. Instrument calibration is achieved by injecting a known mass of Hg vapor through each trap, using the instrument's internal Hg permeation source, or manually via a syringe and external Hg vapor source.

The Tekran® 2537 analyzer is often held to be a total gaseous mercury (TGM) analyzer (Ebinghaus et al., 1999; GMOS, 2011; Landis et al., 2002; Munthe et al., 2001; Schroeder et al., 1995; Temme et al., 2003), meaning that it captures and detects both GEM and GOM with high efficiency. This requires that in addition to complete amalgamation on the gold traps, GEM and GOM are also thermally desorbed and totally *decomposed* to Hg^0 vapor, as detection by CVAFS relies on the very specific UV fluorescence of single elemental Hg atoms at 253.7 nm. Compounds of Hg are transparent to UV at 253.7 nm and do not fluoresce, so their detection depends on a reductive analytical step such as high temperature pyrolysis or a reducing chemical reaction (Schroeder and Jackson, 1985). While desorption at 500 °C is sufficient to release 100% of adsorbed Hg, whether total decomposition is achieved for all Hg compounds at this temperature has not been demonstrated.

Ambient GEM concentrations can also be measured using AAS- based analyzers, such as the Ohio-Lumex® RA-915+ Mercury Analyzer (Ohio-Lumex®). This type of analyzer does not use a pre-concentration step, and as such detection limits are ~ 1 ng m^{-3}, more suitable for industrial measurements or areas with high background concentrations. Lacking a thermal desorption step,

there is no question that the AAS systems provide a pure GEM measurement unless a deliberate pre-pyrolysis is included.

Measurement of GEM is routine in many atmospheric monitoring networks to a nominal level of standardization (UNEP, 2016). However, practically achievable instrument uncertainty may average around 10%, with some inter-instrument biases as high as 20% (Gustin and Jaffe, 2010; Slemr et al., 2015). The difference between measuring TGM and GEM, presupposing the analytical system possesses such a capability, is also dependent on the sample inlet system at a particular site. Most sites deploy a fine particulate filter at the front of the sample line as well as at the instrument sample inlet port (0.2 μm PTFE), and it is also routine to include a soda lime trap in the sample line to scrub halogens or acid aerosols that would otherwise damage and passivate the gold traps. The combination of particulate filters and soda lime likely scrub much if not all RM, and therefore the majority of ambient monitoring sites are almost certainly measuring primarily GEM (Angot et al., 2016a; Steffen et al., 2008; Steffen et al., 2002).

The measurement of RM is more uncertain than for GEM and currently depends on isolating GOM and PBM, separately or together, from a usually much larger GEM signal. Various methods have attempted to do this, including mist chambers (Sheu and Mason, 2001; Stratton et al., 2001), manual denuders (Feng et al., 2003; Sheu and Mason, 2001; Xiao et al., 1997), multi-stage filtration (Bloom et al., 1996; Ebinghaus et al., 1999; Mason et al., 1997; Sheu and Mason, 2001), and by GEM/TGM difference (Ambrose et al., 2013; Lyman and Jaffe, 2009; Lyman and Jaffe, 2012; Swartzendruber et al., 2009).

The principle commercially available apparatus for measuring Hg speciation is the Tekran® 1130/1135 Mercury Speciation System. It should be noted that the Tekran® system does not in fact produce a true "speciation" measurement, as individual Hg compounds cannot be

discriminated. The term "fractionation" is a more appropriate description of the Tekran® measurement, as detailed by International Union of Pure and Applied Chemistry (IUPAC) terminology guidelines. However, as the Tekran® system and terminology are widely applied, "speciation" is herein retained over "fractionation" as a matter of conceptual and textual clarity, versus pure semantic accuracy.

The Tekran® system uses a denuder and particulate filter to separate (i.e. "fractionate") GOM and PBM, respectively, from GEM (Fig. 2.2, Landis et al., 2002). The system is designed to operate at a total sample flow of 10 Lpm, through a Teflon-coated glass elutriator inlet with a 2.5 μm size cut-point. The 1130 denuder module utilizes a quartz glass annular denuder with an active laminar flow section coated in potassium chloride (KCl) to capture GOM from the sample air stream. Downstream of the denuder module is the 1135 particulate module, which contains a 0.1 μm quartz fiber filter to collect fine particulate Hg (< 2.5 μm). All glassware, including the inlet, is heated to 50 ºC (or more) during sampling, during which time GEM passes through the speciation system to a Tekran® 2537 unit, which pulls off the 10 Lpm sample line at the normal sample rate of 1.0 Lpm. The GOM and PBM are quantified after a sufficient sample time (1-3 h), by thermal desorption at 500 and 800 °C from their respective collection media, followed by downstream pyrolysis at 800 ºC for conversion to Hg^0 and detection by the 2537 unit.

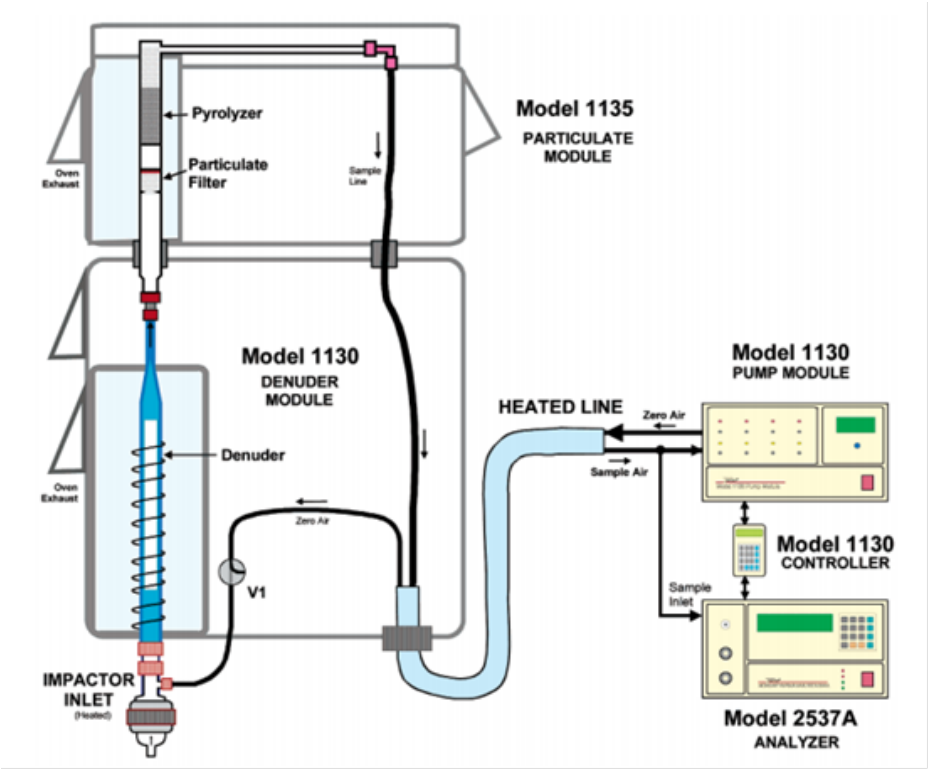

Figure 2.2 *Schematic of the Tekran® 2537/1130/1135 Mercury Speciation System (from Tekran® Instruments Corp).*

The variable levels of success in measuring atmospheric RM have been detailed in recent critical reviews (Cheng and Zhang, 2017; Gustin et al., 2015; Jaffe et al., 2014). In particular, the potassium chloride (KCl) coated denuder used in the Tekran® 1130 system for GOM collection has been shown to suffer interferences from ozone and water vapor, resulting in systematic under quantification (Ambrose et al., 2013; Lyman et al., 2010; McClure et al., 2014). The particle size cut-point at 2.5 μm certainly excludes PBM on larger particles, which will produce an underestimate of total PBM in some conditions (Kos et al., 2013; Talbot et al., 2011). There are also possible PBM measurement artifacts associated with KCl denuders, such as trapping of fine particulate Hg on the rough KCl coating, or decomposition of PBM and subsequent detection as GOM or GEM (Lynam and Keeler, 2005; Rutter et al., 2008).

One alternative method that has been used with some success to selectively measure RM concentrations in ambient air is a cation exchange membrane (CEM) filter system (Bloom et al., 1996; Ebinghaus et al., 1999; Huang and Gustin, 2015a; Huang et al., 2017; Huang et al., 2013; Marusczak et al., 2017; Mason et al., 1997; Pierce and Gustin, 2017; Sheu and Mason, 2001). The use of CEM type filters (then referred to as 'two-ion exchange membranes') was first described in a presentation at the 4th International Conference on Mercury as a Global Pollutant (Bloom et al., 1996). This presentation referred in part to an evaluative deployment of ion exchange membranes (made at the time by Gelman Sciences Inc) as part of a field-based international comparative study of RM measurement techniques in September, 1995 (Ebinghaus et al., 1999). The Gelman ion exchange membranes were also deployed in a 1996 winter/spring field campaign for determining the speciation of atmospheric Hg in the Chesapeake Bay area (Mason et al., 1997). These early studies deployed the ion exchange material as part of a multi filter sampling train, utilizing quartz fiber filters to first capture particulate matter and PBM, while passing GEM and GOM. The pore size of the ion exchange filters used was not reported, though it is expected to be in the range of 0.2-1.0 μm.

The performance of the Gelman ion exchange membranes in this type of sampling configuration was evaluated in a comparative study focusing exclusively on RM measurement techniques (Sheu and Mason, 2001). Specific but unconfirmed concerns included physical particle breakthrough, re-evolution of gas-phase Hg^{2+} from PBM captured on the upstream particulate filters passing downstream to the ion exchange membranes, possible adsorption of GOM compounds to the particulate filters, as well as a possible GEM collection artifact on the CEM filters themselves. However, the Gelman membranes were used as an independent verification of a mercuric chloride permeation source with apparently satisfactory results, though data is not shown (Landis et al., 2002). It can be inferred from this study that the Gelman membranes

exhibited good selectivity and collection efficiency for $HgCl_2$, with no GEM artifact. However, with the development and validation of the automatic Tekran® speciation system as reported by Landis et al. (2002), further work with the ion exchange membrane method entered a hiatus until adapted for use as a surrogate surface for RM dry deposition measurements (Lyman et al., 2007).

The manufacturer of the original ion exchange membranes, Gelman Sciences Inc, was acquired by Pall Corporation in October 1996, and some evolution of the CEM material has occurred since that time. Pall phased out (or re-branded) the original Gelman product at an unknown point and began manufacturing a CEM material termed I.C.E. 450 (referring to a pore size of 0.45 μm). The I.C.E. 450 membranes were eventually discontinued as well (~2013), and a different cation exchange material (Mustang® S, pore size 0.8 μm) was offered as a substitute (Huang and Gustin, 2015b).

The I.C.E 450 material had been utilized in development of passive RM dry deposition samplers, with results indicating it did not adsorb significant quantities of GEM, but did selectively uptake gas-phase Hg^{2+} species (Lyman et al., 2007). The I.C.E. 450 material was subsequently adapted for use in active sample flow systems, with the presumption of continued inertness to GEM and selectivity for GOM (Huang et al., 2013), but it was after this initial work that the I.C.E. 450 material was discontinued, necessitating a change to the Mustang® S product (Huang and Gustin, 2015a, b). It is unclear how the changes in product manufacturing may have affected results between studies, and GEM uptake rates during active flow regimes were never reported in the literature for any of the CEM materials.

Recent CEM based sampling systems typically use a pair of CEM disc filters (Mustang® S version) in 47 mm Teflon filter assemblies, without a pre-particulate filter, a method pioneered by the University of Nevada-Reno Reactive Mercury Active System (UNRRMAS) (Gustin et al.,

2015; Gustin et al., 2016; Huang et al., 2017). In the paired deployment, the first CEM filter serves as a primary RM collection surface, and the second filter captures potential breakthrough. The paired filters are deployed at a controlled flow rate of 1.0 Lpm for 1 to 2 weeks and then collected for analysis by digestion in an oxidizing acid solution, reduction to Hg^0, gold amalgamation, and final quantification by CVAFS (EPA Method 1631, modified, Appendix A). The total Hg measured on each sample CEM filter is divided by the calculated sample volume to arrive at an integrated RM concentration. Generally, 2-3 replicate filter pairs are deployed together, and 1-3 blank CEM filters are collected with every deployment. Method detection limits (MDL) and method uncertainty (3x MDL) hinge on these blank CEM values. In this study, blank Hg mass on the CEM averaged approximately 50 pg, giving an MDL of roughly 2.5 pg m^{-3} over a typical 2-week sample period.

While sample collection times are regrettably long based on the current methodological approach, the CEM filter method does possess the advantages of simplicity, robustness, redundancy, and cost efficiency. The system places minimal technical burdens on site operators, a benefit that is difficult to overstate. Even the basic automated GEM measurement requires deep familiarity with the instrumentation in order to produce reliable and consistent results, and variability in operator skill and technique can be a major source of error (Slemr et al., 2015). Maintaining the full Tekran® 2537/1130/1135 speciation system imposes many additional complexities, including routine cleaning, preparation, and replacement of the speciation glassware, and rigorous weekly QA/QC checks. This becomes something of a fulltime job for a skilled technician, which combines with the high upfront capital cost to make the system prohibitively expensive for many research groups or monitoring agencies. In contrast, the CEM filter system can be setup for several hundred USD, deployed anywhere that minimum power can be delivered to the sample pumps, and requires only one hour every two weeks to collect and

deploy filter sets. While attention to detail is still paramount, no demand is placed on the operator other than standard trace-clean sample collection, careful documentation, and basic assessments of system performance and integrity. As such, CEM filters are an excellent method for quickly acquiring preliminary data for locations in which RM concentrations are unknown or in which a full automated speciation system is impracticable.

2.6 Monitoring of Atmospheric Mercury

Several global and regional networks exist for measuring and monitoring atmospheric Hg (Sprovieri et al., 2016; UNEP, 2016). Such monitoring is extensive in the Northern Hemisphere, including the Atmospheric Mercury Network (AMNet), part of the US National Atmospheric Deposition Program, and the European Monitoring and Evaluation Program (EMEP). In contrast, only a handful of sites operate continuously in the Southern Hemisphere, for the most part within the last decade (summarized in Table 2.2 and shown in Fig. 2.3). The longest atmospheric Hg record in the Southern Hemisphere is from Cape Point, South Africa, with manual GEM measurements extending back to 1995, and an automated mercury analyzer in operation since 2007 (Brunke et al., 2016; Martin et al., 2017). Other long term, continuous, mid-latitude GEM monitoring locations in the Southern Hemisphere, for which data are available, are Amsterdam Island in the southern Indian Ocean (Angot et al., 2014), Cape Grim on the island of Tasmanian south of the Australian mainland (Slemr et al., 2015), Gunn Point in northern Australia (Howard et al., 2017), and Bariloche National Park in the Andean foothills of Argentina (Diéguez et al., 2017). All other Southern Hemisphere ground-based monitoring sites are on the Antarctic continent (Angot et al., 2016a; Angot et al., 2016b; Ebinghaus et al., 2002; Pfaffhuber et al., 2012).

Table 2.2

Location	Coordinates	Duration	GEM/TGM* (ng m^{-3})	GOM (pg m^{-3})	PBM (pg m^{-3})	Reference
Antarctica						
Troll Station	-72.012 S 2.532 W	Feb 2007 - June 2011	0.93 ± .19			Pfaffhuber et al. 2012
		2011-2013	1.018 ± 0.04			Slemr et al. 2015
Neumayer Station	-70.677 S 8.272 W	Jan. 2000 - Jan. 2001	1.06 ± 0.23*			Ebinghaus et al. 2002
		Dec. 2000 - Feb. 2001	1.08 ±0.29*	5 - 300	15 - 120	Temme et al. 2003
Dumont d'Urville Station	-66.663 S 140.002 E	Jan. 2012 - May 2015	0.87 ± 0.23			Angot et al. 2016a
Concordia Station	-75.099 S 123.332 E	2015	1.06 ± 0.41			Angot et al. 2016b
Mid Latitude						
Amsterdam Island	-37.796 S 77.551 E	Jan. 2012 - Dec. 2013	1.03 ± 0.08	0 - 4.1	0 - 12.7	Angot et al. 2014
Gunn Point, Australia	-12.249 S 131.046 E	June 2014 - March 2016	0.95 ± 0.12			Howard et al. 2017
Cape Grim, Australia	-40.683 S 144.690 E	2011 - 2013	0.89 ± 0.06			Slemr et al. 2015
Cape Point, South Africa	-34.353 S 18.489 E	2007-2012	1.01 ± 0.06			Brunke et al. 2016
Bariloche, Argentina	-41.129 S 71.420 W	Oct. 2012 - May 2016	0.89 ± 0.15			Diéguez et al. 2017

Table 2.2 Summary of continuous ground-based atmospheric Hg measurements in the Southern Hemisphere.

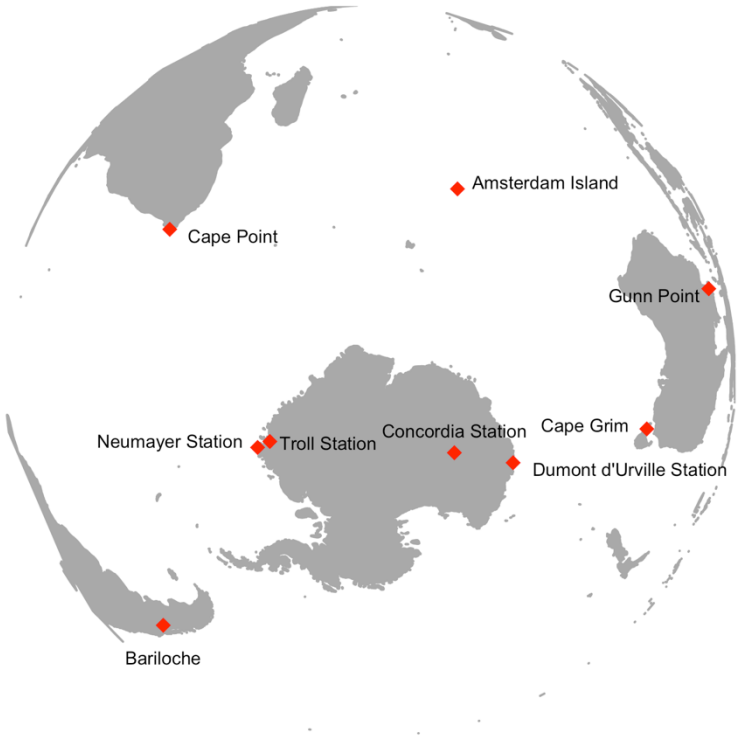

Figure 2.3 *Long-term atmospheric Hg monitoring sites in the Southern Hemisphere.*

Long term RM data is more sparse, with only one mid-latitude dataset available from Amsterdam Island in the southern Indian Ocean (Angot et al., 2014), as well as some short term campaign studies in Antarctica (Brooks et al., 2008; Sprovieri et al., 2002; Temme et al., 2003). Edwards et al. (2018, in preparation) have recently operated a full Tekran® 1130/1135 speciation system at Macquarie University in Sydney, Australia, a temperate mid-latitude location. Long-term results from Amsterdam Island indicate very low GOM/PBM concentrations < 1 pg m^{-3}, with measurements frequently below instrument detection (Angot et al., 2014). However, these results may suffer from the low bias reported for the Tekran® 1130/1135 system. In a maritime environment such as Amsterdam Island, RM is likely to be predominantly in a course sea-salt aerosol fraction (Angot et al., 2014; Feddersen et al., 2012; Malcolm and Keeler, 2007), and would be excluded by the 2.5 μm inlet cut point on the Tekran®.

2.7 Measurement of Air-Surface Mercury Exchange

From the atmosphere, Hg can collect on virtually any surface through a variety of physiochemical deposition processes. As Hg^0 is chemically inert and only weakly soluble, deposition is generally facilitated by oxidation to Hg^{2+} which has an enhanced capability for sorption/dissolution in atmospheric aerosols and wash out in precipitation (wet deposition), and direct sorption onto/into terrestrial, foliar, or aquatic surfaces (dry deposition) (Lin and Pehkonen, 1999; Lindberg et al., 2007; Lindqvist and Rodhe, 1985; Schroeder and Munthe, 1998; Schroeder et al., 1991). Elemental Hg may also react directly with a surface and deposit to it (Gustin et al., 2006; Gustin et al., 2000).

Once Hg has deposited to a surface, it can be re-emitted (Hintelmann et al., 2002; Schroeder et al., 1989). Surface emissions are dominated by volatile Hg^0 which readily enters the gas phase. The availability of surface Hg^0 is mediated by photochemical and aqueous-phase reduction

reactions, with solar radiation (Carpi and Lindberg, 1997; Gustin et al., 2002; Gustin et al., 1999; Moore and Carpi, 2005), temperature (Edwards et al., 2001; Gustin et al., 1997), and moisture (Briggs and Gustin, 2013; Gustin and Stamenkovic, 2005; Lindberg et al., 1999) all thought to contribute to the emission process. It is also possible that some Hg is emitted directly from surfaces as GOM or PBM (Schroeder and Munthe, 1998). Removal from the cycle of emission/deposition requires sequestration, sedimentation, and burial.

Differentiating primary versus re-emitted Hg is not practicable, and so all emissions from surfaces that are not specifically anthropogenic are simply classified as natural emissions (Mason, 2009). Mercury emissions from natural surfaces remain loosely constrained and constitute the largest source of uncertainty in the global mercury budget (Obrist et al., 2018). Hence, quantifying the net exchange of Hg between surface compartments and the atmosphere is an important area for measurement improvement. The rate of transfer in either direction (flux) between air and surface can be measured in the field using two primary *in situ* techniques: the micrometeorological (MM) method and the dynamic flux chamber (DFC) method (Osterwalder et al., 2018; Rasmussen et al., 2005; Sommar et al., 2013; Zhu et al., 2015). Both methods have advantages and disadvantages, which are discussed below. Additionally, neither the DFC nor MM flux methods have previously allowed for direct measurements of reactive Hg fluxes, and the only data on RM air-surface exchange is inferential and very limited (Zhang et al., 2009).

Micrometeorological methods (flux gradient, relaxed eddy accumulation) have the advantages of minimal interference with ground surface dynamics and a large integrated flux area that can provide a representative spatial average. However, strict meteorological and site constraints limit the applicability of these methods in many areas and make them impossible to use in an enclosed

laboratory study (Bash and Miller, 2009; Edwards et al., 2001; Edwards et al., 2005; Fritsche et al., 2008; Kim et al., 1995; Marsik et al., 2005; Pierce et al., 2015; Skov et al., 2006).

The dynamic flux chamber approach involves physically enclosing a target surface and measuring the resulting concentration differences. The DFC method is widely employed due to portability and relative simplicity (Agnan et al., 2016; Edwards et al., 2001; Kim and Lindberg, 1995; Rasmussen et al., 2005; Schroeder et al., 1989). Chambers are constructed of a transparent and chemically inert material such as Pyrex glass or Teflon, in order to reduce chamber blanks and admit a natural solar spectrum to the substrate surface (Carpi and Lindberg, 1998; Edwards et al., 2005). Regardless of material or design, an inherent limitation of the DFC method is the unavoidable impact of the chamber itself. Deploying the chamber is likely to create some level of surface disturbance, and the area enclosed by the chamber is inevitably separated to some degree from true ambient conditions. None the less, the DFC method provides the best approach for assessing the effect of small-scale surface manipulations on Hg flux.

There is a relatively large extant body of GEM flux data compiled using both methods (but mostly the DFC method), and these studies have provided important insight into some of the mechanisms controlling air-surface Hg exchange and magnitude (Agnan et al., 2016; Eckley et al., 2016; Zhu et al., 2016). However, in summarizing Hg flux data from 132 separate published studies, Agnan et al. (2016) show that a majority of measurements have been biased towards Hg enriched soils (63% of total), and there is a strong geographical bias towards sites in North America, Europe, and East Asia (Fig. 2.4). This geographical bias is presumably due to a preponderance of relatively well-funded, well-equipped research groups in the industrialized nations of the Northern Hemisphere. On a global scale, Hg flux data is lacking in general, and many areas report a complete absence of any Hg data at all. The Indo-Pacific region is a

particular unknown, with only two flux studies recently reported from Australia (Edwards and Howard, 2013; Howard and Edwards, 2018).

As the DFC method allows for measurement from small surface areas, it is ideal for laboratory experimentation. The determination of Hg flux by the DFC method is achieved by measuring the difference in air Hg concentration entering and exiting the chamber as it sits on a surface. The flux is proportional to this concentration difference (ΔC), the enclosed surface area, and the flow rate through the chamber. Flux is calculated using the equation:

$$F = (Q * \Delta C) / A$$

where F is the net Hg flux (ng m^{-2} h^{-1}), Q is the flow rate through the chamber (m^3 h^{-1}), C_o is the internal chamber Hg concentration (ng m^{-3}), C_i is the external ambient Hg concentration, and A is the area of the substrate under the chamber (m^2). The sign of ΔC (C_o - C_i) indicates the direction of flux. The concentration of Hg in air may be measured using a variety of methods, but is typically achieved using the Tekran® 2537 analytical platform.

Chamber flow and hence chamber volume turn-over-time (TOT) has been shown to be a major source of variability in calculated Hg flux values (Eckley et al., 2010; Gillis and Miller, 2000; Lindberg et al., 2002b; Wallschläger et al., 1999). The flow rate effect is real only to the extent that it impacts the chamber concentration (C_o) parameter, as chamber area is constant, and C_i is measured external to the chamber. For high Hg emitting materials, a low TOT can lead to Hg accumulating in the chamber volume, resulting in unreasonably elevated C_o values and warranting an increased flow rate, though the artificially large ΔC is offset somewhat by the low Q parameter.

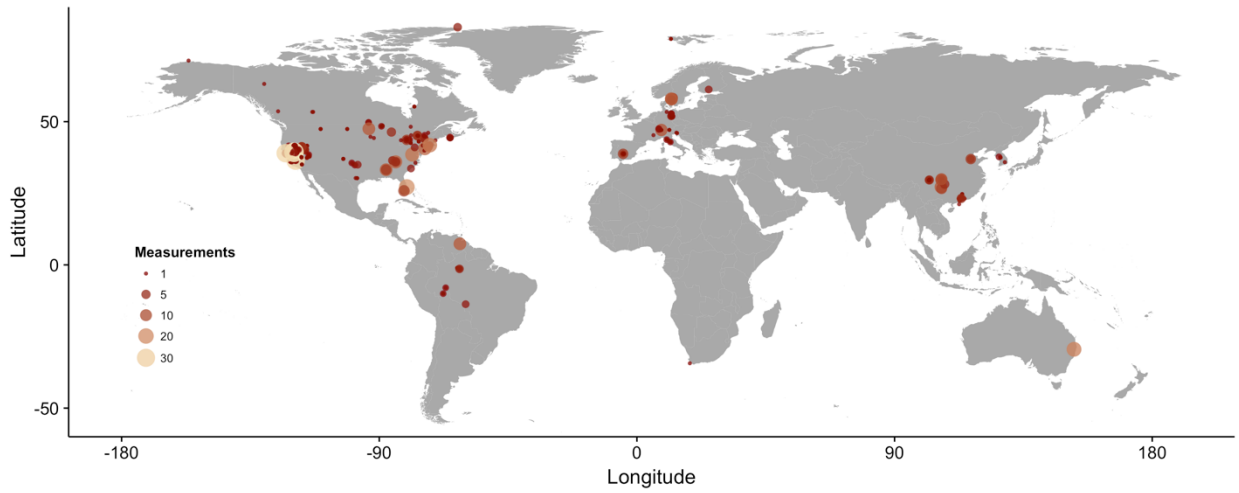

Figure 2.4 *Global distribution of 132 reported Hg flux study sites and the number of measurements at each, adapted from Agnan et al. (2016).*

Beyond the point where steady-state diffusive conditions have been created (evident by a decreasing rate of change in C_o with respect to change in Q), further increases in flow have a diminishing effect on C_o and only serve as an artificial multiplier in the flux equation. In addition, high flow rates introduce high shear velocities and turbulent eddy formation in the chamber volume, which artificially enhances Hg flux through advective transfer of Hg out of the stable surface layer (Eckley et al., 2010). At the extreme, the highest flow rates may begin to introduce negative pressure conditions and entrain particulate into the sample system. The operating parameters of any flux study must be selected to best address the specific research needs, while appropriately balancing the limitations and advantages inherent to any particular methodology.

2.8 Mercury Measurement Techniques Used in this Project

Both atmospheric Hg and air-surface exchange of Hg were measured for the experimental work described in this dissertation project. Atmospheric GEM was measured using the standard Tekran® 2537 A/B system, which was also used in a relatively routine configuration to measure GEM flux. Reactive mercury measurements were made using the CEM filter methodology describe above, with some improvements.

Ambient RM was measured using an adaptation of the University of Nevada Reactive Mercury Active System (UNRRMAS, Gustin et al., 2015; Gustin et al., 2016; Huang et al., 2017). The system was deployed at two sites in Australia: Cape Grim Baseline Air Pollution Station on the north-western point of Tasmania (-40.683 S 144.690 E), and at the Macquarie University Automatic Weather Station in the northern suburban area of Sydney, New South Wales (-33.765 S 151.118 E).

Several improvements were made to the UNRRMAS setup for its application to this dissertation project. For ambient CEM filter deployments, a custom-machined anodized aluminum weather shield provided a significant advantage in mounting and durability versus the previous plastic installations (Fig. 2.5). We adopted 2-stage PFA filter assemblies (Savillex©) that each held two 47 mm filters in-series, as opposed to deploying two separate single-stage filter assemblies in-series (Pierce and Gustin, 2017). The single 2-stage assembly simplifies filter deployment and collection and reduces the number of fittings and potential leaks. Sample filters were collected into new, sterile 50 mL polypropylene sample tubes (Corning™ Falcon™), as opposed to re-cleaning and re-using 125 mL glass jars (Thermo Scientific I-Chem™) as done in previous studies, reducing the chances of high filter blanks or contamination.

Figure 2.5 *Ambient reactive mercury filter deployment setup at Cape Grim Baseline Air Pollution Station, improved upon from the University of Nevada Reno Reactive Mercury System (photo by author).*

The CEM filter-based flux system centered on cylindrical FEP Teflon DFCs operated in conjunction with Tekran® 2537A analyzers after the methods of Eckley et al. (2010; 2011) and Miller et al. (2011). In this system, C_o is the mean concentration of two consecutive 5 min chamber outlet air samples (ng m^{-3}), and C_i is the mean concentration of inlet air in the samples before and after C_o, which provides a 20 min GEM flux value. GEM in each 5-min sample volume was quantified automatically by the 2537A analyzer. For RM flux measurement, the DFC inlet and outlet sample lines are fitted with paired CEM filters in 2-stage filter assemblies. The amount of Hg on the chamber inlet and outlet filter represented $C_{i(RM)}$ and $C_{o(RM)}$, respectively, which allowed calculation of a ΔC_{RM} parameter. With CEM filters deployed on the sample lines, and a particulate filter at the rear inlet of the analyzer, all Hg measured by the 2537A was definitively in GEM form. The RM flux filter samples were collected and analyzed in the same manner as the ambient filter samples.

Filter sample collection was achieved according to trace-clean protocols in designated clean areas, using only Teflon wrapped stainless steel tweezers to contact the filters. All flux filter samples were collected by the author. Site technicians collected the ambient air sample filters according to a provided standard operating procedure. All CEM filters were analyzed by the author, using a Tekran® 2600 system (flow-based configuration w/ phase separator). Operator consistency in terms of sample collection and analysis was deemed highly important to minimize possible sources of error. Overall, we feel that our methodological improvements were borne out by superior filter blanks, improved detection limits, and a relatively unbroken time-series over our dataset.

References

Agnan, Y., T. L. Dantec, C. W. Moore, G. C. Edwards, and D. Obrist, 2016, New Constraints on Terrestrial Surface–Atmosphere Fluxes of Gaseous Elemental Mercury Using a Global Database: Environmental Science & Technology, v. 50, p. 507-524.

Ambrose, J. L., S. N. Lyman, J. Huang, M. S. Gustin, and D. A. Jaffe, 2013, Fast Time Resolution Oxidized Mercury Measurements during the Reno Atmospheric Mercury Intercomparison Experiment (RAMIX): Environmental Science & Technology, v. 47, p. 7285-7294.

Amos, H., D. Jacob, C. Holmes, J. Fisher, Q. Wang, R. Yantosca, E. Corbitt, E. Galarneau, A. Rutter, M. Gustin, A. Steffen, J. Schauer, J. Graydon, V. St Louis, R. Talbot, E. Edgerton, Y. Zhang, and E. Sunderland, 2012, Gas-particle partitioning of atmospheric Hg(II) and its effect on global mercury deposition: Atmospheric Chemistry and Physics, v. 12, p. 591-603.

Amos, H. M., J. E. Sonke, D. Obrist, N. Robins, N. Hagan, H. M. Horowitz, R. P. Mason, M. Witt, I. M. Hedgecock, E. S. Corbitt, and E. M. Sunderland, 2015, Observational and Modeling Constraints on Global Anthropogenic Enrichment of Mercury: Environmental Science & Technology, v. 49, p. 4036-4047.

Andersson, M. E., K. Gårdfeldt, I. Wängberg, and D. Strömberg, 2008, Determination of Henry's law constant for elemental mercury: Chemosphere, v. 73, p. 587-592.

Angot, H., M. Barret, O. Magand, M. Ramonet, and A. Dommergue, 2014, A 2-year record of atmospheric mercury species at a background Southern Hemisphere station on Amsterdam Island: Atmospheric Chemistry and Physics, v. 14, p. 11461-11473.

Angot, H., A. Dastoor, F. De Simone, K. Gårdfeldt, C. N. Gencarelli, I. M. Hedgecock, S. Langer, O. Magand, M. N. Mastromonaco, C. Nordstrøm, K. A. Pfaffhuber, N. Pirrone, A. Ryjkov, N. E. Selin, H. Skov, S. Song, F. Sprovieri, A. Steffen, K. Toyota, O. Travnikov, X. Yang, and A. Dommergue, 2016a, Chemical cycling and deposition of atmospheric mercury in polar regions: review of recent measurements and comparison with models: Atmos. Chem. Phys., v. 16, p. 10735-10763.

Angot, H., I. Dion, N. Vogel, M. Legrand, O. Magand, and A. Dommergue, 2016b, Multi-year record of atmospheric mercury at Dumont d'Urville, East Antarctic coast: continental outflow and oceanic influences: Atmos. Chem. Phys., v. 16, p. 8265-8279.

Ariya, P., H. Skov, M. Grage, M. Goodsite, S. Jr, and E. Brandas, 2008, Gaseous elemental mercury in the ambient atmosphere: Review of the application of theoretical calculations and experimental studies for determination of reaction coefficients and mechanisms with halogens and other reactants: Advances in Quantum Chemistry, Vol 55: Applications of Theoretical Methods To Atmospheric Science, v. 55, p. 43-55.

Ariya, P. A., M. Amyot, A. Dastoor, D. Deeds, A. Feinberg, G. Kos, A. Poulain, A. Ryjkov, K. Semeniuk, M. Subir, and K. Toyota, 2015, Mercury Physicochemical and Biogeochemical Transformation in the Atmosphere and at Atmospheric Interfaces: A Review and Future Directions: Chemical Reviews, v. 115, p. 3760-3802.

Ariya, P. A., A. Khalizov, and A. Gidas, 2002, Reactions of gaseous mercury with atomic and molecular halogens: Kinetics, product studies, and atmospheric implications: Journal of Physical Chemistry A, v. 106, p. 7310-7320.

Aspmo, K., P.-A. Gauchard, A. Steffen, C. Temme, T. Berg, E. Bahlmann, C. Banic, A. Dommergue, R. Ebinghaus, C. Ferrari, N. Pirrone, F. Sprovieri, and G. Wibetoe, 2005, Measurements of atmospheric mercury species during an international study of mercury depletion events at Ny-Ålesund, Svalbard, spring 2003. How reproducible are our present methods?: Atmospheric Environment, v. 39, p. 7607-7619.

Bagnato, E., G. Tamburello, G. Avard, M. Martinez-Cruz, M. Enrico, X. Fu, M. Sprovieri, J. Sonke, G. Zellmer, M. Edmonds, and S. Straub, 2015, Mercury fluxes from volcanic and geothermal sources: an update: Role of Volatiles in the Genesis, Evolution and Eruption of Arc Magmas, v. 410, p. 263-285.

Bakir, F., S. F. Damluji, L. Amin-Zaki, M. Murtadha, A. Khalidi, N. Y. Al-Rawi, S. Tikriti, H. I. Dhahir, T. W. Clarkson, J. C. Smith, and R. A. Doherty, 1973, Methylmercury Poisoning in Iraq: Science, v. 181, p. 230.

Balabanov, N. B., and K. A. Peterson, 2003, Mercury and Reactive Halogens: The Thermochemistry of Hg + {Cl2, Br2, BrCl, ClO, and BrO}: The Journal of Physical Chemistry A, v. 107, p. 7465-7470.

Bash, J. O., and D. R. Miller, 2009, Growing season total gaseous mercury (TGM) flux measurements over an Acer rubrum L. stand: Atmospheric Environment, v. 43, p. 5953-5961.

Benoit, J. M., C. C. Gilmour, A. Heyes, R. P. Mason, and C. L. Miller, 2002, Geochemical and Biological Controls over Methylmercury Production and Degradation in Aquatic Ecosystems, Biogeochemistry of Environmentally Important Trace Elements: ACS Symposium Series, v. 835, American Chemical Society, p. 262-297.

Biester, H., R. Bindler, A. Martinez-Cortizas, and D. Engstrom, 2007, Modeling the past atmospheric deposition of mercury using natural archives: Environmental Science & Technology, v. 41, p. 4851-4860.

Bloom, N., and W. F. Fitzgerald, 1988, Determination of volatile mercury species at the picogram level by low-temperature gas chromatography with cold-vapour atomic fluorescence detection: Analytica Chimica Acta, v. 208, p. 151-161.

Bloom, N., E. Prestbo, and E. VonderGeest, 1996, Determination of atmospheric gaseous Hg(II) at the pg/m 3 level by collection onto cation exchange membranes, followed by dual

amalgamation/cold vapor atomic fluorescence spectrometry, 4th International Conference on Mercury as a Global Pollutant, Hamburg.

Braman, R. S., and D. L. Johnson, 1974, Selective absorption tubes and emission technique for determination of ambient forms of mercury in air: Environmental Science & Technology, v. 8, p. 996-1003.

Briggs, C., and M. Gustin, 2013, Building upon the Conceptual Model for Soil Mercury Flux: Evidence of a Link Between Moisture Evaporation and Hg Evasion: Water Air and Soil Pollution, v. 224.

Brooks, S., S. Lindberg, G. Southworth, and R. Arimoto, 2008, Springtime atmospheric mercury speciation in the McMurdo, Antarctica coastal region: Atmospheric Environment, v. 42, p. 2885-2893.

Brunke, E., C. Labuschagne, R. Ebinghaus, H. Kock, and F. Slemr, 2010, Gaseous elemental mercury depletion events observed at Cape Point during 2007-2008: Atmospheric Chemistry and Physics, v. 10, p. 1121-1131.

Brunke, E.-G., C. Walters, T. Mkololo, L. Martin, C. Labuschagne, B. Silwana, F. Slemr, A. Weigelt, R. Ebinghaus, and V. Somerset, 2016, Mercury in the atmosphere and in rainwater at Cape Point, South Africa: Atmospheric Environment, v. 125, p. 24-32.

Calvert, J. G., and S. E. Lindberg, 2003, A modeling study of the mechanism of the halogen–ozone–mercury homogeneous reactions in the troposphere during the polar spring: Atmospheric Environment, v. 37, p. 4467-4481.

Calvert, J. G., and S. E. Lindberg, 2005, Mechanisms of mercury removal by O3 and OH in the atmosphere: Atmospheric Environment, v. 39, p. 3355-3367.

Canil, D., P. W. Crockford, R. Rossin, and K. Telmer, 2015, Mercury in some arc crustal rocks and mantle peridotites and relevance to the moderately volatile element budget of the Earth: Chemical Geology, v. 396, p. 134-142.

Carpi, A., and S. E. Lindberg, 1997, Sunlight-Mediated Emission of Elemental Mercury from Soil Amended with Municipal Sewage Sludge: Environmental Science & Technology, v. 31, p. 2085-2091.

Carpi, A., and S. E. Lindberg, 1998, Application of a teflon™ dynamic flux chamber for quantifying soil mercury flux: Tests and results over background soil: Atmospheric Environment, v. 32, p. 873-882.

Cheng, I., and L. Zhang, 2017, Uncertainty Assessment of Gaseous Oxidized Mercury Measurements Collected by Atmospheric Mercury Network: Environmental Science & Technology, v. 51, p. 855-862.

Clever, H. L., S. A. Johnson, and M. E. Derrick, 1985, The Solubility of Mercury and Some Sparingly Soluble Mercury Salts in Water and Aqueous Electrolyte Solutions: Journal of Physical and Chemical Reference Data, v. 14, p. 631-680.

Compeau, G. C., and R. Bartha, 1985, Sulfate-Reducing Bacteria: Principal Methylators of Mercury in Anoxic Estuarine Sediment: Applied and Environmental Microbiology, v. 50, p. 498-502.

Dibble, T., M. Zelie, and H. Mao, 2012, Thermodynamics of reactions of ClHg and BrHg radicals with atmospherically abundant free radicals: Atmospheric Chemistry and Physics, v. 12, p. 10271-10279.

Diéguez, M. C., P. E. Garcia, M. Bencardino, F. D'Amore, J. Castagna, S. Ribeiro Guevara, and F. Sprovieri, 2017, Four years of atmospheric mercury records in Northwestern Patagonia (Argentina): potential sources, concentration patterns and influence of environmental variables observed at the GMOS EMMA station: Atmos. Chem. Phys. Discuss., v. 2017, p. 1-18.

Dommergue, A., F. Sprovieri, N. Pirrone, R. Ebinghaus, S. Brooks, J. Courteaud, and C. Ferrari, 2010, Overview of mercury measurements in the Antarctic troposphere: Atmospheric Chemistry and Physics, v. 10, p. 3309-3319.

Donohoue, D. L., D. Bauer, B. Cossairt, and A. J. Hynes, 2006, Temperature and Pressure Dependent Rate Coefficients for the Reaction of Hg with Br and the Reaction of Br with Br: A Pulsed Laser Photolysis-Pulsed Laser Induced Fluorescence Study: The Journal of Physical Chemistry A, v. 110, p. 6623-6632.

Driscoll, C. T., R. P. Mason, H. M. Chan, D. J. Jacob, and N. Pirrone, 2013, Mercury as a Global Pollutant: Sources, Pathways, and Effects: Environmental Science & Technology, v. 47, p. 4967-4983.

Dumarey, R., R. Dams, and J. Hoste, 1985a, Comparison of the collection and desorption efficiency of activated charcoal, silver, and gold for the determination of vapor phase atmospheric mercury: Analytical Chemistry, v. 57, p. 2638-2643.

Dumarey, R., E. Temmerman, R. Dams, and J. Hoste, 1985b, The accuracy of the vapor injection calibration method for the determination of mercury by amalgamation and cold vapour atomic absorption spectrometry: Analytica Chimica Acta, v. 170, p. 337-340.

Ebinghaus, R., S. G. Jennings, W. H. Schroeder, T. Berg, T. Donaghy, J. Guentzel, C. Kenny, H. H. Kock, K. Kvietkus, W. Landing, T. Muhleck, J. Munthe, E. M. Prestbo, D. Schneeberger, F. Slemr, J. Sommar, A. Urba, D. Wallschlager, and Z. Xiao, 1999, International field intercomparison measurements of atmospheric mercury species at Mace Head, Ireland: Atmospheric Environment, v. 33, p. 3063-3073.

Ebinghaus, R., H. H. Kock, C. Temme, J. W. Einax, A. G. Löwe, A. Richter, J. P. Burrows, and W. H. Schroeder, 2002, Antarctic Springtime Depletion of Atmospheric Mercury: Environmental Science & Technology, v. 36, p. 1238-1244.

Eckley, C. S., M. Gustin, C. J. Lin, X. Li, and M. B. Miller, 2010, The influence of dynamic chamber design and operating parameters on calculated surface-to-air mercury fluxes: Atmospheric Environment, v. 44, p. 194-203.

Eckley, C. S., M. Gustin, F. Marsik, and M. B. Miller, 2011, Measurement of surface mercury fluxes at active industrial gold mines in Nevada (USA): Science of the Total Environment, v. 409, p. 514-522.

Eckley, C. S., M. T. Tate, C.-J. Lin, M. Gustin, S. Dent, C. Eagles-Smith, M. A. Lutz, K. P. Wickland, B. Wang, J. E. Gray, G. C. Edwards, D. P. Krabbenhoft, and D. B. Smith, 2016, Surface-air mercury fluxes across Western North America: A synthesis of spatial trends and controlling variables: Science of The Total Environment, v. 568, p. 651-665.

Edwards, G. C., and D. A. Howard, 2013, Air-surface exchange measurements of gaseous elemental mercury over naturally enriched and background terrestrial landscapes in Australia: Atmos. Chem. Phys., v. 13, p. 5325-5336.

Edwards, G. C., P. E. Rasmussen, W. H. Schroeder, R. J. Kemp, G. M. Dias, C. R. Fitzgerald-Hubble, E. K. Wong, L. Halfpenny-Mitchell, and M. S. Gustin, 2001, Sources of variability in mercury flux measurements: Journal of Geophysical Research: Atmospheres, v. 106, p. 5421-5435.

Edwards, G. C., P. E. Rasmussen, W. H. Schroeder, D. M. Wallace, L. Halfpenny-Mitchell, G. M. Dias, R. J. Kemp, and S. Ausma, 2005, Development and evaluation of a sampling system to determine gaseous Mercury fluxes using an aerodynamic micrometeorological gradient method: Journal of Geophysical Research: Atmospheres, v. 110.

Ent, H., I. v. Andel, M. Heemskerk, P. v. Otterloo, W. Bavius, A. Baldan, M. Horvat, J. C. B. Richard, and C. R. Quétel, 2014, A gravimetric approach to providing SI traceability for concentration measurement results of mercury vapor at ambient air levels: Measurement Science and Technology, v. 25, p. 115801.

Feddersen, D. M., R. Talbot, H. Mao, and B. C. Sive, 2012, Size distribution of particulate mercury in marine and coastal atmospheres: Atmos. Chem. Phys., v. 12, p. 10899-10909.

Feng, X., J. Sommar, K. Gardfeldt, and O. Lindqvist, 2000, Improved determination of gaseous divalent mercury in ambient air using KCl coated denuders: Fresenius Journal of Analytical Chemistry, v. 366, p. 423-428.

Feng, X. B., J. Y. Lu, Y. J. Hao, C. Banic, and W. H. Schroeder, 2003, Evaluation and applications of a gaseous mercuric chloride source: Analytical and Bioanalytical Chemistry, v. 376, p. 1137-1140.

Fitzgerald, W. F., D. R. Engstrom, R. P. Mason, and E. A. Nater, 1998, The case for atmospheric mercury contamination in remote areas: Environmental Science & Technology, v. 32, p. 1-7.

Fitzgerald, W. F., and G. A. Gill, 1979, Subnanogram determination of mercury by two-stage gold amalgamation and gas phase detection applied to atmospheric analysis: Analytical Chemistry, v. 51, p. 1714-1720.

Fitzgerald, W. F., and C. H. Lamborg, 2014, 11.4 - Geochemistry of Mercury in the Environment A2 - Holland, Heinrich D, *in* K. K. Turekian, ed., Treatise on Geochemistry (Second Edition): Oxford, Elsevier, p. 91-129.

Friedli, H. R., A. F. Arellano, S. Cinnirella, and N. Pirrone, 2009, Mercury emissions from global biomass burning: spatialand temporal distribution, *in* R. Mason, and N. Pirrone, eds., Mercury Fate and Transport in the Global Atmosphere: Emissions, Measurements and Models: Boston, MA, Springer US, p. 193-220.

Fritsche, J., D. Obrist, M. Zeeman, F. Conen, W. Eugster, and C. Alewell, 2008, Elemental mercury fluxes over a sub-alpine grassland determined with two micrometeorological methods: Atmospheric Environment, v. 42, p. 2922-2933.

Gillis, A., and D. R. Miller, 2000, Some potential errors in the measurement of mercury gas exchange at the soil surface using a dynamic flux chamber: Science of The Total Environment, v. 260, p. 181-189.

GMOS, 2011, GMOS Standard Operational Procedure: Methods for the determination of TGM and GEM, http://www.gmos.eu/public/GMOS%20SOP%20TGM_GEM.pdf.

Goldwater, L. J., 1972, Mercury - A history of quicksilver: Baltimore, York Press, 318 p.

Goodsite, M. E., J. M. C. Plane, and H. Skov, 2004, A Theoretical Study of the Oxidation of Hg0 to HgBr2 in the Troposphere: Environmental Science & Technology, v. 38, p. 1772-1776.

Goodsite, M. E., J. M. C. Plane, and H. Skov, 2012, Correction to A Theoretical Study of the Oxidation of Hg0 to HgBr2 in the Troposphere: Environmental Science & Technology, v. 46, p. 5262-5262.

Gratz, L. E., J. L. Ambrose, D. A. Jaffe, V. Shah, L. Jaegle, J. Stutz, J. Festa, M. Spolaor, C. Tsai, N. E. Selin, S. Song, X. Zhou, A. J. Weinheimer, D. J. Knapp, D. D. Montzka, F. M. Flocke, T. L. Campos, E. Apel, R. Hornbrook, N. J. Blake, S. Hall, G. S. Tyndall, M. Reeves, D. Stechman, and M. Stell, 2015, Oxidation of mercury by bromine in the subtropical Pacific free troposphere: Geophysical Research Letters, v. 42, p. 9.

Gustin, M., and D. Jaffe, 2010, Reducing the Uncertainty in Measurement and Understanding of Mercury in the Atmosphere: Environmental Science & Technology, v. 44, p. 2222-2227.

Gustin, M. S., 2003, Are mercury emissions from geologic sources significant? A status report: Science of The Total Environment, v. 304, p. 153-167.

Gustin, M. S., H. M. Amos, J. Huang, M. B. Miller, and K. Heidecorn, 2015, Measuring and modeling mercury in the atmosphere: a critical review: Atmos. Chem. Phys., v. 15, p. 5697-5713.

Gustin, M. S., H. Biester, and C. S. Kim, 2002, Investigation of the light-enhanced emission of mercury from naturally enriched substrates: Atmospheric Environment, v. 36, p. 3241-3254.

Gustin, M. S., M. Engle, J. Ericksen, S. Lyman, J. Stamenkovic, and M. Xin, 2006, Mercury exchange between the atmosphere and low mercury containing substrates: Applied Geochemistry, v. 21, p. 1913-1923.

Gustin, M. S., J. Huang, M. B. Miller, C. Peterson, D. A. Jaffe, J. Ambrose, B. D. Finley, S. N. Lyman, K. Call, R. Talbot, D. Feddersen, H. Mao, and S. E. Lindberg, 2013, Do We Understand What the Mercury Speciation Instruments Are Actually Measuring? Results of RAMIX: Environmental Science & Technology, v. 47, p. 7295-7306.

Gustin, M. S., S. Lindberg, F. Marsik, A. Casimir, R. Ebinghaus, G. Edwards, C. Hubble-Fitzgerald, R. Kemp, H. Kock, T. Leonard, J. London, M. Majewski, C. Montecinos, J. Owens, M. Pilote, L. Poissant, P. Rasmussen, F. Schaedlich, D. Schneeberger, W. Schroeder, J. Sommar, R. Turner, A. Vette, D. Wallschlaeger, Z. Xiao, and H. Zhang, 1999, Nevada STORMS project: Measurement of mercury emissions from naturally enriched surfaces: Journal of Geophysical Research: Atmospheres, v. 104, p. 21831-21844.

Gustin, M. S., S. E. Lindberg, K. Austin, M. Coolbaugh, A. Vette, and H. Zhang, 2000, Assessing the contribution of natural sources to regional atmospheric mercury budgets: Science of The Total Environment, v. 259, p. 61-71.

Gustin, M. S., S. E. Lindberg, and P. J. Weisberg, 2008, An update on the natural sources and sinks of atmospheric mercury: Applied Geochemistry, v. 23, p. 482-493.

Gustin, M. S., A. M. Pierce, J. Huang, M. B. Miller, H. A. Holmes, and S. M. Loria-Salazar, 2016, Evidence for Different Reactive Hg Sources and Chemical Compounds at Adjacent Valley and High Elevation Locations: Environmental Science & Technology, v. 50, p. 12225-12231.

Gustin, M. S., and J. Stamenkovic, 2005, Effect of Watering and Soil Moisture on Mercury Emissions from Soils: Biogeochemistry, v. 76, p. 215-232.

Gustin, M. S., G. E. Taylor, and R. A. Maxey, 1997, Effect of temperature and air movement on the flux of elemental mercury from substrate to the atmosphere: Journal of Geophysical Research: Atmospheres, v. 102, p. 3891-3898.

Hall, B., 1995, The gas phase oxidation of elemental mercury by ozone: Water, Air, and Soil Pollution, v. 80, p. 301-315.

Harada, M., 1995, Minamata Disease: Methylmercury Poisoning in Japan Caused by Environmental Pollution: Critical Reviews in Toxicology, v. 25, p. 1-24.

Hintelmann, H., R. Harris, A. Heyes, J. P. Hurley, C. A. Kelly, D. P. Krabbenhoft, S. Lindberg, J. W. M. Rudd, K. J. Scott, and V. L. St.Louis, 2002, Reactivity and Mobility of New and Old Mercury Deposition in a Boreal Forest Ecosystem during the First Year of the METAALICUS Study: Environmental Science & Technology, v. 36, p. 5034-5040.

Holmes, C. D., D. J. Jacob, E. S. Corbitt, J. Mao, X. Yang, R. Talbot, and F. Slemr, 2010, Global atmospheric model for mercury including oxidation by bromine atoms: Atmos. Chem. Phys., v. 10, p. 12037-12057.

Holmes, C. D., D. J. Jacob, R. P. Mason, and D. A. Jaffe, 2009, Sources and deposition of reactive gaseous mercury in the marine atmosphere: Atmospheric Environment, v. 43, p. 2278-2285.

Holmes, C. D., D. J. Jacob, and X. Yang, 2006, Global lifetime of elemental mercury against oxidation by atomic bromine in the free troposphere: Geophysical Research Letters, v. 33, p. n/a-n/a.

Horowitz, H., D. Jacob, Y. Zhang, T. Dibble, F. Slemr, H. Amos, J. Schmidt, E. Corbitt, E. Marais, and E. Sunderland, 2017, A new mechanism for atmospheric mercury redox chemistry: implications for the global mercury budget: Atmospheric Chemistry and Physics, v. 17, p. 6353-6371.

Howard, D., and G. C. Edwards, 2018, Mercury fluxes over an Australian alpine grassland and observation of nocturnal atmospheric mercury depletion events: Atmos. Chem. Phys., v. 18, p. 129-142.

Howard, D., P. F. Nelson, G. C. Edwards, A. L. Morrison, J. A. Fisher, J. Ward, J. Harnwell, M. van der Schoot, B. Atkinson, S. D. Chambers, A. D. Griffiths, S. Werczynski, and A. G. Williams, 2017, Atmospheric mercury in the Southern Hemisphere tropics: seasonal and diurnal variations and influence of inter-hemispheric transport: Atmos. Chem. Phys., v. 17, p. 11623-11636.

Huang, J., and M. S. Gustin, 2015a, Uncertainties of Gaseous Oxidized Mercury Measurements Using KCl-Coated Denuders, Cation-Exchange Membranes, and Nylon Membranes: Humidity Influences: Environmental Science & Technology, v. 49, p. 6102-6108.

Huang, J., and M. S. Gustin, 2015b, Use of Passive Sampling Methods and Models to Understand Sources of Mercury Deposition to High Elevation Sites in the Western United States: Environmental Science & Technology, v. 49, p. 432-441.

Huang, J., M. B. Miller, E. Edgerton, and M. Sexauer Gustin, 2017, Deciphering potential chemical compounds of gaseous oxidized mercury in Florida, USA: Atmos. Chem. Phys., v. 17, p. 1689-1698.

Huang, J., M. B. Miller, P. Weiss-Penzias, and M. S. Gustin, 2013, Comparison of Gaseous Oxidized Hg Measured by KCl-Coated Denuders, and Nylon and Cation Exchange Membranes: Environmental Science & Technology, v. 47, p. 7307-7316.

Hynes, A. J., D. L. Donohoue, M. E. Goodsite, and I. M. Hedgecock, 2009, Our current understanding of major chemical and physical processes affecting mercury dynamics in the atmosphere and at the air-water/terrestrial interfaces, *in* R. Mason, and N. Pirrone, eds., Mercury Fate and Transport in the Global Atmosphere: Emissions, Measurements and Models: Boston, MA, Springer US, p. 427-457.

Jaffe, D. A., S. Lyman, H. M. Amos, M. S. Gustin, J. Huang, N. E. Selin, L. Levin, A. ter Schure, R. P. Mason, R. Talbot, A. Rutter, B. Finley, L. Jaeglé, V. Shah, C. McClure, J. Ambrose, L. Gratz, S. Lindberg, P. Weiss-Penzias, G.-R. Sheu, D. Feddersen, M. Horvat, A. Dastoor, A. J. Hynes, H. Mao, J. E. Sonke, F. Slemr, J. A. Fisher, R. Ebinghaus, Y. Zhang, and G. Edwards, 2014, Progress on Understanding Atmospheric Mercury Hampered by Uncertain Measurements: Environmental Science & Technology, v. 48, p. 7204-7206.

Jiao, Y., and T. S. Dibble, 2017, First kinetic study of the atmospherically important reactions BrHg[radical dot] + NO2 and BrHg[radical dot] + HOO: Physical Chemistry Chemical Physics, v. 19, p. 1826-1838.

Johnson, D. L., and R. S. Braman, 1974, Distribution of atmospheric mercury species near ground: Environmental Science & Technology, v. 8, p. 1003-1009.

Jones, C. P., S. N. Lyman, D. A. Jaffe, T. Allen, and T. L. O'Neil, 2016, Detection and quantification of gas-phase oxidized mercury compounds by GC/MS: Atmos. Meas. Tech., v. 9, p. 2195-2205.

Keeler, G., G. Glinsorn, and N. Pirrone, 1995, Particulate Mercury in the Atmosphere: Its Significance, Transport, Transformation and Sources, *in* D. B. Porcella, J. W. Huckabee, and B. Wheatley, eds., Mercury as a Global Pollutant: Proceedings of the Third International Conference held in Whistler, British Columbia, July 10–14, 1994: Dordrecht, Springer Netherlands, p. 159-168.

Khalizov, A., B. Viswanathan, P. Larregaray, and P. Ariya, 2003, A theoretical study on the reactions of Hg with halogens: Atmospheric implications: Journal of Physical Chemistry a, v. 107, p. 6360-6365.

Kim, K.-H., S. E. Lindberg, and T. P. Meyers, 1995, Micrometeorological measurements of mercury vapor fluxes over background forest soils in eastern Tennessee: Atmospheric Environment, v. 29, p. 267-282.

Kim, K. H., and S. E. Lindberg, 1995, Design and initial tests of a dynamic enclosure chamber for measurements of vapor-phase mercury fluxes over soils: Water, Air, and Soil Pollution, v. 80, p. 1059-1068.

Kocman, D., and M. Horvat, 2011, Non-point source mercury emission from the Idrija Hg-mine region: GIS mercury emission model: Journal of Environmental Management, v. 92, p. 2038-2046.

Kocman, D., M. Horvat, N. Pirrone, and S. Cinnirella, 2013, Contribution of contaminated sites to the global mercury budget: Environmental Research, v. 125, p. 160-170.

Kos, G., A. Ryzhkov, A. Dastoor, J. Narayan, A. Steffen, P. Ariya, and L. Zhang, 2013, Evaluation of discrepancy between measured and modelled oxidized mercury species: Atmospheric Chemistry and Physics, v. 13, p. 4839-4863.

Krabbenhoft, D. P., and E. M. Sunderland, 2013, Global Change and Mercury: Science, v. 341, p. 1457.

Landis, M. S., R. K. Stevens, F. Schaedlich, and E. M. Prestbo, 2002, Development and characterization of an annular denuder methodology for the measurement of divalent inorganic reactive gaseous mercury in ambient air: Environmental Science & Technology, v. 36, p. 3000-3009.

Laurier, F., and R. Mason, 2007, Mercury concentration and speciation in the coastal and open ocean boundary layer: Journal of Geophysical Research-Atmospheres, v. 112.

Laurier, F. J. G., R. P. Mason, L. Whalin, and S. Kato, 2003, Reactive gaseous mercury formation in the North Pacific Ocean's marine boundary layer: A potential role of halogen chemistry: Journal of Geophysical Research: Atmospheres, v. 108, p. n/a-n/a.

Lin, C.-J., and S. O. Pehkonen, 1999, The chemistry of atmospheric mercury: a review: Atmospheric Environment, v. 33, p. 2067-2079.

Lin, C. J., P. Pongprueksa, S. E. Lindberg, S. O. Pehkonen, D. Byun, and C. Jang, 2006, Scientific uncertainties in atmospheric mercury models I: Model science evaluation: Atmospheric Environment, v. 40, p. 2911-2928.

Lindberg, S., R. Bullock, R. Ebinghaus, D. Engstrom, X. Feng, W. Fitzgerald, N. Pirrone, E. Prestbo, and C. Seigneur, 2007, A synthesis of progress and uncertainties in attributing the sources of mercury in deposition: Ambio, v. 36, p. 19-32.

Lindberg, S. E., S. Brooks, C. J. Lin, K. J. Scott, M. S. Landis, R. K. Stevens, M. Goodsite, and A. Richter, 2002a, Dynamic Oxidation of Gaseous Mercury in the Arctic Troposphere at Polar Sunrise: Environmental Science & Technology, v. 36, p. 1245-1256.

Lindberg, S. E., and W. J. Stratton, 1998, Atmospheric mercury speciation: Concentrations and behavior of reactive gaseous mercury in ambient air: Environmental Science & Technology, v. 32, p. 49-57.

Lindberg, S. E., H. Zhang, M. Gustin, A. Vette, F. Marsik, J. Owens, A. Casimir, R. Ebinghaus, G. Edwards, C. Fitzgerald, J. Kemp, H. H. Kock, J. London, M. Majewski, L. Poissant, M. Pilote, P. Rasmussen, F. Schaedlich, D. Schneeberger, J. Sommar, R. Turner, D.

Wallschläger, and Z. Xiao, 1999, Increases in mercury emissions from desert soils in response to rainfall and irrigation: Journal of Geophysical Research: Atmospheres, v. 104, p. 21879-21888.

Lindberg, S. E., H. Zhang, A. F. Vette, M. S. Gustin, M. O. Barnett, and T. Kuiken, 2002b, Dynamic flux chamber measurement of gaseous mercury emission fluxes over soils: Part 2—effect of flushing flow rate and verification of a two-resistance exchange interface simulation model: Atmospheric Environment, v. 36, p. 847-859.

Lindqvist, O., K. Johansson, M. Aastrup, A. Andersson, L. Bringmark, G. Hovsenius, L. Hakanson, A. Iverfeldt, M. Meili, and B. Timm, 1991, Mercury in the Swedish environment - Recent research on causes, consequences and corrective methods: Water Air and Soil Pollution, v. 55, p. R11-&.

Lindqvist, O., and H. Rodhe, 1985, Atmospheric mercury-a review: Tellus B: Chemical and Physical Meteorology, v. 37, p. 136-156.

Lu, J., W. Schroeder, T. Berg, J. Munthe, D. Schneeberger, and F. Schaedlich, 1998, A device for sampling and determination of total particulate mercury in ambient air: Analytical Chemistry, v. 70, p. 2403-2408.

Lyman, S., and D. Jaffe, 2009, High Time Resolution Measurements of Gaseous Oxidized Mercury from Ground and Aircraft Platforms: Session A06: Pathways of Mercury Transport and Exposure at Multiple Scales.

Lyman, S., and D. Jaffe, 2012, Formation and fate of oxidized mercury in the upper troposphere and lower stratosphere: Nature Geoscience, v. 5, p. 114-117.

Lyman, S., C. Jones, T. O'Neil, T. Allen, M. Miller, M. S. Gustin, A. M. Pierce, W. Luke, X. Ren, and P. Kelley, 2016, Automated Calibration of Atmospheric Oxidized Mercury Measurements: Environmental Science & Technology, v. 50, p. 12921-12927.

Lyman, S. N., M. S. Gustin, E. M. Prestbo, and F. J. Marsik, 2007, Estimation of Dry Deposition of Atmospheric Mercury in Nevada by Direct and Indirect Methods: Environmental Science & Technology, v. 41, p. 1970-1976.

Lyman, S. N., D. A. Jaffe, and M. S. Gustin, 2010, Release of mercury halides from KCl denuders in the presence of ozone: Atmospheric Chemistry and Physics, v. 10, p. 8197-8204.

Lynam, M. M., and G. J. Keeler, 2005, Artifacts associated with the measurement of particulate mercury in an urban environment: The influence of elevated ozone concentrations: Atmospheric Environment, v. 39, p. 3081-3088.

Malcolm, E. G., and G. J. Keeler, 2007, Evidence for a sampling artifact for particulate-phase mercury in the marine atmosphere: Atmospheric Environment, v. 41, p. 3352-3359.

Mao, H., I. Cheng, and L. Zhang, 2016, Current understanding of the driving mechanisms for spatiotemporal variations of atmospheric speciated mercury: a review: Atmospheric Chemistry and Physics, v. 16, p. 12897-12924.

Marsh, D., T. Clarkson, C. Cox, G. Myers, L. Aminzaki, and S. Altikriti, 1987, Fetal Methylmercury poisoning - Relationship between concentration in single strands of maternal hair and child effects: Archives of Neurology, v. 44, p. 1017-1022.

Marsik, F. J., G. J. Keeler, S. E. Lindberg, and H. Zhang, 2005, Air–Surface Exchange of Gaseous Mercury over A Mixed Sawgrass–Cattail Stand within the Florida Everglades: Environmental Science & Technology, v. 39, p. 4739-4746.

Martin, L., C. Labuschagne, E. Brunke, A. Weigelt, R. Ebinghaus, and F. Slemr, 2017, Trend of atmospheric mercury concentrations at Cape Point for 1995-2004 and since 2007: Atmospheric Chemistry and Physics, v. 17, p. 2393-2399.

Marusczak, N., J. E. Sonke, X. Fu, and M. Jiskra, 2017, Tropospheric GOM at the Pic du Midi Observatory—Correcting Bias in Denuder Based Observations: Environmental Science & Technology, v. 51, p. 863-869.

Mason, R., N. Lawson, and K. Sullivan, 1997, The concentration, speciation and sources of mercury in Chesapeake Bay precipitation: Atmospheric Environment, v. 31, p. 3541-3550.

Mason, R. P., 2009, Mercury emissions from natural processes and their importance in the global mercury cycle, *in* R. Mason, and N. Pirrone, eds., Mercury Fate and Transport in the Global Atmosphere: Emissions, Measurements and Models: Boston, MA, Springer US, p. 173-191.

Mason, R. P., and G. R. Sheu, 2002, Role of the ocean in the global mercury cycle: Global Biogeochemical Cycles, v. 16, p. 40-1-40-14.

McClure, C. D., D. A. Jaffe, and E. S. Edgerton, 2014, Evaluation of the KCI Denuder Method for Gaseous Oxidized Mercury using HgBr2 at an In-Service AMNet Site: Environmental Science & Technology, v. 48, p. 11437-11444.

Mergler, D., H. Anderson, L. Chan, K. Mahaffey, M. Murray, M. Sakamoto, and A. Stern, 2007, Methylmercury exposure and health effects in humans: A worldwide concern: Ambio, v. 36, p. 3-11.

Miller, M. B., M. S. Gustin, and C. S. Eckley, 2011, Measurement and scaling of air-surface mercury exchange from substrates in the vicinity of two Nevada gold mines: Science of the Total Environment, v. 409, p. 3879-3886.

Moore, C., and A. Carpi, 2005, Mechanisms of the emission of mercury from soil: Role of UV radiation: Journal of Geophysical Research: Atmospheres, v. 110, p. n/a-n/a.

Moore, C., D. Obrist, A. Steffen, R. Staebler, T. Douglas, A. Richter, and S. Nghiem, 2014, Convective forcing of mercury and ozone in the Arctic boundary layer induced by leads in sea ice: Nature, v. 506, p. 81-+.

Munthe, J., I. Wangberg, N. Pirrone, A. Iverfeldt, R. Ferrara, R. Ebinghaus, X. Feng, K. Gardfeldt, G. Keeler, E. Lanzillotta, S. E. Lindberg, J. Lu, Y. Mamane, E. Prestbo, S. Schmolke, W. H. Schroeder, J. Sommar, F. Sprovieri, R. K. Stevens, W. Stratton, G. Tuncel, and A. Urba, 2001, Intercomparison of methods for sampling and analysis of atmospheric mercury species: Atmospheric Environment, v. 35, p. 3007-3017.

Nelson, P. F., A. L. Morrison, H. J. Malfroy, M. Cope, S. Lee, M. L. Hibberd, C. P. Meyer, and J. McGregor, 2012, Atmospheric mercury emissions in Australia from anthropogenic, natural and recycled sources: Atmospheric Environment, v. 62, p. 291-302.

Nerentorp Mastromonaco, M., K. Gårdfeldt, B. Jourdain, K. Abrahamsson, A. Granfors, M. Ahnoff, A. Dommergue, G. Méjean, and H. W. Jacobi, 2016, Antarctic winter mercury and ozone depletion events over sea ice: Atmospheric Environment, v. 129, p. 125-132.

NPI, 2017, Australian National Pollutant Inventory, Australian Government.

NRC, 2000, Toxicological Effects of Methylmercury, Washington, DC, The National Academies Press, p. 368.

Obrist, D., J. Kirk, L. Zhang, E. Sunderland, M. Jiskra, and N. Selin, 2018, A review of global environmental mercury processes in response to human and natural perturbations: Changes of emissions, climate, and land use: Ambio, v. 47, p. 116-140.

Obrist, D., E. Tas, M. Peleg, V. Matveev, X. Fain, D. Asaf, and M. Luria, 2011, Bromine-induced oxidation of mercury in the mid-latitude atmosphere: Nature Geoscience, v. 4, p. 22-26.

Osterwalder, S., J. Sommar, S. Åkerblom, G. Jocher, J. Fritsche, M. B. Nilsson, K. Bishop, and C. Alewell, 2018, Comparative study of elemental mercury flux measurement techniques over a Fennoscandian boreal peatland: Atmospheric Environment, v. 172, p. 16-25.

Pacyna, J., O. Travnikov, F. De Simone, I. Hedgecock, K. Sundseth, E. Pacyna, F. Steenhuisen, N. Pirrone, J. Munthe, and K. Kindbom, 2016, Current and future levels of mercury atmospheric pollution on a global scale: Atmospheric Chemistry and Physics, v. 16, p. 12495-12511.

Pal, B., and P. A. Ariya, 2004, Studies of ozone initiated reactions of gaseous mercury: kinetics, product studies, and atmospheric implications: Physical Chemistry Chemical Physics, v. 6, p. 572-579.

Parson, M., and J. Percival, eds., 2005, A brief history of mercury and its environmental impacts: Mercury: Sources, Measurements, Cycles, and Effects, v. 34: Ottaw, Mineralogical Association of Canada, 1-20 p.

Peleg, M., V. Matveev, E. Tas, M. Luria, R. Valente, and D. Obrist, 2007, Mercury depletion events in the troposphere in mid-latitudes at the Dead Sea, Israel: Environmental Science & Technology, v. 41, p. 7280-7285.

Peleg, M., E. Tas, D. Obrist, V. Matveev, C. Moore, M. Gabay, and M. Luria, 2015, Observational Evidence for Involvement of Nitrate Radicals in Nighttime Oxidation of Mercury: Environmental Science & Technology, v. 49, p. 14008-14018.

Pfaffhuber, K., T. Berg, D. Hirdman, and A. Stohl, 2012, Atmospheric mercury observations from Antarctica: seasonal variation and source and sink region calculations: Atmospheric Chemistry and Physics, v. 12, p. 3241-3251.

Pierce, A., C. Moore, G. Wohlfahrt, L. Hortnagl, N. Kljun, and D. Obrist, 2015, Eddy Covariance Flux Measurements of Gaseous Elemental Mercury Using Cavity Ring-Down Spectroscopy: Environmental Science & Technology, v. 49, p. 1559-1568.

Pierce, A. M., and M. S. Gustin, 2017, Development of a Particulate Mass Measurement System for Quantification of Ambient Reactive Mercury: Environmental Science & Technology, v. 51, p. 436-445.

Pirrone, N., S. Cinnirella, X. Feng, R. Finkelman, H. Friedli, J. Leaner, R. Mason, A. Mukherjee, G. Stracher, D. Streets, and K. Telmer, 2010, Global mercury emissions to the atmosphere from anthropogenic and natural sources: Atmospheric Chemistry and Physics, v. 10, p. 5951-5964.

Prestbo, E., and N. Bloom, 1995, Mercury speciation adsorption (MESA) method for combustion flue gas: methodology, artifacts, intercomparison, and atmospheric implications Water Air and Soil Pollution, v. 80, p. 145-158.

Raofie, F., and P. A. Ariya, 2004, Product Study of the Gas-Phase BrO-Initiated Oxidation of Hg0: Evidence for Stable Hg1+ Compounds: Environmental Science & Technology, v. 38, p. 4319-4326.

Rasmussen, P., G. Edwards, W. Schroeder, S. Ausma, A. Steffen, J. Kemp, C. Fitzgerald-Hubble, L. El Bilali, and G. Dias, 2005, Measurement of gaseous mercury fluxes in the terrestrial environment: Mercury: Sources, Measurements, Cycles, and Effects, v. 34: Ottawa, Mineralogical Association of Canada, 123-136 p.

Rice, K. M., E. M. Walker, M. Wu, C. Gillette, and E. R. Blough, 2014, Environmental Mercury and Its Toxic Effects: Journal of Preventive Medicine and Public Health, v. 47, p. 74-83.

Rutter, A., K. Hanford, J. Zwers, A. Perillo-Nicholas, J. Schauer, and M. Olson, 2008, Evaluation of an offline method for the analysis of atmospheric reactive gaseous mercury and particulate mercury: Journal of the Air & Waste Management Association, v. 58, p. 377-383.

Rutter, A., K. Shakya, R. Lehr, J. Schauer, and R. Griffin, 2012, Oxidation of gaseous elemental mercury in the presence of secondary organic aerosols: Atmospheric Environment, v. 59, p. 86-92.

Rytuba, J., 2003, Mercury from mineral deposits and potential environmental impact: Environmental Geology, v. 43, p. 326-338.

Rytuba, J. J., ed., 2005, Geogenic and mining sources of mercury to the environment: Mercury: Sources, Measurements, Cycles, and Effects, v. 34: Ottawa, Mineralogical Association of Canada, 21-41 p.

Scheulhammer, A., M. Meyer, M. Sandheinrich, and M. Murray, 2007, Effects of environmental methylmercury on the health of wild birds, mammals, and fish: Ambio, v. 36, p. 12-18.

Schroeder, W., and R. Jackson, 1985, An instrumental analytical technique for speciation of atmospheric mercury: International Journal of Environmental Analytical Chemistry, v. 22, p. 1-18.

Schroeder, W., G. Keeler, H. Kock, P. Roussel, D. Schneeberger, and F. Schaedlich, 1995, International field intercomparison of atmospheric mercury measurement methods: Water Air and Soil Pollution, v. 80, p. 611-620.

Schroeder, W. H., K. G. Anlauf, L. A. Barrie, J. Y. Lu, A. Steffen, D. R. Schneeberger, and T. Berg, 1998, Arctic springtime depletion of mercury: Nature, v. 394, p. 331.

Schroeder, W. H., and J. Munthe, 1998, Atmospheric mercury - An overview: Atmospheric Environment, v. 32, p. 809-822.

Schroeder, W. H., J. Munthe, and O. Lindqvist, 1989, Cycling of mercury between water, air, and soil compartments of the environment: Water, Air, and Soil Pollution, v. 48, p. 337-347.

Schroeder, W. H., G. Yarwood, and H. Niki, 1991, Transformation processes involving mercury species in the atmosphere — results from a literature survey: Water Air & Soil Pollution, v. 56, p. 653-666.

Seigneur, C., P. Karamchandani, K. Lohman, K. Vijayaraghavan, and R. Shia, 2001, Multiscale modeling of the atmospheric fate and transport of mercury: Journal of Geophysical Research-Atmospheres, v. 106, p. 27795-27809.

Selin, N. E., 2009, Global Biogeochemical Cycling of Mercury: A Review: Annual Review of Environment and Resources, v. 34, p. 43-63.

Shah, V., L. Jaegle, L. Gratz, J. Ambrose, D. Jaffe, N. Selin, S. Song, T. Campos, F. Flocke, M. Reeves, D. Stechman, M. Stell, J. Festa, J. Stutz, A. Weinheimer, D. Knapp, D. Montzka, G. Tyndall, E. Apel, R. Hornbrook, A. Hills, D. Riemer, N. Blake, C. Cantrell, and R. Mauldin, 2016, Origin of oxidized mercury in the summertime free troposphere over the southeastern US: Atmospheric Chemistry and Physics, v. 16, p. 1511-1530.

Shepler, B., and K. Peterson, 2003, Mercury monoxide: A systematic investigation of its ground electronic state: Journal of Physical Chemistry a, v. 107, p. 1783-1787.

Shepler, B. C., N. B. Balabanov, and K. A. Peterson, 2007, Hg+Br→HgBr recombination and collision-induced dissociation dynamics: The Journal of Chemical Physics, v. 127, p. 164304.

Sheu, G. R., and R. P. Mason, 2001, An examination of methods for the measurements of reactive gaseous mercury in the atmosphere: Environmental Science & Technology, v. 35, p. 1209-1216.

Skov, H., S. B. Brooks, M. E. Goodsite, S. E. Lindberg, T. P. Meyers, M. S. Landis, M. R. B. Larsen, B. Jensen, G. McConville, and J. Christensen, 2006, Fluxes of reactive gaseous mercury measured with a newly developed method using relaxed eddy accumulation: Atmospheric Environment, v. 40, p. 5452-5463.

Slemr, F., H. Angot, A. Dommergue, O. Magand, M. Barret, A. Weigelt, R. Ebinghaus, E. Brunke, K. A Pfaffhuber, G. Edwards, D. Howard, J. Powell, M. Keywood, and F. Wang, 2015, Comparison of mercury concentrations measured at several sites in the Southern Hemisphere: Atmospheric Chemistry and Physics, v. 15, p. 3125-3133.

Slemr, F., and E. Langer, 1992, Increase in global atmospheric concentrations of mercury inferred from measurements over the Atlantic ocean: Nature, v. 355, p. 434-437.

Slemr, F., G. Schuster, and W. Seiler, 1985, Distribution, speciation, and budget of atmospheric mercury: Journal of Atmospheric Chemistry, v. 3, p. 407-434.

Slemr, F., W. Seiler, C. Eberling, and P. Roggendorf, 1979, The determination of total gaseous mercury in air at background levels: Analytica Chimica Acta, v. 110, p. 35-47.

Snider, G., F. Raofie, and P. A. Ariya, 2008, Effects of relative humidity and CO(g) on the O3-initiated oxidation reaction of Hg0(g): kinetic & product studies: Physical Chemistry Chemical Physics, v. 10, p. 5616-5623.

Soerensen, A. L., H. Skov, D. J. Jacob, B. T. Soerensen, and M. S. Johnson, 2010a, Global Concentrations of Gaseous Elemental Mercury and Reactive Gaseous Mercury in the Marine Boundary Layer: Environmental Science & Technology, v. 44, p. 7425-7430.

Soerensen, A. L., E. M. Sunderland, C. D. Holmes, D. J. Jacob, R. M. Yantosca, H. Skov, J. H. Christensen, S. A. Strode, and R. P. Mason, 2010b, An Improved Global Model for Air-Sea Exchange of Mercury: High Concentrations over the North Atlantic: Environmental Science & Technology, v. 44, p. 8574-8580.

Sommar, J., W. Zhu, C.-J. Lin, and X. Feng, 2013, Field Approaches to Measure Hg Exchange Between Natural Surfaces and the Atmosphere—A Review: Critical Reviews in Environmental Science and Technology, v. 43, p. 1657-1739.

Sprovieri, F., N. Pirrone, M. Bencardino, F. D'Amore, F. Carbone, S. Cinnirella, V. Mannarino, M. Landis, R. Ebinghaus, A. Weigelt, E. G. Brunke, C. Labuschagne, L. Martin, J. Munthe, I. Wängberg, P. Artaxo, F. Morais, H. D. M. J. Barbosa, J. Brito, W. Cairns, C. Barbante, M. D. C. Diéguez, P. E. Garcia, A. Dommergue, H. Angot, O. Magand, H. Skov, M. Horvat, J. Kotnik, K. A. Read, L. M. Neves, B. M. Gawlik, F. Sena, N. Mashyanov, V. Obolkin, D. Wip, X. B. Feng, H. Zhang, X. Fu, R. Ramachandran, D. Cossa, J. Knoery, N. Marusczak, M. Nerentorp, and C. Norstrom, 2016, Atmospheric mercury concentrations observed at ground-based monitoring sites globally distributed in the framework of the GMOS network: Atmos. Chem. Phys., v. 16, p. 11915-11935.

Sprovieri, F., N. Pirrone, I. M. Hedgecock, M. S. Landis, and R. K. Stevens, 2002, Intensive atmospheric mercury measurements at Terra Nova Bay in Antarctica during November and December 2000: Journal of Geophysical Research: Atmospheres, v. 107, p. ACH 20-1-ACH 20-8.

Steffen, A., T. Douglas, M. Amyot, P. Ariya, K. Aspmo, T. Berg, J. Bottenheim, S. Brooks, F. Cobbett, A. Dastoor, A. Dommergue, R. Ebinghaus, C. Ferrari, K. Gardfeldt, M. E. Goodsite, D. Lean, A. J. Poulain, C. Scherz, H. Skov, J. Sommar, and C. Temme, 2008, A synthesis of atmospheric mercury depletion event chemistry in the atmosphere and snow: Atmos. Chem. Phys., v. 8, p. 1445-1482.

Steffen, A., W. Schroeder, J. Bottenheim, J. Narayan, and J. D. Fuentes, 2002, Atmospheric mercury concentrations: measurements and profiles near snow and ice surfaces in the Canadian Arctic during Alert 2000: Atmospheric Environment, v. 36, p. 2653-2661.

Stratton, W. J., S. E. Lindberg, and C. J. Perry, 2001, Atmospheric mercury speciation: Laboratory and field evaluation of a mist chamber method for measuring reactive gaseous mercury: Environmental Science & Technology, v. 35, p. 170-177.

Streets, D. G., M. K. Devane, Z. Lu, T. C. Bond, E. M. Sunderland, and D. J. Jacob, 2011, All-Time Releases of Mercury to the Atmosphere from Human Activities: Environmental Science & Technology, v. 45, p. 10485-10491.

Streets, D. G., H. M. Horowitz, D. J. Jacob, Z. Lu, L. Levin, A. F. H. ter Schure, and E. M. Sunderland, 2017, Total Mercury Released to the Environment by Human Activities: Environmental Science & Technology, v. 51, p. 5969-5977.

Subir, M., P. Ariya, and A. Dastoor, 2011, A review of uncertainties in atmospheric modeling of mercury chemistry I. Uncertainties in existing kinetic parameters - Fundamental limitations and the importance of heterogeneous chemistry: Atmospheric Environment, v. 45, p. 5664-5676.

Subir, M., P. Ariya, and A. Dastoor, 2012, A review of the sources of uncertainties in atmospheric mercury modeling II. Mercury surface and heterogeneous chemistry - A missing link: Atmospheric Environment, v. 46, p. 1-10.

Sundseth, K., J. Pacyna, E. Pacyna, N. Pirrone, and R. Thorne, 2017, Global Sources and Pathways of Mercury in the Context of Human Health: International Journal of Environmental Research and Public Health, v. 14.

Swartzendruber, P. C., D. A. Jaffe, and B. Finley, 2009, Development and First Results of an Aircraft-Based, High Time Resolution Technique for Gaseous Elemental and Reactive (Oxidized) Gaseous Mercury: Environmental Science & Technology, v. 43, p. 7484-7489.

Swartzendruber, P. C., D. A. Jaffe, E. M. Prestbo, P. Weiss-Penzias, N. E. Selin, R. Park, D. J. Jacob, S. Strode, and L. Jaegle, 2006, Observations of reactive gaseous mercury in the free troposphere at the Mount Bachelor Observatory: Journal of Geophysical Research-Atmospheres, v. 111.

Talbot, R., H. Mao, D. Feddersen, M. Smith, S. Kim, B. Sive, K. Haase, J. Ambrose, Y. Zhou, and R. Russo, 2011, Comparison of Particulate Mercury Measured with Manual and Automated Methods: Atmosphere, v. 2, p. 1-20.

Talbot, R., H. Mao, E. Scheuer, J. Dibb, and M. Avery, 2007, Total depletion of Hg° in the upper troposphere–lower stratosphere: Geophysical Research Letters, v. 34, p. n/a-n/a.

Telmer, K. H., and M. M. Veiga, 2009, World emissions of mercury from artisanal and small scale gold mining, *in* R. Mason, and N. Pirrone, eds., Mercury Fate and Transport in the Global Atmosphere: Emissions, Measurements and Models: Boston, MA, Springer US, p. 131-172.

Temme, C., J. W. Einax, R. Ebinghaus, and W. H. Schroeder, 2003, Measurements of Atmospheric Mercury Species at a Coastal Site in the Antarctic and over the South Atlantic Ocean during Polar Summer: Environmental Science & Technology, v. 37, p. 22-31.

Tossell, J. A., 2003, Calculation of the Energetics for Oxidation of Gas-Phase Elemental Hg by Br and BrO: The Journal of Physical Chemistry A, v. 107, p. 7804-7808.

Trasande, L., P. J. Landrigan, and C. Schechter, 2005, Public Health and Economic Consequences of Methyl Mercury Toxicity to the Developing Brain: Environmental Health Perspectives, v. 113, p. 590-596.

Turekian, K., and K. Wedepohl, 1961, Distribution of the Elements in Some Major Units of the Earth's Crust: GSA Bulletin, v. 72, p. 175-192.

UNEP, 2013a, Global Mercury Assessment 2013: Sources, Emissions, Releases and Environmental Transport, Geneva, United Nations Environment Programme.

UNEP, 2013b, Minamata Convention on Mercury.

UNEP, 2016, Global Review of Mercury Monitoring Networks, Geneva, Switzerland, United Nations Environment Programme, p. 48.

USGS, 1970, Mercury in the Environment, US Geological Survey Professional Paper 713, p. 67.

Varekamp, J. C., and P. R. Buseck, 1984, The speciation of mercury in hydrothermal systems, with applications to ore deposition: Geochimica et Cosmochimica Acta, v. 48, p. 177-185.

Wallschläger, D., R. Turner Ralph, J. London, R. Ebinghaus, H. Kock Hans, J. Sommar, and Z. Xiao, 1999, Factors affecting the measurement of mercury emissions from soils with flux chambers: Journal of Geophysical Research: Atmospheres, v. 104, p. 21859-21871.

Wang, F., A. Saiz-Lopez, A. Mahajan, J. Martin, D. Armstrong, M. Lemes, T. Hay, and C. Prados-Roman, 2014, Enhanced production of oxidised mercury over the tropical Pacific Ocean: a key missing oxidation pathway: Atmospheric Chemistry and Physics, v. 14, p. 1323-1335.

Weiss-Penzias, P., H. Amos, N. Selin, M. Gustin, D. Jaffe, D. Obrist, G. Sheu, and A. Giang, 2015, Use of a global model to understand speciated atmospheric mercury observations at five high-elevation sites: Atmospheric Chemistry and Physics, v. 15, p. 1161-1173.

White, D. E., M. E. Hinkle, and I. Barnes, 1970, Mercury contents of natural thermal and mineral fluid, US Geological Survey Professional Paper 713, p. 25-28

Wolfe, M. F., S. Schwarzbach, and R. A. Sulaiman, 1998, Effects of mercury on wildlife: A comprehensive review: Environmental Toxicology and Chemistry, v. 17, p. 146-160.

Xiao, Z., J. Sommar, S. Wei, and O. Lindqvist, 1997, Sampling and determination of gas phase divalent mercury in the air using a KCl coated denuder: Fresenius Journal of Analytical Chemistry, v. 358, p. 386-391.

Zhang, L., S. Lyman, H. Mao, C. Lin, D. Gay, S. Wang, M. Gustin, X. Feng, and F. Wania, 2017, A synthesis of research needs for improving the understanding of atmospheric mercury cycling: Atmospheric Chemistry and Physics, v. 17, p. 9133-9144.

Zhang, L. M., L. P. Wright, and P. Blanchard, 2009, A review of current knowledge concerning dry deposition of atmospheric mercury: Atmospheric Environment, v. 43, p. 5853-5864.

Zhu, W., C. Lin, X. Wang, J. Sommar, X. Fu, and X. Feng, 2016, Global observations and modeling of atmosphere-surface exchange of elemental mercury: a critical review: Atmospheric Chemistry and Physics, v. 16, p. 4451-4480.

Zhu, W., J. Sommar, C. J. Lin, and X. Feng, 2015, Mercury vapor air–surface exchange measured by collocated micrometeorological and enclosure methods – Part I: Data comparability and method characteristics: Atmos. Chem. Phys., v. 15, p. 685-702.

CHAPTER 3:

Testing and modeling the influence of reclamation and control methods for reducing nonpoint mercury emissions associated with industrial open pit gold mines

Matthieu B. Miller[1] and Mae S. Gustin[2]

[1]Department of Environmental Sciences, Faculty of Science and Engineering, Macquarie University, Sydney, NSW, 2113, Australia

[2]Department of Natural Resources and Environmental Sciences, University of Nevada, Reno NV, 89557, United States

Statement of Authorship

This paper originated from a project sponsored by the Nevada Division of Environmental Protection and the Nevada Mining Association. Its goal was to explore possible ways in which fugitive Hg emissions from aerially extensive mining-related materials might be mitigated. I designed the experimental plan as a research assistant in collaboration with Dr Gustin, and personally collected all field samples from the selected active mining sites. I completed preparation of substrates and determination of total Hg concentrations, as well as all laboratory-based GEM flux measurements, experimental manipulations, and data processing and analysis. In addition, I planned and conducted the field campaigns measuring in-situ GEM flux at select mine locations and completed the predictive emission model analysis. The manuscript was written with assistance from Dr. Gustin. This paper is included in this dissertation (with permission, Appendix B) as it describes the provenance, collection, and characteristics of materials used in the subsequent investigations of reactive mercury flux described in Chapters 5 and 6, providing background information not covered elsewhere. While it predates other work in this dissertation by several years, it has not been used in full or part for any previous degree. Due to a unique set of circumstances I have remained the intellectual and experimental custodian of the aforementioned materials, a position which lead in large part to the greater body of work in this dissertation, and as such this paper is considered foundational to all subsequent work.

Study Design: 50% • Data Collection: 95% • Data Analysis: 90% • Writing: 75%

Journal of the Air & Waste Management Association
Publication details, including instructions for authors and subscription information:
http://www.tandfonline.com/loi/uawm20

Testing and modeling the influence of reclamation and control methods for reducing nonpoint mercury emissions associated with industrial open pit gold mines

Matthieu B. Miller [a] & Mae S. Gustin [a]
[a] University of Nevada Reno , Reno , Nevada , USA
Accepted author version posted online: 12 Mar 2013.Published online: 22 May 2013.

To cite this article: Matthieu B. Miller & Mae S. Gustin (2013) Testing and modeling the influence of reclamation and control methods for reducing nonpoint mercury emissions associated with industrial open pit gold mines, Journal of the Air & Waste Management Association, 63:6, 681-693, DOI: 10.1080/10962247.2013.778221

To link to this article: http://dx.doi.org/10.1080/10962247.2013.778221

TECHNICAL PAPER

Testing and modeling the influence of reclamation and control methods for reducing nonpoint mercury emissions associated with industrial open pit gold mines

Matthieu B. Miller* and Mae S. Gustin
University of Nevada Reno, Reno, Nevada, USA
**Please address correspondence to: Matthieu B. Miller, University of Nevada Reno, 1664 N Virginia St., Reno, NV 89557, USA; e-mail: matthieum@unr.edu*

Industrial gold mining is a significant source of mercury (Hg) emission to the atmosphere. To investigate ways to reduce these emissions, reclamation and dust and mercury control methods used at open pit gold mining operations in Nevada were studied in a laboratory setting. Using this information along with field data, and building off previous work, total annual Hg emissions were estimated for two active gold mines in northern Nevada. Results showed that capping mining waste materials with a low-Hg substrate can reduce Hg emissions from 50 to nearly 100%. The spraying of typical dust control solutions often results in higher Hg emissions, especially as materials dry after application. The concentrated application of a dithiocarbamate Hg control reagent appears to reduce Hg emissions, but further testing mimicking the actual distribution of this chemical within an active leach solution is needed to make a more definitive assessment.

Implications: Laboratory and field measurements of mercury flux from materials typically found at large open pit gold mines in Nevada indicate that non-point-source mercury emissions are a significant component of total mercury emissions, but that these nonpoint emissions can be significantly reduced by postmining capping and reclamation, and possibly by chemical treatments of leach ore and tailings waste.

Introduction

The state of Nevada is a leading mineral industry producer, ranking first in the United States in gold, barite, and lithium production, and fourth overall in world gold production. There were more than 45 large-scale industrial mining operations active in the state in 2010, 22 of which were metal mines, and the total value of all mining extracted commodities was $7.7 billion, driven predominantly by high gold prices. Proven and probable gold reserves were 81 million ounces at the end of 2010, an amount that could sustain current extraction levels for 15 years and that insures that the mining industry will remain an important part of the Nevada economy for the foreseeable future (Driesner and Coyner, 2011).

Mercury (Hg) is often found in mineralogical association with gold and is frequently abundant in other metal-hosting ore bodies (Rytuba, 2005). It is unique among metallic elementals in being liquid at ambient Earth-surface conditions, and readily volatilizing to an atmospheric gas phase. Once in the atmosphere, it is susceptible to a host of chemical and photo-induced transformations (Schroeder and Munthe, 1998; Seigneur et al., 2006). Consequently, Hg naturally occurring in mineral deposits is a pollutant of concern for the mining industry at every stage of ore extraction and processing. In 2010, approximately 2,425 kg of Hg was estimated to be released from gold mining-related point sources in Nevada (NDEP, 2011). Work by Eckley et al. (2011a) showed that nonpoint sources can be between 14 and 56% of the total Hg emissions from a mine. Taking this work into consideration, total emissions from an active open pit mining operation could be twice the reported point-source emissions.

As mercury is a potentially hazardous neurotoxin and persistent environmental contaminant, with a propensity for bioaccumulation in aquatic food webs even in remote and otherwise pristine ecosystems (Fitzgerald et al., 1998), mitigating the release of Hg from anthropogenic sources is an important goal of modern civilization. Though total Hg emissions from mining operations in Nevada are relatively small compared to the global anthropogenic total (2.4 versus 2,900 Mg yr^{-1}; Pirrone et al., 2009), and are similar to estimated emissions from naturally Hg-enriched areas within Nevada (4 Mg yr^{-1}; Gustin et al., 2008), the mining industry has been very proactive in exploring and implementing ways to reduce Hg releases.

Eckley et al. (2011b) showed that the most significant emission surfaces at two previously investigated gold mines were the heap leach pads and the tailings ponds, rather than more areally extensive waste rock materials. Non-ore-bearing waste rock is

Journal of the Air & Waste Management Association, 63(6):681–693, 2013. ISSN: 1096-2247 print
DOI: 10.1080/10962247.2013.778221

typically used for postmining capping and reclamation, and suitable material is specifically set aside for this task. Heap leach material is oxidized (does not contain carbon or sulfur) gold ore of low grade (~0.05 oz gold/ton). It is not cost-effective to mill process this material, so it is stacked in 5- to 10-m benches that are irrigated with a dilute cyanide leach solution (0.03–0.05% NaCN) to extract gold (Heinen et al., 1978). Tailings are the remains of processed high-grade ore, which may include both oxidized and refractory ore (containing carbon or sulfur) from a variety of locations. Ore is milled to a silt-sized powder, thermally and/or chemically treated (i.e., autoclaved, roasted, vat leached), and piped as a slurry to contained impoundments. Due to the high capital and operating costs, not all mines have mill facilities, and ore from one mine may be shipped to another mine for processing. As a result, tailings impoundments often contain a geochemically heterogeneous mixture of materials.

This paper explores several existing reclamation and control strategies that, while perhaps not intended exclusively or even at all for reducing Hg flux to the atmosphere, could prove effective in reducing non-point-source Hg emissions from large areas of mining. Previous work (cf. Eckley et al., 2011a, 2011b) has shown that wetting and material age affect the magnitude of Hg released from specific materials. Since both could be important components of mine material management strategies, we investigated the influence of these factors on Hg releases and addressed the following questions: (1) Does capping of leach and tailings materials reduce Hg emissions? (2) Does application of dust control solutions reduce Hg emissions? (3) Would the addition of an Hg control reagent (sodium dimethyldithiocarbamate) to a heap leach material reduce Hg emissions? The latter has been added to cyanide leach systems to remove Hg from the leaching solution. To determine the utility of these methods on a larger scale we applied the model developed by Eckley et al. (2011a) to estimate potential Hg emission reduction for two mines using results from the reclamation experiments.

Methods

Laboratory materials

Mining substrates (tailings, heap leach, and cap material) were obtained from four large industrial gold mines in Nevada: Newmont Mining Corporation's Twin Creeks (TC) and Lone Tree (LT) mines, and Barrick Gold Corporation's Cortez-Pipeline (CP), and Goldstrike (GS) mines (Figure 1). Samples of heap leach, tailings, and a material used for reclamation and capping were collected from each mine during the fall of 2010. University of Nevada Reno (UNR) personnel collected the materials at TC, LT, and CP, while at GS materials were collected by mine personnel. Materials were transported to the lab in sealed 5-gal containers, where each material was homogenized and transferred to replicate trays (50 × 50 × 7 cm plywood lined with 3-mil polyvinyl film). Three to five trays of 5 cm depth were made of each material. For two materials, CP leach and GS tailings, 10-cm-deep trays were prepared to test possible effects of depth on flux. Two solutions used to suppress dust at the mines were obtained. These consisted of a 50/50 solution of magnesium chloride ($MgCl_2$) and water from TC, and an organic binding agent (GE Dustreat DC9112) from CP. The sodium diethyl dithiocarbamate solution was obtained from Cherokee Chemicals, Inc. (Hg Control Reagent UNR 1221, $NaS_2CN(C_2H_5)_2 + H_2O$).

Flux measurements and material characterization

Air Hg concentrations were measured using Tekran 2537A Hg Analyzers (Tekran, Toronto, Canada; 0.1 ng m^{-3} detection limit). Three 2537A analyzers were set to identical flow, timing, and heating parameters, and were calibrated so that the analytical response factors were roughly equivalent, to avoid differences in sensitivity. The clock and cycle times were synchronized so that measurements were directly comparable. Hg fluxes were

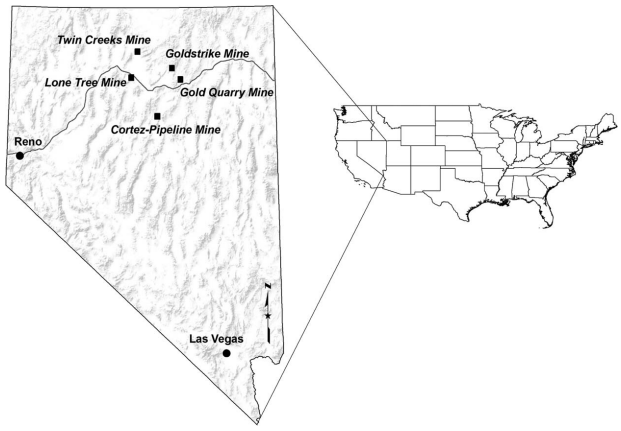

Figure 1. Location map of study sites, Nevada.

measured using the Tekran 2537A in conjunction with a Tekran Automated Dual Sampling Unit (TADS) linked to cylindrical Teflon dynamic flux chambers (DFC) through ~2 m of exposed PFA Teflon tubing. The flux chambers were constructed of thin Teflon film (0.19 mm thickness) overlying a more rigid Teflon frame (1.5 mm thickness), and were designed to be as transparent to visible and ultraviolet (UV) radiation as possible. In total, 16 air inlet holes (1.0 cm diameter) were drilled every 2.5 cm around the base of the chambers. Air was pulled out of the chamber through an opening (0.635 cm diameter) in the top center of the chamber. A complete description of these chambers and rigorous comparisons with other chamber materials and designs can be found in Eckley et al. (2010). Chamber inlet and outlet air were sequentially sampled over 10-min intervals. Hg flux was calculated using the equation:

$$F = Q \times (C_o - C_i)/A \quad (1)$$

where F is the total flux (ng m^{-2} hr^{-1}), Q is the sampling flow rate (m^3 hr^{-1}), A is the chamber footprint (m^2), C_o is the mean Hg concentration (ng m^{-3}) of two consecutive outlet samples, and C_i is the mean Hg concentration (ng m^{-3}) of the 5-min inlet samples collected before and after C_o. The value $C_o - C_i$ is referred to as ΔC. A positive ΔC indicates emission, and a negative ΔC indicates deposition. The sampling flow rate was 1.0 L min^{-1}, and the turnover time for air in the DFC was approximately 2.0 minutes. This turnover time was chosen based on the work of Eckley et al. (2010). Data is presented as a total 24-hr flux (ng m^{-2} day^{-1}) unless otherwise stated.

Meteorological parameters were measured in synchronicity with Hg flux and logged in 5-min intervals using a Campbell Scientific CR10x Datalogger. The parameters measured included incident solar radiation (LiCor Li200X), temperature and relative humidity (Campbell Scientific HMP45C), and in a lab setting volumetric soil moisture (Decagon ECH_20 EC-5 probe). The moisture probe was inserted into the soil through holes drilled into the side of the trays, at a point where the probe would be approximately 3 cm below the material surface.

Solid samples were collected from the top 2 cm of substrate into plastic sample bags using a stainless-steel trowel. These samples were then sieved at 2 mm into glass vials, lyophilized for 48 hr, and stored frozen at –22°C until analysis. Soil moisture samples were collected into glass vials, and then transferred to weighing trays and dried for 1 week in a greenhouse room to determine percent soil moisture by mass.

Total Hg in solid lab and field mining substrates was determined using atomic adsorption spectrometry with a DMA-80 Direct Mercury Analyzer (U.S. Environmental Protection Agency [EPA] Method 7473). NIST traceable standard reference materials (NIST 2709 San Joaquin Soil 1400 ± 80 ng g^{-1}, NIST 2711a Montana Soil 7420 ± 180 ng g^{-1}) were analyzed before and after sets of 10 mine samples (mean recovery = 108 ± 6 %, n = 54). Total Hg in water applied to lab substrates was determined using cold vapor atomic fluorescence spectrometry (U.S. EPA Method 1631). Total Hg in the other mining solutions ($MgCl_2$ etc.) was determined using the DMA-80 method. Organic carbon was determined using a loss-on-ignition (LOI) method (Heiri et al., 2001). Samples were dried for 12–18 hr at 105°C and then combusted at 550°C for 2 hr. The mass loss from dry samples after combustion is approximately equivalent to the mass of organic carbon.

Experimental manipulations

Initially flux from each set of three trays containing the same material was measured and compared to determine how homogeneous each material was with respect to Hg flux. Then, to address each research question, the following experiments were carried out. Two trays of each material (A and B in Figure 2) were unaltered and used to assess influence of watering and aging over the duration of the project (one year). These also served as experimental controls for evaluation of the specific treatments. The third tray (C in Figure 2) of each material was used to test the effect of capping. As application of the dust control treatment is only practical and relevant for areas of heavy equipment use (i.e., active heap leach), a fourth tray (D in Figure 2) of leach material

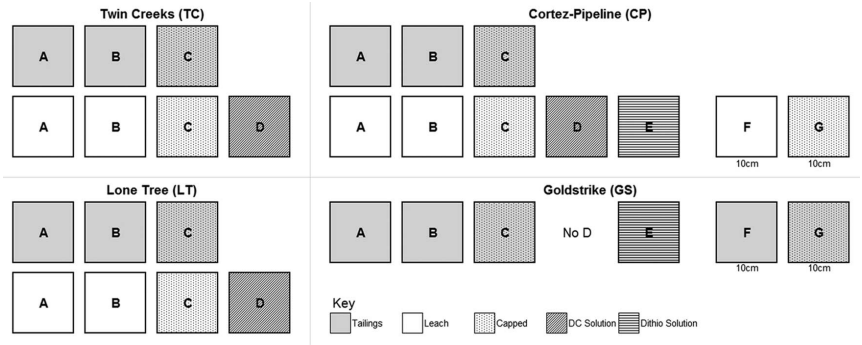

Figure 2. Experimental arrangement of laboratory materials for flux measurements and tests described in the text. Letters represent replicate trays of same material, DC is dust control, and Dithio is dithiocarbamate Hg control reagent.

from TC, LT, and CP was treated with the dust-control solutions used at these mines ($MgCl_2$ used for TC and LT and Dustreat for CP). Trays (E) of CP Leach and GS Tails were treated with the dithiocarbamate Hg control reagent. Additional trays of CP Leach and of GS Tails were filled to 10 cm depth (F and G) to test the effect of material depth on Hg flux.

All tray flux measurements were made within a state-of-the-art greenhouse in the College of Agriculture Biotechnology and Natural Resources Agricultural Experiment Station, in order to provide a controlled environment for manipulating the mine materials without the impact of uncontrollable winds or precipitation. For this experiment, the greenhouse was programmed to maintain a day time temperature range of 18.3 to 23.8, and 12.8 to 18.3°C during the night, to maintain consistent diel temperature changes so that the materials and analytical instruments were not subjected to sudden changes or extremes. Materials received full sun exposure during the day, though total solar energy input, specifically ultraviolet light, was attenuated by the greenhouse glass. The greenhouse temperature was regulated through a natural gas heater and a cooling system of corrugated cellulose evaporative pads and large exhaust blower fans. Measurements were made on the air intake side of the greenhouse so that relatively stable ambient air passed over the materials during flux measurements. All materials were stored together in the same greenhouse space, open to light and air, over the duration of the experiment. Because there were more than 40 trays of material and only three Tekran instruments, it was not possible to carry out continuous measurements. The specific measurements and the sequence in which they were made are described in the following.

All materials were transferred to their respective trays over a period of 2 days. Based on the work of Eckley et al. (2011a) it was suggested that ~7 days were necessary for material flux to stabilize once placed in a tray. To monitor this stabilization and verify that the materials were no longer showing signs of disturbance, flux was measured from one tray of each material type (cap, leach, and tailings) over a period of 7 days immediately following transfer to the trays. After stabilization, all material types from each mine (cap, leach, and tailings) were measured in triplicate (Tray A, B, C) for 24-hr periods to establish a mean daily flux as a reference baseline.

Capping. Capping experiments were performed by covering one tray of leach and tailings material, from each mine, with 2 cm of cap material from the same mine. Based on the results of the disturbance tests, capped trays were allowed to rest for 1 week before flux measurements were begun. Flux measurements were made simultaneously from two uncapped (trays A and B) and one capped tray (tray C) simultaneously for 24 hr. These same measurements were repeated after approximately 1 year.

Watering. Capped and uncapped materials were watered to volumetric soil moisture (VSM) of approximately 15%, using a spray applicator. Materials with higher porosity required a greater mass of water to reach the same VMC as materials with lower porosity. Flux was measured for six consecutive days after the first wetting to capture changes in flux versus VSM. The wetting measurements were repeated after approximately 1 year, but for only 48 hr duration. Tap water (pH 7) was sampled for total Hg analyses before watering each material.

Dust control application. The 50/50 $MgCl_2$ solution was applied to leach ore from TC and LT, and the Dustreat was applied to leach ore from CP. Control trays A and B were watered to equivalent moisture (15% VSM). Flux was measured for 24 hr after application, and at day 60 and day 205 from time of application.

Dithiocarbamate application. For this study, this chemical was applied in solution to previously unaltered trays of CP leach and GS tailings trays E, in conjunction with an equivalent addition of water to control trays A and B (15% VSM). Flux was measured for the first 24 hr after application, and again at day 200 from time of application.

Depth. Two materials were selected for additional measurements of flux from a greater material depth of 10 cm. Flux was measured from two 5-cm trays and one 10-cm tray simultaneously for 24 hr. This was followed by watering to 15% VSM and measuring flux for another 4 days.

Aging. The unaltered A and B trays of each material were used to assess the effects of aging in conjunction with the repetition of the dry and wet capping measurements. Dry materials were measured in January 2011 and again in November 2011. Wet measurements were made January–February–March 2011, and again in December 2011–January 2012.

Model testing

Eckley et al. (2011a) developed a model for estimation of non-point-source emissions using empirical data collected at the Twin Creeks and Cortez Pipeline mines. In this study we verified this model by doing the reverse, that is, predicting field emissions using the model and then measuring flux in the field to determine how well the model predicted flux. This was done in cooperation with Barrick's Goldstrike Mine and Newmont's Gold Quarry Mine.

The Eckley et al. (2011a) model estimates an annual non-point-source Hg emission that is relevant for the surface area of a mine for the time period of interest, and specific environmental conditions. Thus, this model can be applied to predict changes in non-point-source Hg releases as mine surfaces change and are reclaimed. The primary data requirements for the calculations and scaling are as follows:

- Mean Hg concentration for materials with a significant surface area present as a result of mining activity.
- Total three-dimensional (3-D) surface area of the relevant mining materials.
- Mean daily solar radiation and volumetric soil moisture, calculated from annual meteorological data sets.
- Estimates of the extent and duration of certain conditions, such as liquid tailings surfaces, active wet leach, and physical disturbances.

Substrate samples (number of samples shown in Table 1) were collected from representative surface areas at each mine in November and December 2010 for total Hg analysis. Digital elevation data was provided by the staff at both mine sites, and a full-year meteorological data set for calendar year 2010 was acquired from the weather station at Gold Quarry Mine. Hourly data from this set were used to produce mean daily values of temperature, relative humidity, solar radiation, and daily precipitation totals. Substrate moisture was calculated for each day using precipitation and an evapo-transpiration model (Hess, 1997).

The two baseline factors influencing Hg flux include Hg concentration and solar radiation. Superimposed upon these two factors is material wetness, which tends to increase Hg flux. Hg fluxes for each substrate type were calculated using the log-transformed regression equations developed in Eckley et al. (2011a). Due to the influence of solar radiation, these equations are divided into three categories (0–140, 141–252, >252 W m^{-2}). Flux from high-carbon and/or -sulfide materials from the mill stockpiles exhibited a different regression equation than that developed for oxidized rock materials, and these were modeled based on the equations developed for the refractory carbonaceous stockpile at Cortez-Pipeline Mine (Eckley et al., 2011a). Mercury fluxes were adjusted upwards by a factor of 4 if the soil moisture was at or greater than 5% and up by a factor of 7 if disturbed. A separate empirical equation developed by Eckley et al. (2011a) was used to estimate Hg flux from active wet heap leach material (Hg flux (ng m^{-2} day^{-1}) = 1221(% moisture) + 1.2(substrate Hg, ng g^{-1}) + 49.9(leach solution Hg, μg L^{-1}) + 56.6(solar radiation, W m^{-2}) – 18,292 [$R^2 = 77$, $p = 0.003$, $n = 14$]). Percent moisture was assumed to average 50%, between 100% liquid solution in the leach pad furrows and low moisture at the ridges. Leach solution concentration was the mean annual value provided by Gold Quarry Mine staff (114.5 μ g L^{-1}, 2010). The mean solar radiation value was applied for each category (70, 190, and 252 W m^{-2}).

Hg flux estimates for moist and liquid tailings are based on limited in situ field data collected by Eckley et al. (2011b). Hg flux from the 100% liquid pond on the tailings was scaled by Hg concentration from an in situ measurement made on the liquid decant pond at Twin Creeks Mine during fall 2008 (Eckley et al., 2011b). At Gold Quarry Mine a single 24-hr flux measurement made on moist fresh tailings in late spring was used to scale up to an annual emission estimate, using an average area of moist tailings indicated by mine staff. At Goldstrike Mine we were limited to measurements on dry tailings that were in closure.

The Hg concentration and meteorological data were used to calculate a total Hg flux (ng m^{-2}) from each material for the number of days in each category (i.e., 89 out of 365 days at Gold Quarry conditions were low solar and wet, and within that period waste rock would emit 208,000 ng m^{-2}). Flux data was scaled to a total annual emission estimate using the 3-D area data from each mine.

Field measurements

In situ Hg flux was measured at each mine in June 2011 (Table 1). At least one full 24-hr measurement was completed at each site, and whenever possible a second full 24-hr measurement was made simultaneously, using the Tekran method described earlier. The number and length of measurements were constrained by the amount of equipment and time available

Table 1. List of field materials, number of samples and flux measurements collected

Mine	Material	Number of substrate samples	Number of flux samples	Description	% LOI
Goldstrike	Waste Rock Reclaimed	6	2	Carlin Formation overburden	–
	Leach Reclaimed	4	–	Carlin Formation overburden	–
	Waste Rock	10	2	Fresh pit waste rock, carbonaceous	2.4
	Tailings	10	2	Old oxide mill tailings, partially capped	1.5
	Stockpile	Mine data	2	Carbonaceous high-grade ore	4.5
	Open pit	Mine data	–	Popovich Formation, bootstrap limestone	–
Gold Quarry	Leach	25	2	Low grade oxide ore	2.5
	Waste rock	20	2	Carlin Formation waste overburden	3.4
	Tailings	10	1	Mill 5/6 process tailings	2.5
	Stockpile	Mine data	2	Carbonaceous high-grade ore	7.4
	Open pit	Mine data	–	Rodeo Creek Unit, Popovich Formation	–

Note: LOI = mass loss on ignition.

for field work. The analytical equipment was housed either in a trailer or in a weatherproof deck box, with sample lines exiting through ports. Electrical power was supplied by gasoline generators placed as far from the flux chamber as allowed by a 15-m extension cord. Substrate samples were collected for total Hg analysis and soil moisture content from below the flux chamber immediately after each flux measurement, using the methods described earlier.

Statistics

The correlation of Hg flux between trays and with environmental parameters was assessed using the Pearson product-moment correlation. Differences between Hg fluxes were assessed by comparing the mean Hg flux from full 24-hr data sets (~68 individual flux values per each 24-hr measurement) using the nonparametric Kruskall–Wallace test and analysis of variance (ANOVA). The 95% prediction intervals were generated using SigmaPlot. Statistical analysis was performed in Microsoft Excel, Minitab, and SigmaPlot.

Results

Experimental manipulations

The effects of the initial disturbance in preparing the trays were apparent for at least 7 days, and decreased steadily over this time. Peak fluxes decreased by a factor of 17 for TC Tails, and by 6.5 for CP Leach between day 1 and day 12 after preparation. GS cap material did not show a measureable decrease in flux. By day 12, daily fluxes had unequivocally stabilized to a consistent diel or 24-hr pattern, after which point the experimental measurements were begun.

Initial baseline measurements were completed immediately after the stabilization period (examples shown in Figure 3). These measurements revealed slightly lower Hg flux values consistently from the A trays, compared to simultaneous measurements from the B and C trays. This bias is likely explained by the random occurrence of slightly lower mean Hg concentrations in most of the A trays (Table 2). Over the course of the laboratory experiments, concurrently measured Hg flux values from the A and B control materials were strongly correlated (Pearson's correlation, $r = 0.90$ dry, $n = 20$; $r = 0.96$ wet, $n = 14$; $P < 0.05$), indicating that statistically the materials and the analytical instruments behaved very comparably, despite the low A tray bias. There were no significant correlations between mean 24-hr values of measured environmental parameters and corresponding 24-hr Hg fluxes (Pearson's correlation, $\alpha = 0.05$), as expected since solar radiation is a major factor controlling flux and Briggs et al. (2012) demonstrated that the impact of light on Hg flux was strongly reduced in a greenhouse setting.

Capping and watering. Hg flux from mining materials was significantly reduced by the addition of the low Hg capping substrate, as 21 out of 28 measurements showed a statistically lower flux from the capped material (ANOVA, Table 2). The reduction was more consistently demonstrated under wet conditions (12 of 14 measurements) compared to dry conditions (9 of 14), and was most apparent for the tailings material.

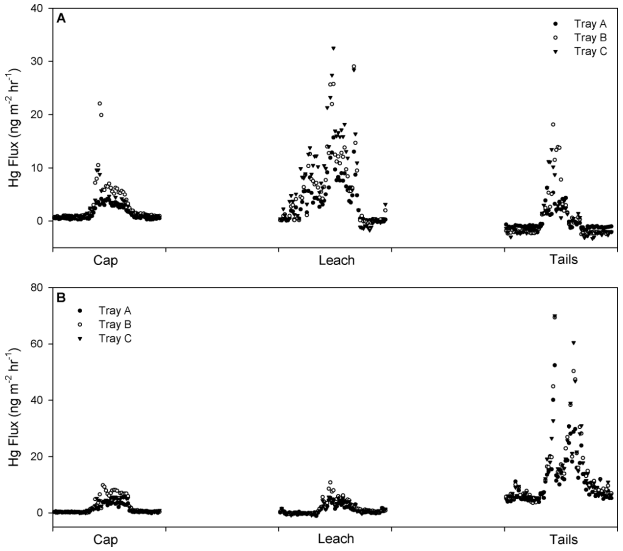

Figure 3. Example of triplicate 24-hr baseline measurements from cap, leach, and tailings material: (A) Twin Creeks Mine; (B) Cortez Pipeline Mine. Marks on *x*-axis indicate 00:00 hr; note difference in scales.

Table 2. Summary of laboratory flux measurements for capped versus uncapped mine material under wet and dry conditions. Initial condition indicates replicate measurements of flux before any manipulation of the trays. Change in flux from the capped C Tray versus uncapped A and B trays is shown as relative percent difference

			Ambient conditions				Hg concentration and flux			
Material (% LOI)	Condition	Date	Solar ($W\ m^{-2}$)	Air temperature (°C ± stdv)	Relative humidity (% ± stdv)	Soil temperature (°C ± stdv)	A	B (Tray Hg ng g^{-1} ± stdv) (Flux ng $m^{-2}\ day^{-1}$)	C	Percent decrease in flux when capped
TC cap (3.1%)	Initial	11/30/2010	19.7	16.8 ± 3.4	31.7 ± 13.2	15.5 ± 3.1		378 ± 48		
							19†	51†	32†	*na*
LT cap (2.7%)	Initial	12/1/2010	22.5	14.7 ± 3.7	31.4 ± 10.9	15.3 ± 4.0		234 ± 109		
							−3	0	−13†	*na*
CP cap (4.1%)	Initial	12/6/2010	26.4	15.0 ± 3.7	33.9 ± 10.7	15.5 ± 3.8		116 ± 59		
							27†	56†	43†	*na*
GS cap (3.9%)	Initial	12/2/2010	23.7	15.5 ± 3.1	40.6 ± 12.2	16.4 ± 3.5		205 ± 118		
							9†	29	35	*na*
TC leach (4.5%)							11,782 ± 273	11,996 ± 1188	14,637 ± 2726	
	Initial	12/8/2010	30.3	15.2 ± 3.9	32.6 ± 6.8	15.6 ± 3.8	88†	160	213	no cap
	Dry 1	1/4/2011	31.3	12.5 ± 4.1	26.4 ± 5.9	13.7 ± 4.1	36	59	52	nsd
	Wet 1	2/12/2011	40.9	15.5 ± 3.5	17.4 ± 5.4	13.6 ± 3.3	1198†	2149†	847†	49
	Dry 2	11/6/2011	32.5	16.0 ± 3.5	31.7 ± 7.9	16.6 ± 4.3	249	248	**52**†	79
	Wet 2	12/15/2011	22.9	15.7 ± 3.4	26.4 ± 5.0	12.9 ± 2.9	8421	9204	**1154**†	87
LT leach (2.7%)							826 ± 143	981 ± 54	1151 ± 547	
	Initial	12/9/2010	14.0	15.7 ± 2.6	42.9 ± 8.0	16.3 ± 3.0	14†	37	26	no cap
	Dry 1	1/5/2011	23.6	12.5 ± 3.7	31.1 ± 7.1	14.2 ± 4.0	−2	−4	**–17**†	462
	Wet 1	2/23/2011	46.6	14.8 ± 3.7	23.0 ± 5.5	13.2 ± 3.9	540†	1074†	**273**†	66
	Dry 2	11/7/2011	32.9	14.4 ± 3.5	26.3 ± 5.1	15.1 ± 3.5	−15	−2	−29	nsd
	Wet 2	12/19/2011	29.5	15.7 ± 4.3	21.3 ± 5.3	12.6 ± 3.5	1922†	653†	**267**†	79
CP leach (2.2%)							436 ± 80	562 ± 1	486 ± 37	
	Initial	12/10/2010	29.8	16.1 ± 3.2	40.9 ± 8.8	17.0 ± 3.8	33†	57	52	no cap
	Dry 1	1/6/2011	18.9	12.0 ± 3.4	32.1 ± 5.6	13.6 ± 3.5	−6	−8	16†	−335
	Wet 1	1/23/2011	35.7	15.2 ± 3.9	29.0 ± 7.1	13.4 ± 3.7	5112†	6268	6168	−8
	Dry 2	11/8/2011	32.1	15.2 ± 3.4	26.5 ± 6.2	16.1 ± 3.9	10	16	6	nsd
	Wet 2	12/13/2011	30.7	15.5 ± 4.2	22.3 ± 5.2	12.4 ± 3.4	5985	6032	10849†	−81
TC Tails (2.8%)							27,786 ± 8363	39,914 ± 1251	37,363 ± 1299	
	Initial	12/14/2010	20.5	14.4 ± 3.4	36.6 ± 11.6	14.7 ± 3.1	−2	7	1	no cap
	Dry 1	1/7/2011	26.1	12.7 ± 3.7	31.1 ± 6.6	14.1 ± 4.1	−8	−19	26†	−290
	Wet 1	3/4/2011	40.9	15.3 ± 2.7	22.0 ± 5.3	14.2 ± 3.6	34,539†	69,014†	1095†	98
	Dry 2	11/10/2011	20.8	15.6 ± 2.7	26.0 ± 5.7	16.0 ± 3.5	260	264	**21**†	92
	Wet 2	12/29/2011	25.1	17.5 ± 3.9	32.1 ± 13.3	14.4 ± 3.6	33,020†	41,298†	**6314**†	83

(*Continued*)

Table 2. (Cont.)

Material (% LOI)	Condition	Date	Ambient conditions: Solar ($W\ m^{-2}$)	Air temperature (°C ± stdv)	Relative humidity (% ± stdv)	Soil temperature (°C ± stdv)	Hg concentration and flux: A	B (Tray Hg ng g^{-1} ± stdv) (Flux ng m^{-2} day^{-1})	C	Percent decrease in flux when capped
LT tails (3.4%)							9494 ± 1486	9682 ± 362	7687 ± 512	
	Initial	12/17/2010	13.0	13.0 ± 2.1	44.2 ± 6.8	13.8 ± 2.6	53	96	97	no cap
	Dry 1	1/8/2011	21.7	13.4 ± 3.8	27.4 ± 5.4	14.5 ± 4.0	51†	96†	**–10**†	113
	Wet 1	1/17/2011	25.1	15.6 ± 3.6	29.2 ± 9.0	13.6 ± 3.2	6958†	9659†	**3643**†	56
	Dry 2	11/20/2011	19.5	16.5 ± 3.5	35.4 ± 8.0	15.6 ± 3.5	123	132	**1**†	99
	Wet 2	1/13/2012	36.9	16.5 ± 4.6	17.3 ± 4.5	13.1 ± 4.1	62,390†	90,439†	**11,847**†	84
CP tails (1.8%)							31,166 ± 17,555	64,023 ± 44,384	25,004 ± 7993	
	Initial	12/19/2010	8.5	11.9 ± 2.0	44.0 ± 6.8	12.2 ± 2.0	260	330	324	no cap
	Dry 1	1/9/2011	27.3	11.9 ± 3.8	23.1 ± 4.1	13.5 ± 4.1	241	323	**26**†	91
	Wet 1	3/16/2011	53.2	16.1 ± 3.4	26.2 ± 6.1	14.3 ± 4.0	4242	4426	**1105**†	75
	Dry 2	11/15/2011	36.3	16.6 ± 2.9	30.4 ± 6.6	16.4 ± 3.2	721†	408†	**0**†	100
	Wet 2	1/11/2012	29.1	16.6 ± 4.5	19.9 ± 5.0	12.8 ± 3.8	27,052†	20,911†	**6092**†	75
GS tails (1.8%)							7931 ± 1744	7121 ± 389	10,873 ± 6301	
	Initial	12/20/2010	21.7	12.9 ± 3.3	36.5 ± 6.2	13.9 ± 3.6	87	171	136	no cap
	Dry 1	1/11/2011	na	na	na	na	27	54	**–29**†	172
	Wet 1	3/24/2011	27.9	14.9 ± 3.1	38.2 ± 6.3	13.0 ± 3.3	29963†	51748†	**317**†	99
	Dry 2	11/18/2011	29.7	16.5 ± 2.5	30.9 ± 8.8	15.8 ± 2.6	345†	259†	**2**†	99
	Wet 2	1/19/2012	14.7	16.1 ± 2.8	30.3 ± 9.0	13.2 ± 2.4	6655†	5970†	**612**†	90

Notes: Initial condition indicates replicate measurements of flux before any manipulation of the trays. Change in flux from the capped C Tray versus uncapped A and B trays is shown as relative percent difference; † indicates statistically significant difference between mean 24-hr flux values (ANOVA $\alpha = 0.05$); boldface indicates decreased flux from C tray; nsd = no significant difference; LOI = mass loss on ignition.

Watering to 15% volumetric soil moisture (VSM) resulted in a higher Hg flux from all materials; however, the following discussion is restricted to the first set of wetting measurements for which a full 6 days of data are available. Evaporation rates after watering followed an asymptotic curve with an initially sharp decline in VSM over the first 24 hr (mean VSM decrease of 5.4 ± 3.1 %, $n = 21$) followed by a relatively constant drop of approximately 2% VSM over each subsequent 24-hr period. Most materials fell below the 5% VSM mark after approximately 72 hr, or during day 4 of the measurements, except TC and LT tailings, which were watered to 20% VSM and did not fall below 5% VSM over the period of flux measurement. For the materials that did show a decrease in VSM from 15 to less than 5%, the 24-hr Hg flux from the first day after watering was on average 3.3 ± 1.7 ($n = 8$) times higher than the 24-hr flux on day four after watering, though the GS tails material showed a much higher (22×) multiplication of Hg flux. Excluding GS tails, the observed increase in flux with moisture agrees well with previous work, indicating a mean factor of 4 increase in Hg flux upon wetting (Eckley et al., 2011a). The Hg concentration in the greenhouse tapwater used to wet the materials was consistently low (1.2 ± 0.7 ng L^{-1}, $n = 65$) over the course of the watering experiments, verifying that the increased flux (hundreds to thousands of nanograms greater; Table 2) was not due to any addition of Hg.

Initial baseline flux measurements of the tailings showed no statistical difference between the three replicate trays, but after capping, flux was significantly lower from the capped versus uncapped tailings, for both wet and dry conditions (TC tails dry 1 was the only exception out of 16 measurements). Under dry conditions, capping reduced Hg flux from tailings between 91 and 100%, and in several cases (GS and LT tails dry 1) the capping substrate changed the surface from a net Hg emitter to a depositional surface. Under wet conditions, Hg fluxes from capped tailings were between 56 and 99% less than the fluxes measured from uncapped equivalents. Total percent loss on ignition (LOI) was higher in three cap materials compared to the tailings substrates (LT tails had a higher LOI content than the LT cap due to vegetation growing on the closed tailings surface at the mine), a factor that likely contributed to the suppression of Hg flux (Table 2).

The impact of capping on Hg flux was more variable for the heap leach materials. For the CP leach material, capping resulted in either no measurable change or an increase in Hg flux, regardless of whether the material was wet or dry. This may be due to the fact that the CP leach had a low total Hg concentration (mean 490 ng g^{-1}), which was not much greater than the concentration of Hg in the capping material (mean 220 ng g^{-1}). The similarity in magnitude of Hg flux from the CP cap and leach materials can clearly be seen in the baseline flux measurements (Figure 3B). The reduction in Hg flux from leach material was more apparent for the higher Hg concentration TC and LT materials, with both showing a significantly smaller flux from capped material under wet conditions (49 to 89% reduction in 4 of 4 measurements) (Table 2). Under dry conditions, capped LT leach showed a strong negative flux (deposition) compared to the uncapped material, and flux from the capped TC leach was either not significantly different (dry 1) or up to 79% lower than uncapped material (dry 2).

Dust control application. The dust control solutions were applied only to leach material, as this was most representative of their actual use at the mine sites. Application of $MgCl_2$ (220 ± 23 ng L^{-1}, $n = 3$) solution resulted in a similar or higher Hg flux from the treated materials while still wet, compared to the leach materials in the A and B trays receiving only water. At day 60 and day 205 after application, when the substrates were completely dry, flux from the $MgCl_2$ treated materials was uniformly higher compared to the untreated materials (Table 3). The Dustreat (326 ± 122 ng L^{-1}, $n = 4$) resulted in an initially lower flux from the treated material while wet, but a significantly higher Hg flux at day 60 and day 205 (Table 3).

Dithiocarbamate application. Application of the dithiocarbamate solution (439 ± 111 ng L^{-1}, $n = 4$) resulted in lower Hg fluxes from the treated materials, especially after materials had dried completely (Figure 4). The initial application of the solution to the CP Leach resulted in a much smaller Hg flux over the first 24 hr, compared to the CP leach materials that received an equivalent volume of water (560 ng m^{-2} day^{-1} versus 3,200 ng m^{-2} day^{-1}). At day 200 after application, flux from the treated CP leach was strongly negative compared to untreated material (–36 ng m^{-2} day^{-1} versus –4 to –9 ng m^{-2} day^{-1}). When the solution was applied to the GS tailings, there was a strong initial spike in Hg flux compared to the two trays that received only water (Figure 4B). The treated material also showed a much higher noonday flux during both the first and second 24-hr periods after application, although flux from the untreated materials was generally higher at night. As a result, total daily flux from the treated GS tailings in the first 24 hr after application was in the range of that measured from the untreated materials (43,500 ng m^{-2} day^{-1} versus 21,000 and 68,000 ng m^{-2} day^{-1}). However, at day 200, flux from the treated GS tails indicated deposition compared to positive emission from the untreated material (–46 versus 23 to 33 ng m^{-2} day^{-1}). The reduction in Hg flux is hypothesized to result from the formation and precipitation from the dithiocarbamate solution of Hg sulfide salts, which are generally less susceptible to volatilization.

Depth. The effect of material depth was variable. Hg flux from the 10-cm-deep tray of CP leach showed lower flux under wet conditions compared to the 5-cm-deep tray (11 vs. 26 ng m^{-2} day^{-1} ANOVA, $\alpha = 0.05$) and was not significantly different under dry conditions (2.5 vs. 1.5 ng m^{-2} day^{-1}). However, the 10-cm-deep tray of GS tails showed significantly higher flux under all conditions (88 vs. 33 ng m^{-2} day^{-1} dry; 2,600 vs. 720 ng m^{-2} day^{-1} wet). Total Hg concentrations from the 5- and 10-cm trays were not significantly different.

Aging. The effect of material aging was uncertain. Of the unaltered A and B control materials, all except LT leach (no change) showed a significant increase (ANOVA, $\alpha = 0.05$) in Hg flux between the dry 1and the dry 2 measurements 10 months later (Table 2). This effect was less apparent when the materials were wet, with only three out of seven cases showing a higher flux compared to the earlier measurement. In contrast, there was not a consistent pattern in flux from the capped trays under dry

Table 3. Summary of laboratory flux measurements, dust-control treated and untreated mine materials

			Ambient conditions				Hg flux			
Material	Days after application	Date	Solar ($W \cdot m^{-2}$)	Air temperature (°C ± stdv)	Relative humidity (% ± stdv)	Soil temperature (°C ± stdv)	A	B (Tray Hg $ng \cdot g^{-1}$ ± stdv) (Flux $ng \cdot m^{-2} \cdot day^{-1}$)	D treated	Percent increase in flux after treatment
CP leach DC							436 ± 80	562 ± 1	421 ± 22	
	1	5/17/2011	71.1	16.3 ± 2.8	34.2 ± 8.9	17.4 ± 5.6	4887†	5841†	1570†	−71
	60	7/6/2011	98.6	22.6 ± 2.8	55.3 ± 14.4	29.2 ± 7.8	43†	85†	127†	98
	205	12/1/2011	29.2	16.3 ± 3.8	18.0 ± 4.4	15.6 ± 4.0	−14†	−11†	5†	140
LT leach DC							826 ± 143	981 ± 54	1068 ± 150	
	1	5/11/2011	109.0	18.1 ± 3.5	33.0 ± 13.1	22.2 ± 9.1	549	716	1475†	133
	60	7/7/2011	116.1	19.8 ± 2.9	48.0 ± 18.6	27.3 ± 9.0	77	68	3086†	4157
	205	11/30/2011	27.8	15.8 ± 3.0	27.1 ± 8.1	15.7 ± 3.4	−11	−6	306†	3700
TC leach DC							11,782 ± 273	11,996 ± 1188	14,310 ± 1798	
	1	5/6/2011	81.4	19.5 ± 3.1	28.9 ± 12.0	22.1 ± 8.1	14,487†	40,821†	27,997†	1.2
	60	7/8/2011	87.4	19.8 ± 2.7	49.1 ± 16.2	23.8 ± 6.0	1681†	3161†	25,005†	933
	205	11/29/2011	27.8	15.8 ± 2.9	26.7 ± 8.1	15.8 ± 3.4	149	170	6062†	3701

Notes: The † indicates statistically significant difference between mean 24-hr flux values (ANOVA $\alpha = 0.05$); treated indicates material that received dust control solution; A and B trays were not treated.

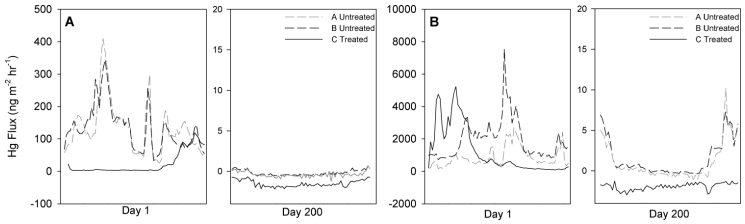

Figure 4. Comparison of Hg flux from untreated materials (dashed lines) and materials treated with Hg control reagent on day 1 after application and day 200 after application: (A) CP leach and (B) GS tails. Note difference in scales between day 1 and day 200.

conditions, with some showing a smaller flux and some a higher flux after an elapse of 10 months (Table 2). However, in six out of seven cases (LT leach was again the exception) flux was significantly higher from the cap material under wet conditions compared to the earlier measurement. There was no change in substrate Hg concentration over time, in either the mine materials or the overlying cap material.

The increase in flux with time from the unaltered materials when dry is believed to be an apparent effect due to the generally colder, darker, drier conditions of the first series of measurements in January 2011 compared to the second set of measurements in November 2011. The increase in Hg flux from capped materials under the wet condition is most likely due to a decrease in effective capping thickness with compaction over time and after repeated wetting. This would bring the underlying mining materials closer to the surface, and when wetted, Hg displaced from the substrate pore spaces would be more readily evaded upward to the atmosphere.

Model testing and emission scaling, now and future

It is important to note that field measurements were restricted to one or two 24-hr measurements from each material during one period in late May to early June 2011. Comparison of these limited in situ flux measurements to fluxes calculated using the predictive regression equations shows a varying degree of predictive fit (Figure 5). In general, the equations calculated flux within the 95% prediction interval for low Hg concentration substrate such as waste rock, but were more variable for substrates that have higher Hg concentrations and/or experience a greater range of conditions, such as heap leach and tailings which may range from fresh to aged and completely liquid to completely dry. The refractory ore stockpile equations predicted stockpile Hg fluxes well at both mines, and the overall lower Hg fluxes observed from these stockpile ore materials agree with their higher LOI content (Table 1).

At Goldstrike Mine, 5 of 6 actual Hg fluxes fell within the 95% prediction interval of the regression equations (Figure 5A). This included fluxes measured from a reclaimed area, waste rock, and from tailings (no heap leach facilities being present at Goldstrike). One of the measured tailings fluxes exceeded the prediction interval. From the stockpile, both of 2 actual fluxes fell within the 95% prediction interval.

At Gold Quarry Mine, 2 of 5 actual fluxes fell within the 95% prediction interval, and these were both measured from low Hg waste rock (Figure 5B). The two actual stockpile fluxes were within the 95% prediction interval. Actual Hg fluxes from heap leach and tailings were higher than predicted. If the disturbance multiplier is applied to the equation, then both actual heap leach fluxes fall on the 95% prediction interval, which may indicate that the location from which these fluxes were measured had undergone some recent unknown physical disturbance.

Since these measurements were made near peak annual solar radiation, and since the equations were developed from an average annual data set, the relatively high solar radiation might account for some of the higher-than-predicted Hg fluxes. Using the regression equations and the appropriate area scaling data from each mine, total annual emission estimates for calendar year 2010 were made for Gold Quarry (81 to 84 kg yr^{-1}) and Goldstrike (14 to 17 kg yr^{-1}). Table 4 shows the upper range of flux estimates from each material and the percent of total Hg emission represented by each major surface. It is estimated that if the active areas at each mine were capped with the lowest Hg concentration waste rock available (excluding the open pit), total

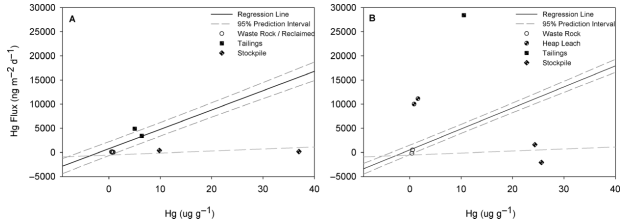

Figure 5. Prediction intervals and actual in situ daily fluxes: (A) Goldstrike Mine; (B) Gold Quarry Mine.

Table 4. Summary of total annual Hg emissions from major surfaces, estimated emissions if materials were capped, and percent reduction in emissions after capping

	Gold Quarry Mine				Goldstrike Mine			
Surface	Flux ($g\ yr^{-1}$)	Percent of total emission	Capped	Percent reduction	Flux ($g \cdot yr^{-1}$)	Percent of total emission	Capped	% Reduction
Waste rock	5261	6	2675	49	960	6	463	52
Reclaimed	–	–	–		4711	28	4711	–
leach	10,023	12	2395	76	–	–	–	–
Tailings	65,775	78	1115	98	8291	49	885	89
Stockpile	−3	0	146	(increase)	8	0	249	(increase)
Pit	2948	4	2948*	–	2954	17	2954*	–
Total	84,004	100	9280	89	16,924	100	9260	45

Notes: *Open pit is not typically capped or reclaimed; capped emission estimates assume lowest Hg material available used for capping.

emissions would drop to 7–9 kg yr^{-1} at Gold Quarry, and 6–9 kg yr^{-1} at Goldstrike. This represents approximately a 90% reduction in non-point-source Hg emissions from the Gold Quarry mine once capping and reclamation are completed on the active mining surfaces. Large areas of the Goldstrike Mine have already been capped and reclaimed, which partly explains the relatively low annual nonpoint emissions (together with the lack of active heap leach facilities). However, complete reclamation of the Goldstrike surfaces could result in a further 47–57% reduction in nonpoint emissions.

Conclusion

Mine operators are required to conduct reclamation activities concurrently with mining when practicable, and immediately upon completion or cessation of mining operations in any area not subject to further disturbance. Restoration of approximate original contour and/or a surface stability and appearance comparable to surrounding areas is the primary goal, and this is usually accomplished in part by capping abandoned mine materials with variable depths of soil substrate followed be revegetating. In addition to restoring the surface condition, capping has the additional benefit of significantly reducing Hg flux from the underlying waste material. In this study, Hg fluxes from mine materials were consistently reduced by 50 to 100% with the addition of 2 cm of capping substrate over 5 cm of soil. This was true especially of high-Hg tailings waste, which is often the largest Hg-emitting surface at any mine. An important caveat to note is that all measurements made in this study were conducted in an enclosed greenhouse on a relatively limited selection of mine materials at a smaller scale, so the numbers presented here may not be directly representative of conditions and results that would occur with capping on actual mine surfaces.

Dust-control solutions are used at mine sites primarily to reduce dust emissions from roads, and on a relatively small area of waste rock, heap leach, and stockpile ore where vehicular traffic is heavy. In this study, the application of typical dust-control solutions to heap leach material exacerbated the release of Hg, both while wet and after drying. This is most likely a result of the high concentration of Hg in solution. Thus, application of these solutions over large areas many not constitute a best management practice. Practically, the areas of traffic where dust-control solutions are applied are small, and any increase in Hg flux resulting from their use is likely negligible compared to total mine emissions.

In cyanide leach systems, the dithiocarbamate Hg control reagent causes Hg to precipitate out of solution as an organic sulfide salt (Wickens, 2000). It was hypothesized that if applied to a material directly, the control reagent would result in the removal of Hg from the material surface and hence in a reduction of Hg flux. The results of this study indicate that Hg flux was indeed reduced after the application of the solution to a leach ore and to tailings, especially as the materials dried, despite the fact that the solution had a higher total Hg concentration than the dust control solutions. Whether this is true when applied in a dilute cyanide solution to active heap leach at a mine is unknown, and additional testing of a larger variety of materials and application methods is needed.

The evaluation of the emission-scaling procedure devised by Eckley et al. (2011a) was not entirely conclusive. When used for predicting daily Hg flux for specific materials on individual days, the model worked very well at the Goldstrike Mine. However, at the Gold Quarry Mine, the modeled values were significantly lower than the actual measurements for heap leach and tailings. Due to the limited number of samples, it is impossible to say whether these values were an anomaly resulting from some unknown environmental factor or disturbance, or whether the model is systematically low for the Gold Quarry materials. A larger number of flux measurements from several seasons is needed for a more definitive assessment.

Acknowledgment

This project was funded by the Nevada Department of Environmental Protection and the Nevada Mining Association. The authors thank personnel from Newmont and Barrick mining companies for providing mining materials and help with field work.

References

Briggs, C.W., R. Fine, M. Markee, and M. Gustin. 2012. Investigation of the potential for mercury release from flue gas desulfurization solids applied as an agricultural amendment. *J. Environ. Qual.* doi:10.2134/jeq2012.0049

Driesner, D., and A. Coyner. 2011. *Major Mines of Nevada 2010*. Nevada Bureau of Mines and Geology Special Publication P-22. http://www.nbmg.unr.edu/dox/mm/mm10.pdf

Eckley, C.S., M. Gustin, M.B. Miller, and F. Marsik. 2011a. Scaling non-point-source mercury emissions from two active industrial gold mines: Influential variables and annual emission estimates. *Environ. Sci. Technol.* 45:392–99. doi:10.1021/es101820q

Eckley, C.S., M. Gustin, F. Marsik, and M.B. Miller. 2011b. Measurement of surface mercury fluxes at active industrial gold mines in Nevada (USA). *Sci. Total Environ.* 409:514–22. doi:10.1016/j.scitotenv.2010.10.024

Eckley, C.S., M. Gustin, C.-J. Lin, X. Li, and M.B. Miller. 2010. The influence of dynamic chamber design and operating parameters on calculated surface-to-air mercury fluxes. *Atmos. Environ.* 44:194–203. doi:10.1016/j.atmosenv.2009.10.013

Fitzgerald, W.F., D.R. Engstrom, R. Mason, and E. Nater. 1998. The case for atmospheric mercury contamination in remote areas. *Environ. Sci. Technol.* 32:1–7. doi:10.1021/es970284w

Gustin, M.S., S. Lindberg, and P. Weisberg. 2008. An update on the natural sources and sinks of atmospheric mercury. *Appl. Geochem.* 23:482–93. doi:10.1016/j.apgeochem.2007.12.010

Heinen, H.J., D.G. Peterson, and R.E. Lindstrom. 1978. *Processing Gold Ores Using Heap Leach-Carbon Adsorption Methods*. U.S. Bureau of Mines Information Circular 8770. http://mines.a2.gov/DigitalLibrary/usbm_ic/USBMIC8770ProcessingGoldOresUsingHeapLeach-CarbonAdsorptionMethods.pdf

Heiri, O., A.F. Lotter, and G. Lemcke. 2011. Loss on ignition as a method for estimating organic and carbonate content in sediments: Reproducibility and comparability of results. *J. Paleolimnol.* 25:101–10. doi:10.1023/A:1008119611481

Hess, T.M. 1997. DAILYET: A computer programme for calculating the daily reference evapotranspiration (ET_o). Cranfield University, Silsoe College, UK (unpublished).

Nevada Division of Environmental Protection. 2011. *Calendar Year 2010 Actual Production/Emission Reporting Form Addendum for Mercury Emissions*. Carson City, NV: Nevada Division of Environment Protection. http://ndep.nv.gov/bapc/hg/docs/2010_AER.pdf (accessed April 2012).

Pirrone, N., S. Cinnirella, X. Feng, R.B. Finkelman, H.R. Friedli, and J. Leaner. 2009. Global mercury emissions to the atmosphere from natural and anthropogenic source. In: Pirrone, N., Mason, R., eds. *Mercury Fate and Transport in the Global Atmosphere: Measurements, Models and Policy Implications*, 3–49. New York, NY: Springer Science+Business Media.

Rytuba, J.J. 2005. Geogenic and mining sources of mercury to the environment. In: Parson, M., Percival, J., eds. *Mercury: Sources, Measurements, Cycles, and Effects*, vol. 34, 21–41. Mineralogical Association of Canada Short Course Series. http://www.mineralogicalassociation.ca/index.php?p=259page=sc34.php

Schroeder, W.H., and J. Munthe. 1998. Atmospheric mercury—An overview. *Atmos. Environ.* 32:809–22. doi:10.1016/S1352-2310(97)00293-8

Seigneur C., K. Vijayarahavan, and K. Lohman. 2006. Atmospheric mercury chemistry: Sensitivity of global model simulations to chemical reactions. *J. Geophys. Res.* 111:1–17. doi:10.1029/2005JD006780

Wickens, J. 2000. Reducing mercury production at Bald Mountain mine. *Workshop on Assessing and Managing Mercury from Historic and Current Mining Activity: U.S. EPA Proceedings and Summary Report*, 137–44.

Zehner, R.E., and M.S. Gustin. 2002. Estimation of mercury vapor flux from natural substrate in Nevada. *Environ. Sci. Technol.* 38:4039–45. doi:10.1021/es015723c

About the Authors

Matthieu B. Miller is a research scientist and **Mae S. Gustin** is a research professor at the University of Nevada, Reno.

CHAPTER 4:

Evaluation of cation exchange membrane performance under exposure to high Hg^0 and $HgBr_2$ concentrations

Matthieu B. Miller[1], Mae S. Gustin[2], Sarrah M. Dunham-Cheatham[2], Grant C. Edwards[1]

[1]Department of Environmental Sciences, Faculty of Science and Engineering, Macquarie University, Sydney NSW, 2113, Australia

[2]Department of Natural Resources and Environmental Sciences, University of Nevada, Reno NV, 89557, United States

Statement of Authorship

This paper originated from a need to conclusively demonstrate that the CEM material does not suffer from a significant GEM measurement artifact, as a GEM artifact of any significant magnitude would render the methodology inadequate for atmospheric RM quantification. The permeation system described in this paper was designed and assembled by me, from commercial and custom-made components, in consultation with Dr. Edwards and Dr. Gustin as well as other experts in the field. The majority of data collection, data analysis, and manuscript preparation were completed by me, with intellectual contribution from co-authors. Dr. Dunham-Cheatham assumed responsibility for the system upon my departure from the University of Nevada-Reno and assisted with final data collection.

Study Design: 90% • Data Collection: 90% • Data Analysis: 95% • Writing: 95%

ABSTRACT

Reactive mercury (RM) is an important component of the global atmospheric mercury cycle, but measurement currently depends on un-calibrated, operationally defined methods with large uncertainty and demonstrated interferences and artifacts. Cation exchange membranes (CEM) provide a promising alternative methodology for quantification of RM, but method validation and improvement are ongoing. For the CEM material to be reliable, uptake of gaseous elemental mercury (GEM) must be negligible for all conditions, and RM compounds must be captured and retained with high efficiency. In this study the performance of CEM material under exposure to high concentrations of GEM (1.43×10^6 to 1.85×10^6 pg m^{-3}) and reactive gaseous mercury bromide ($HgBr_2$ ~ 5000 pg m^{-3}) was explored, using a custom-built mercury vapor permeation system, with quantification of total permeated Hg accomplished via pyrolysis at 600 °C and detection using a Tekran® 2537A. Permeation tests were conducted for 24 to 72 hours in clean laboratory air, with absolute humidity levels ranging from 0.1-10 g m^{-3} water vapor. Gaseous elemental mercury uptake by the CEM material averaged no more than 0.004% of total exposure for all test conditions, which equates to a non-detectable GEM artifact for typical ambient air sample concentrations. Recovery of $HgBr_2$ on CEM filters was >100 % compared to calculated total permeated $HgBr_2$, suggesting incomplete thermal decomposition at the pyrolyzer, as the CEM material collected $HgBr_2$ with less than 1% downstream breakthrough on average, implying a high collection efficiency.

4.1 Introduction

Mercury (Hg) is a persistent environmental contaminant with a significant atmospheric life time, and the form and chemistry of Hg is an important determinant of its biogeochemical cycling. Mercury in the atmosphere is found in three forms: gaseous elemental mercury (GEM), gaseous oxidized mercury (GOM), and particulate bound mercury (PBM). PBM and GOM are often quantified together as reactive mercury (RM = GOM + PBM)(Gustin et al., 2015; Weiss-Penzias et al., 2015). Atmospheric GEM, at an average global background concentration of 1-2 ng m^{-3}, can be reliably measured with calibrated analytical instruments (Gustin et al., 2015; Slemr et al., 2015). The measurement of GOM and PBM requires detection at the part per trillion (pg m^{-3}) level and depends on un-calibrated operationally defined methods with demonstrated interferences and artifacts, and concomitant large uncertainty. Recent reviews (Gustin et al., 2015; Zhang et al., 2017) detail the shortcomings, difficulties, and needed developments for atmospheric RM measurements.

As an alternative methodology, cation exchange membranes (CEM) have been used to selectively measure GOM concentrations in ambient air (Bloom et al., 1996; Ebinghaus et al., 1999; Huang and Gustin, 2015a; Huang et al., 2017; Huang et al., 2013; Marusczak et al., 2017; Mason et al., 1997; Pierce and Gustin, 2017; Sheu and Mason, 2001). The use of CEM type filters for this purpose was first documented in the literature in a conference presentation (Bloom et al., 1996), although such membranes (then referred to as 'ion exchange membranes') were deployed earlier in a field-based international comparative study of RM measurement techniques in September, 1995 (Ebinghaus et al., 1999). In the comparative study, one participating lab deployed a series of ion exchange membranes (for GOM) behind a quartz fiber filter (for PBM) at a sample flow rate of 9-10 Lpm, for 24 h measurements (filter pore sizes were not reported).

Results for PBM and GOM were in similar ranges of 4.5- 26 pg m^{-3} and 13-23 pg m^{-3} , respectively (Ebinghaus et al., 1999).

The ion exchange membrane method was also applied in a 1995-96 field campaign for determining the speciation of atmospheric Hg in the Chesapeake Bay area (Mason et al., 1997). This study used a 5-stage Teflon filter pack system that included one up front quartz fiber filter (0.8 μm pore size) to remove particulate, and four downstream Gelman ion exchange membranes (pore size not reported) to 1) capture GOM, 2) capture GOM breakthrough, 3) serve as deployment blanks, and 4) isolate the filter train on the downstream side (Mason et al., 1997). Concentrations of GOM were reported to be 5-10 pg m^{-3}, essentially at or below the method detection limit and it was speculated that even this small amount may have been an artifact from fine particulate Hg passing through the 0.8 μm quartz fiber filter (Mason et al., 1997). The 3rd-in-series ion exchange membrane blanks were reported to be not significantly different in Hg concentration from unused membrane material, indicating that breakthrough was not a phenomenon that extended past the second ion exchange filter position.

The particulate Hg artifact problem was subsequently elaborated on in a further comparative study focusing exclusively on RM measurement techniques. Specific concerns included physical particle breakthrough, re-evolution of gas-phase Hg^{2+} from PBM captured on the upstream particulate filters passing downstream to the ion exchange membranes, possible adsorption of GOM compounds to the particulate filters, or a GEM collection artifact on the ion exchange membranes (Sheu and Mason, 2001). None of these concerns were proven or disproven conclusively.

Recent CEM based sampling systems typically deploy a pair of CEM disc filters without a pre-particulate filter, in replicates of 2 to 3 at a flow rate of 1.0 Lpm (Gustin et al., 2016). Each pair

of filters constitutes one sample, the first filter serving as the primary RM collection surface, and the second filter capturing breakthrough. Filters are deployed for 1-to-2 weeks and then collected for analysis (CVAFS, EPA Method 1631, modified) (Huang et al., 2017). The CEM material consists of a negatively charged polyethersulfone coated matrix (Pall Corporation), and at least one manufacturing evolution has occurred (Huang and Gustin, 2015b). Prior CEM material versions (I.C.E. 450) had a pore size of 0.45 μm, while the current CEM material (Mustang® S) has a manufacturer reported pore size of 0.8 μm.

Previous work with the I.C.E 450 material indicated it does not adsorb significant quantities of GEM in passive exposures, but can selectively uptake gas-phase Hg^{2+} species (Lyman et al., 2007). The CEM material was subsequently adapted for use in active sample flow systems, with the presumption of continued inertness to GEM and selectivity for GOM (Huang and Gustin, 2015a; Huang et al., 2013). These studies and others (Lyman et al., 2016) have shown better GOM recovery on CEM material compared to potassium chloride (KCl) coated denuder methods.Despite these tests, the transparency of the CEM material to GEM uptake has not been conclusively demonstrated for active sampling flow rates, nor for high GEM concentrations, though limited data using low concentration manual Hg^0 injections through CEM filters suggests little or no GEM uptake (Lyman et al., 2016). However, even small rates of GEM uptake by the CEM material could result in a significant measurement artifact (e.g. a modest 1-2% GEM uptake could easily overwhelm detection of typical ambient GOM concentrations). It is therefore of critical importance that such a GEM artifact be ruled out if the CEM material is to be successfully deployed for ambient RM measurements, first and foremost under controlled laboratory conditions in the absence of confounding variables.

Additionally, previous studies have observed significant amounts of "breakthrough" GOM on the secondary filter. The amount of breakthrough is not consistent, neither as a constant mass, with total Hg ranging from zero to as high as 400 pg (Huang et al., 2017), nor as a percentage of Hg collected on the primary filter, ranging from 0-40% (Pierce and Gustin, 2017). Similar variable breakthrough issues were observed in the earliest field-based CEM measurements as well (Mason et al., 1997). In contrast to ambient measurements, previous laboratory experiments have reported only minor (0-16%) or no breakthrough (Huang and Gustin, 2015a; Huang et al., 2013). Limited experimental work with flow rates of 1.0 and 16.7 Lpm in ambient air could not provide an explanation for differing breakthrough rates (Pierce and Gustin, 2017).

In this paper we investigate the potential for GEM uptake on CEM material using a custom-built permeation system. In addition, the ability of the CEM material to capture and retain a representative GOM compound (mercury bromide, $HgBr_2$) is discussed with a view to estimate collection efficiency and explain or rule out possible mechanisms of breakthrough for both dry and humid conditions

4.2 Methods

A Tekran® 2537A ambient mercury analyzer was integrated with a custom-built permeation system designed to enable controlled exposures of GEM and GOM to CEM filters (Fig. 4.1). The 2537A analyzer was calibrated at the beginning and periodically throughout the study and checked for accuracy by manual Hg^0 injections (mean recovery 101.1% ± 4.3, n = 10, Appendix

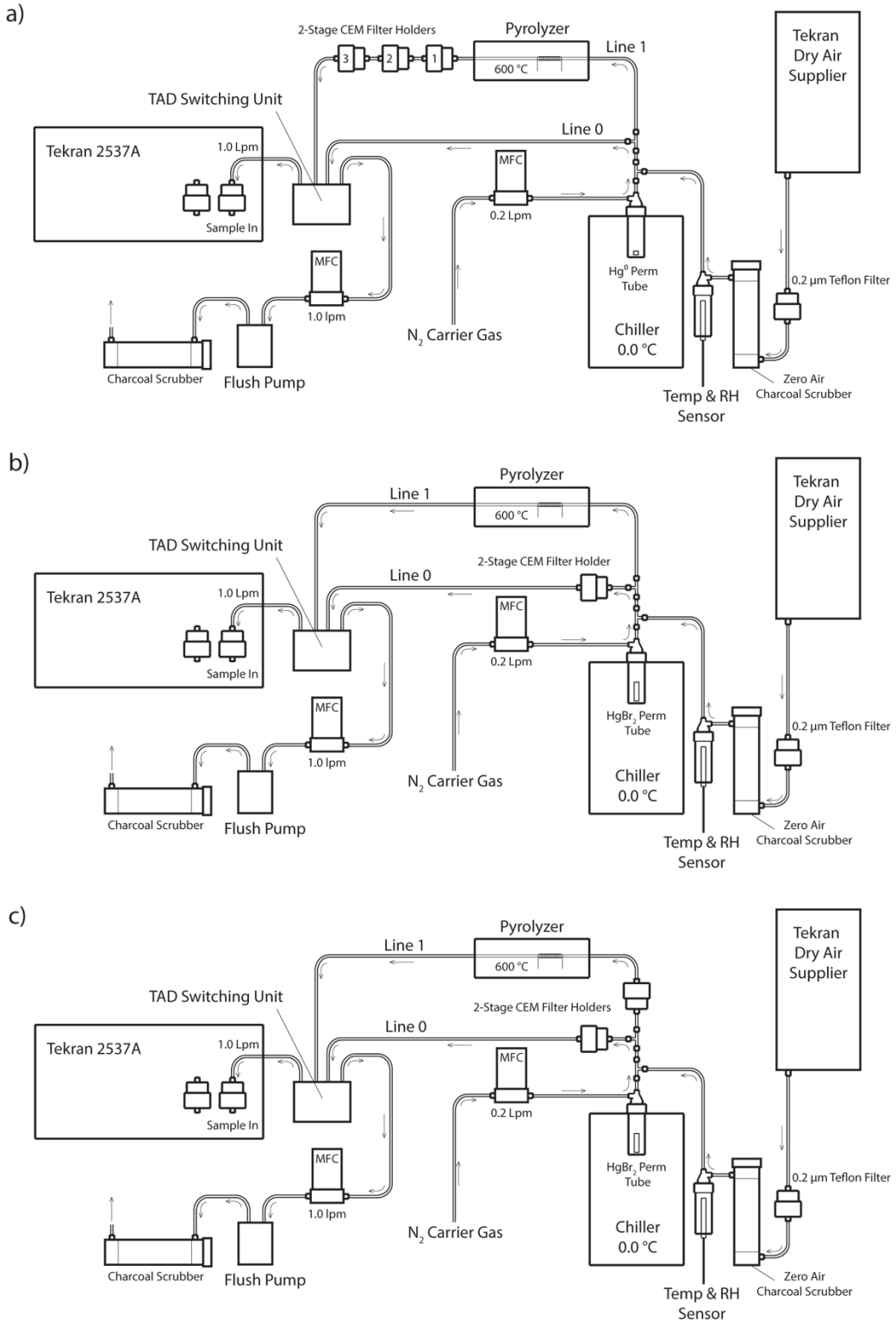

Figure 4.1 *Schematic of Hg vapor permeation system configurations for: a) GEM permeations, b) $HgBr_2$ permeations, and c) simultaneous $HgBr_2$ loading on two sample lines. Note dry air supplier disconnected for ambient and elevated humidity $HgBr_2$ permeations, with sample path starting at 0.2 µm Teflon particulate filter and water bath inserted immediately in front of the charcoal scrubber. All tubing is chemically inert PTFE, except for the quartz glass pyrolyzer tube, and PFA filter holders.*

C, SI Fig. 4.1). The entire system was checked for Hg contamination in clean air prior to permeation tests, and periodically during sampling (Appendix C, SI Fig. 4.2). All tubing and connections used in the permeation system were polytetrafluoroethylene (PTFE), except for the quartz glass pyrolyzer tube and perfluoroalkoxy (PFA) filter holders. Each of these materials is known to be chemically inert, virtually nonporous, and to have a low coefficient of friction. For these reasons, PTFE/PFA plastic and quartz glass are the standard materials employed in almost all Hg sampling systems, as GEM passes over or through these surfaces without loss (Gustin et al., 2015). Given its reactive nature, some GOM inevitably adsorbs to internal line surfaces, but the capacity of these materials to sorb and retain GOM is not infinite and a steady state of adsorption/desorption is expected after 5-6 hours of exposure to a stable concentration (Gustin et al., 2013; Xiao et al., 1997).

Sample flow through the system was alternated between two PTFE sample lines (designated Line 0 and Line 1) using a Tekran® Automated Dual Switching (TADS) unit. Sample air was constantly pulled through each line at 1.0 Lpm by the internal pump and mass flow controller in the 2537A, or by an external flush pump (KNF Laboport® N86 KNP) and mass flow controller (Sierra Smart-Trak® 2). Laboratory air was pulled through a single inlet at the combined rate of 2.0 Lpm, passing through a 0.2 μm PTFE particulate filter and an activated charcoal scrubber to produce clean sample air. Additionally, for dry air permeations sample air was pulled through a Tekran® 1102 Air Dryer installed upstream of the particulate filter, and for elevated humidity permeations sample air was pulled through the headspace of a distilled water bath (DIW, < 0.2 ng L^{-1} total Hg) that was located upstream from the charcoal scrubber to eliminate the DIW being a potential Hg source to the system. Temperature and relative humidity (RH) were measured in-line (Campbell Scientific CS215) and used for calculation of absolute humidity.

Pure liquid Hg^0 and crystalline $HgBr_2$ (purity > 99.998% Sigma-Aldrich®) were used as Hg vapor sources. The elemental Hg^0 bead was contained in a PTFE vial. Solid $HgBr_2$ crystals were packed in thin-walled PTFE heat-shrink tubing (O.D. 0.635 cm) with solid Teflon plugs in both ends to create a perm tube with an active permeation length of 2 mm (Huang et al., 2013). The $HgBr_2$ permeation tube was also placed in the bottom of a PTFE vial, and the permeation vials were submerged in a temperature-controlled laboratory chiller (0.06 ± 0.13 °C, Cole Parmer Polystat®). A low source temperature was favored both because higher temperatures would have produced unacceptably high concentrations, and because there is evidence that at higher temperatures a small amount of Hg^0 can be evolved from Hg^{2+} compounds (Xiao et al., 1997).

An ultra-high purity nitrogen (N_2) carrier gas was passed through the permeation vials at 0.2 Lpm to carry the target Hg vapor into the main sample line through a PTFE T-junction. The main sample line was split into Line 0 and Line 1 immediately downstream from the permeation flow junction. Line 0 proceeded directly to the 2537A without modification during GEM permeations (Fig. 4.1a), but housed CEM filters during the $HgBr_2$ permeations (Fig. 4.1b, 4.1c). Line 1 held a pyrolyzer unit composed of a quartz glass tube (O.D. 0.625 cm) packed with a 3 cm section of quartz wool heated to 600 °C using a nichrome wire coil (Appendix C, SI Fig. 4.3). The goal of the pyrolyzer was to convert all Hg to GEM for detection on the Tekran® 2537A.

CEM filters were deployed in 2-stage, 47 mm disc PFA filter holders (Savillex©). The primary "A" filter in the 2-stage holder is the first to be exposed to the permeated Hg, with the secondary "B" filter mounted immediately behind the A filter (A to B distance ~3 mm) to measure potential breakthrough. For GEM permeations, three 2-stage filter holders were placed in-series on Line 1 behind the pyrolyzer unit (Fig. 4.1a), while total Hg coming through the system was measured on Line 0 with no filters in place. This allowed simultaneous exposure of 6 CEM filters in one GEM

sample exposure. The first CEM filter in-line served to scrub any small residual RM passing through the system and pyrolyzer, and these first in-line filters were removed for the calculations of GEM uptake (Appendix C. SI Fig. 4.4).

For determining the potential for GOM breakthrough, two system configurations were used. In the first configuration (Fig. 4.1b), the total Hg concentration of air that passed through the pyrolyzer on Line 1 was measured without any filters, while Line 0 held one 2-stage CEM filter pair for $HgBr_2$ loading. This configuration allowed for real time (10 min interval) quantification of the $HgBr_2$ permeation concentration through Line 1 using the 2537A, and comparison with total Hg loading on the CEM filters on Line 0. In the second configuration, replicate filters were concurrently loaded with $HgBr_2$ by placing 2-stage CEM filter holders on both Line 0 and Line 1 (upstream of the pyrolyzer, Fig. 4.1c). In all $HgBr_2$ exposures, the filter holders were placed as close to the permeation vial as possible, with a total distance from vial to filter surface of approximately 20 cm. Mercury bromide permeation was conducted in dry air and elevated humidity air. The difference between one line being fully open to the $HgBr_2$ permeation flow (configuration Fig. 4.1b) and then closed by deployment of the CEM filters (configuration Fig. 4.1c) enabled a rough determination of the amount of $HgBr_2$ line-loss within the system.

After permeation, CEM filters were collected into clean, sterile polypropylene vials and analyzed for total Hg by digestion in an oxidizing acid solution, reduction to Hg^0, gold amalgamation, and final quantification by cold vapor atomic fluorescence spectrometry (CVAFS, EPA Method 1631, Rev. E) using a Tekran® 2600 system. This analysis provided for comparison of total Hg filter loading, and verification of in-line results. A to B filter breakthrough was calculated by comparison of total Hg recoveries on the primary and secondary CEM filters, using Eq. (1):

$$\%\ Breakthrough = 100 * CEM_{2nd}/(CEM_{1st} + CEM_{2nd}) \quad (1)$$

Blank CEM filters were collected and analyzed in the same manner with every set of sample filters deployed on the permeation system, and the mean filter blank value was subtracted from all total Hg values to calculate the final blank-corrected Hg values used for data analysis. All data were analyzed in Microsoft® Excel (version 16.12) and RStudio® (version 3.2.2).

4.3 Results

4.3.1 Elemental mercury uptake on cation exchange membranes

Elemental Hg uptake on CEM material was negligible for permeated Hg^0 vapor concentrations ranging from 1.43×10^6 to 1.85×10^6 pg m^{-3} (Fig. 4.2). High GEM concentrations were employed in this study under the logic that if no GEM uptake was observed at high concentrations, a similar lack of GEM uptake can be expected for all lower concentrations. The mean Hg mass on blank CEM filters was 50 ± 20 pg (n = 28). For permeations into dry sample air of 0.5 ± 0.1 g m^{-3} water vapor (WV), total mean Hg^0 permeation exposures of 2.7×10^6 pg (24 h) and 7.3×10^6 pg (72 h) resulted in total (blank-corrected) Hg recoveries on the CEM filters of 100 ± 40 pg (n = 10) and 280 ± 110 pg (n = 5), respectively.

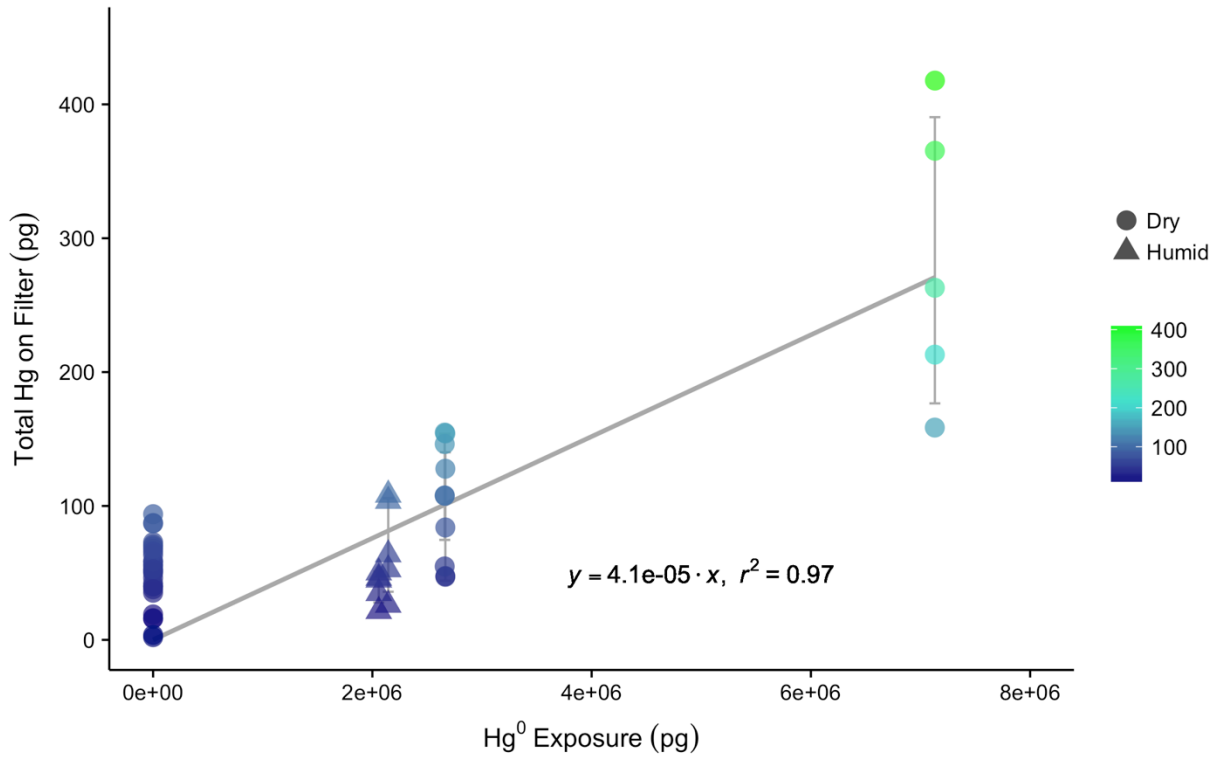

Figure 4.2 *Total Hg recovered on CEM material for blank filters (Hg exposure = 0 pg) and different Hg^0 vapor permeations in dry (0.5 ± 0.1 g m^{-3} WV) and humid air (2-4 g m^{-3} WV). Circles represent dry air permeations, triangles represent humid air exposures, and all permeation exposures were blank-corrected. The regression line shows the relationship between total Hg^0 exposure and blank-correct mean total Hg recovered on CEM filters (error bars ± one standard deviation), with a slope of 4.1x10^{-5} indicating a linear uptake rate of 0.004%.*

These quantities of total recovered Hg equate to a mean GEM uptake rate on the CEM filters of 0.004 ± 0.002%. For GEM permeations into ambient humidity sample air (2-4 g m^{-3} WV), at a slightly lower total mean permeated Hg^0 24 h exposure of 2.1×10^6 pg, total (blank-corrected) Hg recoveries on the CEM filters were 55 ± 30 pg (n =10), equating to a GEM uptake rate of 0.003 ± 0.001%. The overall GEM uptake rate was linear (r^2 = 0.97) for the range of concentrations used in this study, indicating a similar low uptake rate can be expected down to lower GEM concentrations.

4.3.2 Mercury bromide uptake on cation exchange membranes

Breakthrough of $HgBr_2$ vapor from the primary (A) to secondary (B) CEM filters was low for all conditions tested in this study (Table 4.1). These conditions included $HgBr_2$ permeated into clean dry laboratory air with < 0.5 g m^{-3} WV, clean air at ambient room humidity (4-5 g m^{-3} WV), and clean air at elevated humidity (10-11 g m^{-3} WV), at line temperatures between 17 to 19 °C. Overall, the mean A to B filter breakthrough ranged from 0 to 0.5% and averaged 0.2 ± 0.2 % (n = 17), with no statistical difference observed in mean breakthrough rates for the three levels of humidity (ANOVA, p = 0.124).

The first $HgBr_2$ permeation in clean dry (< 0.5 g m^{-3} WV) laboratory air was over a 96 h period, using the system configuration in Figure 1B to establish an approximately permeation rate (Fig. 4.3). Total Hg reaching the 2537A through the pyrolyzer on Line 1 (red line, Fig. 3) indicates an average $HgBr_2$ exposure concentration of 4540 pg m^{-3}, or about 4.5 pg min^{-1} from the permeation tube. After this permeation, total blank-corrected $HgBr_2$ loading on the primary CEM filter on Line 0 was 49400 pg, but only 50 pg on the secondary CEM filter, indicating a breakthrough rate of approximately 0.1%. Total Hg reaching the 2537A through the CEM filters on Line 0 (black line, Fig. 4.3) over this time period was 15 pg, mostly at the beginning of the deployment when some ambient Hg entered the opened system. The low concentrations of Hg measured downstream in Line 0 on the 2537A corroborates that breakthrough of $HgBr_2$ was low. These data also demonstrate that the CEM material did not saturate with a $HgBr_2$ loading of ~ 50000 pg, a loading far higher than could be expected in ambient conditions.

Table 1.

Sample	Start	End	Sample Time (min)	Sample Flow (lpm)	Sample Volume (m^3)	Total Hg on CEM (pg)	Blank Correct (pg)	Total Hg @ Tekran (pg)	A to B Filter Brkthru (%)
Mean CEM Filter Blank							54		
					Clean Dry Air (0.3 ± 0.05 g m^{-3} wv)				
HgBr 1P	*9/21/17 13:25*	*9/25/17 10:25*	*5580*	*1.00*	*5.580*	*na*	*na*	*25181*	*na*
HgBr 1A	9/21/17 13:25	9/25/17 10:25	5580	1.00	5.580	49478	49424	15	0.10
HgBr 1B						101	47		
HgBr 2A	9/25/17 10:30	9/26/17 10:30	1440	1.00	1.440	8901	8847	0	0.20
HgBr 2B						71	17		
HgBr 3A	*9/25/17 10:30*	*9/26/17 10:30*	*1440*	*1.00*	*1.440*	*9125*	*9072*	*1155*	*0.36*
HgBr 3B						*86*	*33*		
HgBr 4A	9/26/17 10:40	9/27/17 10:25	1425	1.00	1.425	8494	8440	0	0.28
HgBr 4B						77	24		
HgBr 5A	*9/26/17 10:40*	*9/27/17 10:25*	*1425*	*1.00*	*1.425*	*8306*	*8253*	*10*	*0.36*
HgBr 5B						*83*	*29*		
HgBr 6A	9/27/17 10:35	9/28/17 10:25	1430	1.00	1.430	8496	8442	0	0.22
HgBr 6B						72	19		
HgBr 7A	*9/27/17 10:35*	*9/28/17 10:05*	*1410*	*1.00*	*1.410*	*8386*	*8333*	*6*	*0.15*
HgBr 7B						*66*	*13*		
					Clean Humid Air (4.4 ± .2 g m^{-3} wv)				
HgBr H1P	*10/2/17 16:10*	*10/3/17 15:20*	*1390*	*1.00*	*1.390*	*na*	*na*	*5888*	*na*
HgBr H1A	10/2/17 16:10	10/3/17 15:20	1390	1.00	1.390	10498	10444	1700	0.25
HgBr H1B						80	27		
HgBr H2A	10/3/17 15:30	10/4/17 14:40	1390	1.00	1.390	8589	8535	164	0.13
HgBr H2B						65	11		
HgBr H3A	*10/3/17 15:30*	*10/4/17 14:40*	*1390*	*1.00*	*1.390*	*8182*	*8129*	*420*	*0.54*
HgBr H3B						*98*	*44*		
HgBr H4A	10/4/17 14:50	10/5/17 11:50	1260	1.00	1.260	7504	7451	0	0.31
HgBr H4B						76	23		
HgBr H5A	*10/4/17 14:50*	*10/5/17 11:50*	*1260*	*1.00*	*1.260*	*7576*	*7522*	*25*	*0.25*
HgBr H5B						*73*	*19*		
HgBr H6P	*10/5/17 12:05*	*10/9/17 10:25*	*5660*	*1.00*	*5.660*	*na*	*na*	*11889*	*na*
HgBr H7A	10/9/17 10:40	10/10/17 10:45	1445	1.00	1.445	9024	8970	105	na
HgBr H7B						2672*	2618*		
HgBr H8A	*10/9/17 10:40*	*10/10/17 10:45*	*1445*	*1.00*	*1.445*	*12359*	*12305*	*397*	*na*
HgBr H8B						*75*	*21*		
					Clean High Humidity Air (10.9 ± 1.7 g m^{-3} wv)				
HgBr H9A	10/10/17 10:50	10/11/17 9:30	1360	1.00	1.360	10920	10866	181	0.22
HgBr H9B						78	24		
HgBr H10A	*10/10/17 10:50*	*10/11/17 9:30*	*1360*	*1.00*	*1.360*	*11413*	*11359*	*308*	*0.00*
HgBr H10B						*53*	*0*		
HgBr H11A	10/11/17 9:35	10/12/17 9:35	1440	1.00	1.440	12001	11947	5	0.00
HgBr H11B						52	0		
HgBr H12A	*10/11/17 9:35*	*10/12/17 9:35*	*1440*	*1.00*	*1.440*	*12579*	*12525*	*40*	*0.29*
HgBr H12B						*90*	*36*		
HgBr H13P	*10/12/17 9:40*	*10/13/17 9:40*	*1440*	*1.00*	*1.440*	*na*	*na*	*1430*	*na*
HgBr H13A	10/12/17 9:40	10/13/17 9:40	1440	1.00	1.440	13152	13099	4	0.12
HgBr H13B						69	16		

Table 4.1 Summary of CEM filter loading and breakthrough during $HgBr_2$ permeations. Samples denoted P indicate approximate permeation rate check through Line 1 via pyrolyzer and Tekran 2537A, italics indicate filter deployments on Line 1, and * indicates high values due to leak around first filter seal.

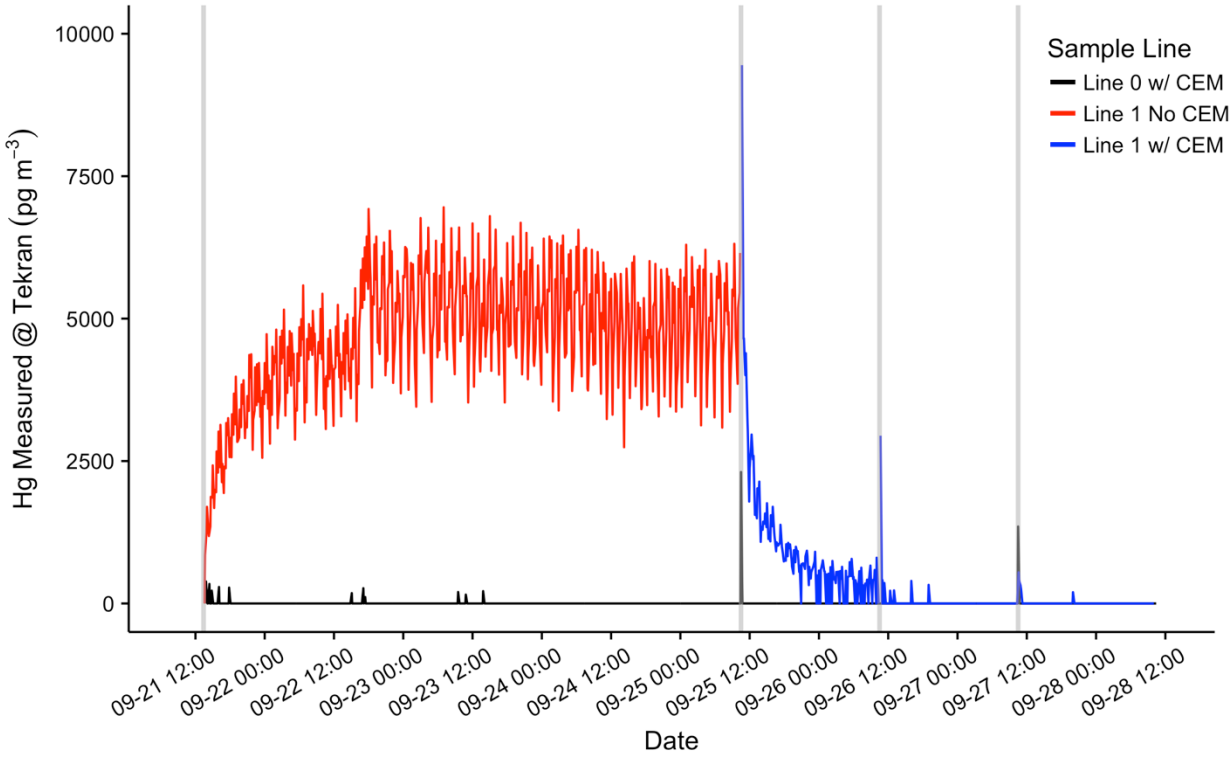

Figure 4.3 *$HgBr_2$ permeations in clean dry lab air using the configuration in Figure 4.1b (red line) and Figure 4.1c (blue line). The red line indicates total Hg released from permeation tube and passing through pyrolyzer on Line 1 before being measured by Tekran 2537A, black line indicates Hg reaching 2537A through CEM filters on Line 0. Vertical grey lines indicate open system during filter deployments.*

Subsequent replicate 24 h $HgBr_2$ permeations in clean dry air resulted in consistent total Hg loading on CEM filters placed on both lines concurrently (8560 ± 320 pg, n = 6, Samples 2-7 Table 4.1), and mean total Hg on the secondary CEM filters was 20 ± 10 pg (average breakthrough of 0.3%). On Line 0 (black line, Fig. 4.3), which was never open to $HgBr_2$ vapor downstream from the CEM filters at any point in the study, Hg measured at the 2537A was zero for all three 24 h permeations, indicating no breakthrough (Samples 2, 4, & 6, Table 4.1). However, on Line 1, which had been exposed to the full $HgBr_2$ vapor concentration of 4540 pg m^{-3} over the duration of the 96 h perm test, 1155 pg of Hg were measured downstream in the first 24 h sample (Sample 3, Table 4.1). The amount of downstream Hg dropped to 10 pg in the second 24 h, and 6 pg in the third 24 h (Samples 5 & 7, Table 4.1). This downstream Hg in Line

1 (compared to the zero Hg simultaneously observed on Line 0) is attributed to re-volatilization of $HgBr_2$ that had stuck to the line material during the open permeation flow. At the moment CEM filters were deployed on Line 1 (red-to-blue transition, Fig. 4.3), a rapid asymptotic decline in the Hg signal began. This decay curve supports drawdown and depletion of a Hg reservoir on the interior line surfaces behind the CEM filters, and not a continuous source such as breakthrough from the permeation tube that was still supplying $HgBr_2$ to both sample lines. The total mass of Hg re-volatized from the interior line surfaces (1155 pg) represents 4-5% of the total $HgBr_2$ that had passed through Line 1 (~25000 pg based on 2537A measurement). Eventually, Hg reaching the 2537A through Line 1 decreased to zero during the same 24 h filter deployment, indicating a majority of $HgBr_2$ line contamination can be expected to flush out within ~12 h.

Additional $HgBr_2$ permeations were made at two levels of in-line humidity. At ambient room humidity (4-5 g m^{-3} WV), mean total Hg measured on the CEM filters was 7910 ± 520 pg (n = 4; Samples H2-5, Table 4.1), with an average breakthrough to the secondary filters of 0.3%. When normalized for sample volume, the mean $HgBr_2$ loading on CEM filters during ambient humidity (5968 ± 125 pg) and dry air (5995 ± 188 pg) permeations was not statistically significantly different (t-test $p = 0.790$). $HgBr_2$ breakthrough rates were also the same (0.3%) as during the dry air permeations, indicating that the permeation system was operating similarly at the two humidity levels, and suggesting that absolute humidity concentrations around 4-5 g m^{-3} WV have insignificant effects on collection of $HgBr_2$ in clean laboratory air by the CEM material.

We observed that an increase in humidity resulted in an initial large increase in Hg measured at the 2537A downstream of the CEM filters on Line 0 (Sample H1, Table 4.1), concurrently with an open $HgBr_2$ permeation flow through Line 1 while both lines were subjected to increased RH. This downstream Hg on Line 0 dropped substantially to zero in ~10 h in the first 24 h

deployment (Sample H2, Table 4.1), and was zero for the duration of the second 24 h deployment (Sample H4, Table 4.1). As this downstream Hg rapidly declined to zero, we believe this was also an off-gassing effect, likely induced by the increased humidity, which perhaps facilitated a heterogeneous surface reduction of $HgBr_2$ to GEM in the short section of line between the perm source and CEM filters, with the GEM then passing through to the 2537A. As the breakthrough rate and the mean $HgBr_2$ loading on the CEM filters did not change between the dry air and ambient humidity permeations, the downstream Hg observed at the 2537A during the ambient humidity permeations cannot be attributed to a loss of Hg from the CEM filters and is more likely due to a process in the sample lines.

As a further test of possible humidity effects, two replicate 24 h CEM filter deployments were conducted in elevated humidity conditions (10-11 g m^{-3} WV) created by an in-line water bath. Mean total Hg loading on the primary CEM filters was higher compared to the previous permeations (11700 ± 720 pg, n = 4, Samples H9-12, Table 4.1), indicating an increase in the effective $HgBr_2$ permeation rate, possibly due to the perturbation caused by a poor filter seal and small leak in the preceding deployment (Sample H7-8, Table 4.1). However, mean total Hg on the secondary CEM filters was 20 ± 20 pg, indicating an average breakthrough of 0.1%, less than the breakthrough observed for the lower humidity permeations.

4.4 Conclusions

GEM uptake on the CEM material was negligible under the laboratory conditions and high GEM loading rates (2 orders of magnitude above ambient) tested in this study, with an overall linear uptake rate of 0.004% for permeated GEM concentrations between 1.43×10^6 to 1.85×10^6 pg m^{-3}. This uptake rate would be insignificant at typical ambient atmospheric Hg concentrations (1-2 ng

m^{-3}). As a hypothetical example, a CEM filter sampling ambient air at an average GEM concentration of 2 ng m^{-3} for a typical 2-week sample period would have a total Hg^0 exposure of ~40000 pg. At the calculated uptake rate of 0.004%, a maximum 1.6 pg of Hg observed on the sample filter could be attributed to GEM artifact and given that blank filters have a mean total Hg mass of 50 ± 20 pg, this amount would be below detection. This corroborates the lack of GEM uptake seen by Lyman et al. (2016) for manual Hg^0 injections on CEM filters at lower total mass loadings of 300-6000 pg.

Mean $HgBr_2$ breakthrough from primary to secondary CEM filters averaged 0.2 ± 0.2% over all test conditions, using $HgBr_2$ as a test GOM compound. A to B filter breakthrough was derived from a comparison between the large amount of $HgBr_2$ permeated onto the primary CEM filters, to the small amount of $HgBr_2$ that collected on the secondary CEM filters, 3 mm immediately downstream. The measurement of 1000s of pg of Hg on the primary filter, and only 10s of pg on the secondary filter, leads to the conclusion that the primary filter removed the majority of $HgBr_2$ from the sample air stream. In addition, low breakthrough was corroborated by downstream measurement of the air stream passing through the CEM filters, using the Tekran® 2537A. The average breakthrough to the 2537A was 0 pg for 24 h permeations in dry air and 0-40 pg in humid air, for those filter deployments than can be considered steady-state (> 24 h without large perturbations).

While the permeation system was not specifically optimized for a quantitative mass balance between permeated $HgBr_2$ and $HgBr_2$ recovered on the CEM filters, a rough estimation of the CEM collection efficiency is possible. Using the $HgBr_2$ permeations conducted in clean dry air (mean loading 8560 pg) and comparing this to the mean Hg concentration measured at the 2537A analyzer during the last 24 h of the 96 h permeation measurement (4680 pg m^{-3}, or 6739

pg per 24 h), the $HgBr_2$ recovery on the CEM filters averaged 127%. Adjusting the expected permeated $HgBr_2$ mass for our estimated line-loss (~4-5%) improves the recoveries to ~123%. Still, $HgBr_2$ loading on the CEM filters was therefore ~23% higher than expected based on the pyrolized total measurement on the 2537A.

The technique of gold amalgamation in general, and specifically including the Tekran® 2537 analyzer, is widely considered to provide a quantitative *total gaseous Hg* measurement, at or very near 100% collection efficiency for Hg^0 and Hg compounds (Dumarey et al., 1985; Landis et al., 2002; Schroeder and Jackson, 1985; Schroeder et al., 1995; Temme et al., 2003). However, to our knowledge collection and desorption efficiencies on gold traps have not been demonstrated for $HgBr_2$. The stated desorption temperature of the Tekran® 2537A gold traps is 500 °C, but temperatures as low as 375 °C have been reported (Gustin et al., 2013), which would likely cause reduced thermal decomposition efficiency for all captured GOM compounds, including $HgBr_2$. We speculate that a combination of incomplete thermal decomposition to Hg^0, at both the 600 °C pyrolyzer and during the best-case 500 °C desorption of the 2537 gold traps, resulted in ~20% non-detection of total permeated $HgBr_2$ as it passed through the CVAFS optical path without generating the necessary fluorescence signal.

While our results validated some basic performance metrics for the CEM material, they did not provide data that could fully explain the higher levels of breakthrough observed for CEM filters deployed in ambient air over the 1 to 2-week sample periods in previous studies. Increasing humidity by itself did not affect observed $HgBr_2$ breakthrough. A $HgBr_2$ loading of ~50000 pg also did not lead to increased breakthrough, indicating there is no saturation effect on CEM filter capacity at a GOM loading far greater than expected from ambient concentrations. It remains unclear, though, whether breakthrough results from different collection efficiencies for GOM

compounds other than $HgBr_2$, or whether breakthrough results from a degradation of GOM retention capacity in the CEM material when exposed to ambient air chemistries not simulated in this study. Also, our experiments were conducted in particulate-free air, which leaves open the possibility that breakthrough is related to capture (or lack thereof) of PBM by the CEM material.

Acknowledgements

The authors would like to acknowledge funding from Macquarie University iMQRES 2015148 and NSF Grant 629679, as well as valuable input and assistance from Dr. Ashley Pierce, Dr. Seth Lyman, and the students of Dr. Gustin's laboratory.

References

Bloom N, Prestbo E, VonderGeest E. Determination of atmospheric gaseous Hg(II) at the pg/m 3 level by collection onto cation exchange membranes, followed by dual amalgamation/cold vapor atomic fluorescence spectrometry. 4th International Conference on Mercury as a Global Pollutant, Hamburg, 1996.

Dumarey R, Dams R, Hoste J. Comparison of the collection and desorption efficiency of activated charcoal, silver, and gold for the determination of vapor phase atmospheric mercury. Analytical Chemistry 1985; 57: 2638-2643.

Ebinghaus R, Jennings SG, Schroeder WH, Berg T, Donaghy T, Guentzel J, et al. International field intercomparison measurements of atmospheric mercury species at Mace Head, Ireland. Atmospheric Environment 1999; 33: 3063-3073.

Gustin MS, Amos HM, Huang J, Miller MB, Heidecorn K. Measuring and modeling mercury in the atmosphere: a critical review. Atmos. Chem. Phys. 2015; 15: 5697-5713.

Gustin MS, Huang J, Miller MB, Peterson C, Jaffe DA, Ambrose J, et al. Do We Understand What the Mercury Speciation Instruments Are Actually Measuring? Results of RAMIX. Environmental Science & Technology 2013; 47: 7295-7306.

Gustin MS, Pierce AM, Huang J, Miller MB, Holmes HA, Loria-Salazar SM. Evidence for Different Reactive Hg Sources and Chemical Compounds at Adjacent Valley and High Elevation Locations. Environmental Science & Technology 2016; 50: 12225-12231.

Huang J, Gustin MS. Uncertainties of Gaseous Oxidized Mercury Measurements Using KCl-Coated Denuders, Cation-Exchange Membranes, and Nylon Membranes: Humidity Influences. Environmental Science & Technology 2015a; 49: 6102-6108.

Huang J, Gustin MS. Use of Passive Sampling Methods and Models to Understand Sources of Mercury Deposition to High Elevation Sites in the Western United States. Environmental Science & Technology 2015b; 49: 432-441.

Huang J, Miller MB, Edgerton E, Sexauer Gustin M. Deciphering potential chemical compounds of gaseous oxidized mercury in Florida, USA. Atmos. Chem. Phys. 2017; 17: 1689-1698.

Huang J, Miller MB, Weiss-Penzias P, Gustin MS. Comparison of Gaseous Oxidized Hg Measured by KCl-Coated Denuders, and Nylon and Cation Exchange Membranes. Environmental Science & Technology 2013; 47: 7307-7316.

Landis MS, Stevens RK, Schaedlich F, Prestbo EM. Development and characterization of an annular denuder methodology for the measurement of divalent inorganic reactive gaseous mercury in ambient air. Environmental Science & Technology 2002; 36: 3000-3009.

Lyman S, Jones C, O'Neil T, Allen T, Miller M, Gustin MS, et al. Automated Calibration of Atmospheric Oxidized Mercury Measurements. Environmental Science & Technology 2016; 50: 12921-12927.

Lyman SN, Gustin MS, Prestbo EM, Marsik FJ. Estimation of Dry Deposition of Atmospheric Mercury in Nevada by Direct and Indirect Methods. Environmental Science & Technology 2007; 41: 1970-1976.

Marusczak N, Sonke JE, Fu X, Jiskra M. Tropospheric GOM at the Pic du Midi Observatory—Correcting Bias in Denuder Based Observations. Environmental Science & Technology 2017; 51: 863-869.

Mason R, Lawson N, Sullivan K. The concentration, speciation and sources of mercury in Chesapeake Bay precipitation. Atmospheric Environment 1997; 31: 3541-3550.

Pierce AM, Gustin MS. Development of a Particulate Mass Measurement System for Quantification of Ambient Reactive Mercury. Environmental Science & Technology 2017; 51: 436-445.

Schroeder W, Jackson R. An instrumental analytical technique for speciation of atmospheric mercury. International Journal of Environmental Analytical Chemistry 1985; 22: 1-18.

Schroeder W, Keeler G, Kock H, Roussel P, Schneeberger D, Schaedlich F. International field intercomparison of atmospheric mercury measurement methods. Water Air and Soil Pollution 1995; 80: 611-620.

Sheu GR, Mason RP. An examination of methods for the measurements of reactive gaseous mercury in the atmosphere. Environmental Science & Technology 2001; 35: 1209-1216.

Slemr F, Angot H, Dommergue A, Magand O, Barret M, Weigelt A, et al. Comparison of mercury concentrations measured at several sites in the Southern Hemisphere. Vol 15, 2015.

Temme C, Einax JW, Ebinghaus R, Schroeder WH. Measurements of Atmospheric Mercury Species at a Coastal Site in the Antarctic and over the South Atlantic Ocean during Polar Summer. Environmental Science & Technology 2003; 37: 22-31.

Weiss-Penzias P, Amos H, Selin N, Gustin M, Jaffe D, Obrist D, et al. Use of a global model to understand speciated atmospheric mercury observations at five high-elevation sites. Atmospheric Chemistry and Physics 2015; 15: 1161-1173.

Xiao Z, Sommar J, Wei S, Lindqvist O. Sampling and determination of gas phase divalent mercury in the air using a KCl coated denuder. Fresenius Journal of Analytical Chemistry 1997; 358: 386-391.

Zhang L, Lyman S, Mao H, Lin CJ, Gay DA, Wang S, et al. A synthesis of research needs for improving the understanding of atmospheric mercury cycling. Atmos. Chem. Phys. 2017; 17: 9133-9144.

CHAPTER 5:

Reactive mercury flux measurements using cation exchange membranes

Matthieu B. Miller[1], Mae S. Gustin[2], Grant C. Edwards[1]

[1]Department of Environmental Sciences, Faculty of Science and Engineering, Macquarie University, Sydney NSW, 2113, Australia

[2]Department of Natural Resources and Environmental Sciences, University of Nevada, Reno NV, 89557, United States

Statement of Authorship

This paper originated from a dialogue between Dr Gustin and Dr Edwards about the possibility of using the CEM filters for quantifying reactive mercury flux. Dr Gustin suggested that the mining materials described in Chapter 3 would make good test substrates, as they were readily available and well characterized. It was suggested that I assist with this work as I was familiar with the materials and the necessary equipment, and that I should proceed with a view towards developing a PhD dissertation. Apart from the initial intellectual genesis between Dr Gustin and Dr Edwards, the study design and experimental setup were driven largely by myself and Dr Edwards in a series of failures and iterative improvements. Once a workable experimental system was established, I completed the majority of flux measurements, filter deployments, analyses, and data processing. The manuscript was drafted with substantive textual contribution from Dr Edwards and editorial insight from Dr. Gustin.

Study Design: 60% • Data Collection: 90% • Data Analysis: 90% • Writing: 80%

ABSTRACT

A novel method was developed to measure reactive mercury (RM) air-surface exchange using dynamic flux chambers (DFCs) in conjunction with cation exchange membrane (CEM) filters. The experimental design and method was developed and tested in a laboratory setting, using materials collected from industrial scale open pit gold mines in central Nevada, USA. These materials include waste rock, heap leach ore, and tailings, with substrate concentrations ranging from 0.1 to 40 μg g^{-1} total mercury (THg). CEM filters were used to capture RM from the DFC sample lines while a Tekran® 2537A analyzer measured GEM concurrently. The method was determined to require a minimum RM concentration difference of 14 pg m^{-3} between DFC inlet and outlet sample air. Positive RM emission rates up to 4000 pg m^{-2} h^{-1} were measured from tailings materials with high Hg substrate concentrations. RM flux was variable for lower Hg concentration substrates, with both emission and deposition observed. For substrates that experienced RM deposition, deposition velocities were in the range 0.01-0.07 cm s^{-1}. These measurements represent the first successful direct quantification of RM air-surface exchange.

5.1 Introduction

In 2013, the United Nations Environment Minamata Convention on Mercury was promulgated with a mission to protect human health and the environment from exposure to the toxic effects of mercury (Hg) and its various compounds (UNEP, 2013). The Convention proposes to fulfill this mission through a strategy of globally coordinated control, scientific research, and ongoing monitoring of Hg in the environment. The mission poses a significant challenge as there are over 3000 known Hg contaminated sites worldwide due to mining and industrial activity, not including legacy and small scale operations involving Hg (Kocman et al., 2013; Krabbenhoft and Sunderland, 2013). Past emissions, including from natural sources but largely dominated by anthropogenic activities, have led to current large reservoirs of Hg in all environmental compartments (Pacyna et al., 2016; Pirrone et al., 2010; Streets et al., 2017). Even in the absence of new anthropogenic emissions, cycling of Hg between different spheres will continue at large scales and in possibly unexpected directions, driven by processes and mechanisms that are not fully understood, and susceptible to increasing human and climate perturbations (Obrist et al., 2018).

The atmosphere, a global common, is the dominant conduit for transport, transformation, emission, deposition, and re-emission of Hg and Hg compounds amongst Earth's ecosystems. Mercury in the atmosphere is classified on the basis of three physiochemical forms: gaseous elemental mercury (GEM), gaseous oxidized mercury (GOM), and particulate bound mercury (PBM), with PBM and GOM defined together as reactive mercury (RM = GOM + PBM)(Gustin et al., 2015; Weiss-Penzias et al., 2015). Atmospheric concentrations of GEM can be measured with well calibrated analytical instruments, whereas the quantification of GOM and PBM has

depended on operationally defined methods with demonstrably large uncertainty (Cheng and Zhang, 2017; Gustin et al., 2015; Gustin et al., 2013; Jaffe et al., 2014; Zhang et al., 2017).

Scientific understanding of the biogeochemical cycling of Hg is currently inadequate due to the large ambiguity in measurements and general difficulty of research on atmospheric Hg chemistry (Jaffe et al., 2014). Atmospheric GEM is relatively inert, has a low deposition rate, and hence a relatively long atmospheric lifetime ranging from 6 months to 1 year (Krabbenhoft and Sunderland, 2013; Zhang et al., 2009). In certain scenarios, GEM has been shown to rapidly deplete in the atmosphere due to fast oxidation of GEM to RM and subsequent deposition to surfaces, and deposition and re-emission on short time scales is an important process driving movement (Howard and Edwards, 2018; Lu et al., 2001; Schroeder et al., 1998; Steffen et al., 2008; Steffen et al., 2002). In contrast to GEM, RM is thought to have high dry deposition velocities (Zhang et al., 2009). Knowledge of concentrations, chemistry, and processes forming atmospheric RM is critical information for understanding how Hg moves and impacts ecosystems globally. Recent research on RM has demonstrated that RM compounds in air vary both spatially and temporally to a considerable extent, pointing to the need for extensive measurements of RM and its specific compounds. (Gustin et al., 2016; Huang and Gustin, 2015b; Huang et al., 2014; Huang et al., 2017).

Fluxes of total gaseous mercury (TGM) and GEM have been successfully measured in many environments, providing insights into the biogeochemical cycling of GEM (Yannick et al., 2016; Zhu et al., 2016). In contrast, there are essentially no direct measurements of RM air-surface exchanges (Zhang et al., 2009). Reactive mercury fluxes reported in the literature are sparse and those reported are largely based on inferential or ambiguous methods (Brooks et al., 2008; Castro et al., 2012; Engle et al., 2005; Lindberg et al., 2002; Lindberg and Stratton, 1998; Lyman et al.,

2009; Lyman et al., 2007; Malcolm and Keeler, 2002; Poissant et al., 2004; Rea et al., 2000; Rothenberg et al., 2010; Sather et al., 2013; Skov et al., 2006; Zhang et al., 2005). A few direct RM-specific air-surface exchange measurements using KCl denuder-based approaches have been undertaken with mixed results (Brooks et al., 2008; Skov et al., 2006). Moreover, recent evaluation of KCl denuder approaches show these methods tend to underestimate RM and are subject to interferences due to ozone and water vapor (Huang and Gustin, 2015a; Lyman et al., 2010; McClure et al., 2014). The current dearth of experimental data on RM air-surface exchange processes is inhibiting our ability to move forward in understanding the biogeochemical cycling of atmospheric Hg.

In this study, we developed and applied a novel experimental approach for direct measurement of RM fluxes using cation exchange membrane (CEM) filters. CEM filters have been successfully deployed to measure RM in ambient air in previous studies (Gustin et al., 2016; Huang et al., 2017; Huang et al., 2013; Marusczak et al., 2017; Pierce and Gustin, 2017), and their use was here modified to allow for the determination of RM air-surface exchange. A series of experiments were conducted to optimize the CEM/RM flux methodology and the resulting method was subsequently applied to determine fluxes over both background waste rock material and Hg enriched mining materials. These data provide new insights into the air-surface exchange process associated with substrates of varying degrees of Hg contamination.

5.2 Methods

5.2.1 Materials

Substrate materials used for measuring Hg flux were acquired from industrial scale, open pit gold mines in central Nevada, and include waste rock, heap leach ore, and tailings. Waste rock is non-mineralized low Hg overburden material consisting of either alluvium or hard rock that

covered the ore body prior to mining. In this study, all such material was selected from the waste rock piles specifically set aside for future capping and site reclamation, and as such is referred to as cap material. Heap leach is low-grade ore blasted from the mine wall and "heaped" on an impoundment for irrigation with dilute cyanide leach solution for gold extraction. Tailings are the waste remnant of high-grade ore that has been pulverized by mechanical ball milling and undergone thermal/chemical treatment to extract gold.

All mining substrate materials were collected in September 2010, for measurements of GEM flux under controlled conditions (Miller and Gustin, 2013). Each material was divided into replicate trays (50 x 50 x 7 cm plywood lined with 3mil polyvinyl sheet) and stored inside a greenhouse bay at the University of Nevada Reno Agricultural Experiment Complex. At the onset of the RM flux experiments described in this paper, the substrates had sat undisturbed for ~3 years, and were completely dry and well compacted/consolidated from previous watering experiments. A circular chamber footprint impression was worn into the material surfaces and provided an excellent existing contact for the chamber base. Comparing GEM flux measurements made in this study with the previous measurements, an overall trend of decreasing GEM flux over time was observed. This fits a hypothesis suggested by Eckley et al. (2011b) of a long term reduction in GEM evasion from a mine substrate as time from disturbance increases.

5.2.2 Methodology

Reactive mercury flux was measured by modifying an existing GEM flux method consisting of a dynamic flux chamber (DFC) and an ambient air Hg analyzer (Tekran® 2537A) after the methods of Eckley et al. (2010; 2011a) and Miller et al. (2011).

The existing GEM flux system modified in this study used a 2537A in conjunction with a cylindrical DFC (footprint 0.036 m^2) made of molded Teflon film (0.19 mm thick) over a rigid Teflon frame (1.5 mm thickness), with a total internal volume of 2.0 Liters (Fig. 5.1). Air enters the chamber through 24 inlet holes (1 cm diameter) spaced 2.5 cm apart around the perimeter and 2.0 cm above the bottom edge. The sample outlet is 0.625 cm diameter PTFE tubing at the top-center of the chamber, and sample inlet air is measured through equivalent tubing at the height of the chamber inlet holes. A Tekran® Automated Dual Switching (TADS) unit was used to cycle the sample flow (1.0 Lpm) between the chamber inlet and outlet lines in sequential 10 min intervals (two 5 min samples on each line). GEM in each 5 min sample volume is quantified automatically by the 2537A analyzer using pre-concentration on gold traps followed by thermal desorption (500 °C) and cold vapor atomic fluorescence spectrometry (CVAFS). The difference in Hg concentration between the outlet and inlet air (C_o - C_i) is referred to as ΔC, and is used to calculate flux by Eq. 1:

$$F = Q * (C_o - C_i)/A \quad (1)$$

where F is the net Hg flux (ng m^{-2} h^{-1}), Q is the flow rate through the chamber (m^3 h^{-1}), C_o is the mean concentration of two consecutive 5 min outlet air samples (ng m^{-3}), C_i is the mean concentration of inlet air in the samples before and after C_o, and A is the area of the substrate under the chamber (m^2). The sign of ΔC indicates the direction of flux.

The modified system involves fitting the DFC inlet and outlet sample lines with 2-stage disc filter assemblies (Savillex© 47 mm PFA Teflon filter assembly) holding two inline polysulfone cation exchange membranes (CEM 0.8 μm, Mustang® S, Pall Corporation). CEMs preferentially

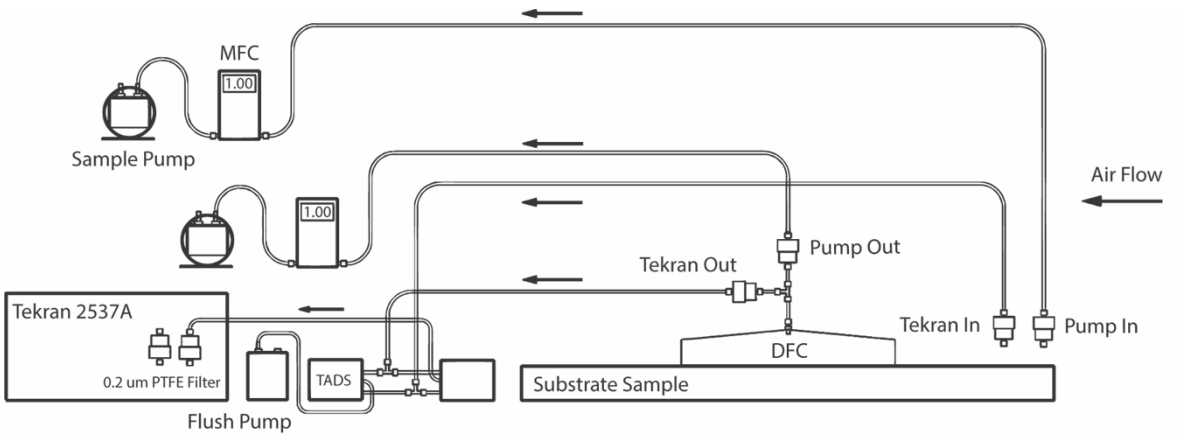

Figure 5.1 *Diagram of one RM filter-based flux system, deployed in duplicate as Systems A and B.*

capture RM compounds while allowing GEM to pass freely (see description below, and Miller et al. submitted). The first upstream CEM serves as the primary collection filter, while the second downstream CEM captures any Hg escaping from or missed by the first filter (referred to as breakthrough). With CEM filters deployed at the front of the sample lines, in conjunction with the 0.2 μm particulate filter at the rear sample inlet of the Tekran®, RM is scrubbed from the sample flow and all Hg measured downstream on the 2537A is in GEM form.

An additional set of inlet and outlet CEM filters was deployed simultaneously, using external sample pumps and mass flow controllers set to match the 2537A sample flow rate (1.0 Lpm, Fig. 1). The external pump outlet sample line pulled from the main DFC outlet line via a T-joint. Two filter assemblies were suspended above the flux system at a height of 2 m to measure background RM concentrations in the greenhouse, sampling at the same flow rate using an equivalent external pump and MFC setup.

With both the Tekran® and external pump controlled CEM sample lines, total flow through the DFC was 2.0 Lpm, which provides a chamber turn over time (TOT) of 1 minute. At this flow rate, flow velocity through the chamber is laminar with no turbulent eddy formation, as

determined through computational fluid dynamic (CFD) modelling of the chamber geometry performed by Eckley et al. (2010). Thus the chamber design of Eckley et al. (2010) is optimal in terms of not disturbing the substrate being studied. With low velocity, non-turbulent flow, particle entrainment from the substrate surfaces in expected to be nil, especially for particle sizes greater than the CEM filter pore size of 0.8 μm.

5.2.3 Cation exchange membrane testing

The possibility of GEM uptake on the CEM material was tested by performing a series of calibrated Hg^0 injections through CEM filters, and by longer duration high concentration Hg^0 permeations. Any GEM uptake on the CEM filters would constitute a serious measurement artifact, and so it was critical to rule out such a possibility.

Elemental Hg injections were made manually via a 250 μL syringe from a Tekran® 2505 Hg vapor source, into the sample air flow of a Tekran® 2537A, upstream of the instrument sample filter. Injection tests were first made through a 0.2 μm PTFE filter to check the recovery of the 2537A, as well as the accuracy of the syringe and vapor source. The PTFE filter was then replaced with CEM filters for a series of Hg^0 injections, at total mass loadings between 0.3 and 6 ng of Hg^0. Loaded filters were analyzed for total Hg (mean 90 ± 24 pg, n = 13), and this was compared to the total Hg on blank filters (mean 85 ± 39 pg, n = 30, Figure 5.2a) collected immediately prior to the injection tests. Results indicate no statistical increase in total Hg on the CEM material after instantaneous exposure to Hg^0 loads equivalent to concentrations up to 2400 ng m^{-3} (Welch t-test, $p = 0.32$, Figure 5.2b).

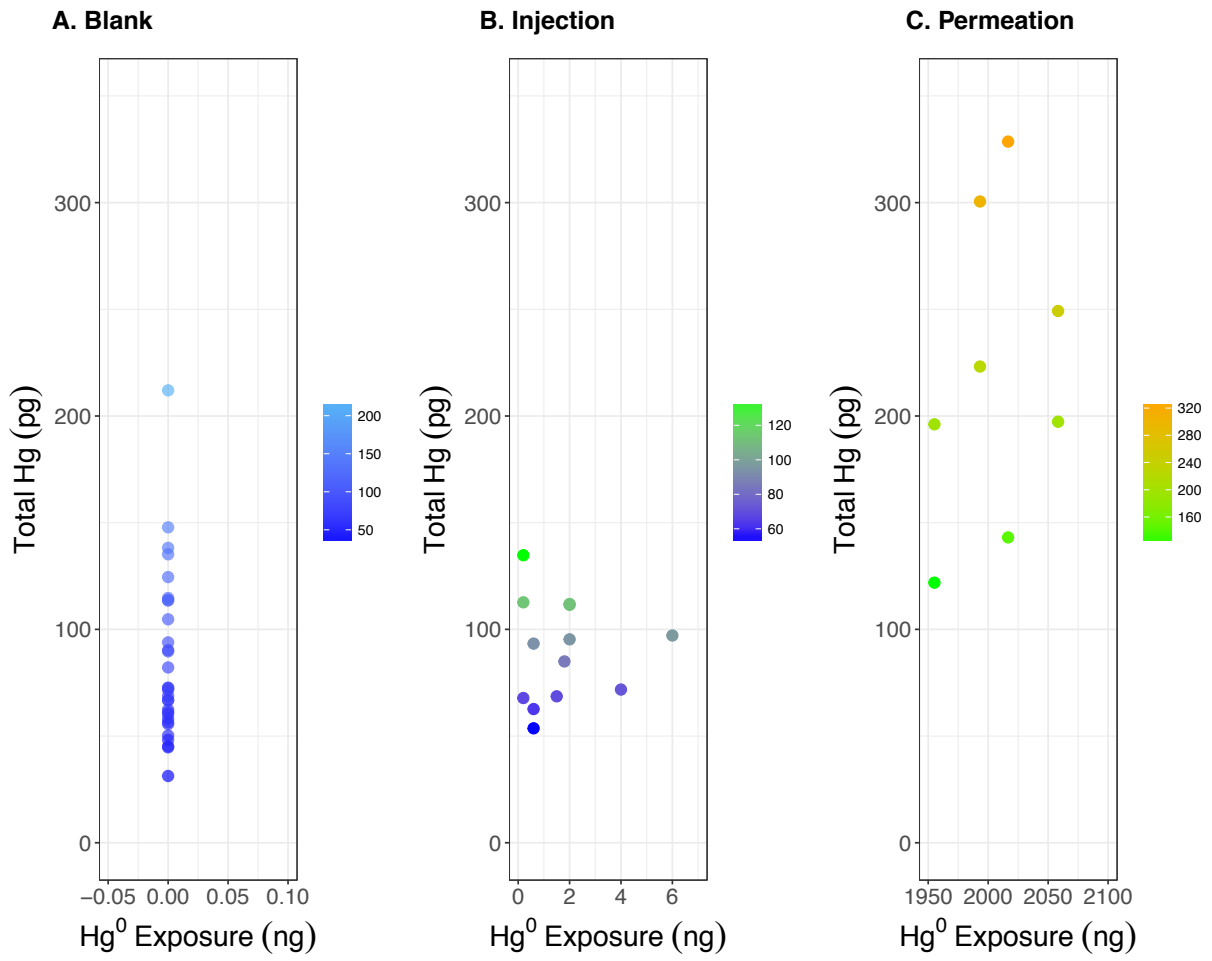

Figure 5.2 *Comparison of total Hg on blank CEM filters (a) versus CEM filters exposed to Hg^0 vapor via syringe injection (b) and continuous permeation (c). Note difference in x-axis scales.*

Elemental Hg permeations were made using a custom-built permeation system. Ambient room air was pulled through a 0.2 µm PTFE particle filter and an activated charcoal zero air canister before passing through a PTFE vial containing a bead of pure Hg^0. The vial was temperature controlled at 2.5 °C using a refrigerated bath (Thermo® NesLAB RTE 7). Sample flow through the permeation vial was controlled by a Tekran® 2537A and TADS unit. The 2537A sample flow was set at 1.0 Lpm, and the flushing flow rate through the TADS unit was also controlled at 1.0 Lpm using an MFC and external pump. The sample flow was split into two channels

immediately downstream of the permeation vial. One channel passed through a quartz wool pyrolyzer tube heated to 600 °C with a Nichrome wire coil, and the other channel flowed directly through the TADS to the 2537A. Each channel was sampled for two consecutive 5 min measurements of total Hg concentration by the 2537A. The test CEM filters were deployed two at a time in a 2-stage Teflon filter holder, placed in-line immediately downstream of the pyrolyzer to ensure that all Hg passing through the membrane material was in the gaseous elemental form. With the combined 2537A and flushing flows, total sample flow through the permeation vial was 2.0 Lpm, producing a mean total Hg concentration of 1380 ± 30 ng m^{-3} as measured by the 2537A. Filter deployments of 24 h duration in the permeation system resulted in an average total pass-through Hg exposure of 2000 ± 40 ng, and the mean mass of total Hg measured on these filters after collection was 220 ± 70 pg (n = 8, Figure 5.2c). This equates to a mean GEM uptake rate of only 0.007 ± 0.004 % on the CEM material, too small to create a significant artifact at the GEM concentrations observed during our measurements. This conclusion is confirmed by more extensive work in Miller et al. (submitted, this thesis).

5.2.4 Analysis

After flux measurements, CEM filters were collected into sterile 50 mL polypropylene centrifuge tubes, and frozen at -20 °C until analyses (within 14 days of collection). Filters were analyzed for total Hg by aqueous digestion and cold vapor atomic fluorescence spectrometry (CVAFS, EPA Method 1631, Rev. E) using a Tekran 2600 system, with total Hg operationally equivalent to total RM. The blank Hg mass that can be expected on an unused CEM filter (median = 68 pg, n = 56) was determined from clean filters collected with every set of measurements, and the median blank value was subtracted from all sample values. Breakthrough is defined as the

amount of Hg on the secondary filter as a percent of the total Hg collected on both filters (after blank correction), and overall median breakthrough was low (4.2%, n = 222).

The RM concentration in the inlet/outlet sample air was calculated by combining the blank-corrected primary and secondary filters into a total Hg mass per sample line and dividing by therespective sample air volume. The difference in RM concentration between the inlet and outlet lines provided a ΔC_{RM}, with this multiplied by sample flow providing the RM emission rate (pg h^{-1}). Reactive Hg flux (pg m^{-2} h^{-1}) was calculated with Eq. 1 using ΔC_{RM} values, the flow rate (1.0 ± 0.005 Lpm) and the chamber footprint (0.036 m^2).

The RM flux detection limit was determined by the minimum statistically resolvable difference between C_o and C_i, i.e. the smallest meaningful ΔC_{RM} that could be measured (Fig. 3). The C_o and C_i concentrations were based on two measurements: total Hg on the CEM filters as determined by analysis on the Tekran® 2600 system, and total sample volume as determined by the mass flow-controlled sample rate and time. The MFC precision was ± 0.5% (± 0.005 Lpm at 1.0 Lpm) and the detection limit of the 2600 was 1 ppt, or about 53 pg per reagent blank in a clean 50 mL collection tube. The median mass of Hg on the blank CEM filters was 68 pg, which subsumes the 53 pg in the reagent/tube blank as the practical detection limit for the method. As distribution of CEM blank values was non-normal and skewed heavily to the right (Fig. 5.3a), the 95% confidence interval around the median (58-73 pg) was used to define a minimum detectable RM concentration (Fig. 5.3b). For example, in a 24 h sample, the minimum detectable RM concentration would be ~3.5 pg m^{-3} to exceed the upper 95% confidence limit of 73 pg for the blank. In a 24 h sample the minimum resolvable ΔC_{RM} would be 13.5 pg m^{-3} (sum of upper + lower confidence intervals, + 3 pg m^{-3} to account for flow precision, converted to 24 h sample volume concentration). This was taken as the upper minimum ΔC_{RM} value.

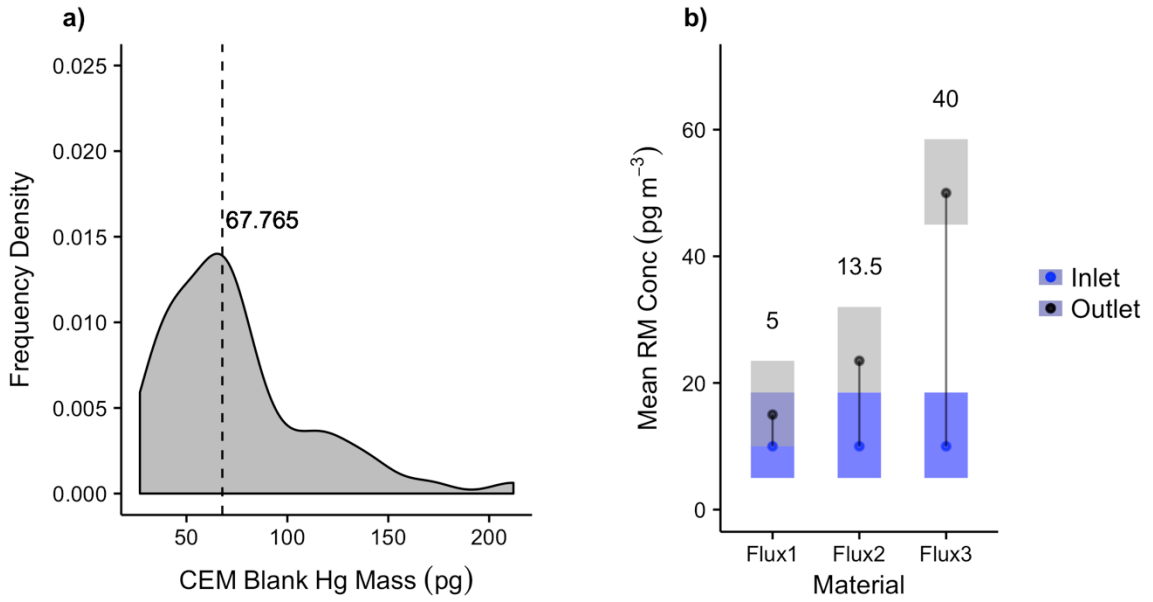

Figure 5.3 *Determination of ΔC_{RM} detection limits: a) distribution of Hg mass on unused "blank" CEM filters (median = 68 pg) and b) hypothetical example of statistically detectable RM flux criteria. Shaded boxes in (b) represent the maximum uncertainty in concentration, based on 95% confidence interval around the median filter blank (58-73 pg), Flux1 represents an insufficiently resolvable ΔC_{RM} in which the 95% confidence intervals around the median blank-corrected C_o and C_i values overlap, Flux2 represents the minimum detectable ΔC_{RM} (13.5 pg m^{-3}), and Flux3 represents an obviously resolvable ΔC_{RM}.*

Chamber blanks were determined for each Teflon DFC (referred to as Chamber A and Chamber B) by measuring flux over a clean Teflon sheet. Chamber blank emission rates were measured immediately following chamber cleanings (24 h acid wash in 10% HNO_3), and then between substrate types (i.e. cap, leach, tailings). For the summer measurement period, the median chamber blank ΔC_{RM} for both Chambers A and B (A = 13 pg m^{-3}, B = 14 pg m^{-3}, n = 12) was at the detection limit, so chamber blanks were not subtracted from material fluxes. For the following winter measurement period, the median chamber blank ΔC_{RM} for both chambers was significantly negative (A = -60 pg m^{-3}, B= -60 pg m^{-3}, n = 6), and the median chamber blank was -215 pg m^{-2} h^{-1}, indicating that the chamber and the blank Teflon sheet were acting as depositional surfaces for RM. For these measurements, the chamber blanks were subtracted. For

materials that demonstrated net RM deposition, the deposition velocity (V_d cm s^{-1}) was calculated using Eq. 2:

$$V_d = \text{flux } (ng\ m^{-2}\ h^{-1}) \text{ / air concentration } (ng\ m^{-3}) * (100/3600) \quad (2)$$

All fluxes were measured in the University of Nevada-Reno Agricultural Experiment Station greenhouse. Meteorological parameters were measured synchronously with flux and recorded in 5 min averages, including temperature and relative humidity (HMP45C, Campbell Scientific®), substrate temperature (C107, Campbell Scientific®), and solar radiation (LI-200X, LiCor®). Rudimentary climate control was provided by ventilation fans pulling outside air across the greenhouse bay from intakes on the opposite side. Fluxes were measured on the "upwind" side of the bay in a variety of orientations (see below).

Data was processed in Microsoft Excel (version 16.22) and RStudio® (version 3.2.2).

5.2.4 Evolution of approach

Two Tekran® 2537A analyzers with associated RM filter systems were used to simultaneously measure flux from two replicate trays (one for each A and B system) of each sample material. The duplicated systems allowed a total of four RM flux measurements to be collected each time a material was tested, two from the Tekran® sample lines and two from the external pump lines. The intention of the duplicate systems was to evaluate consistency and repeatability of the measurements. However, during the initial method testing it became apparent that the position of the trays and the inlet sample lines was an important variable. For example, strong RM emission from an "upwind" tray could substantially increase the inlet RM concentration of the "downwind" tray, resulting in a negative ΔC_{RM} and apparent deposition. Such contradictory results compelled us to test a variety of orientations for the two systems. The best results were

achieved in the final design by placing both trays all the way against the clean intake wall of the greenhouse bay, and separating them laterally by 1.5 meters, with all equipment located downwind. This configuration provided the most uniform inlet air concentrations for both systems.

5.2.5 Limitations of method

The use of filter membranes in conjunction with a DFC to measure RM flux has several limitations. Given the low concentrations of RM, a relatively long sampling time of at least 24 h is required to capture a sufficient mass for quantification. The low temporal resolution limits analysis of the factors controlling RM flux, factors which likely operate on a diel cycle similar to observations of GEM flux. Hence, much of the variability in our observed RM fluxes we cannot explain.

A necessary condition of the DFC method is the placement of flux chambers directly on a material, resulting in artificial modification of surface conditions and a presumptive influence on the magnitude of flux. In our study, this limitation is immaterial, as the entire experimental setup constitutes an artificial environment, and we are more interested in 1) our ability to experimentally detect measurable RM flux, and 2) the qualitative direction of flux versus absolute quantification. As the method develops, it will become necessary to more thoroughly evaluate the effects of the DFC on RM flux.

5.3 Results

5.3.1 Reactive mercury flux measurement repeatability

The first test of the optimized configuration was a set of replicate measurements made on a single material, to assess method repeatability. The material used for this test was a heap leach

ore of intermediate total Hg concentration (TCL, 13.2 ± 2.0 μg g^{-1}). Filters were deployed in three consecutive sample sets of approximately 72 h each, for a total of 12 replicate filter flux measurements (i.e. two RM flux measurements on two separate replicate trays, three times). The mean GEM flux from all samples was 170 ± 60 ng m^{-2} h^{-1} (n = 6). The duplicate measurements of background greenhouse RM showed a mean concentration of 13 ± 7 pg m^{-3} (n = 12). The ΔC_{RM} was well above detection for all measurements (median 100 pg m^{-3}, n = 12), and the mean RM flux over all 12 samples was 370 ± 80 pg m^{-2} h^{-1} (n = 12) and ranged from 240 to 490 pg m^{-2} h^{-1} (Fig. 5.4). The mean relative percent difference (RPD) of RM flux measured between Pump and Tekran sample lines on the same tray was 6.5 ± 3.9%, and mean RPD between trays was 21.4%. These replicate measurements of a single material consistently showed the same direction and magnitude of RM flux with good agreement.

5.3.2 Reactive mercury flux measurement over expanded range of materials: Summer

Following the triplicate measurement of TCL (May), follow up testing was conducted on a series of three additional materials (July – August): a low to intermediate Hg cap material and heap leach ore (TCC 0.2 μg g^{-1}, LTL 0.6 μg g^{-1}), and a high Hg tailings (TCT 36 μg g^{-1}). Measurement time was reduced to 48 h for this series of materials, as the previous deployments had total RM loading well above detection. However, several of the LTL and TCC flux measurements resulted in insignificant ΔC_{RM} values (Fig. 5.5). In these cases, RM flux could not be discriminated, and these values were excluded from subsequent analysis.

A comparison of RM flux measured by the replicate sample lines on each system (Tekran® sample flow and external pump sample flow) show a relationship of 1:1 (Fig. 5.6), which indicates that CEM filters on two independent flow channels were capturing equivalent amounts

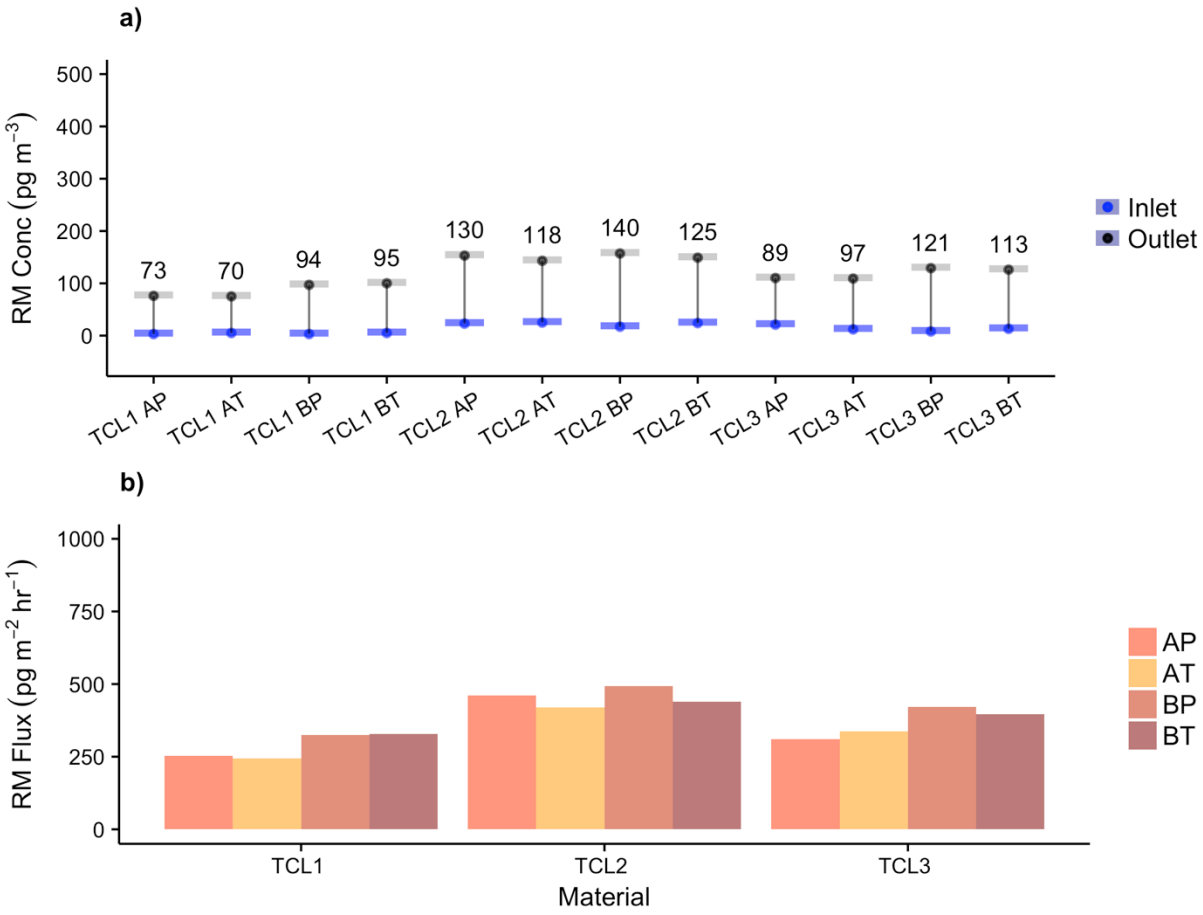

Figure 5.4 *Test 72 h replicate measurements of TCL material: a) ΔC_{RM} values, grey points indicate chamber concentration (C_o), blue points indicate inlet air concentration (C_i), ΔC_{RM} is represented by the grey line between points, and the numeric value of ΔC_{RM} is shown above. b) RM flux from TCL material in three consecutive 72 h measurements, no chamber blank correction. Sample line labels: PA = Pump A, PB = Pump B, TA = Tekran A, TB = Tekran B.*

of RM. This equivalency was true for both of the replicate systems (System A and B), which were each simultaneously measuring flux from replicate trays of the same material. The high level of replication displayed by the system, both in general and in detail, for multiple substrate types, increases confidence that these measurements represent a real net surface exchange of RM.

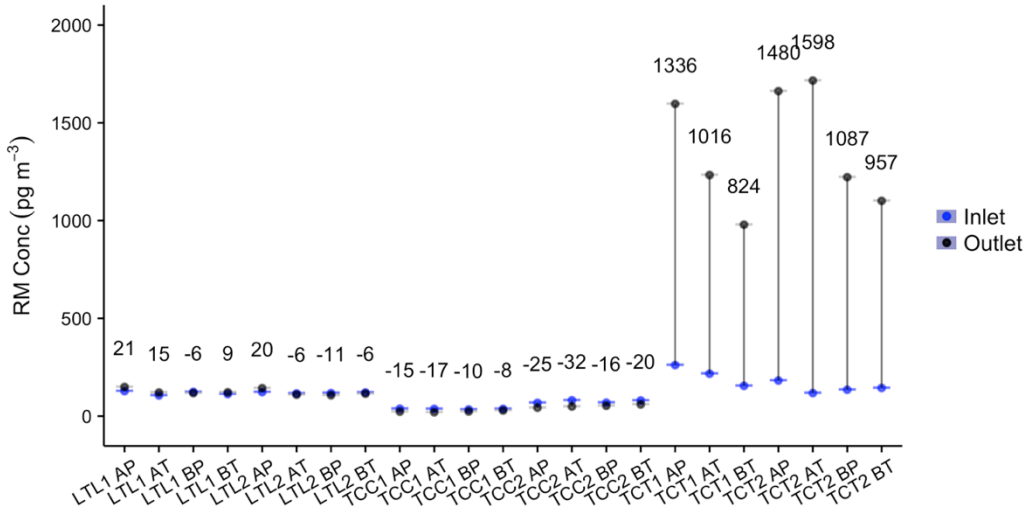

Figure 5.5 *Expanded set of RM flux measurements for select materials during summer. ΔC_{RM} was below detection for 5 of 8 LTL measurements, and 2 of 8 TCC measurements, and these values were excluded from subsequent analysis.*

Positive RM fluxes were associated with the higher substrate concentration materials (TCL, TCT). The low Hg TC cap experienced net RM deposition, with a mean V_d of 0.03 ± 0.01 cm s^{-1} (n = 6). The 3x higher Hg concentration LT leach showed either no net flux or slightly positive RM emission (60 ± 10 pg m^{-2} h^{-1}, n = 3). The very high substrate Hg concentration TC tailings materials showed uniformly high RM emission (4060 ± 1000 pg m^{-2} h^{-1}, n = 7).

The mean ambient RM in the greenhouse during this summer period was 130 ± 55 pg m^{-3} (n = 24), however there was a distinct trend of increasing ambient RM over the course of measurements. During the TC cap measurements, ambient RM concentration in the greenhouse was 70 ± 20 pg m^{-3} (n = 8). This increased to 150 ± 20 pg m^{-3} (n = 8) during the LT leach measurements, and up to 180 ± 40 pg m^{-3} (n = 8) during the TC tailings measurement. It is possible that this increase was due to an actual increase in outside ambient air RM concentrations, but it is more likely that the increasing RM emissions seen over the course of measurements was also captured in the background CEM filter deployments.

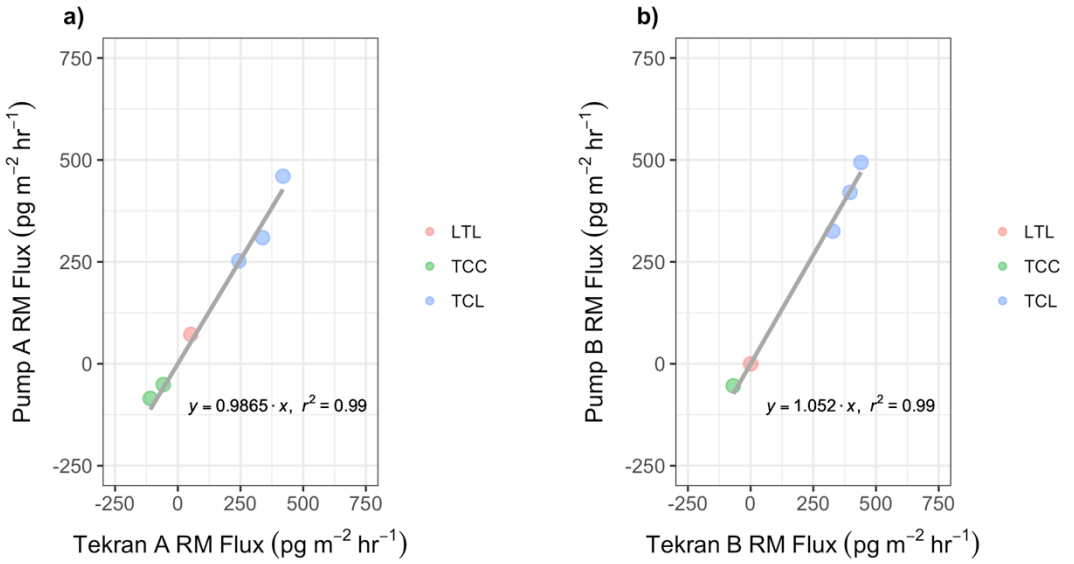

Figure 5.6 *Comparison of RM fluxes measured by Tekran controlled flow sample lines and external pump flow-controlled sample lines, for a) System A and b) System B using TCL, TCC, LTL, and TCT summer measurements. Note TCT data not graphed, as fluxes were an order of magnitude higher and skew the regression r^2 towards 1.*

5.3.3 Reactive mercury flux measurement over complete range of materials: Winter

A full set of 24 h RM flux measurements including all the available mining materials was made in the following winter period (January – March, 2016). Ambient RM concentration in greenhouse air was 51 pg m^{-3} (n = 16), much lower than in the summer months. Mean RH and solar radiation were similar between the summer and winter periods, due to the attenuating effect of the greenhouse. However, mean air and substrate temperatures were significantly lower in the winter (Table 5.1).

All measured fluxes were above the ΔC_{RM} detection limit (Fig. 5.7a). The relationship between RM flux measured on the A and B systems was slightly less than 1:1 (B = 0.87*A) and not as strong (r^2 = 0.74) as during the summer measurements. Without chamber blank correction, RM fluxes were uniformly negative for all materials except the very high Hg TC tails (Fig. 5.7b, orange shades). However, with the chamber blank correction applied, RM flux from the cap

Table I.

	Material	Sample	Date	Substrate Conc ($ng\ g^{-1}$)	GEM Flux ($ng\ m^{-2}\ h^{-1}$)	RM Flux ($ng\ m^{-2}\ h^{-1}$)	RM Inlet ($ng\ m^{-3}$)	RM V_d ($cm\ s^{-1}$)	Ambient RM ($ng\ m^{-3}$)	Temp (°C)	RH (%)	Solar ($W\ m^{-2}$)	Soil Temp (°C)
	Leach	TCL1*	5/16-5/19	11900	134	0.29	0.01	-	0.01				
		TCL2*	5/19-5/22		151	0.45	0.03	-	0.03	na	na	na	na
		TCL3*	5/22-5/25		215	0.37	0.02	-	0.01				
Summer 2015	Cap	TCC1A P	7/21-7/23	230	10	-0.05	0.04	0.04	0.05	22.6	41.6	15.8	23.9
		TCC1A T				-0.06	0.04	0.04					
		TCC1B P			12	na	0.03	na					
		TCC1B T				na	0.04	na					
		TCC2A P	7/29-7/31		4	-0.09	0.07	0.03	0.09	24.8	28.7	15.8	26.4
		TCC2A T				-0.11	0.08	0.04					
		TCC2B P			13	-0.05	0.07	0.02					
		TCC2B T				-0.07	0.08	0.02					
	Leach	LTL1A P	8/12-8/14	590	105	0.07	0.13	-	0.16	23.8	30.2	17.4	26.5
		LTL1A T				0.05	0.11	-					
		LTL1B P			87	na	0.12	na					
		LTL1B T				na	0.11	na					
		LTL2A P	8/14-8/16		100	0.07	0.12	-	0.13	23.4	24.1	17.3	25.6
		LTL2A T				na	0.12	na					
		LTL2B P			99	na	0.12	na					
		LTL2B T				na	0.12	na					
	Tailings	TCT1A P	8/26-8/28	35750	483	4.46	0.26	-	0.22	23.8	31.4	16.6	24.2
		TCT1A T				3.37	0.22	-					
		TCT1B P			370	na	0.15	-					
		TCT1B T				2.76	0.16	-					
		TCT2A P	8/28-8/31		702	5.02	0.18	-	0.16	22.0	33.3	13.9	22.1
		TCT2A T				5.43	0.12	-					
		TCT2B P			457	3.02	0.13	-					
		TCT2B T				2.57	0.14	-					
Winter 2016	Cap	TCCA	1/6/16	230	1	-0.24	0.18	0.07	0.04	15.0	37.6	2.7	14.5
		TCCB				1	0.05	0.06	-				
		LTCA	1/7/16	150	0	0.00	0.09	-	0.03	14.5	38.6	9.7	11.8
		LTCB				-1	0.07	0.06	-				
		CPCA	1/20/16	120	-1	0.00	0.13	-	0.02	14.5	31.7	12.9	15.6
		CPCB				na	0.06	0.05	-				
		GSCA	1/21/16	200	-1	-0.12	0.13	0.02	0.03	14.6	26.6	11.0	15.8
		GSCB				-1	-0.20	0.14	0.04				
	Leach	TCLA	1/26/16	11900	29	0.11	0.14	-	0.04	13.4	35.3	9.3	15.2
		TCLB				30	0.11	0.12	-				
		CPLA	1/29/16	310	-18	0.00	0.08	-	0.04	13.9	34.9	16.5	15.3
		CPLB				-12	0.00	0.09	-				
		LTLA	2/2/16	590	-4	0.13	0.02	-	0.01	11.7	25.5	14.6	14.2
		LTLB				-3	0.07	0.04	-				
	Tailings	CPTA	2/9/16	21150	4	0.00	0.08	-	0.03	14.1	37.5	18.9	15.7
		CPTB				5	0.25	0.04	-				
		GSTA	2/10/16	6960	16	0.16	0.11	-	0.05	14.4	39.3	11.6	13.8
		GSTB				-1	0.11	0.09	-				
		LTTA	3/20/16	11020	2	-0.45	0.28	0.05	0.07	19.8	23.1	31.0	22.3
		LTTB				2	-0.08	0.24	0.01				
		TCTA	3/22/16	35750	51	0.52	0.20	-	0.06	17.0	26.6	37.4	19.3
		TCTB				71	0.79	0.14	-				

Table 5.1. Summary of GEM and RM flux and ambient parameters for all measurements. Fluxes are chamber blank-corrected where applicable, and V_d values are based on corrected fluxes (- indicates no deposition, *na* indicates non-detectable flux).

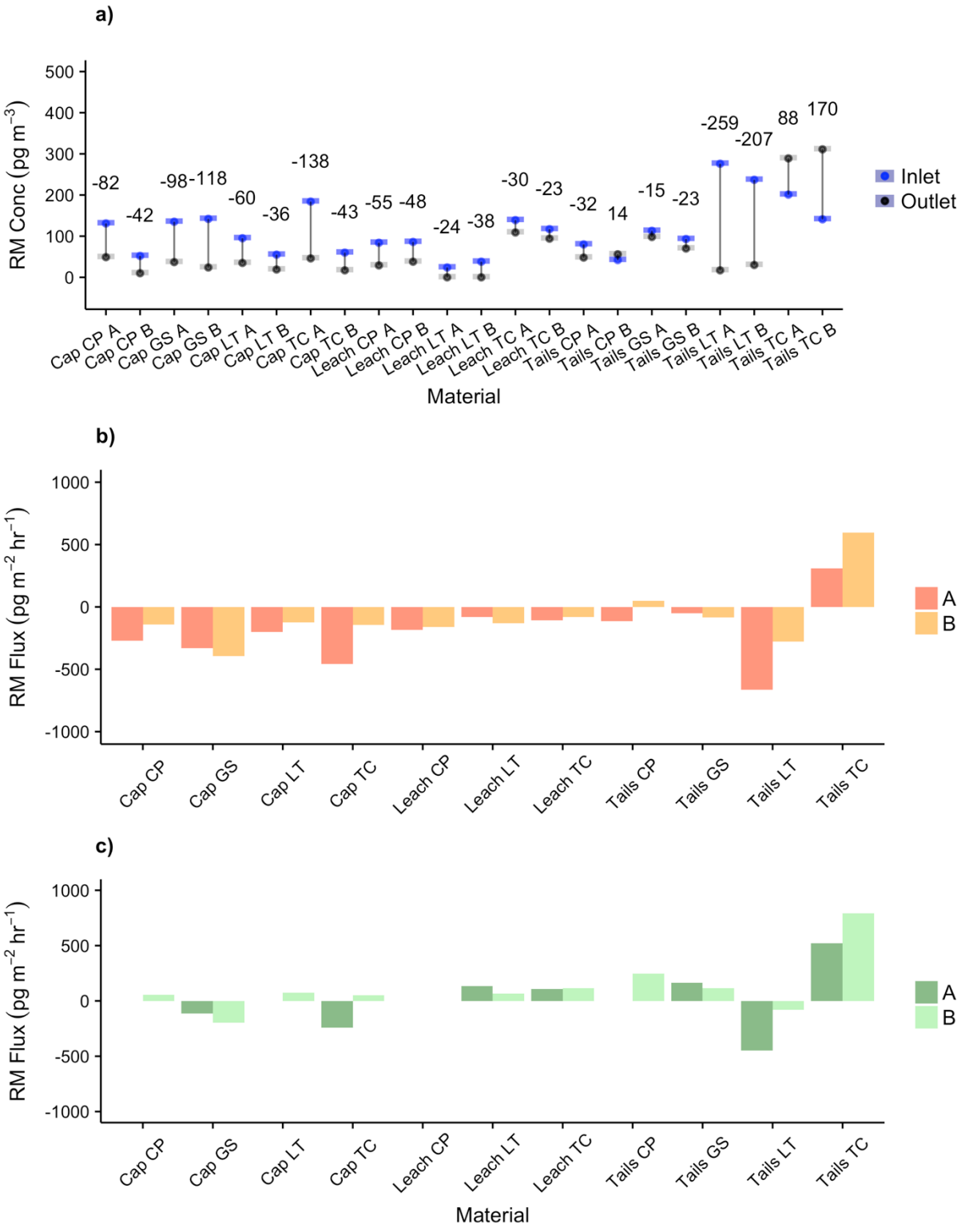

Figure 5.7 *RM flux measurements for all materials, winter 2016. a) ΔC_{RM}, above detection limit for all measurements b) RM flux, no chamber blank correction (shaded orange), and c) RM flux, with chamber blank correction (shaded green).*

materials became ambiguous (i.e. both deposition and emission observed) and positive for all leach and tailings materials except the LT tailings (Fig. 5.7c, green shades).

Three materials had entirely unambiguous fluxes, with or without blank correction: GS cap (RM deposition, V_d = 0.02-0.04 cm s^{-1}, corrected), LT tails (RM deposition, V_d = 0.01-0.05 cm s^{-1}, corrected), and TC tails (strong RM emission). The GS mine exploits a predominantly carbonaceous ore deposit, and much of the mine and surrounding areas are subject to carbon loading from aerial dust deposition. The carbon in the GS waste rock and ore likely facilitate deposition of Hg and RM. The LT tailings material is from a non-active tailings impoundment that was partially revegetated at the time of collection, versus the entirely barren surface typical of active tailings. Although the LTT Hg concentration was high (11 μg g^{-1}), the surface was old, and it is possible this material behaved more as a background substrate. The TC tailings material was collected from an actively filling tailings impoundment that collected process waste from a variety of ore types, from multiple mine sites, and had the highest Hg concentration of the materials used in this study, which likely explains its tendency to by a strong emitter of both GEM and RM, a conclusion also made by Eckley et al. (2011a).

An interesting point is that background and inlet RM concentrations were very similar during the summer measurements (Fig. 5.8a), but inlet concentrations were 3x higher than background during the winter measurements (Fig. 5.8b). The lower winter background RM (50 pg m^{-3}) compared to summer (110 pg m^{-3}) may partially explain this. However, the distance between the inlet and background sampling heights was only ~ 1 m, which implies a strong vertical gradient in RM concentration in the greenhouse air, likely caused by less mixing as circulation fans shut down at 13 ºC. The relatively high inlet level RM concentrations during the winter possibly drove the apparent deposition observed in the chamber blank measurements during this time.

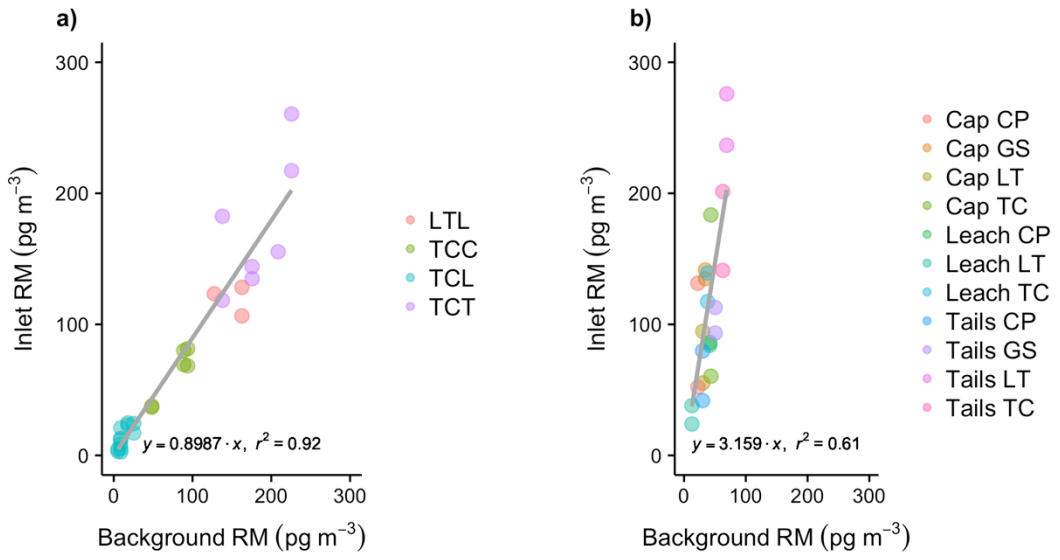

Figure 5.8 *Comparison of ambient background RM concentrations measured at 2 m height in the greenhouse, vs RM concentrations measured at the chamber inlet, for a) Summer 2015 and b) Winter 2016. Background vs inlet concentrations were comparable during Summer measurements, but inlet concentrations were much higher relative to background in the winter.*

5.4 Conclusions

Overall, the new method developed here for direct measurement of RM air-surface exchange was successful. This study presents the first direct RM flux measurements using a CEM filter technique and provides a first analysis of whether the necessary measurements of small differences in RM concentration were possible using a DFC method. Measurements of RM flux were above calculated detection limits in most cases, and both intra- (Tekran vs Pump sample) and inter- (A vs B) system replicate measurements showed very good agreement. After initial trials at 72 h and 48 h, a 24 h sample time was found to be generally sufficient for detecting RM flux on the mining materials used in this study, some of which were similar to background soils. It would be possible to operate the system at higher flow rates, to decrease sample time and improve the temporal resolution of the flux measurements. However, sample deployment and

collection require 20-30 min and to some extent perturbs the system, so ultimately the flux resolution is limited by practical operational constraints. The 24 h measurement at least serves to capture net flux over a full diel cycle without continuous interruptions.

We specifically refer to our measurement as a *reactive mercury* flux to include both GOM and PBM, as it is not possible to explicitly discriminate between the two using a single step filter train. That said, as particulate Hg is not *emitted* from a surface in the volatile sense, and particle entrainment is negligible at the low flow velocities generated in the flux chambers, we posit that RM concentrations measured at the chamber outlet CEM filters are dominated by GOM. If ambient air RM concentrations are primarily PBM, at a size fraction large enough to be captured by the CEM filters (i.e. > 0.8 μm), it will undeniably be captured at the chamber inlet filters. However, PBM at this size would likely deposit to the substrate surface within the chamber, and we will reliably measure that deposition as a smaller RM loading on the C_o filters versus the C_i filters.

Flux measured from low Hg, non-mineralized cap materials tended to be ambiguous for both GEM and RM, with low positive and negative values oscillating around a net zero flux. The observed GEM deposition velocities were typical of non-vegetated surfaces, while RM deposition occurred at V_d values (0.01-0.07 cm s^{-1}) on the low end of the suggested range (Zhang et al., 2009). The higher Hg concentration leach and tailings material (except LT tails) also showed net RM emission, when corrected for chamber blank flux. The highest RM emissions were consistently observed for the highest Hg concentration substrate, TC tailings, in both summer and winter conditions. The implications of these results are that RM fluxes may be directly measured from select substrates, especially areas of Hg contamination, such as mine

tailings impoundments, and such areas can act as a direct emission source of reactive mercury compounds to the atmosphere.

Acknowledgements

The authors would like to acknowledge funding from Macquarie University iMQRES 2015148, National Science Foundation Grant 629679, Barrick Gold Corp and Newmont Mining Corp for donating substrate materials, and Dr. Ashley Pierce for invaluable assistance in preparing this manuscript.

References

Brooks S, Arimoto R, Lindberg S, Southworth G. Antarctic polar plateau snow surface conversion of deposited oxidized mercury to gaseous elemental mercury with fractional long-term burial. Atmospheric Environment 2008; 42: 2877-2884.

Castro MS, Moore C, Sherwell J, Brooks SB. Dry deposition of gaseous oxidized mercury in Western Maryland. Sci Total Environ 2012; 417-418: 232-40.

Cheng I, Zhang L. Uncertainty Assessment of Gaseous Oxidized Mercury Measurements Collected by Atmospheric Mercury Network. Environmental Science & Technology 2017; 51: 855-862.

Eckley CS, Gustin M, Lin CJ, Li X, Miller MB. The influence of dynamic chamber design and operating parameters on calculated surface-to-air mercury fluxes. Atmospheric Environment 2010; 44: 194-203.

Eckley CS, Gustin M, Marsik F, Miller MB. Measurement of surface mercury fluxes at active industrial gold mines in Nevada (USA). Science of the Total Environment 2011a; 409: 514-522.

Eckley CS, Gustin M, Miller MB, Marsik F. Scaling Non-Point-Source Mercury Emissions from Two Active Industrial Gold Mines: Influential Variables and Annual Emission Estimates. Environmental Science & Technology 2011b; 45: 392-399.

Engle MA, Sexauer Gustin M, Lindberg SE, Gertler AW, Ariya PA. The influence of ozone on atmospheric emissions of gaseous elemental mercury and reactive gaseous mercury from substrates. Atmospheric Environment 2005; 39: 7506-7517.

Gustin MS, Amos HM, Huang J, Miller MB, Heidecorn K. Measuring and modeling mercury in the atmosphere: a critical review. Atmos. Chem. Phys. 2015; 15: 5697-5713.

Gustin MS, Huang J, Miller MB, Peterson C, Jaffe DA, Ambrose J, et al. Do We Understand What the Mercury Speciation Instruments Are Actually Measuring? Results of RAMIX. Environmental Science & Technology 2013; 47: 7295-7306.

Gustin MS, Pierce AM, Huang J, Miller MB, Holmes HA, Loria-Salazar SM. Evidence for Different Reactive Hg Sources and Chemical Compounds at Adjacent Valley and High Elevation Locations. Environmental Science & Technology 2016; 50: 12225-12231.

Howard D, Edwards GC. Mercury fluxes over an Australian alpine grassland and observation of nocturnal atmospheric mercury depletion events. Atmos. Chem. Phys. 2018; 18: 129-142.

Huang J, Gustin MS. Uncertainties of Gaseous Oxidized Mercury Measurements Using KCl-Coated Denuders, Cation-Exchange Membranes, and Nylon Membranes: Humidity Influences. Environmental Science & Technology 2015a; 49: 6102-6108.

Huang J, Gustin MS. Use of Passive Sampling Methods and Models to Understand Sources of Mercury Deposition to High Elevation Sites in the Western United States. Environmental Science & Technology 2015b; 49: 432-441.

Huang J, Lyman SN, Hartman JS, Gustin MS. A review of passive sampling systems for ambient air mercury measurements. Environmental Science: Processes & Impacts 2014; 16: 374-392.

Huang J, Miller MB, Edgerton E, Sexauer Gustin M. Deciphering potential chemical compounds of gaseous oxidized mercury in Florida, USA. Atmos. Chem. Phys. 2017; 17: 1689-1698.

Huang J, Miller MB, Weiss-Penzias P, Gustin MS. Comparison of Gaseous Oxidized Hg Measured by KCl-Coated Denuders, and Nylon and Cation Exchange Membranes. Environmental Science & Technology 2013; 47: 7307-7316.

Jaffe DA, Lyman S, Amos HM, Gustin MS, Huang J, Selin NE, et al. Progress on Understanding Atmospheric Mercury Hampered by Uncertain Measurements. Environmental Science & Technology 2014; 48: 7204-7206.

Kocman D, Horvat M, Pirrone N, Cinnirella S. Contribution of contaminated sites to the global mercury budget. Environmental Research 2013; 125: 160-170.

Krabbenhoft DP, Sunderland EM. Global Change and Mercury. Science 2013; 341: 1457.

Lindberg SE, Brooks S, Lin CJ, Scott KJ, Landis MS, Stevens RK, et al. Dynamic Oxidation of Gaseous Mercury in the Arctic Troposphere at Polar Sunrise. Environmental Science & Technology 2002; 36: 1245-1256.

Lindberg SE, Stratton WJ. Atmospheric mercury speciation: Concentrations and behavior of reactive gaseous mercury in ambient air. Environmental Science & Technology 1998; 32: 49-57.

Lu J, Schroeder W, Barrie L, Steffen A, Welch H, Martin K, et al. Magnification of atmospheric mercury deposition to polar regions in springtime: the link to tropospheric ozone depletion chemistry. Geophysical Research Letters 2001; 28: 3219-3222.

Lyman SN, Gustin MS, Prestbo EM, Kilner PI, Edgerton E, Hartsell B. Testing and Application of Surrogate Surfaces for Understanding Potential Gaseous Oxidized Mercury Dry Deposition. Environmental Science & Technology 2009; 43: 6235-6241.

Lyman SN, Gustin MS, Prestbo EM, Marsik FJ. Estimation of Dry Deposition of Atmospheric Mercury in Nevada by Direct and Indirect Methods. Environmental Science & Technology 2007; 41: 1970-1976.

Lyman SN, Jaffe DA, Gustin MS. Release of mercury halides from KCl denuders in the presence of ozone. Atmospheric Chemistry and Physics 2010; 10: 8197-8204.

Malcolm EG, Keeler GJ. Measurements of mercury in dew: atmospheric removal of mercury species to a wetted surface. Environ Sci Technol 2002; 36: 2815-21.

Marusczak N, Sonke JE, Fu X, Jiskra M. Tropospheric GOM at the Pic du Midi Observatory—Correcting Bias in Denuder Based Observations. Environmental Science & Technology 2017; 51: 863-869.

McClure CD, Jaffe DA, Edgerton ES. Evaluation of the KCI Denuder Method for Gaseous Oxidized Mercury using HgBr2 at an In-Service AMNet Site. Environmental Science & Technology 2014; 48: 11437-11444.

Miller MB, Gustin MS. Testing and modeling the influence of reclamation and control methods for reducing nonpoint mercury emissions associated with industrial open pit gold mines. Journal of the Air & Waste Management Association 2013; 63: 681-693.

Miller MB, Gustin MS, Eckley CS. Measurement and scaling of air-surface mercury exchange from substrates in the vicinity of two Nevada gold mines. Science of the Total Environment 2011; 409: 3879-3886.

Obrist D, Kirk J, Zhang L, Sunderland E, Jiskra M, Selin N. A review of global environmental mercury processes in response to human and natural perturbations: Changes of emissions, climate, and land use. Ambio 2018; 47: 116-140.

Pacyna J, Travnikov O, De Simone F, Hedgecock I, Sundseth K, Pacyna E, et al. Current and future levels of mercury atmospheric pollution on a global scale. Atmospheric Chemistry and Physics 2016; 16: 12495-12511.

Pierce AM, Gustin MS. Development of a Particulate Mass Measurement System for Quantification of Ambient Reactive Mercury. Environmental Science & Technology 2017; 51: 436-445.

Pirrone N, Cinnirella S, Feng X, Finkelman R, Friedli H, Leaner J, et al. Global mercury emissions to the atmosphere from anthropogenic and natural sources. Atmospheric Chemistry and Physics 2010; 10: 5951-5964.

Poissant L, Pilote M, Xu X, Zhang H, Beauvais C. Atmospheric mercury speciation and deposition in the Bay St. Francois wetlands. Journal of Geophysical Research-Atmospheres 2004; 109.

Rea AW, Lindberg SE, Keeler GJ. Assessment of Dry Deposition and Foliar Leaching of Mercury and Selected Trace Elements Based on Washed Foliar and Surrogate Surfaces. Environmental Science & Technology 2000; 34: 2418-2425.

Rothenberg SE, McKee L, Gilbreath A, Yee D, Connor M, Fu X. Evidence for short-range transport of atmospheric mercury to a rural, inland site. Atmospheric Environment 2010; 44: 1263-1273.

Sather ME, Mukerjee S, Smith L, Mathew J, Jackson C, Callison R, et al. Gaseous oxidized mercury dry deposition measurements in the Four Corners area and Eastern Oklahoma, U.S.A. Atmospheric Pollution Research 2013; 4: 168-180.

Schroeder WH, Anlauf KG, Barrie LA, Lu JY, Steffen A, Schneeberger DR, et al. Arctic springtime depletion of mercury. Nature 1998; 394: 331.

Skov H, Brooks SB, Goodsite ME, Lindberg SE, Meyers TP, Landis MS, et al. Fluxes of reactive gaseous mercury measured with a newly developed method using relaxed eddy accumulation. Atmospheric Environment 2006; 40: 5452-5463.

Steffen A, Douglas T, Amyot M, Ariya P, Aspmo K, Berg T, et al. A synthesis of atmospheric mercury depletion event chemistry in the atmosphere and snow. Atmos. Chem. Phys. 2008; 8: 1445-1482.

Steffen A, Schroeder W, Bottenheim J, Narayan J, Fuentes JD. Atmospheric mercury concentrations: measurements and profiles near snow and ice surfaces in the Canadian Arctic during Alert 2000. Atmospheric Environment 2002; 36: 2653-2661.

Streets DG, Horowitz HM, Jacob DJ, Lu Z, Levin L, ter Schure AFH, et al. Total Mercury Released to the Environment by Human Activities. Environmental Science & Technology 2017; 51: 5969-5977.

UNEP. Minamata Convention on Mercury, 2013.

Weiss-Penzias P, Amos H, Selin N, Gustin M, Jaffe D, Obrist D, et al. Use of a global model to understand speciated atmospheric mercury observations at five high-elevation sites. Atmospheric Chemistry and Physics 2015; 15: 1161-1173.

Yannick A, Théo Le D, Christopher WM, Grant CE, Daniel O. New Constraints on Terrestrial Surface–Atmosphere Fluxes of Gaseous Elemental Mercury Using a Global Database. Environmental Science & Technology 2016; 50: 507-524.

Zhang HH, Poissant L, Xu X, Pilote M. Explorative and innovative dynamic flux bag method development and testing for mercury air–vegetation gas exchange fluxes. Atmospheric Environment 2005; 39: 7481-7493.

Zhang L, Lyman S, Mao H, Lin C, Gay D, Wang S, et al. A synthesis of research needs for improving the understanding of atmospheric mercury cycling. Atmospheric Chemistry and Physics 2017; 17: 9133-9144.

Zhang LM, Wright LP, Blanchard P. A review of current knowledge concerning dry deposition of atmospheric mercury. Atmospheric Environment 2009; 43: 5853-5864.

Zhu W, Lin C, Wang X, Sommar J, Fu X, Feng X. Global observations and modeling of atmosphere-surface exchange of elemental mercury: a critical review. Atmospheric Chemistry and Physics 2016; 16: 4451-4480.

CHAPTER 6:

Effect of moisture content on air surface exchange of reactive mercury from mining substrates

Matthieu B. Miller[1], Mae S. Gustin[2], Harald Biester[3], Grant C. Edwards[1]

[1]Department of Environmental Sciences, Faculty of Science and Engineering, Macquarie University, Sydney NSW, 2113, Australia

[2]Department of Natural Resources and Environmental Sciences, University of Nevada, Reno NV, 89557, United States

[3]Institute of Geoecology, Technical University of Braunschweig, Braunschweig, 38106, Germany

Statement of Authorship

This manuscript is a continuation of the reactive mercury flux measurements described in Chapter 5, and as such has the same ultimate origination in conceptual dialogue between Dr Gustin and Dr Edwards. Over the course of the RM flux method development, we became interested in the possible effects of substrate moisture on the RM flux measurements, and so designed a controlled experiment to evaluate this. As before, I performed all flux measurements, experimental manipulations, and filter deployments and analyses, as well as data processing. Dr Biester had previously performed solid phase speciation analysis on related mining materials for a tangential project that was not ultimately published, and so here did an up-to-date re-analysis of Hg speciation specifically for the substrates used in this study. The manuscript was largely written by myself with editorial input from co-authors.

Study Design: 75% • Data Collection: 85% • Data Analysis: 85% • Writing: 95%

ABSTRACT

Air-surface exchange of mercury (Hg) is a poorly constrained component of the global mercury cycle, especially for reactive mercury (RM). Diffuse areas of ore and waste materials resulting from mining activities often have elevated concentrations of Hg and can constitute significant local or regional non-point emission sources of Hg to the atmosphere. We measured RM air-surface exchange from a variety of mining-related materials using a novel cation exchange membrane (CEM) filter-based method in conjunction with a traditional dynamic flux chamber system for gaseous elemental Hg (GEM). In general, RM was deposited to low Hg concentration substrates (< 600 ng g^{-1}) and emitted from higher Hg concentration (> 600 ng g^{-1}) substrates when dry. Wet materials tended to have the same direction of RM flux but smaller magnitude compared to the equivalent dry material, indicating some suppression of RM flux due to aqueous phase processes. For both wet and dry conditions, high Hg concentration tailings materials demonstrated the highest RM emissions, ranging from 1000 and 36000 pg m^{-2} h^{-1}. GEM flux was significantly enhanced from wet material versus dry materials in the majority of samples.

6.1 Introduction

The liberation of mercury (Hg) from its natural geogenic occurrence as a native element and mineral results in a persistent and globally pervasive biogeochemical cycle affecting all spheres of the environment. As a unique semi-volatile liquid metal, elemental Hg^0 is readily emitted to the atmosphere in the gas phase, where it is transported widely and subject to a number of physiochemical processes. As a result, atmospheric Hg varies between several forms that are not easily differentiated: gaseous elemental mercury (GEM), gaseous oxidized mercury (GOM), and particulate bound mercury (PBM). When GOM and PBM are not convincingly distinguishable, they can be quantified together as reactive mercury (RM), a more general term encompassing all Hg^{2+} compounds in the atmosphere (Gustin et al., 2015; Weiss-Penzias et al., 2015) and conveying the fact that these compounds are more chemically reactive and have higher rates of both wet and dry deposition to terrestrial surfaces (Lindberg et al., 2007; Schroeder and Munthe, 1998).

Large reservoirs of Hg exist in terrestrial substrates, in some areas due to primary geogenic sources, but mainly as a result of atmospheric inputs originating from anthropogenic emissions over many centuries (Amos et al., 2015; Streets et al., 2017). Regardless of source, once an atom of Hg in surface substrates is emitted to the atmosphere, it may be deposited and re-emitted many times over (Schroeder and Munthe, 1998). Whether this ongoing air-surface exchange is ultimately a net source or sink of Hg is determined by many different substrate characteristics and environmental parameters, and consequently the mechanisms and magnitude of surface Hg fluxes are one of the least constrained components of the global Hg cycle (Obrist et al., 2018; Song et al., 2015). A variety of in-situ measurement techniques are used to determine net air-surface exchange of Hg and a large body of measurements has been generated from a number of environments, which are summarized in several recent reviews (Eckley et al., 2016; Yannick et

al., 2016; Zhu et al., 2016). Sparsely vegetated terrains are generally a net source of Hg to the atmosphere, especially in mineralized Hg-enriched areas (Eckley et al., 2016; Ericksen et al., 2006; Hartman et al., 2009).

In mineralized areas, Hg frequently occurs in association with base and precious metals, dominantly as mercury sulfide (HgS, cinnabar), but also as free elemental Hg^0 and in a number of other mineral forms such as meta-cinnabar, a low temperature polymorph of HgS (Rytuba, 2005). As metals are obviously a target for extractive industries, Hg is often an unavoidable by-product of hard rock metal mining. In addition to typical point-source process emissions (ore roasting, autoclaving, smelting), industrial-scale mining activities can result in very large, diffuse areas of newly excavated rock, crushed ore, and waste materials from which natural geogenic Hg can be liberated to the atmosphere at an enhanced rate relative to the original natural surface (Eckley et al., 2011a; Miller et al., 2011).

Primary ore deposits typically include reduced mineral phases not in equilibrium with the low temperature, low pressure, oxidative surface environment. Most sulfide minerals readily oxidize at the earth surface, forming sulfate anions (SO_4^-) and free cations (Jambor et al., 2000). In Carlin-type disseminated gold (Au) deposits of central Nevada, USA, Au and associated Hg are often deposited within iron sulfide (FeS, pyrite), both as structurally bound cations and in native elemental form (Muntean et al., 2011). Such ore deposits are frequently oxidized to some extent through natural weathering processes where they crop out near the surface (Fraser et al., 1991), and oxidation processes are rapidly accelerated during mining operations. The oxidation of FeS in the presence of air and water places Fe^{2+} and other trace metal inclusions such as Au and Hg into solution with sulfate ions (Jambor et al., 2000; Rimstidt and Vaughan, 2003). Mercury sulfate ($HgSO_4$) is among the possible products.

Diffuse mining areas can have high rates of GEM emission (Eckley et al., 2011b; Garcia-Sanchez et al., 2006; Gustin et al., 2003; Wang et al., 2005). Oxidized Hg^{2+} compounds may also volatize directly to a gas-phase, forming GOM (Schroeder and Munthe, 1998). Pure $HgSO_4$ crystals have been used in low temperature, ambient-pressure laboratory permeation systems as a GOM vapor source (Huang and Gustin, 2015), and $HgSO_4$ is speculated to be a component of atmospheric GOM (Gustin et al., 2015; Zhang et al., 2017). In the enriched environment of a major ore deposit, $HgSO_4$ or other oxidized Hg minerals might be a source of GOM to the atmosphere.

In this study we used a novel technique employing cation exchange membranes (CEM) for measuring RM flux to investigate the potential for RM emissions from several mining materials with a variety of total Hg concentrations, under dry and wet conditions. The CEM filters were integrated with an existing dynamic flux chamber (DFC) flux system that enabled simultaneous measurement of GEM air-surface exchange. Solid phase thermal desorption speciation (SPTD) was used to determine the speciation of Hg compounds within the substrates in order to better understand how the chemical form of Hg affected gaseous emissions.

6.2 Methods

6.2.1 Materials

The materials used as test substrates in this study were collected for a previous study of GEM flux and are described in detail in Miller and Gustin (2013) and Miller et al. (submitted, this thesis). Briefly, all materials were collected from four active industrial-scale open pit gold mines in central Nevada, USA. The mining materials fall into three broad categories, in which specific rock type, mineral composition, and Hg concentration may vary widely, even from the same mine location. The categories include low Hg concentration "cap" material derived from non-

mineralized alluvium and/or hard-rock overburden, moderate to high Hg concentration "leach" material collected from low grade ores that undergo passive extraction by cyanide leach solution, and high Hg concentration "tailings" material composed of the waste rock slurry created by mechanical milling and thermochemical processing of high grade ores.

The mining materials were sorted into replicate trays (50 x 50 x 7 cm) and stored in the University of Nevada Reno Agricultural Experiment Station greenhouses for controlled experimental measurements. Total Hg in the substrates was determined in detail by Miller and Gustin (2013) and again by Miller et al. (submitted, this thesis) using a Milestone® DMA- 80 Direct Mercury Analyzer (EPA Method 7473). The most recent substrate Hg values from Miller et al. (submitted, this thesis) are shown in Table 6.1.

An additional substrate parameter measured in this study was Hg speciation, determined by solid phase thermal desorption (SPTD) analysis using the method of Biester et al. (2000; 1999; 2002; Biester and Scholz, 1997). Individual Hg compounds volatilize and/or decompose at different temperatures, so known reference Hg compounds are used to generate reference thermal desorption profiles (Appendix D, SI Fig. 6.1). The desorption profiles generated from sample materials are compared to the reference profiles to determine the speciation of Hg in the sample, using peak desorption temperature range as the primary differentiator between Hg species. The SPTD method is a somewhat indirect and qualitative determination of Hg speciation, as the fraction of total Hg released over a temperature range is used to infer the presence of a specific Hg compound.

6.2.2 Measurements

Reactive mercury flux was measured using the modified GEM flux method described by Miller et al. (submitted, this thesis), based on the DFC flux methods of Eckley et al. (2010; 2011a; 2011b) and Miller et al. (2011).

The foundation of the modified RM/GEM flux system is a Tekran® 2537A Ambient Air Mercury Analyzer operated in conjunction with a cylindrical Teflon DFC (footprint 0.036 m^2, internal volume 2.0 Liters, Fig. 6.1). A thorough description of the chambers can be found in previous studies (Eckley et al., 2010; Eckley et al., 2011a; Miller et al., 2011). Briefly, air is pulled into the chamber through inlet holes (24, 1 cm dia.) around the perimeter, and air is pulled out of the chamber through a single outlet line (0.625 cm O.D. PTFE tubing) at the top-center. The concentration of the inlet air is sampled through equivalent tubing at the height of the chamber inlets. Sample flow (1.0 Lpm) is cycled between the chamber inlet and outlet lines in 10 min intervals (two 5 min samples on each line) using a Tekran® Automated Dual Switching (TADS) unit. An external flush pump and MFC maintains constant flow through the sample line not actively pulling to the 2537A. GEM in each 5 min sample volume pulled to the 2537A analyzer is quantified via pre-concentration on gold traps followed by thermal desorption (500 °C) and cold vapor atomic fluorescence spectrometry (CVAFS). The difference in Hg concentration between the outlet and inlet air is referred to as ΔC (C_o - C_i). Flux is calculated using Eq. 1:

$$F = Q * (C_o - C_i)/A \quad (1)$$

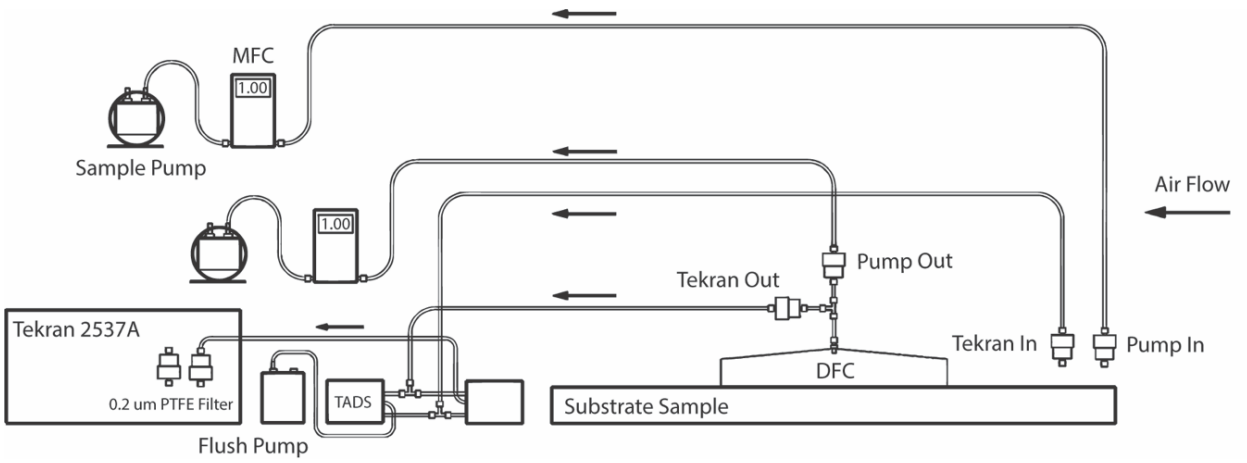

Figure 6.1 *Diagram of one RM filter-based flux system adapted from Miller et al. (submitted, this thesis). Flux systems were deployed in exact duplicate as Systems A and B. Sample line designations indicate whether a chamber inlet ("In") or outlet ("Out"), and the source of sample flow control ("Tekran" or "Pump").*

in which F is the net Hg flux (ng m^{-2} h^{-1}), Q represents flow rate through the chamber (m^3 h^{-1}), A is the area of the chamber footprint over the substrate (m^2), C_o is the mean concentration of two consecutive 5 min outlet air samples (ng m^{-3}), and C_i is the mean concentration of inlet air in the two 5 min samples bracketing the C_o samples. A positive or negative ΔC indicates the direction of flux, i.e. emission or deposition.

Modifying the system to include RM flux was achieved by fitting the DFC inlet and outlet sample lines with polyethersulfone CEM filters (pore size 0.8 μm, Mustang® S, Pall Corporation). Two CEM filters were deployed in-series on each sample line using 2-stage 47 mm PFA filter assemblies (Savillex®). In the 2-stage deployment, the upstream CEM acts as the primary collection filter, while the secondary downstream CEM captures breakthrough Hg. The CEM material has been demonstrated to have negligible GEM uptake at high concentrations (Miller et al., submitted, this thesis), and good selectivity for RM compounds (Huang and Gustin, 2015; Huang et al., 2013; Lyman et al., 2016). As the CEM filters scrub RM with high efficiency, all Hg measured downstream of the filters on the Tekran® 2537A was in GEM form.

The entire RM flux system was duplicated using a second Tekran® 2537A, DFC, and external sample pumps and MFCs (duplicate systems were designated System A and B). The 2537A analyzers were coordinated to the same method parameters and were calibrated from their built-in internal Hg vapor sources before and periodically throughout the study. The internal source calibrations were verified by an external Hg vapor source (Tekran® 2505) via manual gas-tight syringe injections (25 μL, Hamilton®). The recoveries on System A were 98.6 ± 8.5% (n = 10), and on System B 94.7 ± 7.0% (n =10). Each 2537A was operated with a 0.2 μm PTFE particulate filter at the rear sample inlet bulkhead.

An additional replicate RM flux measurement was also made simultaneously within each system by using external sample pumps and mass flow controllers set to match the 2537A sample flow rate (1.0 Lpm, Fig. 6.1). The external pump outlet sample line pulled from the main DFC outlet line via a T-joint. In this study, the duplicate flux sample lines were used to deploy nylon membrane filters (0.2 μm polyamide, Sartorius®), which have been used in previous studies to attempt speciated atmospheric RM measurements (Gustin et al., 2016; Huang and Gustin, 2015; Huang et al., 2017; Huang et al., 2013). Two filter assemblies (one CEM, one nylon) were also suspended above the flux systems at a height of 2 m to measure background RM concentrations in the greenhouse, sampling at the same flow rate using an equivalent external pump and MFC setup. Nylon filter data was ultimately excluded due to very low collection efficiencies and possible GEM collection artifacts.

With two RM flux sample lines per chamber, total flow through the DFC was 2.0 Lpm, with a resulting total turn-over-time (TOT) of 1.0 min. At this flow rate, flow velocity through the chamber is laminar with no turbulent eddy formation (Eckley et al., 2010). As such, particle

entrainment from the substrate surfaces is expected to be low, especially for particle sizes greater than the CEM filter pore size of 0.8 μm.

6.2.3 Experimental manipulations

The replicate A and B flux systems were used to measure flux from a dry and wet material of the same type simultaneously. All watering was done on System B while System A served as the dry control measurement. Volumetric soil moisture (VSM) was measured with a dielectric VSM probe (ECH_2O™ EC-5) inserted horizontally through the side of the trays at mid depth in the substrate material. Distilled water (< 1 ng L^{-1} total Hg) was slowly added to the materials using a misting applicator, to a VSM of 20 - 25% as measured in real time by the soil moisture probe. The DFC was carefully placed on the material after watering was complete.

6.2.4 Analysis

Following flux measurement, CEM filters were collected into sterile 50 mL polypropylene centrifuge tubes, and frozen at -20 °C prior to analysis, which was completed within a maximum of 14 days from collection. Filters were analyzed for total Hg on a Tekran® 2600 system, by aqueous digestion and cold vapor atomic fluorescence spectrometry (CVAFS, EPA Method 1631, Rev. E). Using this technique, total Hg on the CEM filters is operationally equivalent to total RM. The mass of Hg on an unused CEM filter (median = 85 pg, n = 17) was determined from blank filters collected with every deployment on the flux system, and the median blank value was subtracted from all sample values. Filter breakthrough was defined as the amount of Hg on the secondary filter as a percent of the total Hg collected on both filters (after blank correction), and overall median breakthrough was relatively low (6.0%, n = 95). The calculation of RM concentration was achieved by combining the blank-corrected primary and secondary

filters into a total Hg mass per sample line and dividing by the sample volume through the line. The concentration difference between the inlet and outlet lines provided a ΔC_{RM}, and RM flux (pg m^{-2} h^{-1}) was calculated with Eq. 1 using the ΔC_{RM} values, the flow rate (2.0 ± 0.01 Lpm) and the chamber footprint (0.036 m^2).

The flux detection limit was determined after the method of Miller et al. (submitted, this thesis) in which the MFC flow precision and the 95% confidence interval of the median blank filter Hg mass is used to calculate the minimum statistically resolvable ΔC_{RM} between the chamber inlet and chamber outlet CEM filters. For all blank CEM filters collected over the course of these measurements, the median blank was 85 pg (n = 17) and the 95% confidence interval was 64-100 pg. The minimum detectable 24 h RM concentration was therefore ~11 pg m^{-3} (~16 pg per 1.44 m^3 sample volume), and the minimum detectable 24 h ΔC_{RM} was 27.5 pg m^{-3} when converted to a 24 h concentration and including ± 3 pg m^{-3} for uncertainty attributable to flow precision. All measurements except two were above the minimum ΔC_{RM} (Fig. 6.2b).

Chamber blanks were determined for both Teflon DFCs (Chamber A and Chamber B) by measuring flux over a clean (24 h in 10% nitric acid bath) Teflon sheet. Chamber blank flux rates were measured immediately before and then between substrate types (i.e. after cap, after leach, after tailings). All chamber blank fluxes had ΔC_{RM} values above the detection limit (Fig. 6.2a). The mean Chamber A blank flux was 190 ± 820 pg m^{-2} h^{-1} for GEM, and 1660 ± 700 pg m^{-2} h^{-1} for RM (Fig. 6.3a). The mean Chamber B blank flux was -1500 ± 1010 pg m^{-2} h^{-1} for GEM, and -850 ± 1140 pg m^{-2} h^{-1} for RM (Fig. 6.3b). All measured fluxes were chamber blank corrected.

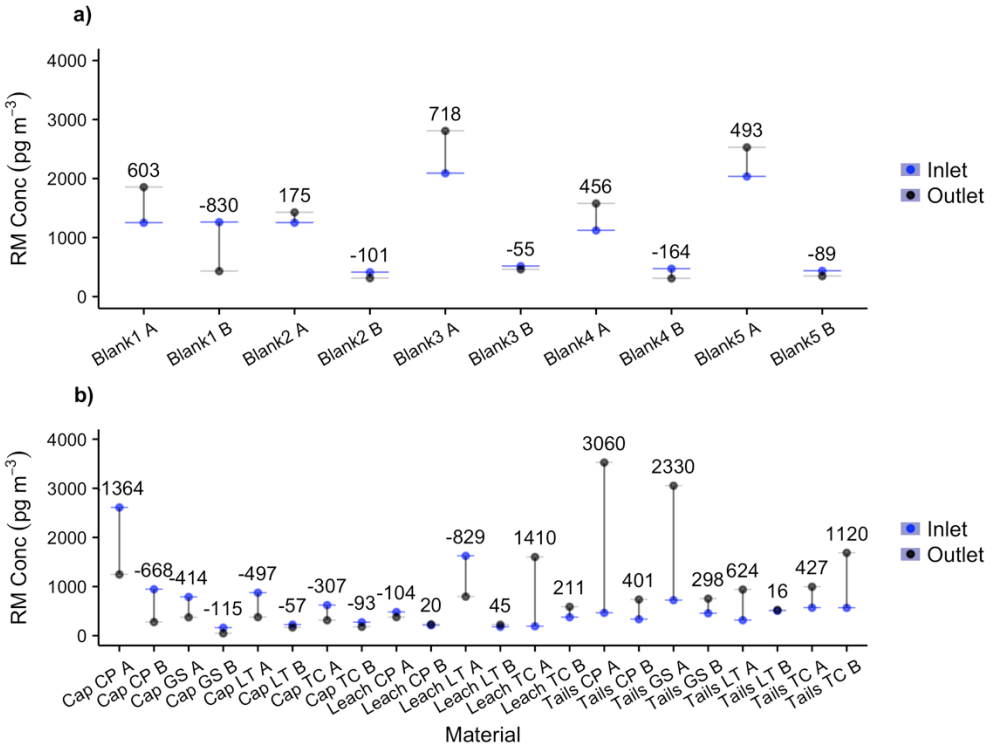

Figure 6.2 *ΔC_{RM} for a) chamber blank fluxes and b) sample fluxes.*

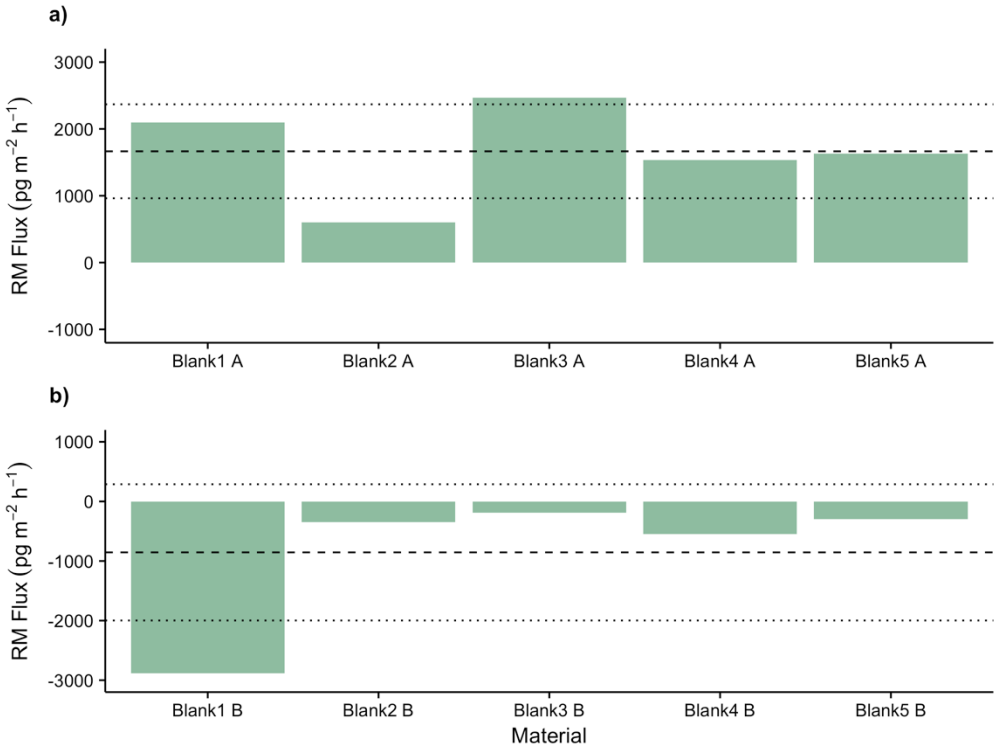

Figure 6.3 *Chamber blank fluxes measured over clean Teflon sheet, for a) System A (mean 1660 ± 700 pg m^{-2} h^{-1}) and b) System B (-850 ± 1140 pg m^{-2} h^{-1}).*

6.3 Results

6.3.1 Greenhouse conditions

The full sequence of mining substrate materials was measured in the summer season between June – August, 2016 (Table 6.1). Conditions in the greenhouse space were relatively uniform over this time period. Mean temperature was 25.5 ± 5.0 °C, and mean RH was 22.7 ± 10.5%. Daily incident solar radiation was attenuated by the greenhouse glass, with mean hourly peak solar radiation of ~400 W m^{-2} between 12:00 – 13:00, falling off rapidly in afternoon shade from structures to the immediate west. Wetted materials were on average 2.2 ± 1.0 °C cooler than equivalent dry substrates due to evaporative heat loss. Mean ambient RM concentrations in the greenhouse air were 180 ± 60 pg m^{-3} based on the background 24 h CEM filter deployments (n = 14), well above the MDL of 11 pg m^{-3} (Fig. 6.4). These were relatively high background RM concentrations compared to previous measurements (64 ± 58 pg m^{-3}) described in Chapter 5.

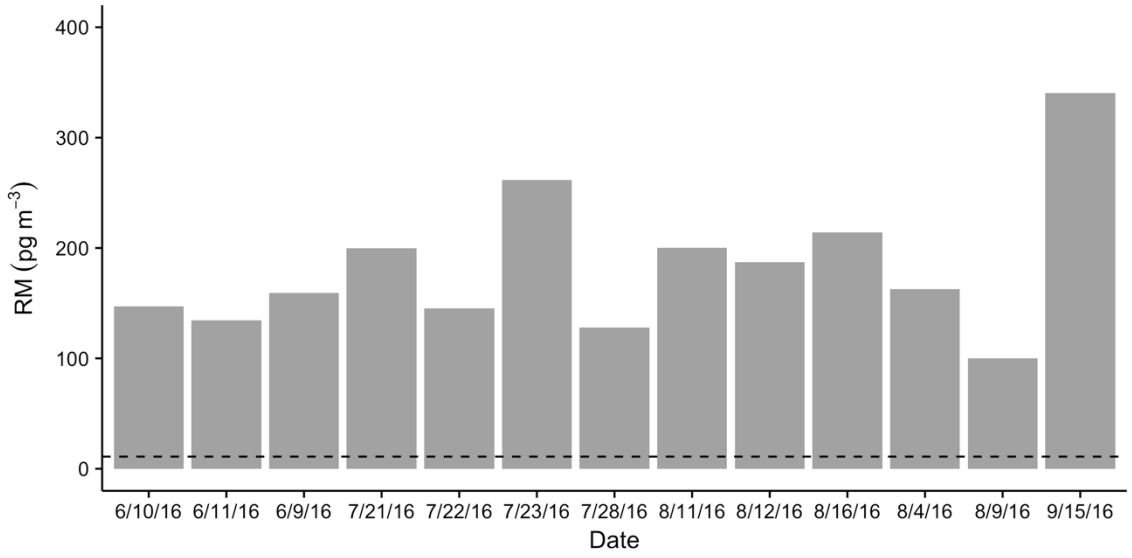

Figure 6.4 *Ambient RM concentrations in greenhouse air at 2 m height. Dashed line is minimum detectable RM concentration.*

Table I. Summary of materials, substrate concentrations, and flux measurements.

	Material	Sample	Date	Substrate Conc ($ng\ g^{-1}$)	GEM Flux ($ng\ m^{-2}\ hr^{-1}$)	RM Flux ($ng\ m^{-2}\ hr^{-1}$)	RM Inlet ($ng\ m^{-3}$)	RM v_d ($cm\ s^{-1}$)	Ambient RM ($ng\ m^{-3}$)	Temp (°C)	RH (%)	Solar ($W\ m^{-2}$)	Soil Temp (°C)	Soil Moisture (%)
Summer 2016	Tailings	TCTA 1	6/9/16		232	0.0	0.57	-	0.16	24.7	23.4	76.1	8.0	0.0
		TCTB 1			1938	4.7	0.57	-					4.7	29.4
		TCTA 2	6/10/16	35750	223	0.0	0.64	-	0.15	23.4	26.8	102.0	7.8	0.0
		TCTB 2			2980	12.8	2.10	-					5.5	24.9
		TCTA 3	6/11/16		283	0.9	0.37	-	0.13	21.6	25.6	102.6	7.2	0.0
		TCTB 3			3948	37.1	1.85	-					6.0	19.7
	Cap	TCCA	7/21/16	230	4	-2.7	0.62	0.12	0.20	24.9	21.6	96.7	6.8	1.6
		TCCB			78	0.0	0.27	-					6.0	11.2
		LTCA	7/22/16	150	3	-3.4	0.87	0.11	0.15	25.6	18.3	95.9	8.4	0.0
		LTCB			237	0.0	0.23	-					7.4	6.8
		CPCA	7/23/16	120	1	-6.3	2.61	0.07	0.26	30.2	8.9	na	12.4	0.1
		CPCB			192	-1.4	0.95	0.04					8.2	22.2
		GSCA	7/28/16	200	20	-3.1	0.79	0.11	0.13	29.6	19.2	91.7	10.1	0.0
		GSCB			44	0.0	0.16	-					8.9	11.1
	Leach	TCLA	8/4/16	11900		3.2	0.19	-	0.16	27.0	19.3	86.9	9.0	0.0
		TCLB				1.6	0.38	-					6.5	21.3
		LTLA	9/15/2016*	600	4	-4.5	1.62	0.08	0.34	24.0	19.6	94.5	7.4	0.0
		LTLB			234	0.0	0.18	-					5.6	6.8
		CPLA	8/9/16	310	1	-2.0	0.48	0.12	0.10	28.2	12.5	103.1	9.7	0.0
		CPLB			760	0.0	0.21	-					8.1	8.3
	Tailings	LTTA	8/11/16	11050	309	0.0	0.31	-	0.20	26.7	24.6	78.2	8.7	0.0
		LTTB			2550	0.0	0.51	-					6.0	9.5
		CPTA	8/12/16	21150	1023	8.6	0.46	-	0.19	24.9	25.5	92.3	8.0	0.0
		CPTB			889	0.0	0.33	-					5.1	16.3
		GSTA	8/16/16	6950	318	6.4	0.72	-	0.21	27.0	24.0	80.1	8.7	0.0
		GSTB			1728	1.9	0.45	-					5.8	11.2

* Measurement Redone

Table 6.1 Summary of GEM and RM fluxes measured from wet and dry mining materials in summer 2016. Material B is always the wetted substrate. Ambient RM is the concentration measured at 2 m height in the greenhouse air above the test substrates.

6.3.2 Substrate Hg speciation

Solid phase thermal desorption speciation revealed multiple mineral forms of Hg in the mining substrates, but no elemental Hg^0 (Fig. 6.5-6.7). In general, the cap materials showed broad Hg desorption profiles indicative of several Hg species, with relatively large proportions of an oxidized Hg species such as $HgSO_4$ (Fig. 6.5). This may be indicative of Hg in the cap materials being derived primarily from atmospheric deposition of oxidized Hg compounds, especially considering the presence of large thermal point source emissions on the mine sites. An exception was the LT cap material, with only meta-HgS present at a peak desorption temperature of 255 °C. Meta-HgS is the less stable polymorph of HgS.

The CP and TC oxidized leach materials were dominated by an oxidized Hg species (likely $HgSO_4$) with peak desorption temperatures around 370 and 405 °C, respectively, and only a secondary amount of meta-HgS and possibly some HgS desorbing in the peak range 240-270 °C (Fig 6.6a and 6.6c). In contrast again, the LT leach material contained a preponderance of meta-HgS at peak desorption temperatures between 180-255 °C, though an oxidized Hg compound was still present to a minor degree at 400-500 °C (Fig. 6.6b).

The GS, CP, and TC tailings materials were composed of meta-HgS and HgS with peak desorption in the range 265-340 °C (Fig. 6.7). LT tailings exhibited a peak desorption temperature of 210 °C indicating primarily meta-HgS. The tailings materials generally showed a trailing section and subsidiary peaks between 350 to 450 or 500 °C on the SPTD profiles, indicating a subordinate proportion of an oxidized Hg compound(s). While dominated by HgS, the high overall Hg concentration of the tailings materials means even subordinate amounts of an oxidized Hg compound would be present at a higher absolute quantity relative to lower Hg concentration materials.

The dominance of mercuric sulfides in the tailings materials is consistent with typical ore processing operations at the mine mill facilities. High grade sulfide ore (the dominant "refractory" process ores at these mines) is typically ball-milled and autoclaved at lowered pH, elevated pressure, and temperatures of 165-175 °C (Fraser et al., 1991). These temperatures are sufficient to vaporize free and bound Hg^0, but are insufficient to break down HgS, which does not thermally decompose until temperatures of 265-345 °C (Leckey and Nulf, 1994), with a peak at ~310 °C (Wu et al., 2011). Mercury oxides would generally not be expected in the reduced ore types that typically receive extensive mill processing to extract gold. Thus, mill processes can be expected to preferentially concentrate mercuric sulfides in tailings materials, with possible secondary fractions of oxidized Hg resulting from the mill process itself (which is intended to be a highly efficient thermochemical oxidation process).

The lower peak temperature meta-HgS identified in all of the LT mine materials was likely due to differences in both ore mineralogy and mine operation. The LT mine primarily exploited an oxidized gold ore deposit, mostly from low grade ores suitable only for heap leach extraction, with limited on-site mill processes. Active mining operations ceased at LT in 2006, so that at the time of collection in 2010, materials were already relatively old. The other mine sites used in this study were still operating at the time of material collection, with heap leaching and active on-site ore processing from a variety of oxidized, sulfide, and carbonaceous ores.

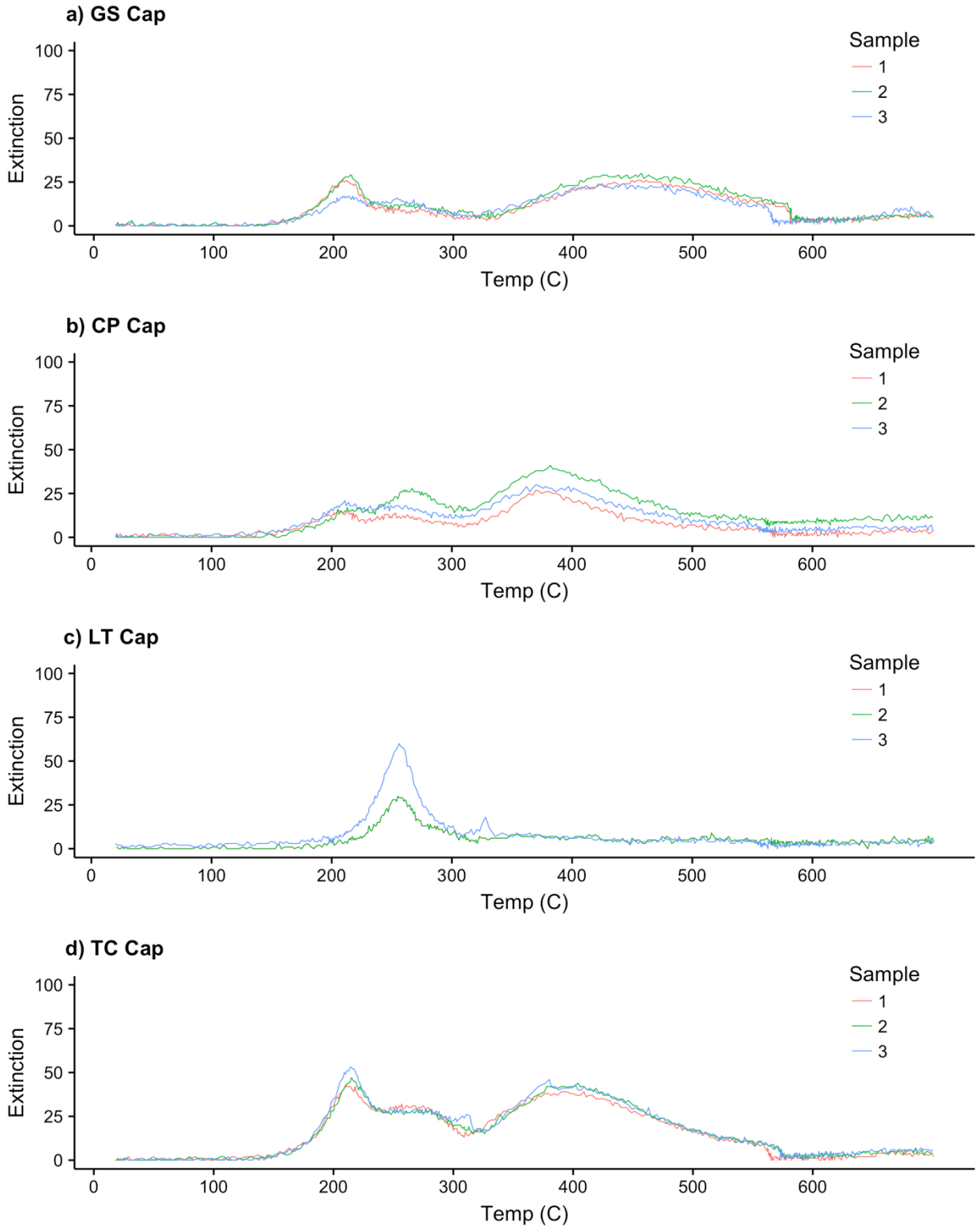

Figure 6.5 *Solid phase thermal desorption profiles for low Hg concentration cap materials: a) CP cap, b) GS cap, c) LT cap, and d) TC cap.*

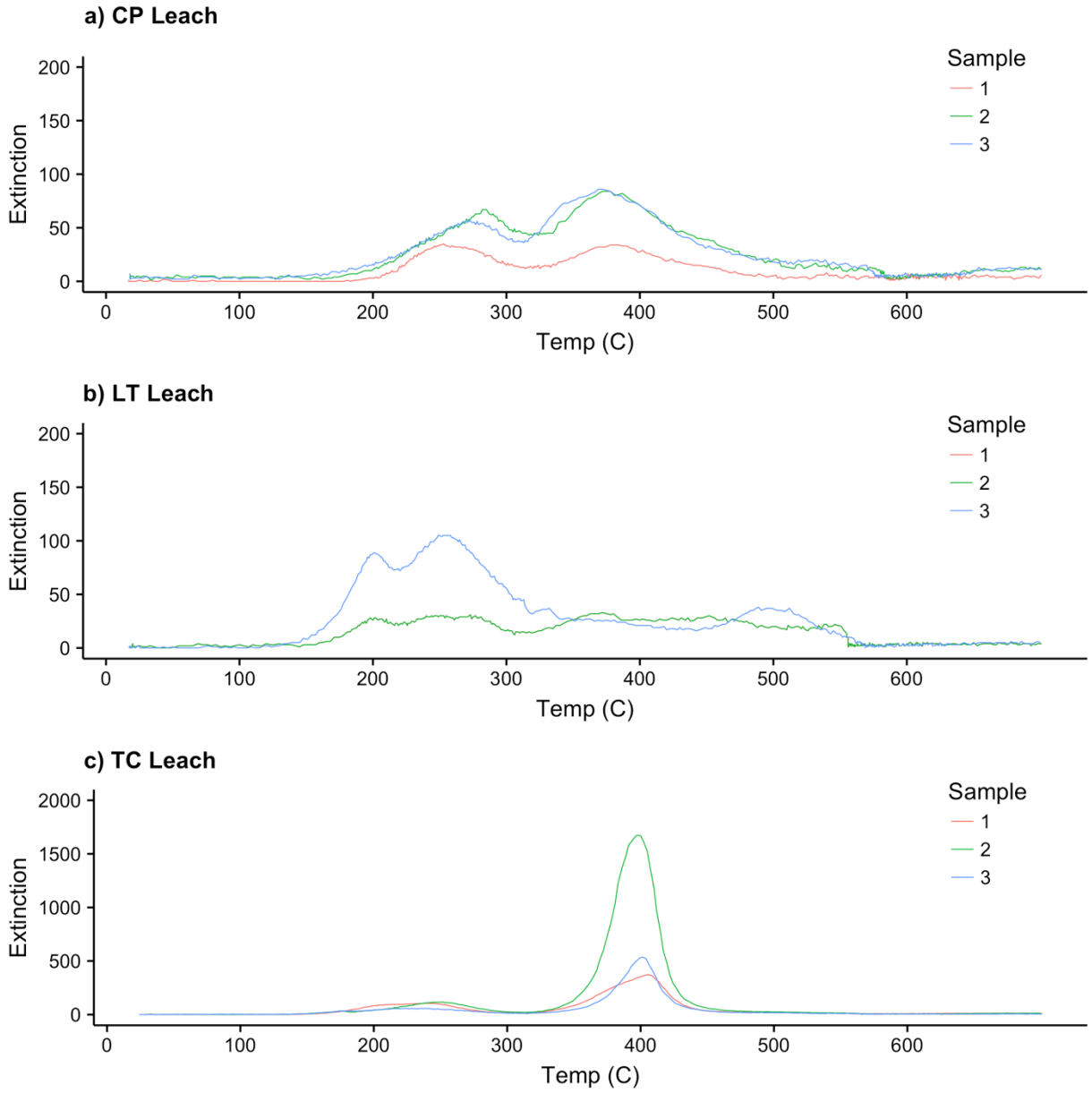

Figure 6.6 *Solid phase thermal desorption profiles for intermediate Hg concentration leach materials: a) CP leach, b) LT leach, and c) TC leach.*

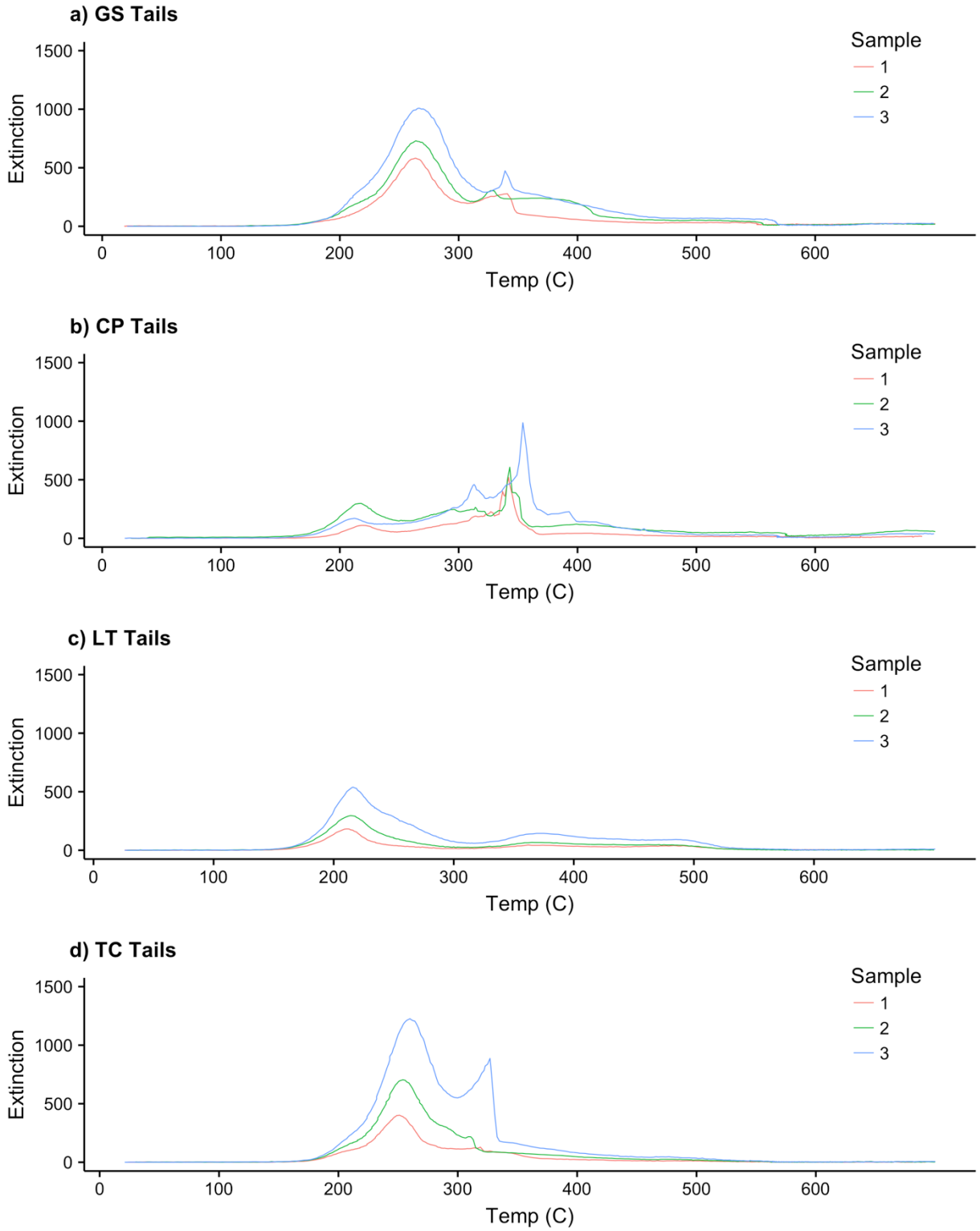

Figure 6.7 *Solid phase thermal desorption profiles for high Hg concentration tailings materials: a) GS Tails, b) CP tails, c) LT tails, and d) TC tails.*

6.3.3 Gaseous elemental mercury flux

Wet materials showed a larger positive GEM flux in comparison to small or no flux from the same dry material (Fig. 6.8). In general, higher GEM fluxes were measured from higher concentration materials, with the tailings materials in particular showing GEM fluxes in the thousands of ng m^{-2} h^{-1} (Table 6.1). These results agree well with expectations based on previous studies using the same or similar materials (Eckley et al., 2011a; Eckley et al., 2011b; Miller and Gustin, 2013; Miller and Gustin, 2015; Miller et al., 2011). Multiple linear regression indicated that four measured variables (substrate Hg concentration, solar radiation, RH, and VSM) explained a majority of the variation in observed GEM fluxes from wet materials ($R^2 = 0.89$, $p = 0.0232$). Relatively humidity was a non-significant variable, but its removal from the MLR model was not supported ($F = 7.953$, $p = 0.0346$). These results are similar to those observed in Eckley et al. (2011b) for similar materials.

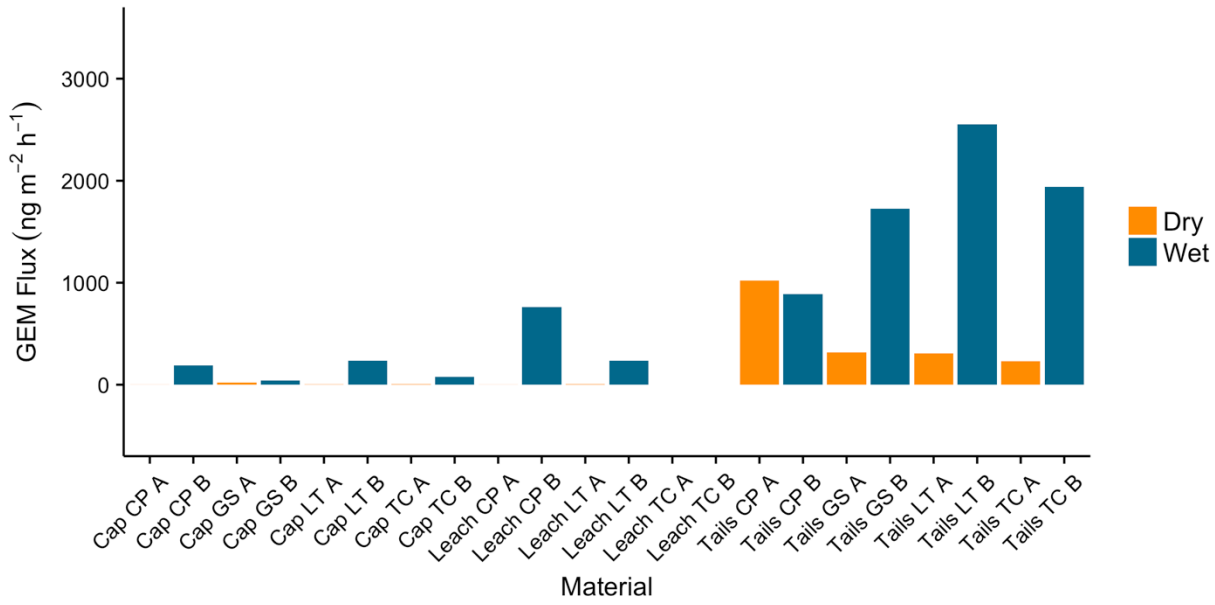

Figure 6.8 *GEM fluxes from all wet and dry materials.*

6.3.4 Reactive mercury flux

Distinct differences in RM flux were observed between substrates with different Hg concentration and between wet and dry substrates (Fig. 6.9). Materials with a substrate Hg concentration ≤ 600 ng g^{-1} experienced net RM deposition when dry, and no RM flux when wet. This was true for all of the low Hg background cap materials (120-230 ng g^{-1}) and the two leach materials with lower Hg concentration (CP leach 310 ng g^{-1}, and LT leach 600 ng g^{-1}). RM deposition to dry materials showed V_d values of 0.10 ± 0.02 cm s^{-1} (n = 8), while the one resolvable measurement of RM deposition to a wet material (Cap CP B) had a V_d of 0.04 cm s^{-1}.

Materials with substrate Hg concentrations > 600 ng g^{-1} generally showed positive RM emission from both wet and dry materials, except for one tailings material (LT tailings) from which a measurable RM flux was not resolvable (discussed below). In general, RM emission was greater from a high Hg material when dry versus the same material when wetted, indicating some suppression of RM flux due substrate moisture content, though the materials were not saturated. Increasing moisture within a substrate is thought to facilitate photochemical reduction to Hg^0 (Gustin and Stamenkovic, 2005), and possibly this occurs to such an extent that the immediate availability of oxidized Hg molecules for direct volatilization is reduced. Increasing moisture content also likely facilitates dissolution of Hg^{2+} compounds into the aqueous phase where they are unavailable for volatilization. As noted, wetted materials were substantially cooler due to evaporation, and these lower temperatures may have contributed to the lower observed RM evasion.

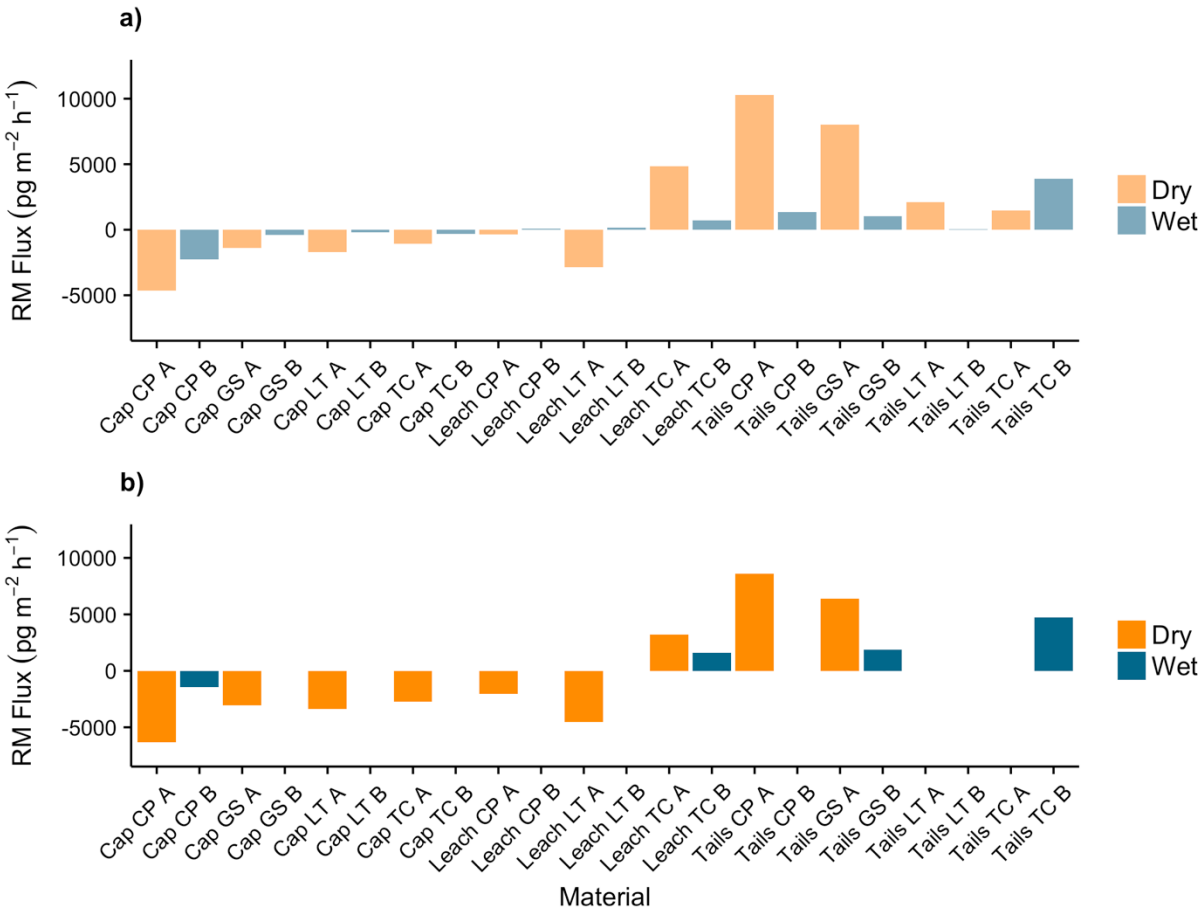

Figure 6.9 *RM flux from wet (blue bar) and dry (orange bar) sample substrates for a) no chamber blank corrections and b) with chamber blank corrections.*

The LT tailings had a relatively high total Hg concentration (11000 ng g^{-1}) and clear high GEM emissions of 300 and 2500 ng m^{-2} h^{-1} from the dry and wet material, respectively, and in this regard was very similar to the other tailings material. It is therefore uncertain why an RM flux was not resolvable. Based on the SPTD speciation determination, LT tailings was the only high Hg material composed dominantly of meta-HgS, with no HgS and a low proportion of oxidized Hg (Fig. 6.7b). Meta-HgS is more readily photo-reduced to Hg^0 versus HgS (Gustin et al., 2002), so a material that contains predominantly meta-HgS might be expected to have preferentially high GEM emission versus low or undetectable RM flux.

A notable exception to the pattern of higher RM emission from dry versus wet substrates was the TC tailings material (total Hg 36000 ng g^{-1}). This material was used in an extended test of wetting and RM flux, in which CEM filters were deployed every 24 h for 3 days, capturing GEM and RM flux as the material dried out (Fig. 6.10). Initial substrate wetting was to a VSM of ~ 32%, and this relatively high initial moisture content (compared to ~ 20-25% for other materials) seems to have suppressed both GEM and RM flux, both of which increased by a factor of 1.5-2 over each subsequent 24 h period as VSM decreased (Table 6.1, Fig. 6.10b-6.10c). A similar suppression of GEM flux from saturated soils has been previously observed, albeit using low Hg background soils (Briggs and Gustin, 2013; Gustin and Stamenkovic, 2005). GEM flux from the dry TC tailings material remained relatively steady over this time at 220-280 ng m^{-2} h^{-1}, while dry RM flux increased from a non-resolvable level to 900 pg m^{-2} h^{-1} in the third 24 h measurement, which may be related to declining background RM concentrations over the same period (Table 6.1). RM flux from the wet TC tailings reached very large concentrations (13000 and 37000 pg m^{-2} h^{-1}) in the second and third 24 h measurements, as VSM dropped below 25 and 20%, respectively. These high RM fluxes may be attributable mainly to the high total Hg concentration of the TC tailings material, as the Hg speciation was not unusual, composed primarily of meta-HgS and HgS.

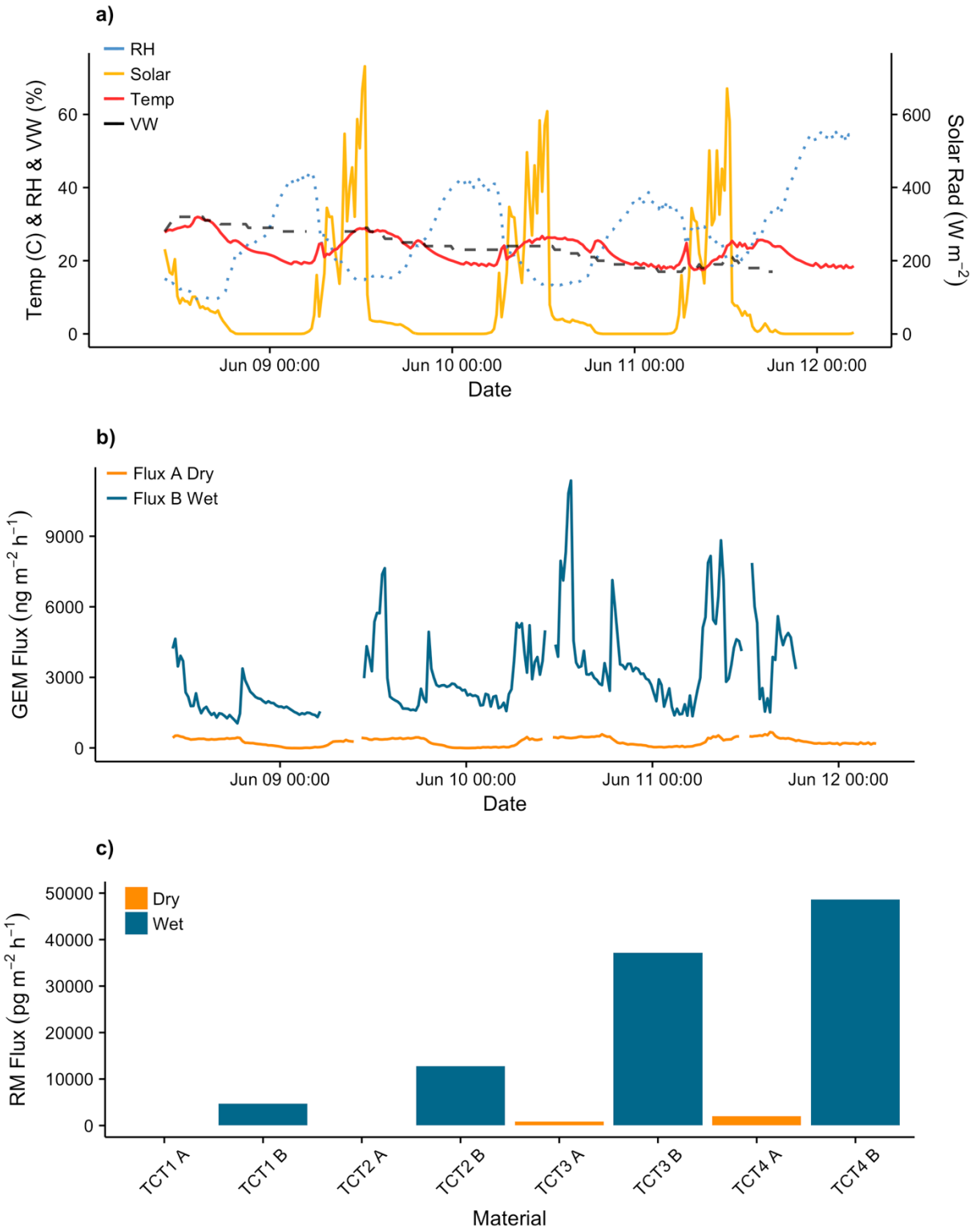

Figure 6.10 *Extended multi-day flux measurement from TC tailings material: a) ambient parameters, b) GEM flux, and c) RM flux.*

6.3.5 Reactive mercury breakthrough on cation exchange membranes

An unresolved question with the CEM filter method in general is what accounts for RM breakthrough form the primary to secondary filters, as breakthrough has been observed to range from zero up to 40% in different studies (Huang et al., 2017; Pierce and Gustin, 2017). The simultaneously deployment of dual CEM filters on multiple sample lines under different conditions allowed us to evaluate possible factors controlling RM breakthrough.

As stated, overall median RM breakthrough observed in this study was relative low (Fig. 6.11a), although some maximum values were in line with the highest values seen in previous studies. There was no significant difference in breakthrough rates between the inlet and outlet sample lines during flux measurements over blank, dry, or wet materials (p values > 0.1, Kruskall-Wallis test). However, breakthrough did vary as a function of material wetness. Specifically, median breakthrough for chamber blank flux measurements (4.3%, range 0-10.2%, n = 20) and fluxes measured over dry material (5.3%, range 0-13.5%, n = 28) were not statistically different (p = 0 .414, Kruskall-Wallis test), but breakthrough for fluxes over wet material (14.4%, range = 0-37.9%, n = 28) was significantly higher (Kruskall-Wallis test p = 0.0003). The median breakthrough from the background RM measurement filters was 9.1% (n = 19, range 0-18.4%), intermediate between the breakthrough rates observed from the dry and wet flux measurements.

There were also differences in RM breakthrough based on material (Fig. 6.11b). The lowest breakthrough rates were measured over low Hg concentration cap materials that generally experienced RM deposition. All of the highest breakthrough rates were observed during flux measurements over higher Hg concentration materials while wet, though not all of these materials had significant RM emissions (i.e. CP and LT tails). Interestingly, RM breakthrough

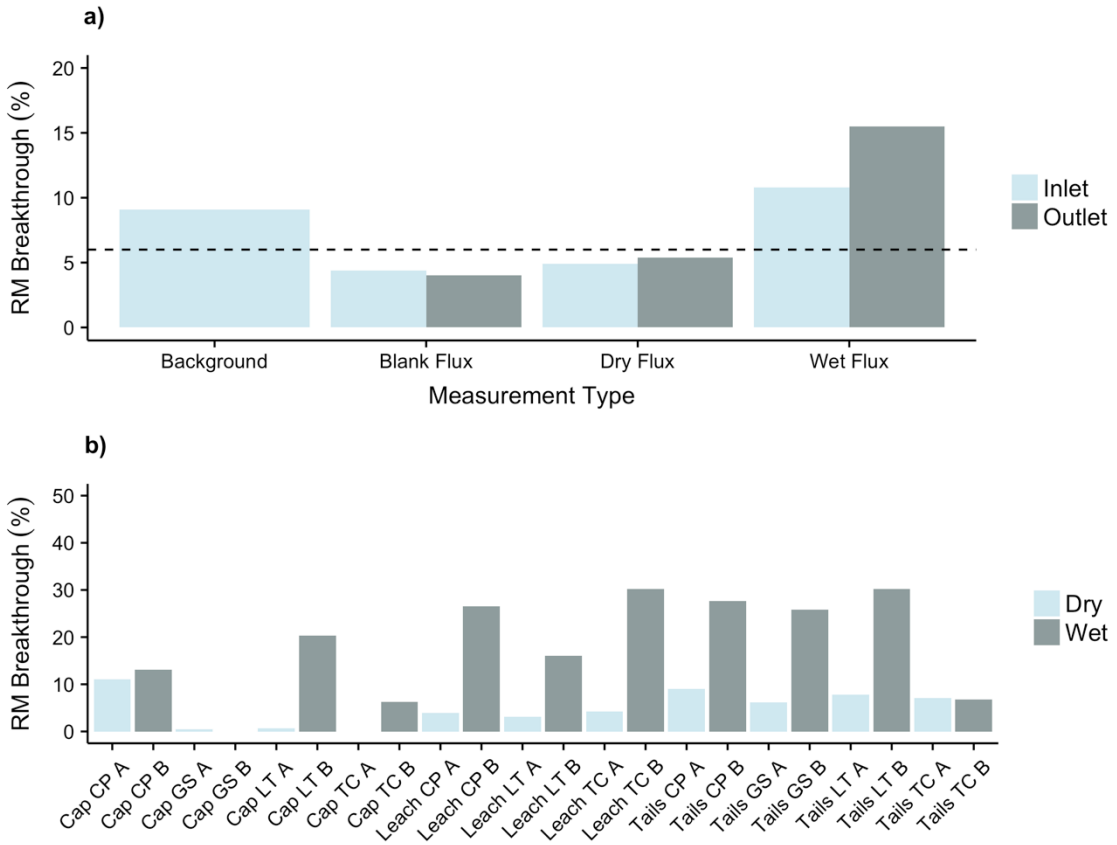

Figure 6.11 *Median RM breakthrough to secondary CEM filters for a) overall breakthrough by measurement type and sample line with overall median breakthrough (6.0%) represented by dashed line, and b) breakthrough by material type.*

was relatively low (median 5.6%, range 0-13.4%, n = 16) for the TC tailings flux measurements under both wet and dry conditions, even though this material had the highest RM emissions. This suggests that breakthrough is not simply a function of higher RM exposure on the primary CEM filter, a result also demonstrated by Miller et al. (submitted, this thesis) in controlled permeation tests on the CEM material using high concentrations of a representative gaseous RM compound ($HgBr_2$).

6.4 Conclusions

A range of GEM and RM fluxes were measured from mining-related materials of differing total Hg concentration (100-36000 ng g^{-1}) and Hg speciation (meta-HgS, HgS, $HgSO_4$), with definite differences in flux behavior between wet and dry substrates. It is important to re-iterate here that the determination of Hg speciation by SPTD is not an exact method, but only a relative indication of the fraction of Hg released over certain temperature ranges. Thus, the interpretation of substrate Hg speciation is somewhat indirect and qualitative, and results must be viewed in that light.

In general, RM deposited to low Hg concentration ($\leq$ 600 ng g^{-1}) substrates when dry (0-2% VSM), and RM flux was below detection from the same materials when wet (15-25% VSM). RM was emitted from higher Hg concentration (> 600 ng g^{-1}) substrates under both wet and dry conditions, though generally to a greater extent from dry materials, with some wet RM fluxes being below detection. In 10 out of 11 measurements, GEM was emitted from wet materials at a significantly enhanced rate relative to the same dry materials, as observed in previous studies.

Breakthrough of RM from the primary to secondary CEM filters was relatively low overall (median 6.0%) but ranged widely from 0 to 38% and was significantly higher during flux measurements over wet material (median 14.4%), especially for the higher Hg concentration substrates that also tended to show net RM emission. Breakthrough was also relatively higher (9.1%) for the CEM filters deployed to measure ambient RM concentrations. Though apparently unrelated to the magnitude of RM flux, the variable rates of RM breakthrough observed between different materials and between wet and dry versions of the same material clearly indicate that some factor or combination of factors is controlling how much RM escapes the primary CEM filter. Our results suggest that moisture plays an important role in the breakthrough mechanism.

Low Hg "cap" materials (120-230 ng g^{-1} total Hg), which of the mining-related substrates can be compared most closely to background soils, had proportionately large amounts of an oxidized Hg compound believed to be $HgSO_4$. This likely indicates a significant contribution from atmospheric deposition of RM, possibly from proximal large point sources on the active mine sites (thermal ore processing facilities, etc.). The exception was a cap material from an inactive mine location, where processing facilities were neither extensive nor continuous, and which therefore did not have a strong local atmospheric input but was instead composed entirely of a geogenic Hg mineral, meta-HgS.

Wetting of a high Hg tailings material to near saturation (32% VSM) resulted in an initial suppression of both GEM and RM flux, with both positively increasing over subsequent 24 h measurements. Suppression of GEM flux from saturated soils has been observed in previous studies (Briggs and Gustin, 2013; Gustin and Stamenkovic, 2005). Gustin and Stamenkovic (2005) suggested that increasing soil water content leads to dissolution of both Hg^0 and Hg^{2+} compounds, which are subsequently transported to the surface as soil pore water evaporates. Dissolution of Hg^{2+} compounds would explain the initial suppression of emissions, and the following mass transfer of Hg^{2+} to the substrate surface may explain the increasing levels of RM flux observed as the TC tailings material dried out.

For high Hg concentration leach and tailings materials that showed a detectable RM emission, total RM emissions could be relatively large. This was especially true for the TC tailings material, for which RM flux approached 40000 pg m^{-2} h^{-1} under wet conditions. This data suggests that active tailings impoundments could constitute large local sources of atmospheric RM, especially as such surfaces undergo repeated wetting and drying as new tailings are added.

Acknowledgements

The authors would like to acknowledge funding from Macquarie University iMQRES 2015148, National Science Foundation Grant 629679, Barrick Gold Corp and Newmont Mining Corp for donating substrate materials, and Dr. Ashley Pierce for invaluable assistance in preparing this manuscript.

References

Amos HM, Sonke JE, Obrist D, Robins N, Hagan N, Horowitz HM, et al. Observational and Modeling Constraints on Global Anthropogenic Enrichment of Mercury. Environmental Science & Technology 2015; 49: 4036-4047.

Biester H, Gosar M, Covelli S. Mercury speciation in sediments affected by dumped mining residues in the drainage area of the Idrija mercury mine, Slovenia. Environmental Science & Technology 2000; 34: 3330-3336.

Biester H, Gosar M, Muller G. Mercury speciation in tailings of the Idrija mercury mine. Journal of Geochemical Exploration 1999; 65: 195-204.

Biester H, Muller G, Scholer H. Binding and mobility of mercury in soils contaminated by emissions from chlor-alkali plants. Science of the Total Environment 2002; 284: 191-203.

Biester H, Scholz C. Determination of mercury binding forms in contaminated soils: Mercury pyrolysis versus sequential extractions. Environmental Science & Technology 1997; 31: 233-239.

Briggs C, Gustin M. Building upon the Conceptual Model for Soil Mercury Flux: Evidence of a Link Between Moisture Evaporation and Hg Evasion. Water Air and Soil Pollution 2013; 224.

Eckley CS, Gustin M, Lin CJ, Li X, Miller MB. The influence of dynamic chamber design and operating parameters on calculated surface-to-air mercury fluxes. Atmospheric Environment 2010; 44: 194-203.

Eckley CS, Gustin M, Marsik F, Miller MB. Measurement of surface mercury fluxes at active industrial gold mines in Nevada (USA). Science of the Total Environment 2011a; 409: 514-522.

Eckley CS, Gustin M, Miller MB, Marsik F. Scaling Non-Point-Source Mercury Emissions from Two Active Industrial Gold Mines: Influential Variables and Annual Emission Estimates. Environmental Science & Technology 2011b; 45: 392-399.

Eckley CS, Tate MT, Lin C-J, Gustin M, Dent S, Eagles-Smith C, et al. Surface-air mercury fluxes across Western North America: A synthesis of spatial trends and controlling variables. Science of The Total Environment 2016; 568: 651-665.

Ericksen JA, Gustin MS, Xin M, Weisberg PJ, Fernandez GCJ. Air–soil exchange of mercury from background soils in the United States. Science of The Total Environment 2006; 366: 851-863.

Fraser KS, Walton RH, Wells JA. Processing of refractory gold ores. Minerals Engineering 1991; 4: 1029-1041.

Garcia-Sanchez A, Contreras F, Adams M, Santos F. Atmospheric mercury emissions from polluted gold mining areas (Venezuela). Environmental Geochemistry and Health 2006; 28: 529-540.

Gustin MS, Amos HM, Huang J, Miller MB, Heidecorn K. Measuring and modeling mercury in the atmosphere: a critical review. Atmos. Chem. Phys. 2015; 15: 5697-5713.

Gustin MS, Biester H, Kim CS. Investigation of the light-enhanced emission of mercury from naturally enriched substrates. Atmospheric Environment 2002; 36: 3241-3254.

Gustin MS, Pierce AM, Huang J, Miller MB, Holmes HA, Loria-Salazar SM. Evidence for Different Reactive Hg Sources and Chemical Compounds at Adjacent Valley and High Elevation Locations. Environmental Science & Technology 2016; 50: 12225-12231.

Gustin MS, Stamenkovic J. Effect of Watering and Soil Moisture on Mercury Emissions from Soils. Biogeochemistry 2005; 76: 215-232.

Gustin SM, Coolbaugh M, Engle M, Fitzgerald B, Keislar R, Lindberg S, et al. Atmospheric mercury emissions from mine wastes and surrounding geologically enriched terrains. Environmental Geology 2003; 43: 339-351.

Hartman JS, Weisberg PJ, Pillai R, Ericksen JA, Kuiken T, Lindberg SE, et al. Application of a Rule-Based Model to Estimate Mercury Exchange for Three Background Biomes in the Continental United States. Environmental Science & Technology 2009; 43: 4989-4994.

Huang J, Gustin MS. Uncertainties of Gaseous Oxidized Mercury Measurements Using KCl-Coated Denuders, Cation-Exchange Membranes, and Nylon Membranes: Humidity Influences. Environmental Science & Technology 2015; 49: 6102-6108.

Huang J, Miller MB, Edgerton E, Sexauer Gustin M. Deciphering potential chemical compounds of gaseous oxidized mercury in Florida, USA. Atmos. Chem. Phys. 2017; 17: 1689-1698.

Huang J, Miller MB, Weiss-Penzias P, Gustin MS. Comparison of Gaseous Oxidized Hg Measured by KCl-Coated Denuders, and Nylon and Cation Exchange Membranes. Environmental Science & Technology 2013; 47: 7307-7316.

Jambor J, Nordstrom D, Alpers C. Metal-sulfate Salts from Sulfide Mineral Oxidation. Reviews in Mineralogy and Geochemistry 2000; 40: 303-350.

Leckey JH, Nulf LE. Thermal decomposition of mercuric sulfide, United States, 1994.

Lindberg S, Bullock R, Ebinghaus R, Engstrom D, Feng X, Fitzgerald W, et al. A synthesis of progress and uncertainties in attributing the sources of mercury in deposition. Ambio 2007; 36: 19-32.

Lyman S, Jones C, O'Neil T, Allen T, Miller M, Gustin MS, et al. Automated Calibration of Atmospheric Oxidized Mercury Measurements. Environmental Science & Technology 2016; 50: 12921-12927.

Miller MB, Gustin MS. Testing and modeling the influence of reclamation and control methods for reducing nonpoint mercury emissions associated with industrial open pit gold mines. Journal of the Air & Waste Management Association 2013; 63: 681-693.

Miller MB, Gustin MS. Gas-exchange chamber analysis of elemental mercury deposition/emission to alluvium, ore, and mine tailings. Chemosphere 2015; 131: 209-216.

Miller MB, Gustin MS, Eckley CS. Measurement and scaling of air-surface mercury exchange from substrates in the vicinity of two Nevada gold mines. Science of the Total Environment 2011; 409: 3879-3886.

Muntean JL, Cline JS, Simon AC, Longo AA. Magmatic–hydrothermal origin of Nevada's Carlin-type gold deposits. Nature Geoscience 2011; 4: 122.

Obrist D, Kirk J, Zhang L, Sunderland E, Jiskra M, Selin N. A review of global environmental mercury processes in response to human and natural perturbations: Changes of emissions, climate, and land use. Ambio 2018; 47: 116-140.

Pierce AM, Gustin MS. Development of a Particulate Mass Measurement System for Quantification of Ambient Reactive Mercury. Environmental Science & Technology 2017; 51: 436-445.

Rimstidt JD, Vaughan DJ. Pyrite oxidation: a state-of-the-art assessment of the reaction mechanism. Geochimica et Cosmochimica Acta 2003; 67: 873-880.

Rytuba JJ. Geogenic and mining sources of mercury to the environment. Vol 34. Ottawa: Mineralogical Association of Canada, 2005.

Schroeder WH, Munthe J. Atmospheric mercury - An overview. Atmospheric Environment 1998; 32: 809-822.

Song S, Selin N, Soerensen A, Angot H, Artz R, Brooks S, et al. Top-down constraints on atmospheric mercury emissions and implications for global biogeochemical cycling. Atmospheric Chemistry and Physics 2015; 15: 7103-7125.

Streets DG, Horowitz HM, Jacob DJ, Lu Z, Levin L, ter Schure AFH, et al. Total Mercury Released to the Environment by Human Activities. Environmental Science & Technology 2017; 51: 5969-5977.

Wang S, Feng X, Qiu G, Wei Z, Xiao T. Mercury emission to atmosphere from Lanmuchang Hg–Tl mining area, Southwestern Guizhou, China. Atmospheric Environment 2005; 39: 7459-7473.

Weiss-Penzias P, Amos H, Selin N, Gustin M, Jaffe D, Obrist D, et al. Use of a global model to understand speciated atmospheric mercury observations at five high-elevation sites. Atmospheric Chemistry and Physics 2015; 15: 1161-1173.

Wu S, Uddin MA, Nagano S, Ozaki M, Sasaoka E. Fundamental Study on Decomposition Characteristics of Mercury Compounds over Solid Powder by Temperature-Programmed Decomposition Desorption Mass Spectrometry. Energy & Fuels 2011; 25: 144-153.

Yannick A, Théo Le D, Christopher WM, Grant CE, Daniel O. New Constraints on Terrestrial Surface–Atmosphere Fluxes of Gaseous Elemental Mercury Using a Global Database. Environmental Science & Technology 2016; 50: 507-524.

Zhang L, Lyman S, Mao H, Lin C, Gay D, Wang S, et al. A synthesis of research needs for improving the understanding of atmospheric mercury cycling. Atmospheric Chemistry and Physics 2017; 17: 9133-9144.

Zhu W, Lin C, Wang X, Sommar J, Fu X, Feng X. Global observations and modeling of atmosphere-surface exchange of elemental mercury: a critical review. Atmospheric Chemistry and Physics 2016; 16: 4451-4480.

CHAPTER 7:

Reactive mercury concentrations in Australia and the Southern Hemisphere

Matthieu B. Miller[1], Dean A. Howard[2], Ashley M. Pierce[1], Kellie Cook[1], Melita Keywood[3], Mae S. Gustin[4], Grant C. Edwards[1]

[1]Department of Environmental Sciences, Faculty of Science and Engineering, Macquarie University, Sydney NSW, 2113, Australia

[2]Department of Environmental, Earth, and Atmospheric Sciences, University of Massachusetts-Lowell, Lowell MA, 01854, United States

[3]Centre for Australian Climate and Weather Research, Australian Commonwealth Scientific and Industrial Research Organization, Melbourne, VIC, Australia

[4]Department of Natural Resources and Environmental Sciences, University of Nevada, Reno NV, 89557, United States

Statement of Authorship

Overall, this chapter represents the most collaborative research effort undertaken as part of this thesis. Though the manuscript and figures were drafted entirely by me, I was assisted with much of the underlying work by both the co-authors and other collaborators, most notably the outstanding technical staff at Cape Grim Baseline Air Pollution Station (CGBAPS).

The chapter is rooted in Dr Edwards' involvement with the atmospheric Hg monitoring program at CGBAPS. There was clear value in expanding the GEM measurements at CGBAPS to include reactive mercury, given the general lack of speciated Hg measurements anywhere in the Southern Hemisphere. Having begun collaboration on the RM flux method described in previous chapters, Dr Edwards and I discussed establishing ambient air monitoring locations in Australia as an additional research component to a full PhD dissertation. Fortuitously, Dr Gustin and her research group at the University of Nevada had originally developed the CEM filter-based sampling method for measuring total RM concentrations in ambient air, and I had played a key role in this development process in an adjunct capacity while engaged on other research projects with Dr Gustin (See Appendix G for relevant publications). As such, I had extensive experience with the system and was able to recommend improvements for a long-term monitoring campaign.

CGBAPS was an obvious first choice as a monitoring location given its excellent infrastructure and full-time support staff, and the Macquarie University Automatic Weather Station (MQAWS) provided the necessary infrastructure and a ready supply of research students. After I had assembled and installed the sampling system at both CGBAPS and MQAWS, most routine sample deployment/collection and maintenance was conducted by on-site personnel according to developed standard operating procedures. Samples were shipped to me for all laboratory analysis and processing.

Routine daily operation of the Tekran® analyzers was carried out by site personnel, while I processed all relevant Tekran® GEM data acquired from the sites for the periods of interest. I also visited the sites for major annual maintenance and troubleshooting, variously assisted by Dr Edwards, Dr Howard, Dr Pierce, and/or PhD student Kellie Cook. The RV Investigator voyage was not originally foreseen as part of this project, and we had no prior insight into how the filter sampling system would work in such an environment. However, given this somewhat unique opportunity as arranged by Dr Melita Keywood with CSIRO, we were able to deploy both the RM filter system and a Tekran® 2537 analyzer, with the help of voyage volunteer Jack Simmons, a Masters candidate at the University of Wollongong.

Ancillary instrumentation and external databases used in this chapter, including meteorology and emission data, are maintained by other responsible parties. The particulate instrumentation at CGBAPS is under the aegis of Dr. Keywood and associates, who provided the dataset used herein. The 120 hr back trajectory calculations for the CGBAPS site were part of a 4-year database (2014-2017, inclusive) assembled by Dr Howard during his PhD project. Back trajectories for selected periods at MQAWS and from the RV Investigator were performed by Dr Pierce as part of her role as a Visiting Scholar at Macquarie University. All such existing or acquired data I have merely manipulated as an end user.

ABSTRACT

Mercury (Hg) and especially reactive Hg (RM) data from the Southern Hemisphere (SH) are limited. In this study we undertook long-term measurements of both gaseous elemental Hg (GEM) and RM at two ground-based monitoring locations in Australia, the Cape Grim Baseline Air Pollution Station (CGBAPS) in Tasmania, and the Macquarie University Automatic Weather Station (MQAWS) in Sydney, New South Wales. GEM was measured using the standard Tekran® 2537 series analytical platform, and RM was measured using cation exchange membranes (CEM) in a filter-based sampling method. The 18-month record of RM concentration obtained at CGBAPS is the longest such record anywhere in the SH, and the first in Australia. Additionally, atmospheric Hg measurements were made on board the Australian RV Investigator (RVI) during an ocean research voyage to the East Antarctic coast. Overall mean RM concentrations at CGBAPS and MQAWS were 15.9 ± 6.7 pg m^{-3} and 17.8 ± 6.6 pg m^{-3}, respectively. For the 10-week austral summer period on RVI, mean RM was 23.5 ± 6.7 pg m^{-3}.

As has been shown for GEM, RM concentrations at CGBAPS were seasonally invariable, though the highest individual RM measurements typically occurred in the late summer and fall, when synoptic wind patterns resulted in a greater occurrence of air masses reaching the site from terrestrial and anthropogenic sources to the east. In contrast to CGABPS, there was a significant difference between summer and winter RM concentrations at MQAWS. This difference was largely attributable to changes in source region driven by synoptic scale winds, with higher winter time concentrations driven by terrestrial/anthropogenic source areas to the west. Cleaner maritime air masses were more prevalent at the site during summer, when the wind was primarily from the east, and these maritime air masses had RM concentrations that were very similar to background concentrations at CGBAPS. During the RVI voyage, RM concentrations

were relatively enhanced along the Antarctic coast (up to 30 pg m^{-3}) and GEM concentrations were highly variable (0.2 to 0.9 ng m^{-3}), suggesting periods of enrichment and depletion. Both RM and GEM were relatively lower farther north of Antarctica, while transiting the Southern Ocean.

RM concentrations measured in this study are higher in comparison to most other reported measurements of RM in the global marine boundary layer (MBL), especially for remote SH locations. While RM concentrations were higher, the lack of observed seasonal RM variability in MBL air is in agreement with other observations of seasonally uniform total gaseous Hg (THg) in the SH. As observations of GEM and RM concentrations inform global ocean-atmosphere model simulations of the atmospheric Hg budget, our results have important implications for understanding of atmospheric THg.

7.1 Introduction

Mercury (Hg) is a pervasive environmental toxin with global distribution via a significant atmospheric cycle that includes emission, deposition, and re-emission. As a unique semi-volatile liquid metal, elemental Hg is readily emitted to the atmosphere in the gas phase, where it is transported widely and subject to a number of physiochemical processes. These processes cause total gaseous Hg (TGM) to fluctuate, usually to a small degree but sometimes radically, between several broad forms that defy easy practical differentiation: gaseous elemental mercury (GEM), gaseous oxidized mercury (GOM), and particulate bound mercury (PBM) or particulate Hg (Hg(p)). GEM is usually thought to comprise the bulk of TGM (>95%), though it is known to convert almost entirely to GOM or PBM under certain oxidative conditions (Ebinghaus et al., 2002; Obrist et al., 2011; Schroeder et al., 1998; Steffen et al., 2002; Temme et al., 2003). Where GOM and PBM are not readily distinguishable with certainty (which is almost all cases using current operationally defined measurement techniques), they can be quantified together as reactive mercury (RM), also referred to as Hg(II) or Hg^{2+} (Weiss-Penzias et al., 2015).

The calibrated measurement of trace concentrations of GEM is technically achievable to high precision (± 3% uncertainty) using pre-concentration and cold vapor atomic fluorescence spectrometry (CVAFS), and the principal analytical instrument for doing so is the Tekran® 2537 A/B/X Automated Ambient Air Analyzer. Measurement of GEM is routine in many atmospheric monitoring networks to a nominal level of standardization (UNEP, 2016). However, practically achievable instrument uncertainty may average around 10%, with some inter-instrument biases as high as 20% (Gustin and Jaffe, 2010; Slemr et al., 2015). There is also a somewhat open question as to whether the 2537 measures GEM or TGM. Part of this question is due to the likelihood that many sample inlet configurations preclude a true TGM measurement but may still

allow some Hg^{2+} to pass through, resulting in an ambiguous value somewhere between GEM and TGM. There is also uncertainty about whether the 500 °C desorption temperature at the 2537 gold traps is really sufficient to decompose all Hg^{2+} that might make it through the sample inlet. For instance, some studies have found that pyrolysis of $HgBr_2$ at temperatures of 500, 550, and even 600 °C has not been sufficient to guarantee total thermal decomposition (Lyman and Jaffe, 2012; Swartzendruber et al., 2009).

The measurement of RM is less straight forward and currently depends on isolating GOM and PBM, separately or together, from a typically much larger GEM signal. Various methods have attempted to do this, the principle commercially available apparatus being the Tekran® 1130/1135 Hg speciation system, which uses a denuder and particulate filter to separate GOM and PBM, respectively, from total gaseous Hg (Landis et al., 2002). The variable levels of success in measuring atmospheric RM have been detailed in recent critical reviews (Cheng and Zhang, 2017; Gustin et al., 2015; Jaffe et al., 2014; Zhang et al., 2017). In particular, the potassium chloride (KCl) coated denuder used in the Tekran® 1130 system for GOM collection has been shown to suffer interferences from ozone and water vapor, resulting in systematic under quantification (Ambrose et al., 2013; Lyman et al., 2010; McClure et al., 2014).

Despite these limitations, the best practicable measurement and monitoring of atmospheric Hg is still vitally necessary to inform environmental and human health policy. Such monitoring is extensive in the Northern Hemisphere, but only a handful of sites operate in the Southern Hemisphere (Sprovieri et al., 2016; UNEP, 2016). Most Southern Hemisphere sites have only been operated continuously within the last several years, and the overall lack of long term atmospheric Hg data in the Southern Hemisphere, especially for reactive Hg species, constitutes a significant knowledge gap. Closing this gap will contribute to ongoing science and policy

needs as expressed in the United Nations Environment Minamata Convention on Mercury (UNEP, 2013).

Currently the primary long term mid-latitude GEM monitoring locations in the Southern Hemisphere (Fig. 7.1) are located at Cape Point in South Africa (Brunke et al., 2016), Amsterdam Island in the southern Indian Ocean (Angot et al., 2014), Bariloché National Park in the Andean foothills of Argentina (Diéguez et al., 2017), Cape Grim on the island of Tasmania south of the Australian mainland (Slemr et al., 2015), and Gunn Point in tropical northern Australia (Howard et al., 2017). Other Southern Hemisphere Hg monitoring sites are primarily in the Antarctic polar region (Angot et al., 2016b; Dommergue et al., 2010; Ebinghaus et al., 2002; Pfaffhuber et al., 2012).

Figure 7.1 *Temperate mid-latitude atmospheric Hg monitoring stations in the Southern Hemisphere*.

Of these active atmospheric Hg monitoring sites in the Southern Hemisphere, almost all are coastal and typically within the marine boundary layer (MBL). Up to 54% of total atmospheric Hg in the Southern Hemisphere is thought to be derived from evasion of Hg^0 from the ocean surface, which is balanced by daytime photo-chemical oxidation to Hg^{2+} and subsequent deposition of resulting RM compounds back to the ocean (Laurier and Mason, 2007; Mason and Sheu, 2002; Strode et al., 2007). The formation of RM within the MBL is generally thought to be dominated by Br oxidation processes (Hedgecock and Pirrone, 2001; Hedgecock et al., 2003; Holmes et al., 2009; Horowitz et al., 2017; Laurier and Mason, 2007; Laurier et al., 2003; Sprovieri et al., 2010; Sprovieri et al., 2002). A large part of RM within the MBL is also believed to be bound with coarse sea-salt aerosols (Feddersen et al., 2012; Holmes et al., 2009; Malcolm and Keeler, 2007; Talbot et al., 2011). Observation of Hg speciation in the MBL is vital information for coupled ocean-atmosphere circulation models that simulate global Hg budgets and inform estimates of atmospheric residence time and emission/deposition processes (Holmes et al., 2010; Horowitz et al., 2017).

Few speciated atmospheric Hg measurements have actually been made in the Southern Hemisphere, with only one year-long continuous data set from Amsterdam Island (Angot et al., 2014), supplemented by shorter term campaign studies in Antarctica (Angot et al., 2016a; Brooks et al., 2008b; Sprovieri et al., 2002; Temme et al., 2003) and a few oceanic research voyages (Angot et al., 2016a; Soerensen et al., 2010; Temme et al., 2003). A major limitation to continuous speciated Hg measurements in the Southern Hemisphere has been suitable site and logistical arrangements for operation of the full Tekran® 2537/1130/1135 speciation system. Furthermore, the demonstrated low measurement bias for GOM and PBM raises concerns about potential under quantification of total RM using the Tekran® system.

Table 7.1

Location & Elevation	Coordinates	Duration	GEM (ng m^{-3})	GOM (pg m^{-3})	PBM (pg m^{-3})	Reference
coastal / marine boundary layer						
Cheeka Peak Obs., USA (492 m)	48.299 N 124.626 W	Sept. 2001 - May 2002	1.55 ± 0.13	MDL - 1.6	MDL - 0.5	Weiss-Penzias et al. 2003
Elkhorn Slough, USA (16 m)	36.819 N 121.736 W	March 2011 - Nov. 2011	1.40 ± 0.2	0.5 ± 1.2	4 ± 5	Wright et al. 2014
		March 2012 - April 2012	na	1.4 ± 1.0	3.6 ± 1.8	Huang et al. 2013
Fukuoka, Japan (20 m)	33.548 N 130.364 E	June 2012 - May 2013	2.33 ± 0.49	5.7 ± 9.4	10 ± 11	Marumoto et al. 2015
Cape Hedo Obs., Japan (20 m)	26.872 N 128.263 E	March 2004 - May 2004	2.04 ± 0.38	4.5 ± 5.4	3.0 ± 2.5	Chand et al. 2008
Galapagos Islands (5 m)	-0.959 S 90.963 W	Feb. 2011 - Oct. 2011	1.08 ± 0.17	MDL - 3.8	MDL - 1.1	Wang et al. 2014
Amsterdam Island (50 m)	-37.796 S 77.551 E	Jan. 2012 - Dec. 2013	1.03 ± 0.08	MDL - 4.1	MDL - 12.7	Angot et al. 2014

Table 7.1 Average GEM and RM concentrations measured using the Tekran® speciation system at select marine boundary layer locations around the Indo-Pacific. MDL is method detection limit.

Many studies using the Tekran® speciation system at MBL locations report extremely low GOM and PBM concentrations (Table 7.1). Angot et al. (2014) reported average GOM and PBM concentrations of < 1 pg m^{-3} for Amsterdam Island, with measurements frequently below detection, similar to many other coastal ground-based RM measurements in the MBL (Chand et al., 2008; Huang et al., 2013; Marumoto et al., 2015; Wang et al., 2014; Weiss-Penzias et al., 2003; Wright et al., 2014). Using data acquired on a circumnavigational voyage measuring atmospheric GEM and GOM using just the Tekran® 2537/1130 , Soerensen et al. (2010) suggested a global mean GOM concentration of 3.1 ± 11 pg m^{-3} in the MBL (4.3 ± 0.14 pg m^{-3} for the SH MBL), in general agreement with other voyage data of 2 to 10 pg m^{-3} (Laurier et al., 2003; Temme et al., 2003).

The explanation for these low RM concentrations in the MBL has generally been rapid deposition of the RM formed by in-situ oxidation processes, due to scavenging by abundant sea-

spray and sea-salt aerosols (Laurier et al., 2003; Mason and Sheu, 2002; Sommar et al., 2010). Some studies have reported much larger RM concentrations in or associated with MBL air, but these are in the minority of observations (Mason et al., 2001; Timonen et al., 2013). There are other scenarios with significant in-situ oxidation of GEM in which the resulting enhancement of RM is typically observable, e.g. coastal polar locations during springtime Atmospheric Mercury Depletion Events (Steffen et al., 2013; Steffen et al., 2008). Similar to the MBL environment, RM formed in polar AMDEs is also thought to rapidly deposit, though more so to ice surfaces than marine aerosols (Angot et al., 2016a; Brooks et al., 2008a; Steffen et al., 2002), yet elevated atmospheric RM concentrations are still measured in spite of high rates of deposition. Why then are the observations of RM in the MBL so modest, or even undetectable? We posit that the low RM measurement bias demonstrated on the Tekran® 1130 system may be contributing to artificially low observations of RM in the MBL.

An alternative method that has been used with some success to selectively measure RM concentrations in ambient air is a cation exchange membrane (CEM) filter system (Huang and Gustin, 2015; Huang et al., 2017; Huang et al., 2013; Marusczak et al., 2017; Pierce and Gustin, 2017; Sexauer Gustin et al., 2016). The CEM filters are inert to GEM uptake (Miller et al. submitted, this thesis) and have good selectivity for RM compounds (Huang et al., 2013; Lyman et al., 2016). The CEM based sampling systems typically deploy replicate paired sets of CEM filters at a controlled flow rate. Each pair of filters constitutes one sample, the first filter serving as the primary collection surface, and the second filter capturing breakthrough. Filters are deployed for 1 to 2 weeks in order to collect a detectable quantity of RM for analysis.

In this study, we report the first continuous measurements of atmospheric RM in Australia, using the CEM filter-based method. RM measurements were made in conjunction with the existing

GEM monitoring program at the Cape Grim Baseline Air Pollution Station (CGBAPS) in Tasmania, and at a new site established at the Macquarie University Automatic Weather Station (MQAWS) in suburban Sydney, New South Wales. In addition, we present RM concentration data from CEM filters deployed on the Australian Research Vessel Investigator (RVI) during an austral summer 2017 voyage in the Southern Ocean, also with concurrent GEM measurement.

7.2 Methods

7.2.1 Field Sites

Atmospheric Hg was measured at two temperate coastal mid-latitude sites in Australia, and on an ocean research voyage transiting the Southern Ocean from southern Australian waters to the East Antarctic coast (Fig. 7.2).

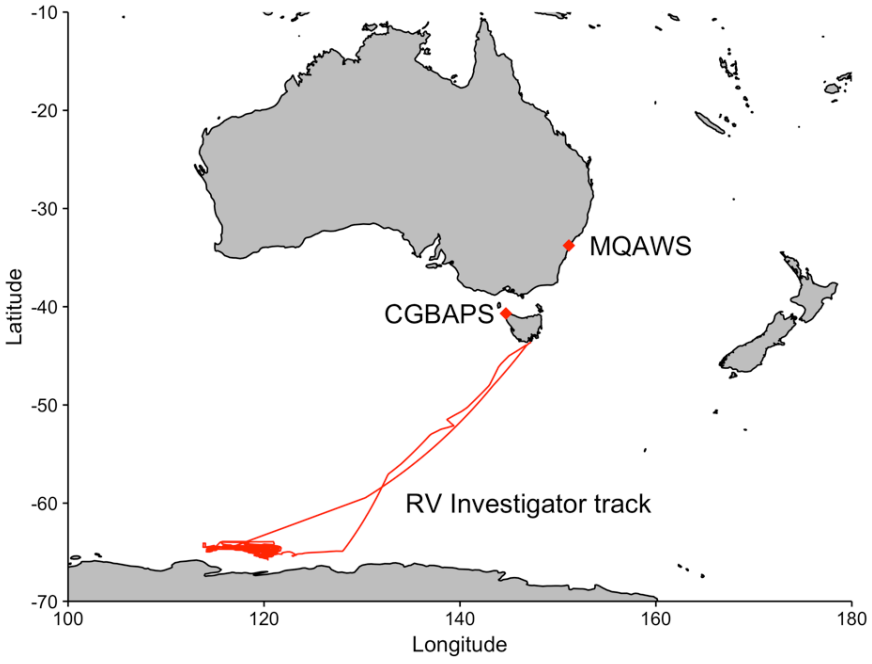

Figure 7.2 *Location map of ambient RM measurement sites in Australia and track of RV Investigator (RVI) research voyage in the Southern Ocean.*

Cape Grim Baseline Air Pollution Station (CGBAPS) is located on the north-western point of Tasmania, Australia (-40.683 S 144.690 E, 94 m a.s.l.), on a sea-side bluff directly overlooking a long westward fetch of the Indian Ocean that is unbroken all the way to South America. The site is coastal with a cool temperate oceanic climate. CGBAPS is jointly administered by the Australian Bureau of Meteorology (BoM) and the Commonwealth Scientific and Industrial Research Organization (CSIRO), and is part of the World Meteorological Organization Global Atmosphere Watch (WMO-GAW) program. The site operates a Tekran® 2537B Ambient Air Mercury Analyzer, and since June 2017 a newer Tekran® 2537X unit.

Macquarie University Automatic Weather Station (MQAWS) is located in the northern suburbs of Sydney, New South Wales, Australia (-33.765 S 151.117 E, 58 m a.s.l.) on part of the campus sport fields, and has previously been used as an "urban background" measurement site as there are no major industrial point sources within 5 km (Mohiuddin et al., 2014). The immediate environment is an open grassy field with denser woodland areas of Lane Cove National Park just to the east, but at larger scale the site is entirely within built up urban areas and a major motorway 400 m to the southwest. Though nominally somewhat inland at 16 km from the pelagic Pacific coast, the site is within the natural Sydney harbor topographical basin and can be considered a near coastal environment with a humid subtropical climate. A Tekran® 2537A has been operated intermittently at the site since May 2016.

The RV Investigator (RVI) is a 94 m state-of-the-art multidisciplinary blue water research vessel operated by CSIRO as part of the Australian Marine National Facility. Voyage 1 of 2017 (January 13 – March 6) transited the Southern Ocean to the sea-ice region off the East Antarctic coast, departing and returning from the southern port of Hobart, Tasmania. The primary scientific mission was a survey of the continental shelf in the area offshore from the Totten

Glacier. Aerosol sampling in the northern Antarctic Atmospheric Polar Cell was an additional mission, and as part of the atmospheric sampling suite a Tekran® 2537A was operated in conjunction with CEM filter deployments over the duration of the voyage. Ship exhaust has not been shown to effect on-board atmospheric Hg measurements (Soerensen et al., 2010; Sommar et al., 2010)

7.2.2 Measurements

Gaseous elemental mercury was measured using a Tekran® 2537A ambient mercury analyzer at MQAWS, and a Tekran® 2537B unit at CGBAPS. The Hg analyzers were operated at a 5 min sample frequency and 1.0 Lpm flow rate. Sample air was pulled through PTFE Teflon tubing (0.625 cm O.D.) at station top roof rail height (~4 m a.g.l.), within a conical PTFE rain shield and an up-front fine particulate filter. At CGBAPS the sample line was maintained at 50 °C from roof to analyzer within an opaque heating jacket. The sample inlet ports on the 2537 units were fitted with 0.2 μm PTFE particulate filters in 47 mm PFA filter assemblies. Soda lime traps (Tekran® p/n 90-13310-06) were placed in-line immediately upstream of the filter assembly to scrub acid and organic aerosols. The attached fine particulate filter and soda lime trap precludes determination of TGM on the 2537 analyzer, and so all Tekran® data is reported as GEM.

At CGBAPS, quality assurance and quality control followed GMOS protocols (Sprovieri et al., 2016). The 2537B analyzer was calibrated from an internal Hg vapor permeation source every 25 h, and a standard addition of Hg vapor was permeated into the sample stream following calibrations to verify Hg recovery efficiency in ambient air. The internal 2537B permeation source was verified via manual injections from a primary Hg vapor source (Tekran® 2505) twice annually. The 5 min GEM data from the 2537 units was averaged to match the 2-week sample periods corresponding to RM filter deployments. Averaging periods for which less than 50% of

data was available were excluded from the final data analysis. Hourly averages of GEM were calculated over the course of the RVI track, and any hour with less than 50% data availability was excluded.

Ambient reactive mercury concentrations were measured using an adaptation of the University of Nevada Reno Reactive Mercury Active System (UNRRMAS)(Gustin et al., 2016; Huang et al., 2017). The RM sampling system consists of 6 sample lines pulling ambient air at a sample flow of 1.0 Lpm, each controlled by a ball valve, with vacuum supplied by pump (AirCadet®). Each sample line was attached to a 2-stage 47 mm PFA filter holder (Savillex®). The primary modification of the UNRRMAS system was to suspend the filter assemblies within a standardized, rigid, durable anodized aluminum weather shield for long term deployments (Fig. 7.3). Six filter assemblies were suspended inlet-down within the weather shield, which was attached to a vertical section of station railing above roof height. In the 2-stage filter deployment, the first upstream "A" filter serves as the primary collection filter, and the secondary downstream "B" filter captures breakthrough. The secondary filter was used to assess how efficiently the primary filter was working, and whether any problems existed such as a rip or otherwise poor seal.

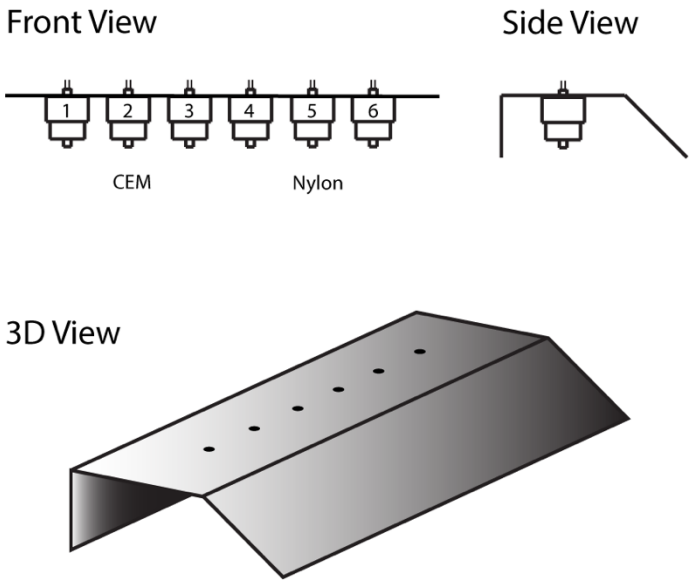

Figure 7.3 *Diagram of modified RM filter-based sampling system*

Cation exchange membrane filters were deployed on Lines 1-3. The CEM filters consist of a negatively charged polyethersulfone coated matrix (0.8 um pore size, Mustang® S, Pall). The CEM material has been shown to have negligible uptake of GEM (Miller et al., this thesis), and good selectivity for GOM compounds (Huang and Gustin, 2015; Huang et al., 2013). Nylon filters (0.2 μm pore size, Sartorius) were deployed on lines 4-6. Sample flow on each line was measured and adjusted at the beginning of each 2-week sample deployment and was again measured immediately preceding filter collection. The average of the beginning and ending sample flows was taken as the flow rate for calculating total sample volume. Damaged or mis-deployed filters (as noted by site operators) were excluded from the dataset, as was any filter pair with higher Hg loading on the secondary filter, always indicative of a poor filter seal or tear.

Atmospheric particle counts at CGBAPS were determined with an Ultrafine Condensation Particle Counter (UCPC, TSI™ Model 3776) sensitive to particle sizes down to 2.5 nm. The UCPC sample inlet was at 10 m a.g.l., with a 10 μm particle size cut-point cyclone inlet. Hourly

average particle counts (particles cm^{-3}) were multiplied by the hourly sample volume through the CEM filters (0.06 m^3) to arrive at number of particles per hour in the sample flow, and these hourly values were summed over each 2-week filter deployment, providing an approximation of 2-week particle loading on the filters.

7.2.3 Analysis

At the end of each deployment, filters were collected into sterile 50 mL polypropylene sample vials using trace clean protocols. A "blank" unused filter of each type was collected with every deployment. The mean blank Hg mass on CEM filters was 60 ± 44 pg at CGBAPS (n = 40), and the minimum detection limit (MDL) for a 2-week sample period (mean sample volume 20.2 m^3) was therefore 5.2 pg m^{-3}. At MQAWS, the mean CEM blank Hg mass was 47 ± 26 pg (n = 31) giving a 2-week MDL of 3.6 pg m^{-3}. The blank Hg values and MDLs are significantly less than reported in previous studies using the CEM filter technique (Gustin et al., 2016; Huang et al., 2017), and this is attributed to the use of new 50 mL vials for each sample filter versus re-cleaned 125 mL glass I-chem jars.

CEM filters were analyzed on a Tekran® 2600 system. Analysis began with an aqueous digestion in a strongly acidic, strongly oxidizing bromine monochloride solution to liberate captured RM from the filter material and bring it into solution within the 50 mL collection vial. Digestion was followed by reduction of the aqueous Hg(II) to Hg^0, which was then purged from solution in an ultra-high purity argon gas flow and pre-concentrated onto gold traps. Finally, the concentrated Hg was thermally desorbed from the gold traps and measured via cold vapor atomic fluorescence spectrometry (CVAFS, EPA Method 1631, Rev. E modified, Appendix A). The total Hg measured on each sample CEM filter was divided by the calculated sample volume to arrive at a

2-week integrated RM concentration. Each 2-week sample period is reported as the mean ± standard deviation of the three sample CEM filters.

Nylon filters were analyzed by stepwise thermal desorption in a Lindberg-Blue® tube furnace from 50 to 200 °C, with released Hg passing downstream through a pyrolyzer (600 °C)and to a Tekran® 2537A sampling at 2.5 min intervals. The release profiles over the stepwise heating provide a qualitative indication of possible RM species, based on desorption profiles for reference Hg compounds (Huang and Gustin, 2015; Huang et al., 2017; Huang et al., 2013). However, a preliminary assessment of total Hg collected on the nylon filters indicated that these collected on average less than 10% of the total Hg recovered on CEM filters. This mass balance was deemed insufficient to justify further deployments.

Seasons were defined according to convention as Summer (Dec-Jan-Feb), Fall (March-April-May), Winter (June-July-Aug), and Spring (Sep-Oct-Nov). Meteorological data was retrieved from CGBAPS in hourly averages and from MQAWS in 15 averages. MQAWS precipitation data was limited and total daily precipitation from a nearby BoM weather station was substituted (Site #066156, 33.78 S 151.11 E). All meteorological data was binned into 2-week intervals corresponding to filter deployments. Wind velocity was assessed seasonally and for each 2-week sample period (Appendix E). In addition, wind velocity at CGBAPS was assigned to a baseline sector (bearing 190 – 280°) based on established station criteria, and the percentage of baseline air in each 2-week sample period was determined.

For select periods of interest, air mass back trajectories were calculated using the NOAA Hybrid Particle Lagrangian Integrated Trajectory (HYSPLIT) model (Draxler and Hess, 1998). Global Data Assimilation System (GDAS) 0.5° meteorological re-analysis data was used for initiating 120 h back trajectory calculations every hour, from a single point at height equal to 0.5x the

mixed layer depth. Any trajectory that bottomed-out at 0 m elevation before reaching the station was removed from analysis.

Anthropogenic point-source Hg emission data was acquired for the 2016/2017 reporting year from the Australian National Pollutant Inventory (NPI, 2017). All point sources less than 100 g yr^{-1} were rounded to 0.1 kg in figures.The occurrence of fire hotspots from biomass burning was identified using thermal anomaly data generated by the Moderate Resolution Imaging Spectroradiometer (MODIS) sensors on NASA's Terra and Aqua satellites. MODIS data (Collection 6, version 6.1, MCD14ML definitive geolocation data set) were retrieved from the NASA Fire Information for Resource Management System (FIRMS) Fire Archive. The location and intensity of bushfire activity was assessed via the Fire Radiative Power (FRP, Watts) data output.

All data was processed and figures generated in Microsoft Excel (version 16.22) and RStudio® (version 3.2.2).

7.3 Results

7.3.1 Overall long-term observations between ground-based monitoring sites

Ambient RM was measured from November 2015 through May 2017 at CGBAPS, and from April 2016 through May 2017 at MQAWS. The overall mean RM concentration was 15.9 ± 6.7 pg m^{-3} at CGBAPS (median = 14.8, range 6.7 - 48.6 pg m^{-3}, n = 39), and 17.8 ± 6.6 pg m^{-3} at MQAWS (median = 16.8, range 7.0 - 32.5 pg m^{-3}, n = 31). Comparing equivalent overlapping sample periods at both sites (April 2016 – May 2017), there was not a statistically significant difference in either mean or median RM concentrations (Welch t-test, p = 0.4063, Kruskall-Wallis test p = 0.4657). This was a somewhat surprising result given the relatively large differences between the sites (i.e. remote undeveloped coast versus major urban area). However, this may stem from a lower absolute number of observations at MQAWS. A frequency distribution of RM concentration by season reveals that a greater percentage of sample periods at MQAWS were at the high range of observations above 25 pg m^{-3} (Fig 7.4). It seems likely that over a longer period of observation RM concentrations at MQAWS might be significantly higher than at CGBAPS.

During the same periods, overall mean GEM concentration was 0.90 ± 0.35 ng m^{-3} (n = 146273 5 min samples) at CGBAPS, and 0.65 ± 0.24 ng m^{-3} (n = 32251) at MQAWS. A detailed discussion of seasonal trends and baseline GEM concentration at CGBAPS for the time period January 2014 to April 2017 is discussed by Howard (Howard, 2018). Technical issues with the 2537 analyzer at MQAWS resulted in less than 50% data availability for many periods, precluding analysis of a complete seasonal dataset and preventing a definite assessment of GEM concentrations at MQAWS.

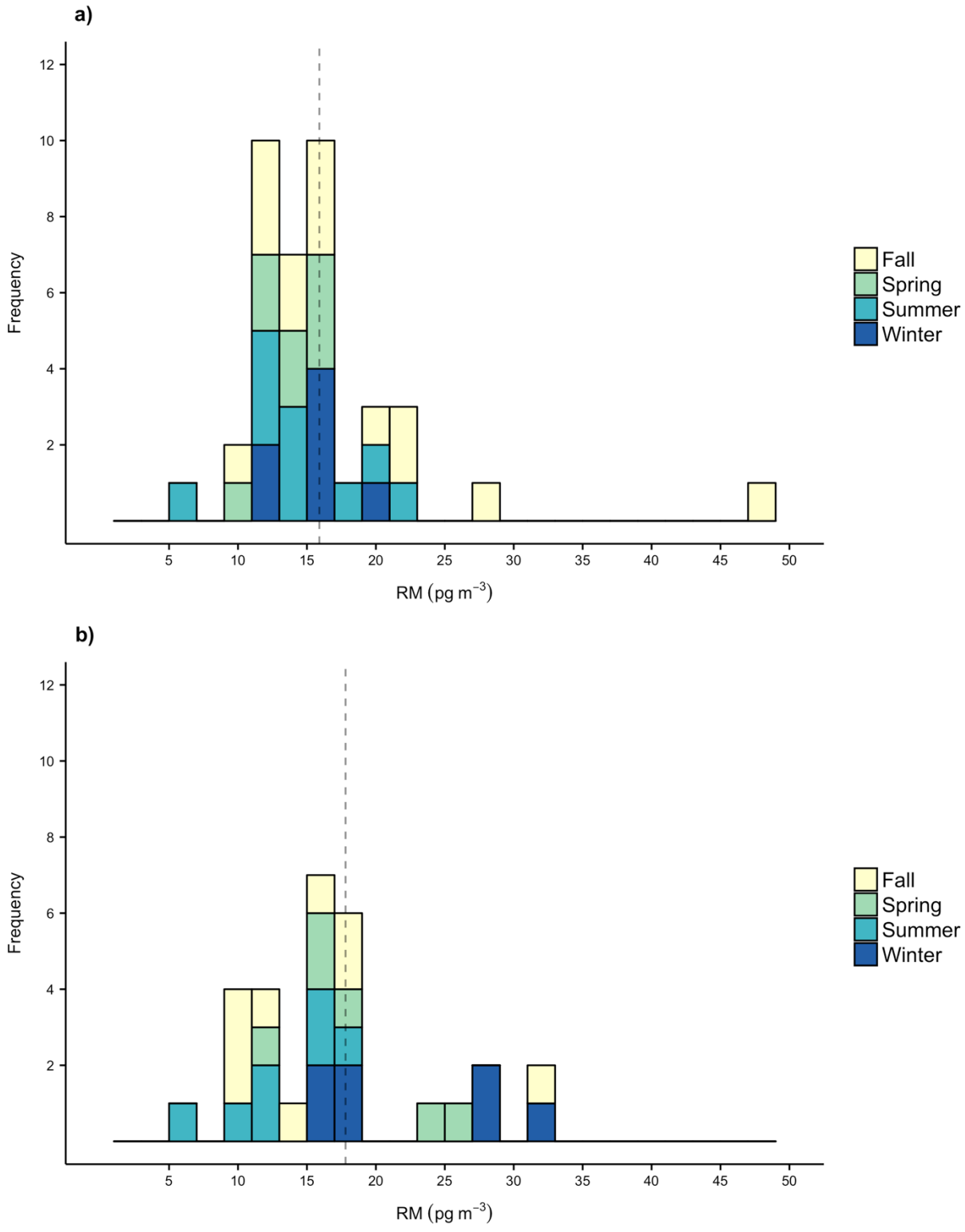

Figure 7.4 *Frequency distribution of observed RM concentrations at a) CGBAPS (n = 39) and b) MQAWS (n = 31). Vertical dashed lines represent overall mean RM concentrations of 15.9 ± 6.7 and 17.8 ± 6.6 pg m^{-3}, respectively.*

7.3.2 Reactive mercury at Cape Grim Baseline Air Pollution Station

The median temperature at CGBAPS was 13.6 °C (range 3.5-25.8 °C), and the median RH was 78.6% (range 41-100%). Total rainfall in 2016 was exceptional at 1124.2 mm (annual median total 734.6 mm). Wind direction was from the west-southwest (195 – 315°) for the majority of time in all seasons (Fig. 7.5). Wind direction was in the baseline sector (190 – 280°) 25% of the time overall, and more so in the winter (34%) and spring (33%) seasons. Wind direction was less consistent in the summer and fall, and the proportion of wind in the baseline sector was less (21% summer, 23% fall). The summer and fall periods also experienced a greater proportion of wind from the eastern sector, which can be expected to have a greater influence from terrestrial and anthropogenic sources.

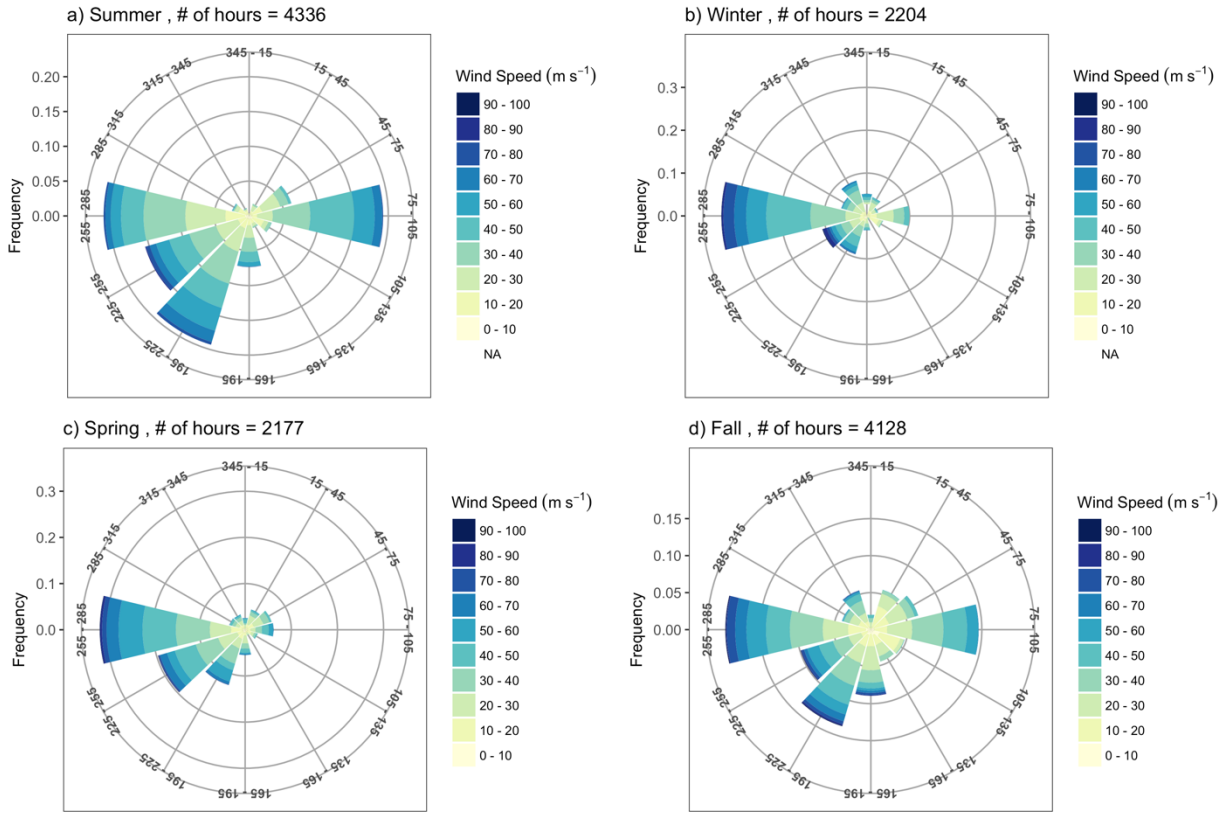

Figure 7.5 *Seasonal wind velocities at CGBAPS. Frequency is represented by circles of increasing radii. The total number of hourly meteorological observations in each season is shown at the top of each chart as '#of hours'.*

Seasonally, the highest mean RM concentrations at CGBAPS were observed in the fall (15.6 ± 3.9 pg m^{-3}), including the two highest individual 2-week RM concentrations of 27.6 and 48.8 pg m^{-3} (Fig. 7.6b) and four of the highest five RM concentrations (Fig. 7.4a). These higher fall season RM concentrations correspond to a greater occurrence of non-baseline wind events from the east. However, overall seasonal mean RM concentrations were not statistically significantly different (Welch t-test, $p > 0.05$), and the occurrence of above-average RM concentration periods in the fall seems to be driven by a greater prevalence of individual events rather than a systematic seasonal increase (see Section 7.3.3 below).

No relationship was apparent between RM concentration and the percent of air arriving from the CGBAPS baseline sector (Fig 7.6c). This is likely a function of the long 2-week sample period for RM, during which source air can obviously be quite variable. Considering the location on a relatively narrow island promontory, it is also likely that in terms of RM the site is dominated by baseline maritime air concentrations even when this air passes over non-baseline surfaces, except for exceptional point-source events (see section 7.3.3 below). However, the top three sample periods with the highest proportion of baseline air (> 40%) did have a somewhat lower mean RM concentration of 12.9 ± 2.1 pg m^{-3}, and this may be more representative of background mid-latitude maritime RM concentrations.

Mean 2-week RM concentrations were also compared to mean 2-week values of GEM, and to median values of temperature, RH, barometric pressure, wind speed, and total 2-week precipitation (SI Fig. 7.1). No relationship between RM concentration and these other variables was discernible at the 2-week temporal resolution (r^2 values < 0.1).

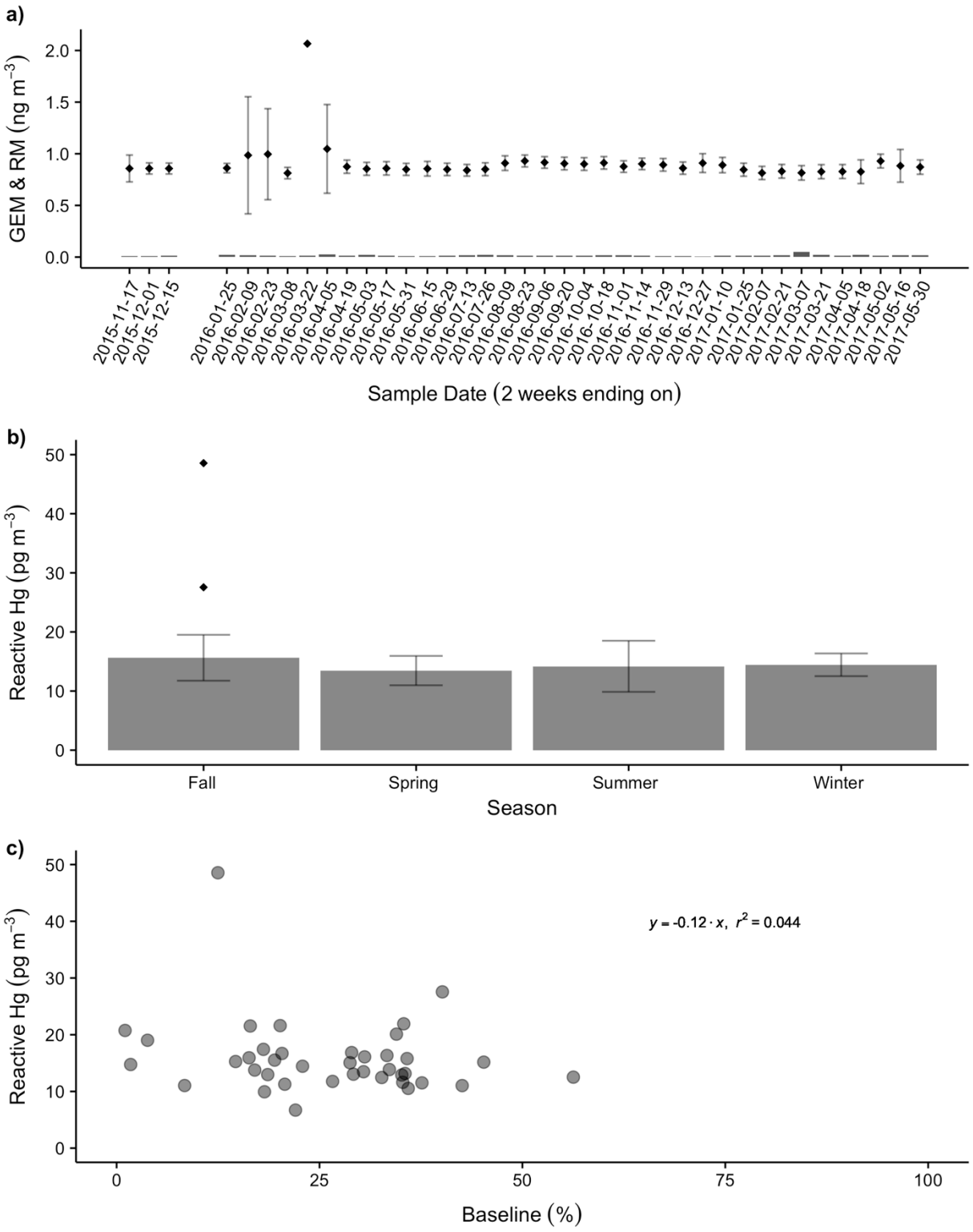

Figure 7.6 *RM and GEM concentrations at CGBAPS for a) 2-week sample periods, b) seasonal averages, and c) in relation to percent of sampled air from baseline wind sector (190 – 280°). Note b) and c) show RM concentrations only.*

7.3.3 Exceptional events: biomass burning and non-baseline sector

A period of widespread bushfire activity occurred in Tasmania during January – March of 2016 (Fig. 7.7). Four 2-week sample deployments in this time period experienced unusually elevated GEM concentrations (Fig. 7.6a). Significant plume events impacted the CGBAPS site on the night of Jan. 25 – 26 with peak GEM of 7.8 ng m^{-3} at 04:25, and on February 12 with peak GEM of 3.8 ng m^{-3} at 05:35 (Howard, 2018; See Appendix E, SI Fig. 7.5). These events were apparent in the 2-week average GEM, but the impact on RM concentration was less clear. The period Jan. 25 – Feb. 9 had an overall mean GEM concentration of 0.99 ± 0.57 ng m^{-3} and a slightly elevated RM concentration of 19.0 ± 0.7 pg m^{-3}. The following period Feb. 9 – 23 had a similar GEM concentration of 1.00 ± 0.44 ng m^{-3} but a relatively low RM concentration of 12.5 ± 0.6 pg m^{-3}.

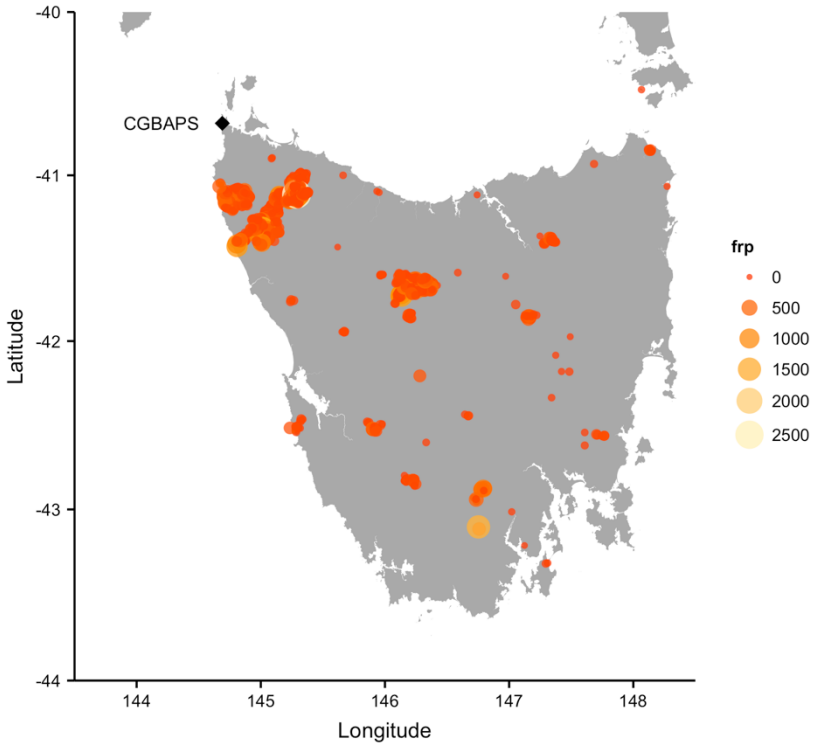

Figure 7.7 *Location and fire radiative power (frp) of Tasmanian bushfires, January – March, 2016. Fire hot spot locations acquired from NASA FIRMS Fire Archive data, retrieved from Aqua MODIS and Terra MODIS satellite sensors.*

Biomass combustion has been demonstrated to release primarily GEM and possibly Hg(p) (Finley et al., 2009; Miller et al., 2015; Weiss-Penzias et al., 2007). The fire plume events observed at CGBAPS were generated proximal to the station (within several hours trajectory travel time) and contained a high proportion of primary combustion products as evidenced by the high CO/CO_2 ratios (Howard, 2018; Appendix E, SI Fig 7.6). As GOM is not a primary combustion product and the primary formation and size of PBM is uncertain, it seems likely that plume arrival times were not sufficiently long to allow secondary oxidative production of RM, especially as both events occurred over night when photochemical oxidation would be at its lowest.

The 2-week sample periods ending March 22 and April 5, 2016, experienced even higher mean GEM concentrations of 2.1 ± 1.9 and 1.1 ± 0.4 ng m^{-3} due to a significant and extended plume event (Fig. 7.5a). Peak 5-min GEM concentrations jumped to ~12 ng m^{-3} on March 17 and remained elevated (> 2.0 ng m^{-3}) until March 23, bracketing the two filter deployment periods. This event is attributable to a renewed flair-up of bushfire activity due south of the station, beginning March 16 and peaking on March 17. Back trajectory calculations during this period show arriving air masses traveling directly over the burn area, in addition to burn areas farther south (Fig. 7.8). The RM concentration for the sample period ending March 22 was not exceptional (14.7 ± 1.5 pg m^{-3}). However, during the following sample period ending April 5, mean RM concentration was 27.6 ± 0.5 pg m^{-3}, the second highest value recorded at CGBAPS, possibly due to an aging and oxidized plume chemistry in the sample further removed in time from primary combustion.

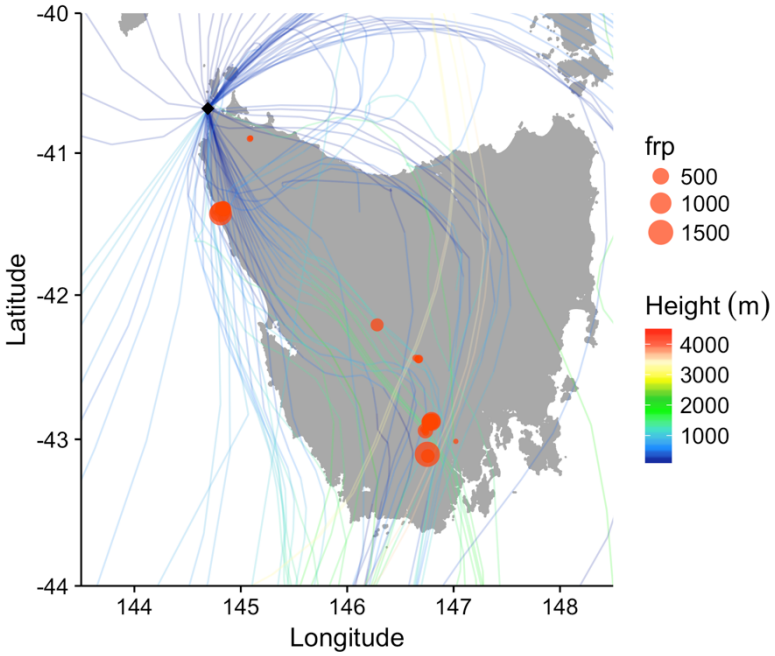

Figure 7.8 *Ensemble of 120 h back trajectory plots for air arriving at CGBAPS during the bushfire plume event of March 16-23, 2016. Trajectories initiated hourly at a single point with height of 0.5x mixed layer depth. Fire locations and fire radiative power (frp) indicated by red circles.*

The highest recorded 2-week RM concentration of 48.6 pg m^{-3} occurred in a period of no major bushfire activity (Feb. 21 – March 7, 2017). This sample period and the next (also above average RM at 20.8 pg m^{-3}, to March 21) were dominated by air flow from the east (75-105°, 42 and 51% of hourly wind directions, respectively), unusual for the CGBAPS site. Back trajectory analysis confirms the easterly flow during this period, with a preponderance of trajectories arriving from the east after traveling over the Bass Straight below 1000 m, well within the mixed depth layer (Fig. 7.9). An iron ore smelting plant (Grange Corp. Port Latta Facility) is located ~61.5 km away from CGBAPS at 108° east bearing (Fig. 7.11) and is a modest source of Hg and RM (5.2 kg y^{-1}, NPI, 2017). Shipping through the Bass Straight to the east-northeast of the site may also be a contributing source during these east-wind periods, similar to an observation made by Sprovieri et al. (2010) for high RM events in the Mediterranean MBL. A similar flow regime was also apparent for the following sample period to March 21 (Fig. 7.10).

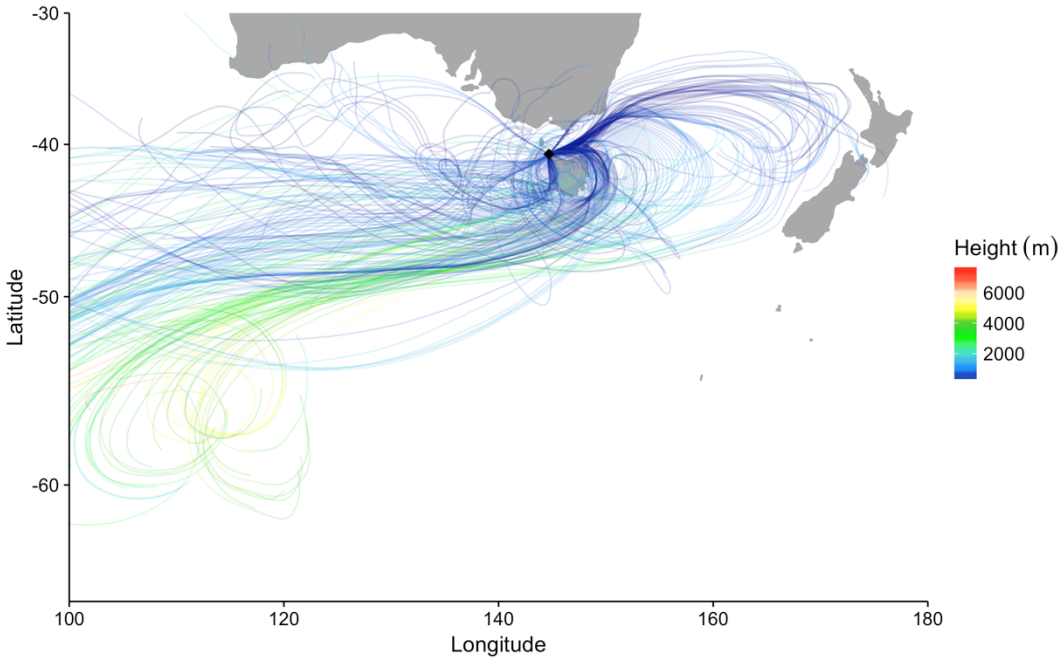

Figure 7.9 *Ensemble of 120 h back trajectory plots for air arriving at CGBAPS during the period Feb. 21 – March 7, 2017. Trajectories initiated hourly from a single point above station with height of 0.5x mixed layer depth.*

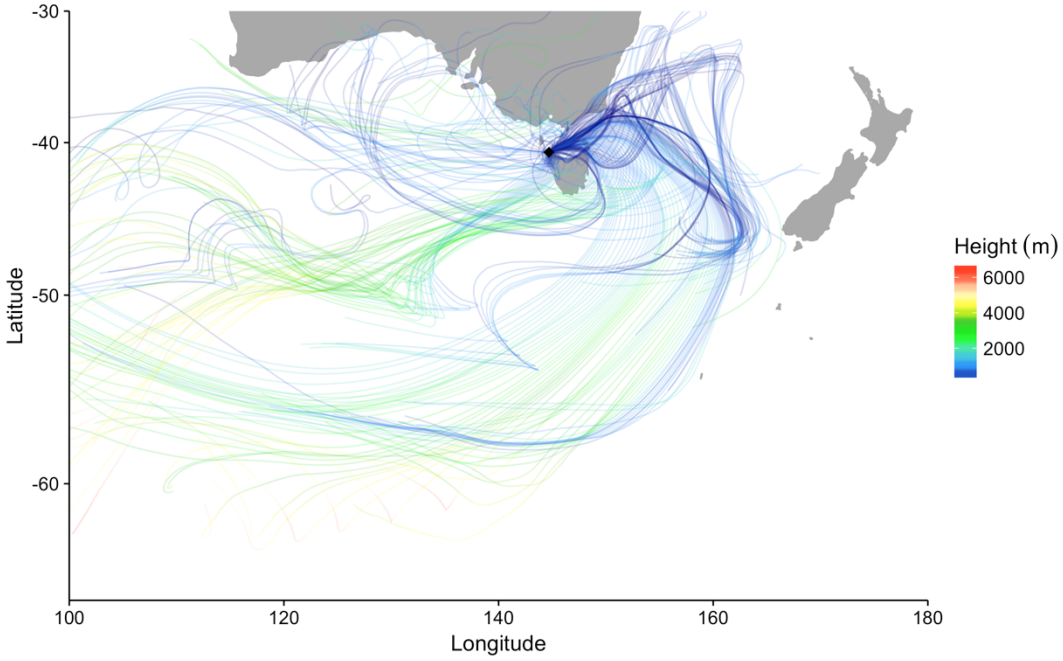

Figure 7.10 *Ensemble of 120 h back trajectory plots for air arriving at CGBAPS during the period March 7 – 21, 2017. Trajectories initiated hourly from a single point above station with height of 0.5x mixed layer depth.*

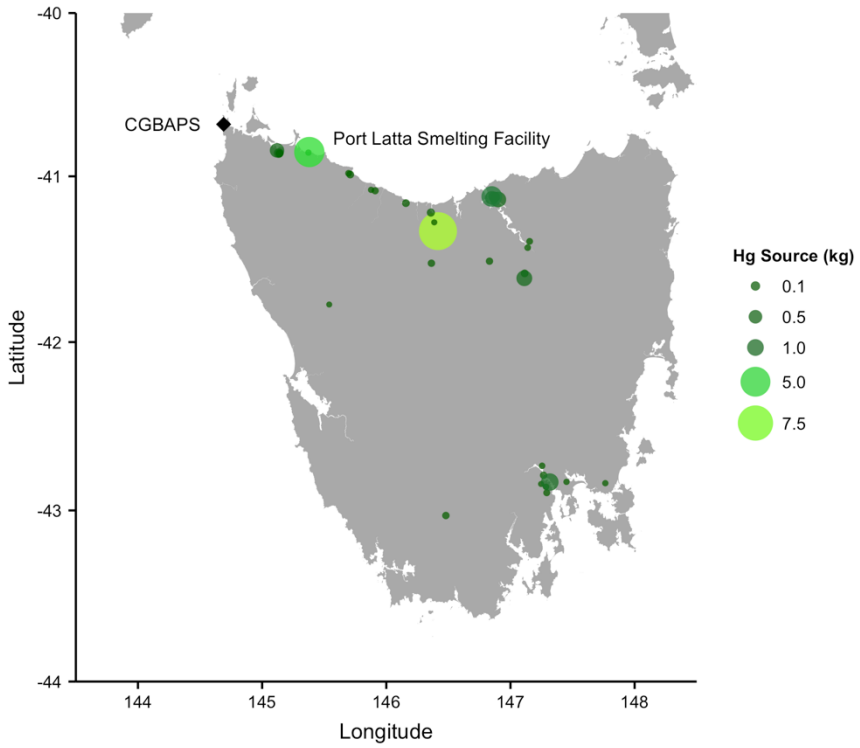

Figure 7.11 *Location and magnitude (kg yr^{-1}) of point source Hg emissions in Tasmania. Data acquired from Australian National Pollutant Inventory 2016/2017 Data Archive.*

7.3.4 Reactive Hg at Macquarie University Automatic Weather Station

In general, the MQAWS site was hotter and more humid than CGBAPS. The median temperature was 17.3 °C (range -0.8 to 42.2 °C), and the median RH was 85% (range 21 to 100%). As is evident from the range in temperature and RH, the site also experienced larger weather extremes compared to the more moderated climate at CGBAPS. Total rainfall in 2016 was above average at 1316.4 mm (annual median total 1122.1 mm). Overall wind velocities were generally low at the MQAWS site, with the dominant wind direction from the west-northwest (225 – 345°) in all seasons except summer when the wind was generally from the east-southeast in the prevailing sea breeze (Fig. 7.12).

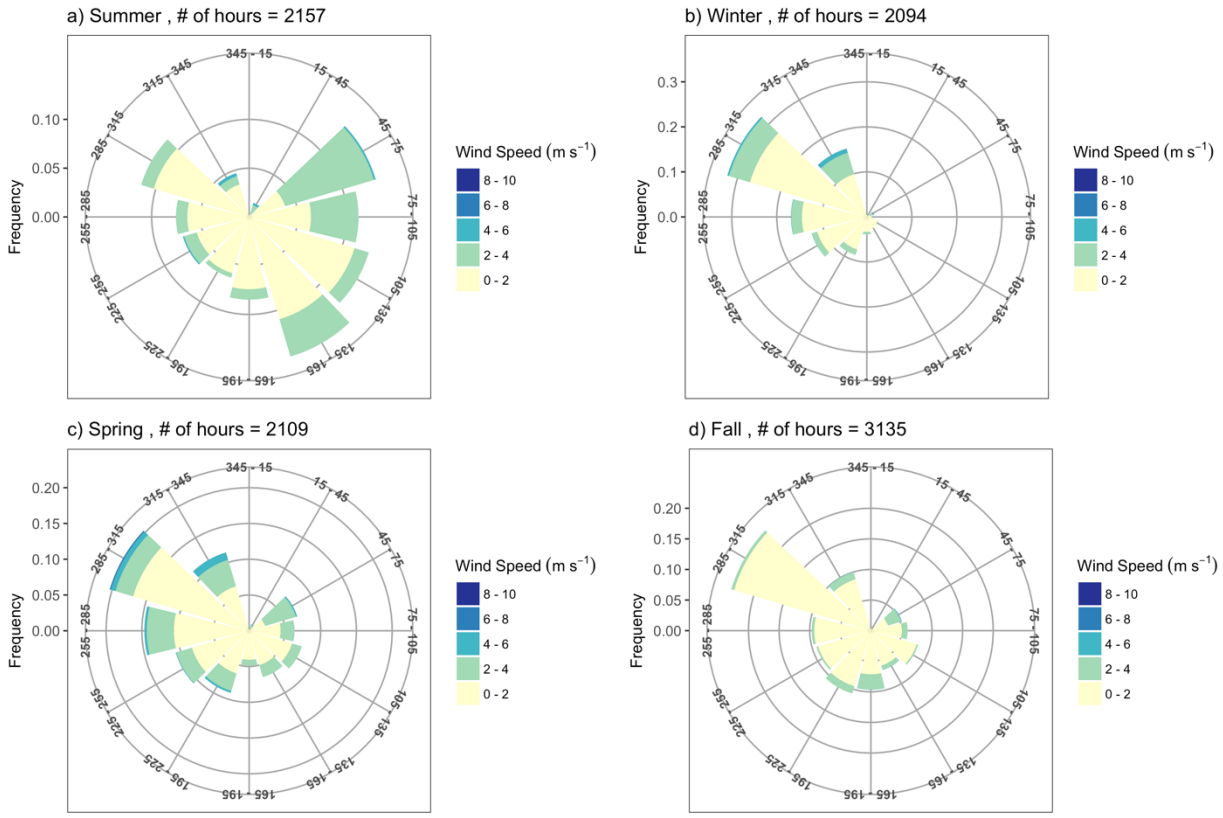

Figure 7.12 *Seasonal wind velocities at MQAWS. Frequency is represented by circles of increasing radii. The total number of hourly meteorological observations in each season is shown at the top of each chart as '#of hours'.*

Seasonally, the lowest mean RM concentrations occurred in the summer (13.3 ± 3.9 pg m^{-3}, n = 7) and the highest RM concentrations occurred in the winter (22.1 ± 6.8 pg m^{-3}, n = 7), a statistically significant difference (Welch t-test, p = 0.015, Fig. 7.13b). Mean RM concentrations during the fall and spring were intermediate between the summer and winter extremes and were not significantly different. As with CGBAPS, mean 2-week RM concentrations were compared to mean 2-week concentrations of GEM, median values of temperature, RH, barometric pressure, and wind speed, as well as total 2-week precipitation (SI Fig. 3), and no relationship between RM concentration and these other variables was discernible at the 2-week temporal resolution (r^2 values < 0.1).

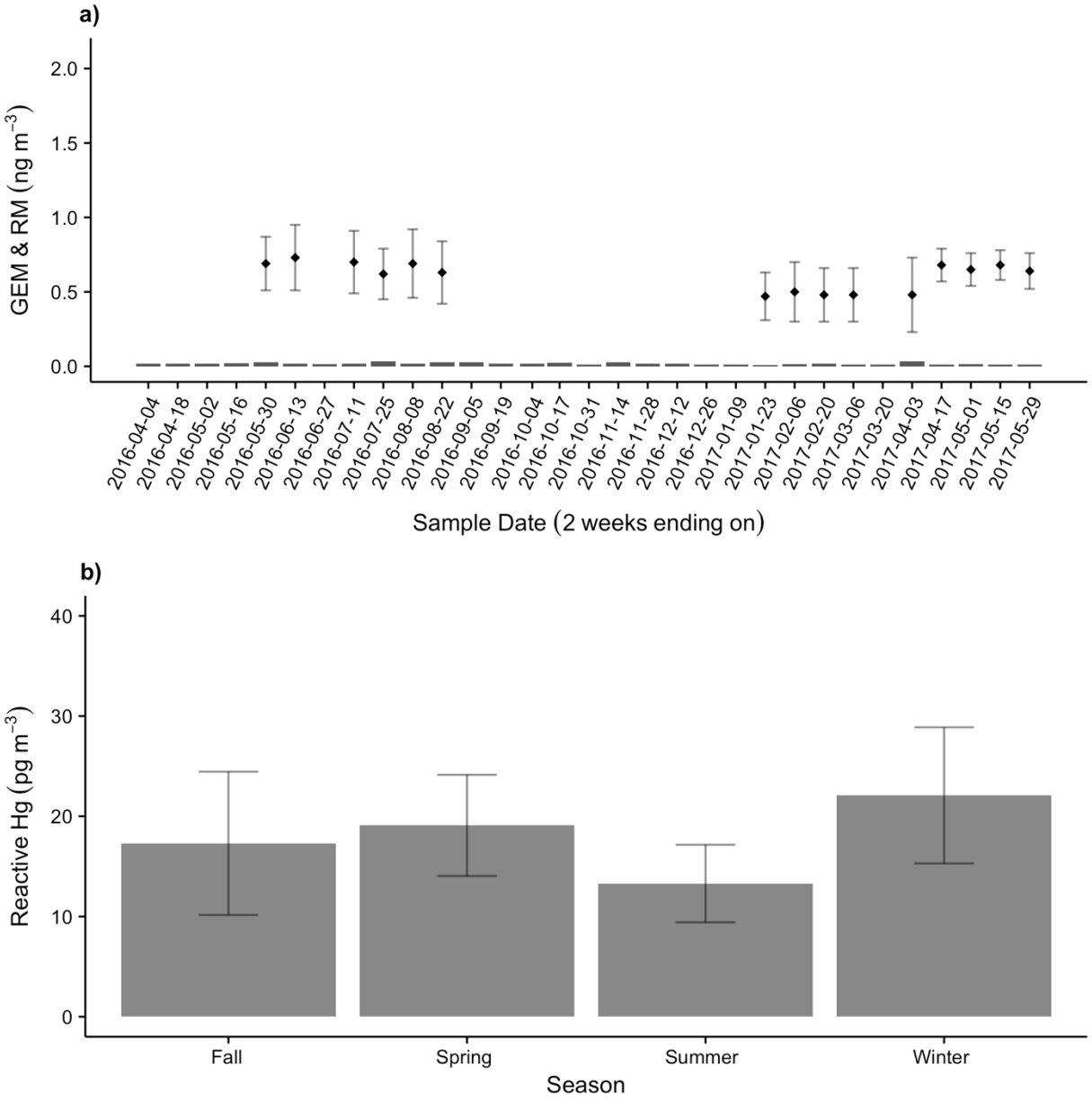

Figure 7.13 *RM and GEM concentrations at MQAWS for a) 2-week sample periods and b) seasonal averages (RM only).*

The difference between summer and winter RM concentrations appears to be largely a function of very different air sources. The relatively high winter RM is associated with ~50% of air flow originating from the west and northwest (Fig 7.12b), a direction that is entirely terrestrial, with varying degrees of urban and industrial development. The majority of significant point source Hg emissions in the Sydney Basin are to the south and west of the MQAWS site, primarily from municipal waste processing, power, generation, and refining (Fig. 7.14). For the reporting period 2016/2017, total Hg emissions in the Sydney area were 43.7 kg, and the largest near-field emitter in the Sydney Basin was the Qenos Olefines polyethylene manufacturing plant in the Botany Bay area (27 kg y^{-1}), south-southeast of MQAWS.

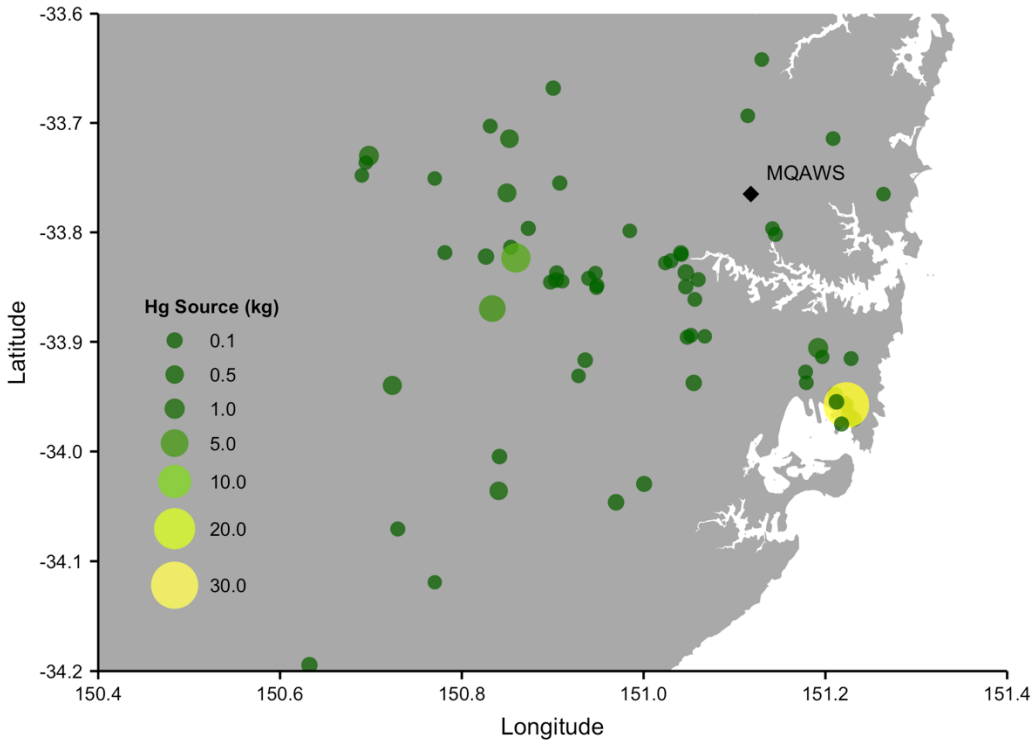

Figure 7.14 *Location and magnitude (kg yr^{-1}) of point source Hg emissions in Sydney area. Data acquired from Australian National Pollutant Inventory 2016/2017 Data Archive.*

Back trajectory calculations for the 2-week sample period with the highest observed RM concentration at MQAWS (32.5 ± 4.4 pg m^{-3}, July 11-25, 2016) demonstrate that a majority of air masses traveled over wide areas of the continent and passed over the urban/industrial areas of western Sydney before reaching the site from the western quadrant (Fig. 7.15). It is likely that in sample periods with this general source area scenario, terrestrial and point source emissions contribute to enhanced RM concentrations.

In contrast to winter patterns, prevailing summertime easterly winds (Fig. 7.12a) originate from maritime air and travel a relatively brief distance over land and the less dense suburban neighborhoods of Northern Sydney, an area with no significant Hg source emissions (Fig 7.14). The lowest observed RM concentration at MQAWS (7.0 ± 1.1 pg m^{-3}) occurred in the summer sample period January 9 – 23, 2017. Back trajectory calculations for this period confirm that air arrived at the site predominantly from the eastern quadrant, having passed through the MBL over the Southern Ocean and Tasman Sea, though a minority of trajectories arrived from a southerly direction (Fig. 7.16).

The more maritime summer-season RM concentrations at MQAWS of 13.3 ± 3.9 pg m^{-3} are very similar to the most representative baseline RM concentrations of 12.9 ± 2.1 pg m^{-3} observed at CGBAPS. Thus, an RM concentration around 13 pg m^{-3} may be representative of an average MBL concentration for coastal waters around southeastern Australia.

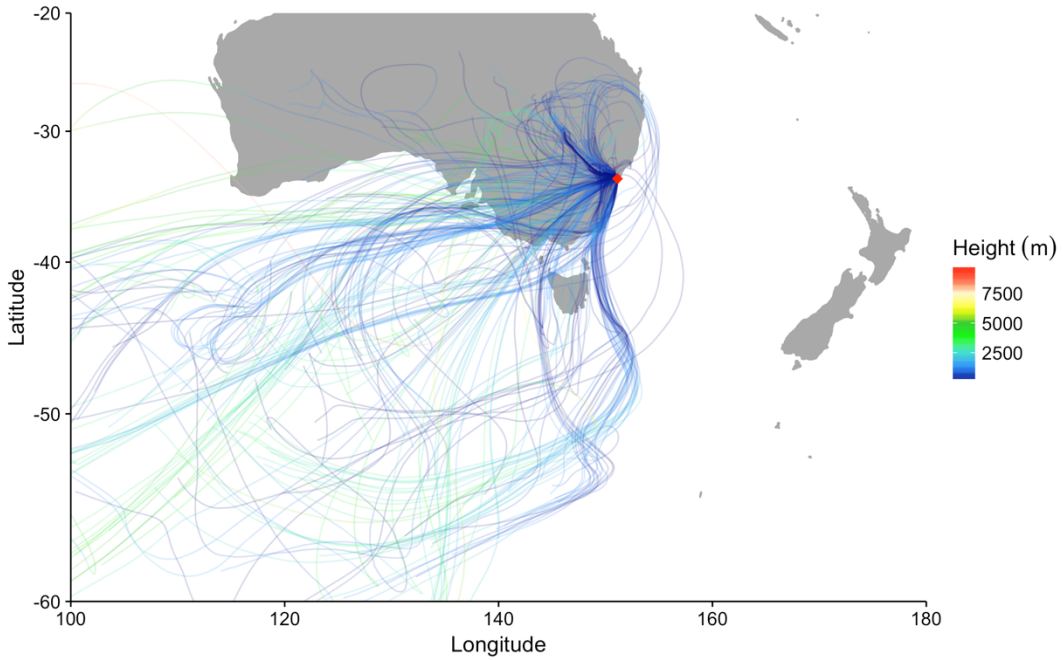

Figure 7.15 *Ensemble of 120 h back trajectory plots for air arriving at MQAWS during a representative winter period (July 11 – 25, 2016). Trajectories initiated hourly from a single point above station with height of 0.5x mixed layer depth.*

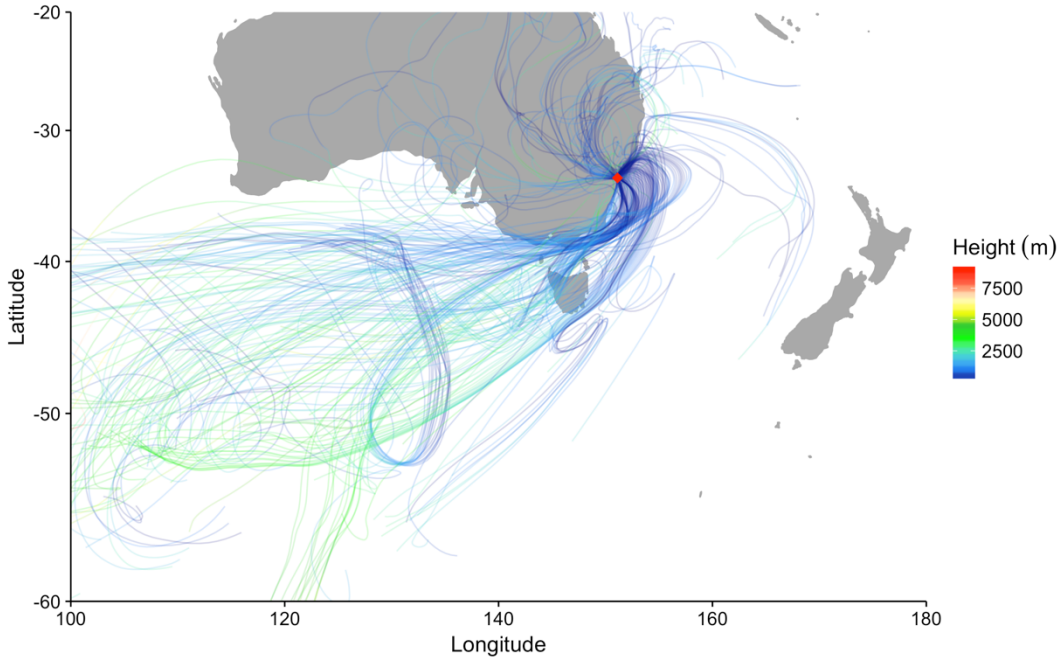

Figure 7.16 *Ensemble of 120 h back trajectory plots for air arriving at MQAWS during a representative summer period (January 9 – 23, 2017). Trajectories initiated hourly from a single point above station with height of 0.5x mixed layer depth.*

7.3.5 Reactive Hg on RV Investigator research voyage

CEM filters were deployed on RVI during an extended research voyage to the East Antarctic coast from January 10 to March 4, 2017. The mean hourly GEM concentration over the entire voyage was 0.53 ± 0.10 ng m^{-3} (n = 978) and ranged from 0.2 to 0.8 ng m^{-3} (Fig. 7.17). GEM concentrations were distinctly and significantly lower (0.42 ± 0.05 ng m^{-3}, n = 134, Welch t-test, $p < 0.000$) between 43.5 – 53.5 ° south latitude compared to the voyage as a whole, for both the outbound and return segments of the voyage. The mean RM concentration over all deployments was 23.5 ± 6.7 pg m^{-3} (n = 4). The mean CEM filter blank was 26.4 ± 8.5 pg, resulting in an average MDL of 1.8 pg m^{-3} for a 2-week sample period, which all filter measurements were well above.

The first filter deployment (January 10 – 26) included four days in the port of Hobart before the voyage south began at approximately 18:00 ship's time, January 14, and so is somewhat compromised by the port environment. The second and third 2-week CEM filter deployments occurred while RVI was on station off the East Antarctic coast between 113-122 °east longitude (ship track and GEM shown Fig. 7.18 and 7.19), and these samples can be considered Antarctic background. Mean RM concentrations were 32.5 ± 3.3 pg m^{-3} (n = 3) in the first 2 weeks, and 21.8 pg m^{-3} (21.2-22.3 pg m^{-3}, n = 2) in the following 2 weeks. The final filter deployment included the transit back to port, and was relatively low at 16.4 ± 2.5 pg m^{-3}

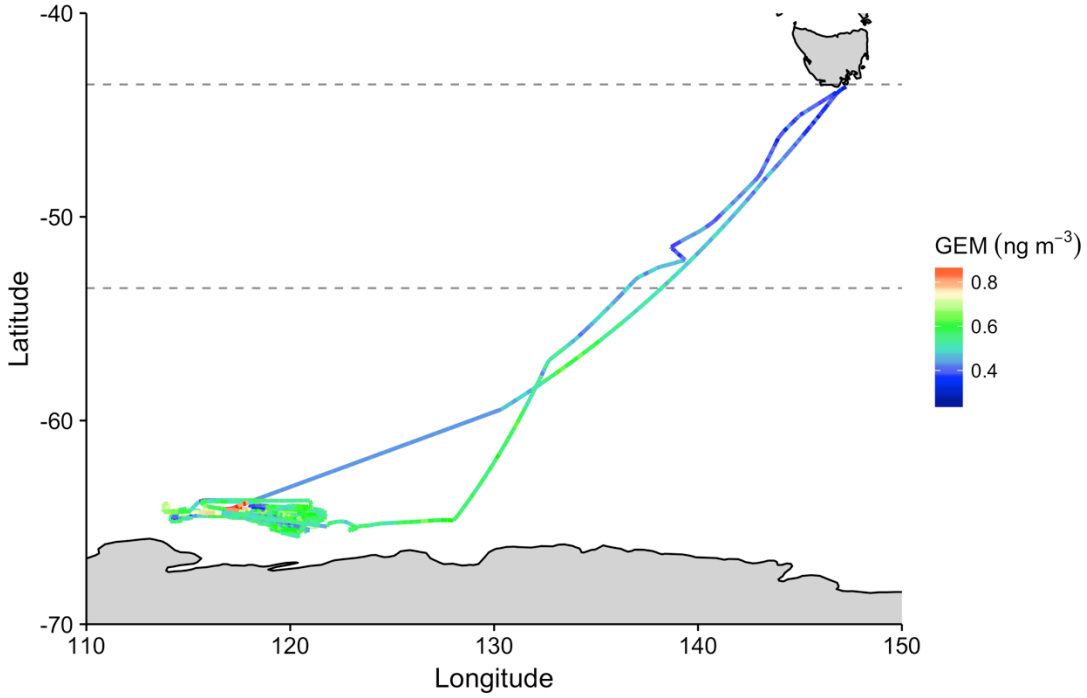

Figure 7.17 *Hourly GEM concentrations along course of RVI voyage in Southern Ocean, January 14 – March 4, 2017. Low GEM values between -43.5 and -53.5 latitudes bracketed by dashed lines. Periods of no data indicated by grey line segments.*

Mean hourly GEM concentrations were highly variable (0.22-0.88 ng m^{-3}) and on average significantly higher while off the East Antarctic coast (0.56 ± 0.11 ng m^{-3}, n = 568, Welch t-test, $p < 0.000$), relative to the overall voyage. An apparent GEM hotspot with hourly concentrations above 0.8 ng m^{-3} was observed around coordinates -64.3 S 117.5 W, during two different transects of the area (January 28 and February 13). Elevated GEM concentrations were also only strongly evident at midday (10:00-16:00), which may indicate a diurnal GEM source mechanism. Back trajectories initiated from RVI's position in the GEM hotspot area on January 28 indicated air masses originating over the Ross Sea and traveling at low altitude along the East Antarctic coast and the Dumont d'Urville Sea (Fig 7.20). This is not easily classifiable as either a maritime or continental air source.

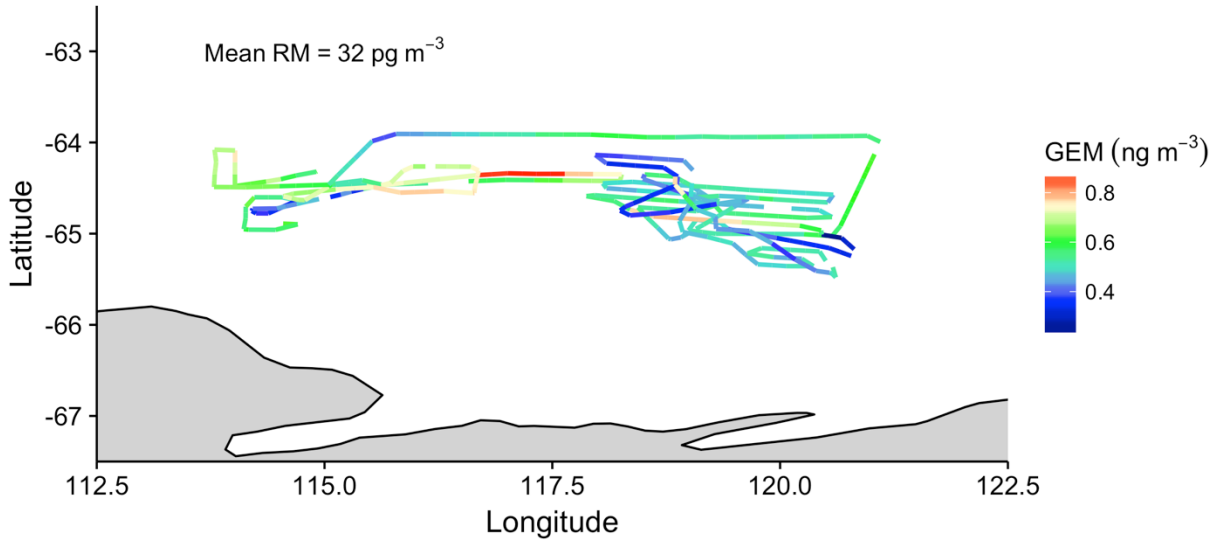

Figure 7.18 *Hourly GEM concentrations along RVI course while on station off the Antarctic coast, CEM filter deployment Jan. 26 – Feb. 8, 2017. GEM hotspot on Jan. 28 13:00-16:00, along -64.3 ° south latitude and between 117.0 and 117.9 ° east longitude.*

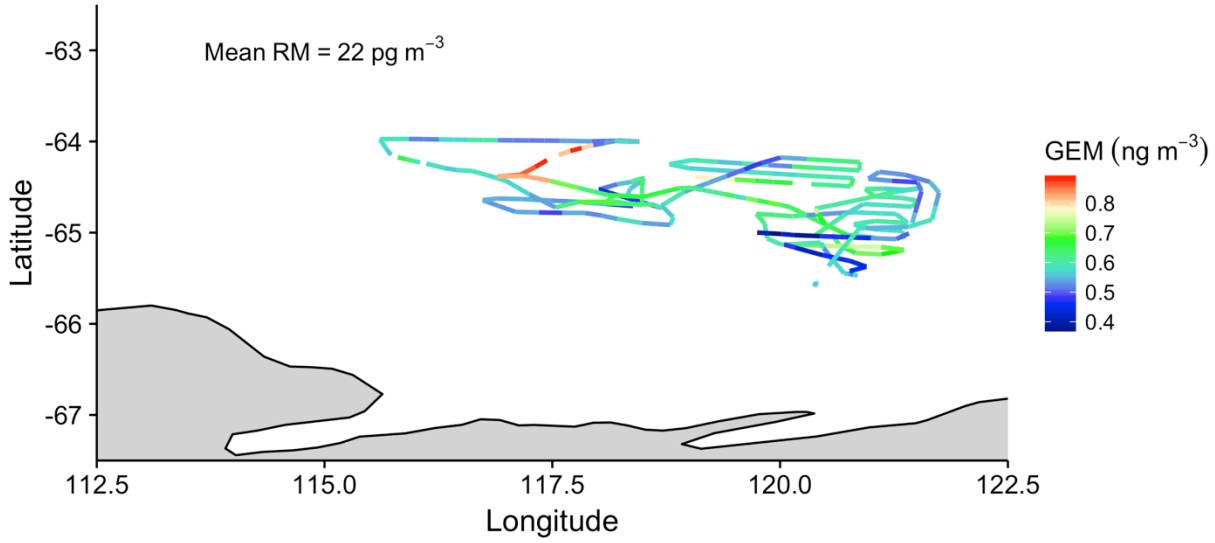

Figure 7.19 *Hourly GEM concentrations along RVI course while on station off the Antarctic coast, CEM filter deployment Feb. 8 – Feb. 20, 2017. GEM hotspot on Feb. 13 10:00-16:00, between -64.0 and -64.3 ° south latitude and between 117.0 and 117.9 ° east longitude.*

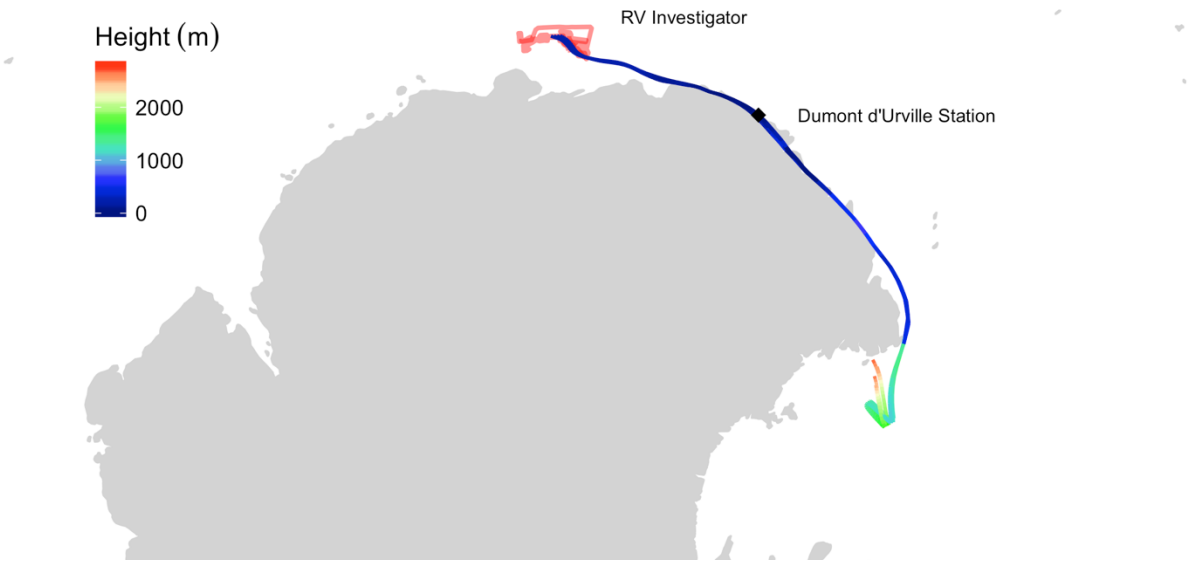

Figure 7.20 *120 h back trajectories arriving at RVI position hourly between 13:00-16:00, Jan. 28, during GEM enhancement.*

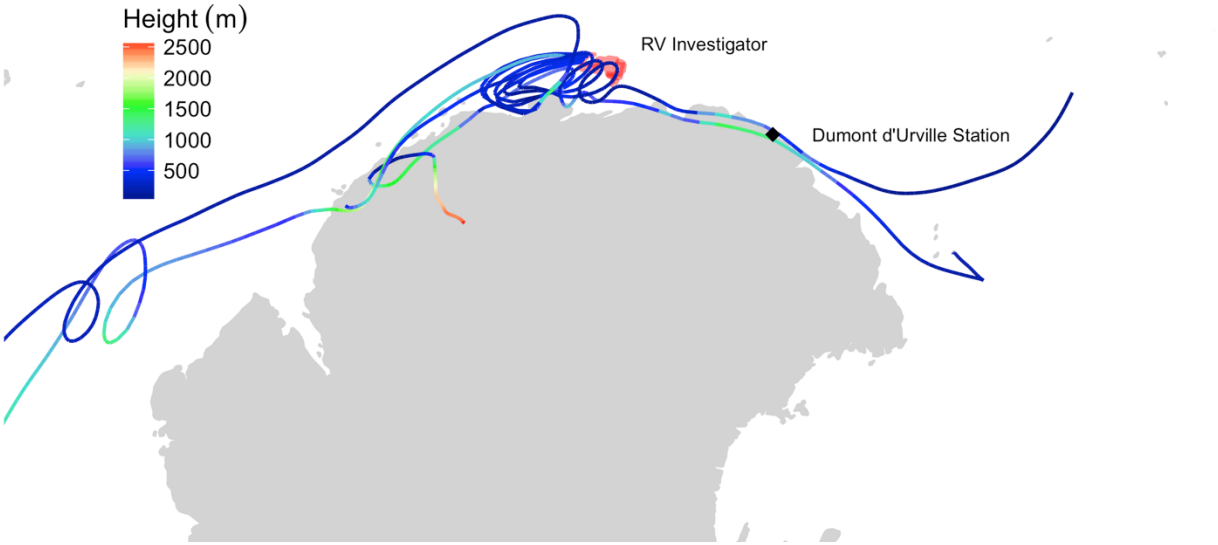

Figure 7.21 *120 h back trajectories arriving at RVI position hourly between 10:00-16:00, Feb. 13, during GEM enhancement.*

Back trajectories from the February 13 GEM enhancement arrive from multiple directions in a cyclonic spiral indicative of a SH low-pressure system. The RVI ship's log confirms storm conditions on February 12-13. It is difficult to ascertain a definite source region for this period, but some of the back trajectories follow the same coastal path as during the January 28 GEM enhancement, and it may be that these two events result from related sources.

Previous observations along this region of the Antarctic coast at Dumont d'Urville Station have also demonstrated high variability in summertime GEM concentrations (0.1 to 3.6 ng m^{-3}), attributed to variations between marine and continental source air, as well as possible diurnal enhancements in GEM concentration due to emissions from snow and ornithogenic (penguin guano) soil surfaces (Angot et al., 2016a; Angot et al., 2016b). In-situ oxidation of GEM to RM is thought to be comparatively low in this region of Antarctica due to less extensive sea ice cover and therefore a lower abundance of available reactive bromine molecules, resulting in less efficient oxidative bromine chemistry. Angot et al. (2016b) have speculated that air enriched in RM species reaches the Dumont d'Urville coast from the high interior Antarctic plateau, where GEM is oxidized in-situ through efficient OH/NOx chemistry. The relatively high RM concentrations measured on RVI may be attributable to a similar transport mechanism from the continental interior, which would likely correspond with the voyage sections where GEM was depleted. Unfortunately, given the long 2-week RM sample time, it is impossible to know with finer resolution exactly when and where in the voyage track the elevated RM concentrations occurred.

7.3.6 Cation exchange membrane performance

Mean RM breakthrough to the secondary CEM filters was 21.1 ± 9.5% (n = 114) at CGBAPS and 17.8 ± 9.9% (n = 92) at MQAWS. These rates of RM breakthrough were statistically significantly different (Welch t-test, $p = 0.01$). At each site, comparison of 2-week median breakthrough values to corresponding 2-week mean concentrations of GEM, median values of temperature, RH, barometric pressure, wind speed, and total 2-week precipitation revealed no correlation. However, MQAWS was overall hotter and more humid than the CGBAPS site, and its possible this contributed to the slightly higher mean rates of RM breakthrough. During the RVI voyage, mean RM breakthrough to the secondary filters was 19.1 ± 5.1% (n = 10), very similar to breakthrough at the ground-based monitoring sites. The voyage was generally cooler but more humid than at either ground site.

There has been speculation that humidity in particular might have an impact on RM collection and possible breakthrough on the CEM material (Huang and Gustin, 2015). Though humidity has not been shown to effect RM breakthrough on CEM filters loaded with a pure GOM compound ($HgBr_2$) in clean, particle-free laboratory air (Miller et al., submitted, this thesis), the effects of RH in ambient air remain unclear. We hypothesized that in ambient air, PBM larger than the CEM pore size (0.8 μm) could be collected and, reacting with other atmospheric constituents such as water vapor, potentially volatilized from the primary filter surface as a gas-phase reactive Hg species, escaping to the secondary filter as breakthrough. However, a comparison of total particle counts in each sample period versus mean % RM breakthrough failed to reveal any relationship (Fig 7.22, $r^2 < 0.000$). However, particle counts included everything down to 0.0025 μm, and a more selective count at sizes larger than the filter pore size might be more relevant.

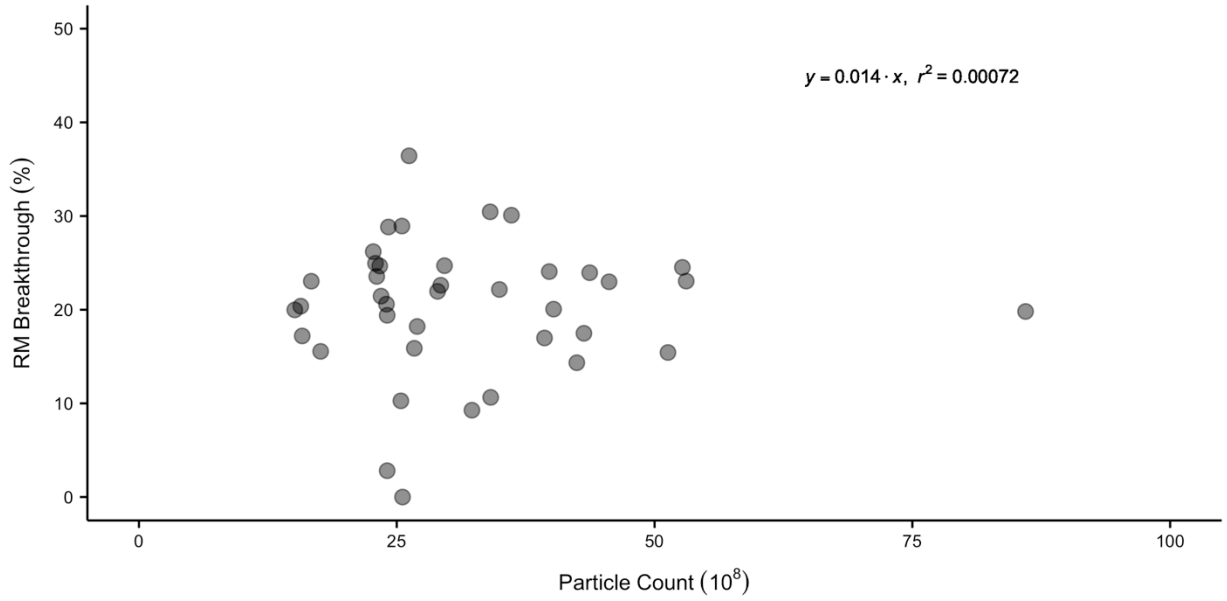

Figure 7.22 *Total 2-week particle counts (0.0025-10 µm particle size) versus mean percent RM breakthrough to secondary CEM filters at CGBAPS.*

7.4 Discussion and Conclusions

Reactive mercury concentrations were relatively uniform between the CGBAPS and MQAWS sites, averaging around 16 and 18 pg m^{-3}, respectively, and ranging from 6 to 48 pg m^{-3}. RM concentrations measured on the RVI voyage in the Southern Ocean were in a similar range (16-32 pg m^{-3}) as the ground-based sites. These results suggest that RM concentrations are relatively stable, likely due to a semi-steady-state equilibrium between in-situ formation and depositional processes within the MBL, as suggested in other studies. However, total RM concentrations measured in this study (overall average 19 pg m^{-3}) were somewhat higher than concentrations reported for the MBL in many previous studies (~2 to 10 pg m^{-3} total RM). We believe this is largely due to the collection of PBM associated with all coarse sea-salt aerosols larger than the CEM filter pore size of 0.8 µm, versus exclusion of coarse aerosols > 2.5 µm by the conventional Tekran® 2537/1130/1135 speciation system.

No samples were below detection limit at the 2-week temporal resolution of the filter samples. In this study there was no discernible correlation between either RM collection or RM breakthrough with humidity or any other measured environmental parameter, including total particle counts at CGBAPS. The mechanism of RM breakthrough in ambient air CEM samples remains unclear, though greater size-selectivity in particle count analysis could be potentially illuminating.

At CGBAPS there was no meaningful seasonal variation in RM concentrations, though isolated periods were occasionally notably higher or lower than average. Widespread bushfire activity in Tasmania and near the CGBAPS site was the largest source of variation in both GEM and RM concentrations but was highly atypical. The overall lack of variation in RM concentration at CGBAPS is likely attributable to the background marine environment, with generally mild conditions, relatively consistent source air, and constant RM source concentrations formed in-situ in the MBL.

In contrast to CGBAPS, the MQAWS site experienced statistically higher RM concentrations in the winter versus the summer. During the summer months, air masses predominantly arrived from the MBL to the east and southeast, versus the prevalence of a northwesterly wind in the winter arriving from terrestrial surfaces. These summertime maritime RM concentrations at MQAWS were comparable to baseline RM concentrations at CGBAPS, suggesting uniform MBL RM concentrations in coastal Australian waters.

High variability in GEM concentrations and elevated RM concentrations were observed from the RV Investigator on transects immediately off the East Antarctic coast. Though in a similar overall range, average RM concentrations off the Antarctic coast were somewhat higher than at the ground-based temperate coastal measurement sites at CGBAPS and MQAWS. The high variability in GEM concentrations (0.2 to 0.9 ng m^{-3}) is in-line with other observations from the

East Antarctic coast, and the relatively high RM concentrations may be due to Antarctic continental outflow.

The RM concentrations measured in this study using the CEM filter-based method are higher relative to most other measurements in the MBL using the Tekran® 2537/1130/1135 Speciation System, and this may have important implications for global ocean-atmosphere models for Hg.

References

Ambrose JL, Lyman SN, Huang J, Gustin MS, Jaffe DA. Fast Time Resolution Oxidized Mercury Measurements during the Reno Atmospheric Mercury Intercomparison Experiment (RAMIX). Environmental Science & Technology 2013; 47: 7285-7294.

Angot H, Barret M, Magand O, Ramonet M, Dommergue A. A 2-year record of atmospheric mercury species at a background Southern Hemisphere station on Amsterdam Island. Atmospheric Chemistry and Physics 2014; 14: 11461-11473.

Angot H, Dastoor A, De Simone F, Gårdfeldt K, Gencarelli CN, Hedgecock IM, et al. Chemical cycling and deposition of atmospheric mercury in polar regions: review of recent measurements and comparison with models. Atmos. Chem. Phys. 2016a; 16: 10735-10763.

Angot H, Dion I, Vogel N, Legrand M, Magand O, Dommergue A. Multi-year record of atmospheric mercury at Dumont d'Urville, East Antarctic coast: continental outflow and oceanic influences. Atmos. Chem. Phys. 2016b; 16: 8265-8279.

Brooks S, Arimoto R, Lindberg S, Southworth G. Antarctic polar plateau snow surface conversion of deposited oxidized mercury to gaseous elemental mercury with fractional long-term burial. Atmospheric Environment 2008a; 42: 2877-2884.

Brooks S, Lindberg S, Southworth G, Arimoto R. Springtime atmospheric mercury speciation in the McMurdo, Antarctica coastal region. Atmospheric Environment 2008b; 42: 2885-2893.

Brunke E-G, Walters C, Mkololo T, Martin L, Labuschagne C, Silwana B, et al. Mercury in the atmosphere and in rainwater at Cape Point, South Africa. Atmospheric Environment 2016; 125: 24-32.

Chand D, Jaffe D, Prestbo E, Swartzendruber PC, Hafner W, Weiss-Penzias P, et al. Reactive and particulate mercury in the Asian marine boundary layer. Atmospheric Environment 2008; 42: 7988-7996.

Cheng I, Zhang L. Uncertainty Assessment of Gaseous Oxidized Mercury Measurements Collected by Atmospheric Mercury Network. Environmental Science & Technology 2017; 51: 855-862.

Diéguez MC, Garcia PE, Bencardino M, D'Amore F, Castagna J, Ribeiro Guevara S, et al. Four years of atmospheric mercury records in Northwestern Patagonia (Argentina): potential sources, concentration patterns and influence of environmental variables observed at the GMOS EMMA station. Atmos. Chem. Phys. Discuss. 2017; 2017: 1-18.

Dommergue A, Sprovieri F, Pirrone N, Ebinghaus R, Brooks S, Courteaud J, et al. Overview of mercury measurements in the Antarctic troposphere. Atmospheric Chemistry and Physics 2010; 10: 3309-3319.

Draxler R, Hess G. An Overview of the HYSPLIT_4 Modelling System for Trajectories, Dispersion on and Deposition. Australian Meteorological Magazine 1998; 47: 295-308.

Ebinghaus R, Kock HH, Temme C, Einax JW, Löwe AG, Richter A, et al. Antarctic Springtime Depletion of Atmospheric Mercury. Environmental Science & Technology 2002; 36: 1238-1244.

Feddersen DM, Talbot R, Mao H, Sive BC. Size distribution of particulate mercury in marine and coastal atmospheres. Atmos. Chem. Phys. 2012; 12: 10899-10909.

Finley BD, Swartzendruber PC, Jaffe DA. Particulate mercury emissions in regional wildfire plumes observed at the Mount Bachelor Observatory. Atmospheric Environment 2009; 43: 6074-6083.

Gustin M, Jaffe D. Reducing the Uncertainty in Measurement and Understanding of Mercury in the Atmosphere. Environmental Science & Technology 2010; 44: 2222-2227.

Gustin MS, Amos HM, Huang J, Miller MB, Heidecorn K. Measuring and modeling mercury in the atmosphere: a critical review. Atmos. Chem. Phys. 2015; 15: 5697-5713.

Gustin MS, Pierce AM, Huang J, Miller MB, Holmes HA, Loria-Salazar SM. Evidence for Different Reactive Hg Sources and Chemical Compounds at Adjacent Valley and High Elevation Locations. Environmental Science & Technology 2016; 50: 12225-12231.

Hedgecock I, Pirrone N. Mercury and photochemistry in the marine boundary layer-modelling studies suggest the in situ production of reactive gas phase mercury. Atmospheric Environment 2001; 35: 3055-3062.

Hedgecock I, Pirrone N, Sprovieri F, Pesenti E. Reactive gaseous mercury in the marine boundary layer: modelling and experimental evidence of its formation in the Mediterranean region. Atmospheric Environment 2003; 37: S41-S49.

Holmes CD, Jacob DJ, Corbitt ES, Mao J, Yang X, Talbot R, et al. Global atmospheric model for mercury including oxidation by bromine atoms. Atmos. Chem. Phys. 2010; 10: 12037-12057.

Holmes CD, Jacob DJ, Mason RP, Jaffe DA. Sources and deposition of reactive gaseous mercury in the marine atmosphere. Atmospheric Environment 2009; 43: 2278-2285.

Horowitz H, Jacob D, Zhang Y, Dibble T, Slemr F, Amos H, et al. A new mechanism for atmospheric mercury redox chemistry: implications for the global mercury budget. Atmospheric Chemistry and Physics 2017; 17: 6353-6371.

Howard D. Aspects of the Biogeochemical Cycling of Mercury in Australia and the Southern Hemisphere. Department of Environmental Science. PhD. Macquarie University, Sydney, Australia, 2018, pp. 160.

Howard D, Nelson PF, Edwards GC, Morrison AL, Fisher JA, Ward J, et al. Atmospheric mercury in the Southern Hemisphere tropics: seasonal and diurnal variations and influence of inter-hemispheric transport. Atmos. Chem. Phys. 2017; 17: 11623-11636.

Huang J, Gustin MS. Uncertainties of Gaseous Oxidized Mercury Measurements Using KCl-Coated Denuders, Cation-Exchange Membranes, and Nylon Membranes: Humidity Influences. Environmental Science & Technology 2015; 49: 6102-6108.

Huang J, Miller MB, Edgerton E, Sexauer Gustin M. Deciphering potential chemical compounds of gaseous oxidized mercury in Florida, USA. Atmos. Chem. Phys. 2017; 17: 1689-1698.

Huang J, Miller MB, Weiss-Penzias P, Gustin MS. Comparison of Gaseous Oxidized Hg Measured by KCl-Coated Denuders, and Nylon and Cation Exchange Membranes. Environmental Science & Technology 2013; 47: 7307-7316.

Jaffe DA, Lyman S, Amos HM, Gustin MS, Huang J, Selin NE, et al. Progress on Understanding Atmospheric Mercury Hampered by Uncertain Measurements. Environmental Science & Technology 2014; 48: 7204-7206.

Landis MS, Stevens RK, Schaedlich F, Prestbo EM. Development and characterization of an annular denuder methodology for the measurement of divalent inorganic reactive gaseous mercury in ambient air. Environmental Science & Technology 2002; 36: 3000-3009.

Laurier F, Mason R. Mercury concentration and speciation in the coastal and open ocean boundary layer. Journal of Geophysical Research-Atmospheres 2007; 112.

Laurier F, Mason R, Whalin L, Kato S. Reactive gaseous mercury formation in the North Pacific Ocean's marine boundary layer: A potential role of halogen chemistry. Journal of Geophysical Research-Atmospheres 2003; 108.

Lyman S, Jaffe D. Formation and fate of oxidized mercury in the upper troposphere and lower stratosphere. Nature Geoscience 2012; 5: 114-117.

Lyman S, Jones C, O'Neil T, Allen T, Miller M, Gustin MS, et al. Automated Calibration of Atmospheric Oxidized Mercury Measurements. Environmental Science & Technology 2016; 50: 12921-12927.

Lyman SN, Jaffe DA, Gustin MS. Release of mercury halides from KCl denuders in the presence of ozone. Atmospheric Chemistry and Physics 2010; 10: 8197-8204.

Malcolm EG, Keeler GJ. Evidence for a sampling artifact for particulate-phase mercury in the marine atmosphere. Atmospheric Environment 2007; 41: 3352-3359.

Marumoto K, Hayashi M, Takami A. Atmospheric mercury concentrations at two sites in the Kyushu Islands, Japan, and evidence of long-range transport from East Asia. Atmospheric Environment 2015; 117: 147-155.

Marusczak N, Sonke JE, Fu X, Jiskra M. Tropospheric GOM at the Pic du Midi Observatory—Correcting Bias in Denuder Based Observations. Environmental Science & Technology 2017; 51: 863-869.

Mason RP, Lawson NM, Sheu GR. Mercury in the Atlantic Ocean: factors controlling air–sea exchange of mercury and its distribution in the upper waters. Deep Sea Research Part II: Topical Studies in Oceanography 2001; 48: 2829-2853.

Mason RP, Sheu GR. Role of the ocean in the global mercury cycle. Global Biogeochemical Cycles 2002; 16: 40-1-40-14.

McClure CD, Jaffe DA, Edgerton ES. Evaluation of the KCI Denuder Method for Gaseous Oxidized Mercury using HgBr2 at an In-Service AMNet Site. Environmental Science & Technology 2014; 48: 11437-11444.

Miller MB, Fine R, Pierce AM, Gustin MS. Identifying sources of ozone to three rural locations in Nevada, USA, using ancillary gas pollutants, aerosol chemistry, and mercury. Science of The Total Environment 2015; 530-531: 483-492.

Mohiuddin K, Strezov V, Nelson PF, Stelcer E. Characterisation of trace metals in atmospheric particles in the vicinity of iron and steelmaking industries in Australia. Atmospheric Environment 2014; 83: 72-79.

NPI. Australian National Pollutant Inventory. Australian Government, 2017.

Obrist D, Tas E, Peleg M, Matveev V, Fain X, Asaf D, et al. Bromine-induced oxidation of mercury in the mid-latitude atmosphere. Nature Geoscience 2011; 4: 22-26.

Pfaffhuber K, Berg T, Hirdman D, Stohl A. Atmospheric mercury observations from Antarctica: seasonal variation and source and sink region calculations. Atmospheric Chemistry and Physics 2012; 12: 3241-3251.

Pierce AM, Gustin MS. Development of a Particulate Mass Measurement System for Quantification of Ambient Reactive Mercury. Environmental Science & Technology 2017; 51: 436-445.

Schroeder WH, Anlauf KG, Barrie LA, Lu JY, Steffen A, Schneeberger DR, et al. Arctic springtime depletion of mercury. Nature 1998; 394: 331.

Sexauer Gustin M, Pierce AM, Huang J, Miller MB, Holmes HA, Loria-Salazar SM. Evidence for Different Reactive Hg Sources and Chemical Compounds at Adjacent Valley and High Elevation Locations. Environmental Science & Technology 2016; 50: 12225-12231.

Slemr F, Angot H, Dommergue A, Magand O, Barret M, Weigelt A, et al. Comparison of mercury concentrations measured at several sites in the Southern Hemisphere. Vol 15, 2015.

Soerensen AL, Skov H, Jacob DJ, Soerensen BT, Johnson MS. Global Concentrations of Gaseous Elemental Mercury and Reactive Gaseous Mercury in the Marine Boundary Layer. Environmental Science & Technology 2010; 44: 7425-7430.

Sommar J, Andersson ME, Jacobi HW. Circumpolar measurements of speciated mercury, ozone and carbon monoxide in the boundary layer of the Arctic Ocean. Atmos. Chem. Phys. 2010; 10: 5031-5045.

Sprovieri F, Hedgecock I, Pirrone N. An investigation of the origins of reactive gaseous mercury in the Mediterranean marine boundary layer. Atmospheric Chemistry and Physics 2010; 10: 3985-3997.

Sprovieri F, Pirrone N, Bencardino M, D'Amore F, Carbone F, Cinnirella S, et al. Atmospheric mercury concentrations observed at ground-based monitoring sites globally distributed in the framework of the GMOS network. Atmos. Chem. Phys. 2016; 16: 11915-11935.

Sprovieri F, Pirrone N, Hedgecock IM, Landis MS, Stevens RK. Intensive atmospheric mercury measurements at Terra Nova Bay in Antarctica during November and December 2000. Journal of Geophysical Research: Atmospheres 2002; 107: ACH 20-1-ACH 20-8.

Steffen A, Bottenheim J, Cole A, Douglas TA, Ebinghaus R, Friess U, et al. Atmospheric mercury over sea ice during the OASIS-2009 campaign. Atmos. Chem. Phys. 2013; 13: 7007-7021.

Steffen A, Douglas T, Amyot M, Ariya P, Aspmo K, Berg T, et al. A synthesis of atmospheric mercury depletion event chemistry in the atmosphere and snow. Atmos. Chem. Phys. 2008; 8: 1445-1482.

Steffen A, Schroeder W, Bottenheim J, Narayan J, Fuentes JD. Atmospheric mercury concentrations: measurements and profiles near snow and ice surfaces in the Canadian Arctic during Alert 2000. Atmospheric Environment 2002; 36: 2653-2661.

Strode S, Jaeglé L, Selin Noelle E, Jacob Daniel J, Park Rokjin J, Yantosca Robert M, et al. Air-sea exchange in the global mercury cycle. Global Biogeochemical Cycles 2007; 21.

Swartzendruber PC, Jaffe DA, Finley B. Development and First Results of an Aircraft-Based, High Time Resolution Technique for Gaseous Elemental and Reactive (Oxidized) Gaseous Mercury. Environmental Science & Technology 2009; 43: 7484-7489.

Talbot R, Mao H, Feddersen D, Smith M, Kim S, Sive B, et al. Comparison of Particulate Mercury Measured with Manual and Automated Methods. Atmosphere 2011; 2: 1-20.

Temme C, Einax JW, Ebinghaus R, Schroeder WH. Measurements of Atmospheric Mercury Species at a Coastal Site in the Antarctic and over the South Atlantic Ocean during Polar Summer. Environmental Science & Technology 2003; 37: 22-31.

Timonen H, Ambrose J, Jaffe D. Oxidation of elemental Hg in anthropogenic and marine airmasses. Atmospheric Chemistry and Physics 2013; 13: 2827-2836.

UNEP. Minamata Convention on Mercury, 2013.

UNEP. Global Review of Mercury Monitoring Networks. United Nations Environment Programme, Geneva, Switzerland, 2016, pp. 48.

Wang F, Saiz-Lopez A, Mahajan A, Martin J, Armstrong D, Lemes M, et al. Enhanced production of oxidised mercury over the tropical Pacific Ocean: a key missing oxidation pathway. Atmospheric Chemistry and Physics 2014; 14: 1323-1335.

Weiss-Penzias P, Amos H, Selin N, Gustin M, Jaffe D, Obrist D, et al. Use of a global model to understand speciated atmospheric mercury observations at five high-elevation sites. Atmospheric Chemistry and Physics 2015; 15: 1161-1173.

Weiss-Penzias P, Jaffe D, Swartzendruber P, Hafner W, Chand D, Prestbo E. Quantifying Asian and biomass burning sources of mercury using the Hg/CO ratio in pollution plumes observed at the Mount Bachelor observatory. Atmospheric Environment 2007; 41: 4366-4379.

Weiss-Penzias P, Jaffe DA, McClintick A, Prestbo EM, Landis MS. Gaseous elemental mercury in the marine boundary layer: Evidence for rapid removal in anthropogenic pollution. Environmental Science & Technology 2003; 37: 3755-3763.

Wright G, Gustin MS, Weiss-Penzias P, Miller MB. Investigation of mercury deposition and potential sources at six sites from the Pacific Coast to the Great Basin, USA. Science of The Total Environment 2014; 470-471: 1099-1113.

Zhang L, Lyman S, Mao H, Lin C, Gay D, Wang S, et al. A synthesis of research needs for improving the understanding of atmospheric mercury cycling. Atmospheric Chemistry and Physics 2017; 17: 9133-9144.

CHAPTER 8:

Inter-comparison of Tekran® 2537 B and X models deployed at the Cape Grim Baseline Air Pollution Station

Matthieu B. Miller[1], Dean A. Howard[2], Melita Keywood[3], Jennifer Powell[3], Sam Cleland[4], Grant C. Edwards[1]

[1]Department of Environmental Sciences, Faculty of Science and Engineering, Macquarie University, Sydney NSW, 2113, Australia

[2]Department of Environmental, Earth, and Atmospheric Sciences, University of Massachusetts-Lowell, Lowell MA, 01854, United States

[3]Centre for Australian Climate and Weather Research, Australian Commonwealth Scientific and Industrial Research Organization, Melbourne VIC, Australia

[4]Cape Grim Baseline Air Pollution Station, Observing Systems and Operations, Bureau of Meteorology, Smithton TAS, 7330, Australia

Statement of Authorship

Dr Edwards' research group has and continues to collaborate with the Cape Grim Baseline Air Pollution Station (CGBAPS) atmospheric Hg monitoring program, providing technical expertise and support for the Hg measurements there. The Tekran® 2537 B and X units at CGBAPS are owned and operated by the Australian Bureau of Meteorology (BoM) and the Commonwealth Scientific and Industrial Research Organization (CSIRO), and as such routine checks, maintenance, and data acquisition are performed by BoM personnel. However, Dr Edwards and past and present group research members (former PhD student Dean Howard, and myself), have undertaken more thorough bi-annual maintenance and verification of the Tekran® analyzers at CGBAPS since 2014. I have been primarily responsible for CGBAPS Tekran® data QA/QC since June 2017, the period of time since installation of the 2537X unit. I completed the majority of raw data processing for this manuscript, including the generation of figures, and the majority of writing was completed by myself. This manuscript is being prepared with a view to publication as a short Technical Note in an atmospheric measurements journal.

Study Design: 80% • Data Collection: 30% • Data Analysis: 90% • Writing: 95%

ABSTRACT

Tekran® 2537 B and X Automatic Ambient Air Analyzers were operated in tandem at the Cape Grim Baseline Air Pollution Station (CGBAPS) in Tasmania, Australia, from June 2017 to June 2018. The mean GEM concentration measured by the 2537B unit during this time period was 0.94 ± 0.09 ng m^{-3}, versus 1.08 ± 0.07 ng m^{-3} measured by the 2537X unit, a systematic high bias of 12.8%. Part of this measurement discrepancy was due to a failing permeation source temperature controller, and after repair the bias between instruments narrowed. However, in the last 6 months of data for which we are confident both analyzers were working optimally, GEM concentrations measured by the 2537X (1.06 ± 0.08 ng m^{-3}) were still 8.6% higher than measured on the 2537B (0.97 ± 0.09 ng m^{-3}). This systematic measurement bias may have important implications for the succession of Tekran® 2537X analyzers at ambient Hg monitoring stations globally.

8.1 Introduction

Mercury (Hg) is globally distributed throughout the earth's atmosphere, from which it pervades the remotest environments and food webs as a bio-accumulative neurotoxic agent (Fitzgerald et al., 1998; Selin, 2009). As a pollutant of concern and through commitments stipulated in the United Nations Environment Minamata Convention on Mercury, monitoring of atmospheric Hg is incumbent upon national science and regulatory agencies around the world (UNEP, 2013). Monitoring of gaseous elemental Hg (GEM) is routine and standardized in many monitoring networks (Sprovieri et al., 2016; UNEP, 2016). The myriad potential forms of reactive Hg (RM) are less easily identified and measured (Gustin et al., 2015; Jaffe et al., 2014; Zhang et al., 2017).

Less ambiguously, single atoms of elemental Hg absorb ultra-violet radiation at a wavelength of 253.7 nm and fluoresce. This characteristic allows for precise detection and quantification of GEM via either atomic absorption spectrometry (AAS) or atomic fluorescence spectrometry (AFS). The CVAFS principle of detection is employed in the Tekran® 2537 A/B/X series of Automated Ambient Air Mercury Analyzers (Tekran® Instrument Corporation, Toronto, Canada). The first Tekran® 2537A model was released in 1992, providing a reliable analytical platform for automated high-time resolution GEM measurement, and replacing tedious manual methods for collection of atmospheric Hg on gold traps (Ebinghaus et al., 1999; Schroeder et al., 1995). In well over two decades of use, the Tekran® 2537 platform has featured in hundreds of studies and publications on atmospheric Hg concentration and speciation, emission sources of Hg, and air-surface exchange of Hg.

The fully redesigned and updated Tekran® 2537X was officially released in May 2012, with improved UV source lamp control and optimization circuitry, internal data logging, improved serial and USB communication interfacing, and network capability for remote access and

control. As of August 2015, Tekran® Instruments Corp. advised that many original components of the 2537 A/B units would become obsolete in the near term, and that repair or replacement of some critical components could not be supported indefinitely. As such the 2537 A/B units will increasingly need to be phased-out of existing atmospheric Hg monitoring sites and replaced by the 2537X.

The Cape Grim Baseline Air Pollution Station (CGBAPS) is a premier remote atmospheric monitoring location on the northwestern cape of Tasmania, Australia (-40.683 S 144.690 E). Directly overlooking a long westward fetch of the Indian Ocean from a 94 m high coastal bluff, the station is ideally situated to sample background Southern Hemisphere air. CGBAPS is administered by the Australian Bureau of Meteorology (BoM) and the Commonwealth Scientific and Industrial Research Organization (CSIRO), and is part of the World Meteorological Organization Global Atmosphere Watch (WMO-GAW) program. The station has operated a Tekran® 2537B since 2011 (Slemr et al., 2015).

With a view towards continuing ambient atmospheric Hg monitoring into the foreseeable future, a Tekran® 2537X unit was installed at CGBAPS on May 31, 2017 and following a 2-week shakedown became operational on June 17, 2017. The 2537X unit has been operated side-by-side with the existing station 2537B, which will eventually be retired pending satisfactory inter-comparison performance. Part of the motivation for this study was a preliminary indication that significant measurement bias was occurring between the 2537X and B analyzers at CGBAPS. Additionally, information gleaned at the 2017 International Conference on Mercury as a Global Pollutant indicated other research groups were experiencing a similar bias between older and newer Tekran® analyzers. As such, we undertook an in-depth analysis of Tekran® analyzer performance at CGBAPS over one year.

8.2 Methods

A Tekran® 2537B and 2537X were operated in tandem from June 2017 to June 2018 at the Cape Grim Baseline Air Pollution Station (CGBAPS) in Tasmania, Australia. The Station is maintained by full time technical staff of the Australian Bureau of Meteorology and is fully climate controlled with backup power generation.

The Tekran® analyzers were operated and maintained according to GMOS protocols, with a sample flow rate of 1.0 Lpm and a sample time of 5 min. Ambient air was pulled from station roof railing height (~4 m a.g.l., ~2.2 m above roof height) through a rain-shield, 0.2 μm PTFE particulate filters (changed every 2 weeks), and heated (50 °C) PTFE tubing (0.625 cm O.D., 0.4 cm I.D.). The sample and zero air inlet ports on each analyzer were filtered with 0.2 μm PTFE filters in single-stage 47 mm PFA filter assemblies. Sample air was also scrubbed with soda lime traps (Tekran® p/n 90-13310-06) placed in-line immediately upstream from the rear-port particulate filters, to remove deleterious compounds such as acid aerosols and halogens that could degrade the analyzer gold traps. Each sampling line was exactly identical between analyzers, and lines were cleaned by de-ionized water purge every 6 months.

Each analyzer was calibrated every 25 h from an internal permeation source (controlled at 50 °C) releasing Hg^0 vapor at a constant rate over 120 s into a charcoal-scrubbed 1 Lpm zero air flow. During ambient sampling, an automated standard Hg^0 vapor addition was permeated into the instrument sample stream every 25 h following auto calibration from the internal permeation source. Automated Hg vapor additions were used to verify Hg vapor recovery efficiency in ambient air. The internal permeation sources were verified twice annually by a series of external Hg vapor injections from a primary Hg vapor source (Tekran® 2505 Calibration Unit) via manual syringe (25 μL, Hamilton®, Reno, NV). The external injections were performed at Hg vapor

masses of 80 pg (equivalent to a concentration of 16 ng m^{-3} in 5 L sample volume), 120 pg (24 ng m^{-3}), and 160 pg (32 ng m^{-3}), bracketing the concentrations generated by the internal permeation sources during calibrations.

During the study period, several major technical problems manifested between the two analytical units. On the 2537B, the internal Hg vapor permeation source temperature controller failed due to a degraded control board capacitor. BoM technical staff at CGBAPS were able to repair the control board on-site with minimal data loss. However, this repair required an adjustment of the internal permeation source rate. On the 2537X unit, a period of high baseline deviation and high variability in GEM concentrations was attributed to a bad electrical wiring harness on the UV source lamp. Unfortunately, this issue could not be immediately addressed, resulting in an extended period of unusable data.

All data was processed in Microsoft Excel (version 16.22) and RStudio® (version 3.2.2).

8.3 Results

8.3.1 First year of operation

Over the first year of operation at CGBAPS, the Tekran® 2537X measured a mean GEM concentration of 1.08 ± 0.07 ng m^{-3} (n = 73658 5 min values). Over the same time period, the 2537B analyzer measured a mean concentration of 0.94 ± 0.09 ng m^{-3} (n = 86790). While the instruments tracked relative GEM fluctuations closely, the 2537X unit reported absolute GEM concentrations that were on average 12.8% higher than those measured by the 2537B (Fig. 8.1). This discrepancy is discussed in detail in the following section.

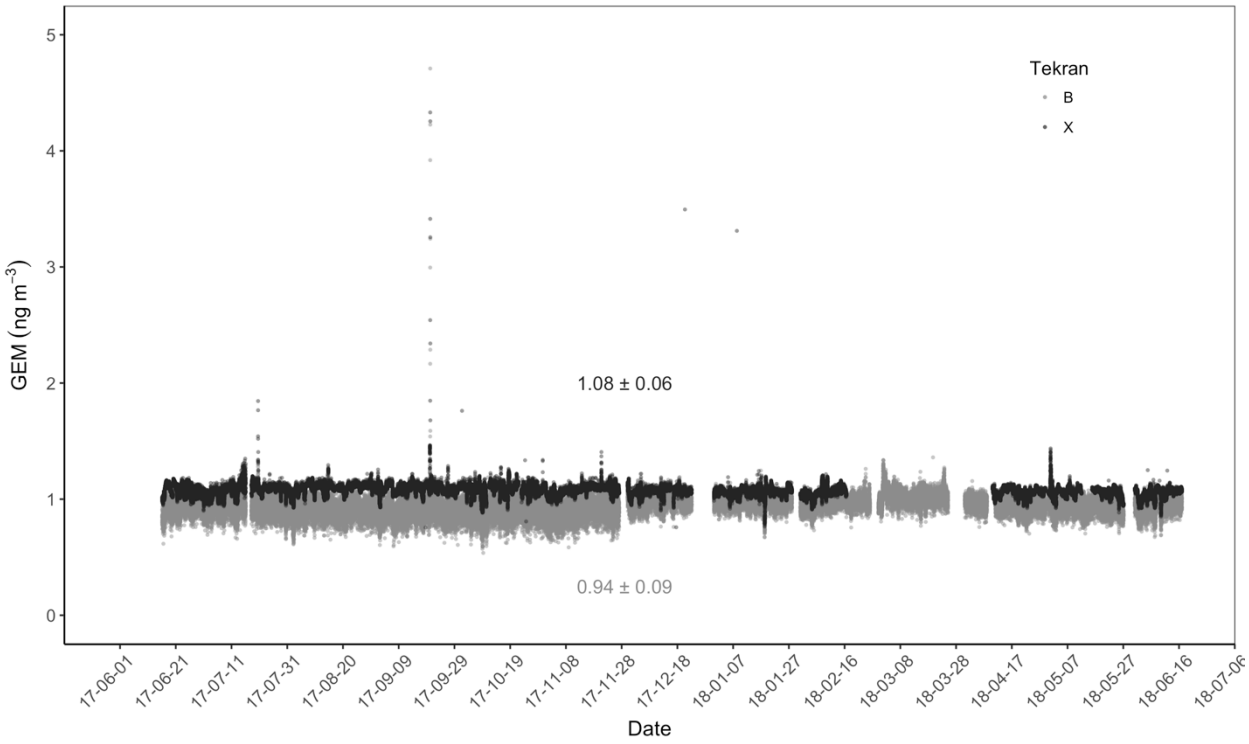

Figure 8.1 *Ambient GEM concentrations (ng m^{-3}) at CGBAPS in the interval June 2017 to June 2018, as measured by Tekran® 2537X (black points) and 2537B (light grey points), with respective overall mean concentrations labeled.*

8.3.2 Measurement discrepancies

During the first 6 months of operation at CGBAPS (June 17 – November 28, 2017), the 2537X measured a mean 5 min GEM concentration of 1.09 ± 0.8 ng m^{-3} (n = 43315), while the 2537B unit measured a mean 5 min GEM concentration of 0.90 ± 0.09 ng m^{-3} (n = 44393). For this time period, the GEM concentration determined by the 2537X was on average 17.0% higher than the 2537B unit. This level of inter-instrument variability was much greater than any inter-site variability observed in Southern Hemisphere atmospheric Hg monitoring sites (Slemr et al., 2015).

In November 2017, bi-annual service and maintenance was completed on both the 2537X and 2537B units at CGBAPS. Initial as-found Hg vapor injections showed that the 2537X unit was

performing in-spec with recoveries of 101.5% (n = 2). However, as-found injections on the 2537B unit resulted in Hg vapor recoveries 109.6% of expected (n = 6). A more thorough examination of the 2537B unit revealed that the permeation source temperature controller was intermittently failing and had likely been progressively degrading over the previous months. A capacitor electrolyte leak was diagnosed as the cause of the failed control board and was replaced on-site. Following repair of the permeation source temperature controller, the internal permeation rate was tested and adjusted based on a full series of manual verification injections.

In the 6 months following maintenance and permeation rate adjustment on the 2537B, the difference between reported GEM concentrations narrowed to 8.6%, indicating that some of the discrepancy between instruments was due to the permeation source performance. However, the 2537X still measured significantly higher ambient GEM concentrations (1.06 ± 0.08 ng m^{-3}, n = 30343) versus the 2537B (0.97 ± 0.09 ng m^{-3}, n = 42963, Welch t-test, $p < 0.000$). This bias was not found to result from the individual sampling lines, as it was still present when both analyzers were plumbed into a single sample line. The performance of the two Tekran® analyzers was otherwise very good, as discussed in the following section.

8.3.3 Performance

Hg^0 vapor recovery efficiency on both Tekran® systems during routine automatic standard Hg additions in ambient air was, on average, within an acceptable ± 4% margin of error (Fig 8.2). The 2537X unit had a mean Hg vapor recovery of 101.8%, while the 2537B unit averaged 96.4% recovery before the permeation rate adjustment, to 103.5% recovery post-adjustment (Fig 8.2). The post-adjustment recovery efficiency on the 2537B was much closer to the 2537X performance and explains the narrowed measurement bias between the two instruments. The measurement precision of the 2537X was much better than that for the 2537B, with a mean difference between 5 min measurement values of 0.03% versus 0.3%, respectively (Fig. 8.3). Precision of the standard Hg vapor additions was also slightly better on the 2537X (± 1.1% recovery efficiency) versus the 2537B (± 1.3%).

Permeation rate verifications for both analyzers indicated that the internal permeation sources were operating within ± 2% of their expected rate, based on a calibration curve constructed from external Hg vapor injections (Fig 8.4). The 2537X internal permeation generated a span concentration of 26.424 ng m^{-3} (equivalent to a span area of 3539243), and the 2537B generated a span concentration of 22.584 ng m^{-3} (span area of 442913). Both of these calibration span areas were within the 95% confidence around the external calibration curve. Further, the 2537X internal calibration span area was only 0.5% different from the expected span area based on the external calibration injections (Fig 8.4a) and the 2537B was 1.8% different (Fig 8.4b).

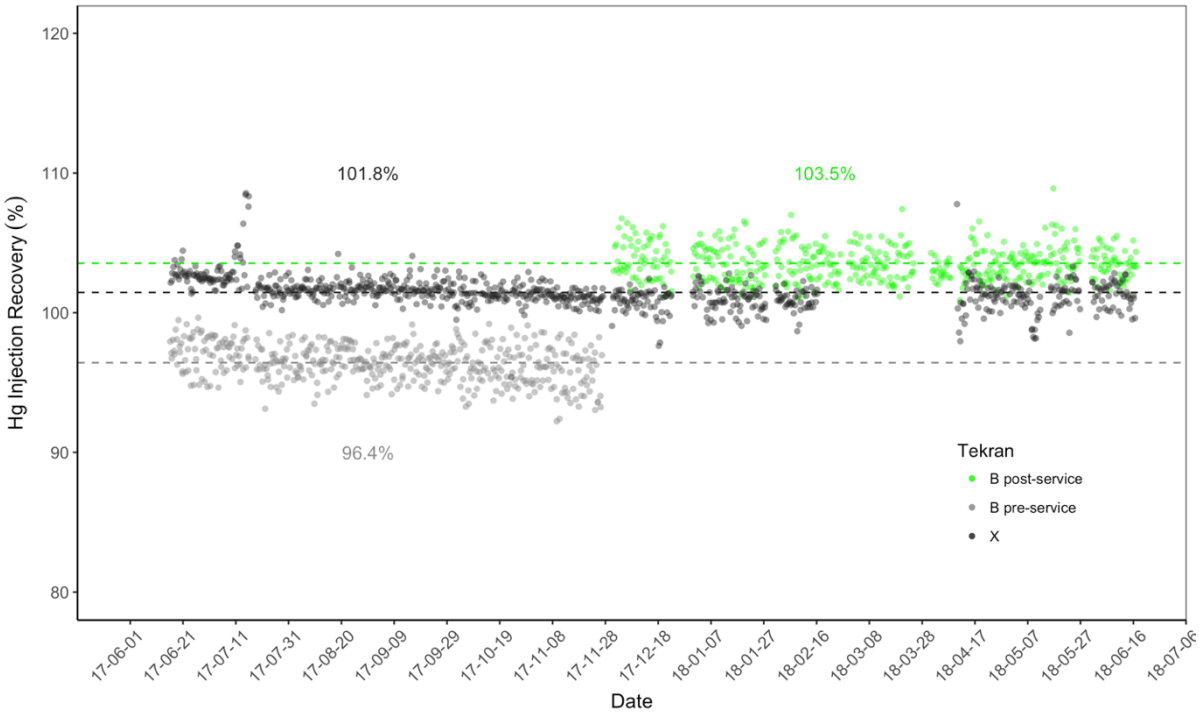

Figure 8.2 *Recovery efficiency (%) of standard Hg vapor additions in ambient air on Tekran® 2537X (black points) and 2537B (grey and green points). Grey points represent injection recoveries prior to maintenance and internal permeation source rate adjustment, and green points represent post-adjustment recoveries. Overall mean injection recoveries are represented by color-coded dashed lines and respective labels.*

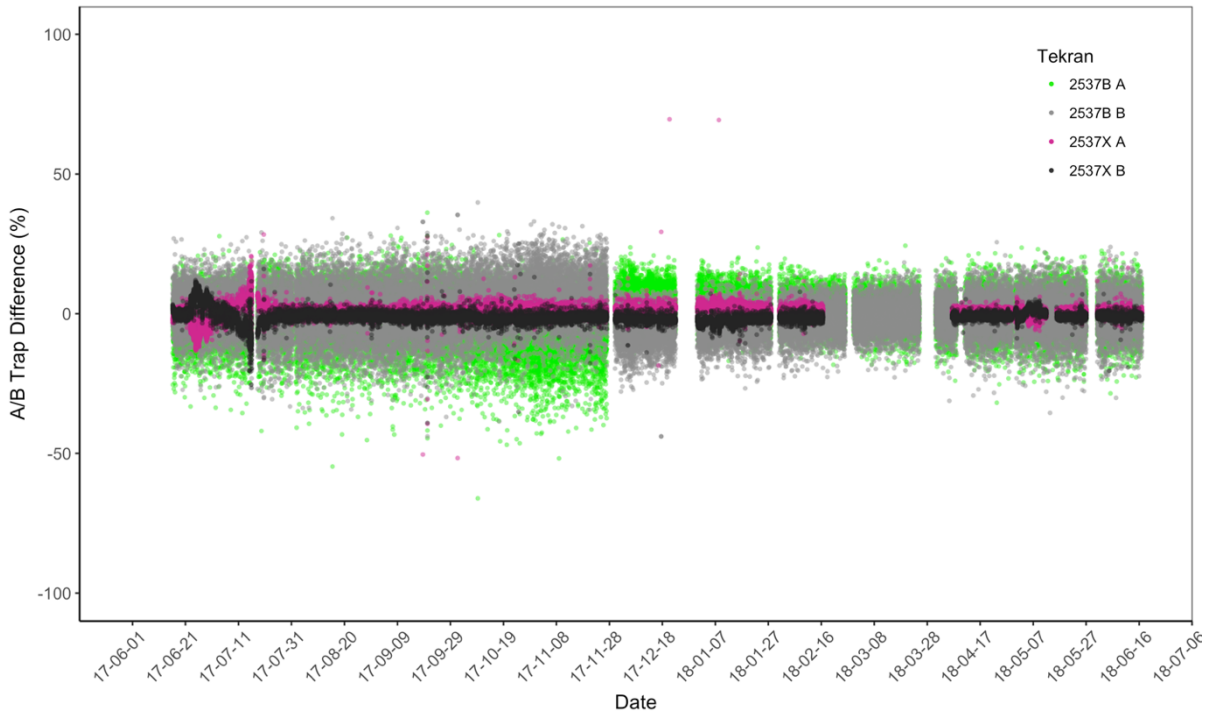

Figure 8.3 *Relative difference between trap A and trap B on the Tekran® 2537 X/B analyzers during ambient air measurements.*

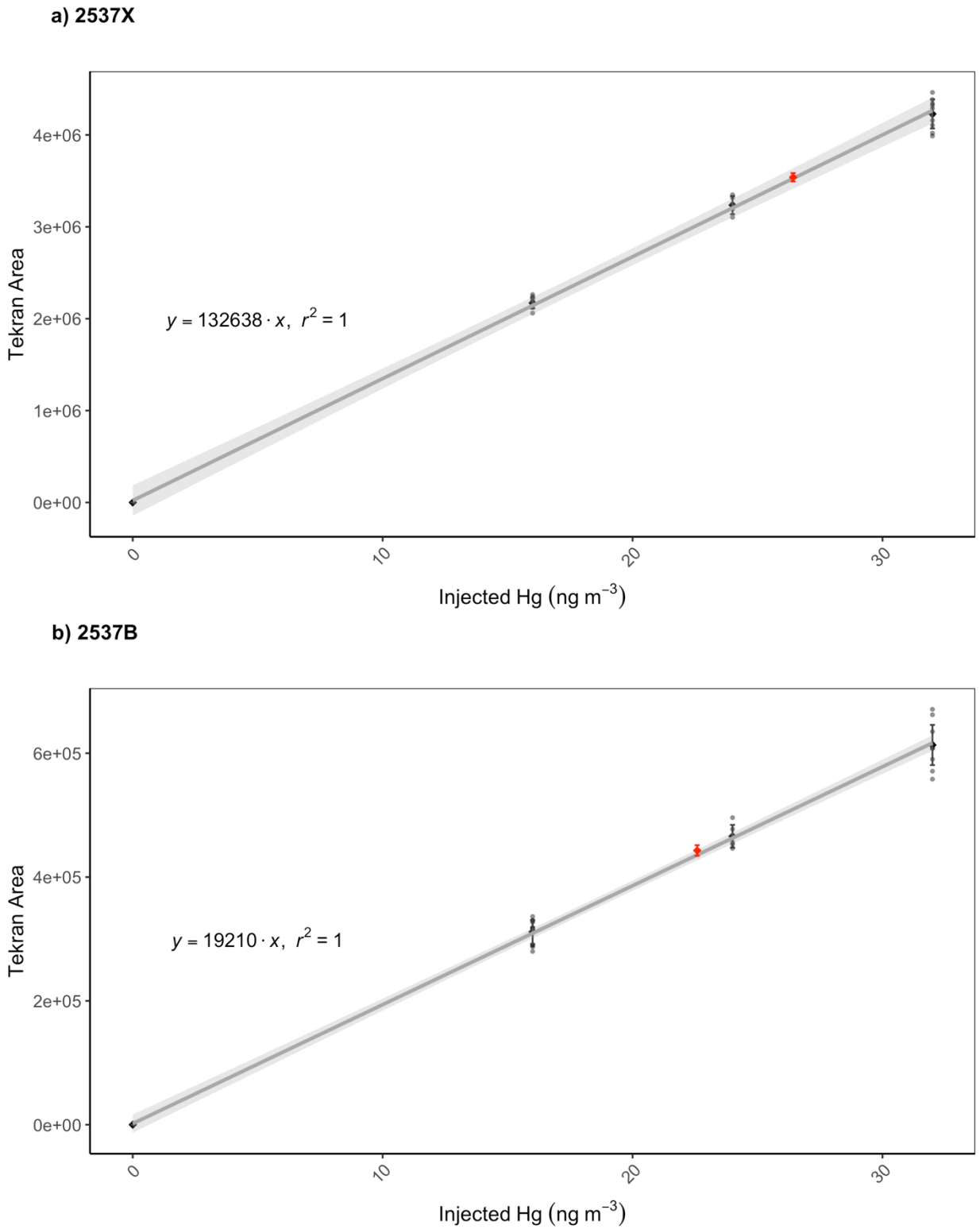

Figure 8.4 *Permeation source rate verifications for Tekran® analyzers: a) 2537X and b) 2537B. Grey points indicate the analytical peak areas measured from individual manual injections, diamonds with error bars indicate average peak area ± standard deviation for each mass of Hg injected, grey line is regression curve with surrounding 95% confidence interval, and red diamond with error bar is average analytical peak area reported by the analyzer during internal calibrations.*

8.4 Conclusions

The concentration of ambient atmospheric GEM measured at CGBAPS over one year using a Tekran® 2537X unit was systematically higher compared to the concentration measured by a co-located 2537B unit. Part of the measurement bias was attributable to a failing permeation source temperature controller on the 2537B unit, and the discrepancy between analyzers narrowed after repairing this controller. However, following repair and adjustment of the 2537B, an average measurement bias of 8.6% still persisted. Extensive maintenance and verification checks in the 6-month period following adjustment lead us to conclude that both analyzers were performing optimally during this time (excepting an interval of excluded data from the 2537X due to a failing UV source lamp). In short, if each analyzer were evaluated alone it would be considered perfectly optimal.

As older Tekran® 2537 A/B units are increasingly obsolescent and technical support will become increasingly limited, ambient air Hg monitoring will be shifting to the newer 2537X analyzer in the near-term. The systematic high measurement bias observed for the 2537X at CGBAPS results in a discrepancy that is larger than any inter-site variability observed for GEM monitoring locations throughout the Southern Hemisphere. Such a bias, if also present in other 2537X analyzers, has important implications for atmospheric Hg monitoring globally.

References

Ebinghaus R, Jennings SG, Schroeder WH, Berg T, Donaghy T, Guentzel J, et al. International field intercomparison measurements of atmospheric mercury species at Mace Head, Ireland. Atmospheric Environment 1999; 33: 3063-3073.

Fitzgerald WF, Engstrom DR, Mason RP, Nater EA. The case for atmospheric mercury contamination in remote areas. Environmental Science & Technology 1998; 32: 1-7.

Gustin MS, Amos HM, Huang J, Miller MB, Heidecorn K. Measuring and modeling mercury in the atmosphere: a critical review. Atmos. Chem. Phys. 2015; 15: 5697-5713.

Jaffe DA, Lyman S, Amos HM, Gustin MS, Huang J, Selin NE, et al. Progress on Understanding Atmospheric Mercury Hampered by Uncertain Measurements. Environmental Science & Technology 2014; 48: 7204-7206.

Schroeder W, Keeler G, Kock H, Roussel P, Schneeberger D, Schaedlich F. International field intercomparison of atmospheric mercury measurement methods. Water Air and Soil Pollution 1995; 80: 611-620.

Selin NE. Global Biogeochemical Cycling of Mercury: A Review. Annual Review of Environment and Resources 2009; 34: 43-63.

Slemr F, Angot H, Dommergue A, Magand O, Barret M, Weigelt A, et al. Comparison of mercury concentrations measured at several sites in the Southern Hemisphere. Vol 15, 2015.

Sprovieri F, Pirrone N, Bencardino M, D'Amore F, Carbone F, Cinnirella S, et al. Atmospheric mercury concentrations observed at ground-based monitoring sites globally distributed in the framework of the GMOS network. Atmos. Chem. Phys. 2016; 16: 11915-11935.

UNEP. Minamata Convention on Mercury. 2018, 2013.

UNEP. Global Review of Mercury Monitoring Networks. United Nations Environment Programme, Geneva, Switzerland, 2016, pp. 48.

Zhang L, Lyman S, Mao H, Lin C, Gay D, Wang S, et al. A synthesis of research needs for improving the understanding of atmospheric mercury cycling. Atmospheric Chemistry and Physics 2017; 17: 9133-9144.

CHAPTER 9:
Concluding Remarks

As the major part of this dissertation, reactive mercury (RM) air-surface exchange was measured directly for the first time using a novel system based around a traditional dynamic flux chamber method. Test materials with high total Hg concentrations such as mine waste tailings showed sometimes high RM emissions up to 40000 pg m^{-2} h^{-1}, while RM deposition was measured over low Hg concentration capping substrates. Material wetness noticeably affected RM flux, generally leading to an attenuation of flux from wet material versus the equivalent dry material. In contrast, GEM flux from wet materials were almost universally higher from wet materials, as has been previously observed. Investigation of potential methods for reducing fugitive Hg evasion from non-point sources typical of large industrial gold mines revealed that the most common reclamation technique, i.e. capping and revegetating, can reduce Hg emissions anywhere from 50 to almost 100%.

All flux measurements were carried out in an artificially controlled laboratory space, from materials with above average total Hg concentrations. Additionally, all measurements were over a minimum of 24 hours, which provides for a net diel air-surface exchange of RM but was too coarse to explore the factors controlling RM flux with much detail. Hence, our flux measurements are not necessarily representative of natural in-situ conditions, and the method as it currently stands may not be suitable for background substrate measurements. However, our primary goal was to determine the feasibility of using the CEM material to detect RM flux, and in this goal we were successful.

The RM flux system could benefit from future improvements that may enable lower detection limits and higher sampling resolution. Adopting a hemi-cylindrical dynamic flux chamber (DFC) with a larger footprint area and chamber flow oriented parallel to the substrate surface would enable higher flow rates while preserving laminar flow and minimizing surface impacts. Higher flow rates provide larger sample volumes in a shorter time. We have also envisioned constructing the DFC of Pyrex glass with thin molded-in silver wire heating filaments, to allow chamber heating while preserving transparency. A heated chamber would promote RM mobility and reduce the possibility of RM deposition to the chamber walls.

Currently, the CEM material is not specifically produced for Hg analysis of any kind and is limited by manufacturer specifications to a pore size of 0.8 μm. In this study, as in all previous studies using the CEM filters, the material has essentially been used as-is from the manufacturer for lack of better alternatives. The material is not always readily available, and the method has potentially suffered as a result of sudden production and supply changes over the years. We suggest that the CEM filter method in general would benefit from improved manufacturing specificity. For instance, we would like to explore the possibility of purpose-coating polyethersulfone onto fine stainless-steel mesh of customizable pore size. If this could be done simply, affordably, and reproducibly in a laboratory setting from stock materials, it would provide the kind of precise discretion over collection-material parameters that is needed for developing a truly robust RM sampling system. At a pore size of 0.1 μm we could more confidently assess total RM concentrations with the inclusion of particulate Hg down to ultra-fine diameters. In addition, by controlling the CEM pore size, we could potentially differentiate gas and particulate phase RM compounds. For example, a multistage filter pack in a cascading configuration of progressively smaller pore sizes might enable a distinction between coarse and

fine particulate Hg. At the very least, such a configuration would enable a more refined analysis of the mechanisms controlling RM breakthrough.

As in previous studies, observations of RM breakthrough across all measurements in this study were highly variable and ranged from 0% (in both laboratory and ambient air) up to roughly 40% (ambient air). RM breakthrough averaged 4-5% during 24 h flux measurements over dry surfaces, but up to 15% over wet surfaces. For the 2-week ambient air deployments in Australia, RM breakthrough averaged ~18% at MQAWS, 21% at CGBAPS, and 19% on the RVI voyage deployments.

One variable that possibly accounts for the observed breakthrough rates is water vapor. Ambient relative humidity (RH) in the UNR greenhouse flux measurements averaged between 23% (summer) to 32% (winter), and overall median RM breakthrough was low at 4 to 6%. In contrast, median RM breakthrough was around 20% for the ambient field sites, where RH averaged around 85% (range 20 to 100%) at MQAWS, and 78% (40 to 100%) at CGBAPS. While there was not necessarily a direct linear relationship between RH and breakthrough over the 2-week sample resolution, there was a clear tendency for higher average rates of breakthrough at higher humidity levels.

However, laboratory tests on CEM filters loaded with high concentrations of $HgBr_2$ and exposed to RH levels of up 80%, in otherwise clean air, showed less than 0.5% breakthrough. These results suggest that pure water vapor by itself does not cause breakthrough, but in ambient air water vapor may be acting synergistically with other gases or aerosols to displace RM molecules. It may be possible that breakthrough is caused by sheer physical impact of particulates or large molecules on the primary filter surface, displacing RM which is subsequently sorbed by the secondary downstream filter. We posit that the breakthrough mechanism is unlikely to involve

reduction of captured RM to GEM, as GEM would pass through the secondary filter undetected. We were also unable to detect GEM downstream of the filters on a Tekran® 2537 analyzer during $HgBr_2$ permeations at high RH, confirming that water vapor was not leading to RM reduction on the filter surface. Work is ongoing to determine the exact mechanism of RM breakthrough.

Whatever the ultimate cause of RM breakthrough, the 2-stage filter deployment minimizes any impact on total RM measurement. As a hypothetical point, if the first filter misses 20% of total RM in a sample volume, then presumably the second filter could miss 20% of the remainder. This means that together two filters would still capture 96% of total RM, and even at the worst case 40% breakthrough, the 2-stage system would capture 84% of total RM. However, if physical impact is indeed the leading cause of breakthrough, then the first filter should attenuate this effect and we expect that the secondary filter is likely capturing the majority of breakthrough RM without additional loss. This conclusion is supported by observations of Mason et al. (2001), who found that the deployment of a third in-line ion exchange filter was not statistically different from their blank filter values. Given these facts, we feel that the 2-stage CEM filter deployment as currently used in the ambient air sampling capacity provides a reasonable measurement of total atmospheric RM that is at least as accurate as any other existing method, and possibly more so in certain conditions.

Using the CEM filter method, ambient atmospheric reactive mercury (RM) concentrations were successfully measured at locations in Australia and the Southern Hemisphere (SH) over a study period of 18 months. Averaging roughly 16 to 18 pg m^{-3}, ambient RM concentrations at the Cape Grim Baseline Air Pollution Station (CGBAPS) and the Macquarie University Automatic Weather Station (MQAWS) were higher than reported for other studies in the SH, though the

amount of data available for comparison is very limited. All previous RM data from the SH has been acquired using the Tekran® 2537/1130/1135 Hg Speciation System, which likely has a low measurement bias due to interferences from water vapor and ozone. Atmospheric Hg measurements made on the Australian Research Vessel Investigator (RVI) off the East Antarctic coast revealed periods of GEM enhancement/depletion, and relatively high RM concentrations compared to sample periods along the transit legs of the voyage at lower latitudes.

Concomitantly with the filter-based RM measurements, high time resolution GEM concentrations were measured using the standard Tekran® 2537 A/B/X Automated Ambient Air Analyzer platform. At MQAWS and on RVI, 2537A analyzers were deployed. At CGBAPS, and 2537B analyzer provided all GEM data used for the study period. Mean GEM concentrations were 0.65 ± 0.24 ng m^{-3} at MQAWS, 0.90 ± 0.35 ng m^{-3} at CGBAPS, and 0.53 ± 0.10 ng m^{-3} on the RVI voyage, indicating some latitudinal variation in GEM concentrations. More recently, a newer 2537X unit was co-located with the existing CGBAPS 2537B for one year (June 2017 to June 2018). The GEM concentration measured by the 2537X analyzer was on average 8.6% higher than the 2537B measurement (1.09 vs 0.94 ng m^{-3}, respectively). This systematic high measurement bias has important implications for ambient atmospheric Hg monitoring. The Tekran® 2537 analytical platform is the primary instrument used at the majority of Hg monitoring sites around the world, and all such sites will need to upgrade to the newer 2537X units as the A/B series becomes increasingly obsolescent.

During the later stages of measurement at MQAWS, a full Tekran® Hg Speciation System was installed at the site and operated in tandem with the filter-based RM measurements there. The results from this inter-comparison are currently in preparation by Cook et al. (in preparation), and regrettably could not be presented as part of this dissertation. However, initial analysis

suggests that the total RM concentrations measured by the both the Tekran® and filter-based systems were comparable. This is in contrast to previous studies reporting up to 3x higher RM collected by the CEM material versus the denuder/RPF combination on the Tekran (Huang et al., 2013).

Measurement of atmospheric RM at CGBAPS is currently ongoing, and the filter-based system there has been further refined. In November 2018, we installed a critical flow orifice (CFO) system to provide innate sample flow control at a constant rate (1.0 Lpm), eliminating the need for manual adjustment by site personnel. The CFO system was also migrated onto the station vacuum manifold, where the necessary pressure differential could be maintained without reliance on individual diaphragm pumps. We expect that the re-designed CFO system will provide more consistent flow rates and hence sample volumes across each set of CEM filters, and we hope to produce a before/after comparison of RM measurement precision using data from the new system.

APPENDICES

Appendix A. Standard operating procedure for filter membrane analysis on the Tekran® 2600-IVS system

Written July 30, 2015 by Matthieu B. Miller and edited by Ashley M. Pierce

Last revised January 10, 2018

STANDARD OPERATING PROCEDURE FOR FILTER MEMBRANE ANALYSIS ON THE TEKRAN 2600-IVS SYSTEM

Revised 01/10/2018 Matthieu Miller

- This SOP is a *guideline* meant to facilitate routine operation of the Tekran® 2600-IVS System. It is not a substitute for adequate training, thorough familiarity with instrument manuals, and a discriminating scientific mindset. The operator must be capable of recognizing and responding to unexpected errors or changes in system performance.

- This procedure is used to analyze samples that may have been collected at a substantial cost in time and resources. It must be done with care and precision or sample data may be irretrievably lost. Always ensure that you have an adequate amount of time, material, and mental acuity for sample prep, and for sample analysis the next day.

1. Summary of Method & Theory of Operation

The standard operating procedure for measurement of mercury (Hg) in aqueous samples (EPA Method 1631, Revision E, Mercury in Water by Oxidation, Purge and Trap, and Cold Vapor Atomic Fluorescence Spectrometry) is here modified to provide a standardized method for quantifying atmospheric Hg captured on filter media, including cation exchange membrane (CEM) and nylon filters. Analysis of filter media for total Hg is accomplished by digesting the filters in an aqueous solution to insure complete oxidation of all Hg compounds to the soluble Hg^{2+} form. The digestion is followed by reduction of all Hg with stannous chloride ($SnCl_2$) to the volatile elemental (Hg^0) form, purging of Hg^0 out of the samples in an argon gas flow and onto gold traps, thermal desorption from the traps, and finally detection of total Hg by cold-vapor atomic fluorescence spectrometry (CVAFS).

The CVAFS method for detection and quantification of trace levels of Hg is an extremely sensitive analytical technique that requires ***precise attention to detail*** at all stages of sample collection, preparation, and analysis. The principle of detection, Atomic Fluorescence, is based on the innate physical property of Hg atoms to become excited under exposure to Ultra Violet (UV) light at 253.7 nm wavelength in which the atoms emit (or fluoresce) photons of light. The Tekran® 2600 exploits this principle by inducing Hg fluorescence with a UV light source and then electronically "counting" the fluoresced photons with a Photo Multiplier Tube (PMT) detector.

Atomic fluorescence is not an absolute quantification method (i.e. individual atoms of Hg are not being counted). The amount of Hg measured in a sample is calculated from a voltage signal generated

as fluoresced photons impact the PMT. The measured voltage is *relative* to the amount of Hg in the sample, but the voltage signal also depends on the intensity of the UV lamp (i.e. higher UV intensity causes more fluorescence from a given amount of Hg) and the sensitivity of the PMT (i.e. lower sensitivity equals a lower voltage signal for a given amount of Hg). Both of these parameters can vary slightly over time. For this reason, the Tekran® 2600 must be calibrated with known Hg standards before every analysis. Each calibration standard provides a reference point that relates a given quantity of Hg to a particular voltage signal. Fluorescence is directly proportional to the quantity of Hg, so a linear calibration curve is produced from which the amount of Hg in any sample can be calculated.

2. Safety Issues Specific to Method

2.1. Mercury Compounds – Only highly trained personnel thoroughly familiar with laboratory procedures should handle pure standards of Hg. Know where Hg spill kits are located and handle all high Hg concentration standards (elemental Hg standards or liquid standards >10 ng/mL) in a fume hood designated for high Hg use. Mercury exposure may cause kidney damage, muscle tremors, spasms, personality changes, depression, irritability, and nervousness.

2.2. Strong Acids – When handling concentrated acids (including BrCl solution), always wear gloves, a lab coat, and safety glasses. Long hair should be pulled back and out of the way.

2.3. BrCl solution – Bromine monochloride solution is very corrosive and the fumes that are off gassed in its making are toxic. Make or use this reagent in a fume hood (not in a laminar clean hood). Always wear gloves, lab coat and safety glasses, and handle reagent carefully.

2.4. Personal hygiene – Hands and forearms should be washed thoroughly after analysis is complete and before breaks, particularly when eating is involved. Observe posted signs and eat and drink only in designated areas.

3. Instrument Working Range and Detection Limits

This method is for determination of Hg in the range of 0.5 to 100 ng/L (Note: 1 ng/L is equal to 1ppt in aqueous samples). Application may be extended to higher concentrations (100 to 1000 ng/L) by dilution of the sample.

4. Sample Collection, Preservation, and Holding Times

The low detection limit of this method depends on the stringent cleaning of equipment and storage containers and careful sample collection. Clean gloves should be replaced if contamination is suspected at any point during handling. Always use clean plastic bags and gloves when handling samples or sampling apparatus. Filter membranes are deployed and collected using the techniques outlined in their respective SOP. In general, filter membranes are collected into new 50 mL polypropylene Falcon tubes, double-bagged, and frozen at -22 °C until analysis.

5. Comments

5.1. Contamination**:** One of the greatest challenges for determination of trace amounts of Hg is prevention of contamination during collection, transport, and analysis. ***Great care to avoid contamination must be exercised by those collecting and preparing samples for analysis***. Contamination may occur when a sample containing a low concentration of Hg is processed immediately after a sample containing a relatively high concentration of Hg. Other potential sources of contamination include metallic labware, containers, equipment, reagents, and reagent water. Atmospheric inputs may contaminate improperly stored samples, equipment, labware, and reagents. In addition, laboratory personnel with Hg amalgam fillings from dental work can potentially contaminate samples by exposing them to exhalation. Reagents and samples should be exposed to possible sources of airborne contamination as little as possible. To avoid exposure to contamination, handle and prepare samples in areas known to be free from contamination, be aware of potential sources of contamination, and pay strict attention to work being done. It is imperative that every piece of labware that is directly or indirectly used in the collection, processing, and analysis of samples be thoroughly clean (in most instances rigorously acid cleaned). Before processing a batch of samples, clean all surfaces and place clean Kim-wipes in areas where analysis will take place. Wear gloves during the handling of apparatus, samples, and blanks, and change gloves if you suspect they have become contaminated.

5.2. Interferences: Filters deployed in especially dirty sample air conditions may contain compounds with a potential to interfere with sample digestion or Hg recovery, such as iodide or carbon dust.

5.3. Destruction of Gold Traps: If free halogens are purged onto gold traps or if gold traps are overheated (>500°C), they may be destroyed. Solutions with more than 20% acid concentration should not be analyzed. In addition, water vapor, acid fumes, and other volatile organic compounds may collect in the gold traps and be released into the fluorescence cell upon desorption. A clean soda lime trap is placed upstream of the gold traps to help remove these compounds from the sample flow.

6. General Preparation Prior to Analysis

6.1. Acid cleaned glassware (volumetric flasks, graduated cylinders, reagent containers): Cleaning consists of a thorough washing with Micro90 (chelating) soap to remove visible residue, followed by rinsing three times with distilled water, and one rinse with acetone. Rinse three more times with ultrapure water, soak in 5% HNO_3 bath overnight, rinse three more times (collecting and neutralizing first rinse) with ultrapure water, and clean with 50:50 HNO_3:H_2O on hot plate (~90°C) for two days. Remove 50:50 HNO_3:H_2O acid and rinse three times (collecting and neutralizing first rinse) with ultrapure water. Acid cleaned glassware is stored in the clean hood or double-bagged in designated drawers for clean glassware. Volumetric flasks are filled with 1% trace grade HCl during storage.

I-Chem vials are cleaned thoroughly with Micro90 soap, followed by rinsing three times with ultrapure water, acetoned to remove labels, and rinsed three more times. The glass jars are soaked for at least 48hr in a 10% HNO_3 bath. The lids are soaked at least 24hr in a 5% HNO_3 bath. Remove the jars and lids from the acid, and rinse three times (collecting and neutralizing first rinse) with ultrapure water. Dry glassware in the clean hood, and once the lids are fully dry, the jars and lids are re-assembled, double-bagged and stored in assigned area.

6.2. The following Check List may be used to verify that you have what you need for analysis:

- A sufficient amount of clean 40 mL sample vials w/ septa
- Argon gas to 2600 system (should read more than 500 psi)
- A sufficient amount of optima HCl to make BrCl
- BrCl, NH_2OH, and $SnCl_2$ reagents
- A sufficient amount of glass wool and soda lime to make a fresh trap.
- Gloves, Kim-wipes, syringes, timers, pipettes, pipette tips, etc.

7. Instrumentation/Equipment and Consumables

7.1. Tekran® Model 2600-IVS mercury analyzer – This instrument consists of a cold vapor atomic fluorescence spectrometry (CVAFS) Hg detection system, with dual stage gold pre-concentration (Figure 1). The 2600-IVS instrument is used in conjunction with Tekran Mercury Data System 2.6 software. For information on replacement parts or troubleshooting, contact Tekran® Instruments Corporation (416-449-3084, www.tekran.com, support@tekran.com).

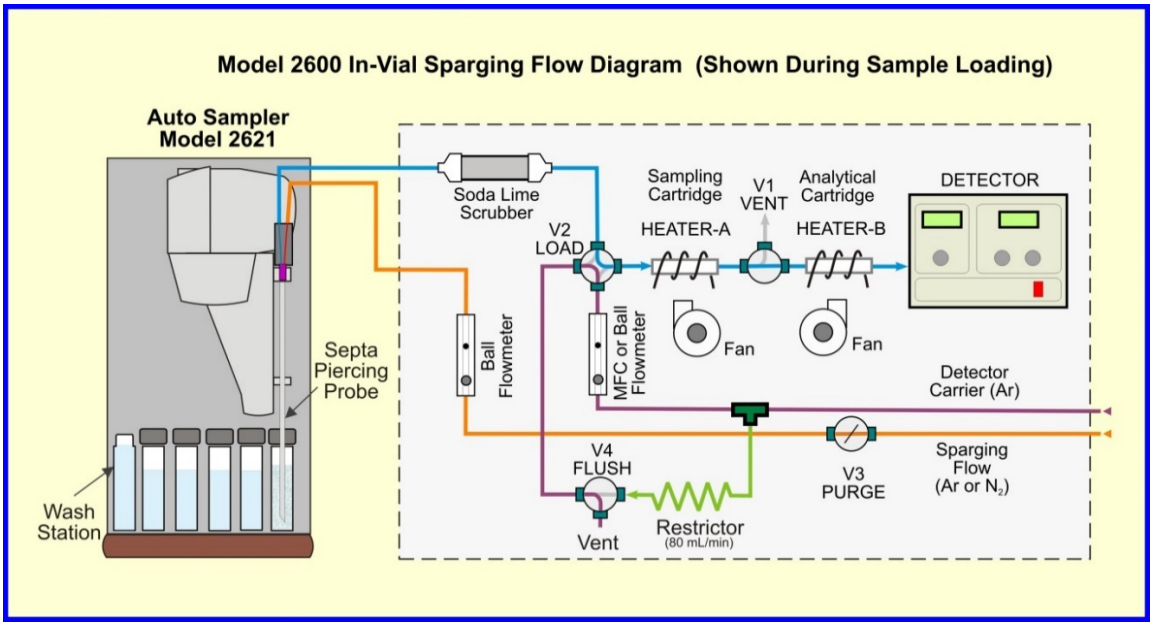

Figure 1. Tekran® 2600-IVS system. The gold traps and soda lime trap are located under the top lid of the instrument.

7.2. Tekran® Model 2621 Auto Sample Changer – This machine allows the 2600 system to automatically draw from successive samples, blanks, and standards.

7.3. Gold Traps – The instrument contains two gold traps. The first trap is at position A of the pre-concentrator, where it bears the brunt of residual halogen and acid vapors from the sample solutions. For this reason, it is composed of gold coated silica sand (Tekran® P/N 35-26510-00), which is relatively inexpensive to replace if the trap is degraded, and should be replaced annually as a matter of course. The second trap, located in position B, contains pure gold (Tekran® P/N35-26500-00), has a much longer lifespan, and is much more expensive to replace.

7.4. Soda Lime Trap – The soda lime should be changed weekly, and always following an extended period of no use. The trap is assembled by placing a glass wool (Supelco P/N 2-0411) plug at one end of the glass tube, located on the pre-concentrator (Figure 1), then filling the body of the tube with soda lime (Fisher P/N AA3659636) followed by another glass wool plug at the other threaded end. The glass tube should be cleaned periodically by scrubbing with microsoap and nanopure water.

7.5. Sample Vials – The automated sampler requires all samples to be in 40 mL I-Chem septa-top glass vials (Fisher P/N 05-719-119).

7.6. Teflon bottles – FEP bottles (Nalgene) of various sizes, typically 500 or 1000 mL size are used depending on the types of analyses that will be performed.

7.7. Filter Media Tubes – Filters are collected, stored and digested in 50 mL polypropylene Falcon tubes. A portion of the digested sample in these jars is transferred into the 40 mL sample vials prior to analysis.

7.8. Other laboratory equipment: top-loading balance, laminar clean hood, fume hood, gas regulators, 100 mL graduated cylinders, 100 mL volumetric flasks, Erlenmeyer flasks with stoppers.

8. Reagents and Standards

8.1. **UHP Argon:**

The argon tank should be changed when gas pressure reads at or below 500 psi. Activation of the argon gas flows are regulated automatically by the 2600 system.

8.2. **Calibration Standards:**

Liquid calibration standards are prepared for each individual run of the 2600 system. The calibration standards are prepared from working Hg solutions. The working Hg standard (10 ng/mL) is prepared by successive dilutions of a NIST certified 1 mg/mL Hg standard (1000 ppm). The dilutions of the stock standard are made in 100 mL volumetric flasks with 10% nitric acid as shown in Table 1. Check pipettes for accuracy and use only pipettes designated for pipetting Hg standards. Invert containers of stock Hg standard solutions several times to assure mixture is homogeneous.

- First, tare a 100 mL volumetric flask, and add ultrapure water to the appropriate mass.
- Add 10 mL of 10% nitric acid to the flask using a 10 mL pipette.
- Add the appropriate amount of Hg standard solution using a designated Hg pipette.

Hg Concentration (ng/mL)	Nanopure Water (mL)	Hg Standard (mL)	10% Nitric Acid (mL)
Stock B (10,000 ng/ml)	89.0	1.0 of Stock A	10
Working Standard (10 ng/ml)	89.9	0.1 of Stock B	10
Working Solution (1.0 ng/ml)	80.0	10 of Working Std.	10
Working Solution (0.1 ng/ml)	89.0	1 of Working Std.	10

Table 1. Preparing Hg working solutions from a stock Hg standard. The far left column indicates the solutions to be prepared, with the three right displaying the amount of each component to add. Stock A solution = 1 mg/mL Hg standard (1000 ppm).

8.2.1. The working 10 ng/mL standard is used to prepare working solutions at 1.0 and 0.1 ng/mL. Calibration standards for the 2600 are made by diluting the working solutions in nanopure water. The typical calibration range is 0 - 100 ng/L, at concentrations of 1.0, 5.0, 10.0, 25.0, and 100.0 ng/L. Calibration standards can be made in any concentration and any quantity necessary for the anticipated sample analysis, although concentrations above 200 ng/L are not recommended (samples anticipated to be in this range should be diluted). Calibration standards must be prepared to exact volumes. As an example, the reagent proportions required for 25 mL of standards at 2% BrCl concentration is shown in Table 2.

Hg Std (ppt or ng/L)	DIW (mL)	BrCl (mL)	Working Hg Solution (mL)	HH (mL)	$SnCl_2$ (mL)
			0.1 ng/ml		
Calblank	24.125	0.5	0	0.125	0.25
0.5	24.000	0.5	0.125	0.125	0.25
1	23.875	0.5	0.25	0.125	0.25
			1.0 ng/ml		
5	24.000	0.5	0.125	0.125	0.25
10	23.875	0.5	0.25	0.125	0.25
25	23.500	0.5	0.625	0.125	0.25
100	21.625	0.5	2.5	0.125	0.25

Table 2. Preparation guide for a typical set of calibration standards. The far left column indicates the standards to be prepared, with the five right columns displaying the amount of each component to add.

The calibration standards *must* be prepared in 40 mL I-Chem vials, weighing out the appropriate mass of ultrapure water on a laboratory scale, and then pipetting the appropriate volume of reagents and Hg solution into the vial. An aliquot of the Hg working solutions should be transferred to small (and clean!) working containers to facilitate pipetting, which is accomplished with the 1000 µL pipette labeled for Hg use. Pipette tips should be changed between preparation of each standard, and care should be exercised to prevent the pipette or pipette tip from touching anything. The working solution should be pipetted directly into the water and not onto the side of the vial.

8.2.2. Calibration blanks should be prepared with the same BrCl that was used to prepare the standards. This can be done by making a 2% BrCl solution in a Teflon bottle, using ultrapure water (500 mL bottle, 487.5 mL DIW, 10 mL BrCl, 2.5 mL HH).

8.2.3. Additional calibration standards should be prepared to serve as IPR (Initial Precision and Recovery) and OPR (Ongoing Precision and Recovery) standards. A standard concentration of 5.0 or 10.0 ng/L is recommended. Enough additional vials should be prepared for one IPR and as many OPRs as needed to bracket every 10-12 samples.

8.3. **Bromine monochloride (BrCl) solution** – BrCl is prepared via an optima HCl solution with 1.8% potassium bromide (KBr) and 1.2% potassium bromate ($KBrO_3$). As an example, to make 300 mL of BrCl, start by adding 150 mL of optima HCl to a clean 500 mL Erlenmeyer flask with clean Teflon stir bar. While the solution is gently mixing, add 5.4g of KBr, followed by an additional 150 mL of optima HCl. Mix for 1 hour in the clean fume hood (keep solution stoppered to prevent contamination). Next, slowly add 3.6g of $KBrO_3$ to the solution while stirring. Caution: this step releases copious amounts of chlorine and bromine gas, which are toxic if inhaled. The solution should be a red-orange color. After fumes have dissipated, stopper the flask to prevent contamination and allow the solution to stir for 15min to 1 hour. A precipitate will form with time, and it is best to use the finished BrCl within 2 hours. Make sure that the tools for making and storing the BrCl solution are completely free of Hg (it is recommended that even acid cleaned flasks be rinsed several times with ultrapure water before using). Do not discard (even after neutralizing) more than ~5 mL of BrCl solution down the drain. Contaminated BrCl solution, which will not be used in analysis, should be submitted as hazardous waste for pick up.

8.4. **1% Optima HCl solution** – Fill a clean 2 L Teflon bottle half full with ultrapure water and in the acid hood (Hood #2), add 20 mL of concentrated trace-grade Optima HCl. Then fill the container to 2 L volume with ultrapure water.

8.5. **Stannous chloride ($SnCl_2$) solution** –Using tin (II) chloride dihydrate crystals (Fisher #T142-500 or equiv.), Optima HCl, and ultrapure water, make a solution that is 20% stannous chloride and 10% HCl. The stannous chloride solution must be purged with a slow flow (~ 20 mL/min) of argon or nitrogen in order to remove any free Hg^0.

1) Weigh out 20 g of $SnCl_2$ crystals and add 10 mL of concentrated HCl. Mix well.
2) Make up volume to 100 mL using reagent grade DI water.
3) Purge overnight with mercury free nitrogen or argon.

8.6. **Hydroxylamine (NH_2OH) solution** – Use the small, acid cleaned bubbler designated for making hydroxylamine solutions. Rinse the apparatus and a Teflon stir bar several times with ultrapure water. Add ~100 mL of ultrapure water to the flask and while the solution is stirring, add 60 g of hydroxyl-amine hydrochloride ($NH_2OH \cdot HCl$) (Fisher #H330-500) and bring the solution to 200 mL volume (as marked on the side of the flask) with ultrapure water. Add 0.1 mL of $SnCl_2$ solution and purge hydroxylamine solution with argon gas overnight. Transfer the solution to a clean container to prevent contamination, and rinse the bubbler apparatus with ultrapure water and place in the clean hood to dry. NH_2OH solution may be stored at room temperature in the laminar clean hood. Pour out a smaller aliquot into a Teflon vial to use as a working solution.

8.7. **Ultrapure water** – deionized water purified with the Millipore system with a minimum of 18.2 MΩ resistivity.

9. Sample Preparation

NOTE: Before you start preparation, determine how many samples you have and calculate how much of all the reagents you will need to run the samples. This is important to ensure that there is enough of everything available before you start and that chemicals are not wasted.

9.1. Have calibration standards and cal blanks prepared as above.

9.2. For filter media, remove Falcon tubes containing filter media from the freezer and add 50 mL of 1% Optima HCl to each tube. Add 3 mL of BrCl to each 50 mL Falcon tube (total volume 53 mL). Recap tubes and shake each for 10 seconds. *Note: this concentration of BrCl has been empirically determined as the most effective concentration for filter digestion.*

9.3. After the BrCl solution has been added, samples must digest for a minimum of 12 hours. Make sure lids are tightly sealed on all vials and tubes. It is important to analyze samples soon after digestion (no more than 1-2 days maximum) because once BrCl has been added, Hg concentrations can increase with time due to atmospheric contamination.

9.4. $SnCl_2$ should be prepared the day before analysis and purged overnight (section 8.5).

10. Analysis of Samples

10.1. **Instrument Set-up:** The 2600 should have been turned on the day before to provide the argon gas flow for purging the $SnCl_2$ solution. In addition, this allows the instrument to warm up and stabilize overnight.

10.1.1 The UV lamp is dependent on a constant temperature and steady voltage to insure a stable output intensity. ***The Lamp Indicator LED on the front panel of the 2600 will illuminate red if the lamp voltage is not in spec***. This indicates that the lamp needs to be adjusted or possibly replaced. The lamp voltage offset, shown on the right side LED readout screen on the 2600 front panel, should be set to approximately 0.100 Volts. This offset voltage must be adjusted back to 0.100 whenever the lamp is adjusted or changed. **If the offset voltage is varying radically, or if it has changed dramatically from 0.100 Volts, the operator should take notice and diagnose the cause**.

10.1.2 During instrument preparation on the day of analysis, a new soda lime trap should be assembled and dried. The drying is accomplished using the 2600 purge flow controller and the free 1/8" Teflon tubing on the left side of the instrument. The soda lime should be dried for 15 minutes prior to analysis.

10.1.3 Argon gas pressure is supplied continuously to the 2600 at the rear panel input bulkheads, and argon flow is controlled automatically via internal valves. When the instrument is powered down, there is no argon flow through the system. When the instrument is on, argon is routed through the detector path and to a valve controlling sparge flow. When a sample is initiated, this valve opens and argon flows through the sparge path. At this time the operator should insure that the sparge flow gauge on the front of the 2600 is at 250 mL/min, and adjust if necessary.

10.2 **Tekran MDS Software Setup:**

10.2.1 Open software: Double click the "TekMDS 2.6" icon on the computer's desktop. The auto-sampler should automatically initialize once the program has opened. Ensure that this has happened by executing a command (i.e. A/S Up or A/S Down) from the drop-down menu titled "Auto Sampler" in the left-hand column of the display. Next, select "new worksheet" from the top ribbon of the screen. Enter a description of what is being analyzed and the operator's initials.

10.2.2 Starting a worksheet: Every new worksheet will begin with a clean cycle, to remove build up in the gold traps. Two clean samples are recommended. Following the clean cycle, the operator must enter the type of sample that is to be analyzed (i.e. calblank, standard, etc.), and the location of that sample. To start the worksheet, click "Run Worksheet," select

EPA1631, then, in the drop down windows labeled Clean ETF and Sample ETF, select "cleandry" and "invial" respectively, and click "Run".

10.3 **Calibration:**

Before samples can be analyzed, a calibration curve must be created. The purpose of the calibration curve is to provide the Tekran software reference values for known amounts of Hg, including a zero or "blank" Hg value. At least seven calibration blanks should be run, followed by at least five standards of known Hg concentration.

10.3.1 Add 0.5% NH_2OH to the blank bottle and standard vials (e.g. 0.125 mL NH_2OH to the 25 mL standard vials), and let the solution react for at least 10 minutes with the caps removed.

10.3.2 For calblanks, fill seven 40 mL vials with 24.75 mL of blank solution, and then add 0.250 mL of $SnCl_2$ (total volume = 25 mL), capping immediately. Wait 10 more minutes for the $SnCl_2$ to react. Place the calblank vials in positions A1 through A7 on the auto-sampler tray.

10.3.3 On the worksheet, highlight seven cells in the SampleID column, right click, and select CalBlank. Next, highlight the seven adjacent cells in the Location column, and click the ellipsis icon in the top cell. This will open a window displaying all locations in the auto-sampler tray. Highlight the location of the blanks (A1 – A7) and click "OK."
NOTE: Seven calblanks is a recommendation, run as many as necessary for the values of at least four calblanks to stabilize. If the calblanks continue to drift it will affect your measurements and OPRs later in the run.

10.3.4 Following the calblanks, run the set of Hg standards (0.5, 1.0, 5.0, 10.0, 25.0, and 100.0 ng/L). $SnCl_2$ should be added to the standard vials at the same time as the calblanks, also at 0.250 mL per vial. This brings the total volume in the standard vials to exactly 25 mL. The 7 calblanks will have taken about 30 minutes to run, and this will be sufficient time for the $SnCl_2$ to reduce the Hg in the standard solutions.

10.3.5 Enter the standards on the worksheet in the SampleID column as type Std followed by the concentration of the standard (i.e. Std1.0, Std5.0, etc.).

10.3.6 Before samples can be analyzed, the calibration curve must have an R^2 value of at least 0.9975, and a CF RSD% value less than 21.0. These values can be found at the top of each worksheet, and will be updated automatically. A minimum of 4 standard values must be represented on the curve, as well as a minimum of 4 calibration blanks. To view the calibration curve click the curve icon in the top-right portion of the worksheet; in the calibration curve window, the values for the blanks and standards which have been run can be added to or removed from the curve. Additional standards can be analyzed throughout the run, as long as an initial calibration curve is present before analysis of samples.

10.3.7 Also before samples can be analyzed, the calibration curve must be checked for accuracy. This is done by analyzing the IPR (Initial Precision & Recovery) standard, which will have been prepared in the same manner as the calibration standards. Type IPR and the concentration (i.e. IPR5.0) in the SampleID column, and select the location of the vial on the worksheet. The software will calculate the percent recovery and display it in the Rec% column. The IPR standard must pass within 5% of the expected concentration. In other words, the Rec% column must show a percent recovery value between 95.0 and 105.0 in order to continue analyzing samples. Multiple IPR standards may be run to obtain a passing value, but if a passing value cannot be achieved, the system must be recalibrated.

WS000000022*

TotalMercury	**Operator:**	TL	**BlankSub:**	177.49053	**Calib Eqn:**	Conc = (Area-177.49053) / 269.	**Run Date:**	2013-03-12	**Blank SD:**	13.85840						
EPA1631	**Worksheet:**	WS000000022	**CalibFactor:**	269.00090	**Status:**	QC Warnings:7/QC Errors:0	**Run Time:**	00:00:00	**Blank RSD%:**	7.80796						
	MethodRev:	2008-05-12	**R:**	0.99999	**R²:**	0.99998			**CF SD:**	7.28750						
	Description:	CGSPR121218, CGSPA121218, CHALKA120911, PVLYR120911, PVLYR130102, NNSSA1							**CF RSD%:**	2.70910						

	Sample/ID	Location	Rinse	Dilute	Blank	Conc (ppt)	MB%	FinalConc	Rec%	QA	RawData	RunEnd	Peak (Raw)	Control (etf)	Flags	RunCount	Commen
1	Clean	...									0079-1.RAW	13:57:34	0.000	Clean	NP	1	
2	Calblank	A1			0.000	3.312					0080-1.RAW	14:01:43	890.940	Sample	OK	1	
3	Calblank	A2			0.000	1.139					0081-1.RAW	14:05:51	306.363	Sample	OK	1	
4	Calblank	A3			0.000	0.862					0082-1.RAW	14:10:00	232.000	Sample	OK	1	
5	Calblank	A4			0.000	0.734					0083-1.RAW	14:14:08	197.502		OK	1	
6	Calblank	A5			0.000	0.637					0084-1.RAW	14:18:17	171.438	Sample	OK	1	
7	Calblank	A6			0.000	0.651					0085-1.RAW	14:22:26	175.075	Sample	OK	1	
8	Calblank	A7			0.000	0.617					0086-1.RAW	14:26:34	165.948	Sample	OK	1	
9	Std1.0 ppt	A8			177.491	0.955			95.47		0087-1.RAW	14:30:43	751.138	Sample	OK	1	
10	Std5.0 ppt	A9			177.491	5.118			102.37		0088-1.RAW	14:34:52	1554.357	Sample	OK	1	
11	Std10.0 ppt	A10			177.491	10.053			100.53		0089-1.RAW	14:39:01	2881.770	Sample	OK	1	
12	Std25.0 ppt	A11			177.491	24.981			99.92		0090-1.RAW	14:43:10	6897.442	Sample	OK	1	
13	Std100.0 ppt	A12			177.491	101.708			101.71		0091-1.RAW	14:47:19	27537.063	Sample	OK	1	
14	OPR10.0	A10			177.491	10.112			101.12		0092-1.RAW	14:51:29	2897.688	Sample	OK	1	
15	CGSPA121218-2	B1			177.491	19.749					0093-1.RAW	14:55:37	5490.012	Sample	OK	1	
16	CHALKA120911-1	B2			177.491	32.824					0094-1.RAW	14:59:46	9007.130	Sample	OK	1	
17	CGSPR121218-2	B3			177.491	6.474					0095-1.RAW	15:03:54	1919.100	Sample	OK	1	
18	PVLYR120911-B	B4			177.491	7.196					0096-1.RAW	15:08:03	2113.323	Sample	OK	1	
19	PVLYR130102-1	B5			177.491	5.046					0097-1.RAW	15:12:11	1534.894	Sample	OK	1	
20	NNSSA121023-1	B6			177.491	71.988					0098-1.RAW	15:16:20	19542.217	Sample	OK	1	
21	PVLYR130102-B	B7			177.491	3.713					0099-1.RAW	15:20:29	1176.387	Sample	OK	1	
22	PVLYR130102-2	B8			177.491	5.108					0100-1.RAW	15:24:37	1551.656	Sample	OK	1	
23	PVLYR120911-1	B9			177.491	6.563					0101-1.RAW	15:28:46	1942.960	Sample	OK	1	
24	CHALKA120911-2	B10			177.491	34.333					0102-1.RAW	15:32:54	9413.000	Sample	OK	1	
25	CGSPA120925-B	B11			177.491	3.988					0103-1.RAW	15:37:03	1250.291	Sample	OK	1	
26	CGSPA120925-2	B12			177.491	86.421					0104-1.RAW	15:41:11	23424.738	Sample	OK	1	
27	OPR1.0	A13			177.491	0.982			98.22		0105-1.RAW	15:45:20	441.710	Sample	OK	1	
28	CGSPR121218-3	B13			177.491	7.276					0111-1.RAW	16:10:10	2134.767	Sample	OK	1	
29	NNSSR121120-1	B14			177.491	28.933					0112-1.RAW	16:14:19	7960.603	Sample	OK	1	
30	NNSSR121120-3	B15			177.491	24.061					0113-1.RAW	16:18:27	6650.035	Sample	OK	1	

Summary

Figure 2. An example worksheet, showing the potential order of calibration blanks, calibration standards, samples, and OPR standards.

10.4 **Analyzing samples**

10.4.1 After running a set of calibration blanks, standards, and a passing IPR standard, samples can be analyzed. Samples should receive NH_2OH to an equivalent of approximately 0.5% of the total sample volume (e.g. in the 50 mL Falcon tubes with 3 mL BrCl, add 0.250 mL NH_2OH), and the solution should react for at least 5 minutes before analysis. Add slightly more NH_2OH if the yellow color is not neutralized to clear.

10.4.2 A 24.75 mL aliquot of each sample must be transferred to a 40 mL I-Chem vial for analysis. Vials should be numbered to match a corresponding number on the sample tubes for identification. The sample solutions should be transferred to the vials using a 10 ml pipette (3 pips at 8.25 mL), using a new pipette tip for each sample.

10.4.3 Once the sample solutions have been added to the vials, add 0.250 mL of $SnCl_2$ to each vial and cap quickly and tightly. Note that the addition of the $SnCl_2$ constitutes a 1% dilution of the sample solution.

10.4.4 On the software worksheet, enter the sample ID in the SampleID column and select its location on the auto-sampler tray. Place the sample vial in the appropriate location. If possible, samples should be run in a logical sequence.

10.4.5 No more than 10-12 samples should be analyzed consecutively without checking the calibration curve with an OPR (Ongoing Precision and Recovery) standard. When possible run a duplicate of one or two samples in each group of 10 samples.

10.4.6 Periodically check the system throughout the analysis. When all samples are analyzed, finish the run with a passing OPR standard.

10.5 **Recording results:**

Click the spreadsheet icon at the top-right portion of the worksheet. A drop-down menu will appear. Click "Complete with Header and QA/QC." This will export the worksheet to an excel spreadsheet. On the spreadsheet, indicate which blanks and standards were used to construct the calibration curve <u>*NOTE:*</u> *include all calblanks and standards even if they were not used*. Print the spreadsheet and add it to the 2600/2700 logbook. Make sure that the worksheet number and R^2 value are visible. Save the spreadsheet in the public drive under CVAFS/Total Hg/ Total Data. Save the worksheet by clicking the save icon on the Tek-MDS program.

11. Quality Control Requirements

11.1 The analyst's initials, date of analysis, the worksheet number, and the R^2 value of the calibration curve must be visible on the spreadsheet and recorded in the logbook.

For each run record in the logbook what was done and if there were any issues or changes made to the setup

11.2 The instrument must be calibrated before every run with a minimum of four different standards (or the calibration was verified with at least two passing standard checks).

11.2.1 The R^2 value of the trendline for the calibration curve must be greater than 0.9975.

11.2.2 The RSD% must be less than 21.0

11.2.3 The calibration must be checked by analyzing an IPR standard after calibration data was entered. And that calibration standard must report ± 5% of the true value before any samples are analyzed.

11.2.4 All samples must be bracketed by OPR calibration checks (one analyzed before and one analyzed after) which have less than 5% error. The maximum number of samples that can be analyzed between OPR checks is 12.

11.3 Calibration blanks must be analyzed along with samples to demonstrate that the process is relatively free of Hg contamination. A good calblank produces a Hg peak area of less than 120. At least seven blanks should be analyzed with at least four included in the calibration curve.

11.4 Data should be validated by someone familiar with this method of analysis. They must verify that appropriate quality control samples were analyzed, and ppt amounts of Hg for samples match those input into the spreadsheet.

11.5 Always note any difficulties or problems with the system or with samples in the logbook.

12. Data Analysis and Calculations

12.1. The Tek-MDS software calculates the peak height or area for Hg analyzed on the 2600 instrument. Standards are analyzed and information is input into the software (calibration) to create a plot of peak area versus ppt Hg amount. With this information the software determines the amount of Hg present in each peak of Hg analyzed.

12.2. Sample dilutions and method blanks must be considered when processing data. In order to calculate the actual mass of Hg in the sample, the ppt Hg concentration reported from the instrument must be divided by the volume of sample used. In addition, there is typically a small amount of Hg in the ultrapure water which is used when any dilutions are made. The amount of Hg in the dilution water must be calculated and subtracted from that of the sample. The calibration blanks can be used to determine the amount of Hg in dilution water.

13. Waste Management

The laboratory is responsible for complying with all federal, state, and local regulations governing waste management, particularly for hazardous materials such as mercury solutions.

13.1. Acid solutions containing HCl or HNO_3 must be neutralized before disposal, or handled as hazardous waste.

13.2. All waste containing reagents used in this method are to be placed in an appropriate hazardous waste container. Contact waste disposal authorities for removal and replacement of waste containers.

13.3. For further information on waste management, consult the appropriate health and safety officer. It is always safer to err on the side of caution.

14. Maintenance

14.1. Cleaning of the sample line – Disconnect the friction fitting from the soda lime trap inlet and squeeze DIW through the sample line. Squeeze methanol through the line to aid with drying. During this cleaning procedure the needle must be in an empty and open vial. After cleaning, install the friction fitting back to soda lime cartridge inlet. In order to speed the drying of the line, activate V4 for a short period from the Hardware Testing menu to purge any remaining fluid from the sample line.

14.2. Replacement of gold traps – The gold-coated sand trap in Position A should be replaced annually.

15. Basic Troubleshooting

- The first 1-3 calibration blanks will often be very high. This is not necessarily a serious issue with the instrument. The reagents in the calblank solution may act to liberate residual Hg in the sparge flow path, causing the initial high blanks. These blanks should not be included in the calibration.

- If concentration results suddenly change or otherwise seem incorrect, check the system. Ensure that the argon flow is working and that the needle probe is functioning correctly.

- If the auto-sampler is not functioning, there may be one of two problems:

- The auto-sampler may not be communicating with the Tek-MDS software. Click "Initialize System" on the right side of the screen.
- The auto-sampler may have experienced a fault. If this is the case, press the "Reset" button (this requires a narrow object, such as the tip of a pencil), located on the side of the auto-sampler above the power switch. If the auto-sampler is obstructed it will not work properly. Ensure that all tubing is properly secured on the instrument and that there is nothing in the way of the auto-sample when it lowers to collect samples.

- If the system is frozen (i.e. the worksheet is unresponsive), exit the program and restart the computer. Data saves automatically, and the worksheet can be resumed once the computer has rebooted.

- Tekran® technical support:
  - A copy of a worksheet experiencing errors can be sent to Tekran's technical support team, by clicking "Help" followed by "Contact Technical Support." The worksheet must be opened for this feature to work. Select "Send Email" or "Save to Disk," and attach the support file to an email. The email address to send to is support2600@tekran.com. In the email, briefly describe the nature of the error, any error messages which were displayed, what the operator has already tried, and at what stage of analysis it occurred.
  - Tekran's toll free telephone number is 1-888-5TEKRAN.

Appendix B. Permission to Reprint Chapter 3

Testing and modeling the influence of reclamation and control methods for reducing nonpoint mercury emissions associated with industrial open pit gold mines

Our Ref: P050818-08/UAWM

08 May 2018

Dear Matthieu Miller on Behalf of Macquarie University,

Material requested: Matthieu B. Miller & Mae S. Gustin (2013)
Testing and Modeling the Influence of Reclamation and Control Methods for Reducing Nonpoint Mercury Emissions Associated with Industrial Open Pit Gold Mines
***Journal of the Air & Waste Management Association*, 63 (6): 681-693.**
DOI: 10.1080/10962247.2013.778221

Thank you for your correspondence requesting permission to reproduce your above mentioned Open Access article in your forthcoming dissertation to be published by Macquarie University.

You are free to use the published version of your article.

We will be pleased to grant you permission free of charge on the condition that:

This permission is limited to non exclusive **English** language rights one time **print & eBook** usage only and permission must be sought for any further use.

E-book rights does not allow our article to be sold as an individual chapter, from your forthcoming publication.

This permission does not cover any third party copyrighted work which may appear in the material requested.

No alterations may be made to our work without written consent.

This license does not cover Taylor & Francis content being republished in a custom publishing program or database.

All reasonable efforts must be made to contact the author(s) to notify them of your intentions and confirm they are happy with the permission being granted.

Full acknowledgement must be included showing author, article title, full Journal title, copyright © the Air & Waste Management Association, www.awma.org, reprinted by permission of Taylor & Francis Ltd, http://www.tandfonline.com on behalf of the Air & Waste Management Association.

Thank you very much for your interest in Taylor & Francis publications. Should you have any questions or require further assistance, please feel free to contact me directly.

Sincerely,

Mary Ann Muller

Permissions Coordinator

E-mail: maryann.muller@taylorandfrancis.com

Telephone: 215.606.4334

530 Walnut Street, Suite 850, Philadelphia, PA 19106 • Phone: 215-625-8900 •
Fax: 215-207-0050
Web: www.tandfonline.com

an informa business

Appendix C. Supporting Information:

Evaluation of cation exchange membrane performance under exposure to high Hg^0 and $HgBr_2$ concentrations

Matthieu B. Miller[1], Mae S. Gustin[2], Sarrah Dunham-Cheatham[2], Grant C. Edwards[1]

[1]Department of Environmental Sciences, Faculty of Science and Engineering, Macquarie University, Sydney, NSW, 2113, Australia

[2]Department of Natural Resources and Environmental Sciences, University of Nevada, Reno NV, 89557, United States

Tekran® 2537 QA/QC

All internal calibrations showed good analyzer zeros, and stable span areas (139875 ± 2.7%) with no drift (SI Fig. 4.1). Every calibration was also checked by external Hg vapor source injections. The system was not operated with a recurring automatic internal calibration, due to the variable timing of the experimental work. System blanks were performed by flowing scrubbed zero air through the entire path of the permeation system, which produced blank values below the Tekran® 2537A detection limit (< 0.1 ng m^{-3}, SI Fig. 4.2 as example). In addition, the system routinely zeroed out when deploying CEM filters on both sample lines during $HgBr_2$ permeations.

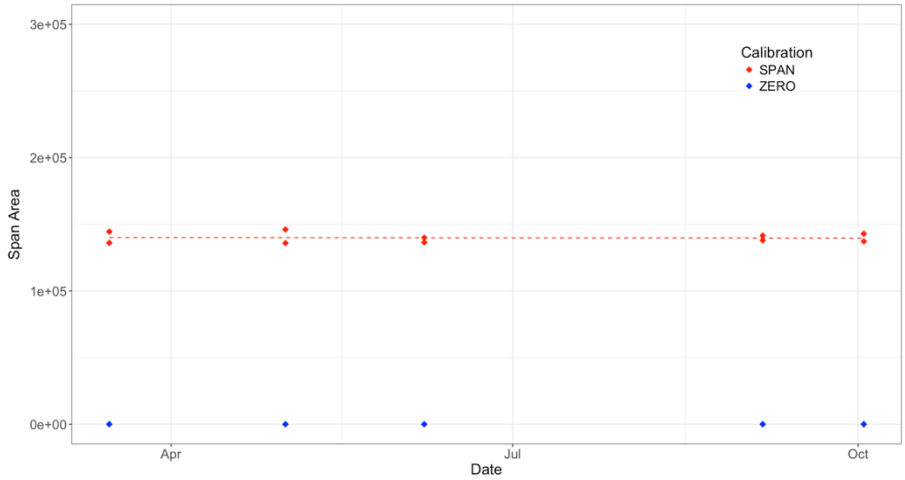

SI Figure 4.1 Tekran 2537A internal calibration data for the duration of the study.

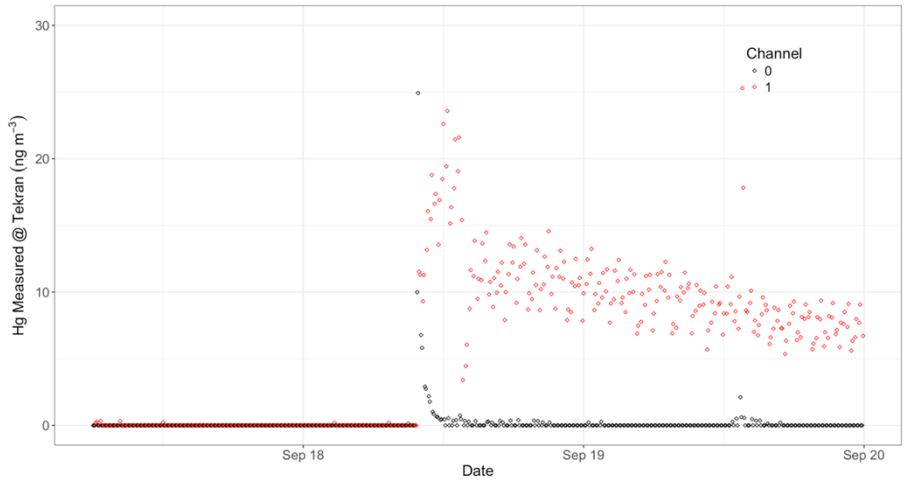

SI Figure 4.2 Example of system zero check prior to turning on $HgBr_2$ permeation source.

Pyrolyzer Design

The pyrolyzer used in the study (SI Fig. 4.3) consisted of a 25.4 cm long quartz glass tube of 0.625 cm diameter (custom, URG Corporation). A loosely packed 3 cm section of quartz wool was lodged in the mid-section of the tube, and this 3 cm section was wrapped with 22 gauge Nichrome wire (18 loops). The quartz tube was closely contained within 2.5 cm thick quartz fiber insulation within a 1.6 mm aluminum casing, except for an enclosed air space around the heated Nichrome coil section. The coil wire was connected to 16 AWG stranded copper wire with all metal dis-connects, which were buried within the quartz fiber insulation to reduce thermal fatigue on the connections. The copper wire insulation was stripped and replaced with higher temperature heat-shrink insulation where the wiring passed through the pyrolyzer case to the external power supply. The tip of a 150 mm long K-type thermocouple (Auber® WRNK-191) was inserted through the insulation into the heated air space next to the coil to provide a temperature feedback for a PID controller (Auber® SYL-1512A). Power to the Nichrome coil was supplied by a 12 VDC transformer through a solid-state relay (Auber® MGR-1D4825) switched by the PID controller.

It was found that the position of the feedback thermocouple in the airspace outside of the heating coil caused a large discrepancy between nominal temperature setpoint and actual temperature inside the heated section of pyrolyzer tube. In general, much higher temperatures are achieved inside the coil than outside. To compensate for this, actual temperature at the heated coil section was verified to 600 °C by external IR sensor and internal thermocouple probe. The pyrolyzer design used in this study was not 100% efficient at thermally reducing $HgBr_2$ to Hg^0, based on the higher total Hg recoveries on the CEM filters versus total Hg measured through the pyrolyzer

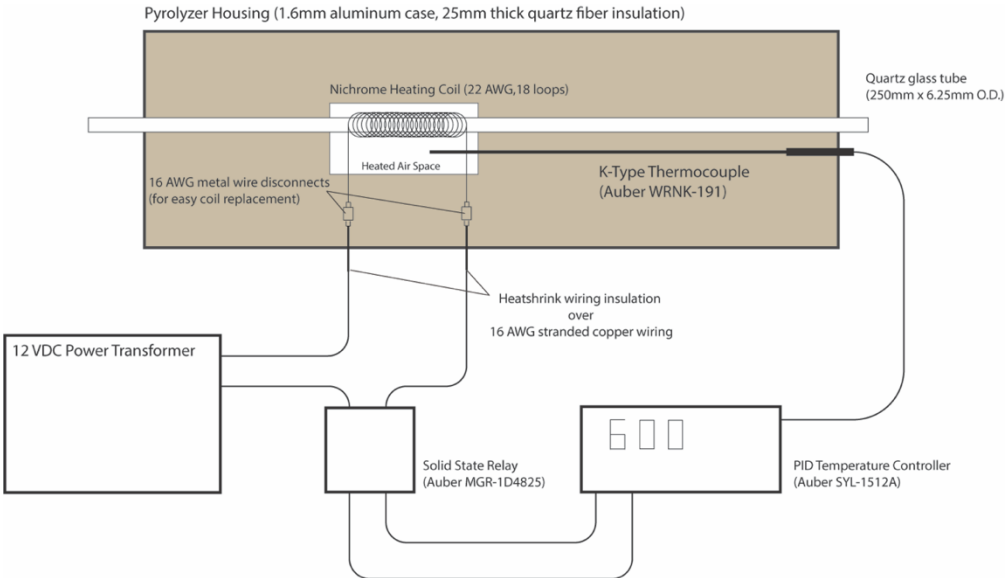

SI Figure 4.3 Detailed schematic of pyrolyzer design.

on the Tekran® 2537. A larger heated section, and higher temperatures than 600 °C would likely improve pyrolyzer efficiency. However, we found that the fine silanized quartz wool used in the pyrolyzer tube began to melt around 700 °C, and so a different tube configuration with quartz chips would be required for higher temperatures.

GEM Permeation

The first CEM filter in line during the GEM permeations always showed more total Hg than the following 5 downstream filters, which were not significantly different from each other (SI Fig. 4.4). We believe it is unlikely that the Hg observed on the first CEM filters results from GEM uptake. Even at the highest GEM permeation level, the first filter captured only ~1700 pg of Hg, out of a total permeated amount of over 7.3 *million* pg (a 0.02 % uptake rate). This means that the downstream CEM filters were still exposed to about 7.2985 *million* pg of GEM but captured less total Hg. The most likely explanation is that the first CEM filters were scrubbing a small component of residual RM that was coming off the system, possibly minor oxidation of the Hg^0 bead. Therefore, the first in-line filters were not included in calculation of GEM uptake rates.

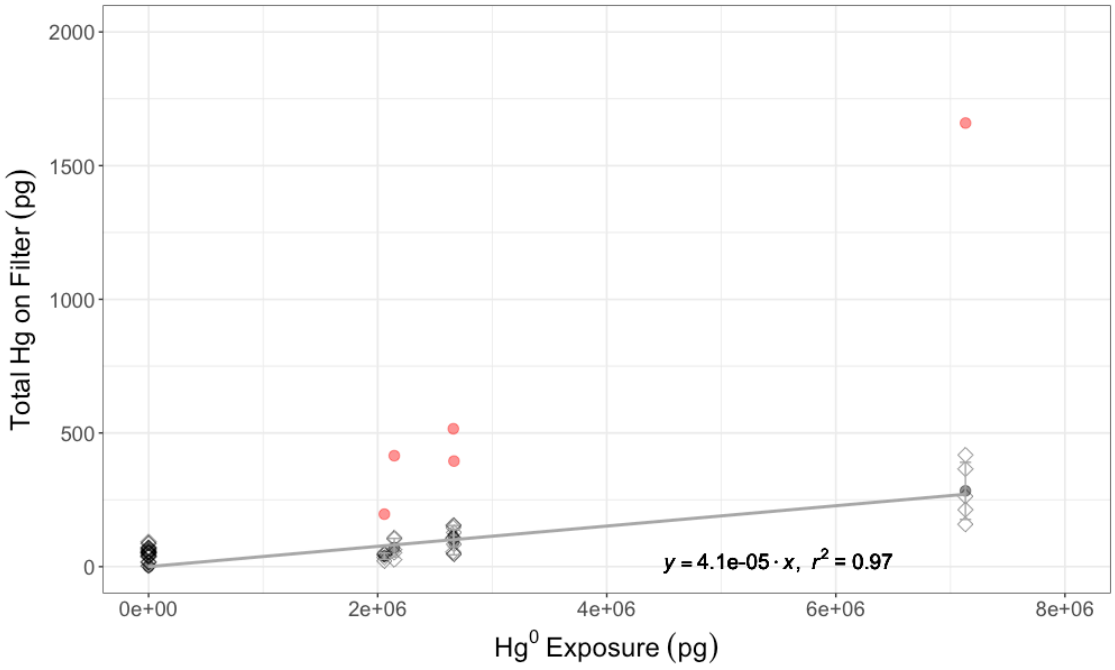

SI Figure 4.4 Hg on first in-line CEM filters (red circles) versus following downstream filters (open diamonds and regression line), during the 5 GEM permeations. These first filters were not used in calculations of GEM uptake, on the strong suspicion they were capturing residual RM from the sample lines.

Appendix D. Supporting Information:

Effect of moisture content on air surface exchange of reactive mercury from mining substrates

Matthieu B. Miller[1], Mae S. Gustin[2], Harald Biester[3], Grant C. Edwards[1]

[1]Faculty of Science and Engineering, Department of Environmental Sciences, Macquarie University, Sydney NSW, 2113, Australia

[2]Department of Natural Resources and Environmental Sciences, University of Nevada, Reno NV, 89557, United States

[3]Institute of Geoecology, Technical University of Braunschweig, Braunschweig, 38106, Germany

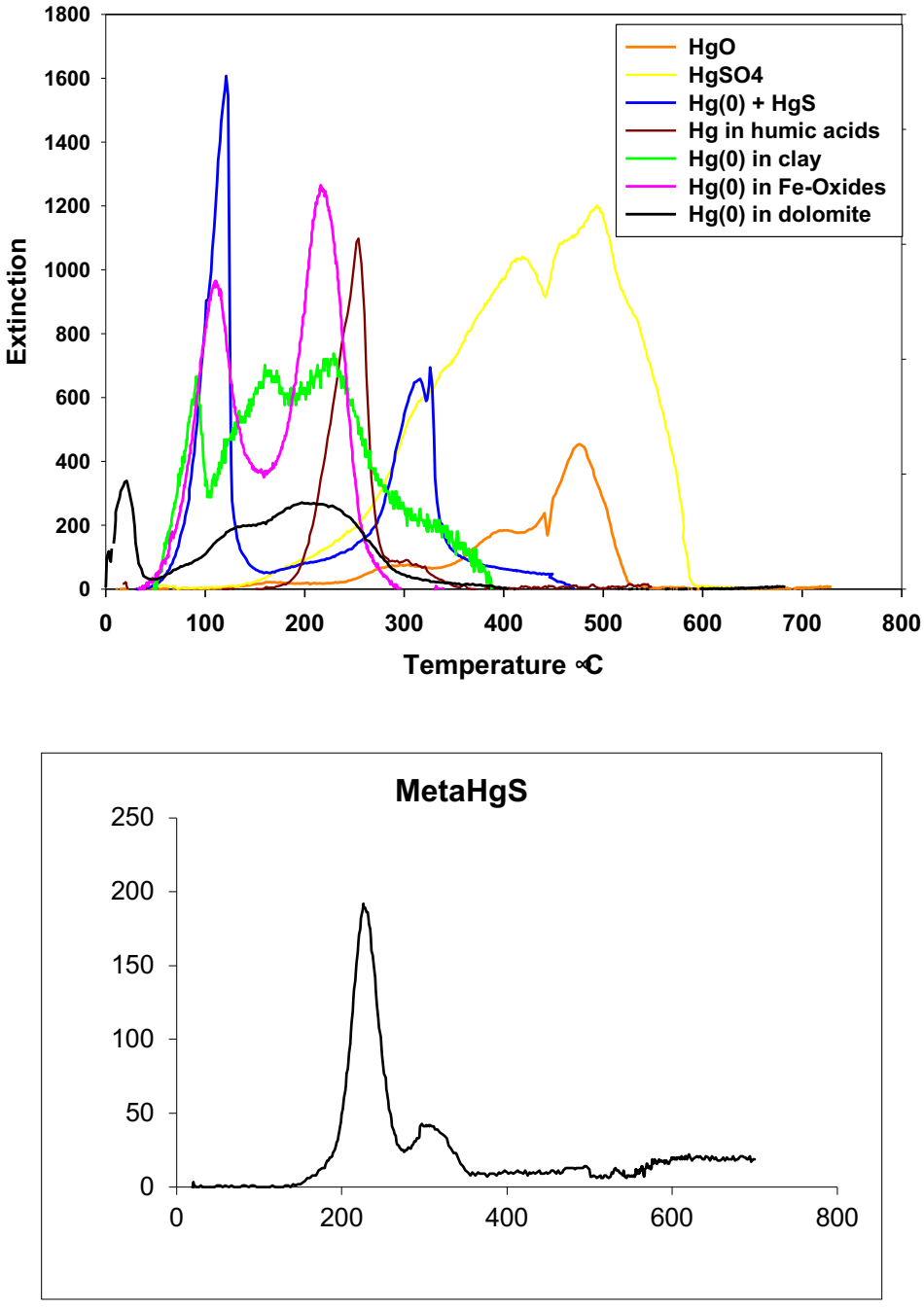

SI Figure 6.1 Reference solid phase thermal desorption profiles for select Hg compounds.

Appendix E. Supporting Information:

Reactive mercury concentrations in Australia and the Southern Hemisphere

Matthieu B. Miller[1], Dean A. Howard[2], Ashley M. Pierce[1], Kellie Cook[1], Melita Keywood[3], Mae S. Gustin[4], Grant C. Edwards[1]

[1]Department of Environmental Sciences, Faculty of Science and Engineering, Macquarie University, Sydney NSW, 2113, Australia

[2] Department of Environmental, Earth, and Atmospheric Sciences, University of Massachusetts-Lowell, Lowell MA, 01854, United States

[3]Centre for Australian Climate and Weather Research, Australian Commonwealth Scientific and Industrial Research Organization, Melbourne, VIC, Australia

[4]Department of Natural Resources and Environmental Sciences, University of Nevada, Reno NV, 89557, United States

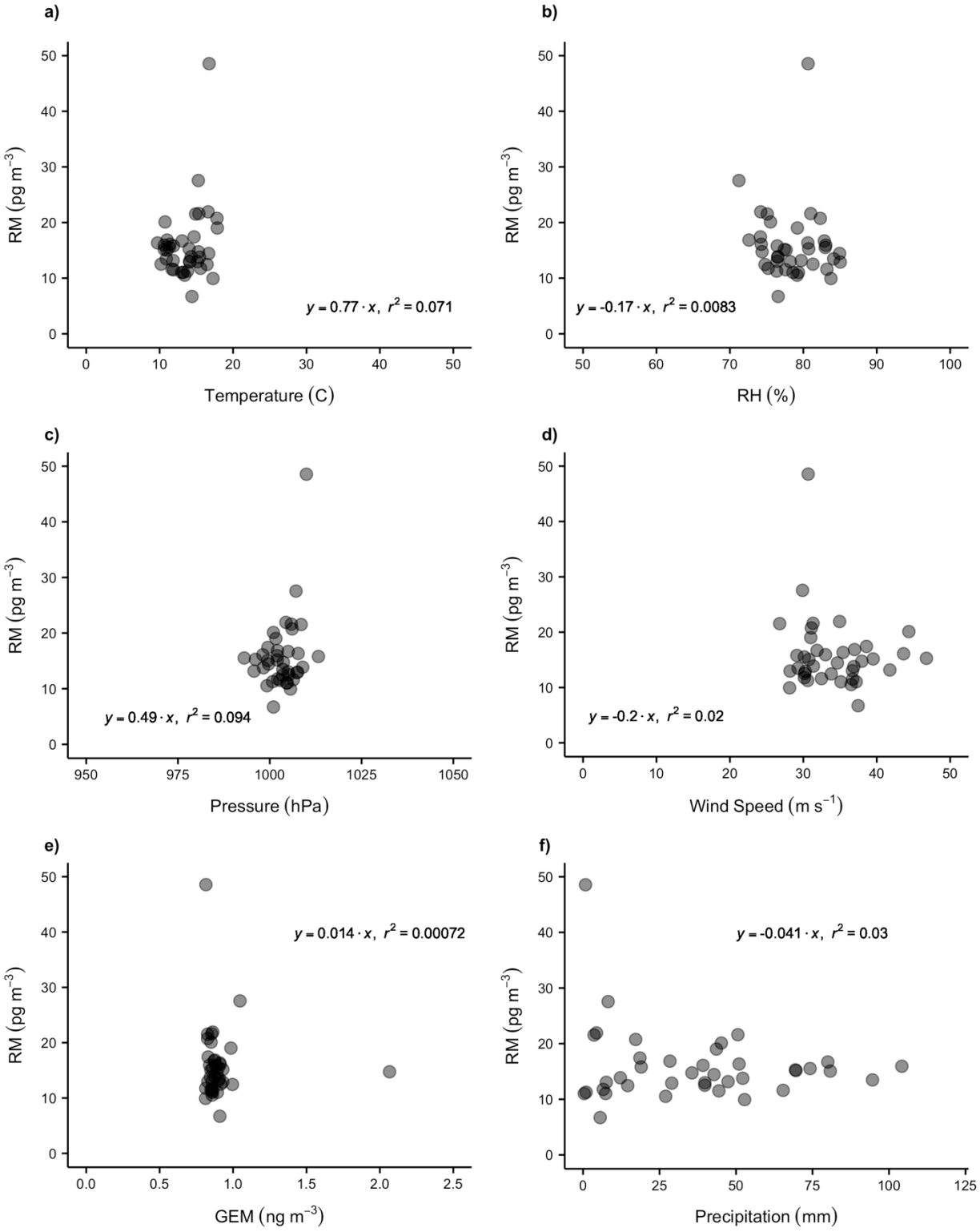

SI Figure 7.1 Relationship between RM concentration (pg m^{-3}) and other parameters measured at CGBAPS: a) Temperature (°C), b) RH (%), c) atmospheric pressure (hPa), d) wind speed (m s^{-1}), e) GEM concentration (ng m^{-3}), and f) total precipitation (mm).

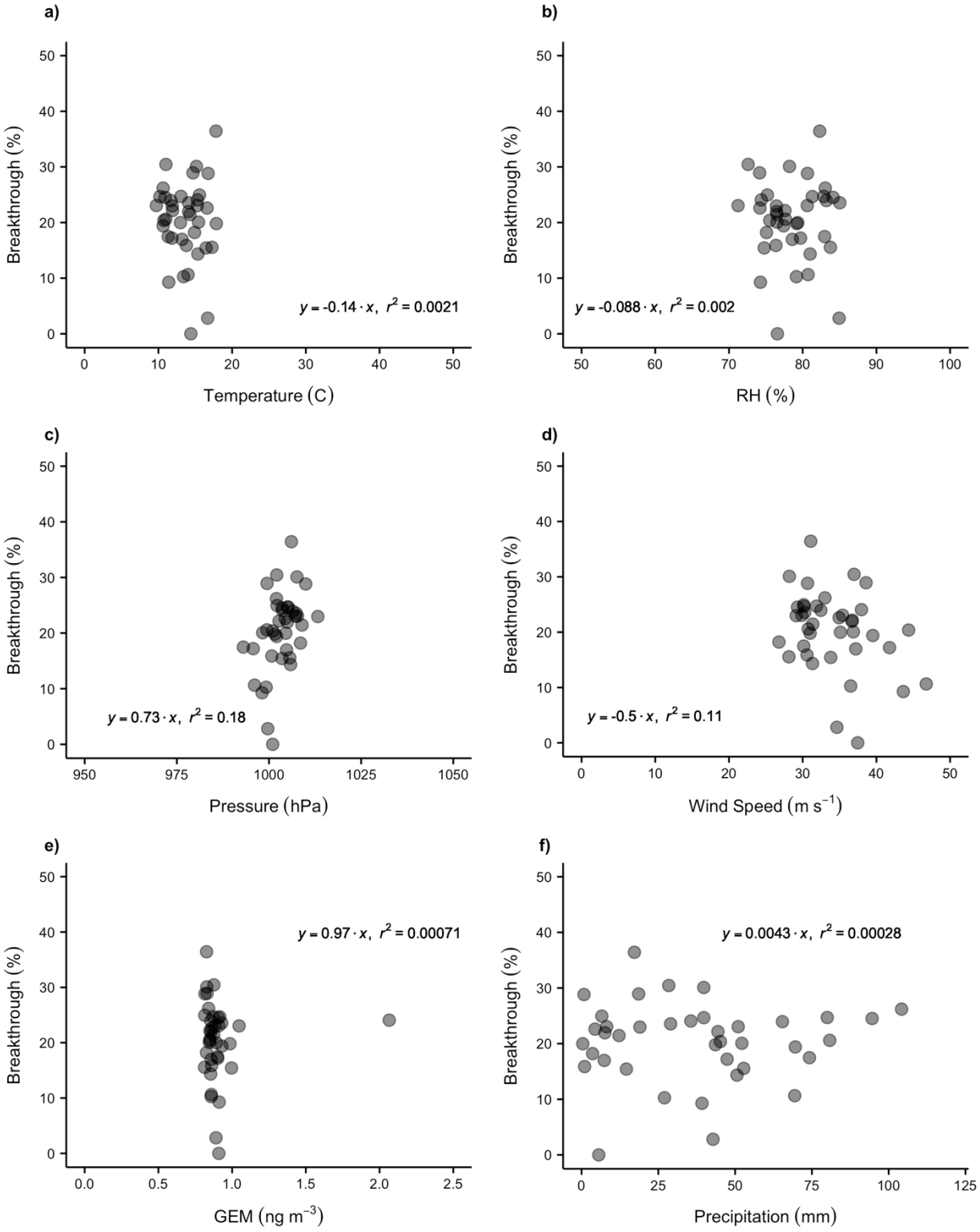

SI Figure 7.2 Relationship between RM breakthrough to the secondary CEM filter (% of total) and other parameters measured at CGBAPS: a) Temperature (°C), b) RH (%), c) atmospheric pressure (hPa), d) wind speed (m s^{-1}), e) GEM concentration (ng m^{-3}), and f) total precipitation (mm).

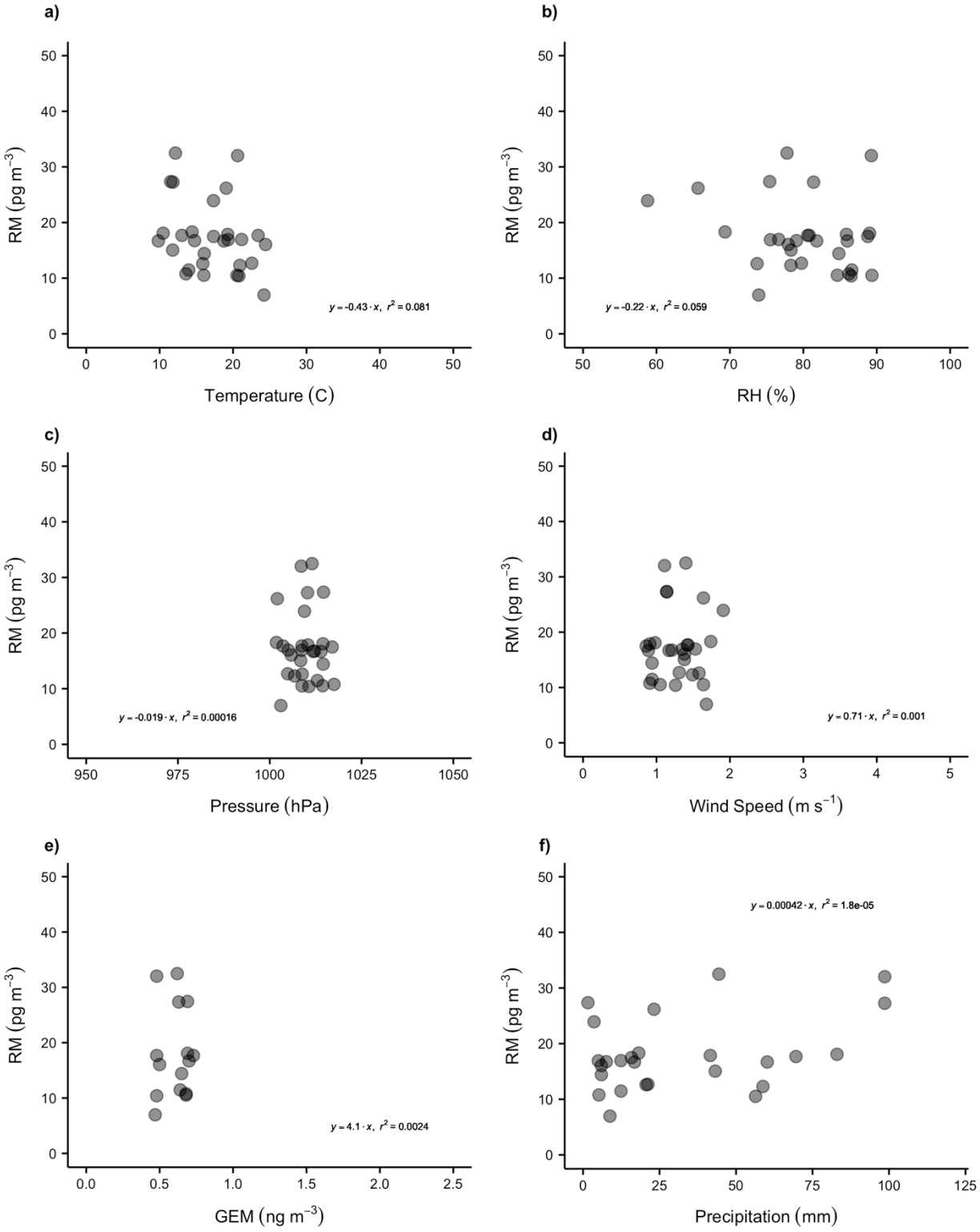

SI Figure 7.3 Relationship between RM concentration (pg m^{-3}) and other parameters measured at MQAWS: a) Temperature (°C), b) RH (%), c) atmospheric pressure (hPa), d) wind speed (m s^{-1}), e) GEM concentration (ng m^{-3}), and f) total precipitation (mm).

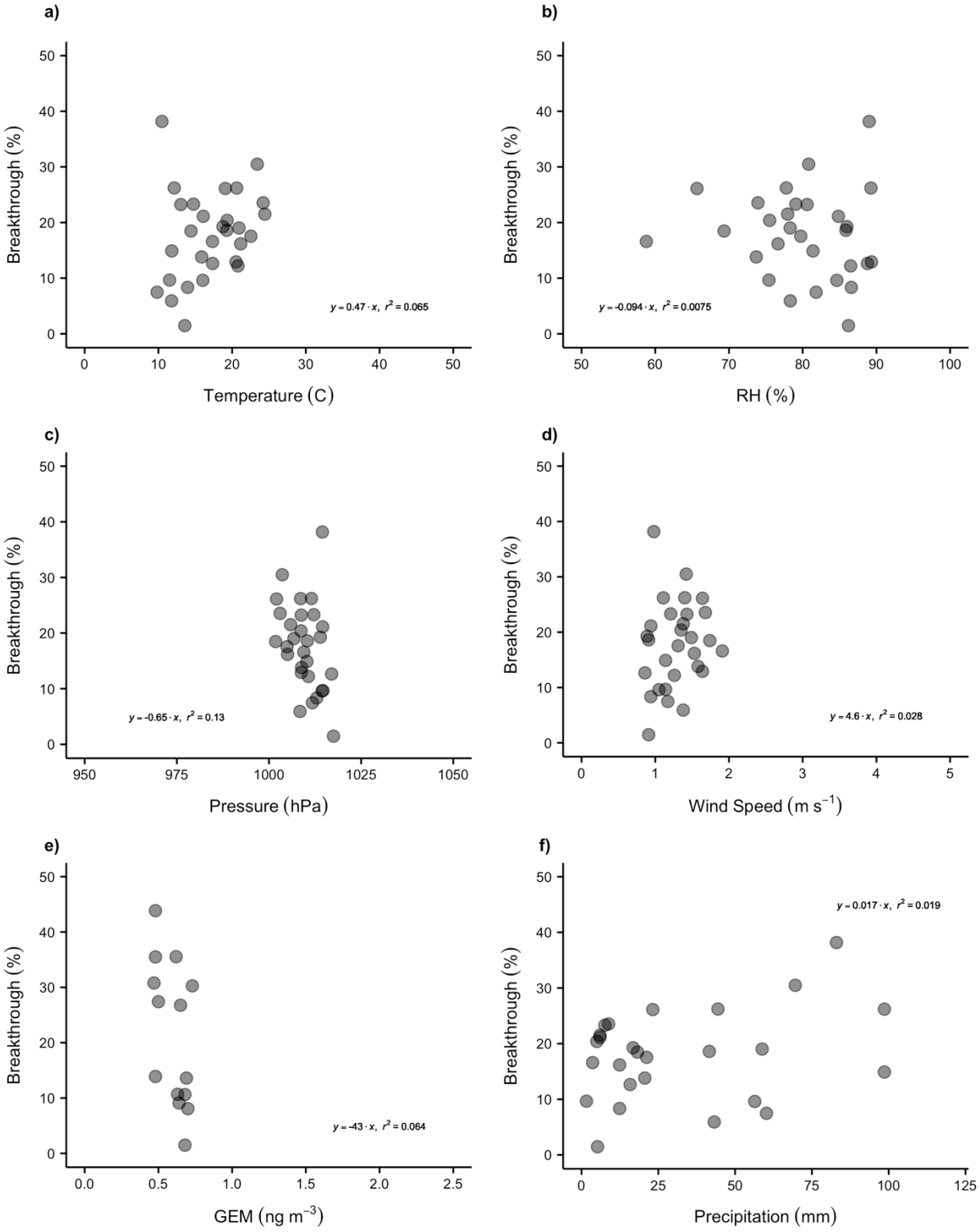

SI Figure 7.4 Relationship between RM breakthrough to the secondary CEM filter (% of total) and other parameters measured at MQAWS: a) Temperature (°C), b) RH (%), c) atmospheric pressure (hPa), d) wind speed (m s^{-1}), e) GEM concentration (ng m^{-3}), and f) total precipitation (mm).

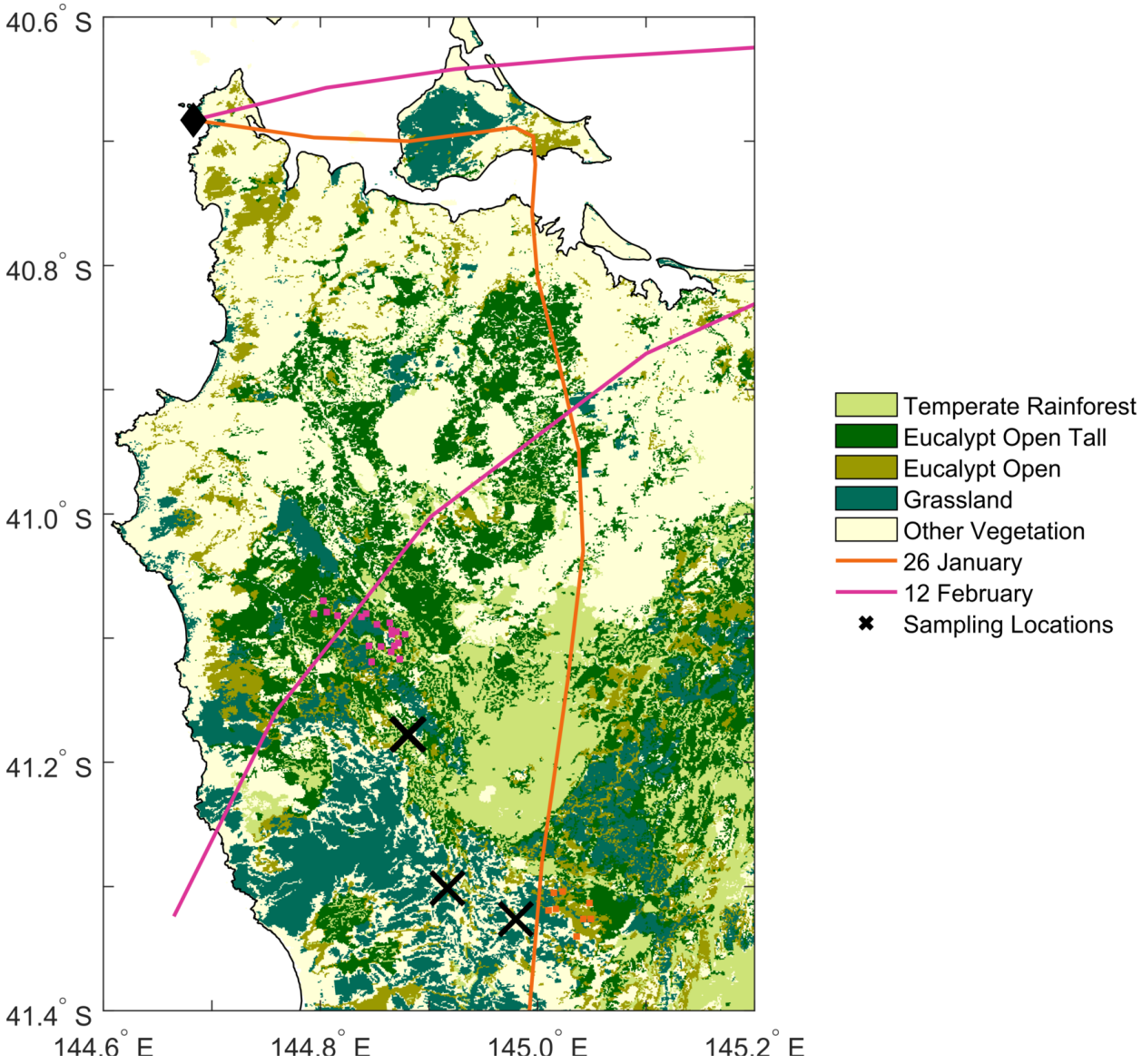

SI Fig 7.5 Back trajectory plots and fire hotspot locations during plume events of January 26 and February 12, 2016. From Howard (2018).

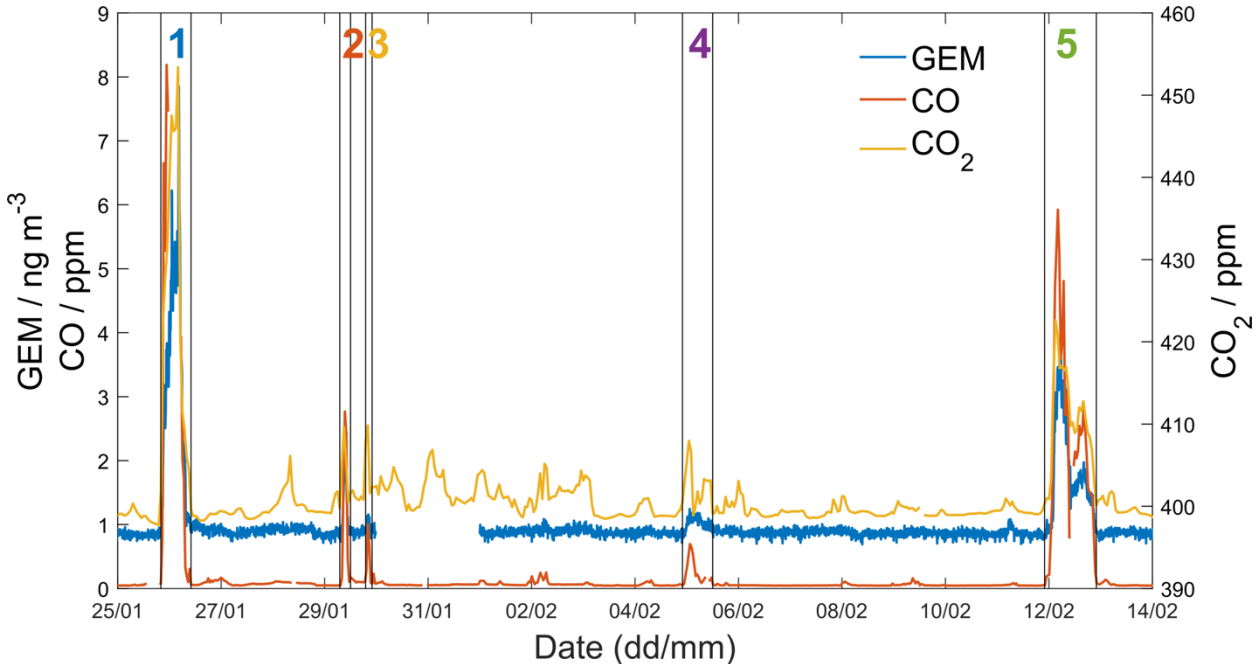

SI Fig 7.6 GEM, CO, and CO2 concentration during plume events between January 25 and February 14, 2016. From Howard (2018).

Wind rose charts for Cape Grim Baseline Air Pollution Station

CG.1 2015-11-17 , # of hours = 271

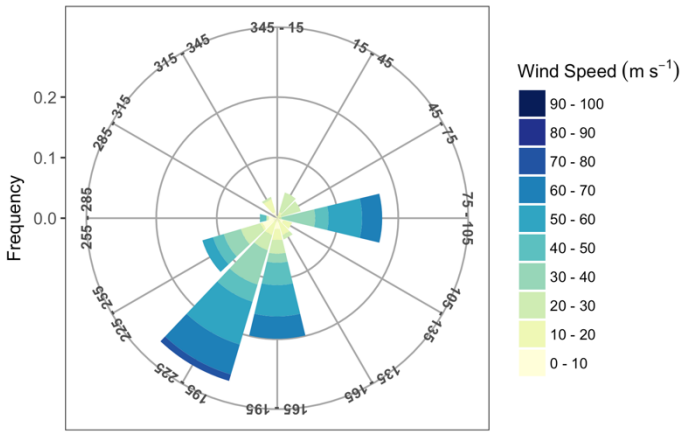

CG.2 2015-12-01 , # of hours = 336

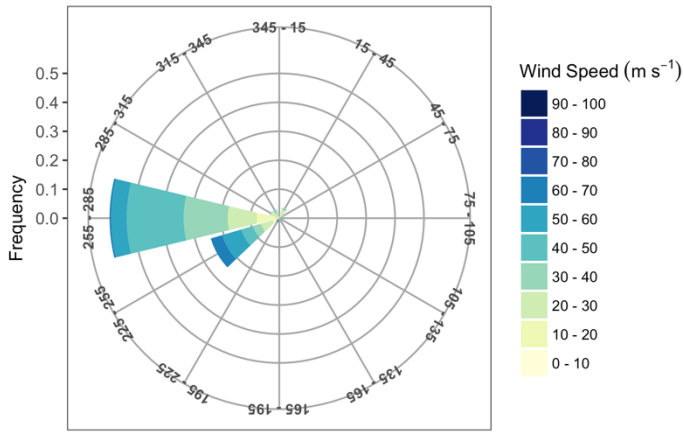

CG.3 2015-12-15 , # of hours = 336

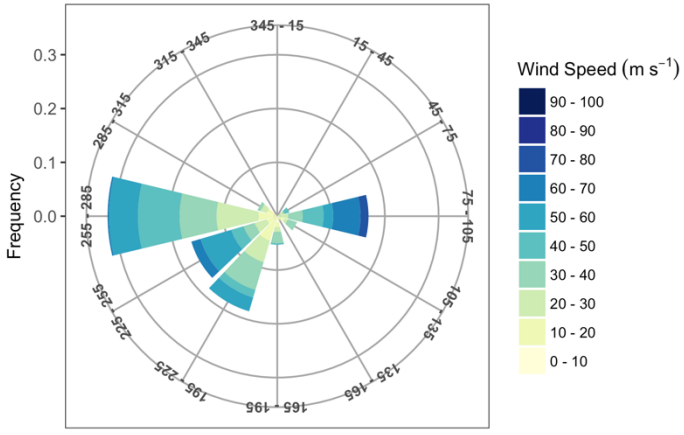

CG.4 2015-12-29 , # of hours = 330

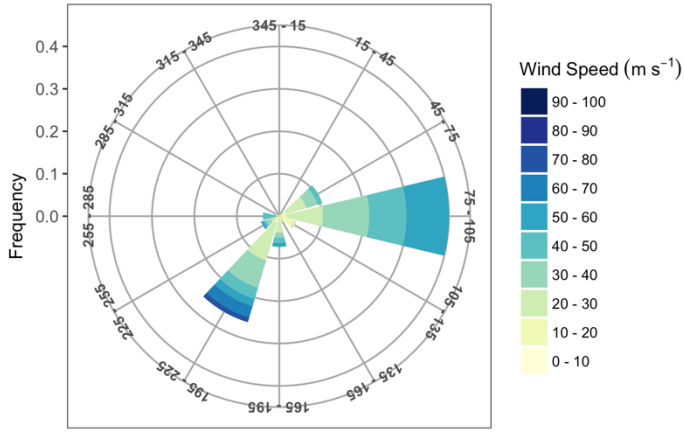

CG.5 2016-01-11 , # of hours = 312

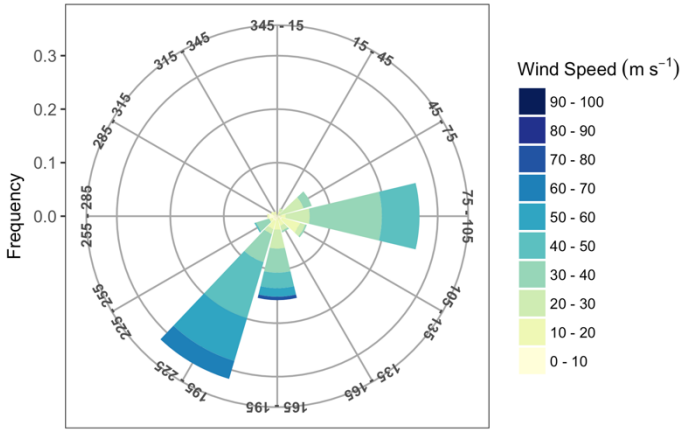

CG.6 2016-01-25 , # of hours = 334

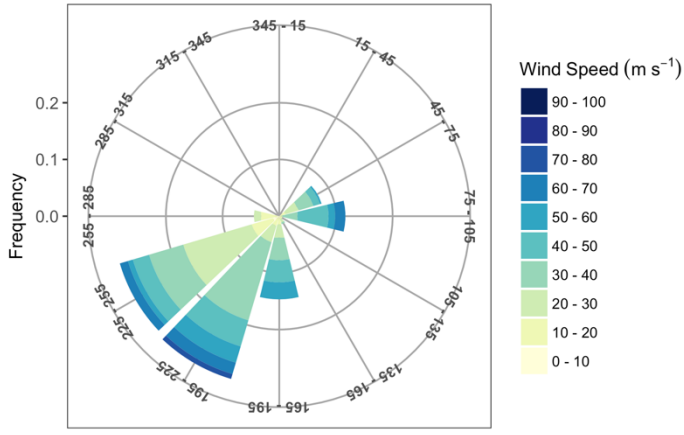

CG.7 2016-02-09 , # of hours = 360

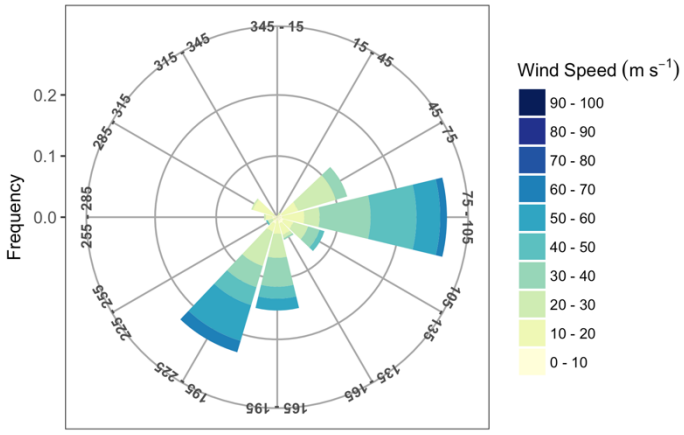

CG.8 2016-02-23 , # of hours = 336

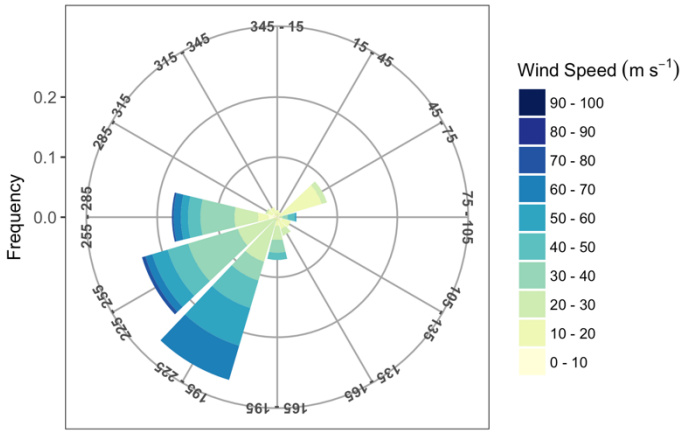

CG.9 2016-03-08 , # of hours = 252

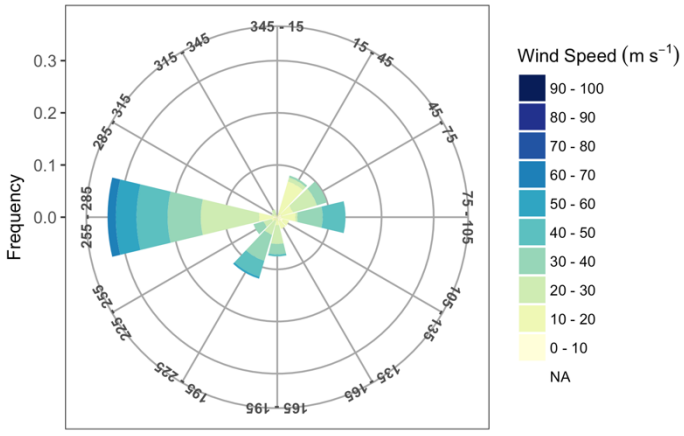

CG.10 2016-03-22 , # of hours = 156

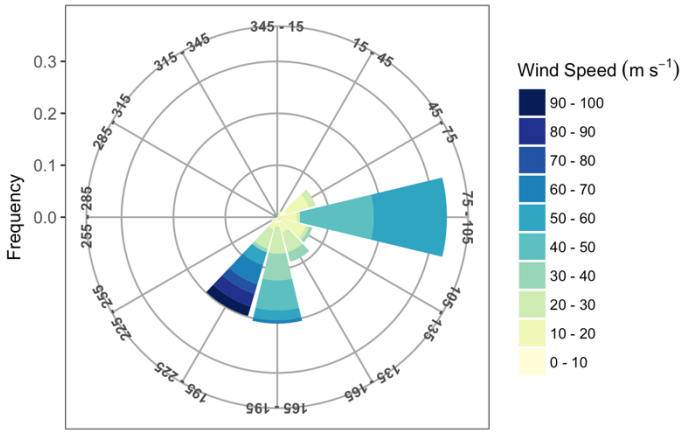

CG.11 2016-04-05 , # of hours = 336

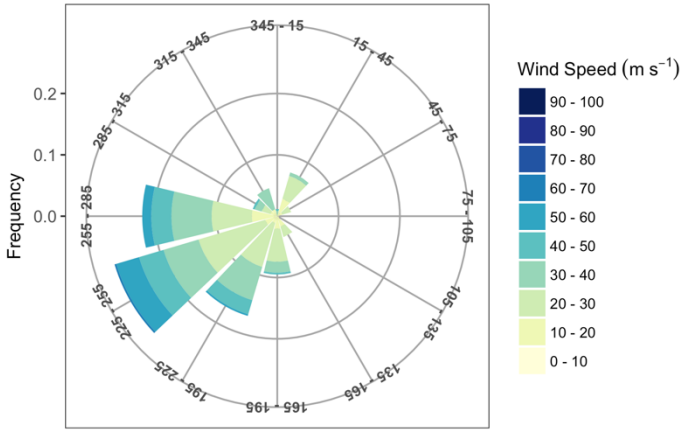

CG.12 2016-04-19 , # of hours = 336

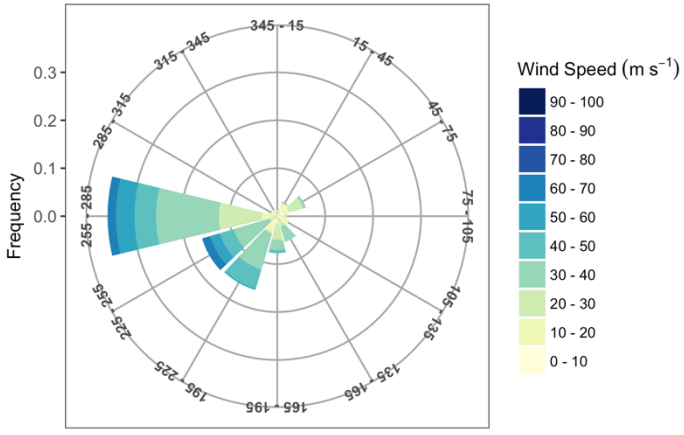

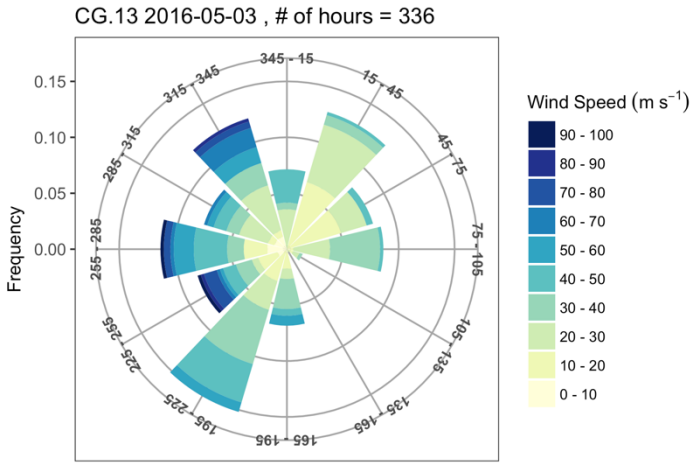
CG.13 2016-05-03 , # of hours = 336
Frequency
0.15
0.10
0.05
0.00
345 - 15
15 - 45
45 - 75
75 - 105
105 - 135
135 - 165
165 - 195
195 - 225
225 - 255
255 - 285
285 - 315
315 - 345
Wind Speed (m s−1)
90 - 100
80 - 90
70 - 80
60 - 70
50 - 60
40 - 50
30 - 40
20 - 30
10 - 20
0 - 10

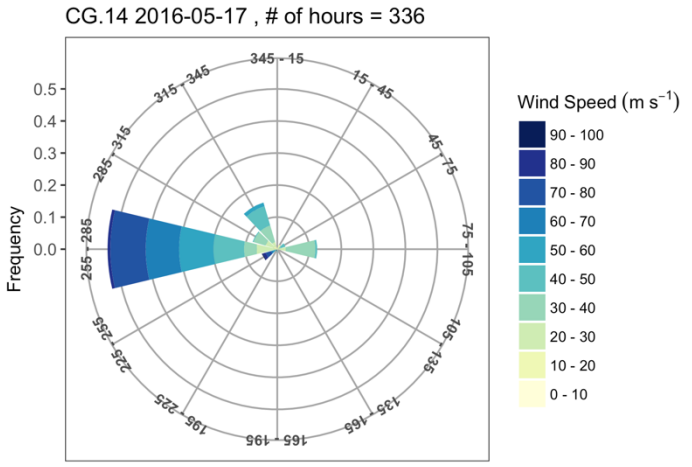
CG.14 2016-05-17 , # of hours = 336
Frequency
0.5
0.4
0.3
0.2
0.1
0.0
345 - 15
15 - 45
45 - 75
75 - 105
105 - 135
135 - 165
165 - 195
195 - 225
225 - 255
255 - 285
285 - 315
315 - 345
Wind Speed (m s−1)
90 - 100
80 - 90
70 - 80
60 - 70
50 - 60
40 - 50
30 - 40
20 - 30
10 - 20
0 - 10

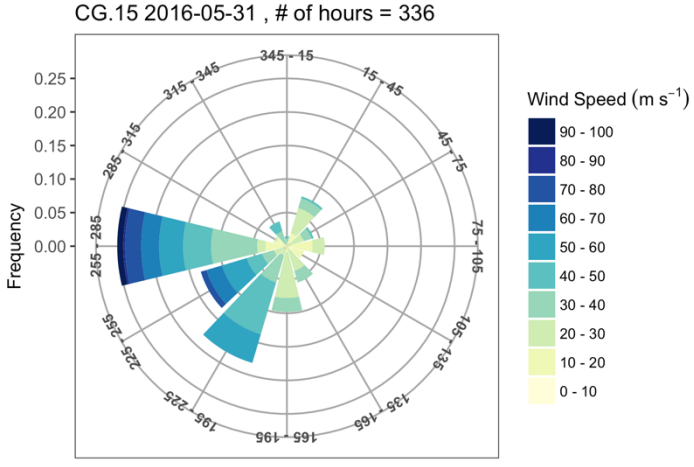
CG.15 2016-05-31 , # of hours = 336
Frequency
0.25
0.20
0.15
0.10
0.05
0.00
345 - 15
15 - 45
45 - 75
75 - 105
105 - 135
135 - 165
165 - 195
195 - 225
225 - 255
255 - 285
285 - 315
315 - 345
Wind Speed (m s−1)
90 - 100
80 - 90
70 - 80
60 - 70
50 - 60
40 - 50
30 - 40
20 - 30
10 - 20
0 - 10

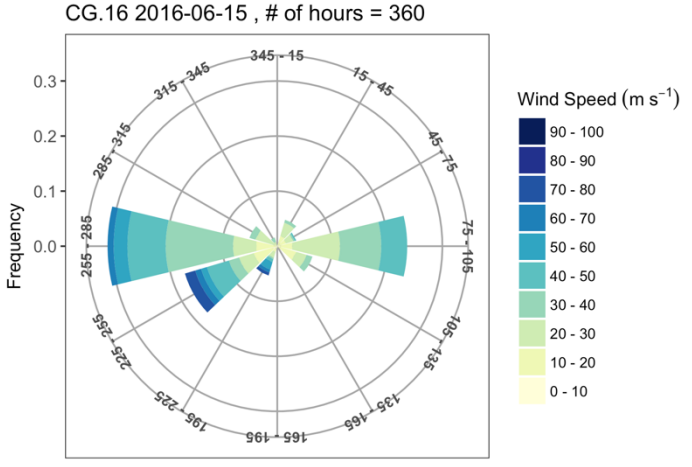
CG.16 2016-06-15 , # of hours = 360
Frequency
0.3
0.2
0.1
0.0
345 - 15
15 - 45
45 - 75
75 - 105
105 - 135
135 - 165
165 - 195
195 - 225
225 - 255
255 - 285
285 - 315
315 - 345
Wind Speed (m s−1)
90 - 100
80 - 90
70 - 80
60 - 70
50 - 60
40 - 50
30 - 40
20 - 30
10 - 20
0 - 10

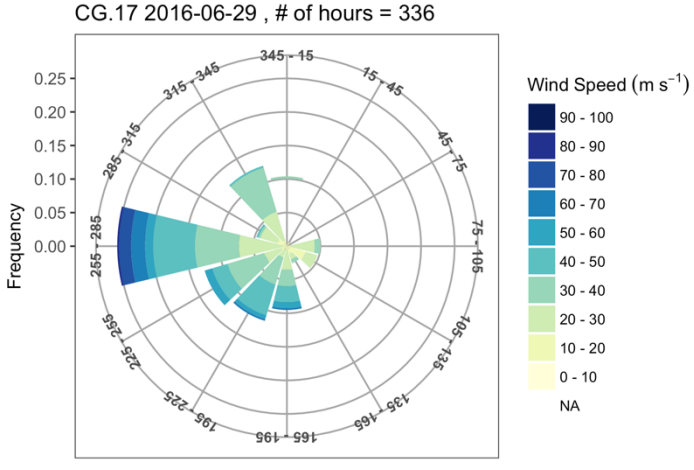
CG.17 2016-06-29 , # of hours = 336
Frequency
0.25
0.20
0.15
0.10
0.05
0.00
345 - 15
15 - 45
45 - 75
75 - 105
105 - 135
135 - 165
165 - 195
195 - 225
225 - 255
255 - 285
285 - 315
315 - 345
Wind Speed (m s−1)
90 - 100
80 - 90
70 - 80
60 - 70
50 - 60
40 - 50
30 - 40
20 - 30
10 - 20
0 - 10
NA

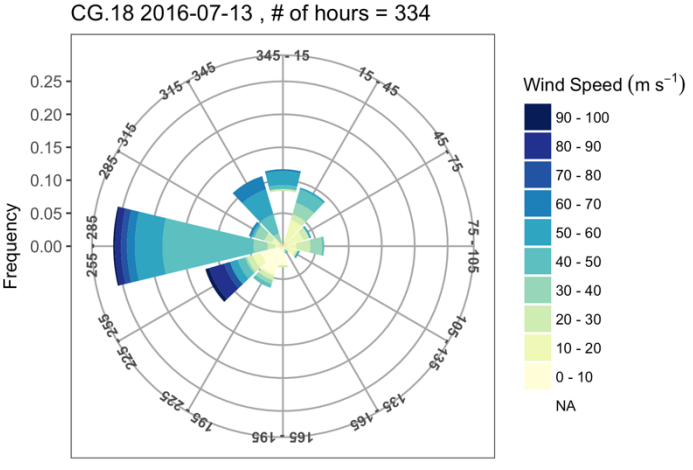
CG.18 2016-07-13 , # of hours = 334
Frequency
0.25
0.20
0.15
0.10
0.05
0.00
345 - 15
15 - 45
45 - 75
75 - 105
105 - 135
135 - 165
165 - 195
195 - 225
225 - 255
255 - 285
285 - 315
315 - 345
Wind Speed (m s−1)
90 - 100
80 - 90
70 - 80
60 - 70
50 - 60
40 - 50
30 - 40
20 - 30
10 - 20
0 - 10
NA

CG.19 2016-07-26 , # of hours = 312

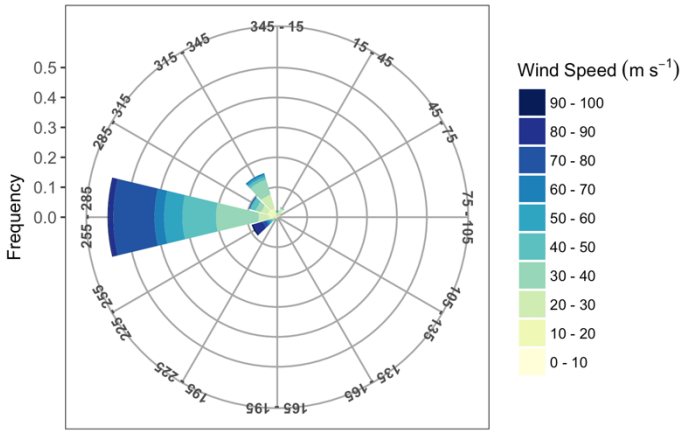

CG.20 2016-08-09 , # of hours = 336

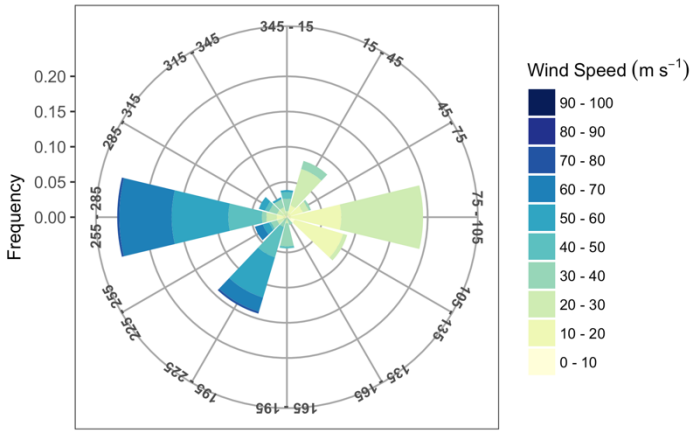

CG.21 2016-08-23 , # of hours = 336

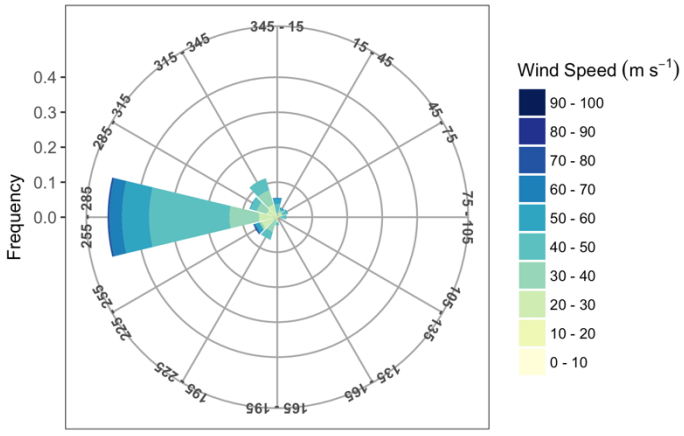

CG.22 2016-09-06 , # of hours = 336

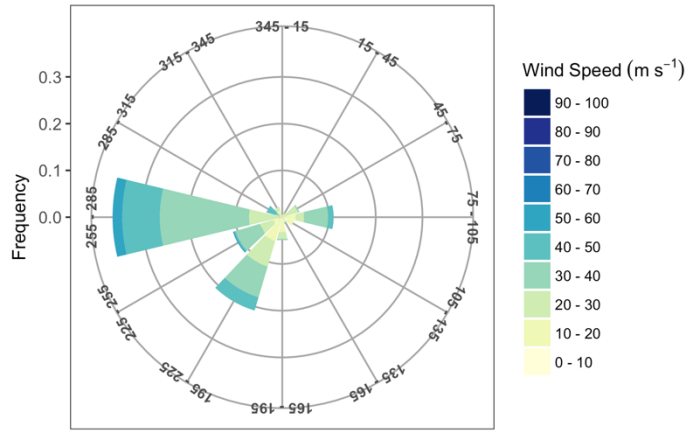

CG.23 2016-09-20 , # of hours = 336

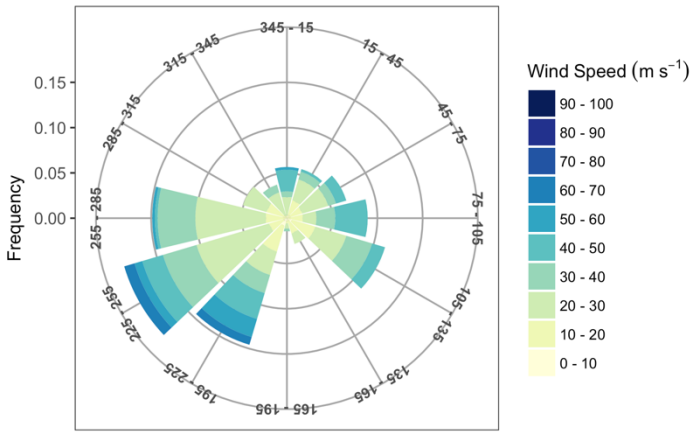

CG.24 2016-10-04 , # of hours = 331

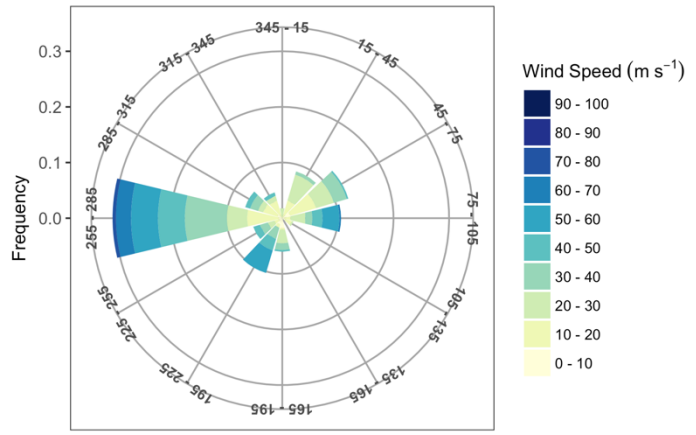

CG.25 2016-10-18 , # of hours = 336

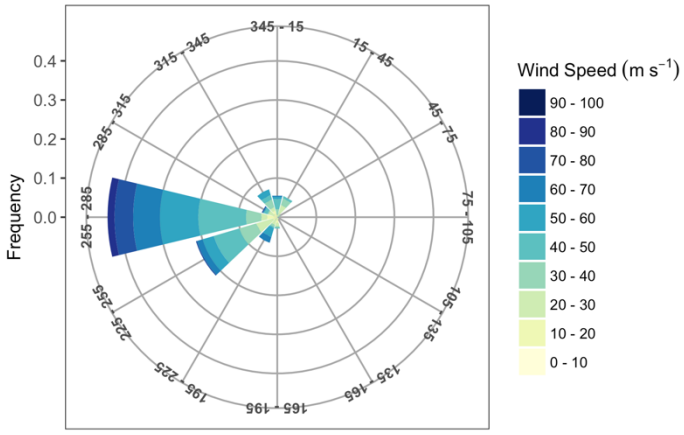

CG.26 2016-11-01 , # of hours = 336

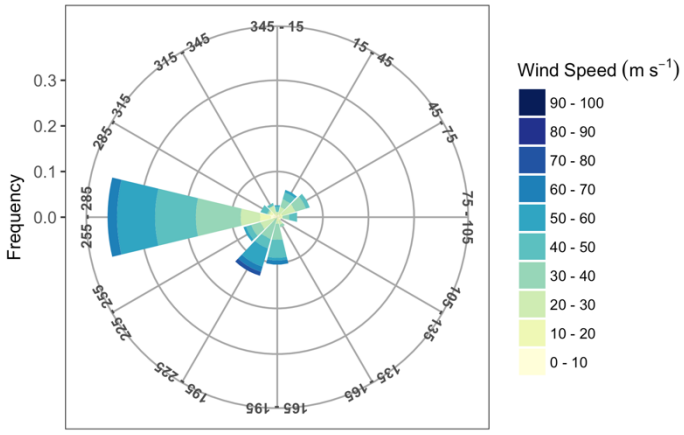

CG.27 2016-11-15 , # of hours = 336

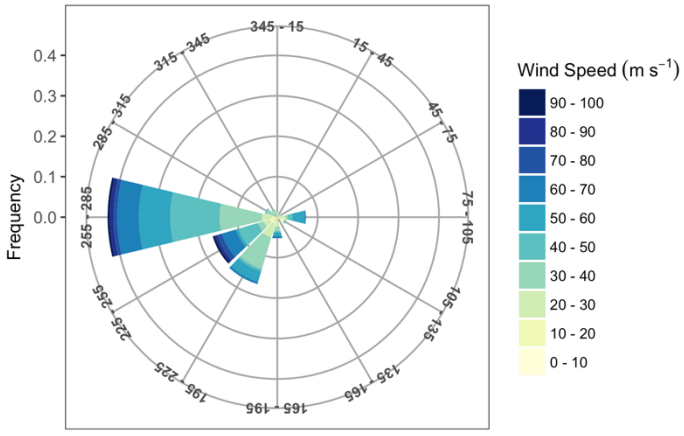

CG.28 2016-11-29 , # of hours = 336

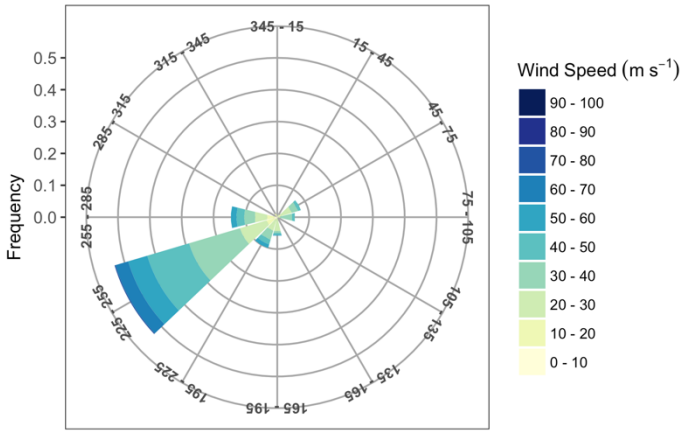

CG.29 2016-12-13 , # of hours = 336

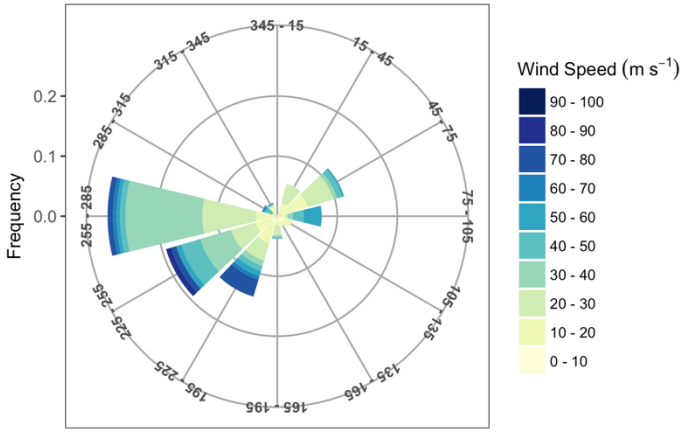

CG.30 2016-12-27 , # of hours = 336

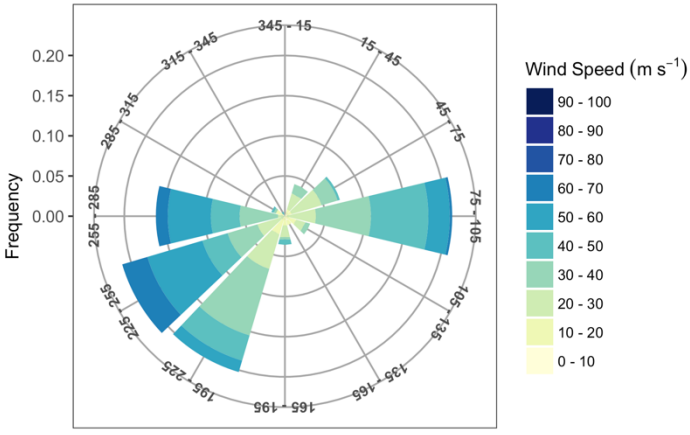

CG.31 2017-01-10 , # of hours = 336

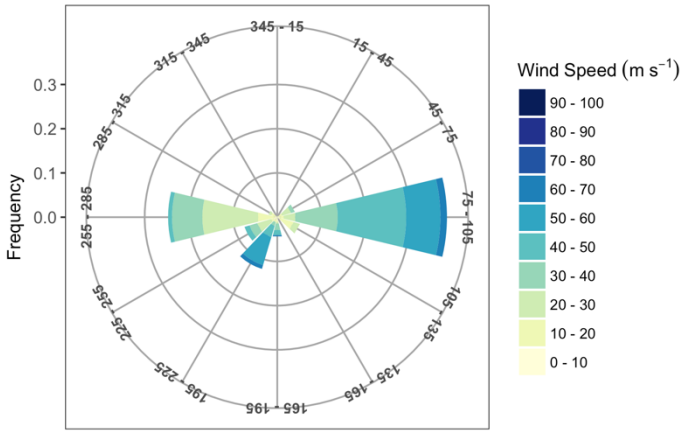

CG.32 2017-01-25 , # of hours = 360

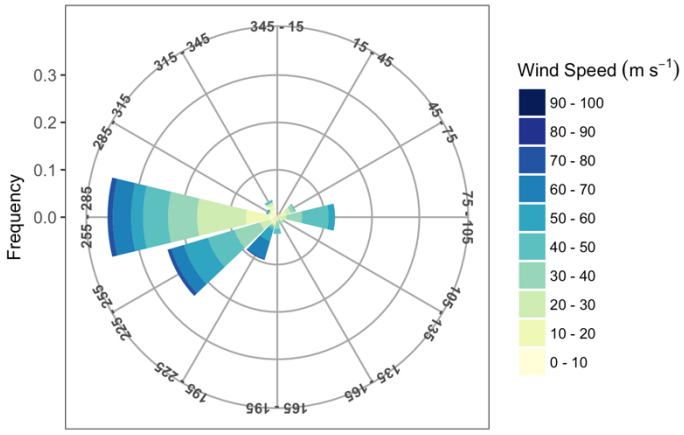

CG.33 2017-02-07 , # of hours = 312

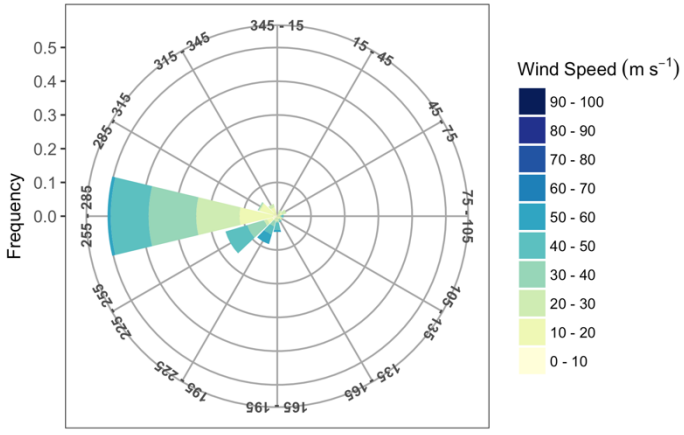

CG.34 2017-02-21 , # of hours = 336

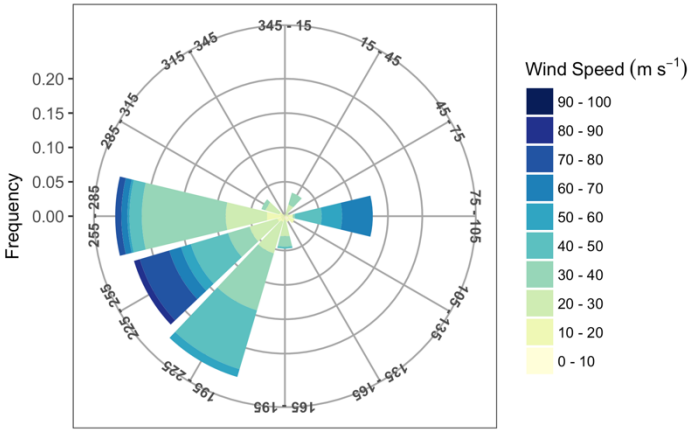

CG.35 2017-03-07 , # of hours = 336

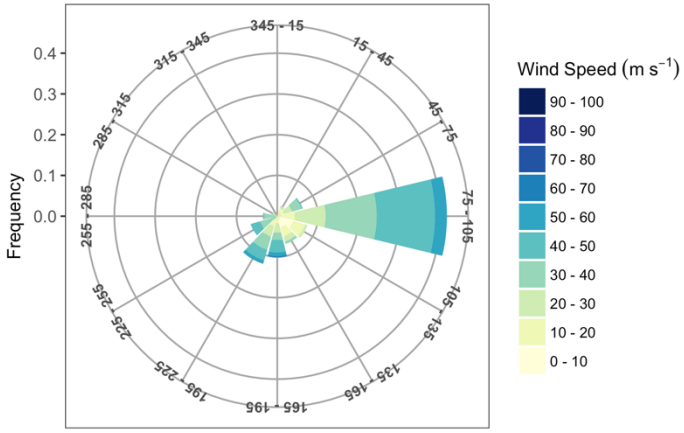

CG.36 2017-03-21 , # of hours = 336

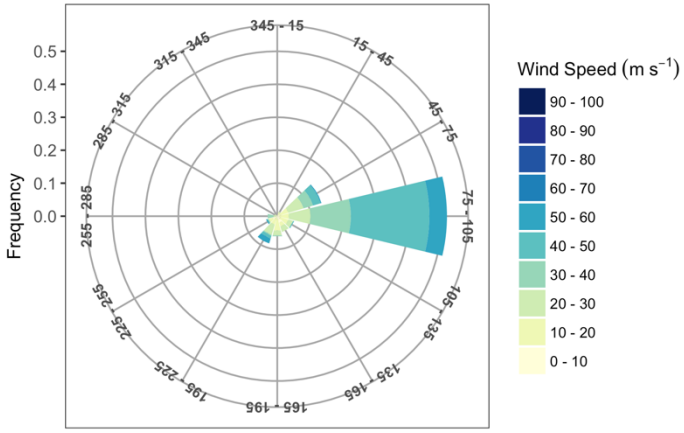

CG.37 2017-04-05 , # of hours = 360

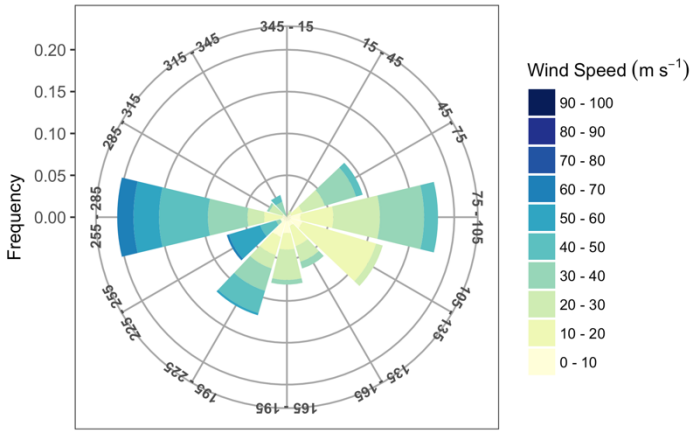

CG.38 2017-04-18 , # of hours = 312

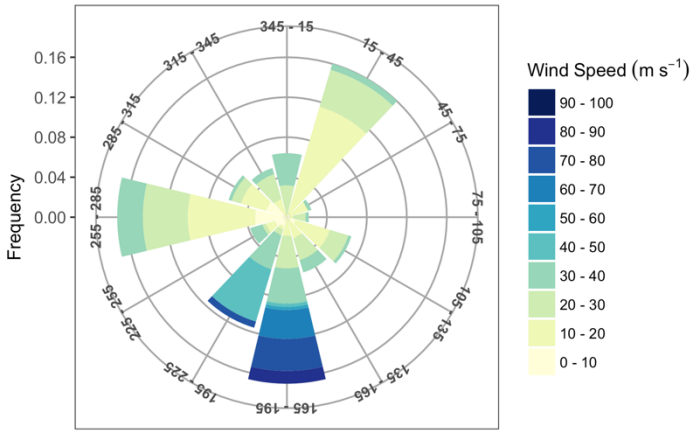

CG.39 2017-05-02 , # of hours = 336

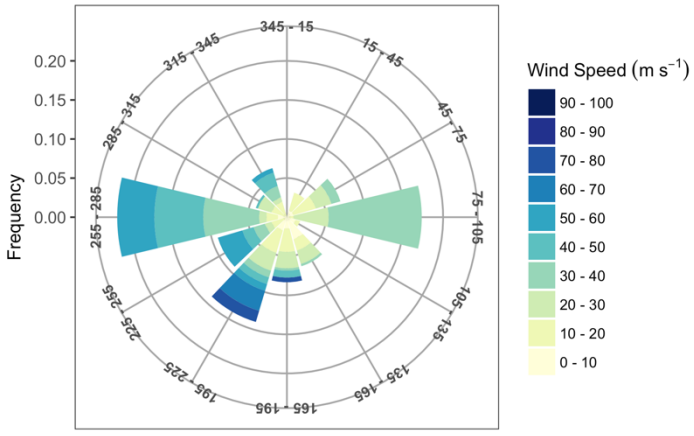

CG.40 2017-05-16 , # of hours = 336

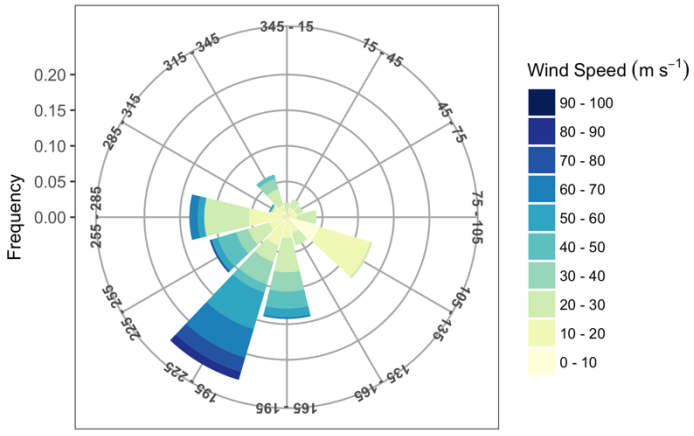

CG.41 2017-05-30 , # of hours = 336

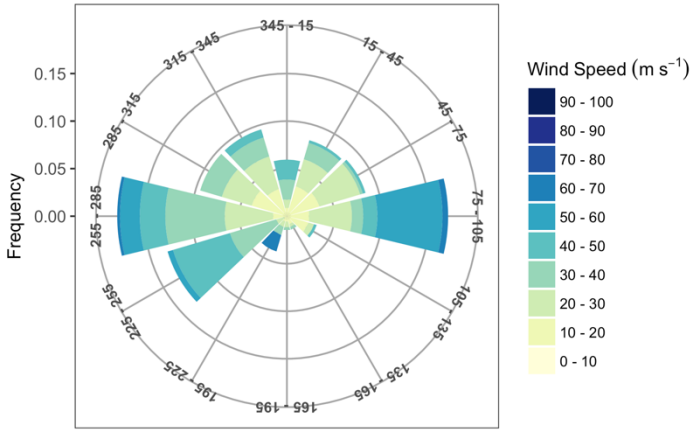

Wind rose charts for Macquarie University Automatic Weather Station

MQ.1 2016-04-04 , # of hours = 293

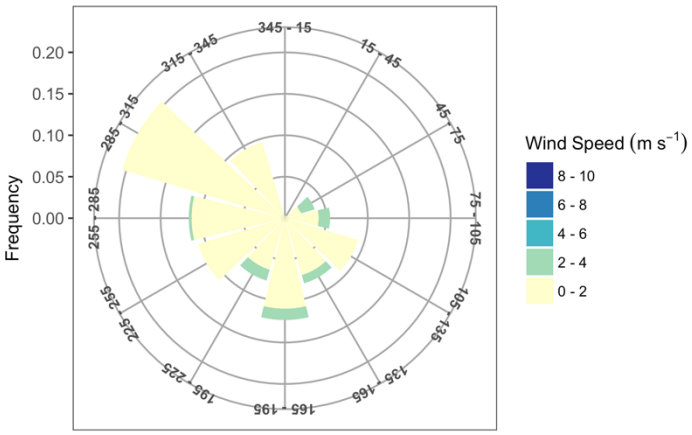

MQ.2 2016-04-18 , # of hours = 336

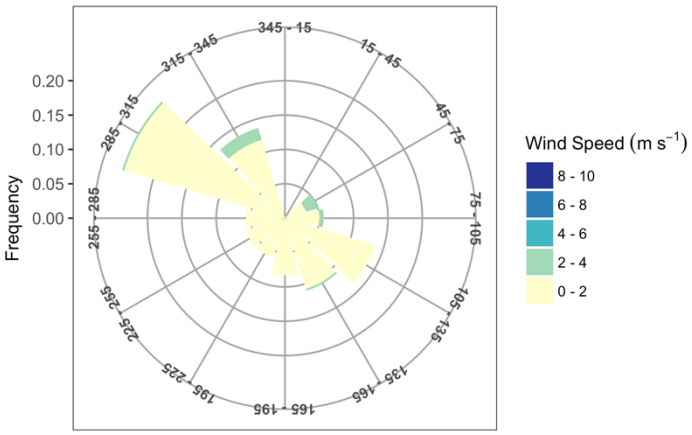

MQ.3 2016-05-02 , # of hours = 288

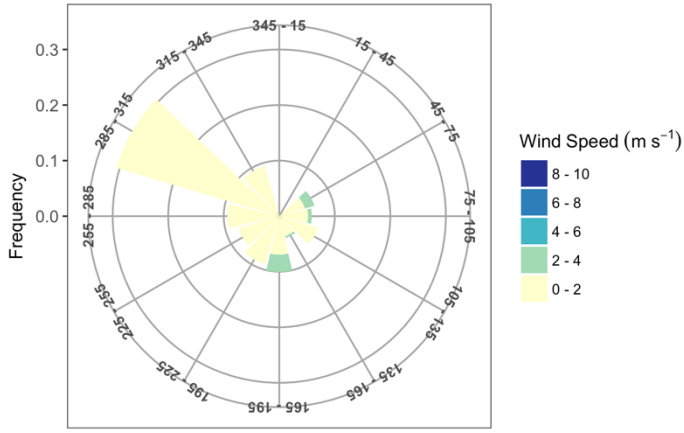

MQ.6 2016-06-13 , # of hours = 288

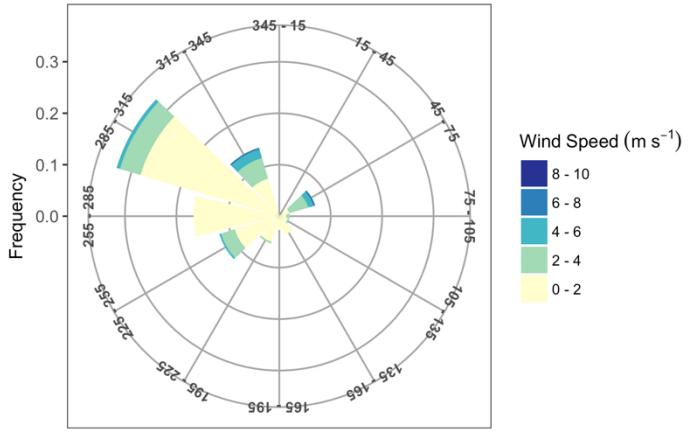

MQ.7 2016-06-27 , # of hours = 336

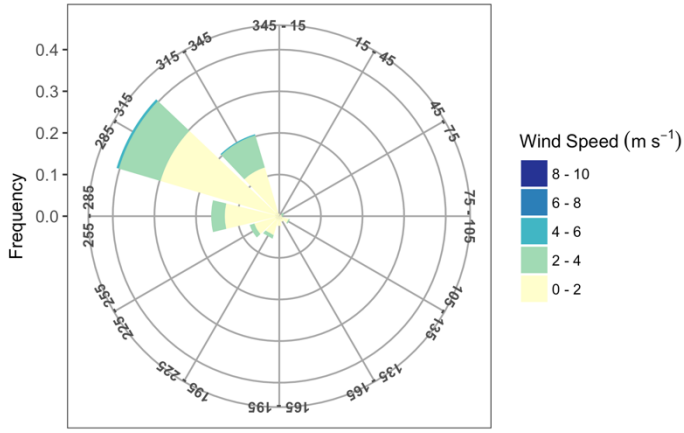

MQ.8 2016-07-11 , # of hours = 336

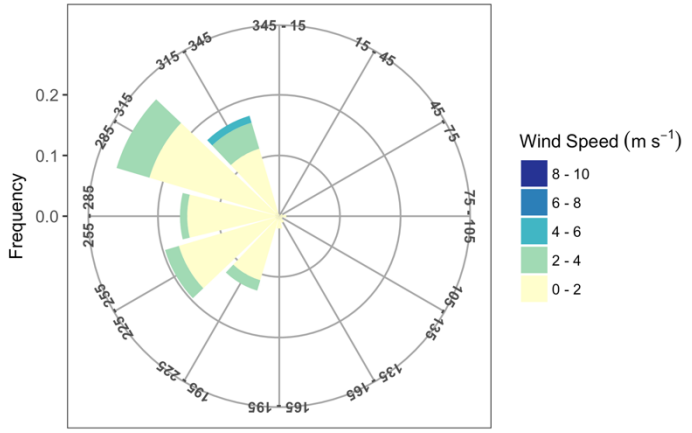

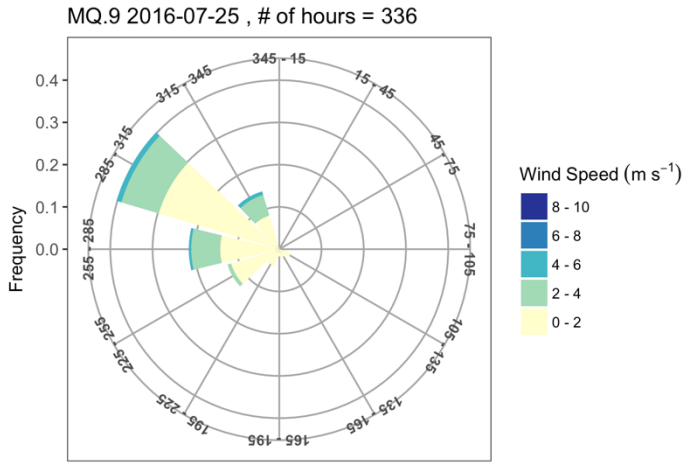
MQ.9 2016-07-25 , # of hours = 336
Frequency
0.4
0.3
0.2
0.1
0.0
345 - 15
15 - 45
45 - 75
75 - 105
105 - 135
135 - 165
165 - 195
195 - 225
225 - 255
255 - 285
285 - 315
315 - 345
Wind Speed (m s^{-1})
8 - 10
6 - 8
4 - 6
2 - 4
0 - 2

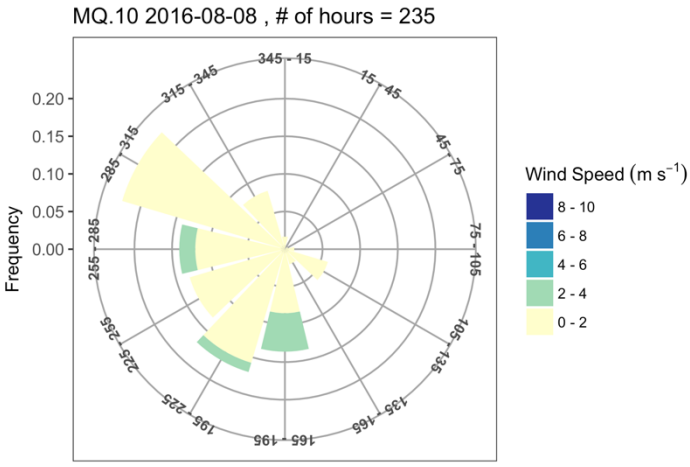
MQ.10 2016-08-08 , # of hours = 235
Frequency
0.20
0.15
0.10
0.05
0.00
345 - 15
15 - 45
45 - 75
75 - 105
105 - 135
135 - 165
165 - 195
195 - 225
225 - 255
255 - 285
285 - 315
315 - 345
Wind Speed (m s^{-1})
8 - 10
6 - 8
4 - 6
2 - 4
0 - 2

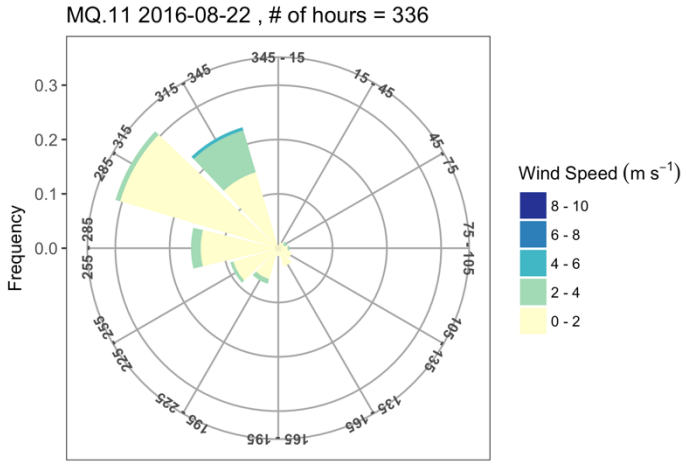
MQ.11 2016-08-22 , # of hours = 336
Frequency
0.3
0.2
0.1
0.0
345 - 15
15 - 45
45 - 75
75 - 105
105 - 135
135 - 165
165 - 195
195 - 225
225 - 255
255 - 285
285 - 315
315 - 345
Wind Speed (m s^{-1})
8 - 10
6 - 8
4 - 6
2 - 4
0 - 2

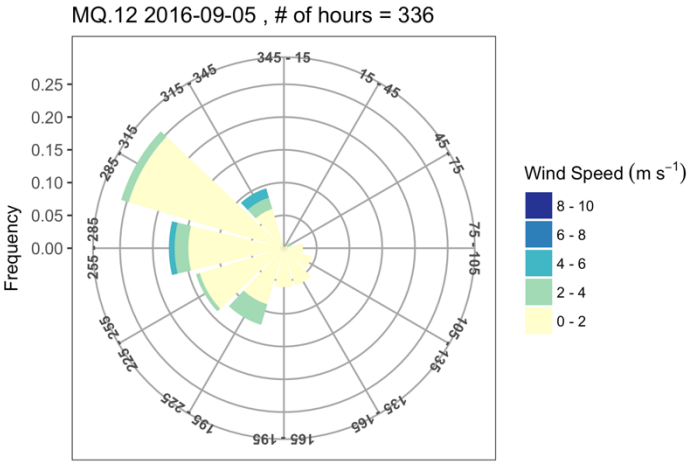
MQ.12 2016-09-05 , # of hours = 336
Frequency
0.25
0.20
0.15
0.10
0.05
0.00
345 - 15
15 - 45
45 - 75
75 - 105
105 - 135
135 - 165
165 - 195
195 - 225
225 - 255
255 - 285
285 - 315
315 - 345
Wind Speed (m s^{-1})
8 - 10
6 - 8
4 - 6
2 - 4
0 - 2

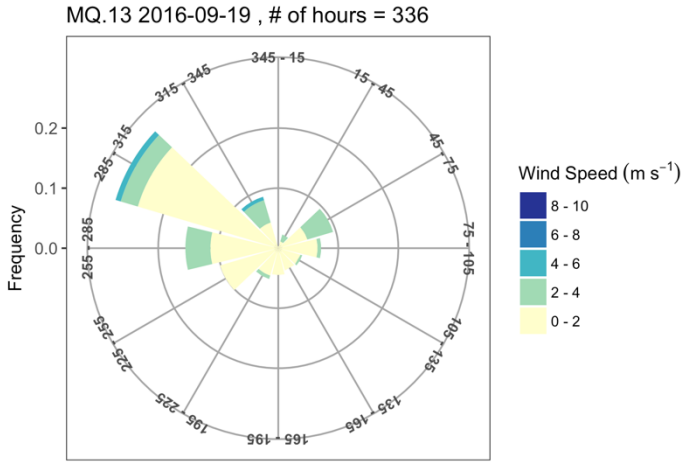
MQ.13 2016-09-19 , # of hours = 336
Frequency
0.2
0.1
0.0
345 - 15
15 - 45
45 - 75
75 - 105
105 - 135
135 - 165
165 - 195
195 - 225
225 - 255
255 - 285
285 - 315
315 - 345
Wind Speed (m s^{-1})
8 - 10
6 - 8
4 - 6
2 - 4
0 - 2

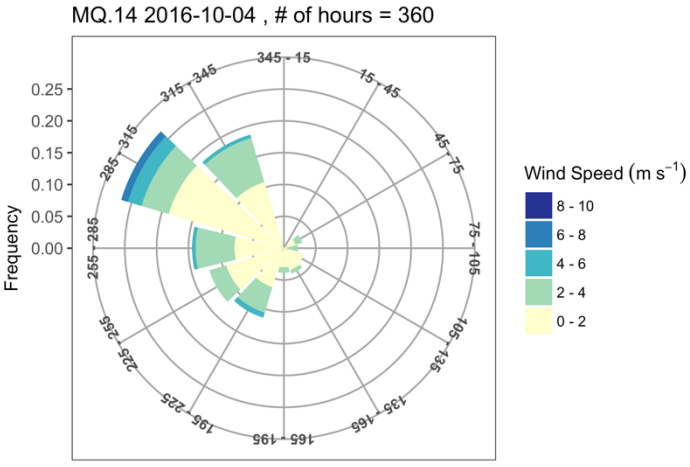
MQ.14 2016-10-04 , # of hours = 360
Frequency
0.25
0.20
0.15
0.10
0.05
0.00
345 - 15
15 - 45
45 - 75
75 - 105
105 - 135
135 - 165
165 - 195
195 - 225
225 - 255
255 - 285
285 - 315
315 - 345
Wind Speed (m s^{-1})
8 - 10
6 - 8
4 - 6
2 - 4
0 - 2

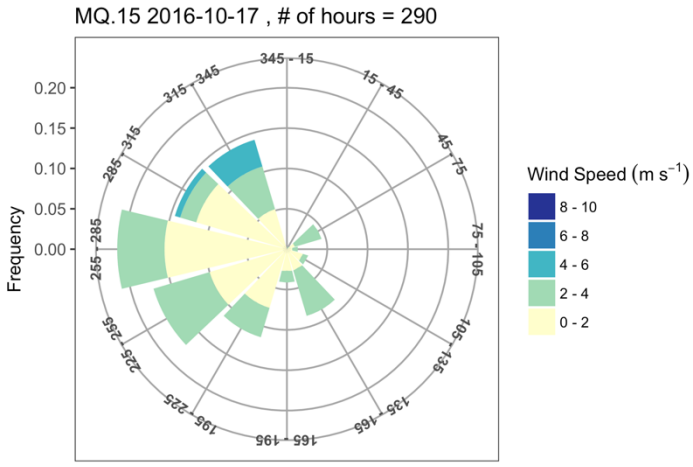
MQ.15 2016-10-17 , # of hours = 290
Frequency
0.20
0.15
0.10
0.05
0.00
345 - 15
15 - 45
45 - 75
75 - 105
105 - 135
135 - 165
165 - 195
195 - 225
225 - 255
255 - 285
285 - 315
315 - 345
Wind Speed (m s^{-1})
8 - 10
6 - 8
4 - 6
2 - 4
0 - 2

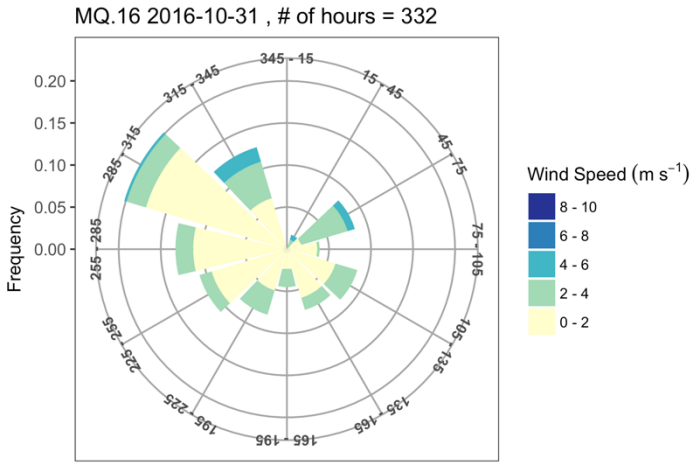
MQ.16 2016-10-31 , # of hours = 332
Frequency
0.20
0.15
0.10
0.05
0.00
345 - 15
15 - 45
45 - 75
75 - 105
105 - 135
135 - 165
165 - 195
195 - 225
225 - 255
255 - 285
285 - 315
315 - 345
Wind Speed (m s^{-1})
8 - 10
6 - 8
4 - 6
2 - 4
0 - 2

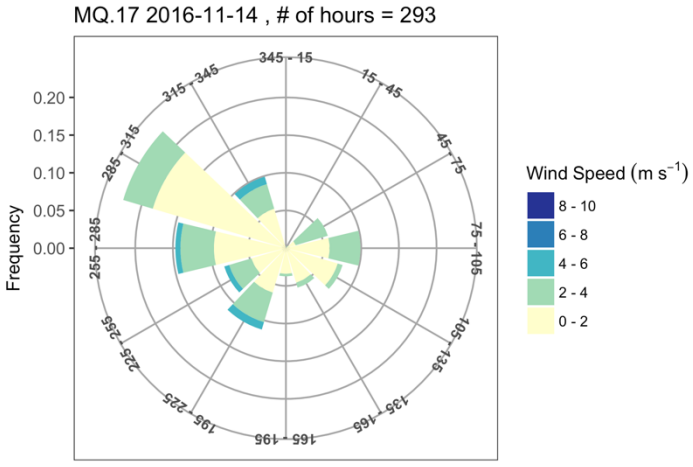
MQ.17 2016-11-14 , # of hours = 293
Frequency
0.20
0.15
0.10
0.05
0.00
345 - 15
15 - 45
45 - 75
75 - 105
105 - 135
135 - 165
165 - 195
195 - 225
225 - 255
255 - 285
285 - 315
315 - 345
Wind Speed (m s^{-1})
8 - 10
6 - 8
4 - 6
2 - 4
0 - 2

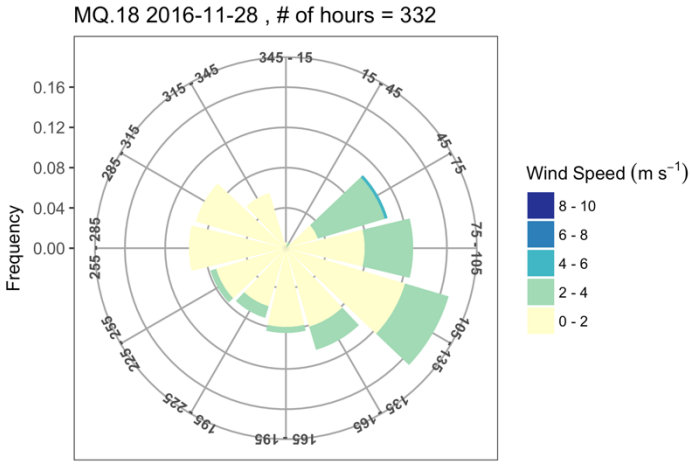
MQ.18 2016-11-28 , # of hours = 332
Frequency
0.16
0.12
0.08
0.04
0.00
345 - 15
15 - 45
45 - 75
75 - 105
105 - 135
135 - 165
165 - 195
195 - 225
225 - 255
255 - 285
285 - 315
315 - 345
Wind Speed (m s^{-1})
8 - 10
6 - 8
4 - 6
2 - 4
0 - 2

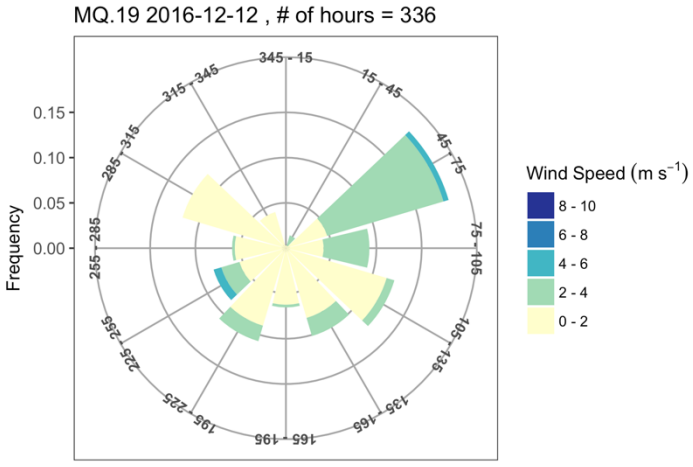
MQ.19 2016-12-12 , # of hours = 336
Frequency
0.15
0.10
0.05
0.00
345 - 15
15 - 45
45 - 75
75 - 105
105 - 135
135 - 165
165 - 195
195 - 225
225 - 255
255 - 285
285 - 315
315 - 345
Wind Speed (m s^{-1})
8 - 10
6 - 8
4 - 6
2 - 4
0 - 2

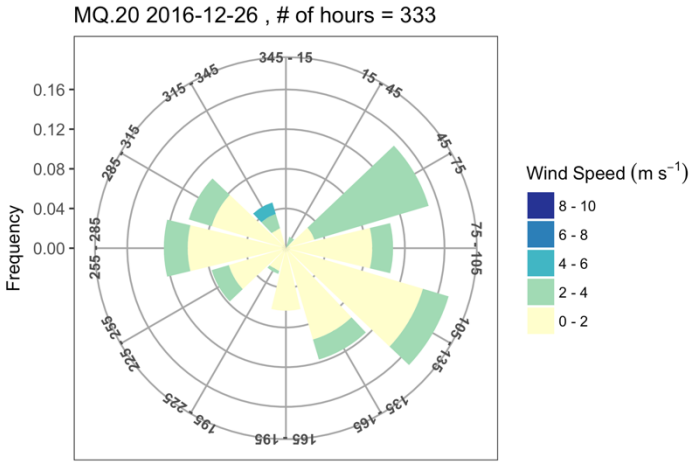
MQ.20 2016-12-26 , # of hours = 333
Frequency
0.16
0.12
0.08
0.04
0.00
345 - 15
15 - 45
45 - 75
75 - 105
105 - 135
135 - 165
165 - 195
195 - 225
225 - 255
255 - 285
285 - 315
315 - 345
Wind Speed (m s^{-1})
8 - 10
6 - 8
4 - 6
2 - 4
0 - 2

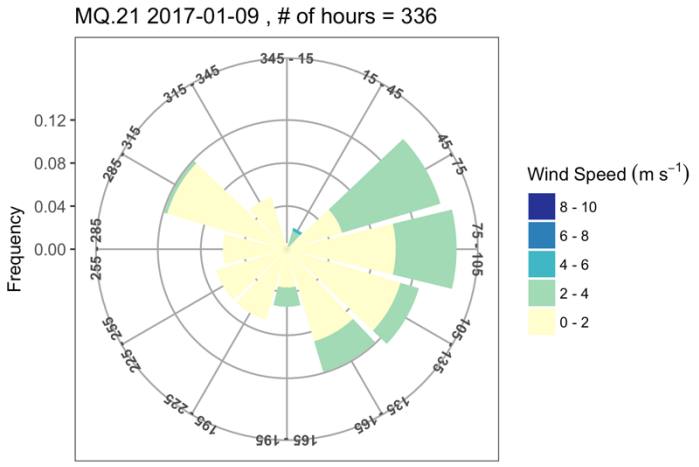
MQ.21 2017-01-09 , # of hours = 336
Frequency
0.12
0.08
0.04
0.00
345 - 15
15 - 45
45 - 75
75 - 105
105 - 135
135 - 165
165 - 195
195 - 225
225 - 255
255 - 285
285 - 315
315 - 345
Wind Speed (m s^{-1})
8 - 10
6 - 8
4 - 6
2 - 4
0 - 2

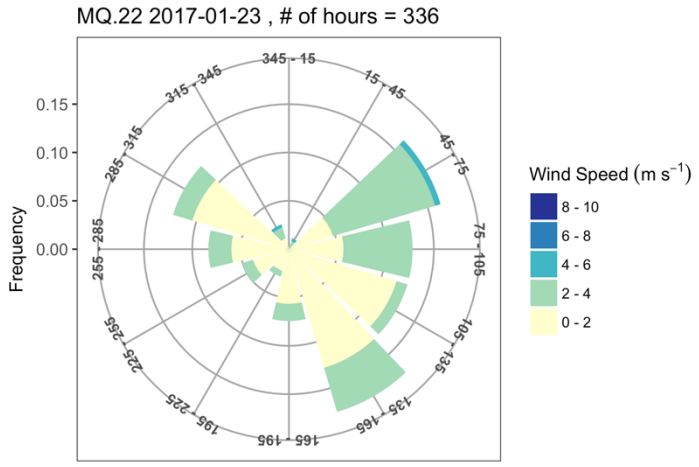
MQ.22 2017-01-23 , # of hours = 336
Frequency
0.15
0.10
0.05
0.00
345 - 15
15 - 45
45 - 75
75 - 105
105 - 135
135 - 165
165 - 195
195 - 225
225 - 255
255 - 285
285 - 315
315 - 345
Wind Speed (m s^{-1})
8 - 10
6 - 8
4 - 6
2 - 4
0 - 2

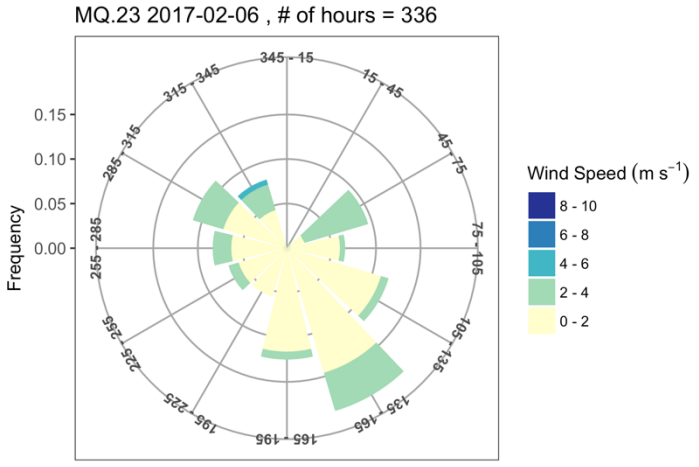
MQ.23 2017-02-06 , # of hours = 336
Frequency
0.15
0.10
0.05
0.00
345 - 15
15 - 45
45 - 75
75 - 105
105 - 135
135 - 165
165 - 195
195 - 225
225 - 255
255 - 285
285 - 315
315 - 345
Wind Speed (m s^{-1})
8 - 10
6 - 8
4 - 6
2 - 4
0 - 2

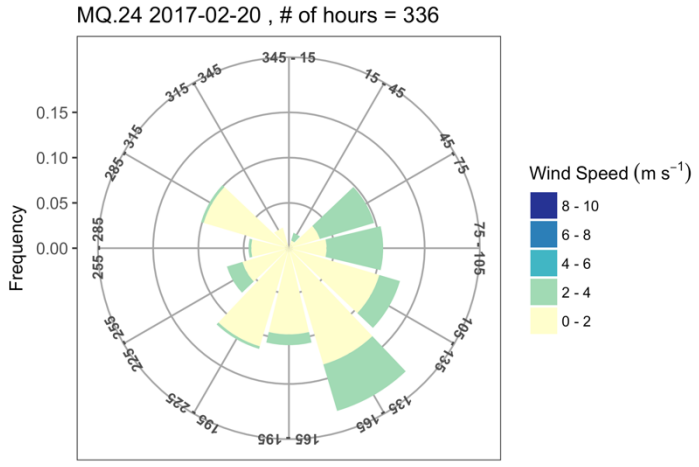
MQ.24 2017-02-20 , # of hours = 336
Frequency
0.15
0.10
0.05
0.00
345 - 15
15 - 45
45 - 75
75 - 105
105 - 135
135 - 165
165 - 195
195 - 225
225 - 255
255 - 285
285 - 315
315 - 345
Wind Speed (m s^{-1})
8 - 10
6 - 8
4 - 6
2 - 4
0 - 2

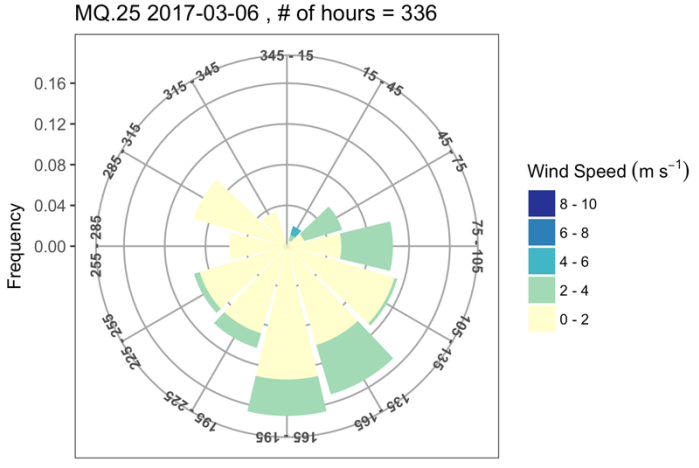
MQ.25 2017-03-06 , # of hours = 336
Frequency
0.16
0.12
0.08
0.04
0.00
345 - 15
15 - 45
45 - 75
75 - 105
105 - 135
135 - 165
165 - 195
195 - 225
225 - 255
255 - 285
285 - 315
315 - 345
Wind Speed (m s^{-1})
8 - 10
6 - 8
4 - 6
2 - 4
0 - 2

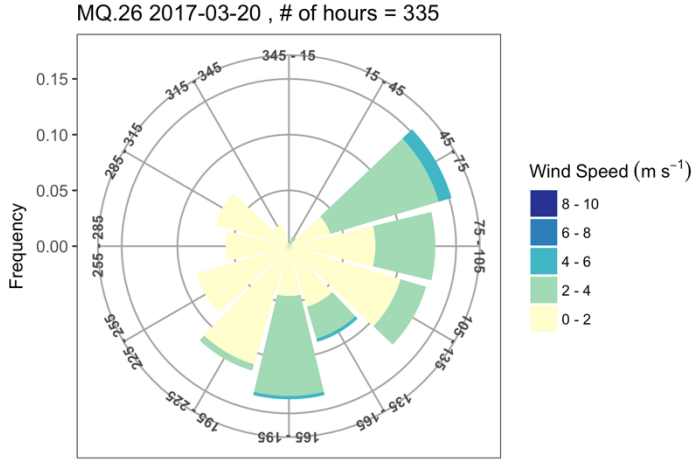
MQ.26 2017-03-20 , # of hours = 335
Frequency
0.15
0.10
0.05
0.00
345 - 15
15 - 45
45 - 75
75 - 105
105 - 135
135 - 165
165 - 195
195 - 225
225 - 255
255 - 285
285 - 315
315 - 345
Wind Speed (m s^{-1})
8 - 10
6 - 8
4 - 6
2 - 4
0 - 2

MQ.27 2017-04-03 , # of hours = 336

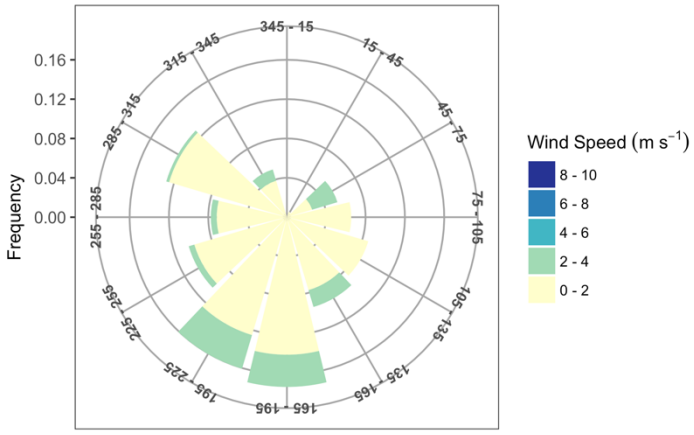

MQ.28 2017-04-17 , # of hours = 336

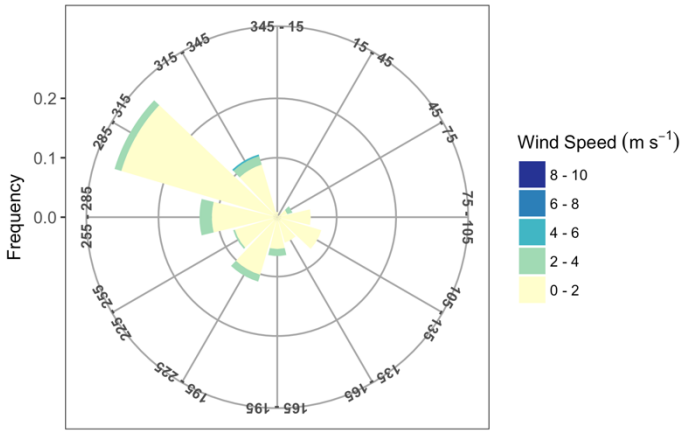

MQ.29 2017-05-01 , # of hours = 336

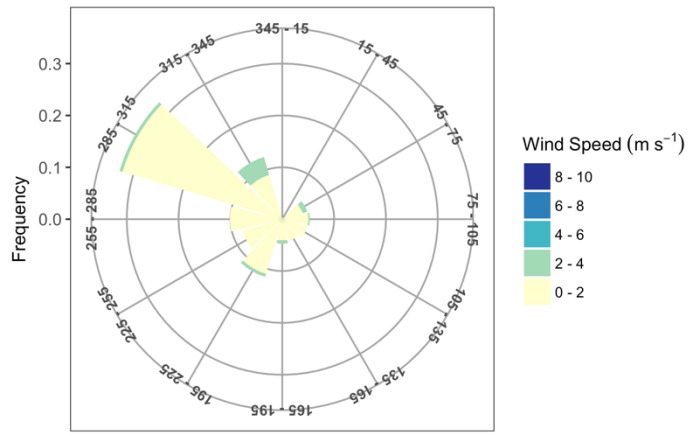

MQ.30 2017-05-15 , # of hours = 336

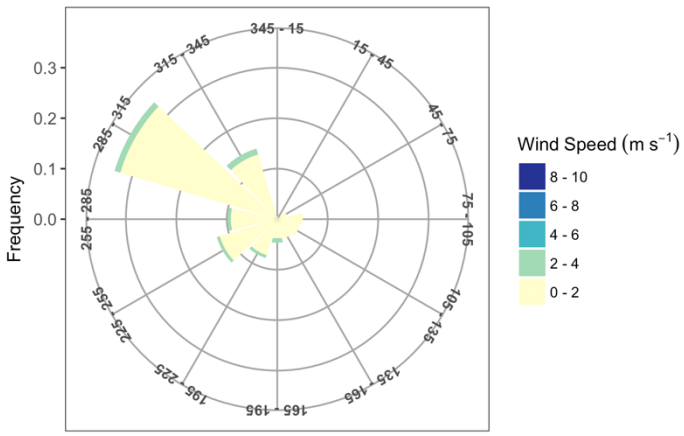

MQ.31 2017-05-29 , # of hours = 336

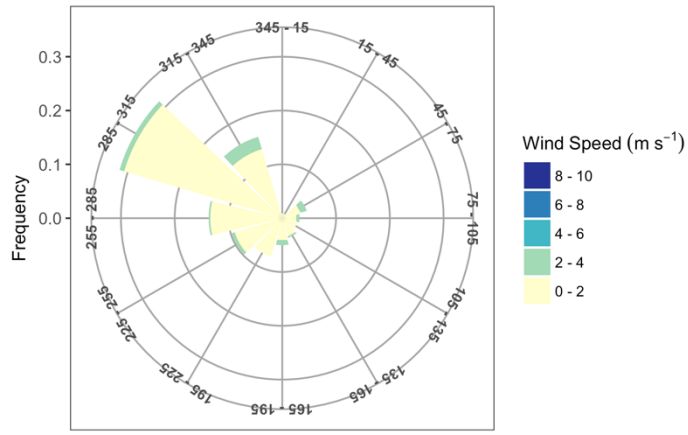

Appendix F. Note

The reader will have noted that the filter-based reactive mercury (RM) sampling systems described in this dissertation included provision for deployment of nylon filters as a possible method for determining gaseous oxidized mercury (GOM) speciation. However, use of nylon filter material was ultimately discontinued and no speciation data is presented as any part of this dissertation, despite much time and energy invested. The decision to exclude this data lies with the author, who points to numerous methodological unknowns and inconsistencies:

1) The possibility that the nylon material sorbs GEM in a way that could interfere with detection of much lower concentrations of GOM has not been convincingly ruled out. Indeed, significant GEM sorption at concentrations above 200 ng m^{-3} was explicitly demonstrated in Huang et al. (2013), reprinted Appendix G.

2) The nylon material does not collect a quantitatively equivalent mass of RM compared to cation exchange membrane (CEM) material. Total RM measured on nylon filters is often less than 10% of the RM measured on CEM filters deployed at the same time and place and *exactly* the same way. The nylon filters have always been used at a reported pore size of 0.2 μm versus the 0.45 or 0.8 μm pore size of the CEM filters, so when deployed in ambient air they should theoretically be collecting *more* Hg at finer particulate-bound size fractions. The author suggests that no meaningful analysis of Hg speciation can be made when over 90% of the Hg is missing and disavows any unsubstantiated assertion that the CEM or nylon filters do not collect ambient particulate matter.

3) Many of the reference thermal desorption profiles for specific GOM species overlap in such a way as to make objective identification impossible. Where desorption peaks overlap significantly (or occur at the same temperature), clear separation and disambiguation of specific compounds is simply not possible. The author points to Figure 3 of Huang et al. (2013) and Figure 2 of Gustin et al. (2015), reprinted in Appendix G.

Given these limitations, extensive additional research and quality assurance is needed before (and if ever) nylon filters can be used for the determination of GOM species with scientific rigor.

Appendix G. Relevant Publications

The following publications are relevant to the work presented in this dissertation and are reprinted here in full (with permission). I have contributed to all of these as a co-author, primarily in the role of instrumentation specialist and field technician. Much of the background and supporting work on the CEM material is covered in these papers. In addition, I have contributed at a lesser extent to the work of Lyman et al. (2010) and Pierce and Gustin (2017) in an acknowledge capacity, primarily with technical field assistance.

Comparison of gaseous oxidized Hg measured by KCl-coated denuders, and nylon and cation exchange membranes

Permission to Reprint

The following article is reprinted with permission from:

Comparison of Gaseous Oxidized Hg Measured by KCl-Coated Denuders, and Nylon and Cation Exchange Membranes, Jiaoyan Huang, Matthieu B. Miller, Peter Weiss-Penzias, and Mae Sexauer Gustin. *Environmental Science & Technology,* 2013, *47* (13), 7307-7316. DOI: 10.1021/es4012349. Copyright (2013) American Chemical Society.

Environmental Science & Technology

Article

pubs.acs.org/est

Comparison of Gaseous Oxidized Hg Measured by KCl-Coated Denuders, and Nylon and Cation Exchange Membranes

Part of the "RAMIX: Reno Atmospheric Intercomparison eXperiment" group

Jiaoyan Huang,[†] Matthieu B. Miller,[†] Peter Weiss-Penzias,[‡] and Mae Sexauer Gustin[†,*]

[†]Department of Natural Resources and Environmental Sciences, University of Nevada, Reno, 1664, N. Virginia Street, Reno, Nevada 89557, United States

[‡]Department of Microbiology and Environmental Toxicology, University of California, Santa Cruz, California 95060, United States

Supporting Information

ABSTRACT: The chemical compounds that make up gaseous oxidized mercury (GOM) in the atmosphere, and the reactions responsible for their formation, are not well understood. The limitations and uncertainties associated with the current method applied to measure these compounds, the KCl-coated denuder, are not known due to lack of calibration and testing. This study systematically compared the uptake of specific GOM compounds by KCl-coated denuders with that collected using nylon and cation exchange membranes in the laboratory and field. In addition, a new method for identifying different GOM compounds using thermal desorption is presented. Different GOM compounds ($HgCl_2$, $HgBr_2$, and HgO) were found to have different affinities for the denuder surface and the denuder underestimated each of these compounds. Membranes measured 1.3 to 3.7 times higher GOM than denuders in laboratory and field experiments. Cation exchange membranes had the highest collection efficiency. Thermodesorption profiles for the release of GOM compounds from the nylon membrane were different for HgO versus $HgBr_2$ and $HgCl_2$. Application of the new field method for collection and identification of GOM compounds demonstrated these vary as a function of location and time of year. Understanding the chemistry of GOM across space and time has important implications for those developing policy regarding this environmental contaminant.

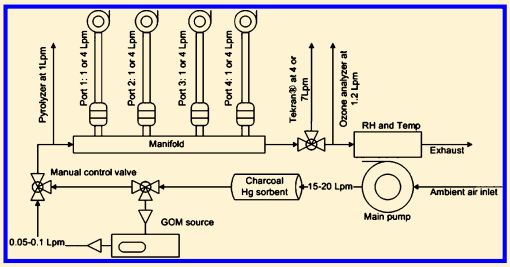

INTRODUCTION

Mercury (Hg) is an unique trace metal that exists in the gas phase as the elemental form and oxidized compounds.[1−3] Dry and wet deposition are important pathways by which Hg is moved from the atmosphere to terrestrial and marine ecosystems.[3] There are three operationally defined "forms" of Hg in the atmosphere, gaseous elemental Hg (GEM), gaseous oxidized Hg (GOM), and particle-bound Hg (PBM).[1] Gaseous oxidized Hg has a short residence time in the atmosphere ranging from hours to weeks.[1] Particle-bound Hg can remain in the atmosphere for days to weeks, and this is dependent upon particle size and interaction with moisture.[1] The chemical compounds of GOM have been suggested to include mercury chloride ($HgCl_2$), mercury bromide ($HgBr_2$), mercury oxide (HgO), mercury sulfate ($HgSO_4$), mercury nitrite ($Hg(NO_2)_2$), and mercury hydroxide ($Hg(OH)_2$).[4−12] Atmospheric measurements in the past have assumed all GOM compounds are captured using a KCl-coated denuder[13,14] and have not attempted to collect them individually. Since different compounds will have different properties (i.e., water solubility, water-octanol partitioning coefficients, deposition velocities, etc.) they could be collected differently by the denuder, and it is important to understand their chemistry (cf. Schroeder et al.;[15] Walschlager;[16] and references cited therein).

Methods applied for measurement of GOM have included KCl-coated tubular and annular denuders;[13,17,18] mist chambers;[19] and cation exchange membranes (CEM).[20−26] Methods applied for PBM measurements include particulate traps[9,27] and filter packs.[28−30] A new method designed for measurement of GOM is the Detector for Oxidized Hg Species (DOHGS).[31−33] These methods have been compared in field settings with conflicting results.[13,14,20,34,35] Gustin et al. and Peterson et al.[34,35] suggested, based on the results of field measurements made in Nevada and Florida, respectively, that discrepancies exist because different compounds of GOM and reactive mercury (RM = GOM + PBM) exist across space and time, and different methods measure different chemical forms. If this assertion is correct, then this has significant consequences for policy makers because current knowledge is based on one measurement method that may have systematic errors.

Received: December 5, 2012
Revised: May 6, 2013
Accepted: May 7, 2013

Ion exchange membranes have been applied for atmospheric gas measurements since the late 19th century, i.e., $SO_{2(g)}$, $NH_{3(g)}$, and $H_2O_{2(g)}$.[36] Polyethersulfone CEMs have been applied for measurement of GOM in the ambient air,[20,24−26] and were tested by Lyman et al.[21,22] and Peterson et al.[35] The KCl-coated denuder was first investigated by Xiao et al. [17] and modified by Landis et al.;[13] however, there were few systematic laboratory tests of this method (cf. Gustin et al.,[34] Supporting Information (SI)). Nylon membranes were first used for nitric acid (HNO_3) measurements 30 years ago.[37,38] Because HNO_3 is often used a surrogate for GOM in models,[39] we hypothesized that this material might be useful for GOM measurements.

The major hypothesis driving this work was that the chemistry of GOM will vary spatially and temporally, and this will be influenced by the different constituents in the atmosphere. In this study, we investigated the collection efficiency of different chemical compounds of GOM by colocated nylon membranes, CEMs, and KCl-coated denuders using a laboratory manifold system. We used scrubbed (activated carbon column) and filtered ambient air, into which HgO, $HgCl_2$, and $HgBr_2$ were systematically permeated. Data derived using a laboratory framework could provide a foundation for determining if there are systematic biases so that previous data sets could be corrected. Samples were collected using these same surfaces in the field at highway impacted (HI), agriculturally impacted (AI), and marine boundary layer (MBL) sites. The ability of a new method, thermal desorption of nylon membranes, to separate different GOM compounds was also investigated.

METHODS

Sampling Systems. *Laboratory Measurements.* Laboratory measurements were made using an eight port glass manifold (not coated; URG custom designed). During this study, only four ports were used. Manual denuders were directly connected to the manifold system using Teflon adaptors (see Supporting Information, SI, Figure SI 1). For each port, Teflon joints at the end of each denuder were used to connect to Teflon tubing (OD: 0.635 cm), a mass flow controller, and vacuum pumps (end of manifold flow rate: 2 to 3 Lpm; total manifold flow 15 to 20 Lpm). Manual denuders were maintained at room temperature (20 to 25 °C).

A Tekran 2537/1130 unit was used to measure GEM and GOM concentrations, respectively, collected through tubing connected to the outlet tubing of the manifold. A Tekran 2537 (constant flow of 1 Lpm) with a quartz wool based pyrolyzer maintained at 650 °C at the instrument inlet (see SI for details), used to convert all Hg to GEM, sampled air at the front of the manifold (Figure SI 1: see SI for QA/QC). Air temperature and relative humidity (RH) in the manifold were monitored using a Campbell Scientific CS 500L at the end of the manifold, and data were logged using a CR10X (Figure SI 1). The RH in the manifold was 9 to 20%. The glass manifold and associated Teflon tubing were heated to 100 °C to increase the mobility of GOM in the system. There was no significant difference in the GOM amounts collected using CEM from different ports (ANOVA-ranked); therefore, we assume that the 100 °C for Teflon and quartz surfaces was sufficient to keep the forms of GOM being tested moving through the manifold system. Ozone (O_3) concentrations were also measured periodically at the end of the manifold using a Thermo 49C (span check at 450 ppb every 3 months, and zero check weekly).

The flow through the Tekran 1130 unit was adjusted to 4 Lpm when the manifold was being used with manual denuders. Manual denuder flow was also 4 Lpm. When sampling using membranes housed in Teflon filter packs in series, the 1130 unit flow was 7 Lpm and flow through the membranes was maintained at 1 Lpm. These differences in flow would not significantly influence the KCl-coated denuder's performance.[34] The flows for the inlet, outlet, and four sampling ports were checked before, during, and after all experiments using an external flow meter (Sierra Instrument Inc., CA). On the basis of the flow mass, balance recoveries were >90% indicating that <10% of the Hg permeated was lost from or deposited to the system.

A manual valve was used to control the flow through the GOM permeation system (described below). This was turned on 24 h prior to sampling to obtain stable target concentrations (based on Tekran measurements). After all experiments, the valve was completely closed, and the manifold was flushed with scrubbed air for 24 h to clean out the system. Manifold blanks before permeations were <20 pg m^{-3}.

GOM Collection Methods. Denuders coated with KCl that have been widely applied [cf., ref 13], were used to collect GOM using both automated and manual systems. In addition, nylon membranes (P/N: EW-36229−04, 0.2 μm, Cole Parmer) and polyethersulfone cation exchange membranes (CEM; I.C.E. 450, 0.45 μm, Pall Corporation) were used to collect GOM. Membrane samples were collected over ∼8 h and little break through was observed on the second membrane in the series (ratios of Hg amount on the first and second membrane for nylon and CEM range from 0 to 6% and 0 to 16%, respectively). There was no significant GEM capture on nylon membranes at low GEM concentrations (<12.6 ng m^{-3}, collection efficiency <1%), but a small amount at higher GEM concentrations (>200 ng m^{-3}, collection efficiency 7 ± 2%). This check was done using the system in Figure SI 5 of the SI. Total Hg on the CEM membranes was determined using EPA method 1631E (see SI).

As part of this study, other collection materials were tested using the manifold system, including Teflon membranes (P/N EW-36229−24, pore size: 0.2 μm, Cole-Parmer), Tenax traps (P/N Tenax TA 60/80, Supelco), and quartz wool traps (∼5 cm in length, P/N 502−177, Leco Corporation). The collection efficiency of these materials for GOM was limited and inconsistent (Hg amount collected on these materials were <1% to 30% of Tekran measurements) and their use was not investigated further (see SI).

Most samples were collected in triplicate; however, for the multiple material comparisons, replicate samples were collected. Since scrubbed (activated charcoal column) or filtered ambient air (glass fiber filter; P/N: GB14047MM, Advantec MFS Inc.) was used in the manifold system, PBM was assumed to be negligible.

GOM Permeation System. Three solid-phase GOM compounds (HgO, $HgCl_2$, and $HgBr_2$; Sigma-Aldrich, purity >99.99%), were packed in thin wall polytetrafluoroethylene (PTFE) heat-shrink tubing (O.D. 0.635 cm, P/N: EW-06851−20, Cole Parmer) with solid Teflon plugs in both ends. An active permeation length of 2 mm existed between the plugs. Permeated Hg was carried by scrubbed air into the manifold at ∼0.05 to 0.1 Lpm to mix with manifold air and to control the

dx.doi.org/10.1021/es4012349 | Environ. Sci. Technol. XXXX, XXX, XXX−XXX

concentrations in manifold. Permeation tubes were contained in a temperature controlled bath at 0 to 10 °C.

Emission rates of $HgBr_2$ at 0, 5, and 10 °C were 61 ± 7, 76 ± 10, and 107 ± 12 pg min^{-1} (mean ± standard deviation calculated based on variation in Hg concentrations and the uncertainty of flow rate 0.1 Lpm), respectively, were determined based on air directed through the pyrolyzer to a Tekran 2537. Finley et al. [40] measured a $HgBr_2$ permeation rate of 126 ± 4 pg min^{-1} at 50 °C using a similar system. Although these data indicate that the permeation rate increased with temperature exponentially, and are stable after ∼25 °C, this needs further investigation. Finley et al. [40] also measured permeation rates using the Tekran 2537 unit after pyrolysis; however, concentrations permeated were >1000 ng m^{-3}. Although the measurement range of the Tekran 2537 unit is from 0.1 to 2000 ng m^{-3}, the linear working range is from 1 to 200 ng m^{-3}. In our study, more dilution zero air was used than that in Finley et al. [40] and concentrations were <200 ng m^{-3}. Emission rates of a $HgBr_2$ permeation tube packed in 2007 were compared with a new one generated in 2012 and a ∼18% difference was observed (50 ± 11 pg min^{-1} at 0 °C for 2007). This could reflect a decline in permeation over time or a difference in tube packing, since there is no current standard protocol for permeation tube generation.

Permeation rates for $HgCl_2$ at 0 °C, and HgO at 10 °C (0.1 Lpm), were 25 ± 18 and 38 ± 20 pg min^{-1}, respectively. Although it has been suggested that HgO will partition into a particulate phase,[5] high GOM concentrations were measured by the Tekran denuder during HgO permeation. Given the purities of the permeation sources provided by the manufacturer, the presence of nontarget compounds would be small. Additionally, since the emitted form passed through thin wall Teflon tubing, it was most likely a gas. We cannot be sure if the chemical compound was HgO or another, such as Hg_2O.[41]

Recent work has also reported that little GEM was detected using similar permeation tubes.[40,42] These results also indicate that gaseous GOM emissions were occurring from the permeation tubes. Thus, it was assumed that no GEM was generated using the GOM permeation tubes under the experimental conditions.

GEM concentrations measured by the Tekran system ranged from <0.5 to ∼2 ng m^{-3} at the highest GOM concentrations in the manifold. This can be explained by the high GOM concentration in the manifold, the lack of complete capture by the denuder, and some deposition in the ∼7.5 m line that was heated to 50 °C and located between the 1130 and the Tekran 2537 unit. Additionally, not all of the denuder flow is diverted to the 2537 unit. Deposition to the sampling lines was observed during the Reno Atmospheric Mercury Intercomparison eXperiment (RAMIX).[34]

Because of the high emission rates from the permeation tubes, and the need to generate low concentrations (range of 150 to 3000 pg m^{-3}) in the manifold, the flow through the permeation oven was only a few mL min^{-1}. Because of the uncertainty associated with measurement of this low flow rate, we focus on the comparison of the GOM collected by the different methods rather than on the exact concentrations in the manifold.

Field Measurements. Field measurements were made using a 6-port sampling system with three housing nylon membranes and three CEMs (described and shown as a schematic and photograph in the SI). Data were collected from highway and agriculturally impacted sites (HI and AI, respectively) and in the marine boundary layer (MBL) (see SI for details). During these measurements, a Tekran 2537/1130/1135 unit was used to make simultaneous measurements, except from November 2011 to January 2012, and during April 2012 at the HI site. During this time period at the HI site, the 1135 unit was replaced with quartz fiber filters after the 1130 denuder. The filters were collected weekly as a surrogate for the PBM measurements and analyzed using EPA Method 1631 (see SI Membrane Analyses). The Tekran 1130/1135 units were set to sample over an hour at the AI and HI sites and for two hours at the MBL site.

In the field and laboratory, GOM was measured by the Tekran system using a one hour desorption cycle.[43] The 2537 units were calibrated every 24 h using instrument autocalibration and an internal permeation source. The calibration of the Tekran 2537 units applied at the HI and AI sites, and in the laboratory, were checked weekly using manual injections of GEM from an external source, while the system operating at the MBL site was manually calibrated only at the beginning of the experiment. Mercury concentrations at the MBL site were corrected for a sampling bias associated with lower trapping efficiency on one of the two gold traps used to alternately collect GEM based on discrete injections of mercury into ambient air (see SI). Detailed information regarding membrane analyses, data analyses, quality assurance, and quality control are provided in SI.

■ RESULTS AND DISCUSSION

On the basis of our sampling configurations, laboratory manifold derived samples are considered to contain only GOM; while data collected at field sites may include some PBM, and as such, are considered RM (PBM + GOM).

Laboratory KCl-Denuder 1-h and 8-h Comparison. Collection of GOM during 1 h measurements made using the Tekran system were compared with those collected over 8 h using denuders connected to the manifold. This was done to check the collection efficiency of the manual denuders over time since the membranes were loaded over 8 h. Concentrations of $HgCl_2$, $HgBr_2$, and HgO measured by manual denuders (8-h) were 30% to 50% lower than those calculated by integrating the area underneath the curve for the 1 h concentrations made over the same 8-h period by the Tekran automated system (Figure 1; see SI Data Analyses, denuder comparison for calculation). The difference (but not statistically significant, ANCOVA, *p*-values range from 0.59 to 0.68) varied as a function of GOM compounds being highest for HgO and $HgBr_2$, and lower for $HgCl_2$. The fact that the KCl-coated denuder collection efficiency was $HgCl_2$ > $HgBr_2$ > HgO demonstrates that uptake and retention will be influenced by the compounds of GOM in the air.

The reason for the variability in the 1- and 8-h measurements, shown in Figure 1, could be that measurements were made using filtered ambient air, and collection and retention of the GOM was affected by air chemistry. An O_3 influence on the denuders has been reported.[34,42] On the basis of measurements made using the laboratory manifold system air containing 5 to 60 ppb of O_3 could have entered the denuders (Figure SI 1 of the SI).

Lyman et al. [42] suggested, in the public discussion, the following potential reaction for $HgCl_2$ and O_3 on the KCl-coated surface:

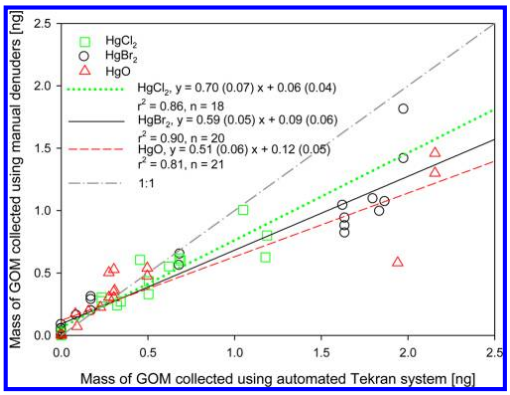

Figure 1. Laboratory comparison of GOM amount (mass ng) as measured by KCl-coated denuders with different exposure times (1 h for every other hour and 8 h) using $HgCl_2$ (green squares), $HgBr_2$ (blank circles), and HgO (red triangles) as permeated sources into filtered ambient air. The slopes and intercepts are presented as mean (standard deviation). The *x*-axis is the extrapolated mass of mercury collected over 8 h based on the sum of 4 individual 1-h measurements taken every other hour. All regression equations are significant at *p*-value <0.01; *n* is the sample number. The fine gray "dotted-dashed" line is the 1:1 comparison. The regression for data when the Hg amount below 1 ng is $y = 0.88x + 0.05$, $r^2 = 0.89$ (all three species together).

$$HgCl_2 + 2O_3 \rightarrow Hg^0 + 2O_2 + ClO \quad (\Delta Gr = -85\ kJ/mole)$$

They also reported that the longer the O_3 exposure the more GOM lost from the KCl-coated surface. This suggests that GOM could be reduced and lost from the denuder surface due to O_3. Lynam and Keeler [30] also showed that O_3 was destroyed by the KCl-coated denuder providing additional evidence for this hypothesis. Data collected during five Hg and O_3 depletion events at Ny-Ålesund, located on the island of Spitsbergen in the Svalbard Archipelago, administered by Norway, using manual denuders that sampled for 1 to 18 h, and Tekran 1130/2537 systems that sampled for 2 h, found the former to collect 25 to 77% of GOM with respect to the latter.[44] These observations indicate that the impact of atmospheric chemistry on the denuder measurements needs to be systematically explored.

Laboratory Tekran System and Membrane Comparison. Tekran measured GOM concentrations during permeations ranged from 150 to 3000 pg m^{-3}. Because we cannot be sure they are accurate, we discuss the relative amounts collected. Comparison of the data collected using the laboratory manifold showed the highest GOM concentrations in scrubbed air were measured by CEMs, followed by nylon membranes, and then the KCl-coated denuder (Figure 2). The slopes for the comparison of the GOM measured by the denuder versus the nylon membranes were similar for all compounds (1.6 to 1.8, ANCOVA, *p*-values for $HgCl_2$ versus $HgBr_2$, $HgCl_2$ versus HgO, and $HgBr_2$ versus HgO were 0.972, 0.121, and 0.211, respectively). Slopes for the comparison of the CEM and KCl-coated denuder varied with HgO > $HgCl_2$ > $HgBr_2$. The slopes varied from 1.6 to 3.7 and *p*-values for $HgCl_2$ versus $HgBr_2$, $HgCl_2$ versus HgO, and $HgBr_2$ versus HgO were 0.49, <0.01, and 0.04, respectively.

In general, all membranes collected >60% more GOM than denuders. The nylon membrane had 60 to 80% higher capture efficiency than the denuder for all three compounds; while the CEM had uptake capacity that was similar to the nylon membrane for $HgBr_2$, and much higher uptake for $HgCl_2$ and HgO relative to the denuder (140 and 270%, respectively). If we use the regression curves in Figure 2, and assume the KCl-coated denuders have the same collection efficiency for individual compounds, then the ratio of the collection efficiencies of $HgCl_2$, $HgBr_2$, and HgO on CEM to the nylon membranes (CEM:nylon membrane) are 1.50, 0.95, and 2.06, respectively. A comparison is made of the slopes of HgO versus

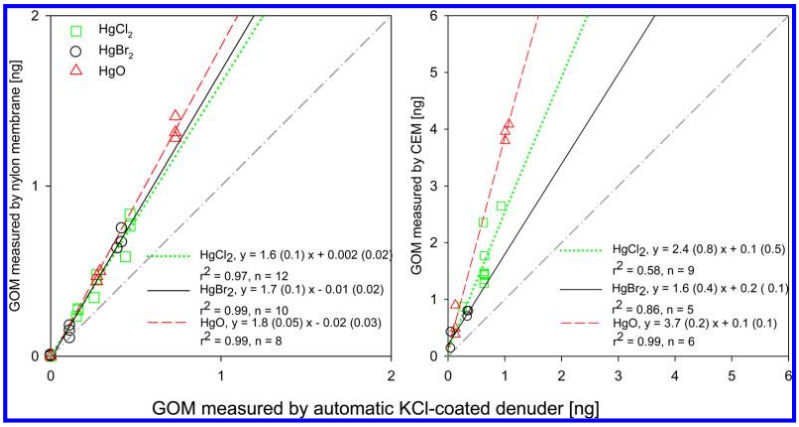

Figure 2. Laboratory comparison GOM measured by Tekran system compared with that measured by the nylon membrane (left) and CEM (right) with $HgCl_2$ (green squares), $HgBr_2$ (blank circles), and HgO (red triangles) as permeated sources into charcoal scrubbed air. Note difference in axis scales. The slopes and intercepts are presented as mean (standard deviation), and regression equations are significant at *p*-value <0.01; *n* is the number of samples. The fine gray "dotted-dashed" line is the 1:1 comparison.

dx.doi.org/10.1021/es4012349 | Environ. Sci. Technol. XXXX, XXX, XXX–XXX

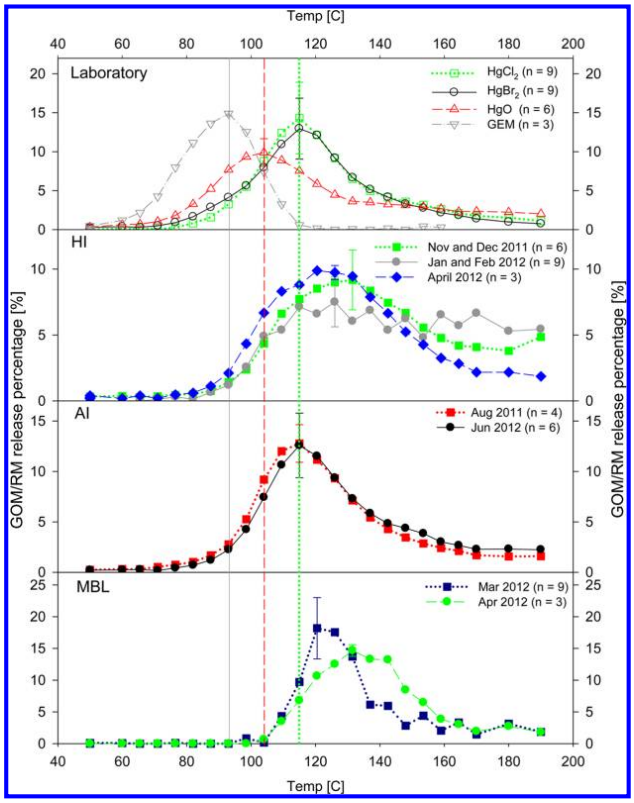

Figure 3. Percent GOM and RM desorption profiles for nylon membranes. Percent released is the amount released at a specific temperature as a function of the total amount released by the membrane. The standard deviation (as $n > 3$) is presented as the error bar in peak of the curve. The error bar for GEM is too small to see (laboratory panel). The open and solid symbols represent the measurements in laboratory and field, respectively. The lower three panels represent desorption profiles for the samples collected at highway impacted (HI), agricultural impacted (AI), and marine boundary layer (MBL) sites. The vertical lines indicate peak desorption temperatures for GEM (gray solid), HgO (red dashed), and $HgCl_2/HgBr_2$ (green dotted). The desorption profile of GEM is based on a high GEM concentration exposure (>200 ng m^{-3}).

$HgCl_2$, and HgO versus $HgBr_2$, for the CEM data shown in Figure 2 (0.65 and 0.41, respectively), and assuming that the CEMs have the same capture efficiency for all three GOM compounds, as shown by Lyman et al. [22] (See Data Analyses, efficiency calculation in the SI); this indicates KCl-coated denuder has highest collection efficiency for $HgBr_2$, followed by $HgCl_2$, and then HgO:

$$y(\text{Hg amount, ng, on CEM membrane}) = 1.5(\text{ng, } HgBr_2 \text{ on denuder}) = 2.4(\text{ng, } HgCl_2 \text{ on denuder}) = 3.7(\text{ng, HgO on denuder})$$

This order of capture efficiency (Br > Cl > O) tracks that of the static average electric dipole polarizabilities for ground state atoms of Br, Cl, and O which are 3.05×10^{-24}, 2.18×10^{-24}, and 0.802×10^{-24} cm^3, respectively.[45] This would influence the GOM uptake on the KCl coating. Polarizability is a "measure of the extent to which the electron cloud of an atom or molecule can be distorted by an external electrical charge."[46] The polarizability also corresponds with an element's Van Der Waals radius. The more easily distorted the electron cloud, the more readily this element would be taken up by the KCl denuder. This would explain the observed order of uptake of the Hg compounds tested.

Sheu and Mason [14] reported GOM concentrations measured by KCl-coated denuders were 51% of those measured by filter packs [that consisted of three CEMs preceded by two Teflon filters (five membranes in-series)]. Although the Teflon filters could have influenced the downstream GOM measurements,[13] laboratory tests of this material showed little affinity for GOM. Notably, we show that KCl-coated denuders collected only 27% to 60% of GOM measured by CEMs, and these numbers are within the range of values obtained for comparison of the Tekran denuder versus a reactive mist chamber (27 to 37%;[13,14]). Recent data collected during RAMIX showed that the Tekran system measured 45 to 54% of spiked $HgBr_2$ compared to that measured by DOHGS, respectively.[34]

Although the CEM showed the highest GOM capture efficiency, it can only be analyzed using wet digestion. These

dx.doi.org/10.1021/es4012349 | Environ. Sci. Technol. XXXX, XXX, XXX–XXX

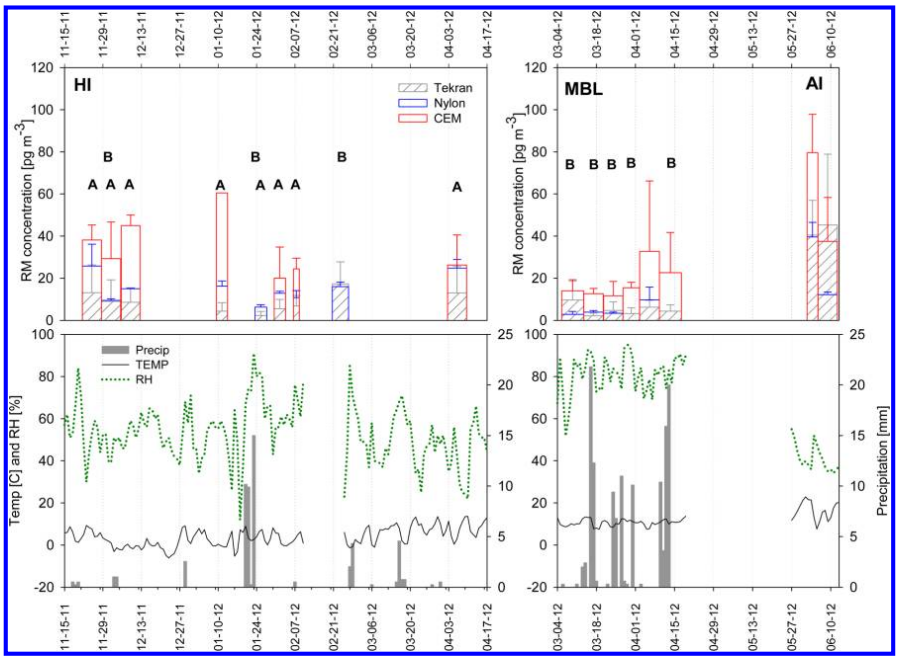

Figure 4. Bar graph showing RM concentrations measured by a Tekran (gray shadow) system, nylon membranes (blue), and CEMs (red) at the three field sites. The whisker indicates standard deviation (or relative percent difference) for triplicate membranes (or replicate membranes) and for 1 to 2 h Tekran measurements over the sampling period. Note the one bar without standard deviation was only a single sample. The width of the bar indicates the length of the sampling period from two to eight days. The 1135 component of the Tekran system was not available during the events marked as A. The events marked as B were time of precipitation. The bottom panels are the meteorological data with precipitation (vertical bar, *y*-axis on the right), temperature (solid line, *y*-axis on left), and relative humidity (dotted line, *y*-axis on left). Tekran data collected at the MBL site during 3/13/2012 and 3/27/2012 were incomplete and subjected to a correction factor.

results indicate that when used in tandem, the CEM can be used to quantify the amount of GOM in air, while nylon membranes can be used to qualitatively identify the chemical compound, since it collected the three compounds with equal capture efficiency.

We tested the hypothesis that if all compounds of GOM are collected on the nylon membrane, then these could be separated as a function of temperature (Figure 3). Tests of GEM release from the nylon membranes, after exposure to high concentrations (>200 ng m^{-3}), showed a sharp desorption curve starting at 60 °C, a peak at ∼95 °C, and all was removed by 120 °C (Figure 3). Tests at lower exposure concentrations <13 ng m^{-3}, and a loading amount of 260 pg, showed that little GEM was collected (<10 pg). The GEM desorption profile was cleaner than that of the GOM desorption profiles with no residual tail. This suggests that GEM bonding on the nylon surface might be due to van der Waals forces, which would be disrupted at lower temperatures. In contrast, GOM release from the nylon membrane started at 75 °C, and peaked at 105 °C for HgO, and 115 °C $HgCl_2$ and $HgBr_2$, respectively (Figure 3). Desorption profiles for these compounds extended to the highest desorption temperature of ∼190 °C. Subsequent analyses of these membranes, by wet digestion and cold vapor atomic fluorescence (EPA method 1631 E), showed little residual Hg, 0.13 ± 0.05 ng, an amount not significantly different from that of the membrane blanks (0.07 ± 0.06 ng n = 4 Mann−Whitney test, p-value = 0.054). Nylon material has a long molecular chain that is dominated by hydrogen bonding, and binding with this surface is driven by electrostatic interactions. We suggest that based on the polarizability of Hg, that is 5.1 to 5.7 × 10^{-24} cm^3,[45] this element was dominant in influencing the binding of GOM compounds.

Desorption profiles of GEM and $HgCl_2$ occurred at temperatures from 60 °C to 120 °C, and 75 °C to 190 °C, respectively, and overlapped the range reported in Feng et al. [9] (the references therein) for these compounds added directly to coal fly ash. Feng et al. [9] added elemental Hg as a gas phase but other compounds were added as solid phases by "dry dilution". Feng et al. [9] reported an HgO single peak at ∼500 °C. The discrepancy between our HgO profile and that of Feng et al. [9] could be due to the different addition methods, and the fact that fly ash contains activated carbon and other impurities (Al_2O_3, K_2O, MgO, SO_3, P_2O, etc.) that would provide different chemical bonding between different compounds of GOM and the collection surfaces. Nylon is a uniform material with a specific physical bonding force that will also influence its ability to collect certain compounds of GOM. If we assume that no particulate phase HgO was present, for this form could be deposited to the manifold,[5,34] then the lower released temperature of "HgO" or another compound (i.e., Hg_2O) from nylon is due to a lower electrostatic charge on this compound relative to $HgBr_2$ and $HgCl_2$.

dx.doi.org/10.1021/es4012349 | *Environ. Sci. Technol.* XXXX, XXX, XXX−XXX

Field Measurements. Field results were similar to those observed in the laboratory with the RM (designated as RM due to uncertainty as to whether aerosols were collected) concentrations measured by CEM being higher than those measured by the Tekran denuder and nylon membranes, except for a measurement made in June 2012 at the AI site (considered an outlier-discussed below) (Figure 4). Statistical comparison of the data showed that the CEM collected a significantly higher amount of GOM relative to the nylon membranes (ANCOVA, p-value <0.01). Since the time resolution of the Tekran measurement (1 h, on average) is different from that of the membrane (1 week), they cannot be statistically compared; however, given that the mean of the Tekran data represents the average of multiple measurements, this strengthens the argument for the lower concentration as measured by this instrument.

Reactive Hg concentrations as measured by nylon membrane were not consistently higher than those measured by the Tekran system at the MBL site, unlike the results observed in the laboratory with scrubbed air. During times of precipitation (marked as B in Figure 4), the ratio of Hg amount measured by nylon membrane to the RM measured by the Tekran system was <1.05 (0.75 ± 0.33). However, during these time periods, the CEM consistently recorded higher concentrations. The CEM is designed for proton exchange. Cation exchange membranes used were hydrophilic and had a neutral surface.[47] This material also wets out (or is impregnated by water) quickly.[48] This suggests that due to the nature of this material it collected RM during humid conditions (cf. Peterson et al. [35]).

Although correlation coefficients comparing the Tekran system derived RM and membrane measurements across all sites are significant (Figure SI 6 of the SI, r^2 = 0.53 to 0.71, p-value <0.01), r^2 values and slopes, were lower than those observed in the laboratory (r^2 = 0.58 to 0.99, p-value <0.01, Figure 2). This may be due to other atmospheric constituents that have stronger polarizability out competing Hg for binding sites on the nylon membrane such as water vapor. Similarly, relative humidity has been suggested to influence the KCl-coated denuder performance,[13,18,24] as moisture could hydrolyze the KCl-coated surface. Water might create another layer for compounds to be transported from air to the collection surface for some materials; however, as mentioned above, RH likely inhibited capture by the nylon membranes but could provide a means by which GOM is captured by the CEM since this material "wets out" quickly. If the data collected using the nylon membranes during precipitation are removed, the following equation is obtained:

$$\text{GOM concentrations on the nylon membrane (ng)} = 1.6\ \text{GOM Tekran denuder(ng)} + 4.8,\ r^2 = 0.88,\ p\text{-value} < 0.01,\ n = 10\ \text{sets}$$

The slope for this equation is the same as that obtained for the nylon membrane-denuder laboratory comparisons (Figure 2).

Since different RM/GOM compounds have different basic chemistry, this will influence their affinity for and retention by the collection surface. Unlike laboratory experiments, in the field, the membranes could collect particulate matter as well as the gaseous compounds. Linear regression analyses comparing membrane field data with RM as measured by the Tekran system showed the CEM measured more RM than the denuder ($y = 1.5x + 17$, $r^2 = 0.53$, p-value <0.01); however, this was not the case for the nylon membrane ($y = 0.89x + 5.1$, $r^2 = 0.71$, p-value <0.01) (Figure SI 6 of the SI). These data analyses included one outlier. Since there were no significant differences in meteorological conditions during the week outlier data were collected at the AI, and the Tekran system data were variable, this data point was removed. Removal of this outlier resulted in the equation $y = 2.0x + 17.5$, $r^2 = 0.45$, p-value <0.01, for the Hg measured on the CEM (assumed to be GOM in Figure SI 7 of the SI) versus the GOM measured by the Tekran 1130; and for the nylon membrane of $y = 1.3x + 4.2$, $r^2 = 0.67$, p-value <0.01. The resulting relationships were similar to those measured using the laboratory manifold. This suggests that the membranes as deployed were measuring primarily GOM.

Particle-bound Hg as measured by the Tekran system was higher at the MBL site (56 to 86% PBM/RM) and AI sites (47 and 63%) relative to that measured at the HI site (35% Tekran based; 0 to 15% quartz filter based; Table SI 1 of the SI). Given the chemical composition of aerosol in the MBL site, the form of GOM could be quite different from that at the HI and AI. This is suggested by the desorption profiles discussed below.

The chemical forms and compounds measured by the Tekran GOM and PBM measurements are uncertain. Gustin et al. [34] and Lynam et al. [30] suggested that GOM can pass through the KCl-coated denuder, be collected on downstream particle filter, and analyzed as PBM. Thus, under certain conditions, the Tekran system might underestimate GOM and overestimate PBM concentrations. It is possible that the denuder, as prepared, results in an alignment of charges across the surface that is more electropositive or negative. This could result in preferential collection of specific forms of GOM. Additionally, as mentioned, KCl is hydroscopic.[13] This means that it attracts and holds on to water molecules. Materials with this property when exposed to water change by increasing in volume, and as such, the denuder coating would lose the ability to capture GOM because the water molecules become suspended between the KCl molecules. This process could limit the ability of the denuder to collect GOM and result in compounds being collected on the downstream particulate measurement. This also suggests the denuder could be passivated quickly, given it is heated to high temperatures during desorption. This would explain the higher PBM measurements made at the MBL site (Table SI 1). In contrast, because of the configuration of the Tekran system (50 °C for entire sampling system), GOM may be deposited within the system.[34] The complexities of the Tekran system make the observations uncertain; and the influence of water on the denuder needs to be systematically investigated.

Other evidence to support that GOM was the primary form collected using nylon membranes, as opposed to PBM, is that the slope of the relationship when using all data at the field sites without PBM was 1.3 ± 0.2, similar to that obtained for the laboratory experiments, with a higher r^2 value (Figure SI 7 of the SI) than for the RM comparison. In addition, the GOM or RM concentrations measured by Tekran system in the field were only ∼20% of those measured by CEM, and this number is consistent with the ambient GOM recovery measured during RAMIX.[31,34] Particle-bound Hg concentrations measured weekly on quartz filters were significantly lower than those measured using the Tekran 1135 system. This also suggests that using quartz filters after KCl-coated denuders for PBM measurements does not collect PBM.

Different desorption profiles were obtained for membranes collected from the three field sites (Figure 3). At the HI site, the RM release started at 75 °C similar to profiles obtained in the laboratory; however, these curves peaked at ∼130 °C, which is 15 °C and 25 °C higher than $HgCl_2$/$HgBr_2$ and HgO (or Hg_2O) collected in laboratory, respectively. Furthermore, there was high residual RM after 150 °C, especially for the samples collected in the coldest time periods (January and February). From late fall to early spring, wood fired stoves are frequently used in Reno, NV, and an inversion layer often occurs due to topography. Huang et al. [49] reported, when using a Tekran system, that PBM was the dominant form of RM measured and suggested that wood combustion for space heating in winter was important. Since PBM is thought to be decomposed at higher temperatures than GOM,[13] and little residual GOM (digested membranes after desorption 0.26 ± 0.13, n = 9; blanks 0.29 ± 0.23 ng, n = 7; total 4 sets of data, 2 for HI and 2 for the MBL site) was measured on the membranes, this suggests that a different form of GOM than permeated in the laboratory was present in the air.

The GOM or RM desorption profile in summer time at the AI site was identical to that of $HgCl_2$ and $HgBr_2$ collected in scrubbed air using the laboratory manifold system. This site could be influenced by NO_3^- and NH_x related chemistry due to nearby livestock, agricultural activities, and/or wastewater treatment and usage. Limited work using $Hg(NO_3)_2$ showed a peak desorption temperature of 110 °C (data is not shown due to limited tests n = 2). This site has also been demonstrated to be impacted by free troposphere air that has been suggested to include $HgBr_2$ (cf. Gustin et al.).[34]

Interestingly, the desorption profile of RM collected at the MBL site showed a significant temperature lag (starting from 105 °C) and peaked from 120 to 135 °C. This pattern is not similar to the GOM compounds permeated, and we suggest that a different form of GOM was present. Engle et al. [50] showed, based on Tekran measurements, that unpolluted air from the MBL site was not a source of GOM and based on limited data PBM was associated primarily with particulate matter >2.5 μm. On the basis of their comparison of Hg concentrations measured as a function of particle size, and the inlet for our sampling system, we would not be sampling this coarse fraction. If one assumes that our field system is only measuring GOM, based on data presented in Figure SI 6 and 7 of the SI, then a similar capture efficiency is shown for GOM compounds by the nylon membrane, and the CEM data are a better indicator of actual concentration. The field data demonstrate that the denuder method underestimates GOM by 2-fold and that GOM compounds other than those tested were being collected; and GOM varies spatially and temporally.

Implications. The use of a KCl-coated annular denuder underestimates the concentrations of $HgCl_2$, $HgBr_2$, and HgO in air. Given the different forms suggested to be present in the atmosphere,[4−6,9−12] and that we do not know all of the compounds present, it is possible that some may not be collected by the denuder as suggested by Gustin et al.[34] On the basis of systematic laboratory experiments, the relative collection efficiency for GOM by the denuders in ambient air is $HgBr_2$ > $HgCl_2$ > HgO. Comparison of denuder-measured concentrations with those measured using the CEM represents the start of a quantitative framework for calibrating past measurements. This framework is supported by understanding the basic chemistry of the anions bound to the Hg. In order to understand and calibrate GOM measurements, permeation rates of GOM compounds, including $HgBr_2$, $HgCl_2$, HgO, and $HgSO_4$, and $Hg(NO_3)_2$ must be developed for a standard system with standard sources. Field and laboratory research are pointing toward KCl denuder interferences with water vapor and O_3. More work is needed to develop calibration factors that will allow us to correct past field measurements using the denuder method for spatial and temporal variations in atmospheric chemistry and GOM compounds.

In scrubbed air experiments, $HgCl_2$ and HgO amounts measured using CEMs were higher than those measured using nylon membranes; however, there was no difference using these two methods during $HgBr_2$ permeation. This indicates that bonding of $HgCl_2$ and $HgBr_2$ is different for these different surfaces, and that the CEM is a more robust collection surface for quantifying total GOM. Furthermore, different desorption profiles were observed for GEM, HgO, and $HgCl_2$/$HgBr_2$; this is due to the overall different affinities between GOM compounds and the nylon surface. Limited field data indicated that PBM was not measured using our field sampling system.

On the basis of thermodesorption profiles, the atmospheric chemistry of GOM varies over space and time. Since GOM has a high deposition velocity and is readily bioavailable, accurate measurements are needed to assess the environmental impacts of this global contaminant.

■ ASSOCIATED CONTENT

Supporting Information

Additional text, Table, 7 Figures, and additional references. This material is available free of charge via the Internet at http://pubs.acs.org.

■ AUTHOR INFORMATION

Corresponding Author

*Phone: 1-775-784-4203; e-mail: mgustin@cabnr.unr.edu.

Notes

The authors declare no competing financial interest.

■ ACKNOWLEDGMENTS

This work was funded by the National Science Foundation (Grant No. 0917934). However, it does not reflect the views of the Agency and no official endorsement should be inferred. Thanks to Bo Kindred, with Nevada Agriculture Experiment Station, for his help with technical support. We thank UNR undergraduate students Larz Bolster, Douglas Yan, Musheng Alishahi, Travis Lyman, and Vanessa Wehrkamp for help with this project. Thanks to the Nevada Division of Environmental Protection for use of their Tekran system. We also thank the five anonymous reviewers whose comments improved the clarity of this manuscript, and to Christianna Peterson for text editing. The last author thanks Michael Gustin for his patience, comments, and questions. All authors of the papers associated with the RAMIX linked papers thank Dr. Jerald Schnoor for handling these submissions.

■ REFERENCES

(1) Schroeder, W. H.; Munthe, J. Atmospheric mercury—An overview. *Atmos. Environ.* **1998**, *32* (5), 809−822.

(2) Seigneur, C.; Vijayaraghavan, K.; Lohman, K.; Karamchandani, P.; Scott, C. Global source attribution for mercury deposition in the United States. *Environ. Sci. Technol.* **2004**, *38* (2), 555−569.

(3) Lindberg, S. E.; Bullock, R.; Ebinghaus, R.; Engstrom, D.; Feng, X.; Fitzgerald, W.; Pirrone, N.; Prestbo, E.; Seigneur, C. A synthesis of

progress and uncertainites in attributing the sources of mercury in deposition. *AMBIO* **2007**, *36*, 19−32.
(4) Hynes, A. J.; Donohoue, D. L.; Goodsite, M. E.; Hedgecock, I. M., Our current understanding of major chemical and physical processes affecting mercury dynamics in the atmosphere and at the air-water/terrestrial interfaces. In *Mercury Fate and Transport in the Global Atmosphere*; Mason, R., Pirrone, N., Eds. Springer: New York, 2009.
(5) Ariya, P. A.; Peterson, K.; Snider, G.; Amyot, M. Mercury chemical transformations in the gas, aqueous and heterogeneous phases: State-of-the-art science and uncertainties. In *Mercury Fate and Transport in the Global Atmosphere*; Mason, R.; Pirrone, N., Eds. Spring: New York, 2009.
(6) Lin, C.-J.; Pongprueksa, P.; Lindberg, S. E.; Pehkonen, S. O.; Byun, D.; Jang, C. Scientific uncertainties in atmospheric mercury models I: Model science evaluation. *Atmos. Environ.* **2006**, *40* (16), 2911−2928.
(7) Subir, M.; Ariya, P. A.; Dastoor, A. P. A review of uncertainties in atmospheric modeling of mercury chemistry I. Uncertainties in existing kinetic parameters: Fundamental limitations and the importance of heterogeneous chemistry. *Atmos. Environ.* **2011**, *45* (32), 5664−5676.
(8) Subir, M.; Ariya, P. A.; Dastoor, A. P. A review of the sources of uncertainties in atmospheric mercury modeling II. Mercury surface and heterogeneous chemistry—A missing link. *Atmos. Environ.* **2012**, *46* (0), 1−10.
(9) Feng, X.; Lu, J. Y.; Grégoire, C. D.; Hao, Y.; Banic, C. M.; Schroeder, W. H. Analysis of inorganic mercury species associated with airborne particulate matter/aerosols: method development. *Anal. Bioanal. Chem.* **2004**, *380*, 683−689.
(10) Calvert, J. G.; Lindberg, S. E. Mechanisms of mercury removal by O_3 and OH in the atmosphere. *Atmos. Environ.* **2005**, *39* (18), 3355−3367.
(11) Lindberg, S. E.; Stratton, W. J. Atmospheric mercury speciation: Concentrations and behavior of reactive gaseous mercury in ambient air. *Environ. Sci. Technol.* **1998**, *32* (1), 49−57.
(12) Seigneur, C.; Abeck, H.; Chia, G.; Reinhard, M.; Bloom, N. S.; Prestbo, E.; Saxena, P. Mercury adsorption to elemental carbon (soot) particles and atmospheric particulate matter. *Atmos. Environ.* **1998**, *32*, 2649−2657.
(13) Landis, M. S.; Stevens, R. K.; Schaedlich, F.; Prestbo, E. M. Development and characterization of an annular denuder methodology for the measurement of divalent inorganic reactive gaseous mercury in ambient air. *Environ. Sci. Technol.* **2002**, *36* (13), 3000−3009.
(14) Sheu, G.-R.; Mason, R. P. An examination of methods for the measurements of reactive gaseous mercury in the atmosphere. *Environ. Sci. Technol.* **2001**, *35* (6), 1209−1216.
(15) Schroeder, W.; Yarwood, G.; Niki, H. Transformation processes involving mercury species in the atmosphere—Results from a literature survey. *Water Air and Soil Pollution* **1991**, *56*, 653−666.
(16) Wallschläger, D. *Speziesanalytische Untersuchungen zur Abschätzung des Remobilisierungspotentials ban Queeksilber aus kontaminierten Elbauen*; University of Bremen: Bremen, Germany, 1996.
(17) Xiao, Z.; Sommar, J.; Wel, S.; Lindqvist, O. Sampling and determination of gas phase divalent mercury in the air using a KCl coated denuder. *Fresenius J. Anal. Chem.* **1997**, *358*, 386−391.
(18) Feng, X.; Sommar, J.; Gårdfeldt, K.; Lindqvist, O. Improved determination of gaseous divalent mercury in ambient air using KCl coated denuders. *Fresenius J. Anal. Chem.* **2000**, *366*, 423−428.
(19) Stratton, W. J.; Lindberg, S. E. Use of a refluxing mist chamber for measurement of gas-phase mercury(II) species in the atmosphere. *Water Air Soil Pollut.* **1995**, *80* (1−4), 1269−1278.
(20) Ebinghaus, R.; Jennings, S. G.; Schroeder, W. H.; Berg, T.; Donaghy, T.; Guentzel, J.; Kenny, C.; Kock, H. H.; Kvietkus, K.; Landing, W.; Mühleckleck, T.; Munthe, J.; Prestbo, E. M.; Schneeberger, D.; Slemr, F.; Sommar, J.; Urba, A.; Wallschläger, D.; Xiao, Z. International field intercomparison measurements of atmospheric mercury species at Mace Head, Ireland. *Atmos. Environ.* **1999**, *33* (18), 3063−3073.
(21) Lyman, S. N.; Gustin, M. S.; Prestbo, E. M.; Marsik, F. J. Estimation of dry deposition of atmospheric mercury in Nevada by direct and indirect methods. *Environ. Sci. Technol.* **2007**, *41* (6), 1970−1976.
(22) Lyman, S. N.; Gustin, M. S.; Prestbo, E. M.; Kilner, P. I.; Edgerton, E.; Hartsell, B. Testing and application of surrogate surfaces for understanding potential gaseous oxidized mercury dry deposition. *Environ. Sci. Technol.* **2009**, *43* (16), 6235−6241.
(23) Lyman, S. N.; Gustin, M. S.; Prestbo, E. M. A passive sampler for ambient gaseous oxidized mercury concentrations. *Atmos. Environ.* **2010**, *44* (2), 246−252.
(24) Huang, J.; Choi, H.-D.; Landis, M. S.; Holsen, T. M. An application of passive samplers to understand atmospheric mercury concentration and dry deposition spatial distributions. *J. Environ. Monitoring.* **2012**, *14* (11), 2976−2982.
(25) Caldwell, C. A.; Swartzendruber, P.; Prestbo, E. Concentration and dry deposition of mercury species in arid south central New Mexico (2001−2002). *Environ. Sci. Technol.* **2006**, *40* (24), 7535−7540.
(26) Castro, M. S.; Moore, C.; Sherwell, J.; Brooks, S. B. Dry deposition of gaseous oxidized mercury in Western Maryland. *Sci. Total Environ.* **2012**, *417*−*418* (0), 232−240.
(27) Lu, J. Y.; Schroeder, W. H.; Berg, T.; Munthe, J.; Schneeberger, D.; Schaedlich, F. A device for sampling and determination of total particulate mercury in ambient air. *Anal. Chem.* **1998**, *70* (11), 2403−2408.
(28) Rutter, A. P.; Schauer, J. J. The impact of aerosol composition on the particle to gas partitioning of reactive mercury. *Environ. Sci. Technol.* **2007**, *41* (11), 3934−3939.
(29) Rutter, A. P.; Schauer, J. J. The effect of temperature on the gas-particle partitioning of reactive mercury in atmospheric aerosols. *Atmos. Environ.* **2007**, *41* (38), 8647−8657.
(30) Lynam, M. M.; Keeler, G. J. Artifacts associated with the measurement of particulate mercury in an urban environment: The influence of elevated ozone concentrations. *Atmos. Environ.* **2005**, *39* (17), 3081−3088.
(31) Ambrose, J. L.; Lyman, S. N.; Huang, J.; Gustin, M.; Jaffe, D. A. Fast time resolution oxidized mercury measurements with the UW detector for oxidized Hg species (DOHGS) during the Reno atmospheric mercury intecomparison experiment. *Environ. Sci. Technol.* **2013**, DOI: 10.1021/es303916v • Publication Date (Web): 20 Feb 2013.
(32) Swartzendruber, P. C.; Jaffe, D. A.; Finley, B. Development and first results of an aircraft-based, high time resolution technique for gaseous elemental and reactive (oxidized) gaseous mercury. *Environ. Sci. Technol.* **2009**, *43* (19), 7484−7489.
(33) Lyman, S. N.; Jaffe, D. A., Formation and fate of oxidized mercury in the upper troposphere and lower stratosphere. *Nat. Geoscience.* 2011, advance online publication.
(34) Gustin, M. S.; Huang, J.; Miller, M. B.; Peterson, C.; Jaffe, D. A.; Ambrose, J.; Finley, B. D.; Lyman, S. N.; Call, K.; Talbot, R.; Feddersen, D.; Mao, H.; Lindberg, S. E. Do we understand what the mercury speciation instruments are actually measuring? Results of RAMIX *Environ. Sci. Technol.* **2013**, DOI: 10.1021/es3039104, Publication Date January 10, 2013 (Article).
(35) Peterson, C.; Alishahi, M.; Gustin, M. S. Testing the use of passive sampling systems for understanding air mercury concentrations and dry deposition across Florida, USA. *Sci. Total Environ.* **2012**, *424* (0), 297−307.
(36) Dasgupta, P. K.; McDowell, W. L.; Rhee, J.-S. Porous membrane-based diffusion scrubber for the sampling of atmospheric gases. *Analyst* **1986**, *111* (1), 87−90.
(37) Appel, B. R.; Tokiwa, Y.; Haik, M. Sampling of nitrates in ambient air. *Atmos. Environ. (1967)* **1981**, *15* (3), 283−289.
(38) Appel, B. R.; Wall, S. M.; Tokiwa, Y.; Haik, M. Simultaneous nitric acid, particulate nitrate and acidity measurements in ambient air. *Atmos. Environ. (1967)* **1980**, *14* (5), 549−554.

(39) Marsik, F. J.; Keeler, G. J.; Landis, M. S. The dry-deposition of speciated mercury to the Florida Everglades: Measurements and modeling. *Atmos. Environ.* **2007**, *41* (1), 136−149.
(40) Finley, B. D.; Jaffe, D. A.; Call, K.; Lyman, S. N.; Gustin, M., Development, testing, and deployment of an air sampling manifold for spiking elemental and oxidized mercury during RAMIX. *Environ. Sci. Technol.* **2013**, DOI: 10.1021/es304185a, Publication Date (Web): 26 Feb 2013.
(41) L'Vov, B. V. Kinetics and mechanism of thermal decomposition of mercuric oxide. *Thermochim. Acta* **1999**, *333* (1), 21−26.
(42) Lyman, S. N.; Jaffe, D. A.; Gustin, M. S. Release of mercury halides from KCl denuders in the presence of ozone. *Atmos. Chem. Phys.* **2010**, *10*, 8197−8204.
(43) NADP Atmospheric Mercury Network (AMNet) Site Operations Manual. http://nadp.sws.uiuc.edu/amn/docs/AMNet_Operations_Manual.pdf
(44) Aspmo, K.; Gauchard, P.-A.; Steffen, A.; Temme, C.; Berg, T.; Bahlmann, E.; Banic, C.; Dommergue, A.; Ebinghaus, R.; Ferrari, C.; Pirrone, N.; Sprovieri, F.; Wibetoe, G. Measurements of atmospheric mercury species during an international study of mercury depletion events at Ny-Ålesund, Svalbard, spring 2003. How reproducible are our present methods? *Atmos. Environ.* **2005**, *39* (39), 7607−7619.
(45) Lide, D. R. *CRC Handbook of Chemistry and Physics*; CRC Press: Boca Raton, 2001.
(46) Kotz, J. C.; Purcell, K. F. *Chemistry and Chemical Reactivity*; Sanders College: Philadelphia, 1987.
(47) Alyssa, N., *Product Applications Specialist, Cole-Parmer*. In 2012.
(48) Pall Scientific http://www.pall.com/main/OEM-Materials-and-Devices/Product.page?id=3949
(49) Huang, J.; Hopke, P. K.; Choi, H.-D.; Laing, J. R.; Cui, H.; Zananski, T. J.; Chandrasekaran, S. R.; Rattigan, O. V.; Holsen, T. M. Mercury (Hg) emissions from domestic biomass combustion for space heating. *Chemosphere* **2011**, *84* (11), 1694−1699.
(50) Engle, M. A.; Tate, M. T.; Krabbenhoft, D. P.; Kolker, A.; Olson, M. L.; Edgerton, E. S.; DeWild, J. F.; McPherson, A. K. Characterization and cycling of atmospheric mercury along the central US Gulf Coast. *Appl. Geochem.* **2008**, *23* (3), 419−437.

Measuring and modeling mercury in the atmosphere: a critical review

Permission to Reprint

The following article is reprinted with permission from:

Gustin, M. S., Amos, H. M., Huang, J., Miller, M. B., and Heidecorn, K.: Measuring and modeling mercury in the atmosphere: a critical review, Atmos. Chem. Phys., 15, 5697-5713, https://doi.org/10.5194/acp-15-5697-2015, 2015.

Atmos. Chem. Phys., 15, 5697–5713, 2015
www.atmos-chem-phys.net/15/5697/2015/
doi:10.5194/acp-15-5697-2015

Atmospheric Chemistry and Physics
Open Access

Measuring and modeling mercury in the atmosphere: a critical review

M. S. Gustin[1], H. M. Amos[2], J. Huang[1], M. B. Miller[1], and K. Heidecorn[1]

[1]Department of Natural Resources and Environmental Science, University of Nevada-Reno, Reno, NV, 89557, USA
[2]Department of Environmental Health, Harvard School of Public Health, Boston, MA, 02115, USA

Correspondence to: M. S. Gustin (mgustin@cabnr.unr.edu)

Received: 9 January 2015 – Published in Atmos. Chem. Phys. Discuss.: 10 February 2015
Revised: 9 April 2015 – Accepted: 4 May 2015 – Published: 26 May 2015

Abstract. Mercury (Hg) is a global health concern due to its toxicity and ubiquitous presence in the environment. Here we review current methods for measuring the forms of Hg in the atmosphere and models used to interpret these data. There are three operationally defined forms of atmospheric Hg: gaseous elemental mercury (GEM), gaseous oxidized mercury (GOM), and particulate bound mercury (PBM). There is relative confidence in GEM measurements (collection on a gold surface), but GOM (collection on potassium chloride (KCl)-coated denuder) and PBM (collected using various methods) are less well understood. Field and laboratory investigations suggest the methods to measure GOM and PBM are impacted by analytical interferences that vary with environmental setting (e.g., ozone, relative humidity), and GOM concentrations measured by the KCl-coated denuder can be too low by a factor of 1.6 to 12 depending on the chemical composition of GOM. The composition of GOM (e.g., $HgBr_2$, $HgCl_2$, HgBrOH) varies across space and time. This has important implications for refining existing measurement methods and developing new ones, model/measurement comparisons, model development, and assessing trends. Unclear features of previously published data may now be re-examined and possibly explained, which is demonstrated through a case study. Priorities for future research include identification of GOM compounds in ambient air and development of information on their chemical and physical properties and GOM and PBM calibration systems. With this information, identification of redox mechanisms and associated rate coefficients may be developed.

1 Introduction

The Minamata Convention for mercury (Hg) has been signed by more than 120 nations and is now being ratified. The primary objective of the convention is to "protect human health and the environment from anthropogenic emissions and releases of mercury and mercury compounds" (UNEP Minamata Convention, 2014). A key challenge for Hg researchers is developing linkages between Hg in the atmosphere, deposition, and ecosystem contamination (Pirrone et al., 2013). Here we review where the science on measuring and modeling atmospheric Hg currently stands and offer suggestions for future research directions that will both advance understanding of Hg cycling in and between environmental reservoirs and better serve the needs of the convention.

Although the atmosphere is a relatively minor reservoir of Hg compared to oceans or soils, it is an important pathway by which Hg is distributed globally over short timescales (≤ 1 year). Atmospheric deposition represents the major pathway of Hg input to terrestrial and aquatic ecosystems outside areas of direct contamination. A variety of environmental archives, including remote lake sediments, ombrotrophic peat bogs, glacial ice, and tree rings, suggests Hg inputs to the atmosphere have increased several fold in the last 150 years (cf. Engstrom et al., 2014; Schuster et al., 2002; Wright et al., 2014a). Measured concentrations of atmospheric Hg have been declining over the last ~ 15 years (Slemr et al., 2011; Cole and Steffen, 2010; Soerensen et al., 2012; Cole and Steffen, 2010; Cole et al., 2014), despite inventories suggesting global anthropogenic emissions have been relatively flat or increasing (AMAP/UNEP, 2013). This conundrum has challenged our understanding of Hg cycling

Published by Copernicus Publications on behalf of the European Geosciences Union.

and emissions, and underscores the need for continued atmospheric Hg monitoring.

Measuring the forms of Hg in the atmosphere is difficult. Mixing ratios are at low parts per quadrillion by volume (ng m^{-3} and pg m^{-3}). Atmospheric Hg is operationally defined as gaseous elemental Hg (GEM), gaseous oxidized Hg (GOM), and particulate bound Hg (PBM) less than 2.5 μm in diameter (Lindberg et al., 2007; Schroeder and Munthe, 1998; Landis et al., 2002). GOM can be present as different forms (Huang et al., 2013, 2015). GOM and PBM have complex fundamental physiochemical properties. Because of the complexity, recent work has combined GOM and PBM concentrations as measured by the Tekran® system and defined this as reactive Hg (RM = GOM + PBM) (cf. Rutter and Schauer, 2007a, b; Gustin et al., 2013; Weiss-Penzias et al., 2015). Previously it was thought that GEM was 95–99 % of Hg in the atmosphere (cf. Schroeder and Munthe, 1998). Recent work is pointing towards GOM being 25 % of total Hg in the boundary layer (see the discussion below). In the Arctic, up to 100 % conversion of GEM to GOM has been observed (Steffen et al., 2014, 2015). In addition, it has been demonstrated that there are different GOM compounds in the air (Huang et al., 2013, 2015).

Here we review current methods for measuring the forms of Hg in the atmosphere and models used to interpret these data. The advantages and limitations of each measurement method are discussed, and a narrative is provided on how we have arrived at our current understanding of the limitations. The number of models that have developed the capacity to simulate atmospheric Hg has multiplied in the last decade. We review major gains in Hg science gleaned from the use of measurements and models together, as well as key open questions. We conclude with a discussion of outstanding problems facing measurement and modeling communities.

2 Methods for measuring atmospheric Hg

2.1 Atmospheric mercury basics

Mercury is typically detected by atomic absorption (AAS) or atomic fluorescence spectroscopy (AFS). In nearly all cases, Hg forms are pre-concentrated on gold-coated surfaces because the sensitivity of AAS and AFS are, with the exception of laser and Zeeman AAS techniques, not sufficient for direct measurements of Hg at ambient concentrations. GOM and PBM are converted to GEM by thermal desorption from the gold surfaces. Gold is the most frequently used and best-studied pre-concentration material for Hg but can become passivated (Huang et al., 2014; Landis et al., 2002). Currently, the Tekran® 2537/1130/1135 system is the most widely adopted method for measurement of atmospheric Hg, and this instrument has been incorporated into monitoring networks, such as the Canadian Mercury Network (CAMNet), Atmospheric Mercury Network (AMNet), and Global Mercury Observation System (GMOS). Alternate measurement methods have been developed, but are currently operated on a limited scale.

An AAS or AFS instrument combined with a pre-concentration on a gold adsorber with an in-line pyrolyzer will provide total gaseous mercury (TGM = GEM + GOM) or total atmospheric mercury (TAM = GEM + GOM + PBM). Since GOM is adhesive, sampling lines are often heated and should be kept short in length to prevent wall loss.

GOM and PBM are in temperature-dependent equilibrium (Rutter and Schauer, 2007b; Amos et al., 2012). Specific PBM sampling has to take account of this, in addition to the usual precautions to prevent size-dependent particle losses. Since it is difficult to achieve separation of PBM and GOM without disturbing the equilibrium, RM is a more accurate measurement to use. In addition, due to lack of capture of GOM by the denuder and collection on the PBM unit (Gustin et al., 2013), discussion of RM is more appropriate.

2.2 Active automated systems

2.2.1 Tekran® system

The Tekran® 2537/1130/1135 system has been widely used to measure atmospheric Hg for the past ∼ 15 years (Landis et al., 2002). The Tekran® 2537 module measures TGM or GEM in ng m^{-3} and was the first component to be developed. The 1130 and 1135 components were added to this system to measure GOM and PBM in pg m^{-3} (Landis et al., 2002), respectively. The instrument pulls air through an elutriator that is heated to 50 °C and removes particles > 2.5 μm, depending on the flow rate (Lyman et al., 2007). This particle size cut is necessary to keep larger particles from depositing on the denuder. GOM is collected on a potassium chloride (KCl)-coated denuder, and PBM on a column of quartz chips and a quartz filter. Air passes through 10 m of heated line with a soda lime trap and Teflon filter at the 2537 inlet and then into the 2537 where GEM is collected on a gold trap. It is not known whether the soda lime trap captures and retains GOM. GOM (500 °C) and PBM (800 °C) are thermally desorbed from their collection surfaces, loaded on the gold traps, and quantified as GEM (gold traps are heated to 350 °C) by cold vapor atomic fluorescence spectrometry (CVAFS). Although the particle cut inlet, coated annular denuder, particle filtration device, and heated line are all held at constant temperatures (50 °C) when sampling, there are temperature drops within the sampling line and GOM may be lost to the walls (Gustin et al., 2013). Recent work has shown that heating of the inlet to 100 °C improves GOM collection (Huang and Gustin, 2015a).

This instrument has high temporal resolution, low limit of detection, and established quality assurance / quality control protocols (Table 1). The CAMNet and AMNet developed best management practices for this instrument (Steffen et al.,

Table 1. Pros and cons of automated and integrative methods used to make Hg measurements.

	Hg form measured/detection limit	Pros	Cons	Suggestion/comments
Automated				
Tekran 2537 gold traps	GEM or TGM; 0.5 ng m^{-3} ambient air	Low detection limit, 2.5 to 5 min resolution; there is a calibration source, standardized by AMNet and CAMNet (cf. Prestbo and Gay, 2009)	Inlet configuration will impact whether measuring GEM or TGM; requires fairly trained technicians, stable electrical source, regular calibration and checks	Suggest using a pyrolyzer at the inlet if TGM measurement is desired
Tekran 1130 KCl denuder	GOM; 1 pg m^{-3}	Good time resolution (1 to 2 h)	No calibration source; coating denuders needs to be done by one operator; does not measure all the GOM in air	New method needs to be developed that measures all forms in air and is not impacted by relative humidity and ozone; a different denuder coating would be useful
Tekran 1135 quartz filter and chips	PBM; 1 pg m^{-3}	Good time resolution (1 to 2 h)	Positive artifact due to measurement of GOM that passes through the denuder; not all PBM is measured due to select grain size capture	Filter method may be best and suggest using cation exchange membranes
Lumex	GEM or TGM; in liquids, solids, air; 1 ng m^{-3}	Good time resolution (seconds); field portable; allows for measurement of Hg concentrations in environmental media in the field	Not calibrated at low air concentrations	Good for industrial applications
Gardis	GEM or TGM; 0.5 ng m^{-3}	Good time resolution (2.5 min)	Requires trained operators	
DOHGS	GEM and TGM; 80 pg m^{-3}	Good time resolution (2.5 min)	Requires highly trained operators and stable environment	Useful as a research instrument
Laser	GEM	Fast time resolution (seconds)	Requires highly trained operators and a stable environment; cannot quantify GOM	Useful as research instrument
Integrated measurements				
GEM sampler activated carbon	GEM or TGM; 10–80 pg m^{-3}	Easy operation	Long time resolution	Good for areas with high concentration gradients
GOM mist chamber	GOM; Blank: 20–50 pg		Complicated operation; needs acidified solution	Useful as a research instrument; needs to be re-evaluated
GOM passive sampler concentration	GOM; 2.3–5 ng m^{-3}	Easy operation	Long time resolution	Needs a new design
GOM passive sampler deposition	GOM; probably PBM; 0.02–0.24 ng m^{-2} h^{-1}	Easy operation; real Hg loading to ecosystem	Long time resolution	Good for worldwide network
Direct particulate matter sampler measurement	PBM; probably GOM	Easy operation	Artifacts from GOM partition; choice of filters important to consider and length of sampling line	
UNR active system	GOM; $\sim$ 30 pg m^{-3}	Easy operation; for quantifying GOM and trying to understand the chemical forms in air	Potentially some PBM measured	Good for networks, and it could be used to help calibrate measurements made by the Tekran system

2012; Gay et al., 2013). Co-located GEM measurement can deviate by 20 to 30 % (Aas, 2006; Gustin et al., 2013). Lyman et al. (2007; Supplement) found that TGM could vary by 7.0 ± 5.3 %. There are no calibration standards for GOM, breakthrough can result in collection on the PBM filter, and collection efficiencies for GOM and PBM are uncertain (cf. Gustin and Jaffe, 2010; Huang et al., 2013; Talbot et al., 2011).

2.2.2 Lumex

Lumex RA-915 and Lumex 915+ (Lumex, St. Petersburg, Russia) units measure GEM and TGM, respectively, with a reported detection limit of $\sim 1\,\mathrm{ng\,m^{-3}}$ for measurements in air. If averaged over the sampling time of the GEM measurement by the Tekran® system (5 min), a detection limit of a few tenths of $\mathrm{ng\,m^{-3}}$ can be achieved. The Lumex uses Zeeman atomic absorption spectrometry with Zeeman background correction. In this instrument, a Hg vapor lamp sits in a magnetic field and generates a 254 nm light wavelength split into three polarized light fields. A photodetector detects light in one field within the Hg absorption wavelength 254 nm and another lying outside of this wavelength. The signals from both fields are equal when Hg is not present (for details see Sholupov et al., 2004). The instrument can be periodically calibrated using a permeation source such as used for internal calibration of the Tekran® instruments. This is not available commercially (F. Slemr, personal communication, 2015).

2.2.3 Gardis

The Gardis Hg analyzer has two gold traps, a concentrating and analytical trap, and measures Hg using CVAAS (Institute of Physics, Lithuania). Having two gold traps might reduce some interferences, such as passivation. This instrument will measure GEM, TGM, or TAM depending on inlet configuration and was developed in 1995 by Urba et al. (1995). In a field comparison, concentrations were similar to that measured by the Tekran® 2537 (Ebinghaus et al., 1999). This unit has had limited use and a reported detection limit of $0.5\,\mathrm{ng\,m^{-3}}$ (Table 1).

2.2.4 University of Houston Mercury system (UHMERC)

UHMERC was designed for measuring GEM and TGM (Talbot et al., 2008). This instrument uses two Tekran® systems that are slightly modified (gold trap heated to 460 °C). The inlet to the instrument measuring GEM consists of a Teflon filter to remove fine particles ($< 2\,\mu$m) with a molecular sieve trap immediately after to remove GOM (Gustin et al., 2013).

2.2.5 Detector for oxidized Hg species (DOHGS)

The DOHGS instrument measures TGM and GEM using two Tekran® 2537 units. The difference between these measurements is interpreted as RM. The original instrument is described in Swartzendruber et al. (2009), and subsequent modifications to the system can be found in Ambrose et al. (2013) and Lyman and Jaffe (2012). The measurement of GEM requires that GOM and PBM be selectively removed from the airstream. In early versions, only GOM was removed using a KCl-coated denuder. This led to the discovery of a discrepancy between GOM collected on KCl-coated denuders and that measured by the difference method (Swartzendruber et al., 2009). The GOM removal method was changed to quartz chips maintained at 650 °C as a pyrolyzer to measure TGM and then quartz wool (Lyman and Jaffe, 2012; Ambrose et al., 2013). More recently a cation-exchange membrane filter has been used to remove RM compounds.

The method detection limit for RM is $\sim 80\,\mathrm{pg\,m^{-3}}$ (Ambrose et al., 2013; Table 1). Extensive testing has been conducted on the DOHGS using calibration sources of Hg^0, $HgBr_2$, and $HgCl_2$. Improving the sensitivity of the underlying CVAFS systems would enable more routine operation of this instrument.

2.2.6 Laser systems

Two laser systems have been developed for measurement of GEM (Faïn et al., 2010; Pierce et al., 2013; Bauer et al., 2002, 2010, 2014). One is a cavity ring-down system, and the other operates on the principle of laser-induced fluorescence. Both are calibrated using Tekran® data. These do not currently have the ability to measure GOM or PBM. If GOM and/or PBM were to be measured, they must be converted to GEM first. The cavity ring-down instrument has interferences with ozone (O_3) (Faïn et al., 2010; Pierce et al., 2013). Laser systems are best applied in laboratory settings given the current sensitivity, need for a consistent electrical supply, and large electrical power use.

During the Reno Atmospheric Mercury Intercomparison eXperiment, the laser-induced fluorescence system operated by University of Miami successfully sampled on 18 days, typically for between 4 and 6 h a day. The longest period of continuous sampling lasted for 26 h. During RAMIX they sampled directly from the manifold and, in addition, at the end of the campaign sampled ambient air independently, including true in situ sampling on the roof of their mobile lab. They also attempted to measure GOM by pyrolyzing the sample air and measuring the difference between Hg(0) and TGM (Bauer et al., 2014; A. Hynes, personal communication, 2015).

2.3 Active manual samplers

Here we briefly review manual sampling methods for GEM/TGM, GOM, and PBM. Manual samplers collect over a specific amount of time, and then the samples collected need to be analyzed using an alternate method. In contrast, automated samplers provide short time (seconds to minutes) resolution measurements and do not need measurements by an alternate method.

2.3.1 Mist chamber method for RM

Stratton and Lindberg (1995), Lindberg and Stratton (1998), Lindberg et al. (2000), and Stratton et al. (2001) described development of a mist chamber for measurement of GOM (termed RGM then). The principle of operation includes pulling air at a high flow rate (15 to 20 Lpm) through a fine mist aerosol made of water, NaCl, and HCl. GOM and PBM accumulate in droplets captured on a membrane. This liquid drains into a chamber and is collected, stored in vials, and analyzed using EPA Method 1631 (EPA Method 1631, 2013).

Sheu and Mason (2001) compared denuders, mist chambers, and a filter pack method for GOM (see the Supplement for details). They showed GOM concentrations in Maryland could be up to 500 pg m^{-3} and that GOM could be up to 30 % of the TGM. Reported daytime concentrations measured by the mist chamber were significantly higher (20 to 700 pg m^{-3}) than the KCl-coated denuder (20 to 70 pg m^{-3}).

2.3.2 UNR active system for GOM

The UNR active system measures ambient GOM concentrations and identifies GOM compounds. It consists of a six-port system each with two in-series Teflon filter holders. Three of the filter holders house nylon membranes and three-cation exchange membranes. Air is pulled using a vacuum pressure pump through the membranes with flow regulated by a mass flow controller at a rate of $\sim$ 1 Lpm. (Huang et al., 2013). This unit is not thought to measure PBM as configured (Huang et al., 2013, 2015).

Cation exchange membranes are analyzed using EPA Method 1631 (EPA Method 1631, 2013) to quantify GOM concentrations. Nylon membranes are thermally desorbed to determine compounds present in the air (Huang et al., 2013, 2015). This method may not collect all GOM compounds (Wright et al., 2014b; Huang et al., 2014; Huang and Gustin, 2015b). The nylon membrane is influenced by relative humidity (RH) (Huang et al., 2013; Huang and Gustin, 2015a). A summary of some advances presented in Huang and Gustin (2015b) associated with this method are described in the Supplement. The active system is currently limited to a resolution of 1 to 2 weeks.

2.3.3 Active manual systems for PBM/RM

Teflon, glass-fiber, and quartz filters have been used in open-faced filter packs, cascade impactors, and Micro-Orifice Uniform Deposition Impactors™ (MOUDIs) to measure atmospheric PBM concentrations (Keeler et al., 1995; Wang et al., 2013; Talbot et al., 2011; Engle et al., 2008; Rutter et al., 2008). PBM will vary depending on the chemistry of the aerosol, the atmosphere, and GOM chemistry along with physical conditions of the atmosphere, such as temperature and relative humidity. PBM measurements will collect some GOM and will be impacted by the filter material, flow rate, and inlet configuration.

2.4 Passive samplers

Passive samplers may be biotic (i.e., mosses, lichens, plant leaves) or abiotic surfaces (membranes, water). Huang et al. (2014) recently reviewed passive sampling methods for atmospheric Hg.

2.4.1 Total gaseous mercury

The method developed by W. Zhang et al. (2012) used an abiotic passive sampler with sulfate-impregnated carbon contained in an axial sampler. Activated carbon was investigated as a sampling material for Hg by Lindberg and Turner (1977), Lindberg et al. (1979), and Lindberg (1980). Other materials that have been applied include silver wires, gold-coated plates, and gold plugs (Gustin et al., 2011; Skov et al., 2007; Huang et al., 2014). Sulfate-impregnated carbon is effective because it retains atmospheric Hg, has a high sorption capacity, and will not become passivated over time (cf. Huang et al., 2014). This sampler is best applied for Hg measurements across significant concentration gradients (e.g., urban to rural). The sampler would need to be deployed for more than 90 days at a remote site. It is not known whether it measures TGM or GEM.

2.4.2 Gaseous oxidized Hg

There are currently two types of passive samplers for GOM. These include surrogate surfaces to measure dry deposition, and a measurement of diffusive uptake as a surrogate for concentration. The most widely adopted dry deposition method uses a cation exchange membrane in a down-facing aerodynamic sampler housing ("Aerohead sampler"; Lyman et al., 2007, 2009) and has been deployed in multiple studies (Castro et al., 2012; Sather et al., 2013, 2014; Peterson et al., 2012; Gustin et al., 2012; Wright et al., 2014b; Huang and Gustin, 2015b). Although there are limitations, such as measurement of only unidirectional flux, dry deposition models also apply a similar flux. Huang and Gustin (2015b) found that the surrogate surface better agreed with models when air concentrations measured by the box sampler and calibrated by the Tekran® system were adjusted by a factor of 3. The

box sampler designed by Lyman et al. (2010b) provides a means for calculating concentrations based on uptake rate. Recent work suggests the box sampler has significant wall loss (80 %) of GOM (Huang and Gustin, 2015b). Lack of calibration is a limitation for all passive samplers. The temporal resolution is coarse and samplers must be deployed for 1 to 2 weeks.

2.5 Calibration methods

One of the major outstanding issues is that the vast majority of GOM and PBM measurements are not calibrated (Jaffe et al., 2014). Calibration of GOM measurements has been done using manifold and chamber systems. Neither is automated or widely adopted. Coal fly ash is available as a standard for PBM, but calibrations have not been done. Laboratory chambers have been developed for calibrating and testing membranes and passive samplers (Gustin et al., 2011; Lyman et al., 2007, 2010b; Skov et al., 2007).

The UNR manifold calibration system is designed so specific Hg compounds can be added at different concentrations as well as O_3, water vapor, and other chemical compounds. A pyrolyzer at the inlet can be used to determine concentrations of Hg being permeated (Huang et al., 2013). The eight-port glass manifold allows for collection of GOM on KCl-coated denuders and different surfaces (Huang et al., 2013). A Tekran® 2537/1130 unit at the end of the manifold is used to measure GEM and GOM concentrations. Manifold calibrations have also been performed by the University of Washington in the laboratory (Finley et al., 2013; McClure et al., 2014) and field (RAMIX; Gustin et al., 2013; Finley et al., 2013). During the RAMIX campaign, transmission efficiencies of GEM and $HgBr_2$ were 92 and 76 %, respectively.

3 Evolution of our understanding of the limitations of speciated Hg measurements

3.1 Are we measuring TAM, TGM, or GEM?

Inlet configuration and local atmospheric chemistry will affect the measurement of TGM versus GEM. Limited work in dry air with uncovered lines (i.e., exposed to sunlight) indicated that the Tekran® 2537 measures TGM (see the Supplement). If GOM is able to pass through the inlet to the Tekran® 2537 and the gold traps are not passivated, the instrument will measure TGM (Gustin et al., 2013; Temme et al., 2002). Passivation of gold surfaces can occur (Barghigiani et al., 1991; Brosset and Iverfeldt, 1989; Gustin et al., 2011; Munthe et al., 1990; Xiao et al., 1991), and when this occurs these surfaces are no longer quantitatively collecting atmospheric Hg. Landis et al. (2002) mentioned passivation of gold traps periodically occurred right after analysis of a denuder, with recovery dropping to 50 %. To measure TAM requires the use of a pyrolyzer at the inlet to the sampling line to convert GOM + PBM to GEM. Field data suggest GOM can constitute up to 25 % of TGM in Nevada, Florida, and Maryland (see Sects. 2.3.1, 3.2.2, 4) and up to 100 % during depletion events in the Arctic (Steffen et al., 2014, 2015).

3.2 PBM measurements and potential artifacts

Relative to GOM and GEM, PBM measurements have received less systematic study. The Tekran® system is currently the most widely used configuration for measuring PBM. Other sampling methods tested include filter-based methods (Rutter et al., 2008; Talbot et al., 2011; Malcolm and Keeler, 2007; Kim et al., 2012). The sign and magnitude of the Tekran® measured PBM bias is presently unclear. Both high and low biases have been reported (Talbot et al., 2011; Rutter et al., 2008; Malcolm and Keeler, 2007; Gustin et al., 2013).

The particle size distribution of PBM is spatially heterogeneous and can include both fine and coarse fractions (Kim et al., 2012; Keeler et al., 1995; Malcolm and Keeler, 2007; Engle et al., 2008). The standard inlet on the Tekran® 2537/1130/1135 excludes particles larger than 2.5 μm (depending on the flow rate; Lyman et al., 2010) in diameter to prevent large particles from depositing on the KCl-coated denuder. Thus in coastal/marine, agricultural, or industrial settings with high concentrations of large particles, reported PBM concentrations represent a lower bound (Malcolm and Keeler, 2007; Kim et al., 2012; Poissant et al., 2005). Surrogate surfaces with cation exchange membranes may collect very small aerosol fractions by diffusion (Lyman et al., 2007; Huang and Gustin, 2015b).

Temperature and atmospheric composition potentially impact PBM measurements. The Tekran® 1135 particulate module is maintained at 50 °C to prevent condensation of water vapor. Based on filter experiments compared with Tekran® PBM, Rutter et al. (2008) suggested there is evaporative loss of PBM. Thermal desorption profiles using nylon membranes showed that Hg(II) compounds are emitted at temperatures ranging from 50 to 200 °C (Fig. 2), depending on charges on the collection surface and the polarizability of the different Hg compounds (Huang et al., 2013). Lynam and Keeler (2005) observed less PBM collected on quartz filters for 12 versus 4 h, and suggested a negative sampling artifact associated with relative humidity or reaction with gases in the air such as O_3.

Breakthrough of GOM from the upstream denuder can result in inadvertent retention of GOM on the PBM collection surface resulting in biased high PBM measurement. In principal, the Tekran® 2537/1130/1135 removes GOM on the KCl-coated annual denuder and then PBM is collected downstream. Field data have shown that GOM compounds not collected by the KCl-coated denuder can be captured by the particulate unit (Gustin et al., 2013). Quartz fiber filters used to collect PBM may also collect GOM (Rutter et al., 2007; see the Supplement for detailed example). Lyman et al. (2007) compared calculated dry deposition fluxes associated with

coated (KCl) and uncoated quartz fiber filters against data collected using cation-exchange membranes, both yielded significantly lower deposition fluxes. GOM breakthrough may not occur in all cases. For example, if there are temperature drops within the instrument, then GOM will deposit to the walls (Gustin et al., 2013). Because of these issues, the authors conclude it is presently more robust to interpret RM rather than PBM and GOM data separately.

3.3 GOM: biases, interferences, and shedding light on the spatiotemporal variability of GOM compounds in air

Based on laboratory and field studies, concentrations of GOM collected on the nylon and cation exchange membranes are higher than those collected by the Tekran® system by 60–1000 % (Huang et al., 2014; Huang and Gustin, 2015a, b). Laboratory and field experiments have demonstrated the collection efficiency of KCl-coated denuders varies with environmental conditions (O_3, RH) and Hg(II) compounds present in air. Below we discuss recent laboratory experiments and field studies that have shaped our understanding of the limitations of GOM measurement methods.

3.3.1 Ozone and relative humidity interferences

Laboratory experiments have confirmed O_3 interferences for KCl-coated denuders and relative humidity interferences for both denuders and nylon membranes (Lyman et al., 2010a; McClure et al., 2014; Huang and Gustin, 2015b). Lyman et al. (2010a) found the collection efficiency of $HgCl_2$ loaded on a KCl denuder was reduced by 3 to 37 % when O_3 concentrations were 6 to 100 ppbv. Lyman et al. (2010a) proposed reduction was occurring on the denuder wall:

$$HgCl_2 + 2O_3 \rightarrow Hg^0 + 2O_2 + ClO. \quad (1)$$

Their results also indicated less GOM was recovered as O_3 exposure time increased (10 to 26 % removed from loaded denuders for 2.5 min and 29 to 55 % for 30 min at 30 ppbv).

In experiments similar to those performed for O_3, McClure et al. (2014) found RH had a similar effect on $HgBr_2$ loaded on KCl-coated denuders. Huang and Gustin (2015a) permeated $HgBr_2$ and water vapor into a Tekran® 2357/1130 system in ambient air and found collection efficiencies dropped during the spikes of RH, and the denuder became passivated over time.

They found the following at RH of 21 to 62 %:

$$\mathrm{RH} = 0.63\,\mathrm{GOM\ loss}\,\% + 18.1,\ r^2 = 0.49,\ p\ \mathrm{value} < 0.01. \quad (2)$$

Huang and Gustin (2015a) found a greater impact of relative humidity than O_3.

3.3.2 Variability of RM composition and concentrations

Here we use comparisons of data collected with a variety of sampling methods to better understand atmospheric Hg concentrations and how measurement discrepancies vary with environmental setting (e.g., RH and O_3) and Hg(II) compounds present in the ambient atmosphere. This includes data collected as part of a large study in Florida (Peterson et al., 2012; Gustin et al., 2012), the RAMIX field campaign (Gustin et al., 2013), recent comparison of KCl-coated denuder data with the UNR active system (Huang et al., 2013, 2015), and laboratory testing (Huang et al., 2013; Huang and Gustin, 2015a, b). For a historical review of additional literature see the Supplement in Gustin et al. (2013), Huang et al. (2014), and this paper.

Peterson et al. (2012) compared passive samplers and Tekran® data from three sites in Florida. The region has high Hg wet deposition but low GOM concentrations (on average 2–8 pg m^{-3} as measured by the Tekran® system). In general, the Aerohead or dry deposition sampling system (described above), showed higher deposition for GOM than that calculated using KCl-coated denuder concentrations and a dry deposition model. Based on passive sampler uptake and calculated deposition velocities, Peterson et al. (2012) suggested the difference could be explained by the presence of different GOM compounds in the air (see the Supplement for additional detail). Examining the data across all seasons, using three Hg measurement methods, criteria pollutants, and meteorology, Gustin et al. (2012) concluded there were different GOM compounds in air that were derived from different primary sources, sources producing different oxidants, and variation across season.

Data from the RAMIX experiment also indicated the KCl-denuder measurements were biased low through spikes of GOM ($HgBr_2$) into a manifold. Ambient air RM concentrations measured by the DOGHS were higher than those measured by the Tekran® system and this instrument recovered 66 % of the $HgBr_2$ spike during RAMIX (Gustin et al., 2013). The experiment also indicated RH caused the denuders to become passivated over time (Gustin et al., 2013). Spike recoveries of $HgBr_2$ by KCl-coated denuders were 2 to 5 times lower than that measured by the DOGHS, with mean values for spikes ranging from 17 to 23 % recovery. Replicate nylon membranes collected 30 to 50 % more RM than the Tekran® system in ambient air. For a concise summary of the results of the RAMIX DOHGS versus Tekran® data and an explanation for a component of the atmospheric chemistry occurring see the Supplement.

Figure 1 and Table 2 show correlations between specific GOM compounds concentrations measured by the nylon and cation exchange membranes versus the KCl-coated denuder in the Tekran® system (see Huang et al. (2013) for detail on the experimental setup). These data demonstrate different compounds have different collection efficiencies by the

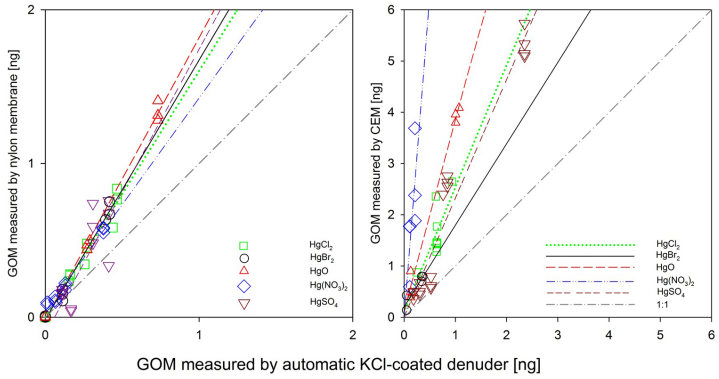

Figure 1. Correlation between GOM concentrations measured by KCl-coated denuder and the nylon and cation exchange membranes in activated charcoal-scrubbed air. Modified from Huang et al. (2013).

Table 2. Regression equations comparing nylon membrane and cation exchange membrane measured GOM concentrations to those measured by the denuder using the UNR laboratory manifold system and charcoal-scrubbed air.

	$HgCl_2$	$HgBr_2$	HgO	$Hg(NO_3)_2$	$HgSO_4$
Nylon membrane (y) KCl denuder (x)	$y = 1.6x + 0.002$ $r^2 = 0.97, n = 12$	$y = 1.7x + 0.01$ $r^2 = 0.99, n = 10$	$y = 1.8x + 0.02$ $r^2 = 0.99, n = 8$	$y = 1.4x + 0.04$ $r^2 = 0.90, n = 12$	$y = 1.9x - 0.1$ $r^2 = 0.6, n = 12$
Cation-exchange membrane (y) KCl denuder (x)	$y = 2.4x + 0.1$ $r^2 = 0.58, n = 9$	$y = 1.6x + 0.2$ $r^2 = 0.86, n = 5$	$y = 3.7x + 0.1$ $r^2 = 0.99, n = 6$	$y = 12.6x - 0.02$ $r^2 = 0.50, n = 6$	$y = 2.3x + 0.01$ $r^2 = 095, n = 18$

denuder. Figure 1 shows the nylon membrane has equal efficiency for all Hg(II) compounds tested, and the cation exchange membrane quantitatively collects the Hg(II) compounds permeated. The collection efficiency of the cation exchange membrane relative to the KCl-coated denuder in a Tekran® 1130 is $HgBr_2$ (1.6) > $HgSO_4$ (2.3) = $HgCl_2$ (2.4) > HgO (3.7) > $Hg(NO_3)_2$ (12.6).

Huang et al. (2013) compared field data collected using the Tekran® system and the UNR active system. Cation-exchange membranes measured concentrations were 1.1 to 3.7 times greater than the nylon membranes and 2 to 6 times greater than Tekran® RM values. Substantial spatial and temporal variability in the difference between the cation-exchange membrane and Tekran® RM values were observed. Thermal desorption profiles from the nylon membranes indicate this is explained by variability in the Hg(II) compounds present in air (Huang et al., 2013, 2015).

Data collected using the UNR Active System can be compared to KCl-coated denuder measurements in different areas and used for understanding the GOM concentrations and chemistry for different areas.

4 Case study demonstrating how we can use past measurements to move forward

In light of the new information about interferences affecting GOM measurements, we may begin to go back and re-examine features of past data that previously could not be explained. Here we explore Weiss-Penzias et al. (2003) as a case study. They measured GEM, GOM, and PBM at Cheeka Peak Observatory (Fig. 3), Washington, USA, in the marine boundary layer and found "air of continental origin containing anthropogenic pollutants contained on average 5.3 % lower GEM levels as compared with the marine boundary". GOM and PBM concentrations in continental air were very low, 0–20 and 1–4 pg m^{-3}, respectively. At the time, the results were "difficult to reconcile". Now we see that the change in GEM concentrations during local anthropogenic pollution events relative to the mean of monthly marine air (−60 to −270 pg m^{-3}) in Weiss-Penzias et al. (2003) are similar to the disparity in concentrations measured during RAMIX between the DOHGS and Tekran® RM measurement.

Retrospectively, we suggest the observed differences between the two air masses reported can be explained by dif-

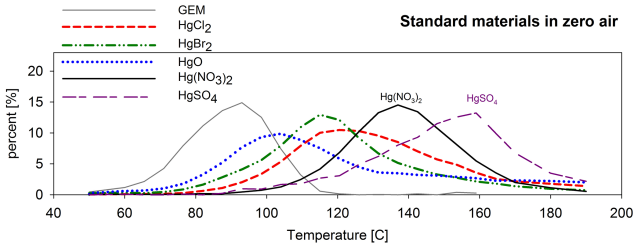

Figure 2. Thermal desorption profiles generated by permeating different Hg compounds. Modified from Huang et al. (2013). Percent indicates the amount released relative to the total. Profiles were developed in activated charcoal-scrubbed air. Compounds being permeated may not be the exact compound in the permeation tube, and this needs to be verified.

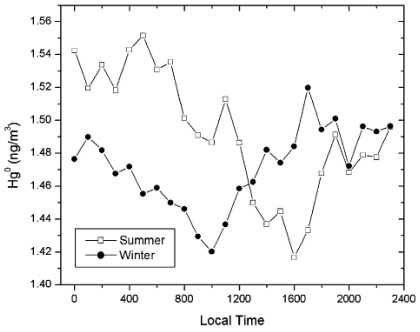

Figure 3. Figure 7 from Weiss-Penzias et al. (2003). Reprinted with permission from Weiss-Penzias et al. (2003), copyright: 1 September 2003 American Chemical Society.

ferences in the mix of oxidants and the resultant Hg(II) compounds formed. GOM and PBM were likely low due to lack of collection efficiency, interferences with O_3, and loss in the sampling line (see the Supplement for details of sampling set up). Significantly lower GEM concentrations in the continental air are indicative of greater oxidation, which is supported by decreases in GEM concentrations coincident with O_3 increases. Eastern Washington is covered by forests, which generate volatile organic compounds that could contribute to O_3 and GOM formation. The marine air masses likely contained $HgBr_2$ or $HgCl_2$, and the continental air Hg-O, Hg-S, and Hg-N compounds associated with industry, agriculture, and mobile sources. The capture efficiency of $HgBr_2$ and $HgCl_2$ is greater than for O, S, and N compounds (Fig. 1; Table 2). The case study exemplifies how we can use the loss of GEM as a means of understanding the amount of GOM present or produced in air.

5 Advancing understanding using Hg measurements and models

Here we discuss several key scientific advancements that have come from comparing models with speciated measurements, as well as the major questions left open by these studies. The number of atmospheric models capable of simulating speciated Hg has multiplied over the last decade (Table 3). Detailed discussion on model/measurement comparisons of RM can be found in Kos et al. (2013). Limitations and uncertainties of the models themselves have been written about at length in original research articles on model intercomparisons (Bullock et al., 2008; Pongprueksa et al., 2008; Lin et al., 2006). Fully acknowledging current limitations, there have still been huge strides made in our scientific understanding of the processes controlling GEM, GOM, and PBM cycling in the atmosphere including: marine boundary layer cycling, plume chemistry, source–receptor relationships, gas–particle partitioning, and vertical distribution.

Our understanding of speciated Hg cycling in the marine boundary layer (MBL) is one example of Hg science advancing as a result of using measurements and models in combination. GOM in the MBL has a diurnal pattern characterized by a midday peak and is depleted through deposition at night (Laurier and Mason, 2007; Laurier et al., 2003; Sprovieri et al., 2003). The use of observations and models together determined that the MBL has bromine photochemistry and was not affected by the hydroxyl (OH) radical. This drives the midday photochemical peak in GOM concentrations in the MBL and that scavenging by sea salt was driving rapid deposition at night (Holmes et al., 2009; Selin et al., 2007; Obrist et al., 2010; Hedgecock and Pirrone, 2001, 2004; Hedgecock et al., 2003; Jaffe et al., 2005; Laurier and Masson, 2007; Laurier et al., 2003; Sprovieri et al., 2003).

Model–observation comparisons consistently suggest models overestimate GOM surface concentrations, sometimes by as much as an order of magnitude (Amos et al., 2012; W. Zhang et al., 2012; Kos et al., 2013; Holloway et al., 2012; Bieser et al., 2014). The measurement–model mis-

Table 3. Atmospheric models with speciated mercury.

Model name	Domain	Type	Explicit or lumped Hg(II)	References
GRAHM	Global	3-D, Eulerian	Explicit ($HgCl_2$, HgO)	Dastoor and Larocque (2004); Ryaboshapko et al. (2007a, b); Dastoor et al. (2008); Durnford et al. (2010); Kos et al. (2013); Dastoor et al. (2014)
GEOS-Chem	Global*	3-D, Eulerian	Bulk Hg(II)	Selin et al. (2008); Selin and Jacob (2008); Holmes et al. (2010); Corbitt et al. (2011); Amos et al. (2012); Y. Zhang et al. (2012); Chen et al. (2014); Kikuchi et al. (2013)
CMAQ-Hg	Continental USA	3-D, Eulerian	Explicit ($HgCl_2$, HgO)	Bullock and Brehme (2002); Vijayaraghavan et al. (2008); Holloway et al. (2012); Bash et al. (2014)
GLEMOS	Variable, global to regional	3-D, Eulerian	Lumped	Travnikov and Ryaboshapko (2002, EMEP report); Travnikov (2010)
ECHMERIT	Global	3-D, Eulerian	$HgO_{(g)}$, $HgCl_{2(g)}$, lumped $Hg(II)_{(aq)}$	De Simone et al. (2014); Jung et al. (2009)
WRF-Chem	Regional	3-D, Eulerian	Lumped	Gencarellia et al. (2014)
MSCE-Hg-Hem	Northern Hemisphere	3-D, Eulerian	$HgO_{(g)}$, $HgCl_{2(g)}$, lumped $Hg(II)_{(aq)}$	Travnikov and Ryaboshapko (2002); Travnikov (2005); Travnikov and Ilyin (2009)
ADOM	North America, Europe	3-D, Eulerian	$HgO_{(g)}$, $HgCl_{2(g)}$, lumped $Hg(II)_{(aq)}$	Petersen et al. (2001)
DEHM	Northern Hemisphere	3-D, Eulerian	$HgO_{(g)}$, $HgCl_{2(g)}$, lumped $Hg(II)_{(aq)}$	Christensen et al. (2004); Skov et al. (2004, EST)
WoRM3	Global	2-D, multi-media	Lumped	Qureshi et al. (2011)
PHANTAS	Arctic	box model	Detailed, explicit Hg(II) compounds	Toyota et al. (2014)
HYSPLIT	Global	3-D, Lagrangian	$HgO_{(g)}$, $HgCl_{2(g)}$, lumped $Hg(II)_{(aq)}$	Cohen et al. (2004)
TEAM	North America	3-D, Eulerian	$HgO_{(g)}$, $HgCl_{2(g)}$, lumped $Hg(II)_{(aq)}$	Bullock et al. (2008, 2009)
CTM-Hg	Global	3-D, Eulerian	$HgO_{(g)}$, $HgCl_{2(g)}$, lumped $Hg(II)_{(aq)}$	Shia et al. (1999); Seigneur et al. (2001, 2003, 2004, 2006); Lohman et al. (2008)
REMSAD	North America	3-D, Eulerian	Explicit ($HgCl_2$, HgO)	Bullock et al. (2008, 2009)
EMAP	Europe	3-D, Eulerian	Lumped	Syrakov et al. (1995)

* The standard GEOS-Chem has a global domain with the option to have a nested high-resolution simulation over North America (Zhang et al., 2012).

match is now understood as being partly explained by a low sampling bias (see Sect. 3), but this alone cannot reconcile the discrepancy. Reduction of GOM to GEM in coal-fired power plant plumes (Edgerton et al., 2006; Lohman et al., 2006) has been invoked as a possible explanation (Amos et al., 2012; W. Zhang et al., 2012; Kos et al., 2013; Holloway et al., 2012; Vijayaraghavan et al., 2008). The mechanism for in-plume reduction (IPR) remains speculative, hindering inference about how in-plume reduction may vary with coal type, control technology, or atmospheric composition. Results from recent field and laboratory data have been mixed, providing evidence for and against IPR (Tong et al., 2014; Landis et al., 2015) (Deeds et al., 2013). The speciation of anthropogenic emission inventories is also being revisited in order to reconcile model–measurement RM mismatches (Wang et al., 2014; Bieser et al., 2014). Improving our understanding of IPR and emission speciation has important implications for the efficacy of domestic regulation such as the US EPA Mercury Air Toxics Standard and for potentially attributing trends in Hg wet deposition over the USA (Y. Zhang et al., 2012).

Derived source–receptor relationships will also be sensitive to uncertainties in IPR and emission speciation. On the whole, Hg models simulate wet deposition fluxes better than surface GOM concentrations, contributing to the relatively high degree of consensus among source–receptor studies. A comparison of source–receptor studies found models agreed within 10 % in terms of the attribution of total wet Hg deposition to a given continental region (e.g., Europe, Asia) (AMAP/UNEP, 2013; Travnikov et al., 2010). Several source–receptor studies have concluded domestic US emissions contribute $\sim$ 20 % to total Hg deposition over the contiguous USA (Selin and Jacob, 2008; Corbitt et al., 2011). W. Zhang et al. (2012) found that including IPR in a model decreased the domestic contribution to wet deposition over the USA from 22 to 10 %.

An additional area of measurement–model study has been gas–particle partitioning of GOM and PBM. Understanding gas–particle partitioning is important because gases and particles are removed from the atmosphere by different physical processes. There is observational and laboratory evidence that gas–particle partitioning between GOM and PBM is driven by air temperature and aerosol concentrations (Rutter and Schauer, 2007a, b; Steffen et al., 2014; Rutter et al., 2008; Amos et al., 2012; Chen et al., 2014). Implementing temperature-dependent gas–particle partitioning in a global model increased simulated annual Hg deposition at higher latitudes (Amos et al., 2012). Aircraft observations suggest

gas–particle partitioning also plays a major role in influencing the vertical profile of Hg, especially in the upper troposphere/lower stratosphere (Swartzendruber et al., 2009; Lyman and Jaffe, 2012; Murphy et al., 2006). Current gas–particle partitioning relationships are derived from surface data. PBM measurements from the summit of Mt. Bachelor suggest these relationships do not capture PBM dynamics aloft (Timonen et al., 2013). Effects of aerosol composition (Rutter and Schauer, 2007b), relative humidity, or even repartitioning of RM within the Tekran® (see Sect. 3.3) could potentially contribute to this deficiency.

Oxidation also plays a central role in Hg cycling at the upper troposphere/lower stratosphere boundary. Comparisons against vertical aircraft profiles of TGM consistently suggest there is too little oxidation in models in the lower stratosphere (W. Zhang et al., 2012; Holmes et al., 2010). Observations show that total Hg is depleted in the lower stratosphere (Holmes et al., 2010; Lyman and Jaffe, 2012; Slemr et al., 2014), which is thought to be the result of rapid oxidation of Hg(0) to Hg(II), partitioning of Hg(II) to sulfate aerosol, and subsequent sedimentation of PBM (Lyman and Jaffe, 2012). Aircraft measurements over Washington and Tennessee, USA, found summertime GOM peaks between 2 and 4 km (Swartzendruber et al., 2009; Brooks et al., 2014). Modeled GOM vertical profiles over the USA have a less pronounced peak and generally place it higher (4–6 km) (Bullock et al., 2008). Correctly modeling the vertical distribution of Hg, particularly GOM and PBM, is essential for simulating deposition and hence Hg loading to surface ecosystems.

Chemistry remains one of the greatest uncertainties in Hg models. Improving measurements to determine the chemistry can help determine the mechanism(s) at play. There is still a general lack of rate coefficients and corresponding step-by-step reaction mechanisms available. The estimated tropospheric lifetime of RM against deposition and reduction is 40 days (Holmes et al., 2010), but the reduction pathway is highly uncertain (Subir et al., 2011; Pongprueska et al., 2008), and the burden of RM in the free troposphere is uncertain by at least a factor of 2 (Selin et al., 2008; De Simone et al., 2014). Improving our knowledge of the reduction and oxidation rates in the atmosphere will allow models to better capture the vertical distribution of Hg and in turn better simulate Hg deposition. The recent AMAP/UNEP (2013) assessment identified this as the highest priority for Hg models due to the importance in the Hg exposure pathway.

A persistent issue is the ambiguity in comparing modeled Hg(II) compounds to GOM and PBM, which are operationally defined. Models either have a lumped Hg(II) tracer or explicitly resolve individual Hg(II) compounds (Table 3). Since different Hg(II) compounds have different collection efficiencies by the KCl coated denuder (Fig. 1), this further confounds how to best construct a GOM-like model quantity to compare against observations. An active dialogue between experimentalists and modelers is encouraged as the community moves forward, so modelers may implement Hg tracers that emulate the Hg compounds measured.

Recent papers have used a three-fold correction factor to adjust the GOM concentrations measured by the Tekran® system to calculate dry deposition using models in the western USA and Florida (cf. Huang and Gustin, 2015a; Huang et al., 2015). Use of this correction factor is based on the discrepancy between denuder measurements in the field and cation exchange membranes dry deposition measurements and concentrations collected using the UNR active system. Weiss-Penzias et al. (2015) found the GEOS-Chem model overestimated RM/GEM by a factor of 2.8 compared to Tekran® RM/GEM, which is roughly in line with this correction factor. These field observations were collected in dry and humid conditions and at O_3 concentrations typically observed in the atmosphere. Additional consideration could be based on the RH and O_3 concentrations and the potential GOM compounds in the air.

6 Outstanding issues

Mercury is present in the atmosphere at pg m^{-3} to ng m^{-3}, and the capability to measure it is a substantial analytical accomplishment. Ongoing measurements of atmospheric Hg will be key in evaluating the environmental benefit of regulation on behalf of the Minimata Convention.

Here we reviewed the current state of the science for measuring and modeling atmospheric Hg concentrations. Recent laboratory and field investigations have shown numerous artifacts and environmental interferences can affect measurement methods. Some environments such as those with low humidity and O_3 may be less susceptible to sampling interferences than others. In light of new information about the limitations of sampling methods, we may revisit and better explain certain features of previous data sets and measurement–model comparison.

Fundamental research is needed on measurement methods and the atmospheric chemistry of Hg. We need to obtain agreement between several methods for understanding the chemical forms and compounds in the air. Only through comparison of multiple calibrated measurements can results be determined to be accurate.

Identifying the chemical compounds of RM in the atmosphere is a top priority. Understanding the final oxidation products are key for resolving questions regarding Hg chemistry. Knowing the dominant compounds would help with the design of measurement methods and determination of deposition velocities. Thermal desorption shows promise and mass spectrometry may be a way to verify compounds.

Development of a standard, field-deployable calibration system is needed. This system should provide spikes into ambient air and allow for studying sampling efficiencies and artifacts associated with ambient air. Lack of calibration is currently a major shortcoming.

A pyrolyzer should be used at the inlet of the 2537 if the goal is to measure TAM. The way the Tekran® 1130/1135 system is configured to capture GOM first and then PBM is the best method to measure these two compounds. However, given the difficulty of separating GOM from PBM, we recommend interpreting the sum of RM instead of PBM alone until separation is improved.

A measurement system that collects GOM on a denuder material demonstrated to work for all compounds of GOM, and a separate measurement on a filter using a cation-exchange membrane could be used for measurement of GOM and RM. Then PBM could be determined by difference. Due to negative artifacts during long sampling times measurements should be done for < 24 h.

A new passive sampler design is needed that quantitatively determines concentrations and is calibrated. Use of a computational fluid dynamics model to help design the sampler could be one successful way forward. Passive samplers and surrogate surfaces have longer time resolution (1 day to weeks), but are relatively inexpensive and easy to operate and could provide an alternative measure of GOM concentrations and dry deposition fluxes in large-scale sampling networks once the above issues are resolved.

The Supplement related to this article is available online at doi:10.5194/acp-15-5697-2015-supplement.

Acknowledgements. This manuscript was initiated by discussions at the "Data Collection, Analysis and Application of Speciated Atmospheric Mercury" workshop coordinated by Leiming Zhang and held on 29 July 2014 in San Francisco, California. Work at UNR was supported by the National Science Foundation (Awards: 0850545, 0917934, 1102336, 1326074), the Electric Power Research Institute, and The Southern Company. We thank Dan Jaffe and Steve Lindberg for comments on an early version of this manuscript. We thank Franz Slemr for his extensive review and constructive comments, two anonymous reviewers for their comments, and Tony Hynes for providing information on his instrument that has now been included in the paper. M. S. Gustin thanks all the undergraduate students who clean glassware and process and analyze samples in the lab, for this work could not have been done without their conscientious efforts, and Michael Gustin for his continued support.

Edited by: L. Zhang

References

Aas, W. (Ed.).: Data quality 2004, quality assurance, and field comparisons, C587 EMEP/CCC-Report 4/2006, NILU, Kjeller, Norway 2006.

AMAP/UNEP: Technical Background Report for the Global Mercury Assessment 2013., Arctic Monitoring and Assessment Program, Oslo, Norway / UNEP Chemicals Branch, Geneva, Switzerland, VI, 263 pp., http://www.unep.org/PDF/PressReleases/GlobalMercuryAssessment2013.pdf (last access: 20 May 2015), 2013.

Ambrose, J. L., Lyman, S. N., Huang, J., Gustin, M., and Jaffe, D. A.: Fast Time Resolution Oxidized Mercury Measurements with the UW Detector for Oxidized Hg Species (DOHGS) during the Reno Atmospheric Mercury Intercomparison Experiment, Environ. Sci. Technol., 47, 7285–7294, 2013.

Amos, H. M., Jacob, D. J., Holmes, C. D., Fisher, J. A., Wang, Q., Yantosca, R. M., Corbitt, E. S., Galarneau, E., Rutter, A. P., Gustin, M. S., Steffen, A., Schauer, J. J., Graydon, J. A., St Louis, V. L., Talbot, R. W., Edgerton, E. S., Zhang, Y., and Sunderland, E. M.: Gas-particle partitioning of atmospheric Hg(II) and its effect on global mercury deposition, Atmos. Chem. Phys., 12, 591–603, doi:10.5194/acp-12-591-2012, 2012.

Barghigiani, C., Ristori, T., and Cortopassi, M.: Air mercury measurement and interference of atmospheric contaminants with gold traps, Environ. Technol., 12, 935–941, 1991.

Bash, J. O., Carlton, A. G., Hutzell, W. T., and Bullock, O. R.: Regional Air Quality Model Application of the Aqueous-Phase Photo Reduction of Atmospheric Oxidized Mercury by Dicarboxylic Acids, Atmosphere, 5, 1–15, doi:10.3390/atmos5010001, 2014.

Bauer, D., Campuzano-Jost, P., and Hynes, A. J.: Rapid, ultrasensitive detection of gas phase elemental mercury under atmospheric conditions using sequential two-photon laser induced fluorescence, Environ. Monit., 4, 339–343, 2002.

Bauer, D., Swartzendruber, P. C., and Hynes, A. J.: Deployment of a compact sequential 2 Photon LIF detection system for gaseous elemental mercury at ambient levels, Geochim. Cosmochim. Ac., 74, A60–A60, 2010.

Bauer, D., Everhart, S., Remeika, J., Tatum Ernest, C., and Hynes, A. J.: Deployment of a Sequential Two-Photon Laser Induced Fluorescence Sensor for the Detection of Gaseous Elemental Mercury at Ambient Levels: Fast, Specific, Ultrasensitive Detection with Parts-Per-Quadrillion Sensitivity, Atmos. Meas. Tech., 7, 4251–4265, doi:10.5194/amt-7-4251-2014, 2014.

Bieser, J., De Simone, F., Gencarelli, C., Geyer, B., Hedgecock, I., Matthias, V., Travnikov, O., and Weigelt, A.: A diagnostic evaluation of modeled mercury wet depositions in Europe using atmospheric speciated high-resolution observations, Environ. Sci. Pollut. Res., 21, 9995–10012, doi:10.1007/s11356-014-2863-2, 2014.

Brosset, C. and Iverfeldt, A.: Interaction of solid gold surfaces with mercury in ambient air, Water Air Soil Poll., 43, 147–168, 1989.

Brooks, S., Ren, X., Cohen, M., Luke, W., Kelley, P., Artz, R., Hynes, A., Landing, W., and Martos, B.: Airborne Vertical Profiling of Mercury Speciation near Tullahoma, TN, USA, Atmosphere, 5, 557–574, 2014.

Bullock Jr., O. R. and Brehme, K. A.: Atmospheric mercury simulation using the CMAQ model: formulation description and anal-

ysis of wet deposition results, Atmos. Environ., 36, 2135–2146, doi:10.1016/S1352-2310(02)00220-0, 2002.

Bullock, O. R., Atkinson, D., Braverman, T., Civerolo, K., Dastoor, A., Davignon, D., Ku, J. Y., Lohman, K., Myers, T. C., Park, R. J., Seigneur, C., Selin, N. E., Sistla, G., and Vijayaraghavan, K.: The North American Mercury Model Intercomparison Study (NAMMIS): Study description and model-to-model comparisons, J. Geophys. Res.-Atmos., 113, D17310, doi:10.1029/2008JD009803, 2008.

Bullock, O. R., Atkinson, D., Braverman, T., Civerolo, K., Dastoor, A., Davignon, D., Ku, J. Y., Lohman, K., Myers, T. C., Park, R. J., Seigneur, C., Selin, N. E., Sistla, G., and Vijayaraghavan, K.: An analysis of simulated wet deposition of mercury from the North American Mercury Model Intercomparison Study, J. Geophys. Res.-Atmos., 114, doi:10.1029/2008JD011224, 2009.

Castro, M. S., Moore, C., Sherwell, J., and Brooks, S. B.: Dry deposition of gaseous oxidized mercury in Western Maryland, Sci. Total Environ., 417, 232–240, 2012.

Chen, L., Wang, H. H., Liu, J. F., Tong, Y. D., Ou, L. B., Zhang, W., Hu, D., Chen, C., and Wang, X. J.: Intercontinental transport and deposition patterns of atmospheric mercury from anthropogenic emissions, Atmos. Chem. Phys., 14, 10163–10176, doi:10.5194/acp-14-10163-2014, 2014

Christensen, J. H., Brandt, J., Frohn, L. M., and Skov, H.: Modelling of Mercury in the Arctic with the Danish Eulerian Hemispheric Model, Atmos. Chem. Phys., 4, 2251–2257, doi:10.5194/acp-4-2251-2004, 2004.

Cohen, M., Artz, R., Draxler, R., Miller, P., Poissant, L., Niemi, D., Ratte, D., Deslauriers, M., Duval, R., Laurin, R., Slotnick, J., Nettesheim, T., and McDonald, J.: Modeling the atmospheric transport and deposition of mercury to the Great Lakes, Environ. Res., 95, 247–265, doi:10.1016/j.envres.2003.11.007, 2004.

Cole, A. S. and Steffen, A.: Trends in long-term gaseous mercury observations in the Arctic and effects of temperature and other atmospheric conditions, Atmos. Chem. Phys., 10, 4661–4672, doi:10.5194/acp-10-4661-2010, 2010.

Cole, A. S., Steffen, A., Eckley, C. S., Narayan, J., Pilote, M., Tordon, R., Graydon, J. A., St Louis, V. L., Xu, X., and Branfireun, B. A.: A Survey of Mercury in Air and Precipitation across Canada: Patterns and Trends, Atmosphere, 5, 635–668, 2014.

Corbitt, E. S., Jacob, D. J., Holmes, C. D., Streets, D. G., and Sunderland, E. M.: Global Source–Receptor Relationships for Mercury Deposition Under Present-Day and 2050 Emissions Scenarios, Environ. Sci. Technol., 45, 10477–10484, doi:10.1021/es202496y, 2011.

Dastoor, A. P. and Larocque, Y.: Global circulation of atmospheric mercury: a modelling study. Atmos. Environ., 38, 147–161, 2004.

Dastoor, A. P., and Durnford, D. A.: Arctic Ocean: Is It a Sink or a Source of Atmospheric Mercury?, Environ. Sci. Technol., 48, 1707–1717, doi:10.1021/es404473e, 2014.

Dastoor, A. P., Davignon, D., Theys, N., Van Roozendael, M., Steffen, A., and Ariya, P. A.: Modeling Dynamic Exchange of Gaseous Elemental Mercury at Polar Sunrise, Environ. Sci. Technol., 42, 5183–5188, 2008.

Deeds, D. A., Banic, C. M., Lu, J., and Daggupaty, S.: Mercury speciation in a coal-fired power plant plume: An aircraft-based study of emissions from the 3640 MW Nanticoke Generating Station, Ontario, Canada, Geophys. Res.-Atmos., 118, 4919–4935, 2013.

De Simone, F., Gencarelli, C. N., Hedgecock, I. M., and Pirrone, N.: Global atmospheric cycle of mercury: a model study on the impact of oxidation mechanisms, Environ. Sci. Poll. Res., 21, 4110–4123, doi:10.1007/s11356-013-2451-x, 2014.

Durnford, D., Dastoor, A., Figueras-Nieto, D., and Ryjkov, A.: Long range transport of mercury to the Arctic and across Canada, Atmos. Chem. Phys., 10, 6063–6086, doi:10.5194/acp-10-6063-2010, 2010.

Ebinghaus, R., Jennings, S. G., Schroeder, W. H., Berg, T., Donaghy, T., Guentzel, J., Kenny, C., Kock, H. H., Kvietkus, K., Landing, W., Mühleck, T., Munthe, J., Prestbo, E. M., Schneeberger, D., Slemr, F., Sommar, J., Urba, A., Wallschläger, D., and Xiao, Z.: International field intercomparison measurements of atmospheric mercury species at Mace Head, Ireland, Atmos. Environ., 33, 3063–3073, 1999.

Edgerton, E. S., Hartsell, B. E., and Jansen, J. J.: Mercury Speciation in Coal-fired Power Plant Plumes Observed at Three Surface Sites in the Southeastern U.S., Environ. Sci. Technol., 40, 4563–4570, doi:10.1021/es0515607, 2006.

Engle, M. A., Tate, M. T., Krabbenhoft, D. P., Kolker, A., Olson, M. L., Edgerton, E. S., DeWild, J. F., and McPherson, A. K.: Characterization and cycling of atmospheric mercury along the central US Gulf Coast, Appl. Geochem., 23, 419–437, 2008.

Engstrom, D. R., Fitzgerald, W. F., Cooke, C. A., Lamborg, C. H., Drevnick, P. E., Swain, E. B., Balogh, S. J., and Balcom, P. H.: Atmospheric Hg Emissions from Preindustrial Gold and Silver Extraction in the Americas: A Reevaluation from Lake-Sediment Archives, Environ. Sci. Technol., 48, 6533–6543, 2014.

EPA Method 1631: http://water.epa.gov/scitech/methods/cwa/metals/mercury/index.cfm, last access: 27 December 2014.

Faïn, X., Moosmüller, H., and Obrist, D.: Toward real-time measurement of atmospheric mercury concentrations using cavity ring-down spectroscopy, Atmos. Chem. Phys., 10, 2879–2892, doi:10.5194/acp-10-2879-2010, 2010.

Finley, B. D., Jaffe, D. A., Call, K., Lyman, S., Gustin, M. S., Peterson, C., Miller, M., and Lyman, T.: Development, Testing, And Deployment of an Air Sampling Manifold for Spiking Elemental and Oxidized Mercury During the Reno Atmospheric Mercury Intercomparison Experiment (RAMIX), Environ. Sci. Technol., 47, 7277–7284, 2013.

Gay, D. A., Schmeltz, D., Prestbo, E., Olson, M., Sharac, T., and Tordon, R.: The Atmospheric Mercury Network: measurement and initial examination of an ongoing atmospheric mercury record across North America, Atmos. Chem. Phys., 13, 11339–11349, doi:10.5194/acp-13-11339-2013, 2013.

Gustin, M. and Jaffe, D.: Reducing the Uncertainty in Measurement and Understanding of Mercury in the Atmosphere, Environ. Sci. Technol., 44, 2222–2227, 2010.

Gustin, M. S. and Lindberg, S. E.: Assessing the contribution of natural sources to the global mercury cycle: The importance of intercomparing dynamic flux measurements, Fresen. J. Anal. Chem., 366, 417–422, 2000.

Gustin, M. S., Lyman, S. N., Kilner, P., and Prestbo, E.: Development of a passive sampler for gaseous mercury, Atmos. Environ., 45, 5805–5812, 2011.

Gustin, M. S., Weiss-Penzias, P. S., and Peterson, C.: Investigating sources of gaseous oxidized mercury in dry deposition at three sites across Florida, USA, Atmos. Chem. Phys., 12, 9201–9219, doi:10.5194/acp-12-9201-2012, 2012.

Gustin, M. S., Huang, J., Miller, M. B., Peterson, C., Jaffe, D. A., Ambrose, J., Finley, B. D., Lyman, S. N., Call, K., Talbot, R., Feddersen, D., Mao, H., and Lindberg, S. E.: Do We Understand What the Mercury Speciation Instruments Are Actually Measuring? Results of RAMIX, Environ. Sci. Technol., 47, 7295–7306, 2013.

Hedgecock, I. M. and Pirrone, N.: Mercury and photochemistry in the marine boundary layer-modeling studies suggest the in situ production of reactive gas phase mercury, Atmos. Environ., 35, 3055–3062, doi:10.1016/s1352-2310(01)00109-1, 2001.

Hedgecock, I. M. and Pirrone, N.: Chasing quicksilver: Modeling the atmospheric lifetime of Hg-(g)(0) in the marine boundary layer at various latitudes, Environ. Sci. Technol., 38, 69–76, doi:10.1021/es034623z, 2004.

Hedgecock, I. M., Pirrone, N., Sprovieri, F., and Pesenti, E.: Reactive gaseous mercury in the marine boundary layer: modelling and experimental evidence of its formation in the Mediterranean region, Atmos. Environ., 37, S41–S49, doi:10.1016/s1352-2310(03)00236-x, 2003.

Holloway, T., Voigt, C., Morton, J., Spak, S. N., Rutter, A. P., and Schauer, J. J.: An assessment of atmospheric mercury in the Community Multiscale Air Quality (CMAQ) model at an urban site and a rural site in the Great Lakes Region of North America, Atmos. Chem. Phys., 12, 7117–7133, doi:10.5194/acp-12-7117-2012, 2012.

Holmes, C. D., Jacob, D. J., Mason, R. P., and Jaffe, D. A.: Sources and deposition of reactive gaseous mercury in the marine atmosphere, Atmos. Environ., 43, 2278–2285, doi:10.1016/j.atmosenv.2009.01.051, 2009.

Holmes, C. D., Jacob, D. J., Corbitt, E. S., Mao, J., Yang, X., Talbot, R., Slemr, F.: Global atmospheric model for mercury including oxidation by bromine atoms, Atmos. Chem. Phys., 10, 12037–12057, 2010, http://www.atmos-chem-phys.net/10/12037/2010/.

Huang, J. and Gustin, M. S.: Impacts of relative humidity on GOM measurements, Environ. Sci. Technol., 49, 6102–6108, doi:10.1021/acs.est.5b00098, 2015a.

Huang, J. and Gustin, M. S.: Use of passive sampling methods and models to understand sources of mercury deposition to high elevation sites in the Western United States, Environ. Sci. Technol., 49, 432–441, doi:10.1021/es502836w, 2015b.

Huang, J. Y., Miller, M. B., Weiss-Penzias, P., and Gustin, M. S.: Comparison of Gaseous Oxidized Hg Measured by KCl-Coated Denuders, and Nylon and Cation Exchange Membranes, Environ. Sci. Technol., 47, 7307–7316, 2013.

Huang, J. Y., Lyman, S. N., Hartman, J. S., and Gustin, M. S.: A review of passive sampling systems for ambient air mercury measurements, Environ. Sci.-Proc. Imp., 16, 374–392, 2014.

Huang, J., Miller, M. B., Edgerton, E., and Gustin, M. S.: Use of Criteria Pollutants, Active and Passive Mercury Sampling, and Receptor Modeling to Understanding the Chemical Forms of Gaseous Oxidized Mercury in Florida, Atmos. Chem. Phys. Discuss., 15, 12069–12105, doi:10.5194/acpd-15-12069-2015, 2015.

Jaffe, D., Prestbo, E., Swartzendruber, P., Weiss-Penzias, P., Kato, S., Takami, A., Hatakeyama, S., and Kajii, Y.: Export of atmospheric mercury from Asia, Atmos. Environ., 39, 3029–3038, doi:10.1016/j.atmosenv.2005.01.030, 2005.

Jaffe, D. A., Lyman, S., Amos, H. M., Gustin, M. S., Huang, J., Selin, N. E., Levin, L., ter Schure, A., Mason, R. P., Talbot, R., Rutter, A., Finley, B., Jaeglé, L., Shah, V., McClure, C., Ambrose, J., Gratz, L., Lindberg, S., Weiss-Penzias, P., Sheu, G.-R., Feddersen, D., Horvat, M., Dastoor, A., Hynes, A. J., Mao, H., Sonke, J. E., Slemr, F., Fisher, J. A., Ebinghaus, R., Zhang, Y., and Edwards, G.: Progress on Understanding Atmospheric Mercury Hampered by Uncertain Measurements, Environ. Sci. Technol., 48, 7204–7206, doi:10.1021/es5026432, 2014.

Keeler, G., Glinsorn, G., and Pirrone, N.: Particulate mercury in the atmosphere: Its significance, transport, transformation and sources, Water Air Soil Poll., 80, 159–168, 1995.

Kikuchi, T., Ikemoto, H., Takahashi, K., Hasome, H., and Ueda, H.: Parameterizing Soil Emission and Atmospheric Oxidation-Reduction in a Model of the Global Biogeochemical Cycle of Mercury, Environ. Sci. Technol., 47, 12266–12274, doi:10.1021/es401105h, 2014.

Kim, P.-R., Han, Y.-J., Holsen, T. M., and Yi, S.-M.: Atmospheric particulate mercury: Concentrations and size distributions, Atmos. Environ., 61, 94–102, 2012.

Kos, G., Ryzhkov, A., Dastoor, A., Narayan, J., Steffen, A., Ariya, P. A., and Zhang, L.: Evaluation of discrepancy between measured and modelled oxidized mercury species, Atmos. Chem. Phys., 13, 4839–4863, doi:10.5194/acp-13-4839-2013, 2013.

Landis, M. S., Stevens, R. K., Schaedlich, F., and Prestbo, E. M.: Development and characterization of an annular denuder methodology for the measurement of divalent inorganic reactive gaseous mercury in ambient air, Environ. Sci. Technol., 36, 3000–3009, 2002.

Landis, M. S., Ryan, J. F., Arnout, F. H., Schure, T., and Laudal, D.: The Behavior of Mercury Emissions from a Commercial Coal-Fired Power Plant: The Relationship Between Stack Speciation and Near-Field Plume Measurements, Environ. Sci. Technol., 48, 13540–13548, 2015.

Laurier, F. J. G. and Mason, R. P.: Mercury concentration and speciation in the coastal and open ocean boundary layer, J. Geophys. Res., 112, D06302, doi:10.1029/2006JD007320, 2007.

Laurier, F. J. G., Mason, R. P., Whalin, L., and Kato, S.: Reactive gaseous mercury formation in the North Pacific Ocean's marine boundary layer: A potential role of halogen chemistry, J. Geophys. Res., 108, 4529, doi:10.1029/2003JD003625, 2003.

Lin, C.-J., Pongprueksa, P., Lindberg, S. E., Pehkonen, S. O., Byun, D., and Jang, C.: Scientific uncertainties in atmospheric mercury models I: Model science evaluation, Atmos. Environ., 40, 2911–2928, 2006.

Lindberg, S. E.: Mercury partitioning in a power plant plume and its influence on atmospheric removal mechanisms, Atmos. Environ., 14, 227–231, 1980.

Lindberg, S. E. and Stratton, W. J.: Atmospheric mercury speciation: Concentrations and behavior of reactive gaseous mercury in ambient air, Environ. Sci. Technol., 32, 49–57, 1998.

Lindberg, S. E. and Turner, R. R.: Mercury emissions from chlorine production solid waste deposits, Nature, 268, 133–136, 1977.

Lindberg, S. E., Jackson, D. R., Huckabee, J. W., Janzen, S. A., Levin, M. J., and Lund, J. R.: Atmospheric emission and plant uptake of mercury from agricultural soils near the Almaden mercury mine, J. Environ. Qual., 8, 572–578, 1979.

Lindberg, S. E., Stratton, W. J., Pai, P., and Allan, M. A.: Measurements and modeling of a water soluble gas-phase mercury

species in ambient air, Fuel Process. Technol., 65, 143–156, 2000.

Lindberg, S. E., Bullock, R., Ebinghaus, R., Engstrom, D., Feng, X., FItzgerald, W., Pirrone, N., Prestbo, E., and Seigneur, C.: A synthesis of progress and uncertainties in attributing the sources of mercury in deposition, AMBIO, 36, 19–32, 2007.

Lohman, K., Seigneur, C., Edgerton, E., and Jansen, J.: Modeling mercury in power plant plumes, Environ. Sci. Technol., 40, 3848–3854, doi:10.1021/es051556v, 2006.

Lyman, S. N. and Jaffe, D. A.: Formation and fate of oxidized mercury in the upper troposphere and lower stratosphere, Nat. Geosci., 5, 114–117, doi:10.1038/ngeo1353, 2012.

Lyman, S. N., Jaffe, D. A., and Gustin, M. S.: Release of mercury halides from KCl denuders in the presence of ozone, Atmos. Chem. Phys., 10, 8197–8204, doi:10.5194/acp-10-8197-2010, 2010a.

Lyman, S. N., Gustin, M. S., and Prestbo, E. M.: A passive sampler for ambient gaseous oxidized mercury concentrations, Atmos. Environ., 44, 246–252, 2010b.

Lyman, S. N., Gustin, M. S., Prestbo, E. M., Kilner, P. I., Edgerton, E., and Hartsell, B.: Testing and Application of Surrogate Surfaces for Understanding Potential Gaseous Oxidized Mercury Dry Deposition, Environ. Sci. Technol., 43, 6235–6241, 2009.

Lyman, S. N., Gustin, M. S., Prestbo, E. M., and Marsik, F. J.: Estimation of dry deposition of atmospheric mercury in Nevada by direct and indirect methods, Environ. Sci. Technol., 41, 1970–1976, 2007.

Lyman, S. N. and Jaffe, D. A.: Formation and fate of oxidized mercury in the upper troposphere and lower stratosphere, Nat. Geosci., 5, 114–117, 2012.

Lynam, M. M. and Keeler, G. J.: Artifacts associated with the measurement of particulate mercury in an urban environment: The influence of elevated ozone concentrations, Atmos. Environ., 39, 3081–3088, 2005.

Malcolm, E. G. and Keeler, G. J.: Evidence for a sampling artifact for particulate-phase mercury in the marine atmosphere, Atmos. Environ., 41, 3352–3359, 2007.

McClure, C. D., Jaffe, D. A., and Edgerton, E. S.: Evaluation of the KCl Denuder Method for Gaseous Oxidized Mercury using HgBr2 at an In-Service AMNet Site, Environ. Sci. Technol., 48, 11437–11444, 2014.

Munthe, J., Schroeder, W. H., Xiao, Z., and Lindqvist, O.: Removal of gaseous mercury from air using a gold coated denuder, Atmos. Environ., 24, 2271–2274, 1990.

Murphy, D. M., Hudson, P. K., Thomson, D. S., Sheridan, P. J., and Wilson, J. C.: Observations of mercury-containing aerosols, Environ. Sci. Technol., 40, 316–3167, doi:10.1021/es052385x, 2006.

Obrist, D., Faïn, X., and Berger, C.: Gaseous elemental mercury emissions and CO_2 respiration rates in terrestrial soils under controlled aerobic and anaerobic laboratory conditions, Sci. Total Environ., 408, 1691–1700, doi:10.1016/j.scitotenv.2009.12.008, 2010.

Petersen, G., Bloxam, R., Wong, S., Munthe, J., Kruger, O., Schmolke, S. R., and Kumar, A. V.: A comprehensive Eulerian modelling framework for airborne mercury species: model development and applications in Europe, Atmos. Environ., 35, 3063–3074, doi:10.1016/s1352-2310(01)00110-8, 2001.

Peterson, C., Alishahi, M., and Gustin, M. S.: Testing the use of passive sampling systems for understanding air mercury concentrations and dry deposition across Florida, USA, Sci. Total Environ., 424, 297–307, 2012.

Pierce, A., Obrist, D., Moosmüller, H., Faïn, X., and Moore, C.: Cavity ring-down spectroscopy sensor development for high-time-resolution measurements of gaseous elemental mercury in ambient air, Atmos. Meas. Tech., 6, 1477–1489, doi:10.5194/amt-6-1477-2013, 2013.

Pirrone, N., Aas, W., Cinnirella, S., Ebinghaus, R., Hedgecock, I. M., Pacyna, J., Sprovieri, F., and Sunderland, E. M.: Toward the next generation of air quality monitoring: Mercury, Atmos. Environ., 80, 599–611, 2013.

Poissant, L., Pilote, M., Beauvais, C., Constant, P., and Zhang, H. H.: A year of continuous measurements of three atmospheric mercury species (GEM, RGM and Hg-p) in southern Quebec, Canada, Atmos. Environ., 39, 1275–1287, 2005.

Pongprueksa, P., Lin, C. J., Lindberg, S. E., Jang, C., Braverman, T., Bullock, O. R., Ho, T. C., and Chu, H. W.: Scientific uncertainties in atmospheric mercury models III: Boundary and initial conditions, model grid resolution, and Hg(II) reduction mechanism, Atmos. Environ., 42, 1828–1845, doi:10.1016/j.atmosenv.2007.11.020, 2008.

Qureshi, A., MacLeod, M., and Hungerbuhler, K.: Quantifying uncertainties in the global mass balance of mercury, Global Biogeochem. Cy., 25, GB4012, Gb4012, doi:10.1029/2011GB004068, 2011.

Ryaboshapko, A., Bullock Jr, O. R., Christensen, J., Cohen, M., Dastoor, A., Ilyin, I., Petersen, G., Syrakov, D., Artz, R. S., Davignon, D., Draxler, R. R., and Munthe, J.: Intercomparison study of atmospheric mercury models: 1. Comparison of models with short-term measurements, Sci. Total Environ., 376, 228–240, 2007a.

Ryaboshapko, A., Bullock Jr, O. R., Christensen, J., Cohen, M., Dastoor, A., Ilyin, I., Petersen, G., Syrakov, D., Travnikov, O., Artz, R. S., Davignon, D., Draxler, R. R., Munthe, J., and Pacyna, J.: Intercomparison study of atmospheric mercury models: 2. Modelling results vs. long-term observations and comparison of country deposition budgets, Sci. Total Environ., 377, 319–333, 2007b.

Rutter, A. P. and Schauer, J. J.: The impact of aerosol composition on the particle to gas partitioning of reactive mercury, Environ. Sci. Technol., 41, 3934-3939, doi:10.1021/es062439i, 2007a.

Rutter, A. P. and Schauer, J. J.: The effect of temperature on the gas-particle partitioning of reactive mercury in atmospheric aerosols, Atmos. Environ., 41, 8647–8657, doi:10.1016/j.atmosenv.2007.07.024, 2007b.

Rutter, A. P., Hanford, K. L., Zwers, J. T., Perillo-Nicholas, A. L., Schauer, J. J., and Olson, M. L.: Evaluation of an offline method for the analysis of atmospheric reactive gaseous mercury and particulate mercury, J. Air Waste Manag. Assoc., 58, 377–383, 2008.

Sather, M. E., Mukerjee, S., Smith, L., Mathew, J., Jackson, C., Callison, R., Scrapper, L., Hathcoat, A., Adam, J., and Keese, D.: Gaseous oxidized mercury dry deposition measurements in the Four Corners area and Eastern Oklahoma, USA, Atmos. Poll. Res., 4, 168–180, 2013.

Sather, M. E., Mukerjee, S., Allen, K. L., Sminth, L., Mathew, J., Jackson, C., Callison, R., Scrapper, L., Hathcoat, A., Adam, J.,

Keese, D., Ketcher, P., Brunette, R., Karlstrom, J., and Jagt, G. V. d. : Gaseous Oxidized Mercury Dry Deposition Measurements in the Southwestern USA: A Comparison between Texas, Eastern Oklahoma, and the Four Corners Area, Sci. World J., accession no. WOS:000334852000001, 2014.

Schroeder, W. H. and Munthe, J.: Atmospheric mercury–An overview, Atmos. Environ., 32, 809–822, 1998.

Schuster, P. F., Krabbenhoft, D. P., Naftz, D. L., Cecil, L. D., Olson, M. L., Dewild, J. F., Susong, D. D., Green, J. R., and Abbott, M. L.: Atmospheric mercury deposition during the last 270 years: A glacial ice core record of natural and anthropogenic sources, Environ. Sci. Technol., 36, 2303–2310, 2002.

Selin, N. E. and Jacob, D. J.: Seasonal and spatial patterns of mercury wet deposition in the United States: Constraints on the contribution from North American anthropogenic sources, Atmos. Environ., 42, 5193–5204, 2008.

Selin, N. E., Jacob, D. J., Park, R. J., Yantosca, R. M., Strode, S., Jaegle, L., and Jaffe, D.: Chemical cycling and deposition of atmospheric mercury: Global constraints from observations, J. Geophys. Res., 112, D02308, doi:10.1029/2006jd007450, 2007.

Seigneur, C., Karamchandani, P., Lohman, K., Vijayaraghavan, K., and Shia, R. L.: Multiscale modeling of the atmospheric fate and transport of mercury, J. Geophys. Res.-Atmos., 106, 27795–27809, doi:10.1029/2000jd000273, 2001.

Seigneur, C., Karamchandani, P., Vijayaraghavan, K., Lohman, K., Shia, R. L., and Levin, L.: On the effect of spatial resolution on atmospheric mercury modeling, Sci. Total Environ., 304, 73–81, doi:10.1016/s0048-9697(02)00558-2, 2003.

Seigneur, C., Vijayaraghavan, K., Lohman, K., Karamchandani, P., and Scott, C.: Global source attribution for mercury deposition in the United States, Environ. Sci. Technol., 38, 555–569, doi:10.1021/es034109t, 2004.

Seigneur, C., Vijayaraghavan, K., and Lohman, K.: Atmospheric mercury chemistry: Sensitivity of global model simulations to chemical reactions, J. Geophys. Res., 111, doi:10.1029/2005JD006780, 2006.

Sheu, G. R. and Mason, R. P.: An examination of methods for the measurements of reactive gaseous mercury in the atmosphere, Environ. Sci. Technol., 35, 1209–1216, 2001.

Shia, R. L., Seigneur, C., Pai, P., Ko, M., and Sze, N. D.: Global simulation of atmospheric mercury concentrations and deposition fluxes, J. Geophys. Res.-Atmos., 104, 23747–23760, doi:10.1029/1999JD900354, 1999.

Sholupov, S., Pogarev, S., Ryzhov, V., Mashyanov, N., and Stroganov, A.: Zeeman atomic absorption spectrometer RA-915 + for direct determination of mercury in air and complex matrix samples, Fuel Process. Technol., 85, 473–485, 2004.

Skov, H., Christensen, J. H., Goodsite, M. E., Heidam, N. Z., Jensen, B., Wahlin, P., and Geernaert, G.: Fate of elemental mercury in the arctic during atmospheric mercury depletion episodes and the load of atmospheric mercury to the arctic, Environ. Sci. Technol., 38, 2373–2382, doi:10.1021/es030080h, 2004.

Skov, H., Sorensen, B. T., Landis, M. S., Johnson, M. S., Sacco, P., Goodsite, M. E., Lohse, C., and Christensen, K. S.: Performance of a new diffusive sampler for atmospheric Hg0 determination, Environ. Chem., 4, 75–80, 2007.

Slemr, F., Brunke, E.-G., Ebinghaus, R., and Kuss, J.: Worldwide trend of atmospheric mercury since 1995, Atmos. Chem. Phys., 11, 4779–4787, doi:10.5194/acp-11-4779-2011, 2011.

Slemr, F., Weigelt, A., Ebinghaus, R., Brenninkmeijer, C., Baker, A., Schuck, T., Rauthe-Schoch, A., Riede, H., Leedham, E., Hermann, M., van Velthoven, P., Oram, D., O'Sullivan, D., Dyroff, C., Zahn, A., and Ziereis, H.: Mercury Plumes in the Global Upper Troposphere Observed during Flights with the CARIBIC Observatory from May 2005 until June 2013, Atmosphere, 5, 342–369, doi:10.3390/atmos5020342, 2014.

Soerensen, A. L., Jacob, D. J., Streets, D. G., Witt, M. L. I., Ebinghaus, R., Mason, R. P., Andersson, M., and Sunderland, E. M.: Multi-decadal decline of mercury in the North Atlantic atmosphere explained by changing subsurface seawater concentrations, Geophys. Res. Lett., 39, L21810, doi:10.1029/2012GL053736, 2012.

Sprovieri, F., Pirrone, N., Gardfeldt, K., and Sommar, J.: Mercury speciation in the marine boundary layer alonga 6000 km cruise path around the Mediterranean Sea, AE, 37, 63–71, 2003.

Steffen, A., Scherz, T., Olson, M., Gay, D., and Blanchard, P.: A comparison of data quality control protocols for atmospheric mercury speciation measurements, Environ. Monit., 14, 752–765, 2012.

Steffen, A., Bottenheim, J., Cole, A., Ebinghaus, R., Lawson, G., and Leaitch, W. R.: Atmospheric mercury speciation and mercury in snow over time at Alert, Canada, Atmos. Chem. Phys., 14, 2219–2231, doi:10.5194/acp-14-2219-2014, 2014.

Steffen, A., Lehnherr, I., Cole, A., Ariya, P., Dastoor, A., Durnford, D., Kirk, J., and Pilote, M.: Atmospheric mercury measurements in the Canadian Arctic Part 1: A review of recent field measurements, Sci. Total Environ., 509–510, 3–15, 2015.

Stratton, W. J. and Lindberg, S. E.: Use of a refluxing mist chamber for measurements of gas phase mercury(II) species in the atmosphere, Water Air Soil Pollut., 80, 1269–1278, 1995.

Stratton, W. J., Lindberg, S. E., and Perry, C. J.: Atmospheric mercury speciation: Laboratory and field evaluation of a mist chamber method for measuring reactive gaseous mercury, Environ. Sci. Technol., 35, 170–177, 2001.

Subir, M., Ariya, P. A., and Dastoor, A. P.: A review of uncertainties in atmospheric modeling of mercury chemistry I. Uncertainties in existing kinetic parameters: Fundamental limitations and the importance of heterogeneous chemistry, Atmos. Environ., 45, 5664–5676, 2011.

Syrakov, D., Gryning, S. E., and Schiermeier, F. A. (Eds.): On a PC-oriented Eulerian Multi-level model for long-term calculations of the regional sulphur deposition, Air pollution modeling and its application, XI, 21, Plenum Press, New York, 645–646, 1995.

Swartzendruber, P. C., Jaffe, D. A., and Finley, B.: Development and First Results of an Aircraft-Based, High Time Resolution Technique for Gaseous Elemental and Reactive (Oxidized) Gaseous Mercury, Environ. Sci. Technol., 43, 7484–7489, doi:10.1021/es901390t, 2009.

Talbot, R., Mao, H., Scheuer, E., Dibb, J., Avery, M., Browell, E., Sachse, G., Vay, S., Blake, D., Huey, G., and Fuelberg, H.: Factors influencing the large-scale distribution of Hg° in the Mexico City area and over the North Pacific, Atmos. Chem. Phys., 8, 2103–2114, doi:10.5194/acp-8-2103-2008, 2008.

Talbot, R., Mao, H., Feddersen, D., Smith, M., Kim, S. Y., Sive, B., Haase, K., Ambrose, J., Zhou, Y., and Russo, R.: Comparison of Particulate Mercury Measured with Manual and Automated Methods, Atmosphere, 2, 1–20, 2011.

Temme, C., Einax Jr., W., Ebinghaus, R., and Schroeder, W. H.: Measurements of Atmospheric Mercury Species at a Coastal Site in the Antarctic and over the South Atlantic Ocean during Polar Summer, Environ. Sci. Technol., 37, 22–31, 2002.

Timonen, H., Ambrose, J. L., and Jaffe, D. A.: Oxidation of elemental Hg in anthropogenic and marine airmasses, Atmos. Chem. Phys., 13, 2827–2836, doi:10.5194/acp-13-2827-2013, 2013.

Tong, Y. D., Eichhorst, T., Olson, M. R., Rutter, A. P., Shafer, M. M., Wang, X. J., and Schauer, J. J.: Comparison of heterogeneous photolytic reduction of Hg(II) in the coal fly ashes and synthetic aerosols, Atmos. Res., 138, 324–329, doi:10.1016/j.atmosres.2013.11.015, 2014.

Toyota, K., Dastoor, A. P., and Ryzhkov, A.: Air-snowpack exchange of bromine, ozone and mercury in the springtime Arctic simulated by the 1-D model PHANTAS – Part 2: Mercury and its speciation, Atmos. Chem. Phys., 14, 4135–4167, doi:10.5194/acp-14-4135-2014, 2014.

Travnikov, O.: Contribution of the intercontinental atmospheric transport to mercury pollution in the Northern Hemisphere, Atmos. Environ., 39, 7541–7548, doi:10.1016/j.atmosenv.2005.07.066, 2005.

Travnikov, O. and Ilyin, I.: The EMEP/MSC-E Mercury Modeling System, Mercury Fate and Transport in the Global Atmosphere: Emissions, Measurements and Models, edited by: Pirrone, N., and Mason, R., Springer, New York, 571–587, 2009.

Travnikov, O. and Ryaboshapko, A.: Modeling of mercury hemispheric transport and depositions, EMEP/MSC-E Technical Report 6/2002, 2002.

Travnikov, O., Ilyin, I., Pirrone, N., and Mason, R. (Eds.): The EMEP/MSC-E mercury modeling system, in: Mercury fate and transport in the global atmosphere, Springer, New York, NY, USA, 571–587, 2009.

Travnikov, O., Lin, C. J., Dastoor, A., Bullock, O. R., Hedgecock, I., Holmes, C., Ilyin, I., Jaegle, L., Jung, G., Pan, L., Pongprueksa, P., Ryzhkov, A., Seigneur, C., and Skov, H.: Global and Regional Modeling, in: Hemispheric Transport of Air Pollution. Part B: Mercury, edited by: Pirrone, N. and Keating, T., United Nations, 97–144, 2010.

UNEP Minamata Convention on Mercury, available at: http://www.mercuryconvention.org/, last access: 15 October 2014.

Urba, A., Kvietkus, K., Sakalys, J., Xiao, Z., and Lindqvist, O.: A new sensitive and portable mercury vapor analyzer GARDIS-1A, Water Air Soil Poll., 80, 1305–1309, 1995.

Vijayaraghavan, K., Karamchandani, P., Seigneur, C., Balmori, R., and Chen, S. Y.: Plume-in-grid modeling of atmospheric mercury, J. Geophys. Res., 113, D24305, doi:10.1029/2008jd010580, 2008.

Wang, Y., Huang, J., Hopke, P. K., Holsen, T. M., Rattigan, O. V., Chalupa, D. C., and Utell, M. J.: Effect of the shutdown of a large coal-fired power plant on ambient mercury species, Chemosphere, 92, 360–367, 2013.

Wang, L., Wang, S., Zhang, L., Wang, Y., Zhang, Y., Nielsen, C., McElroy, M., B., and Hao, J.: Source apportionment of atmospheric mercury pollution in China using the GEOS-Chem model, Environ. Poll., 190, 166–175, doi:10.1016/j.envpol.2014.03.011, 2014.

Weiss-Penzias, P., Jaffe, D. A., McClintick, A., Prestbo, E. M., and Landis, M. S.: Gaseous elemental mercury in the marine boundary layer: Evidence for rapid removal in anthropogenic pollution, Environ. Sci. Technol., 37, 3755–3763, 2003.

Weiss-Penzias, P., Amos, H. M., Selin, N. E., Gustin, M. S., Jaffe, D. A., Obrist, D., Sheu, G.-R., and Giang, A.: Use of a global model to understand speciated atmospheric mercury observations at five high-elevation sites, Atmos. Chem. Phys., 15, 1161–1173, doi:10.5194/acp-15-1161-2015, 2015.

Wright, G., Woodward, C., Peri, L., Weisberg, P. J., and Gustin, M. S.: Application of tree rings dendrochemistry for detecting historical trends in air Hg concentrations across multiple scales, Biogeochemistry, 120, 149–162, 2014a.

Wright, G., Gustin, M. S., Weiss-Penzias, P., and Miller, M. B.: Investigation of mercury deposition and potential sources at six sites from the Pacific Coast to the Great Basin, USA, Sci. Total Environ., 470, 1099–1113, 2014b.

Xiao, Z. F., Munthe, J., and Lindqvist, O.: Sampling and determination of gaseous and particulate mercury in the atmosphere using gold-coated denuders, Water Air Soil Poll., 56, 141–151, 1991.

Zhang, W., Tong, Y. D., Hu, D., Ou, L. B., and Wang, X. J.: Characterization of atmospheric mercury concentrations along an urban-rural gradient using a newly developed passive sampler, Atmos. Environ., 47, 26–32, 2012.

Zhang, Y., Jaeglé, L., van Donkelaar, A., Martin, R. V., Holmes, C. D., Amos, H. M., Wang, Q., Talbot, R., Artz, R., Brooks, S., Luke, W., Holsen, T. M., Felton, D., Miller, E. K., Perry, K. D., Schmeltz, D., Steffen, A., Tordon, R., Weiss-Penzias, P., and Zsolway, R.: Nested-grid simulation of mercury over North America, Atmos. Chem. Phys., 12, 6095–6111, doi:10.5194/acp-12-6095-2012, 2012.

Automated calibration of atmospheric oxidized mercury measurements

Permission to Reprint

The following article is reprinted with permission from:

Automated Calibration of Atmospheric Oxidized Mercury Measurements, Seth Lyman, Colleen Jones, Trevor O'Neil, Tanner Allen, Matthieu Miller, Mae Sexauer Gustin, Ashley M. Pierce, Winston Luke, Xinrong Ren, and Paul Kelley *Environmental Science & Technology,* 2016 *50* (23), 12921-12927. DOI: 10.1021/acs.est.6b04211 Copyright (2016) American Chemical Society.

Environmental Science & Technology

Article

pubs.acs.org/est

Automated Calibration of Atmospheric Oxidized Mercury Measurements

Seth Lyman,*[,†] Colleen Jones,[†] Trevor O'Neil,[†] Tanner Allen,[†] Matthieu Miller,[‡,§] Mae Sexauer Gustin,[§] Ashley M. Pierce,[§] Winston Luke,[∥] Xinrong Ren,[∥,⊥] and Paul Kelley[∥,⊥]

[†]Bingham Research Center, Utah State University, Vernal, Utah 84322, United States

[‡]Macquarie University, North Ryde, New South Wales Australia

[§]Department of Natural Resources and Environmental Science, University of Nevada, Reno, Reno, Nevada 89557, United States

[∥]Air Resources Laboratory, National Oceanic and Atmospheric Administration, College Park, Maryland 20742, United States

[⊥]Cooperative Institute for Climate and Satellites, University of Maryland, College park, Maryland 20742, United States

ABSTRACT: The atmosphere is an important reservoir for mercury pollution, and understanding of oxidation processes is essential to elucidating the fate of atmospheric mercury. Several recent studies have shown that a low bias exists in a widely applied method for atmospheric oxidized mercury measurements. We developed an automated, permeation tube-based calibrator for elemental and oxidized mercury, and we integrated this calibrator with atmospheric mercury instrumentation (Tekran 2537/1130/1135 speciation systems) in Reno, Nevada and at Mauna Loa Observatory, Hawaii, U.S.A. While the calibrator has limitations, it was able to routinely inject stable amounts of $HgCl_2$ and $HgBr_2$ into atmospheric mercury measurement systems over periods of several months. In Reno, recovery of injected mercury compounds as gaseous oxidized mercury (as opposed to elemental mercury) decreased with increasing specific humidity, as has been shown in other studies, although this trend was not observed at Mauna Loa, likely due to differences in atmospheric chemistry at the two locations. Recovery of injected mercury compounds as oxidized mercury was greater in Mauna Loa than in Reno, and greater still for a cation-exchange membrane-based measurement system. These results show that routine calibration of atmospheric oxidized mercury measurements is both feasible and necessary.

1. INTRODUCTION

Over the past two decades, atmospheric mercury speciation has been measured routinely at dozens of locations around the world with the Tekran 1130/1135/2537 speciation system (Tekran Instruments Corporation, Toronto, Canada; referred to herein as "Tekran system" or "Tekran speciation system").[1−5] This system measures atmospheric mercury as three fractions: gaseous elemental mercury (Hg^0, also often referred to as GEM), gaseous oxidized mercury (GOM, also called reactive gaseous mercury, or RGM), and particulate-bound mercury (PBM). It collects Hg^0 on gold traps with periodic thermal desorption into an atomic fluorescence detector. GOM and PBM are collected onto a KCl-coated quartz denuder and quartz fiber filter, respectively, both of which are periodically thermally desorbed at a temperature sufficient to decompose Hg compounds, and the resultant Hg^0 is analyzed by the same gold traps and atomic fluorescence detector.[6]

Unfortunately, a growing body of research is showing that the Tekran speciation system is unable to quantify GOM and PBM consistently. Rutter and Schauer, Talbot et al., and Gustin et al. showed that the system does not accurately distinguish between GOM and PBM.[7−9] Lyman et al. demonstrated that ozone can decompose oxidized mercury compounds from KCl-coated denuders to Hg^0 such that injected oxidized mercury compounds are quantified by the system as Hg^0,[10] and McClure et al. confirmed this finding in the laboratory and in ambient air.[11] McClure et al. also demonstrated that humidity reduces the amount of GOM recovered by KCl-coated denuders in a Tekran system, as has been shown by Huang and Gustin.[12]

Discovery of bias in Tekran system measurements did not occur until after the instruments were in use for at least a decade, at least in part because no system existed for routine verification of atmospheric mercury speciation measurements in ambient air. Such a system has been called for repeatedly.[10,13−15] High-concentration oxidized mercury calibrators are available for measurements in flue gas (i.e., Thermo model 81i and Tekran model 3310/3321), which work by combining Hg^0 with chlorine gas to generate mercuric chloride. However, no commercial calibration system exists that is capable of producing stable, ambient levels of oxidized mercury (zero to hundreds of pg m^{-3}). Some studies have accomplished injections of Hg compounds into mercury measurement

Received: August 19, 2016
Revised: November 3, 2016
Accepted: November 7, 2016
Published: November 7, 2016

DOI: 10.1021/acs.est.6b04211
Environ. Sci. Technol. 2016, 50, 12921−12927

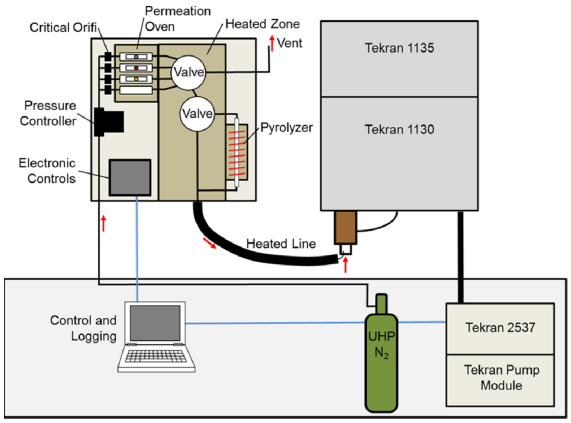

Figure 1. Schematic of the calibrator.

systems with manual permeation tube-based calibrators.[10−12,16,17] Adding standards manually is time-consuming and has not been done routinely, however.

We have developed a permeation tube-based calibrator that is capable of providing automated injections of Hg^0 and Hg compounds at atmospherically relevant concentrations into the inlet of mercury analyzers (patent pending). We integrated this calibrator with Tekran speciation systems in Reno, Nevada and Mauna Loa, Hawaii, resulting in the first routine verification of atmospheric mercury speciation measurements.

2. EXPERIMENTAL SECTION

2.1. Sampling Locations. The calibrator was deployed at the College of Agriculture, Biotechnology, and Natural Resources Valley Road Greenhouse Facility at the University of Nevada, Reno campus near downtown Reno, Nevada, and at the Mauna Loa Observatory in Hawaii. For work reported herein, the instrument operated in Reno from 27 February until 7 June 2015 and from 7 May until 3 June 2016, and at Mauna Loa from 7 August until 28 September 2015.

2.2. Calibrator Construction and Operation. *2.2.1. Permeation Oven.* The core of the mercury calibrator was a permeation oven that housed four stainless steel tubes of 5 mm internal diameter coated with deactivated fused silica (Figure 1). Three of these tubes contained permeation tubes, while the fourth was empty, allowing for flushing of mercury-free nitrogen through the system. Upstream of the 5 mm internal diameter tubes were critical orifices designed for a flow of 100 mL min^{-1} (for the Mauna Loa deployment and the 2016 deployment in Reno, a flow of 25 mL min^{-1} was used). No additional flow was provided through the calibrator, so the flow of gas across the permeation tubes was the same as the flow from the calibrator into the measurement system being calibrated. The pressure upstream of the critical orifices was controlled by an Alicat pressure controller. High purity nitrogen from a compressed gas cylinder (Airgas UHP N_2; 99.999% pure, < 1 ppm of O_2, < 1 ppm of H_2O, < 0.5 ppm THC, < 1 ppm of CO + CO_2) provided flow through the tubes. Flow through the tubes was directed either to a vent (with an activated charcoal scrubber) or to the outlet line of the calibrator.

The permeation oven was maintained at 100 °C. In previous work with HgX_2 permeation tubes, investigators have kept permeation ovens cooler than this,[11,17] but recent work has shown that HgX_2 passes more efficiently through tubing and decomposes to Hg^0 less when kept at higher temperatures.[18] Also, our own observations and data presented by McClure et al.[11] show permeation rates of permeation tubes maintained at low temperatures may not be stable over time.

The permeation oven housed permeation tubes for Hg^0, $HgBr_2$, and $HgCl_2$ (obtained from Sigma-Aldrich, purity >99.9%). Other mercury compounds besides $HgBr_2$ and $HgCl_2$ may exist in ambient air, and while the compounds that exist in ambient air are not known with certainty, many studies have speculated that halogen-containing mercury compounds exist.[19−21] Furthermore, $HgBr_2$ and $HgCl_2$ are readily available commercially, can survive well in the valve and tubing materials used for the calibrator,[18] and Hg compounds emitted from $HgBr_2$ and $HgCl_2$ permeation tubes have been shown by mass spectrometry to be $HgBr_2$ and $HgCl_2$ (this has not been shown for HgO and $Hg(NO_3)_2$).[18]

All three permeation tubes were constructed from 3 mm internal diameter thin-wall PTFE tubing with 3 mm diameter solid PTFE plugs. The permeable length of the $HgCl_2$ and $HgBr_2$ permeation tubes (i.e., the distance between the plugs where the solid-phase mercury compounds were contained) was 1 mm. For the Hg^0 permeation tube, a 1 mm diameter, 1 mm deep hole was drilled into the solid PTFE plug, the hole was filled with Hg^0, and the plug was then covered with the thin-wall PTFE tubing, sealing the Hg^0 into the tubing. After reaching the set temperature, the permeation tubes required about 24 h to stabilize prior to use.

2.2.2. Pyrolyzer. A pyrolyzer allowed for decomposition of permeated mercury compounds to Hg^0 to determine total mercury permeation rates. The pyrolyzer consisted of a U-shaped 6 mm outer-diameter quartz tube filled with quartz wool, with quartz frits on either end to retain quartz wool in the tube. The pyrolyzer was maintained at 700 °C.

DOI: 10.1021/acs.est.6b04211
Environ. Sci. Technol. 2016, 50, 12921−12927

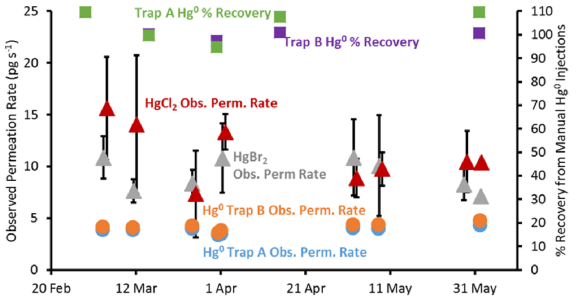

Figure 2. GOM+PBM recovered by the Tekran speciation system from injections of $HgBr_2$ and $HgCl_2$ by the calibrator while operated in Reno, Nevada. Recovery of Hg^0 from injections of Hg^0 by the calibrator and % recovery from manual injections of Hg^0 from a temperature-controlled Hg vapor source are also shown. Whiskers represent 95% confidence intervals. n = 2–5 for each point shown.

2.2.3. Valves and Tubing. VICI GC valves were used to select among the permeation tubes (flow was passed to vent when permeation tubes were not in use), and to select whether the permeated Hg would pass through the pyrolyzer prior to exiting the calibrator. Valves were constructed of deactivated fused silica-coated stainless steel, and valve rotors were composed of Valcon T (a polyimide/PTFE/carbon composite). All connecting tubing consisted of 1.6 mm outer diameter deactivated fused silica-coated stainless steel.

A heated outlet line was also composed of 1.6 mm outer diameter deactivated fused silica-coated stainless steel tubing. The outlet line was insulated except for the final 20 mm, which was bent upward and placed inside the Tekran speciation system's elutriator inlet. This allowed the Tekran system to sample ambient air without a sampling manifold and allowed all injections from the calibrator to be carried out in ambient air.

Valves and tubing, including the outlet line, were maintained at 200 °C. This temperature maximized HgX_2 transmission and minimized decomposition to Hg^0 in tests performed by Jones et al.[18]

2.2.4. Housing. The calibrator was installed outdoors next to the Tekran speciation system to minimize the transport distance of permeated mercury compounds. The calibrator was housed in a weatherproof box with a temperature-controlled fan that ventilated the box if the box temperature increased above 30 °C. Communication cables connected the calibrator to an indoor computer with a custom LabVIEW executable file that controlled the calibrator and connected the calibrator to the digital data output from the Tekran 2537.

2.2.5. Software. Through the LabVIEW executable, the calibrator was programmed to inject Hg^0, $HgCl_2$, or $HgBr_2$ for a set number of seconds, and would repeat the programmed injection over a set time interval (1–24 h) on a daily or weekly basis. The Tekran systems in this study sampled ambient air for 1 h and then desorbed and analyzed their denuder and pyrolyzer for the next hour. The Hg^0 measurement interval for the Tekran 2537s was 5 min. The calibrator injected a selected calibration gas according to a programmed schedule. Injections only occurred when the Tekran data output received by the calibrator indicated that the instrument had been sampling ambient air for at least 10 min. The calibrator began injections at the beginning of each 5 min measurement period.

Injections of $HgCl_2$ and $HgBr_2$ lasted for 7–100 s, and only occurred once during the hour-long ambient air sampling period. Hg^0 was injected at the start of each 5 min sampling period for the duration of the ambient air sampling hour, and injections lasted for 100–300 s. After $HgCl_2$ and $HgBr_2$ injections were completed, the selection valve switched the flow path to the 5 mm stainless tube that was empty, allowing mercury-free nitrogen to flush through the calibrator and into the measurement system inlet for the remainder of the ambient air sampling hour. The nitrogen flush after Hg^0 injections only lasted for the balance of the 5 min interval. Following the flush, the selection valve switched to a closed position and flow through the outlet line ceased.

In 5 min intervals, the LabVIEW executable recorded the date and time; the temperatures of the permeation oven, valves and tubing, pyrolyzer, outlet line, and housing; the data output from the Tekran 2537; the number of seconds the permeation tube selection valve spent in each possible position; and the time the pyrolyzer selection valve spent in each possible position.

2.3. Tekran Speciation System Measurements. The Tekran system in Mauna Loa is operated as part of the Atmospheric Mercury Network (AMNet) and follows AMNet protocols.[22] The Tekran system in Reno was also operated following AMNet protocols.

2.4. Cation-Exchange Membrane-Based Measurements. In addition to injections into the Tekran system, we used the calibrator to inject $HgCl_2$ and $HgBr_2$ into a cation-exchange membrane-based manual measurement system. The system consisted of an activated poly(ether sulfone) cation exchange membrane (Mustang S, Pall Corporation), that was housed in a 47 mm PFA filter holder, to collect GOM, followed by a 4 mm inner diameter quartz tube, the center 2–4 cm of which was filled with gold-coated quartz beads, to collect Hg^0. A pump pulled ambient air through the membrane and then the tube at 1 L min^{-1}. The calibrator injected Hg compounds into the PFA filter holder while the pump pulled ambient air through the system. The pump began pulling air through the system 30 s before the injection began, and then for 30 s after the injection finished.

Membranes were handled and analyzed by EPA Method 1631, as described by Huang and Gustin.[12] Gold traps were analyzed by atomic fluorescence spectrometry, as in Gustin et al.[23]

2.5. Data Processing and Reporting. The amount of Hg recovered from calibrator injections is reported in this work as

DOI: 10.1021/acs.est.6b04211
Environ. Sci. Technol. 2016, 50, 12921–12927

total pg or pg s^{-1} (the observed permeation rate). For Hg^0 injections, the total pg recovered was calculated by correcting for measured ambient Hg^0 concentrations (measured during the first 10 min of each 1 h ambient air sampling cycle, units of ng m^{-3}), then multiplying by (1) the m^3 of air sampled by the Tekran speciation system during each 5 min measurement period and (2) 1000 pg ng^{-1}.

For $HgCl_2$ and $HgBr_2$ injection periods, total GOM recovered from desorption of the KCl denuder and PBM recovered from desorption of the particulate filter (units of pg m^{-3}) were added together, ambient air concentrations of GOM and PBM from previous and subsequent sampling periods were subtracted, and the resultant value was multiplied by the m^3 of air sampled during the 1 h ambient air sampling period. Hg^0 recovered during $HgCl_2$ and $HgBr_2$ injection periods was calculated in the same way as during Hg^0 injection periods, except that Hg^0 enhancements above ambient levels were calculated and summed for each 5 min measurement period subsequent to injection.

The permeation rates of the permeation tubes used in the calibrator were not verified independently of the measurement systems being calibrated, so percent recoveries are not reported for automated calibrator results. Instead, recovered pg or observed permeation rates are reported. Coefficient of determination (r^2) values shown in this work were determined by ordinary least-squares regression, and p values shown for comparison of two data sets were calculated using student's t tests. Statistical significance was determined at $\alpha = 0.05$.

3. RESULTS AND DISCUSSION

3.1. Repeatability and Variability. Figure 2 shows the recovery of Hg^0, $HgBr_2$ and $HgCl_2$ injected by the calibrator into the Tekran system while it was deployed in Reno, as well as the recovery of Hg^0 injected manually from a temperature-controlled Hg vapor source.None of the injected compounds exhibited a statistically significant change in recovery over the measurement period. A slight (but statistically insignificant) decreasing trend was observed for recovery of GOM + PBM from $HgCl_2$ and $HgBr_2$ injections in Figure 2. A weak but statistically significant increase in dew point occurred over the same period ($r^2 = 0.09$; $p < 0.01$), possibly accounting for the decreasing trend (see discussion about dew point below). Recovery from $HgBr_2$ injections at Mauna Loa did not exhibit a temporal trend. $HgCl_2$ and Hg^0 injections were only performed at the beginning of the Mauna Loa deployment, so temporal trends could not be established.

GOM and PBM results from the Tekran system were summed for Figure 2 and elsewhere in this work because GOM and PBM both increased when $HgCl_2$ or $HgBr_2$ was injected into the Tekran, and because the ability of the Tekran to distinguish quantitatively between GOM and PBM is in question.[7−9] Twenty ±4% (mean ±95% confidence interval) of GOM + PBM recovered from $HgBr_2$ injections was PBM, and an average of 18 ± 3% of GOM + PBM recovered from $HgCl_2$ injections was PBM.

Recovery of Hg^0 from manual injections in Reno was 101.9 ± 5.9% for gold trap A and 104.3 ± 8.3% for gold trap B. Hg^0 injections from the calibrator exhibited similar variability, with 96.2 ± 6.5% recovery for trap A and 103.8 ± 7.4% recovery for trap B (percent recovery calculated as the recovered amount divided by the average recovery for both traps over the operation period). The amount of the variability in recovery that was due to the calibrator versus the Tekran system cannot be ascertained from this data set.

The majority of $HgCl_2$ and $HgBr_2$ injected into the Tekran System in Reno was recovered as Hg^0, and the amount recovered as Hg^0 was consistent for the 2015 and 2016 deployments (Figure 3). The percentage of injected Hg that

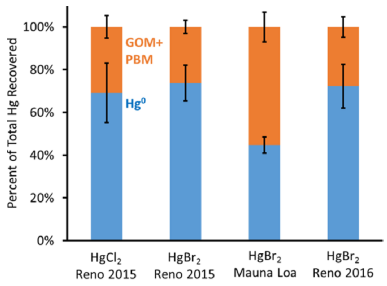

Figure 3. Average percent of total Hg recovered as Hg^0 and GOM +PBM by the Tekran system for injections of $HgBr_2$ and $HgCl_2$ in Reno during 2015, injections of $HgBr_2$ in Reno during 2016, and injections of $HgBr_2$ in Mauna Loa during 2015. Whiskers show 95% confidence intervals. $n = 28$ for $HgCl_2$, 25 for $HgBr_2$ in Reno 2015, 82 for Mauna Loa, and 44 for $HgBr_2$ in Reno 2016.

was recovered as Hg^0 was greater for $HgBr_2$ than for $HgCl_2$, though the difference was not statistically significant ($p = 0.11$). Hg−Br bonds require less energy to break than Hg−Cl bonds,[24] so reactions that decompose Hg compounds could affect $HgBr_2$ more strongly than $HgCl_2$. In contrast with Reno, the majority of Hg recovered from $HgBr_2$ injections in Mauna Loa was GOM + PBM, perhaps because of differences in air chemistry at the two locations (see discussion below). Calibrations in Reno occurred during spring, while calibrations in Mauna Loa occurred during late summer and early fall. More study is needed to determine whether oxidized Hg recovery by the Tekran system exhibits seasonality.

3.2. Recovery Under Different Conditions. In Reno and Mauna Loa, no statistically significant relationships were observed between ozone and GOM+PBM recovery from Hg compound injections or for the percent of recovered Hg that was Hg^0 (p values for correlations were all greater than 0.24). Laboratory studies have established that ozone leads to reduction of Hg halides on KCl denuders to Hg^0,[10,11] and McClure and Jaffe[11] noted a negative correlation between ambient ozone and recovery of injected $HgBr_2$ by a Tekran system, but, using data from their Table S2, that correlation was also not statistically significant ($r^2 = 0.23$; $p = 0.08$).

McClure et al. report a significant correlation between ambient specific humidity and recovery of $HgBr_2$ by a Tekran system in the Southeast United States ($r^2 = 0.70$; $p < 0.01$).[11] Huang and Gustin also showed that water vapor negatively impacts the retention of Hg compounds by KCl denuders.[12] In this study, recovery of GOM+PBM from $HgBr_2$ injections in Reno decreased and the percent of total recovered Hg that was Hg^0 increased with increasing specific humidity (Figure 4). The intercept for this relationship (i.e., zero water vapor in ambient air) was 61% Hg^0 in total Hg recovered, higher than the % Hg^0 in Hg recovered from $HgBr_2$ injections at Mauna Loa. This

DOI: 10.1021/acs.est.6b04211
Environ. Sci. Technol. 2016, 50, 12921−12927

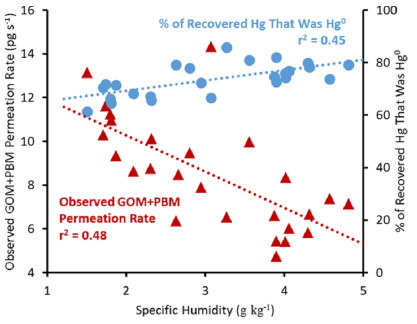

Figure 4. GOM+PBM recovery from $HgBr_2$ injections in Reno and percent of recovered Hg that was Hg^0 versus ambient specific humidity.

indicates that something other than water vapor likely also decreased the recovery of $HgBr_2$ as GOM + PBM in Reno.

The r^2 value for the relationship of specific humidity with GOM+PBM recovery was not significant for $HgCl_2$, but a significant relationship was observed between specific humidity and percent Hg^0 in total Hg recovered from $HgCl_2$ injections (r^2 = 0.19, p = 0.02).

Surprisingly, the percent Hg^0 in total Hg recovered from $HgBr_2$ injections in Mauna Loa was weakly negatively correlated with specific humidity (Figure 5; p < 0.01). Percent

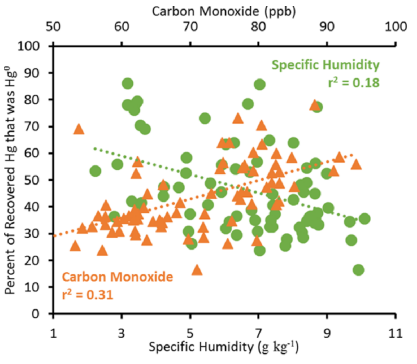

Figure 5. Percent of recovered Hg that was Hg^0 versus ambient specific humidity and ambient carbon monoxide at Mauna Loa Observatory.

Hg^0 in total Hg recovered was positively correlated with carbon monoxide in Mauna Loa (Figure 5; p < 0.01), and specific humidity and carbon monoxide were inversely correlated with each other (r^2 = 0.24; p < 0.01). It is possible that some anthropogenic pollutant for which carbon monoxide is a tracer led to the conversion of injected $HgBr_2$ to Hg^0 at Mauna Loa, obscuring the impact of water vapor. It may be that the relatively pristine atmosphere at Mauna Loa led to the improved recovery of injected $HgBr_2$ as GOM + PBM relative to Reno (Figure 3). No meaningful correlations between carbon monoxide concentrations and $HgBr_2$ recovery were observed in Reno (r^2 < 0.001; carbon monoxide range of 137–1034 ppb).

Recovery of GOM+PBM was inversely correlated with the percent of total recovered Hg that was Hg^0 (r^2 = 0.52 for $HgBr_2$ injections in Reno), and the total Hg recovered did not vary with specific humidity (p = 0.31), indicating that, while some of the injected Hg compounds were likely converted to Hg^0 under ambient conditions, the total amount of Hg recovered by the Tekran system was conserved.

Figure 6 shows the average concentration of Hg^0 measured by the Tekran system during sampling periods when $HgCl_2$ was

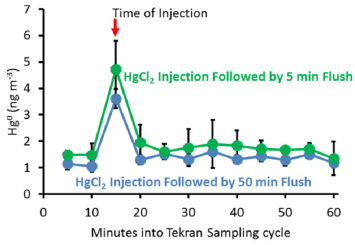

Figure 6. Average 5 min Hg^0 measurements collected by the Tekran system for hours during which $HgCl_2$ was sampled. $HgCl_2$ injections followed by a 5 min flush and a 50 min flush are shown. Whiskers show 95% confidence intervals. n = 4–5 for each point shown.

injected. Hg^0 increased above the ambient level for the 5 min period during which the injections occurred, and while it decreased again following the injection period, it stayed statistically significantly above ambient Hg^0 for the remainder of the 1 h ambient air sampling period (p = 0.01). Under normal operation, after the calibrator injected $HgCl_2$ ($HgCl_2$ injections lasted 20 s for the results shown in Figure 6), it flushed the outlet line with nitrogen for the remainder of the sampling period. While Figure 4 provides evidence that conversion of some injected $HgCl_2$ to Hg^0 within the Tekran system did occur, continued release of Hg^0 from the calibrator during flushing could also explain the excess Hg^0 after the initial injection period shown in Figure 6. We tested this by manually ending the calibrator flush 5 min after some injections (Figure 6). The increase in Hg^0 after injections was not statistically significantly different for the two flush times (p = 0.87), showing the increase was likely due to $HgCl_2$ breakdown within the Tekran system, rather than from Hg^0 introduced by the calibrator during flushing. The amount of excess Hg^0 collected in the 45 min following injection was ~120 pg, which is ~18% of the total Hg recovered from $HgCl_2$ injections.

3.3. Comparison With a Cation-Exchange Membrane System. The Tekran system captured 34% less of injected $HgBr_2$ and $HgCl_2$ as GOM+PBM relative to the cation exchange membrane and gold trap-based system (Figure 7). Ambient air flowed through the membrane system for just a few minutes during each injection, rather than for the 1 h Tekran ambient air sampling period. Thus, only the Hg^0 recovered from the Tekran system in the 5 min during which injections occurred were used in Figure 7.

Injections of Hg^0 from a temperature-controlled Hg vapor source through a membrane and into a Tekran 2537 mercury analyzer showed the same amount of Hg^0 whether a cation-

DOI: 10.1021/acs.est.6b04211
Environ. Sci. Technol. 2016, 50, 12921–12927

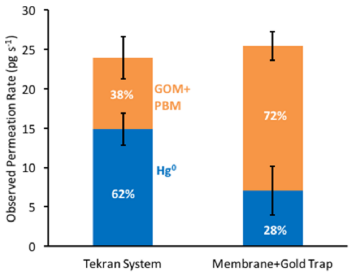

Figure 7. Average recovery of injected $HgCl_2$ and $HgBr_2$ as Hg^0 and GOM+PBM by the Tekran system (subset of data from 9 to 10 May 2015) versus a cation exchange membrane (CEM) followed by a trap filled with gold-coated quartz beads (injections performed on 7 May 2015). Whiskers show 95% confidence intervals. n = 6 for the Tekran system, 4 for the membrane + gold trap system.

exchange membrane or Teflon membrane was installed (p = 0.74; 120.36 ± 0.77 ng m^{-3} recovered), indicating that the cation-exchange membranes did not adsorb a detectable amount of Hg^0. In tests with two cation-exchange membranes in series, Huang and Gustin did not observe any measurable breakthrough of permeated Hg compounds in activated carbon-scrubbed air,[12] while tests with ambient Hg in ambient air resulted in a median breakthrough of 25%.[25] If breakthrough of $HgBr_2$ or $HgCl_2$ did occur, the percent of recovered Hg that was Hg^0 could be overestimated for the membrane and gold trap system. Some evidence exists that recovery of Hg compounds by cation-exchange membranes may depend on ambient conditions,[12] and the membrane system is not definitive. In fact, no method for collection of Hg compounds has been shown to be unbiased by ambient conditions. This comparison shows, however, that the membrane system was better able to recover injected Hg compounds as GOM than the Tekran system.

3.4. Limitations. The automated calibrator was stable over time, was useful for determination of the influence of ambient conditions on Hg recovery, and provided for comparisons among Hg measurement methods. The calibrator's ability to inject directly into the Tekran system's inlet allowed for the addition of Hg compounds into ambient air without the use of a manifold, since manifolds have been shown to retain Hg compounds.[17] However, this inlet design did not allow for injection into zero air (e.g., air scrubbed with activated carbon), which rendered us unable to compare recoveries in ambient vs zero air. A system is needed that will allow for injections in zero and ambient air, and yet still perform injection of Hg compounds without a manifold. The calibrator injected Hg compounds at the tip of the Tekran inlet, allowing for a realistic determination of passage of Hg compounds through the entire inlet system. The Tekran system can provide zero air to the inlet, but it adds zero air downstream of the inlet's elutriator and particle impactor, where previous research has shown that more than 30% of injected $HgCl_2$ is lost.[26] Thus, injection by the calibrator downstream of the Tekran system's zero air port would likely lead to unrealistic calibration results.

Since Tekran systems can quantitatively recover injected $HgBr_2$ and $HgCl_2$ in zero air,[6,11] comparisons of calibration results in zero and ambient air will allow for a more quantitative determination of the Tekran instrument's bias in ambient conditions, and for determination of the amount of Hg emitted from permeation tubes that is Hg^0. However, National Institute of Standards and Technology (NIST)-traceable standards that are independent of measurement systems being calibrated are still needed to provide definitive calibration of Hg measurement instrumentation. Our $HgCl_2$ and $HgBr_2$ permeation tubes emitted about 30 pg s^{-1} of Hg (Figure 3), equivalent to 18 μg week^{-1}. This is adequate to verify permeation rates gravimetrically with a μg-sensitivity scale, as has been done by others.[27] Gravimetric verification of permeation rates could make permeation tubes for Hg compounds traceable to NIST gravimetric standards if the speciation of Hg emitted from the tubes can be reliably and independently determined. Unfortunately, the amount of Hg^0 emitted from permeation tubes used in this study is unclear, since the amount of injected Hg recovered as Hg^0 varied with ambient conditions. A standardized, independent method (independent of permeation tubes *and* the measurement systems to be calibrated by permeation tubes) is needed to determine the speciation of Hg emitted from $HgCl_2$ and $HgBr_2$ from permeation tubes.

In order to provide an independent, NIST-traceable, reliable source of Hg compounds in the gas phase, permeation tubes need to be (1) stable over time, (2) emit enough Hg to be gravimetrically verifiable, and (3) emit very little Hg^0 (or at least the amount of Hg^0 emission needs to be independently verifiable). Our calibrator achieves the first two benchmarks, but work is needed on the third. Some low-temperature Hg compound permeation tubes have achieved the third, but not the first two.[10,17,26]

The calibrator's pyrolyzer was designed to provide simple, real-time verification of total Hg permeation rates by converting permeated Hg compounds to Hg^0,[16] followed by detection with the Tekran system's 2537 analyzer. Passing permeated Hg^0, $HgCl_2$, and $HgBr_2$ through the pyrolyzer resulted in total Hg recoveries that were not significantly different from unpyrolyzed Hg (p = 0.11 to 0.56), though some of the pyrolyzed Hg was still recovered as GOM + PBM (average of 7% for $HgBr_2$ and $HgCl_2$ injections). It is not clear whether pyrolyzed Hg that was recovered as GOM + PBM was due to inefficient pyrolysis or contamination of the pyrolysis system with $HgBr_2$ or $HgCl_2$.

3.5. Implications. Similar to other studies, automated calibrations in this study showed that Hg compounds are converted to Hg^0 within the Tekran system, resulting in GOM + PBM measurements that are biased low. This study also showed, however, that Tekran systems deployed in different locations can have different levels of bias, perhaps because of differences in atmospheric chemistry. Relationships between Tekran recovery and atmospheric conditions were not consistent across the two study locations, indicating that more research is needed to understand the mechanisms that lead to bias in Tekran systems.

These results show that the bias in Tekran speciation system-based measurements is not consistent spatially or temporally. This suggests that the spatial and temporal trends in Hg speciation observed in previous studies could be due, at least in part, to instrument bias, rather than real changes in atmospheric Hg chemistry. It also implies that correction of Tekran system data that were collected without routine calibration may only be able to be accomplished if adequate ancillary data are available. While improvements to the automated calibrator presented here are needed, it is clear that routine calibration of atmospheric Hg measurement instrumentation will increase the validity and utility of collected data.

DOI: 10.1021/acs.est.6b04211
Environ. Sci. Technol. 2016, 50, 12921−12927

AUTHOR INFORMATION

Corresponding Author

*E-mail: seth.lyman@usu.edu.

ORCID

Seth Lyman: 0000-0001-8493-9522

Notes

The authors declare no competing financial interest.

ACKNOWLEDGMENTS

We are grateful to the U.S. National Science Foundation (Grant 1324781) and the Utah Science, Technology and Research Initiative for funding this work. We are also grateful to NOAA staff for facilitating the deployment of the calibrator at Mauna Loa Observatory.

REFERENCES

(1) Valente, R. J.; Shea, C.; Lynn Humes, K.; Tanner, R. L. Atmospheric mercury in the Great Smoky Mountains compared to regional and global levels. *Atmos. Environ.* **2007**, *41* (9), 1861−1873.

(2) Slemr, F.; Brunke, E.-G.; Ebinghaus, R.; Kuss, J. Worldwide trend of atmospheric mercury since 1995. *Atmos. Chem. Phys.* **2011**, *11* (10), 4779−4787.

(3) Cole, A.; Steffen, A.; Pfaffhuber, K. A.; Berg, T.; Pilote, M.; Poissant, L.; Tordon, R.; Hung, H. Ten-year trends of atmospheric mercury in the high Arctic compared to Canadian sub-Arctic and mid-latitude sites. *Atmos. Chem. Phys.* **2013**, *13* (3), 1535−1545.

(4) Angot, H.; Barret, M.; Magand, O.; Ramonet, M.; Dommergue, A. A 2-year record of atmospheric mercury species at a background Southern Hemisphere station on Amsterdam Island. *Atmos. Chem. Phys.* **2014**, *14* (20), 11461−11473.

(5) Fu, X.; Zhang, H.; Yu, B.; Wang, X.; Lin, C.; Feng, X. Observations of atmospheric mercury in China: a critical review. *Atmos. Chem. Phys.* **2015**, *15*, 9455−9476.

(6) Landis, M. S.; Stevens, R. K.; Schaedlich, F.; Prestbo, E. M. Development and characterization of an annular denuder methodology for the measurement of divalent inorganic reactive gaseous mercury in ambient air. *Environ. Sci. Technol.* **2002**, *36* (13), 3000−3009.

(7) Rutter, A. P.; Schauer, J. J. The effect of temperature on the gas-particle partitioning of reactive mercury in atmospheric aerosols. *Atmos. Environ.* **2007**, *41* (38), 8647−8657.

(8) Talbot, R.; Mao, H.; Feddersen, D.; Smith, M.; Kim, S. Y.; Sive, B.; Haase, K.; Ambrose, J.; Zhou, Y.; Russo, R. Comparison of Particulate Mercury Measured with Manual and Automated Methods. *Atmosphere* **2011**, *2* (1), 1−20.

(9) Gustin, M. S.; Huang, J.; Miller, M. B.; Peterson, C.; Jaffe, D. A.; Ambrose, J.; Finley, B. D.; Lyman, S. N.; Call, K.; Talbot, R. Do we understand what the mercury speciation instruments are actually measuring? Results of RAMIX. *Environ. Sci. Technol.* **2013**, *47* (13), 7295−7306.

(10) Lyman, S. N.; Jaffe, D. A.; Gustin, M. S. Release of mercury halides from KCl denuders in the presence of ozone. *Atmos. Chem. Phys.* **2010**, *10* (17), 8197−8204.

(11) McClure, C. D.; Jaffe, D. A.; Edgerton, E. S. Evaluation of the KCl denuder method for gaseous oxidized mercury using HgBr2 at an in-service AMNet site. *Environ. Sci. Technol.* **2014**, *48* (19), 11437−11444.

(12) Huang, J.; Gustin, M. S. Uncertainties of Gaseous Oxidized Mercury Measurements Using KCl-Coated Denuders, Cation-Exchange Membranes, and Nylon Membranes: Humidity Influences. *Environ. Sci. Technol.* **2015**, *49* (10), 6102−6108.

(13) Jaffe, D. A.; Lyman, S.; Amos, H. M.; Gustin, M. S.; Huang, J.; Selin, N. E.; Levin, L.; Ter Schure, A.; Mason, R. P.; Talbot, R. Progress on understanding atmospheric mercury hampered by uncertain measurements. *Environ. Sci. Technol.* **2014**, *48* (13), 7204−7206.

(14) Gustin, M.; Jaffe, D. Reducing the Uncertainty in Measurement and Understanding of Mercury in the Atmosphere. *Environ. Sci. Technol.* **2010**, *44* (7), 1573−2932.

(15) Gustin, M. S.; Amos, H. M.; Huang, J.; Miller, M. B.; Heidecorn, K. Measuring and modeling mercury in the atmosphere: a critical review. *Atmos. Chem. Phys.* **2015**, *15* (10), 5697−5713.

(16) Lyman, S. N.; Jaffe, D. A. Elemental and oxidized mercury in the upper troposphere and lower stratosphere. *Nature Geosci.* **2012**, *5*, 114−117.

(17) Finley, B. D.; Jaffe, D. A.; Call, K.; Lyman, S.; Gustin, M. S.; Peterson, C.; Miller, M.; Lyman, T. Development, testing, and deployment of an air sampling manifold for spiking elemental and oxidized mercury during the Reno Atmospheric Mercury Intercomparison Experiment (RAMIX). *Environ. Sci. Technol.* **2013**, *47* (13), 7277−7284.

(18) Jones, C. P.; Lyman, S. N.; Jaffe, D. A.; Allen, T.; O'Neil, T. L. Detection and quantification of gas-phase oxidized mercury compounds by GC/MS. *Atmos. Meas. Tech.* **2016**, *9* (5), 2195−2205.

(19) Gratz, L.; Ambrose, J.; Jaffe, D.; Shah, V.; Jaeglé, L.; Stutz, J.; Festa, J.; Spolaor, M.; Tsai, C.; Selin, N. Oxidation of mercury by bromine in the subtropical Pacific free troposphere. *Geophys. Res. Lett.* **2015**, *42*, 10494−10502.

(20) Holmes, C. D.; Jacob, D. J.; Corbitt, E. S.; Mao, J.; Yang, X.; Talbot, R.; Slemr, F. Global atmospheric model for mercury including oxidation by bromine atoms. *Atmos. Chem. Phys.* **2010**, *10* (24), 12037−12057.

(21) Coburn, S.; Dix, B.; Edgerton, E.; Holmes, C. D.; Kinnison, D.; Liang, Q.; ter Schure, A.; Wang, S.; Volkamer, R. Mercury oxidation from bromine chemistry in the free troposphere over the southeastern US. *Atmos. Chem. Phys.* **2016**, *16* (6), 3743−3760.

(22) *Atmospheric Mercury Network Site Operations Manual*, Version 1.2, National Atmospheric Deposition Program: Champaign, IL, 2015, http://nadp.sws.uiuc.edu/lib/manuals/AMNet_Operations_Manual_v1-2.pdf.

(23) Gustin, M. S.; Taylor, G. E.; Leonard, T. L. High Levels of Mercury Contamination in Multiple Media of the Carson River Drainage Basin of Nevada: Implications for Risk Assessment. *Environ. Health Perspect.* **1994**, *102* (9), 772−778.

(24) Tacey, S. A.; Xu, L.; Mavrikakis, M.; Schauer, J. J. Heterogeneous Reduction Pathways for Hg (II) Species on Dry Aerosols: A First-Principles Computational Study. *J. Phys. Chem. A* **2016**, *120* (13), 2106−2113.

(25) Gustin, M. S.; Pierce, A. M.; Huang, J.; Miller, M. B.; Holmes, H.; Loria-Salazar, S. M. Evidence for different reactive Hg sources and chemical compounds at adjacent valley and high elevation locations. *Environ. Sci. Technol.* **2016**, DOI: 10.1021/acs.est.6b03339.

(26) Feng, X.; Lu, J. Y.; Hao, Y.; Banic, C.; Schroeder, W. H. Evaluation and applications of a gaseous mercuric chloride source. *Anal. Bioanal. Chem.* **2003**, *376* (7), 1137−1140.

(27) Maria, P.-C.; Gal, J.-F.; Balza, M.; Peré-Trepat, E.; Tumbiolo, S.; Couret, J.-M. Using thermogravimetry for weight loss monitoring of permeation tubes used for generation of trace concentration gas standards. *Anal. Chem.* **2002**, *74* (1), 305−307.

DOI: 10.1021/acs.est.6b04211
Environ. Sci. Technol. 2016, 50, 12921−12927

Evidence for different reactive Hg sources and chemical compounds at adjacent valley and high elevation locations

Permission to Reprint

The following article is reprinted with permission from:

Evidence for Different Reactive Hg Sources and Chemical Compounds at Adjacent Valley and High Elevation Locations, Mae Sexauer Gustin, Ashley M. Pierce, Jiaoyan Huang, Matthieu B. Miller, Heather A. Holmes, and S. Marcela Loria-Salazar. *Environmental Science & Technology,* 2016, *50* (22), 12225-12231. DOI: 10.1021/acs.est.6b03339. Copyright (2016) American Chemical Society.

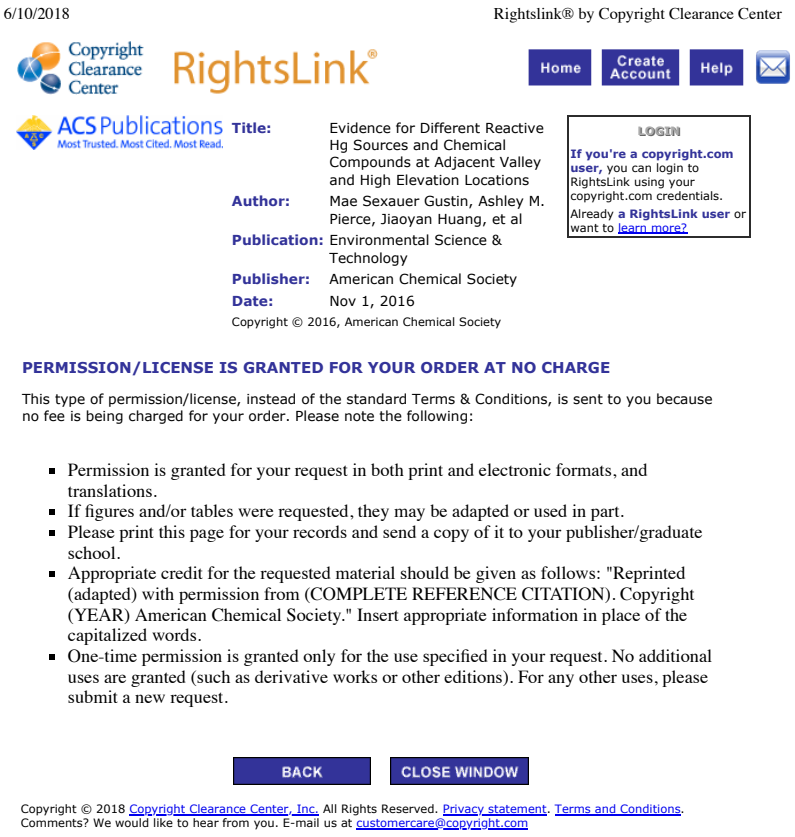

6/10/2018 Rightslink® by Copyright Clearance Center

Copyright Clearance Center RightsLink®

Home | Create Account | Help

ACS Publications Most Trusted. Most Cited. Most Read.

Title: Evidence for Different Reactive Hg Sources and Chemical Compounds at Adjacent Valley and High Elevation Locations

Author: Mae Sexauer Gustin, Ashley M. Pierce, Jiaoyan Huang, et al

Publication: Environmental Science & Technology

Publisher: American Chemical Society

Date: Nov 1, 2016

Copyright © 2016, American Chemical Society

LOGIN

If you're a copyright.com user, you can login to RightsLink using your copyright.com credentials.

Already **a RightsLink user** or want to learn more?

PERMISSION/LICENSE IS GRANTED FOR YOUR ORDER AT NO CHARGE

This type of permission/license, instead of the standard Terms & Conditions, is sent to you because no fee is being charged for your order. Please note the following:

- Permission is granted for your request in both print and electronic formats, and translations.
- If figures and/or tables were requested, they may be adapted or used in part.
- Please print this page for your records and send a copy of it to your publisher/graduate school.
- Appropriate credit for the requested material should be given as follows: "Reprinted (adapted) with permission from (COMPLETE REFERENCE CITATION). Copyright (YEAR) American Chemical Society." Insert appropriate information in place of the capitalized words.
- One-time permission is granted only for the use specified in your request. No additional uses are granted (such as derivative works or other editions). For any other uses, please submit a new request.

BACK CLOSE WINDOW

Copyright © 2018 Copyright Clearance Center, Inc. All Rights Reserved. Privacy statement. Terms and Conditions.
Comments? We would like to hear from you. E-mail us at customercare@copyright.com

Environmental Science & Technology

Article

pubs.acs.org/est

Evidence for Different Reactive Hg Sources and Chemical Compounds at Adjacent Valley and High Elevation Locations

Mae Sexauer Gustin,*[,†] Ashley M. Pierce,[†] Jiaoyan Huang,[†] Matthieu B. Miller,[†] Heather A. Holmes,[‡] and S. Marcela Loria-Salazar[‡]

[†]Department of Natural Resources and Environmental Science and [‡]Atmospheric Sciences Program, Department of Physics University of Nevada−Reno, Reno, Nevada 89557, United States

Supporting Information

ABSTRACT: The spatial distribution of chemical compounds and concentration of reactive mercury (RM), defined as the sum of gaseous oxidized mercury (GOM) and <3 μm particulate bound mercury (PBM), are poorly characterized. The objective of this study was to understand the chemistry, concentration, and spatial and temporal distribution of GOM at adjacent locations (12 km apart) with a difference in elevation of ∼1000 m. Atmospheric GOM measurements were made with passive and active samplers using membranes, and at one location, a Tekran mercury measurement system was used. The chemistry of GOM varied across time and location. On the basis of data collected, chemistry at the low elevation site adjacent to a highway was primarily influenced by pollutants generated by mobile sources (GOM = nitrogen and sulfur-based compounds), and the high elevation site (GOM = halogen-based compounds) was affected by long-range transport in the free troposphere over the marine boundary layer into Nevada. Data collected at these two locations demonstrate that different GOM compounds exist depending on the oxidants present in the air. Measurements of GOM made by the KCl denuder in the Tekran instrument located at the low elevation site were lower than that measured using membranes by 1.7−13 times. Accurate measurements of atmospheric concentrations and chemistry of RM are necessary for proper assessment of environmental impacts, and field measurements are essential for atmospheric models, which in turn influence policy decisions.

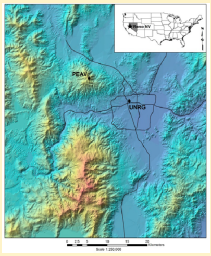

INTRODUCTION

Mercury exists as three forms in the atmosphere: gaseous elemental (GEM), particulate bound (PBM), and gaseous oxidized (GOM). Understanding the relative abundance and chemistry are critical for assessing the potential for impacts on human and ecological health.[1,2] Current estimates suggest that the total amount of mercury input into the atmosphere is ∼5.8 Gg yr^{-1}, with direct anthropogenic release of Hg responsible for 23% of atmospheric deposition.[3] Natural emissions from oceans, geologic sources, and volcanoes are estimated to be ∼10% of the total emitted each year. Once released into the environment, Hg becomes part of the global pool and is redistributed as well as recycled between the biosphere, lithosphere, atmosphere, and hydrosphere. Recycled Hg accounts for ∼60% of the total Hg emissions each year.[4]

The chemistry of atmospheric Hg is complex and not well understood.[5,6] For many years, Hg researchers have considered gaseous elemental Hg to be fairly inert, representing ≥99% of Hg in the atmosphere.[7,8] However, reactive mercury (RM, defined as GOM + PBM) can be as high as 25 to ∼100% in the planetary boundary layer, depending on the location and oxidants present.[9,10] The amount of GOM is impacted by the oxidant chemistry (i.e., ozone [O_3], bromine [Br], hydroxyl radical [OH]), temperature, and relative humidity of the area.[11] GEM has been estimated to have a mean residence in the atmosphere of 100 days to 1.5 years.[1,11−13] This may be shorter for a molecule emitted locally that could be oxidized quickly (minutes to hours), depending on the chemistry of the atmosphere and surfaces available.[10,14,15] GEM can be oxidized to Hg(I) and Hg(II) compounds, and form a variety of inorganic compounds (i.e., $HgSO_4$, $Hg(NO_3)_2$, $HgBr_2$, and $HgCl_2$) and organic compounds such as dimethyl and methyl Hg ($(CH_3)_2Hg$ and $(CH_3Hg)^+$).[5,6]

Recently, PBM and GOM concentrations have been combined in discussions as reactive Hg due to current uncertainties in automated measurement methods.[9,16,17] In addition, it has been demonstrated using data developed with surrogate surfaces that GOM concentrations measured by KCl-coated denuders in Tekran systems are not useful for determining dry deposition.[18−20] GOM collected by the denuder can decompose to GEM in the presence of O_3 and water vapor due to heterogeneous reactions.[21−24] GOM and GEM can be collected as PBM.[14,25] Other collection surfaces, such as nylon and cation exchange membranes (CEM), have been shown to collect more GOM relative to that collected by the denuder in the Tekran 2537/1130/135 system by up to 60−1000%, but they also have limitations.[9]

Mercury is input to ecosystems through wet and dry deposition.[1] GOM dry deposition can comprise 20−70% of

Received: July 4, 2016
Revised: October 6, 2016
Accepted: October 19, 2016
Published: October 19, 2016

DOI: 10.1021/acs.est.6b03339
Environ. Sci. Technol. 2016, 50, 12225−12231

that deposited, depending on location.[9,19,20,26] A range in deposition velocities have been reported (0.5−6 cm s^{-1}).[26,27] These observations indicate that the chemistry of GOM can vary temporally and spatially.[20,23]

The major hypothesis for this work was as follows: because oxidant chemistry varies across space and time, GOM chemistry and concentrations will vary depending on the oxidants present in the air at adjacent locations. This was tested through collection of data at a high elevation remote site and a lower elevation highway-impacted urban site. HYSPLIT analyses were done to understand sources when certain compounds were present, and planetary boundary layer height was determined to understand potential for convective mixing to impact GOM measured at the high elevation location.

MATERIALS AND METHODS

The high elevation location was on the top of Peavine Peak, NV (PEAV) at 2515 m above sea level (asl) (39°35′21.79″N, 119°55′43.72″W). The low elevation location (UNRG) was outside the University of Nevada College of Agriculture Biotechnology and Natural Resources Valley Road Greenhouse Facility at 1377 m asl (39°32′14.87″N, 119°48′16.93″W) in Reno adjacent to US Interstate 80, where >8500 vehicles travel per day[29] (see abstract graphic). These sites are 12 km apart. For details on each location and criteria air pollutant and meteorological measurements, see the Supporting Information. The predominant wind direction in this area of Nevada is from west to east.[30]

Nylon and cation exchange membranes (47 mm) were used in the University of Nevada— Reno Reactive Mercury Active System (UNRRMAS). Nylon membranes are polyamide filters (hydrophilic and chemically resistant to alkaline solutions and organic solvents (P/N: 25007-47-N, 0.2 μm, Sartorius Stedim Biotech).[23] Cation exchange membranes (CEM) are medium-hydrophilic cationic poly(ether sulfone) membranes (Mustang S, 0.2 μm Pall Corporation, Port Washington, NY).[23] An automated Tekran 2537/1130/1135 Hg speciation system was collocated with the UNRRMAS at the UNRG site. Box samplers for passive sampling GOM were also deployed at both locations (see Supporting Information and refs 19 and 31).

The UNRRMAS consists of six sample ports with three containing nylon filters (two in series in separate PFE Teflon filter cartridges (Savillex, P/N 401-21-47-10-21-2)) and three being CEM, also in a series of two. This allowed for measuring potential breakthrough. Sample ports were contained in a plastic box modified to serve as a weather shield.

Potential chemical forms of GOM on the nylon membranes were determined using thermal desorption.[20,13] Sample thermal desorption profiles were compared against reference GOM profiles generated from five solid phase GOM compounds ($HgBr_2$, $HgCl_2$, $HgN_2O_6{\cdot}H_2O$, $HgSO_4$, and HgO), elemental Hg[0] and methylmercury(II) chloride directly added to membranes (Alfa Aesar; CH_3HgCl 1000 ppm in water, see Supporting Information). It is important to note $HgN_2O_6{\cdot}H_2O$ was the compound used in all our other work and was mislabeled as $Hg(NO_3)_2$.[9,23]

To test for remnant Hg after desorption, nylon membranes were analyzed after thermal desorption by digestion using a modified EPA method 1631 E (Tekran 2600, Tekran Corp., Ontario, Canada; http://www.tekran.com/files/EPA_1631.pdf). Filters were digested in 100 mL of 18 MΩ Milli-Q water with 1% Optima HCl and 6 mL of 0.2 M BrCl solution for <24 h. CEM in the UNRRMAS and passive samplers were analyzed using the same method. CEM were not used in thermal desorption analyses. For details, see the Supporting Information.

Data Analyses. Tekran data were used when >50% of the data were available. This included passing QA/QC protocols associated with AMNET. For the CEM and nylon membranes, the median blank for all samples was subtracted from all filter concentrations. The median was not different from the mean. The equation used to calculate the total concentration was:

$$[(\text{concn of first filter (A)} + \text{concn of second filter (B)}) - (2 \times \text{median blank})]/(\text{mean flow rate} \times 1000) \quad (1)$$

Median concentration, standard deviation, and skewness and kurtosis for the UNRG CEM blanks were 0.2 ± 0.3 ng, 2.6, and 8.6 (n = 96), respectively, and for PEAV, the values were lower. For the nylon membrane, the values were 0.006 ± 0.02 ng, 6.0, and 2.3 (n = 80), respectively.

Calculation of the relative percent difference (RPD) was used to determine if there were potential outliers in the triplicate samples. To do this, concentration of one filter was compared to the mean of the other two filter concentrations during the same sampling period.[18] If the RPD was >75%, it was considered an outlier. Outliers could be due to a ripped or contaminated filter, improperly working pump, or filter pack not being properly sealed. For the passive samplers, a value of >90% was applied due to low concentrations.

Percent breakthrough was calculated using the following equation with A being the first membrane in series and B being the second:

$$\frac{(\text{B} - \text{blank})}{((\text{B} - \text{blank}) + (\text{A} - \text{blank}))} \times 100 \quad (2)$$

For the CEM, mean breakthrough was 25 (median 25) ± 12% (25−75th percentile range 21−36%, n = 149 samples). For the nylon membrane, mean breakthrough was 48 (median 46%) ± 22% (range 34−71%, n = 32). The method detection limit for the CEM using 3 times the standard deviation of blanks, excluding outliers and using the 75th percentile as a specific value, resulted in a detection limit of 0.3 ng. The method detection limit for the nylon membrane was 0.006 ng.

Global Data Assimilation System (GDAS) 1° × 1° meteorology was applied with a starting height at 1000 m above ground at each location. This was done so that the general flow of air into this area of complex terrain was modeled (see abstract graphic). During every selected event or sampling period, back trajectories were calculated 4 times a day to capture a daily air parcel transport (0400, 1000, 1600, and 2200 h, local standard time) during the entire period. Two different trajectory analyses were used: gridded frequency distributions (GFDs) and cluster analysis.[20,26,32,33] For GFDs, trajectories were calculated back 240 h; however, for cluster analysis, the trajectories were calculated back 120 h. On the basis of previous work, uncertainties of back trajectories were 20% of their traveling distances.[34,35] Cluster and GFDs were plotted using ArcGIS.

Planetary boundary layer heights were calculated using radiosonde data from the Reno National Weather Service and the HYSPLIT model.[28] The Reno National Weather Service is 1516 m asl (39°34′04.8″N, 119°47′45.6″W). Data were compiled into the same sampling periods as the highway impacted site from January 2014 to May 2015. Balloon sounding measurements were from the 1600 h Pacific Standard

DOI: 10.1021/acs.est.6b03339
Environ. Sci. Technol. 2016, 50, 12225−12231

Time (PST) launch times. Soundings at this time provide an idea of the height of convective mixing in the atmospheric boundary layer. Balloon sounding and HYSPLIT data were plotted in MATLAB version 8.5, R2015a (MathWorks Inc., MA, United States).

RESULTS AND DISCUSSION

Criteria Air Pollutants. At PEAV, mean CO concentrations were ~150 ppbv in the summer, and in the fall, median concentrations increased starting at noon to 1700 PST h to ~200 ppbv; O_3 concentrations were fairly constant with median concentrations of ~50 ppbv in the summer and 45 ppbv in the fall (see Figure S1). In contrast, CO concentrations at the UNRG site were 244 ± 98, 397 ± 286, 529 ± 384, and 261 ± 143 ppbv, and O_3 concentrations were 25 ± 17, 23 ± 19, 17 ± 17, and 44 ± 24 ppbv in the summer, fall, winter, and spring, respectively (Table S1). The lack of overlap of the O_3 and CO concentrations at UNRG and PEAV, a typical diel pattern for atmospheric pollutants associated with traffic at UNRG, and lower O_3 and higher CO concentrations at the UNRG site suggests little connectedness and different air masses at these two sites (Table S1 and Figures S1 and S2). This fits with the location of the site that was not in the center of the valley and close to a ridge (cf. ref 30 and abstract graphic). Previous work at multiple locations in Nevada has shown that sampling location significantly influences data collected in complex terrain.[30]

Biweekly Concentrations Measured by Tekran, UNRRMAS, and Passive Sampler Uptake. Concentrations discussed represent A + B CEM UNRRMAS membranes added together. At UNRG, GOM concentrations measured by the Tekran system (20 ± 10 pg m^{-3}) were always lower than those measured by the UNRRMAS. There were two occasions when the Tekran RM (42 ± 43 pg m^{-3}) measurement was similar to the active CEM concentration (Figure S3); however, this may be due to lack of Tekran data, because, for these two dates (March 7 and December 16, 2014), only ~50% of the Tekran data were available. Huang et al.[24] showed that the concentration on the CEM was always higher than the Tekran RM measurement at the UNRG site. At the UNRG site, CEM GOM concentrations were 86 ± 48 pg m^{-3} (mean ± standard deviation, median 70 pg m^{-3}, n = 42). Mean breakthrough on the backup CEM was 25 ± 8% (0.7 standard error) (21.0 ± 4.8 pg m^{-3}). There was no correlation between concentration and breakthrough. Nylon membranes do not quantify GOM concentrations.[9] However, there were times when the nylon membrane total concentration was greater than that of CEM (see Figure S4).

Correlation between UNRRMAS GOM concentrations and GOM uptake rate at UNRG was r^2 = 0.4 (p = 0.006, n = 31, Figure 1). The intercept for zero GOM uptake by the passive sampler was 50 pg m^{-3}. This may be due to the fact the passive sampler has design limitations and does not efficiently collect GOM, as pointed out in Huang and Gustin[19]. The mean passive sampler uptake rate was 1.1 ± 0.9 pg h^{-1} (n = 32) (Figure 2).

CEM concentrations were not correlated with Tekran measured RM, GEM, maximum RM, or PBM; however, they were correlated with GOM (r^2 = 0.51, P < 0.001), and concentrations measured by the CEM were 1.7−13 times higher than those in the Tekran system. GOM measured by the CEM was up to 10% of GEM. Gustin et al.[14] pointed out that the ratios of GOM concentrations for different GOM

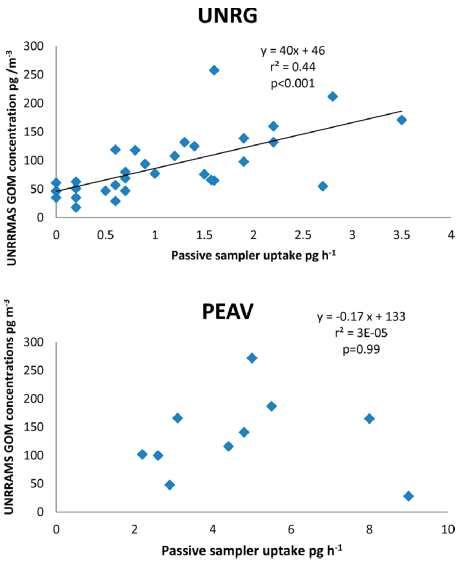

Figure 1. Correlation between GOM measured by the UNRRMAS and the passive box sampler at the College of Agriculture, Biotechnology, and Natural Resources Valley Road Experiment Station (UNRG) site and the Peavine Peak (PEAV) site. Note the difference in scale between the two graphs.

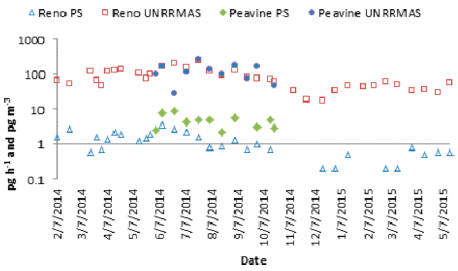

Figure 2. Passive sampler uptake (pg h^{-1}) and UNRRMAS GOM concentration (pg m^{-3}). Note the log scale.

compounds measured using the CEM/Tekran system are $HgBr_2$ (1.6), $HgSO_4$ (2.3), $HgCl_2$ (2.4), HgO (3.7), and $HgN_2O_6{\cdot}H_2O$ (12.6). These ratios were derived from laboratory experiments in charcoal scrubbed air, but provide insight into how CEM GOM concentrations would be compared to those of the Tekran system. Field samples differ from the laboratory ratios, because of atmospheric chemistry impacting KCl-denuder measurements and/or other GOM compounds potentially being present on the membranes.

At PEAV, passive sampler uptake was 4.7 ± 2.1 pg h^{-1} and mean CEM GOM air concentration was 147 ± 73 pg m^{-3} (n = 11) that were higher than those at UNRG. Unlike UNRG, PEAV data from these methods were not correlated. No data were collected using the Tekran system at PEAV. Similar to

DOI: 10.1021/acs.est.6b03339
Environ. Sci. Technol. 2016, 50, 12225−12231

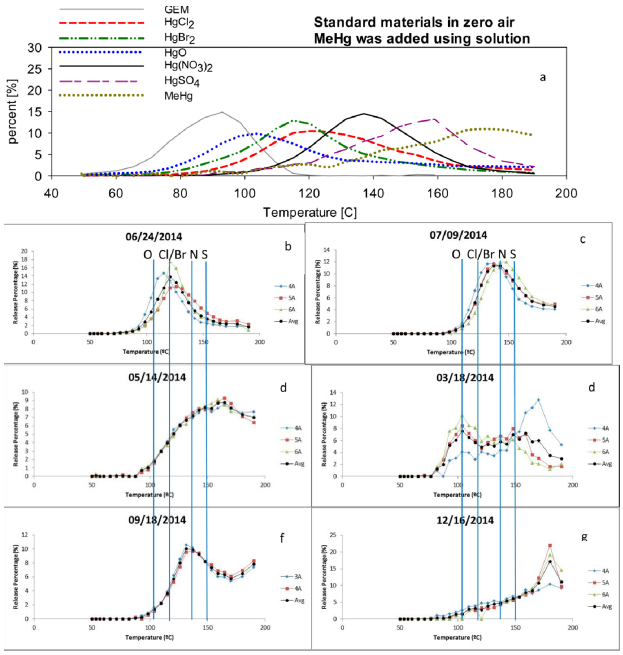

Figure 3. Thermal desorption profiles. Top graph is permeation from standard materials in zero air modified from Gustin et al.[9] with methylmercury profile added (a). The following are graphs showing a triplicate and an average profile. Panel b (6/24) shows $HgCl_2/HgBr_2$, and panel c (7/09)shows Hg, sulfur, and nitrogen compounds at PEAV. Panel d (5/14) shows a mixture of compounds. Panel e (3/18) shows HgO, Hg-nitrogen, and sulfur compounds. Panel f (9/18) shows Hg-nitrogen compounds with an unknown compound producing a high residual tail, and panel g (12/16) shows a gradual increase with an unknown peak from UNRG. Note Hg $(NO_3)_2$ = $HgN_2O_6{\cdot}H_2O$.

that at UNRG, CEM membrane concentration was higher than that of the nylon membrane by 2−13 times (see Figure S5).

Thermal Desorption Profiles. As data from this system has been analyzed, we realized there are several issues that need to be considered. The current design of the system is not as efficient as possible and needs to be modified. Preliminary work has demonstrated a method for better resolution of peaks (data not shown). On the basis of the comparison concentrations measured by the CEM, the nylon membrane does not capture all GOM (Figure S4 and 5). Because laboratory tests show the nylon membrane collects forms being permeated, it is considered a qualitative measure. It also could possibly not measure all compounds; however, compounds permeated so far have been measured in the laboratory. Because of the current broad peaks, identification of specific compounds is difficult. At high humidity, the CEM can collect more GOM. Both methods have limitations, but are steps toward developing new methods for quantifying GOM and identification of the compounds. In addition, it must be remembered that exact compounds being permeated for the standard compounds are not known. Given these limitations, profiles of the potential compounds are qualitative. Peak temperatures measured in this study correspond with those from desorbed compounds as follows: 100−105 °C HgO, 115 and 120 °C $HgBr_2$ and $HgCl_2$, respectively, $HgN_2O_6{\cdot}H_2O$ at 140 °C, and $HgSO_4$ at 150−160 °C (Figure 3a; Table 1). There were two profiles that started at 100 °C that either immediately increased and plateaued with a high residual tail or gradually increased (Figures 3d and f). The first of these indicates a wide variety of compounds in air (Table 1 and Figure 3). Observed profiles demonstrate that compounds at UNRG were primarily nitrogen- and sulfur-based or a variety of compounds in the spring and winter.

At PEAV, 9 out of 11 two-week periods had clear peaks that overlapped with $HgCl_2/HgBr_2$ desorption profiles (Figure 3b). Three of these profiles also had a peak at HgO (Table 1). For 10 overlapping time periods at UNRG, the profiles were indicative of a mixture of compounds or had N and S compound peaks that would be expected at a highway location (Figures 3d and e), and this suggests rapid oxidation. This was suggested to occur based on samples collected from a manifold during the Reno Atmospheric Mercury Intercomparison eXperiment (RAMIX[14]) and a study in Florida.[20]

Distinct $HgBr_2/HgCl_2$ peaks were observed only at UNRG in June 2014, and $HgBr_2/HgCl_2$ peak patterns were observed at PEAV. Profiles at the two locations in July were similar to Hg-nitrogen and -sulfur compounds dominating (Figure 3 c; Table 1). During the June measurement, cluster trajectories indicated that most of the air at PEAV and UNRG was from >2000 m (Figures S6 and S7). Air was moving fast based on the 120 h back-trajectories. During July, the distribution of the trajectories

DOI: 10.1021/acs.est.6b03339
Environ. Sci. Technol. 2016, 50, 12225−12231

Table 1. Summary of Thermal Desorption Profiles from UNRG and PEAV[a]

start date	RENO	PEAV
12/6/2013	S	
12/27/2013	N/S	
1/17/2014	100^	
1/24/2014	100^	
2/7/2014	S/N	
3/18/2014	O/S	
3/35/2014	Cl/Br	
4/1/2014	O 150^	
4/8/2014	100 plateau	
4/23/2014	100 plateau	
5/7/2014	O high tail	
5/14/2014	100 ^plateau	
5/23/2014	100^plateau	
5/28/2014	100 ^plateau	
6/4/2014	100^plateau	O/Cl
6/11/2014	Cl/Br	O/Cl/Br
6/25/2014	Cl/Br	O/Cl/Br
7/9/2014	N/S	N
7/23/2014	N/S	N/high tail
8/6/2014		Cl/Br
8/20/2014	N/S	Cl/Br
9/4/2014		Cl/Br
9/18/2014	N/S	100^plateau
9/30/2014	N/S	Cl/Br/N
10/16/2014	N/S	Cl/Br/residual
10/30/2014	N/S	Cl/Br
11/17/2014	N/S	
12/16/2014	100^gradual	
12/31/2014	100^gradual	
1/15/2015	100^gradual	
2/2/2015	100^gradual	
2/15/2015	100^plateau	
2/28/2015	100^gradual	
3/15/2015	100^plateau	
3/31/2015	100^gradual	
4/15/2015	N/S	
5/1/2015	N/S	
5/15/2015	100^plateau	

[a]When distinct profiles were observed, they are indicated. Cl/Br indicates curves that point to $HgCl_2$ and $HgBr_2$ compounds. N/S indicates curves of nitrogen and sulfur compounds permeated. 10$\hat{0}$ indicates an increase in concentrations of GOM compounds off of the nylon membranes at 100 °C. The profile then either increased significantly and plateaued, indicating a variety of compounds (plateau), or increased gradually (gradual). Residual indicates a residual tail associated with the peaks observed.

was more localized (Figure S8). During both of these periods, planetary boundary layer height was 2−3 km above the valley floor, which would encompass PEAV (Figure S9). However, given the prevailing wind direction from west to east, any mixing to PEAV would have been limited due to its location on the western edge of the basin (cf. ref 30 and abstract graphic).

During July 2014, GOM chemistry indicated that local pollution from the valley floor in UNRG could be mixed up to PEAV. During this time, trajectories were short, and the frequency distribution showed a more localized stationary air mass (Figure S8). Calculated planetary boundary layer height also supports this (Figure S9).

On the basis of GOM chemistry, some mixing was observed for sampling that overlapped for the UNRG and PEAV sites. During August and September, GOM compounds were $HgCl_2$/$HgBr_2$ at PEAV, and nitrogen- and sulfur-based compounds were at UNRG. Despite the calculated boundary layer height (Figure S9), the chemistry of GOM indicates lack of mixing between the two sites. This is due to the location of the UNRG site on the west side of a complex valley that is small in size, limiting deep mixing, and prevailing winds from west to east in the free troposphere (cf. ref 30 and abstract graphic). This is also supported by CO and O_3 data.

Implications. Chemistry of GOM can vary at sites in close proximity, depending on the air masses at each location. The UNRRMAS CEM GOM concentrations were always higher than the KCl-coated denuder GOM measurements from the Tekran system at UNRG. The presence of $HgCl_2$ and $HgBr_2$ compounds at PEAV suggests marine boundary interactions and/or transport from free troposphere where Br compounds reside.[11,36] High concentrations observed at PEAV (Figure 2) support other work that measured high GOM concentrations in the free troposphere.[11,19,20,26,30,32,33,36] GOM concentrations were also high at UNRG, and the chemical profile suggests the impact of mobile sources on GOM chemistry.[16] Passive samplers were observed to have higher uptake rates at the PEAV site due to the higher wind speed at this location. Lyman et al.[31] demonstrated an impact on wind speed on uptake. Passive sampler uptake rates and CEM concentrations were moderately correlated at the UNRG site due to both being exposed to similar concentrations of Hg-nitrogen- and Hg-sulfur-based compounds. At PEAV, wind speed would affect passive sampler uptake, but this does not occur at UNRRAMS. A difference in compounds at each location is supported by thermal desorption profiles from each site.

Chemical compounds measured at PEAV (Table 1) indicate compounds that could form as polluted air mass plumes from Asia travel over the ocean and react, forming Hg-oxide compounds[17] and also halogenated compounds that could indicate transport and reaction with the marine boundary layer[36] or compounds concentrated at the tropopause.[37,11] In July, the overlap of PEAV and UNRG suggests GOM compounds generated due to local oxidants.[14,20] This is supported by CO and ozone data that indicate little connectedness between the two locations.

Currents models do not use all potential oxidation reaction mechanisms and are limited to certain reactions and low/inaccurate Tekran GOM KCl denuder measurements. A better understanding of the array of chemical compositions of GOM is important for refining atmospheric mercury chemistry. Because models affect policy decisions, without accurate data, this global contaminant will not be properly assessed. This will also significantly affect dry deposition estimates.

■ ASSOCIATED CONTENT

Supporting Information

The Supporting Information is available free of charge on the ACS Publications website at DOI: 10.1021/acs.est.6b03339.

Additional text, tables, and figures, including site details, membrane preparation, the Tekran system, sample collections, condition summaries, and additional analyses (PDF)

DOI: 10.1021/acs.est.6b03339
Environ. Sci. Technol. 2016, 50, 12225−12231

AUTHOR INFORMATION

Corresponding Author

*Phone: 775-784-4203; e-mail: mgustin@cabnr.unr.edu.

Notes

The authors declare no competing financial interest.

ACKNOWLEDGMENTS

Funding for this work was provided by the National Science Foundation (Grant 629679). The authors thank the students that helped collect and analyze samples, including Keith Heidecorn, Jennifer Arnold, Matt Peckham, Jen Schoener, and Douglas Yan.

REFERENCES

(1) Lindberg, S.; Bullock, R.; Ebinghaus, R.; Engstrom, D.; Feng, X.; Fitzgerald, W.; Pirrone, N.; Prestbo, E.; Seigneur, C. A Synthesis of Progress and Uncertainties in Attributing the Sources of Mercury in Deposition. *Ambio* **2007**, *36*, 19−32.

(2) Selin, N. E. Global Biogeochemical Cycling of Mercury: A Review. *Annual Review of Environment and Resources* **2009**, *34*, 43−63.

(3) Song, S.; Selin, N. E.; Soerensen, A. L.; Angot, H.; Artz, R.; Brooks, S.; Brunke, E. G.; Conley, G.; Dommergue, A.; Ebinghaus, R.; Holsen, T. M.; Jaffe, D. A.; Kang, S.; Kelley, P.; Luke, W. T.; Magand, O.; Marumoto, K.; Pfaffhuber, K. A.; Ren, X.; Sheu, G. R.; Slemr, F.; Warneke, T.; Weigelt, A.; Weiss-Penzias, P.; Wip, D. C.; Zhang, Q. Top-down constraints on atmospheric mercury emissions and implications for global biogeochemical cycling. *Atmos. Chem. Phys.* **2015**, *15*, 7103−7125.

(4) UNEP. *Global Mercury Assessment 2013: Sources, Emissions, Releases and Environmental Transport*; UNEP Chemicals Branch: Geneva, Switzerland, 2013.

(5) Subir, M.; Ariya, P. A.; Dastoor, A. P. A review of uncertainties in atmospheric modeling of mercury chemistry I. Uncertainties in existing kinetic parameters − Fundamental limitations and the importance of heterogeneous chemistry. *Atmos. Environ.* **2011**, *45*, 5664−5676.

(6) Lin, C.-J.; Pehkonen, S. O. Oxidation of elemental mercury by aqueous chlorine (HOCl/OCl−): Implications for tropospheric mercury chemistry. *Journal of Geophysical Research: Atmospheres* **1998**, *103*, 28093−28102.

(7) Slemr, F.; Schuster, G.; Seiler, W. Distribution, speciation, and budget of atmospheric mercury. *J. Atmos. Chem.* **1985**, *3*, 407−434.

(8) Schroeder, W. H.; Munthe, J. Atmospheric mercury - An overview. *Atmos. Environ.* **1998**, *32*, 809−822.

(9) Gustin, M. S.; Amos, H. M.; Huang, J.; Miller, M. B.; Heidecorn, K. Measuring and modeling mercury in the atmosphere: a critical review. *Atmos. Chem. Phys.* **2015**, *15*, 5697−5713.

(10) Steffen, A.; Lehnherr, I.; Cole, A.; Ariya, P.; Dastoor, A.; Durnford, D.; Kirk, J.; Pilote, M.; et al. Atmospheric mercury in the Canadian Arctic. Part I: A review of recent field measurements. *Sci. Total Environ.* **2015**, *509*, 3−15.

(11) Holmes, C. D.; Jacob, D. J.; Corbitt, E. S.; Mao, J.; Yang, X.; Talbot, R.; Slemr, F. Global atmospheric model for mercury including oxidation by bromine atoms. *Atmos. Chem. Phys.* **2010**, *10*, 12037−12057.

(12) Radke, L. F.; Friedli, H. R.; Heikes, B. G. Atmospheric mercury over the NE Pacific during spring 2002: Gradients, residence time, upper troposphere lower stratosphere loss, and long-range transport. *J. Geophys. Res.* **2007**, *112*, D19305.

(13) Seigneur, C.; Lohman, K. Effect of bromine chemistry on the atmospheric mercury cycle: Journal of Geophysical Research. *J. Geophys. Res.* **2008**, *113*, D23309.

(14) Gustin, M. S.; Huang, J.; Miller, M. B.; Peterson, C.; Jaffe, D. A.; Ambrose, J.; Finley, B. D.; Lyman, S. N.; Call, K.; Talbot, R.; Feddersen, D.; Mao, H.; Lindberg, S. E. Do We Understand What the Mercury Speciation Instruments Are Actually Measuring? Results of RAMIX. *Environ. Sci. Technol.* **2013**, *47*, 7295−7306.

(15) Engle, M. A.; Sexauer Gustin, M.; Lindberg, S. E.; Gertler, A. W.; Ariya, P. A. The influence of ozone on atmospheric emissions of gaseous elemental mercury and reactive gaseous mercury from substrates. *Atmos. Environ.* **2005**, *39*, 7506−7517. (15) Engle, M. A.; Sexauer Gustin, M.; Lindberg, S. E.; Gertler, A. W.; Ariya, P. A. The influence of ozone on atmospheric emissions of gaseous elemental mercury and reactive gaseous mercury from substrates. *Atmos. Environ.* **2005**, *39*, 7506−7517.

(16) Gustin, M. S.; Huang, J. Y.; Miller, M. B.; Peterson, C.; Jaffe, D. A.; Ambrose, J.; et al. Do We Understand What the Mercury Speciation Instruments Are Actually Measuring? Results of RAMIX. *Environ. Sci. Technol.* **2013**, *47*, 7295−7306.

(17) Weiss-Penzias, P.; Amos, H. M.; Selin, N. E.; Gustin, M. S.; Jaffe, D. A.; Obrist, D.; Sheu, G. R.; Giang, A. Use of a global model to understand speciated atmospheric mercury observations at five high-elevation sites. *Atmos. Chem. Phys.* **2015**, *15*, 1161−1173.

(18) Peterson, C.; Alishahi, M.; Gustin, M. S. Testing the use of passive sampling systems for understanding air mercury concentrations and dry deposition across Florida, USA. *Sci. Total Environ.* **2012**, *424*, 297−307.

(19) Huang, J.; Gustin, M. S. Use of Passive Sampling Methods and Models to Understand Sources of Mercury Deposition to High Elevation Sites in the Western United States. *Environ. Sci. Technol.* **2015**, *49*, 432−441.

(20) Huang, J.; Miller, M. B.; Edgerton, E.; Gustin, M. S. Use of criteria pollutants, active and passive mercury sampling, and receptor modeling to understand the chemical forms of gaseous oxidized mercury in Florida: Atmos. *Atmos. Chem. Phys. Discuss.* **2015**, *15*, 12069−12105.

(21) Lyman, S. N.; Jaffe, D. A.; Gustin, M. S. Release of mercury halides from KCl denuders in the presence of ozone. *Atmos. Chem. Phys.* **2010**, *10*, 8197−8204.

(22) McClure, C. D.; Jaffe, D. A.; Edgerton, E. S. Evaluation of the KCl Denuder Method for Gaseous Oxidized Mercury using HgBr2 at an In-Service AMNet Site. *Environ. Sci. Technol.* **2014**, *48*, 11437−11444.

(23) Huang, J. Y.; Gustin, M. S. Uncertainties of Gaseous Oxidized Mercury Measurements Using KCl-Coated Denuders, Cation-Exchange Membranes, and Nylon Membranes: Humidity Influences. *Environ. Sci. Technol.* **2015**, *49*, 6102−6108.

(24) Huang, J. Y.; Miller, M. B.; Weiss-Penzias, P.; Gustin, M. S. Comparison of Gaseous Oxidized Hg Measured by KCl-Coated Denuders, and Nylon and Cation Exchange Membranes. *Environ. Sci. Technol.* **2013**, *47*, 7307−7316.

(25) Luke, W. 2016 NOAA report. ftp://ftp.arl.noaa.gov/.mercury-workshop [ftp.arl.noaa.gov] (accessed June 2016).

(26) Gustin, M.; Weiss-Penzias, P.; Peterson, C. *Investigating sources of gaseous oxidized mercury in dry deposition at three sites across Florida*; Atmospheric Chemistry & Physics: United States, 2012; Vol. *12*, pp. 9201−9219.

(27) Zhang, L.; Wright, L. P.; Blanchard, P. A review of current knowledge concerning dry deposition of atmospheric mercury. *Atmos. Environ.* **2009**, *43*, 5853−5864.

(28) Draxler, R. R.; Hess, G. D. HYSPLIT 4 USER's Guide. In *NOAA Technical Memorandum ERL ARL-230*; NOAA: Washington, DC, 2005.

(29) NDOT. https://www.nevadadot.com/reports_pubs/traffic_report/ (accessed 25 October 2016).

(30) Gustin, M. S.; Fine, R.; Miller, M.; Jaffe, D.; Burley, J. The Nevada Rural Ozone Initiative (NVROI): Insights to understanding air pollution in complex terrain. *Sci. Total Environ.* **2015**, *530*−*531*, 455−470.

(31) Lyman, S. N.; Gustin, M. S.; Prestbo, E. M. A passive sampler for ambient gaseous oxidized mercury concentrations. *Atmos. Environ.* **2010**, *44*, 246−252.

(32) Huang, J. Y.; Gustin, M. S. Evidence for a Free Troposphere Source of Mercury in Wet Deposition in the Western United States. *Environ. Sci. Technol.* **2012**, *46*, 6621−6629.

DOI: 10.1021/acs.est.6b03339
Environ. Sci. Technol. 2016, 50, 12225−12231

(33) Weiss-Penzias, P.; Gustin, M. S.; Lyman, S. N. Observations of speciated atmospheric mercury at three sites in Nevada: Evidence for a free tropospheric source of reactive gaseous mercury. *J. Geophys. Res.* **2009**, *114*, D14302.
(34) Stohl, A. Computation, accuracy and applications of trajectories - a review and bibliography. *Atmos. Environ.* **1998**, *32*, 947−966.
(35) Stohl, A.; Forster, C.; Eckhardt, S.; Spichtinger, N.; Huntrieser, H.; Heland, J.; Schlager, H.; Wilhelm, S.; Arnold, F.; Cooper, O. A backward modeling study of intercontinental pollution transport using aircraft measurements. *J. Geophys. Res.* **2003**, *108*, 4370.
(36) Timonen, H.; Ambrose, J. L.; Jaffe, D. A. Oxidation of elemental Hg in anthropogenic and marine airmasses. *Atmos. Chem. Phys.* **2013**, *13*, 2827−2836.
(37) Lyman, S. N.; Jaffe, D. A. Formation and fate of oxidized mercury in the upper troposphere and lower stratosphere. *Nat. Geosci.* **2011**, *5*, 114−117.

DOI: 10.1021/acs.est.6b03339
Environ. Sci. Technol. 2016, 50, 12225−12231